University of Sheffield

Department of Civil
and Structural Engineering

The geotechnical behaviour of ballast materials for railway track maintenance

By

Peter Fair

Supervisor: Professor W.F. Anderson

A thesis submitted to
The University of Sheffield
Department of Civil and Structural Engineering
for the degree of Doctor of Philosophy

July 2003

SUMMARY

The search for an improved mechanised method of maintaining railway track to the correct level and alignment led to the development of the stoneblower, a machine that lifts the rail and attached sleepers and pneumatically injects the required amount of 20mm stone into the void created, creating a two-layer granular foundation. Stoneblowing minimises disturbance to the existing well-compacted ballast and reduces the amount of particle breakage normally associated with maintenance. By 1999 a fleet of stoneblowers was fully operational across the UK rail network and achieving target rates of track maintenance. However in some cases the track quality appears to have been left in worse condition than it was pre-maintenance.

To investigate the deformation characteristics of the foundations directly below the sleepers a programme of large scale triaxial tests on 20mm stone, 50mm ballast and two-layer specimens was carried out under monotonic, cyclic and post cyclic monotonic loading. It was perceived that the amount of volume change, which was partly dependent on the amount of particle breakage, was critical to the overall permanent strain.

From the laboratory testing it was found that particle breakage behaviour had an important role to play in the performance of the ballast, even at relatively low pressures. The specimens were particularly sensitive to the moisture content and to the variation in the subgrade modulus, both of which were related to an increase in the amount of particle breakage occurring in the test. In the two-layer specimens there was an increase in the resilient modulus and a decrease in the amount of breakage.

Complementary to the laboratory work in-depth analysis of track quality data and of data downloaded from the stoneblower was undertaken. Detailed analysis of the data gave a better understanding of the performance and provided guidance for optimising the deployment of the stoneblower fleet and the stoneblowing procedures.

ACKNOWLEDGEMENTS

"A wife of noble character who can find? She is worth far more than rubies....
She watches over the affairs of her household and does not eat the bread of laziness.
Her children arise and call her blessed; her husband also, and he praises her.
Many women do noble things, but you surpass them all.
Charm is deceptive and beauty is fleeting;
but a women who fears the Lord is to be praised
Give her the reward she has earned,
and let her works bring her praise at the city gate."

The Bible – Proverbs 31

I would like to take this opportunity to give my sincere thanks to my wife who has stood by me during this difficult period of our lives. Frankie, I am eternally indebted to you. To my two sons Shem and Joel, you are very precious to me and I love you.

I would also like to thank my supervisor Prof. Bill Anderson, who has worked extremely hard to keep to my timescale during the few weeks prior to submission; his time, help and support have been priceless. The help and advice from the laboratory technicians was much appreciated, especially that of Paul Osborne, Mark Foster and Tim Robinson.

The research was mainly funded by the E.P.S.R.C. This was raised to a CASE award funded project with the support of Railtrack, thanks to Peter McMichael and the Stoneblower Project Team.

Specific thanks is due to our friends and families, although to list everyone who has been a support and help to me (and Frankie) would be too long, but you most certainly know who you are. However I will name a few – Mary for all those hours you have looked after the boys, Ed and Kath, Sam and Naomi, Simon and Lorna, Kirsty, Alex and Tom for your invaluable drawing skills, Jon, Jill and John, Big Shem, Adrian,....

And most importantly to God, for strength and daily bread.

"Because the foolishness of God is wiser than men;
and the weakness of God is stronger than men."

The Bible, 1 Corinthians 1 vs. 25

"It's best to know what you're looking for before you look for it."
"Sometimes the more you think, the more there is no real answer."

Quotes by Pooh. The House at Pooh Corner. A.A. Milne

Table of Contents

LIST OF TABLES

LIST OF FIGURES

LIST OF PLATES

LIST OF SYMBOLS

α, β, γ	=	Coefficients
ε	=	Total permanent strain after N cycles
ε_1	=	First load cycle plastic strain
ε_a	=	Axial strain
ε_{ar}	=	Resilient axial strain
ε_P	=	Cumulative plastic strain
ε_r	=	Radial strain
ε_R	=	Resilient/recoverable strain
ε_{rr}	=	Resilient radial strain
ε_{sr}	=	Resilient shear strain
ε_v	=	Volumetric strain
ε_{vr}	=	Resilient volumetric strain
φ'	=	Angle of shearing resistance
φ'_{peak}	=	Peak angle of shearing resistance
θ	=	Sum of principle stresses ($\sigma_1 + \sigma_2 + \sigma_3$)
σ	=	Characteristic tensile strength / principle stress
σ_0	=	Characteristic tensile strength
σ_1	=	Principle stress
σ_2	=	Principle stress
σ_3	=	Principle stress
σ_a	=	Tensile stress at the first asperity breakage
σ_c	=	Crushing stress
σ_d	=	Deviator stress
σ_f	=	Average particle tensile stress at failure
σ_{sp}	=	Average characteristic tensile stress in a single particle
$\Delta V_{\varepsilon,b}$	=	Volumetric strain due to breakage alone
$\Delta V_{\varepsilon,s}$	=	Volumetric strain due to shearing alone
$\Delta V_{\varepsilon,total}$	=	Observed total volumetric strain
ΔV_b	=	Volume change due to breakage alone
ΔV_s	=	Volume change due to shearing alone
ΔV_{total}	=	Total change in volume

A_0	=	Original area
a_1	=	Material parameter
b	=	Ballast material component
B_p	=	Breakage potential
B_r	=	Relative breakage
B_s	=	Breakage score
B_t	=	Total breakage
B_{TBS}	=	Total breakage score
C	=	Dimensionless constant controlling the rate of growth of deformation
c'	=	Cohesion intercept
C_a	=	Average co-ordination number
d	=	Diameter of particle
$\bar{d}$	=	Mean particle size
d_a	=	Particle diameter at first asperity breakage
d_f	=	Particle diameter at particle fracture
d_{max}	=	Maximum particle size
D	=	Specimen diameter
e	=	Void ratio
E_s	=	Secant modulus taken at 250kPa
E_t	=	Tangent modulus at zero strain
F	=	Force applied
F_a	=	Force at first asperity breakage
F_c	=	Force at initial asperity breakage (Nakata et al, 1999)
F_f	=	Peak force at major splitting / Force at failure
F_{sp}	=	Force acting on a single particle
H	=	Specimen height
h_0	=	Original height of the square based pyramid
h_b	=	Approximate height of breakage (broken off from the square based pyramid)
k_1, k_2	=	Material parameters
k_a	=	Coefficient for ballast durability
k_f	=	Coefficient for initial degree of ballast fouling
k_w	=	Coefficient for wheel load
m	=	Weibull modulus
M_r	=	Resilient modulus

n	=	Number of specimens
n	=	Porosity of the material
n_0	=	Theoretical maximum value of porosity when $M_r = 0$
n_b	=	Number of broken particles
n_i	=	Number of particles in the original specimen
N	=	Number of load repetitions
N	=	Number of particles in a cross sectional area of the specimen
N_{total}	=	Total number of particles tested
p'	=	Normal effective stress
P_0	=	Atmospheric pressure of 100kPa
P_1	=	Initial high frequency impact force caused by a dipped joint
P_2	=	Low frequency unsprung mass caused by a dipped joint
P_s	=	Static wheel load
$P_s(d)$	=	Probability of survival
q	=	deviator stress
R^2	=	Coefficient of conformity
R_a	=	Cross sectional area of the particle
s	=	Standard deviation of the specimens
$SE(\overline{X})$	=	Standard error of the mean
t	=	Traffic (in the same units as P_s)
v_i	=	Volume of original specimen
V_s	=	Volume of solids
V_s	=	Volume of the solids
V_{sbp}	=	Volume of a square based pyramid, where the height is the same length as the sides of the base (ie V_{sbp} = 1/3 height^3)
V_{sp}	=	Volume of single particle
x	=	Repeated number of loads or tonnage carried by the track
y	=	Settlement

CHAPTER 1

Introduction

1.1 Preface

For efficient running of trains and for passenger comfort railway track must be maintained to the correct level and alignment for the speed of traffic that uses the track. Movements from the ideal position occur for a number of reasons including subgrade settlement, densification of the ballast and ballast particle breakdown due to the repeated loading, lateral spread of the ballast, and deterioration of the sleepers and their fixings. When the track quality deteriorates beyond certain limits maintenance for re-levelling and re-alignment is necessary.

Two such mechanised maintenance techniques are known as stoneblowing and tamping. The stoneblower was one of a number of projects that came out of a drive in the 1970s by British Rail to overcome a phenomenon known as 'ballast memory'. Ballast memory is where the track, maintained using the normal tamping technique, returns with trafficking to its original, pre-maintenance geometry (see Section 2.2.4.1).

The stoneblower took over twenty years to "achieve fruition", when the first machine came into full operation in 1997. Railtrack, who carried on the project after British Rail, are convinced that it offers major benefits to the rail industry (McMichael, 1998). With 13 machines now operating across the network there are consistent reports of good quality maintenance and track durability of three to four times better than previously experienced.

With the passage of traffic, a section of railway track will undergo differential settlement and become uneven; this reduces train speeds and gives rise to poor levels of passenger comfort. To realign the geometric track profile back to the desired level the stoneblower injects a thin layer of smaller stone under the sleeper, on top of the existing ballast, giving rise to a two-layer granular foundation. The principles are based on the old measured shovel packing technique, where one gang of labourers lifted up the track and another gang shovelled a pre-determined amount of 6mm stone between the ballast and the sleeper. Although effective, measured shovel packing was labour intensive and time consuming.

The performance of the stoneblower is not fully understood and in some cases it would appear that the track has been left in worse condition than it was pre-maintenance. To gain further insight into the mechanisms that control the performance of the stoneblower fundamental laboratory based studies involving element testing and individual particle testing were carried out coupled with detailed data analysis of the maintenance process and also of the track quality pre- and post-maintenance.

1.1.1 Laboratory specimen testing

As mentioned by Key (1998), the stoneblower was developed mainly by mechanical engineers and there was little work done on the "geotechnical aspects of the operation". Key carried out a parametric study into the fundamental behaviour of two-layer track foundation as set up by the stoneblower, looking into the effects of varying the lateral pressures, stone sizes and layer thickness.

With Key's work as a background it was decided to extend this research, again looking at the fundamental behaviour of the material. This work has been advanced in four main areas i) by improving the test apparatus, ii) by adapting the data acquisition software to record more data at specifically targeted points within cyclic load tests, iii) by gathering detailed information on the individual particles during preparation and dismantling of the test specimens, and iv) by considering and applying some of the more recent theories in soil mechanics.

Monotonic load triaxial tests were used in the test programme to develop the basic geotechnical understanding of the material and cyclic load triaxial tests to simulate the passing of railway traffic.

1.1.2 Stoneblower data analysis

The High Speed Track Recording Car (HSTRC) travels over the majority of the UK main line track periodically, from which data is collected and the track quality is calculated. The stoneblower also records track data during the measurement and maintenance runs. This combined data allows the maintenance site to be analysed in full, the performance of each maintenance run to be determined and any track geometry with time to be assessed.

Over 1400 stoneblower maintenance sites have been analysed, which includes assessment of the stoneblower performance during the maintenance run (using the data

downloaded off the machine) and assessment of the track quality for the 12 months pre-maintenance and the 12 months post-maintenance.

1.2 Aims and objectives

The aim of this project was to deepen and broaden the understanding of the behaviour of granular materials under repeated loading, in particular the passing of railway traffic and the two-layer foundation typical of that set up by the stoneblowing maintenance process. This was split into two distinct elements;

i) Laboratory testing was carried out to investigate the behaviour of granular materials in a controlled environment.
ii) Detailed data analysis was undertaken to develop the understanding of the factors that control the in-situ behaviour.

To meet this aim the following objectives were set:

1) To investigate the volume change behaviour and the associated particle breakage behaviour of a large sized uniform granular material under monotonic and repeated loading of the individual materials and of layered systems.
2) To consider and simulate some of the other factors that may affect the stiffness and long term settlement of the track within a controlled laboratory environment.
3) To investigate the quality and durability of the track maintenance undertaken by the stoneblower so that improvements in management and maintenance quality may be achieved.

1.3 Scope

A review of the theoretical background and literature relevant to this work is presented in Chapter 2. This covers information related to the railway environment and research carried out by railway engineers into the deterioration of track quality. Research by academics into the fundamental behaviour of cohesionless soils has also been presented. Chapters 3 and 4 look at the experimental programme as carried out at the University of Sheffield. The original development of the equipment and the addition of new apparatus is summarised in Chapter 3. The specifications for the materials used, instrumentation and data acquisition are also included in Chapter 3 along with an overview of the testing procedure. Chapter 4 provides details of instrument calibrations, data corrections and describes the initial analysis undertaken after each test.

Triaxial test results are presented in Chapter 5. In Chapter 6 the results from single-particle crushing tests and the particle breakage occurring during the triaxial tests are given.

Chapter 7 draws all the laboratory test results together, that is the triaxial test behaviour and the particle breakage behaviour, and presents the conclusions from the laboratory work.

The stoneblower data analysis is presented in Chapter 8. This includes a review into the way the machine works and the data recorded by the machine, a discussion of the reliability of both the data from the track recording car and the stoneblower, and an overview of the methods used to assess the quality impact of the maintenance. The results, discussions and conclusions from the data analysis are also included in Chapter 8.

Chapter 9 presents a closing discussion, which brings together both the laboratory testing and the stoneblower data analysis. This work is completed in Chapter 10 with the presentation of the overall conclusions and recommendations for further work.

CHAPTER 2

Literature Review

2.1 Introduction

A review of the literature related to the geo-mechanical behaviour of granular materials in a railway environment has been carried out. The four main sections of literature considered were the railway environment itself, work and research carried out by railway engineers including site investigations and field work, academic related research and finally some more recently developed geo-mechanical theories.

2.2 The railway

The railways are a harsh environment and it is especially difficult for the track formation to remain within serviceability limits. This is due to each section of main line track receiving millions of load cycles, accumulating into millions of mega tonnes per year.

2.2.1 Track components

The track and its foundations can be split into several easily identifiable components; the track superstructure includes the rails, fastenings, pads and sleepers; and the substructure includes the ballast, sub ballast and subgrade (Figure 2.1). For good track quality to be sustained it is essential that the substructure was initially correctly designed and is well maintained (Evans, 1992).

It has been stated by Evans (1992) that "Railway track formation design is probably one of the most complex soil:structure interactions to analyse.". The various elements of this system comprise of: multi axle loading, which varies in magnitude and frequency; deformable rails attached to deformable sleepers with flexible fixings; varied sleeper spacing; a range of ballast properties and thicknesses; sub ballast; prepared subgrade; and underlying subgrade layers.

Interfaces between all the different track superstructure components and substructure layers are subject to repeated load reversals (also referred to as cyclic loading), resulting in degradation to all the materials. The properties and rates of deterioration for the track superstructure are generally known. However, the performance of the man-made

substructure layers is uncertain. According to Cope (1992) this uncertainty increases i) in the specific areas of compaction at the ballast:subgrade interface, and ii) with the performance of the substructure with varying moisture contents.

The four main components of the track and also the smaller 20mm stone used by the stoneblower are reviewed below.

2.2.1.1 Rail

Starting at the top of the structure the vehicle loads are transferred via the wheels to the rail. Due to impact loading occurring at the joints on 'fish-plate' jointed track, super- and substructure track maintenance costs are high. On the main lines, flat bottomed continuously welded rails (CWR) are now generally used. Using CWR has significantly reduced the impact loading over rail joints; however impact loads are still encountered due to discontinuities in the rail level and flat areas on the wheels. Eisenmann et al (1993) estimated, through the use of acoustic counting, that the occurrence of such impact loads due to wheel flats was 1 in 300 to 1 in 500 load cycles. Heavy and fast traffic can quickly turn a small dip in the track profile into a serious problem leading to sleeper and fastening damage and associated ballast failure (Morris, 1992). The rail sits on a rubber pad and together they are fastened to the sleeper using a clip.

2.2.1.2 Sleeper

On the main lines the sleepers will usually be pre-cast pre-tensioned concrete. The dimensions vary although the normal European concrete sizes are 250-300mm wide and 2300-2600mm long, with wooden sleepers being slightly narrower but longer. Concrete sleepers will usually be at a spacing of between 600 and 700mm on the UK mainline. Supporting the sleeper is a continuous bed of ballast.

2.2.1.3 Ballast (nominal 50mm diameter)

The ballast has four main functions:

i) Load distribution – to distribute the load to the subgrade,

ii) Drainage – to prevent the accumulation of water around the base of the sleeper,

iii) Adjustability – to allow for realignment of the track and,

iv) Fines reservoir – to allow fines, from particle breakdown or spillage, to be washed to the bottom of the ballast (Evans, 1992).

Furthermore the ballast also provides lateral restraint, with the crib ballast (in between the sleepers) and the shoulder ballast (by the side of the track – see Figure 2.1). A minimum ballast depth of 230mm below the sleeper base is specified for main line track in the UK, although for the most heavily used lines this is increased to 300mm (Morris, 1992).

Ballast used in the UK is of a coarse uniform particle size of 28–50mm crushed stone (grading to be shown later in Figure 3.1). The coarse particle size results in fewer contact points than that of a well graded material. Therefore with the high stresses involved abrasion occurs leading to particle attrition and breakage. However the large voids are required to allow rapid drainage of rainfall from the track surface, most of which runs down through the ballast and sub ballast.

There have been four main areas of track substructure inadequacy outlined in the literature (Evans, 1992):

i) Ballast contamination,
ii) Subgrade erosion,
iii) Subgrade strength failure, and
iv) Soft, very hard or variable subgrade stiffness.

The area of ballast contamination leading to poor track quality is of most relevance to this field of research.

The voids in the ballast gradually become filled with fine grained material from particle breakdown, materials that may have fallen onto the track or from subgrade erosion. This build up of fines results in poor drainage and allows the build up of pore water pressures under repeated loading that cannot dissipate due to the low permeability. A reduction of internal friction occurs, allowing particle movement under loading, which naturally leads to rapid deterioration and degradation (Evans, 1992).

Work carried out in the early 1990's revealed the main sources of fines that accumulate in the ballast (Table 2.1). The amounts of fines quoted are typical and will naturally depend on the traffic and the route. A limit has been set for ballast failure criterion that when 30% passes a 14mm sieve then it is deemed unacceptable. When this limit is passed the ballast is either cleaned or replaced.

2.2.1.4 20mm Stone

The 20mm stone, which is used by the stoneblower, has a grading between 14 – 20mm (grading to be shown later in Figure 3.1). The stone is blown under the sleepers where

the highest stresses accumulate in the ballast. This smaller stone gives a greater number of contact points, thus lowering the contact stresses and the possibility of breakdown. Where inspections have been made on stoneblown track, there has been little evidence of particle breakdown (Chrismer, 1990).

2.2.1.5 Subgrade

The subgrade must be stable and provide adequate support to the ballast, sometimes the natural subgrade will provide this, otherwise extra layers will be required (as shown in Figure 2.1). These layers will further distribute the load to prevent over stressing of the natural subgrade, they will help to prevent contamination of the ballast from the subgrade, and will direct water away from the subgrade to prevent softening (Evans, 1992).

2.2.2 Track forces

Track structure should be designed and maintained to minimise the dynamic forces produced both vertically and horizontally by trains (Cope, 1992).

2.2.2.1 Vertical forces

Vertical forces are imposed on the track from the vehicles through the wheels. Both the wheel support and the track support act as suspension and dampers. With a stationary vehicle the static forces are passed down via the wheels through the superstructure and ballast into the formation, with the load being spread so that the pressure is not greater than the bearing capacity of the natural ground. The load is the mass of the vehicle divided by the number of wheels. Within the UK the static axle loads are limited to 25.5 Tonnes. However, a typical high speed passenger coach will weigh approximately 16 Tonnes. Figure 2.2 shows the P_1 and P_2 forces that are used in vehicle characterisation. The P_1 force is the initial high frequency force of the wheel load as it crosses a dip in the track. The P_2 force is the much more damaging force of the unsprung mass of the vehicle. The maximum allowable P_2 force in the UK is 340kN. Figure 2.2 also shows the difference in the load transmitted through to the substructure between the wood and the concrete sleepers. These have been calculated using a finite element package named GEOTRACK (Li and Selig, 1995).

The magnitude of individual loads and the repetition of loading are the main two features that control the overall loading of the track. With routine traffic the magnitude of load is less than critical, and it is the repetition of load that is the main problem for

the track substructure. Such loading causes a build up of plastic strains in, and degradation to, the substructure.

Therefore Li and Selig (1995) used an equation that takes into account the maximum dynamic wheel load and the total number of repetitions. Equation 2.1 gives the equivalent number of load repetitions, *N*:

$$N = \frac{t}{4P_S} \qquad \text{Equ. 2.1}$$

where: P_s = static wheel load,

t = traffic (in the same units as P_s).

However, a large number of repetitions of wheel load less than the maximum magnitude of dynamic wheel load may also have significant effects on the accumulation of plastic deformation. Therefore Li and Selig (1995) determined the equivalent number of load repetitions could be calculated by adding up $N_1 + N_2 + \ldots$ for each load case.

2.2.2.2 Horizontal forces

Horizontal forces act in both principal planes. Longitudinally during acceleration and braking (and also a small component due to steering), and transversely due to hunting and when cornering (Morris, 1992).

2.2.3 Terms and definitions

In this section a description of the terms and definitions which are commonly used within track quality analysis and in particular referred to in Chapter 8 have been included.

High Speed Track Recording Car (HSTRC): In the UK the quality of the track is periodically monitored, mainly by using the High Speed Track Recording Car (HSTRC) which records the vertical profile of each rail, the track centreline position, the gauge, the cross level, the cant and the track curvature.

Infrastructure Maintenance Contractors (IMCs): The companies that have contracts to maintain the railway track.

Eighths: Within the railway industry the track is broken down into eighth miles sections (roughly equated to 200m).

Filters: The ride quality in terms of passenger comfort is not only related to the 'longitudinal and transverse inhomogeneities' but also related to the speed of the train. Undulations in the track (both in the vertical and horizontal planes) are all related to

'waves' of specific lengths – wavelength. At low speeds the short wavelengths control passenger comfort. At higher speeds the longer wavelengths become more critical. Selig and Waters (1994) give the following example, at train speeds of 100km/h, it is unlikely that undulations in track having a wavelength in excess of 30m will have a damaging effect on either passenger comfort or the ride quality. Similarly, at 200km/h, it is unlikely that wavelengths in excess of 50m will be significant." Both the vertical top and the lateral alignment profiles are therefore passed through filters to remove the longer wavelengths thus leaving the relevant data.

Wavelength: Typically the track is measured by four standard parameters that are used to assess the quality of the track.

- The track level with wavelengths over 35m filtered out ('35m level')
- The track level with wavelengths over 70m filtered out ('70m level')
- The track alignment with wavelengths over 35m filtered out ('35m line')
- The track alignment with wavelengths over 70m filtered out ('70m line')

Standard Deviation (SD): This is the standard deviation (SD) calculated from 'continuous' measurements in mm over each consecutive 200m length of track (approximately an eighth of a mile) on the filtered profile. This value is used as a measure of track quality for that specific eighth. The higher the SD value the worse the track quality.

Running standard deviation: The running SD is used in this analysis to calculate the SD value over 200m of track at each measurement location throughout the site (approximately every metre).

Ramping: At the beginning and end of the site the stoneblower has to ramp in and out of the maintenance. This happens to allow the machine to align, both vertically and horizontally, the track that has been maintained with track that has not. Ramping may also occur in the middle of a site, e.g. at switches and crossings, where the stoneblower cannot maintain. At such points the stoneblower will ramp out to the fixed point and then back in again. Over this length the track will not be maintained to optimum design and the SD for that particular eighth will increase.

End eighths: These are the eighths at each end of the maintained site in which the machine ramps in and out of the maintenance.

Design category: The crew sets the design category on the night of maintenance. The design category dictates the value of each parameter used in the maintenance design of

the track. The design categories are ranked from A* to D, where A* is the best design for high quality track and D is a 'catch design' for miscellaneous maintenance sites (Table 2.2).

Versine: The versine is defined as the offset from a chord of length L to a circle of radius R.

TrackMaster™: TrackMaster is a management tool designed by AEA Technology (Rail), which runs off a database containing track quality data from across the whole network. In Chapter 8 TrackMaster has been used to view track quality, cant, curvature and structures information for each site of interest.

Engineers Line Reference (ELR): The UK network is split into sections of track, e.g. SPC is the line from St Pancras to Chesterfield.

Track ID: A number that refers to a specific line within the ELR. A piece of track with a Track ID 1100 means that it is the Up Fast line, a piece of track with a Track ID of 1200 means it is the Up Slow line. Similarly 2100 means the Down Fast line and 2200 means the Down Slow line.

2.2.3.1 Group Standards

Group Standards are used as a benchmark for track quality throughout the UK. Table 2.3 shows the track quality bands taken from the Track Maintenance Handbook GC/EH0005 (British Railways Board, 1993). The standards are referred to as standard deviations in mm. The 50%, 90% and 100% SD's indicate the target percentage of track which should be better than or equal to these values to produce acceptable ride comfort. Prior to the introduction of Table 2.3 BR used four quality bands (A – D) as shown in Table 2.2. The algorithm used by the stoneblower to design the maintenance was programmed to these (McMichael, 2001). The enhanced A* design category was introduced at a later date.

2.2.4 Maintenance

To keep the track operating at the required speed and with a reasonable level of passenger comfort the track has to be maintained to a certain standard both vertically and horizontally. The main factors that affect track degradation are the deterioration of the rails, sleepers and fastenings, the densification and breakage of the ballast and lateral spread of the ballast, and subgrade settlement. Tamping has until recently been

the normal process of carrying out the re-levelling and re-aligning of the track. However, the new maintenance process of stoneblowing challenges this dominance.

The effectiveness of maintenance needs to be measured by both the quality of the track immediately after maintenance and by the durability of the track long term. As tamping has becoming better understood it has become apparent that the effects of tamping are destructive to the ballast and the benefits can often be short lived.

2.2.4.1 Tamping

Figure 2.3 illustrates the maintenance technique known as tamping. As the tamper lifts the track up, tines are inserted on the outside of the rails and on either side of the sleeper. Using large mechanical forces they are driven into the ballast and are then drawn together with the aid of vibration. In theory shoulder ballast is pushed into the voids under the sleepers, and supports the sleeper at the required profile. In practice this does not happen and it has been recognised that the track soon returns to its pre-maintenance profile. This is a phenomenon known as 'ballast memory'. Figure 2.4 shows a typical result for a tamped site and the effects of ballast memory. Instead of ballast being compacted under the sleeper, as the theory would suggest, the process disturbs and dilates the densely packed ballast, so under vibration the void is filled with 'loose' ballast. This is what causes the inherent track profile ('ballast memory'), where ballast, under trafficking, soon returns to its previous compact arrangement. When maintained by tamping the decay in track geometry is found to get faster with each cycle of maintenance (Wright, 1983; Figure 2.5). Eventually the ballast must be completely renewed.

BR Research investigated the damage caused by the tamping process and found that tamping was the main cause for ballast damage. Evans (1992) reported that a typical 'tamp' produces 4kg fines/tamp/sleeper (Table 2.1). Furthermore Hellawell (1997) comments that stoneblowing would result in less than 0.5kg of dirt being produced. Initial results suggest that with the stoneblower ballast damage would be cut by up to 50%. Similarly McMichael (1999) argues that stoneblowing has negligible affect on ballast damage and that ballast life could be doubled by a change in the maintenance process. Research has also found that tamping has resulted in a decrease of ballast density and bearing strength (Selig et al., 1982 and Johnson, 1983). It would appear therefore that tamping is not only an inefficient method of maintaining the track, but also causes a large amount of ballast damage and a reduction in ballast life (Chrismer, 1991).

2.2.4.2 Stoneblowing

The concept of stoneblowing has been around for a significant amount of time with the journal of 'Compressed Air' (June 1897, cited by McMichael, 1998) reporting a 'Railroad Ballast Injector' operating with 'great nicety'. The stoneblower has been developed primarily to overcome the phenomenon of ballast memory. This is achieved by blowing a layer of smaller, single sized (20mm) stone under a raised sleeper leaving the sleeper at the desired level and the compact ballast virtually undisturbed. Stoneblower maintenance thus creates a two-layer granular foundation on which the sleeper sits (Figure 2.6). This method originally proved to be successful with the use of measured shovel packing, where one gang of labourers lifted up the track and another gang shovelled a pre-determined amount of 6mm stone between the ballast and the sleeper.

With the stoneblower 0.45kg (1lb) of 20mm stone is injected under the sleeper for every 0.8mm (1/32 inch) the sleeper is raised - each injector receives half the amount of stone. Examinations have shown that the support area is about 230mm by 460mm (9 by 18 inches), which is about the same area as the tamping tines affect (Chrismer 1990).

In its early days the stoneblowing process came under criticism concerning migration of the 20mm stone into the ballast causing the blocking of voids. Research by Key (1998) looked at the effect of different sizes of stone and also different types of stone. He found through a series of triaxial tests and scale model tests, migration of stone through the ballast only occurred with smaller size stone and that there was no evidence of migration of the 20mm stone. The stone does not percolate through the ballast, as the voids are smaller than the stone size and BR have found no stone percolation after several years (Chrismer 1991). This is in accordance with the work carried out by Cedergren (1989) on the erodibility of granular materials. He postulated that if three perfect spheres had a diameter greater than 6.5 times the diameter of the smaller sphere, then the smaller sphere would be able to pass through them (Figure 2.7). Although this is a very generalised statement, it implies that for 50mm ballast a maximum particle size to pass through would be less than 9mm in diameter, significantly less than the 20mm used by the stoneblower. In fact there is evidence that stoneblowing improves the drainage properties of the track. McMichael (1998) hypothesised that this was probably due to reducing the pumping effects caused by poorly supported sleepers.

2.2.5 Stoneblower performance research

2.2.5.1 AEA Technology (Rail)

Some early data analysis was carried out by AEA technology (Rail) for the stoneblower Project Team. This work reviewed the immediate pre- and post-maintenance track quality data collected from the HSTRC machines, to determine the improvements in track quality achieved (Baulk, 1999). The analysis looked at five machines that operated within the Southern and Great Western Zones.

The data covered all 77 sites that had been stoneblown in these two zones between July 1998 and January 1999. The analysis compared standard deviation over eighth mile sections of track. There were a total of 403 eighth mile sections. However discrete track faults were not considered. This work therefore gave a broad overview of the effectiveness of the stoneblower, and may not be representative of the true ability of the machine.

Separate analysis was conducted for the four main track quality parameters: 35m level, 70m level, 35m line and 70m line (see Section 2.2.3). For the analysis AEA looked at the standard deviation (SD) before and after stoneblowing. The data showed the following general trends:

i) The overall improvements in track quality could be seen. However there was considerable scatter in the results, e.g. a pre-maintenance SD of 4mm may leave a post-maintenance SD of between 1.5mm and 5mm. (Showing signs of significant improvement to the track and also of deterioration to the track quality respectively. Figure 2.8).

ii) Generally the track quality improvements from the Great Western Zone were better than those of the Southern Zone. It was suggested in the report (Baulk, 1999) that this may be a reflection of the Great Western Zone generally starting with better quality track due to the higher line speeds.

iii) The worst site treated was improved from 6.8 to 2.3mm SD (35m level). From a SD outside of the safety maximum to well within the allowable limits respectively.

iv) Ramping in and out (at the ends of a site or due to restrictions mid site) appeared to have significant effects on the results. Figure 2.9 shows that around a third of the results from these specific eighth mile sections leave the track in a worse condition. However that implies that two thirds still have an improved post-maintenance SD.

It is therefore difficult to draw conclusions on the effect of ramping in and out from this data.

The AEA report concluded with three comments. The first was that further detailed recording of specific sites is needed to draw reliable conclusions in the track quality deterioration rate. Secondly it is important to know about all work that goes on on the track, especially on sites already stoneblown. Thirdly a similar exercise needs to be carried out on conventional maintenance tamping to allow for a proper comparison of the two maintenance processes to be made (Baulk, 1999).

2.2.5.2 Maintenance Contractors

Many of the contractors (those who maintain the track) want to share their experiences and information on best practice to enhance the development of the stoneblowing process.

GTRM, who first used the stoneblower in mid 1998 and carried out 160 miles of stoneblowing in 15 months, picked up on several areas that they believed to be important for good performance of the stoneblower (Nutbrown and Nicholas, 1999), three of which have been highlighted below.

i) Selection and training of the machine operators is important. They found that it is often down to the operators/maintainers and supervisors to get good performance and high reliability from the stoneblower.

ii) Planning, site preparation and marking up, was mentioned as being important- including two extra chains either end of the selected section for ramping in/out, replacing broken sleepers, fastenings etc. and checking all height and width clearances to limit unnecessary ramping out/in mid site. It is best to do this during the day – pre-maintenance.

iii) The benefits of stoneblowing on the track quality improvement and durability could be seen. GTRM noted a vast improvement on several sections of track which used to require tamping every three months, which, at the time the paper was written, had lasted 12 months after being stoneblown.

Nutbrown and Nicholas finished the report by saying that 'sections of track which have been stoneblown need to be clearly marked up to ensure that it is not tamped and to allow reliable track monitoring'.

2.2.6 Data analysis

2.2.6.1 Reliability of data

Raymond and Bathurst (1994) suggest there are three main uses of track quality data:

i) Locating exceptions to the track standard,

ii) Characterisation of present conditions,

iii) Predicting future deterioration.

However as McMichael (1999b) comments there are several inherent difficulties with the data analysis including:

i) The Engineers Line References do not always match up.

ii) The machine can only be accurate to within about 200mm in original positioning along the track.

iii) The start and end data does not always tally with distance measured or the distance maintained.

iv) Phase shifts in the data due to different filters being used by different types of machine/analysis.

v) Machine difficulties; auger jams, tube jamming, sticking transducers, and machine maintenance issues.

vi) End eighths and other eighths where the machine has had to ramp in and out. Also at points where there are restrictions around the track, e.g. a confined bridge or tunnel, where the machine will have to ramp out and back in, in the middle of a run. At such points the track will not get maintained to the required level and alignment, including up to 70 metres either side of the restriction.

There appear to be three main issues that need to be addressed regarding the reliability of the data. Firstly that of the machine (mechanical) errors as mentioned above. These occur due to malfunctions of the machine and may therefore cause the track to be left in a worse condition than expected. Secondly that of positioning of the stoneblower; it appears that especially with the earlier data the machine may not always have been in the intended position, in one instance up to 2m out. These kinds of errors can leave the track in a considerably worse state than it was pre-maintenance as sleepers not due for stone to be blown under may get stone and others sleepers needing stone may not get any. The third area is that of comparing the data between the different vehicles that record the data, i.e. the stoneblower and the HSTRC. Although these machines are all required to be calibrated they show variation between each other and with repeated runs on the same machine.

Furthermore, care has to be taken with the interpretation of data over a long period of time, as there could be unrecorded maintenance work performed, especially on sites of poor track quality (Baulk, 1999).

2.3 Laboratory tests

The geotechnical practices of pavement engineering have over the years become different from those of other geotechnical applications in several ways. Two of the main differences as suggested by Brown (1996) are:

i) Soil and granular fills are subject to a large number of load applications at stress levels well below their shear strength (known as cyclic loading or repeated loading), and

ii) Under a single load application, a pavement's response is essentially resilient. However, irrecoverable plastic strain can accumulate under repeated loading.

The latter allows the analysis to be separated into two parts, those of elastic strains and those of plastic strains. In a statement about granular material response to repeated loading, Brown further comments "Non-linear stress-strain characteristics are a particular feature of the problem and have to be catered for in design and evaluation."

2.3.1 Triaxial tests

As this research project follows on from that of Key (1998), it is important that his work is considered in depth. Within his research Key, under a limited budget, designed and assembled his equipment. Using a large triaxial cell available at the University of Sheffield he conducted drained monotonic, cyclic and post cyclic monotonic load tests on 236mm diameter and 455mm high specimens. The cyclic load tests were carried out up to a total of 100,000 load cycles. In addition Key carried out model tests using a half sleeper rig at Scientifics Ltd., Derby, under 1,000,000 cycles, approximating to one year's main line traffic in the UK.

With the background of stoneblowing in mind, Key (1998) also researched the behaviour of 20mm, 14mm, 10mm and 6mm granite and also the use of rounded river gravel. These materials were tested in a two-layer system with nominal 50mm ballast at the bottom and the smaller stone at the top of the test specimen.

2.3.1.1 Specimen preparation

Work by Salman (1994) suggests that a minimum D/d_{max} ratio of 6 is required for a specimen to be representative of the in-situ soil (where D = specimen diameter and d_{max} = maximum particle size). Details of the D/d_{max} ratio from other research are given in Table 2.4. As can be seen from Table 2.4 Key (1998) had a D/d_{max} ratio of 4.7, this was limited by the size of the cell. Sweere (1990) said that with a D/d_{max} of less than 10 inaccuracies were obtained. In work by Bishop and Green (1965), they determined that a specimen with a height to diameter ratio (H/D) of 2 or more did not require any form of end lubrication. This applied to all of the tests reported in Table 2.4.

Table 2.5 shows from the research reviewed the range of densities of railway ballast used in tests. Unfortunately the specific gravities for the majority of the materials were not given and it is probable that the range of densities reported is a reflection of different mineralogies (or specific gravities). It may also be due to varying gradings or particle shapes.

On investigating the ballast vertical heterogeneity in the track bed, Lopez Pita and Fonseca Teixeira (2002) show that density levels ranged from $1.5Mg/m^3$ to $2.1Mg/m^3$ in less than 25cm below track bed depth.

2.3.1.2 Procedures

There has been little reported about actual specimen preparation directly related to ballast type aggregate in the available literature.

From the testing carried out by Key (1998), the following main points were highlighted:

i) The usual procedure of compacting a granular material in layers was not considered suitable for ballast, due to the size and shape of the material, which may cause artificial planes of weakness to develop.

ii) Key considered the height of drop of the particle during specimen preparation to be crucial to the overall density of the specimen. He chose to drop the particles from a height of 0.75m above the material surface whilst the specimen was vibrating. He found the density was relatively insensitive to the timing of the drop.

iii) Surcharging the specimen with more than 20kg had little effect. Key therefore chose 20kg to surcharge the specimen for 1min on a vibrating table.

iv) With the 20mm stone he added the material steadily over a period of one minute, whilst the specimen was vibrating, left it to settle for 15sec and then surcharged it with 20kg for 30sec on the vibrating table.

v) After the specimen was prepared he measured the height of the material surface from the top of the supporting mould enclosing the specimen at three points around the circumference. He allowed these three points to be within 2mm (1/100 – 0.5°) of each other, otherwise the specimen was discarded.

2.3.1.3 Loading

For monotonic loading Key (1998) used a rate of strain of 0.22%/minute in both the monotonic and post cyclic monotonic load tests. This loading rate of 0.96mm/min was the highest rate of strain available. This was considered to be reasonable as with the large grain size and no water in the pore spaces there would be no build up of pore pressure.

Considering the cyclic load tests Shenton (1975) suggested that the maximum pressure in the ballast below the sleeper for a 100kN load is between 200-300kPa. This is also in agreement with Esveld (1989), Raymond and Bathurst (1994) and Eisenmann and Mattner (1989). Key (1998) used a deviator stress cycling between a nominal 12.5kPa and 250kPa (0.5 – 12kN) in compression, and a cycle rate of 0.16Hz for the first 50 cycles then of 0.5Hz for the rest – completing 100,000 load cycles in total. Lopez Pita and Fonseca Teixeira (2002) considered confining pressures of up to 30kPa or 35kPa would adequately represent field conditions.

2.3.1.4 Instrumentation

Many have commented on the 'poor accuracy' of conventional external strain measurement equipment, which is not reliable for strains of less than 1%. Pappin et al. (1992) used on specimen measurements, four LVDT's and three strain gauged epoxy resin rings to measure axial and radial strain respectively. Kolisoja (1997) used on specimen instrumentation for both axial and radial strain measurements. Brown (1996) used a partial internal vacuum to provide the constant confining stress (after Cheung 1994), thus allowing the triaxial cell to be dispensed with and easy access to on specimen equipment. The cell size was a limiting factor in the work carried out by Key (1998), which meant that on sample equipment was not an option.

2.3.1.4.1 Axial strain

There are a number of arguments for the use of local measurement of axial strain and as Goto et al. (1991) commented "it is crucial to measure 'local' axial strain", where the strain is measured over a certain length of the specimen excluding all bedding errors.

Several authors have found that, especially with small strains ($10^{-4}\varepsilon$), the specimen stiffness is underestimated with external axial measurement. In the Table 2.6 Scholey et al. (1995) carried out a comprehensive review on the sources of error that occur when measuring strains with conventional equipment. Goto et al. (1991) looked at the sources of errors due to external measurement, addressing specifically shear banding, and tilting of the top cap. They commented that as the specimen reached a few percent strain, the external strain measurement was 'good enough'.

2.3.1.4.2 Radial strain

In a paper reviewing the different instrumentation, Dawson and Gillett (1998) looked particularly at instrumentation to measure the radial displacement. Proximity transducers were mainly used on the smaller finer materials, where the measurements were taken at mid-height, on opposite sides of the specimen. On some of the larger specimens the radial displacements were measured by calliper Plexiglas rings held by blocks glued onto the specimen with a proximity transducer across the jaws of the hinged callipers. Two such rings were used at one-third and two-thirds of the specimen height. A further radial measurement apparatus was a 'necklace-style string-of-wheels', which went around the mid height and had an LVDT measuring across an opening, alternatively a chain could have been used in place of the string-of-wheels. A fourth method used was epoxy resin hoops fitted onto the holdings of axial LVDT's providing strain measurements at a quarter and three quarters of the specimen height. The hoops were resistant wire strain gauges and as the specimen expands/contracts the resistance in the strain gauges changes. Others have used spring loaded LVDT's set in the cell wall, which react against the fixings attached to the specimen as described above (Dawson and Gillett, 1998). This final method is similar to that used by Key (1998).

From their research Dawson and Gillett (1998) drew the following conclusions "that intimate connection of the instrumentation with the soil or aggregate specimen appears almost essential to measure radial strain." and "For axial strain entirely on specimen instrumentation is preferred."

2.3.1.4.3 Volumetric strain

For dry specimens the axial strain and the radial strains are often used to calculate the volumetric strain of the specimen. This however relies on the assumption of the specimen remaining a right-angled cylinder.

Aruruna et al. (1995) reviewed the use of a volume change measurement device based on a differential pressure transducer. A more complex device, which also used a differential pressure transducer, is reviewed by Ng et al. (2002). Both of these methods were based on the measurement of the change on the cell fluid volume.

2.3.1.5 Membrane correction

Indraratna et al. (1998) found when a 4mm rubber membrane was used in his tests with a similar set up to those described by Key (1998), that even with low confinement, membrane correction was minimal. Key looked at ways to carry out membrane correction using methods by Henkel and Gilbert (1952), La Rochelle et al. (1988) and Keubris and Vaid (1990). Based on these he found that the corrections were minimal due to the scale of the testing and therefore did not include such corrections in his results.

2.4 Behaviour of cyclically loaded aggregates

In the following sections the behaviour of aggregates under repeated loading has been split into three types of behaviour. These have been categorised as the resilient modulus behaviour (Section 2.4.1), the permanent plastic strain behaviour (Section 2.4.2), and the particle breakage behaviour during both cyclic and monotonic loading (Section 2.6). Each type of behaviour has then been subdivided into parameters that may have an effect on that particular type of behaviour. The behaviour of the specimens in the monotonic load tests has been included in Section 2.5.

2.4.1 Resilient modulus

Seed et al. (1967) calculated the resilient modulus as 'the magnitude of the repeated deviator stress divided by the resilient axial strain', which makes it equivalent to the resilient Young's modulus. Key (1998) further explained the resilient modulus (M_r) as the gradient of the load-unload loop.

For triaxial tests the resilient modulus (M_r) can be calculated from:

$$M_r = \frac{\sigma_d}{\varepsilon_R} \qquad \text{Equ. 2.2}$$

where: σ_d = deviator stress

ε_r = resilient or recoverable strain

Kolisoja (1997) used a kθ-model from Brown and Pell (1967) to determine the resilient modulus (M_r).

$$M_r = k_1 p_0 \left(\frac{\theta}{p_0} \right)^{k_2} \qquad \text{Equ. 2.3}$$

where: θ = the sum of the principle stresses, $\theta = \sigma_1 + \sigma_2 + \sigma_3$

p_0 = atmospheric pressure, 100kPa, and

k_1, k_2 = material parameters.

(with $k_2 = 0.5$ there is virtually no loss of accuracy).

However this has several short comings, the main one being that it assumes a constant Poisson's ratio, which has been shown to vary with stress by Hicks and Monismith (1971), Brown and Hyde (1975), Sweere (1990), and Kolisoja (1997). Furthermore it does not include the effects of shear strain induced by the deviator stress. Uzan (1985) included the deviator stress (q) into the above model as follows:

$$M_r = k_1 p_0 \left(\frac{\theta}{p_0} \right)^{k_2} \left(\frac{q}{p_0} \right)^{k3} \qquad \text{Equ. 2.4}$$

The resilient response of unbound aggregates can be affected by several parameters, seven of which are reviewed below.

2.4.1.1 Effect of stress level

From the early 1960's up to recent studies the stress level has been understood to have the most significant impact on the resilient properties of granular materials (Kolisoja, 1997). Many including Hicks and Monismith (1971), Uzan (1985) and Sweere (1990) have shown that the resilient modulus is highly dependent on the degree of confining pressure or the bulk stress. Although Hicks and Monismith have suggested that, within reason, the magnitude of the deviator stress has limited effect on the resilient modulus.

Ping and Yang (1998) found that with Panama sand (fine sand) the resilient modulus remained constant or increased slightly with an increased deviator stress. Yet with Alachua sand (silty sand) the opposite occurred and the resilient modulus decreased with an increase in deviator stress.

Dawson & Gomes Correia (1987) commented, "in order to be as close as possible to the stress field the cyclic load triaxial test should perform both cyclic vertical and confining stresses, yet commented that the rotation of principle stress 'did not affect very much the elastic behaviour of the material'. Work by Brown and Hyde (1975) suggested that it was not necessary to cyclic both the vertical and confining stresses as long as the

constant cell pressure was equal to the mean of the cyclic cell pressure that would otherwise be applied.

2.4.1.2 Effect of density

It is well documented that, under monotonic loading, an increase in density significantly increases the stiffness and the strength of a specimen. However it would appear that the effect on cyclic loading is less well understood (Lekarp et al., 2000a). Hicks and Monismith (1971) and Kolisoja (1997) suggest that an increase in density results in an increase in resilient modulus. This was understood to be due to the increase in co-ordination number and therefore a reduction in inter-particle contact stress. However Thom and Brown (1988) and Brown and Selig (1991) suggest that the density is relatively insignificant. Hicks and Monismith do report that the significance of the density is however reduced with an increase in fines content.

Kolisoja (1997) found that the test material density had a marked effect on the resilient modulus value (Figure 2.10). Traditionally density has been described by a reference datum e.g. the Proctor compaction test, however this method often has shortcomings, as mentioned by Kolisoja. In his research he found that the best way to describe material density was via porosity (n), or void ratio (e).

From this he concluded that within reason the resilient modulus was directly proportional to the porosity of the material. The equation that he used to express this was:

$$M_r = a_1(n_0 - n)p_0\left(\frac{\theta}{p_0}\right)^{0.5} \qquad \text{Equ. 2.5}$$

where: n = porosity of the material

n_0 = theoretical maximum value of porosity when $M_r = 0$

a_1 = material parameter

Equation 2.5 above takes into account the material composition (such as moisture, particle size distribution and rock type) in the parameter a_1. There is an exponential form of this equation, which better takes into account the extremes of the range of possible densities, yet within the normal range of densities the above equation is comparable. Unfortunately there was no further clarification on what was considered to be of normal density.

2.4.1.3 Effect of grading and grain size

From the literature reviewed there was not a clear consensus on the effect of the fines content on the resilient modulus of the material. However it was clear that the resilient modulus is affected by both the particle size and distribution, which is therefore related to the number of particle contacts (co-ordination number). Kolisoja (1997) reported that an increase in the maximum particle size led to an increase in the resilient modulus. This was apparently due the reduced co-ordination number, and a reduced number of particles in the column of particles transmitting the load (as explained in Section 2.6.1.6), which would reduce the amount of displacement resulting in a higher modulus.

Thom and Brown (1988) considered the effects of particle size distribution of crushed limestone on the resilient modulus. They concluded that uniform aggregates had a higher resilient modulus than well graded aggregates. This would appear to be in parity to the explanation offered by Kolisoja above, as a uniformly distributed material would have a lower co-ordination number than well graded material.

2.4.1.4 Effect of moisture content

The effect of moisture content on the resilient modulus of an aggregate was reasonably conclusive in the literature reviewed. However there were still areas that were in need of clarification, some of which are discussed here. Lekarp et al. (2000a) suggested that when a specimen is either dry or partially saturated then the effect on the resilient response is limited. Yet as the specimen approaches saturation then the resilient modulus can reduce quite significantly. Hicks and Monismith (1971), Dawson and Gomes Correia (1996), Khogali and Zeghal (2000) and Ping and Yang (1998) all showed that the resilient behaviour was highly dependant on the moisture content at high cell pressures. They found that as the moisture content increased, the resilient modulus decreased. Hicks and Monismith suggested that this effect only occurred above the optimum moisture content. Furthermore Dawson and Gomes Correia (1996) found that at moisture contents below optimum the resilient modulus increased, possibly due to the increase in suction. Raad et al. (1992) demonstrated that the effect of moisture content was most significant in well graded aggregates with higher proportions of fines, again confirming the above suggestion.

It would appear that much of this research was based on highway subgrades where the granular materials may still be susceptible to the build up of pore pressures. This would lead to a decrease in the effective stress, resulting in lower strength and stiffness.

However Thom and Brown (1987) showed that in crushed rock where there was no detectable build up of pore water pressure, there was still a decrease in the resilient modulus with increased moisture content. They proposed that this was due to the moisture acting as a lubricant between the particles. Similarly Awoleye (1998) comments that water and fines collecting in the ballast act as lubricant between the ballast particles, significantly reducing the interlocking between particles, which effectively reduced the resilient modulus. Lekarp et al. (2000a) argued that this may not have been due to lubrication as such but more a reduction of localised pore suctions as the moisture content was increased. This would lead to lower inter-particle contact forces.

Kolisoja (1997) also looked at the effect of moisture content on the resilient modulus. He found, contrary to the above findings, that the resilient modulus of the 'very open graded test material' was insensitive to variations in moisture content. Similarly Boyce (1976) and Pappin et al. (1992) concluded, from tests on a well graded crushed limestone with a maximum particle size of 40mm, that where full drainage was allowed the resilient strain behaviour of a saturated specimen was the same as that of a dry specimen.

2.4.1.5 Effect of stress history and the number of load cycles

Past research would suggest that the resilient modulus is affected by the stress history. Key (1998) found that the resilient modulus increased rapidly during the first few cycles and that the rate of change reduced with an increased number of loadings, stabilising after about 40,000 load cycles. It would appear that this effect is due to the compaction of the specimens under particle rearrangement and particle crushing. Boyce et al. (1976) demonstrated that stress history effects could be reduced by a few cycles of pre-loading, although, as reported by Brown and Hyde (1975), there is little effect on the resilient response of the material as long as the deviator stress is kept relatively low, i.e. by limiting large permanent axial strains.

Post cyclic monotonic load tests carried out by Key (1998) after 100,000 load cycles showed an increase in the specimen stiffness compared to the normal monotonic test by up to 100% with a 40kPa cell pressure. This would appear to be due to the compaction of the specimen during the cyclic load test. From this Key suggested that a form of controlled pre-loading after railway track maintenance may have long term benefits on the permanent settlement of the track.

2.4.1.6 Effect of particle shape and aggregate type

The resilient modulus depends on the material used although there is little reported in the literature relating this directly to the cyclic load behaviour of soils.

Hicks and Monismith (1971) and Thom and Brown (1989) showed that angular to subangular crushed rock have a higher resilient modulus than subrounded or round particles. This was reported to be due to the angular and subangular particles 'spreading the load better' and therefore reducing the inter-particle stresses.

2.4.1.7 Effect of loading duration and frequency

Boyce and Brown (1976), Seed et al. (1967), and Thom and Brown (1987) showed that the loading duration and frequency have little or no effect on the resilient properties of a material. Lekarp et al. (2000a) comments that the loading frequency could have an effect on the resilient modulus when the material is close to saturation, possibly due to increased pore pressures.

As previously stated Brown (1996) comments that the resilient characteristics of large sized granular materials was insensitive to the frequency of loading.

2.4.2 Permanent strain

Due to the nature of permanent strain tests which require long testing times and the necessity of separate specimens for each test, advances in understanding of the development of plastic strains have not be so forthcoming as those of resilient modulus where much information can be gathered from one specimen. Similar to the seven factors that affected the resilient modulus above five factors have been reviewed for their effects on the permanent strains in granular materials.

Many models have been suggested over the years to determine the development of permanent strain with cyclic loading, however they have all been limited. Lerkarp et al. (2000b) suggests this is because failure in cyclic load tests is not sudden as in monotonic load tests, but is an incremental process as the deviator stress in cyclic load tests is often well below that of the failure stress in monotonic load tests.

2.4.2.1 Effect of stress level and history

As with the resilient modulus the literature suggests that stress level is one of the most important factors that affects the permanent deformation in granular soils, depending on both the deviator stress and the cell pressure. Lashine et al. (1971) and Brown and

Hyde (1975) indicate that permanent axial strains reached a constant value related to the ratio of the deviator stress and cell pressure.

From the literature it would appear that permanent strains would be increased with the rotation of the principal stresses as in the hollow cylinder apparatus beyond that seen in a triaxial test specimen (Ansell and Brown 1978, and Chan and Brown, 1994). However there is a limitation due to the maximum particle size that can be tested in such apparatus.

Limited research has been conducted on the effect of the stress history on the plastic strain of the material. Although Stewart (1986) reported that the maximum stress to which the specimen has been subjected in the past controlled the future response. Key (1998) noted that under repetitive loading the specimen densified and gradually increased in strength and so was able to better resist the applied stress of the following cycles.

2.4.2.2 Effect of density

The density of the specimen has been found to be significant in the long term plastic behaviour of granular materials under repeated loading as reported by Barksdale (1972) and Thom and Brown (1988). With increased density the permanent strains are significantly reduced, Lekarp et al. (2000b).

2.4.2.3 Effect of grading and aggregate type

The grading of a material will naturally have a direct influence on the overall density, where the densest mix results in the least deformation (Dawson and Gomes Correia, 1996). However the plastic strain may increase as the amount of fines increases according to Barksdale (1972) and Thom and Brown (1988).

The shape of the aggregate has a significant influence on the permanent strains with the more rounded particles having less resistance to strain than angular ones (Key, 1998). However Leung et al. (1996) found that the more angular particles were more susceptible to creep.

Raymond and Bathurst (1994) tested 7 selected ballasts, plus a soft rock for a control. 500,000 load cycles were applied to the specimens at a frequency of 1Hz. Each material was tested for characteristics such as hardness, toughness and particle size distribution. Figure 2.11 shows the development of axial strain with the number of

cycles. From this they commented that the differences are only really apparent after 10,000 cycles so tests needed to be continued to at least 500,000 cycles.

2.4.2.4 Effect of moisture content

There would appear to be two aspects to the effects of moisture on the plastic strains occurring in a specimen. Firstly, should pore water pressures build up under repeated loading this leads to lower effective stresses and a reduction in the resistance to plastic deformation (Barksdale, 1972; Thom and Brown, 1988 and Dawson and Gomes Correia, 1996). Secondly, in granular materials with a high void ratio and limited chance of the build up of pore water pressure the increase in moisture content would appear to cause an increase in the plastic strain (Thom and Brown, 1988 and Key, 1998).

Key (1998) carried out a drained triaxial test with wet ballast under cyclic loading. He found that after 100,000 load cycles the wet specimen had undergone a 67% increase in non-recoverable plastic strain compared to a similarly prepared dry specimen. Eisenmann et al (1993) found that in model tests when the ballast was wetted there was an increase of settlement similar to an increase of 100kPa in the cyclic stress. Using triaxial tests Gidel et al (2000) noted that both the stiffness and the permanent axial strains depended on the moisture content.

Freeme and Servas (1985) considered the influence of water ingress on the material response was. They found that with the injection of water into the granular layer there was an associated build up of permanent deformation. Figure 2.12 also illustrates the importance of good quality ballast and the influence of effective drainage. G1, in Figure 2.12, represents the behaviour of good quality ballast with an open grading and G4 represents the behaviour of poor quality ballast where most of the voids have been infilled with fines.

2.4.2.5 Loading duration and frequency

Research by Lee and Vernese (1978) concluded that in most cases, frequency and loading waveform had no effect on the results. Cheung (1994) used a manually operated hydraulic actuator on granular material (40mm maximum particle size) for simple repeated load tests. This was considered to be reasonable as Brown, (1996) suggests granular materials are not sensitive to loading rates. However Gaskin et al. (1978) and Sato (1995) suggest that the peak acceleration is a dominant factor in the ballast settlement (i.e. the loading waveform). A square wave used by Key (1998)

would therefore give higher accelerations and have an increased effect on the ballast settlement. Although the rate of loading may influence the behaviour of the granular materials it would appear that the frequency would have little effect.

2.4.3 Layered specimens

Key (1998) carried out layered triaxial tests where a nominal 20mm stone overlaid a nominal 50mm ballast. He found that a thin layer of stone reduced the amount of axial displacement. Anderson et al (2001) speculated from this work that the interface friction between the top platen (or sleeper) and the stone may reduce permanent deformation.

Using the scale model tests, Anderson and Key (2000), looked at how the depth of layer of the 20mm stone affected the resilient modulus and the permanent deformation. They concluded that with larger lifts the results were similar to those from bed disturbance similar to that caused by tamping maintenance. It was clear that as the added material thickness passed a certain level the amount of settlement increased dramatically. It appeared that with reduced lateral restraint the stones around the edge of the added material may have fallen away – therefore leaving a smaller area to transfer the load, increased stresses in the ballast and excessive settlement – greater than the actual thickness of added material. A further test, where lateral confinement was arranged around the thick layer of added stone showed a significant reduction in the settlement. Therefore larger lifts require adequate confinement, which should possibly come from the crib ballast.

Claisse and Calla (2003) also reviewed model scale tests on two-layer ballast beds. In their system the crib ballast was replaced by the smaller stone, and where voids appear below the sleeper then the small crib ballast falls into the void maintaining the track without the need for maintenance. Again the original ballast below the sleeper is left undisturbed. This work is still in its early stages with the intention of carrying out field tests in the near future.

2.5 Behaviour of monotonically loaded materials

Monotonic load behaviour in triaxial tests is well documented in literature (e.g. Bishop, 1966 and Atkinson, 1993). Key (1998) showed that under monotonic load triaxial test conditions, the stress-strain behaviour for a dense granular specimen was more akin to that of a loose specimen. Bishop (1966) also demonstrates this in Figure 2.13, where

axial strains of up to 25% are reached in dense sands before the peak stresses were recorded. Hall and Gordan (1963) quoted strains of between 15%-20% were required before failure was reached. Datta et al (1979) observed similar behaviour when testing four different calcareous sands and an Ottawa sand.

Oldecop and Alonso (2001) presented a very interesting piece of work on some oedometer tests that were carried out on rockfill compressibility. In a review of many papers based on many different soil mechanics tests they concluded that the main cause of rockfill settlement was particle breakage, which would appear to be accentuated in the presence of water. They suggested that the factor that determines collapse behaviour of rockfill could be due to the reduction in the strength of the rock upon wetting. In the paper Oldecop and Alonso introduced a macroscopic constitutive model for rockfill that includes the effect of water on compressibility and collapse phenomena. It was based on the understanding that rockfill has two sets of voids. Firstly, there is the set of interlinked voids between the individual particles (termed rockfill voids). Secondly, there are the voids within the rock particles themselves (termed rock pores, which the author understands to also include surface cracks). They carried out five tests, the results of which are shown in Figure 2.14 and summarised here. Some specimens were inundated with water at specific points (test 1, 2 and 3) filling the rockfill voids. Test 4, which had a very similar expression of collapse as seen in test 3 was not inundated with water but rather had its relative humidity raised, inducing collapse gradually as the water content was increased. Passing humid air through the specimen raised the relative humidity and the suction pressures within the rock pores caused the water to pass from the rockfill voids into rock pores by molecular diffusion. The amount of water in the rock pores was controlled by controlling the relative humidity of the air being passed through the specimen. Even though the water content in test 4 (inducing collapse) was only 3.2% compared with nearly 20% in the flooded specimen (test 3) the amount of collapse in test 3 and test 4 was the same. Test 5 was used to verify the proposed model by causing two partial collapses due to limiting the amount of relative humidity in the specimen.

The interpretation of these results by Oldecop and Alonso was as follows. i) A unique normal compression line exists at any given water content. ii) The effect of moisture on a specimen is influenced by the stress, as at low stresses there is a tendency for the specimen to swell slightly before compressing, whereas at higher stresses collapse occurs. iii) Saturation of the rock pores has the same effect as flooding the whole

specimen on the collapse of the specimen. iv) There are three boundaries where the water content does not effect the behaviour of the specimen; a) where the stress level is below the clastic yield stress as defined by McDowell and Bolton (1998), this was 0.29MPa for the Pancrudo slate, b) at very dry states, where the water content is less than or equal to 0.45%, and c) where the water content is greater than full saturation of the rock pores, which was 3.2%.

2.6 Particle crushing

Particle crushing occurs when the stress imposed on a particle exceeds its strength. Throughout the review of the literature there has been no clear use of specific terms such as breakage, fracturing, splitting and crushing. Generally breakage and crushing have been used simultaneously, although crushing sometimes referred to the crushing of individual particles beyond recognition. Festag and Katzenbach (2001) refer to breakage as the dissection of grains, which only occurs with high stress levels, and abrasion when small particles break off from the main grain, which is independent of stress level.

In recent years much work has been carried out into the relationship between the behaviour of sands and the breakage of particles mainly focusing on one dimensional tests and monotonic load triaxial tests. It would appear that with those sands tested and with a variety of initial void ratios all tend towards the normal consolidation line (NCL) at high stresses (Figure 2.15) (Coop and Lee, 1993; Lade et al, 1996; Pestana and Whittle, 1995). It is accepted that the yield point (during one-dimensional compression) is related to the initiation of particle crushing (Nakata et al., 2001a).

Lade et al. (1996) explained the importance of particle breakage as follows; "The most important engineering properties of granular materials such as stress-strain and strength behaviour, volume change and pore pressure developments, and variation in permeability depend on the integrity of the particles or the amount of particle crushing that occurs due to changes in stress." Furthermore breakage and the crushing of contacts decrease the rate of dilation in triaxial or simple shear tests, which lower the peak compressive strength and hence the angle of shearing resistance.

Many authors have identified certain characteristics on which the breakage of soil particles depend. Hardin (1985) comments that the stress-strain behaviour is greatly affected by the degree of particle breakage and suggests seven parameters that influence the amount of breakage in an element of soil under stress. "i) particle size distribution,

ii) particle shape, iii) state of effective stress, iv) effective stress path, v) void ratio, vi) particle hardness, and vii) the presence or absence of water."

In a review of literature on particle breakage Lee and Farhoomand (1967) concluded their investigations by writing "The scattered available data suggest that both the compression and particle breakage appear to be accelerated by the addition of water and to increase with: (a) increasing grain size, (b) increasing uniformity of a soil sample, (c) increasing angularity of particles, (d) decreasing strength of individual particles, (e) increasing confining pressure, and (f) increasing shear stress at one confining pressure." In the discussion following this paper, Insley (1963) comments that the factors (e) confining pressure, and (f) shear stress, are not major causes of compression and breakage, but are rather related to (d) the strength of individual particles.

Nakata et al. (2001b) refine the above lists, saying that particle crushing is affected by particle size, initial density, particle shape and mineral composition and McDowell et al. (1996) put crushing down to a function of particle size, co-ordination number and stress, where the co-ordination number is a reflection of the void ratio.

2.6.1 Effects of breakage on material behaviour

When a specimen is sheared, plastic volumetric strains occur partly as a result of the crushing of the material. At high pressures particle breakage apparently dominates the change in volume, whereas at low pressures it would be the rearrangement of particles that dominates. Chandler (1985) comments that when these two effects cancel each other out then the specimen has reached critical state. Ramamurthy et al. (1974) report that due to crushing the observed dilatancy at low stresses disappears and at higher stresses, during shear, significant volume contraction occurs. Luzzani and Coop (2001) concluded from their work on a carbonate sand and a quartz sand, that the volumetric compression appeared to be directly related to the amount of particle breakage.

Similarly, Miura et al. (1984) commented that particle breakage caused a decrease in the dilatancy effect, which in turn caused a decrease in the shear strength of sand. Thus on a stress-strain plot any peak in the deviator stress was reduced and the axial strain at the peak increased due to the effect of particle crushing.

In the following sections parameters that may affect the amount of breakage are considered in turn.

2.6.1.1 Effect of particle size distribution

Roberts and de Souza (1958) observed that a uniformly graded soil 'crushed' more than a well graded soil. This has since been supported by Hall and Gordon (1963), Lee and Farhoomand (1967), and Al-Hussaini (1983). Hagerty et al. (1993), Hyde and Nakata (2001), and Nakata et al. (2001a) noted that there was a much more marked yield point for uniformly graded sands than well graded sands, resulting in a steeper curve after yielding on a void ratio versus log stress plot from an oedometer test.

2.6.1.2 Effect of particle size

Hardin (1985) states "the potential for breakage of a soil particle increases with particle size." The reason for this is two fold i) as the size increases the normal contact forces increase as there are fewer paths for the stress to travel though the specimen (see Section 2.6.1.6 on the effects of stress path), ii) the probability of defects increases with the size of the particle – known as Griffiths Law (Griffith, 1920). Marsal (1966), reporting on drained triaxial tests on broken rock and gravel, comments that greater compression and particle breakdown was observed in the coarse material than the fine material. This was also noted by Lee and Farhoomand (1967), De Souza (1958), Hendron (1963), Datta et al (1979), and Raymond and Diyaljee (1979). Hagerty et al. (1993) confirmed this in tests with glass beads where an increase in the mean particle size led to an increase in the amount of crushing, which they understood to be due to a lower co-ordination number.

Lee (1992) found the average tensile strength (σ_f) of a particle to be a function of the size (d), which was also evident in tests reported by Braddick (1963) and Billam (1972).

The reduction in strength with the increase in particle size would appear to be similar to the statistical variation in the strength of brittle ceramics as detailed by Weibull (1951). He found with tests on ceramic materials that there were fewer flaws in smaller ceramic pieces and therefore less variation in the strength.

McDowell and Bolton (1998) argued that if the larger particles, being inherently weaker than the smaller particles, are most likely to break, then with the compression of a coarse grained material a uniform matrix of fine grained particles would evolve. However this was not found by Sammis et al. (1987) who, when testing gouge material, found that the larger particles had not all been crushed and that the particle size distribution was self-similar (of fractal nature).

Similarly Nakata et al. (2001a) found that with well graded sands, smaller particles underwent more severe damage than the larger ones. This was thought to be due to a lower co-ordination number for the smaller particles in a well graded material. Therefore, although the smaller particles are stronger, in a matrix their probability for survival is lower than for the larger particles.

There are therefore two opposing effects of particle survival; these are the particle size versus the co-ordination number (McDowell and Bolton, 1998).

2.6.1.3 Effect of particle shape

In one-dimensional compression tests Roberts and de Souza (1958) noted that at moderately low pressures angular sands crushed and compressed more than rounded sands, yet at higher pressures very little difference was observed between the two types of sand. With tests on loose and dense sands, Lee and Seed (1967) found that well-rounded Ottawa sand was considerably more resistant to crushing than either fine subangular or subrounded sands. They also found this to be true for different types of soil.

Lee and Farhoomand (1967) observed that the proportions of fines produced is greater for angular sands than round sands, and Datta et al (1979) found that crushing increased with angularity in tests on calcareous sands.

In experiments with glass ballotini (G.B.) and crushed glass particles (A.G.), Nakata et al. (2001b) confirmed that the angular particles yielded at a much lower vertical stress (6MPa) than the rounded particles (20MPa) (Figure 2.16). This confirmed similar work by Hagerty et al. (1993). However, although the e - $\log\sigma_v$ curves took very different paths, at very high stresses the curves for both types of glass merge onto a single normal compression line. It was also noted that as the angularity of a particle increased so did the variability of the strength of the individual particles.

Bowman et al. (2001), using Fourier shape descriptors, showed that the particle roughness did not change when breakage occurred in some sands.

2.6.1.4 Effect of particle hardness / mineralogy

Marsal (1966) found, not surprisingly, that greater compression and particle breakage was observed in weaker particles.

One-dimensional compression tests by Nakata et al. (2001b) investigated the effect of the mineral composition of three sands (where the composition of individual particles

was made up of quartz and feldspar). They found that for specimens where the particles had a high quartz content (the stronger mineral) the yield stress was higher than for those where the particles contained lower amounts of quartz. However, for each of the three sands tested the e - logσ_v curves merged onto a single post-yielding curve at high stresses.

Festag and Katzenbach (2001) noted, in cyclic load triaxial tests, that quartz sand showed significantly less breakage and hence less axial displacement than gabbro sand (a volcanic material) (Figure 2.17).

2.6.1.5 Effect of the state of effective stress

Vesic and Barksdale (1963) carried out triaxial tests on a medium grained sand over a wide range of confining pressures up to a maximum of 10,000lb/sq.in (approximately 69000kPa). They observed that the amount of particle crushing increased with increased confining pressure, over half of the crushing occurring during the shearing stage of the test after isotropic consolidation. This has also been observed by several authors including Bishop (1966), Lee and Seed (1967), and Ueng and Chen (2000).

Yamamuro and Lade (1996), from drained triaxial tests on dense Cambria sand, the results of which are shown in Figure 2.18, found that as the confining pressure was increased (in different tests), there was a defined stress magnitude at which the volumetric strain and axial strain curves rapidly increased. This was shown to be directly related to a rapid increase in the amount of particle breakage. Beyond a further significant confining stress the slope of the volumetric and axial strain curves decreased; again this was shown to be directly related to a point at which there was no further occurrence of breakage.

2.6.1.6 Effect of the stress path

Nakata et al. (1999) noted that the transmission of the forces through the material was important and when using models such as that of Cundall and Strack (1979) there were strong lines of force running through the specimen at intervals of 2-3 particle diameters as shown in Figure 2.19a. Furthermore Nakata et al. (2001b) found that the ratio of the single particle strength to the particle characteristic tensile strength was an indicator of the ratio of the 'active' to 'non active' particles.

Work on agglomerate strength by Adams et al. (1994), shows very clearly the lines of concentrated force which travel through the material in the direction of the principle

stress (Figure 2.19b), again showing many of the particles carry little, or no, load. Therefore the failure of one particle will cause a concentration of stress on its neighbours, leading to an increase in the possibility of fracture of the particles nearby (Steacy & Sammis, 1991).

2.6.1.7 Effect of the void ratio

A decrease in the initial void ratio, i.e. an increase in the relative density and therefore an increase in the number of particle contacts (co-ordination number) would reduce the inter-particle contact force and hence reduce the amount of crushing (Hardin, 1985).

The void ratio vs. vertical stress plots seen in Figure 2.20 show that as the initial void ratio decreased the stress at which the specimen started to yield increased. This was perhaps as explained by Nakata et al. (2001b) and analysis by Jaeger (1967), that the tensile stress for a particle in a matrix decreases with an increased co-ordination number. Field (1963) and Oda (1977) both showed that as the void ratio decreased there was an increase in the average number of contact points per particle. That is, the average co-ordination number (C_a), which was defined by Field (1963) as:

$$C_a = \frac{12}{1+e} \qquad \text{Equ 2.6}$$

Therefore the yield stress for a specimen with a higher void ratio is lower due to the decrease in the co-ordination number (Oda, 1977 and Jaeger, 1967). Bolton and McDowell (1996) call the behaviour about the point of yielding 'clastic yielding', whereby major irrecoverable strains occur due to the fracturing of particles. Following on from that the clastic yield stress is the value of the applied stress which causes the maximum rate of grain fracture, i.e. the point of maximum curvature on the e - $\log\sigma_v$ plot.

Al-Hussaini (1983) noted that a medium dense specimen tended to undergo more particle crushing than a dense specimen. Although at increased cell pressures Lee and Seed (1967) and Vesic and Clough (1968) have found that the influence of the initial void ratio on the breakage in compression tests was significantly diminished.

It is important to recognise that the reduction in the void ratio is dependent on the volume of voids being reduced, i.e. the filling of the voids. Hence for a soil to be fractal it is essential that the small particles fracture to fill the void spaces. However, where a large particle fractures, there may not be a large void for it to fill (McDowell and Daniell, 2001). This is a circular argument as where there is a large void space there

will presumably be several large particles nearby and hence a low co-ordination number. In other words where there are only small voids then there will be plenty of particles near by (both small and large) and the larger particles will therefore have a higher co-ordination number and are less likely to fracture.

2.6.1.8 Effect of moisture content

Hardin (1985) investigated the effect of moisture content on a saturated and a dry Antioch sand. He concluded that water (saturated tests) greatly increased the crushability, or possibly decreased the particle hardness for that specific sand. Sowers et al. (1965), in laboratory tests on broken rock observed that the addition of water increased the rate and the amount of crushing. On work related to rockfill dams, Nobari and Duncan (1972) found that further particle crushing was caused when particles were introduced to water. They found that the amount of collapse occurring when the material was flooded was reduced when there had been a higher initial water content. Lee and Coop (1995) showed that particle breakage of Dog's Bay sand is greater when the soil is wet than when it is dry.

Lee and Coop (1995), as shown in Figure 2.21, used the critical state framework to describe their results on decomposed granite soils where particle breakage was the principal means of plastic volumetric compression. They found that a state boundary surface for the dry soil developed outside that of the surface formed by the saturated and partially saturated soil (i.e. stronger). This was put down to the dry soil undergoing a smaller amount of breakage (also found by Miura and O'Hara, 1979). Lee and Coop proposed this reduced amount of breakage allowed greater dilation and increased peak strength. However, when a dry specimen, whose state was outside that of the saturated boundary, was flooded, large strains occurred and the soil state quickly returned onto and followed the saturated surface. Furthermore, when soils have inter-particle bonds due to the drying out of specimens that were compacted at optimum moisture content (i.e. denser), their peak strengths lay further still from the saturated state boundary than for the loose dry soils. With wetting there is an immediate collapse of the soil back to the saturated state surface. The collapse of both afore mentioned soils is associated with occurrence of an increase in the amount of particle breakage. The behaviour of the saturated and partially saturated soils were found not to differ significantly. Also, the critical state friction angle was shown not to differ between the different moisture contents.

Miura and Yamanouchi (1975) in high pressure triaxial tests on sand showed that water affected the settlement occurring in the specimen. They speculated that this was because the surface energy reduced in already existing cracks in the particles thus inducing extra breakage. This is in agreement with the conclusions drawn by Oldecop and Alonso (2001) on rockfill material.

2.6.1.9 Curved failure envelope

Yamamuro and Lade (1996) found that with a dense sand the curvature of the Mohr-Coulomb failure envelope at low stresses was greater than a loose sand. This is where at higher pressures the angle of shearing resistance (φ') decreases and becomes stable. This was also found to be true by several other authors including Vesic and Barksdale (1963), Marachi et al (1972), Billam (1971), Ramamurthy et al (1974), Charles and Watts (1980), Al-Hussaini (1983), and Indraratna et al. (1993). However some have found that the friction angle reaches a low point before rising again (Bishop, 1966; and Lee and Seed, 1967). Hall and Gordan (1963) carried out tests on gravels and found that the angle of shearing resistance was 5° to 6° higher at low stress than those obtained at higher stresses. With rockfill material Marsal (1967) also quoted figures of between 5° to 6°.

Bishop (1966) comments that curvature of the failure envelope is most marked for soils where:

i) the specimens are initially dense or heavily compacted,
ii) the particle grading is uniform, and
iii) if the specimen is undisturbed, then where it is heavily over consolidated.

He further comments that the curvature of the failure envelope in specimens with coarser grained granular material is linked with the crushing of particles. Marsal (1967) also made this link when carrying out large scale tests on rockfill material, as did Datta et al (1979) with tests on calcareous sands. With dense granular materials this meant a reduction in the rate of volumetric strain and a reduction of angle of shearing resistance (φ'_{peak}). Although there have been calculations relating the rate of volumetric strain with φ' (Taylor, 1948; Bishop, 1950; Hafiz, 1950; and Bishop and Eldin, 1953), the effect of particle crushing is usually omitted (Bishop, 1966).

Lee and Farhoomand (1967) could hear audible cracking sounds from the cell after each stress increase and occasional further cracking sounds during the following two hours. A two hour time period was chosen between each successive load increment as Lee and

Seed (1967) suggested that most of the significant volume change would occur within the first two hours after the load was applied. These further cracking sounds would indicate that breakage as well as compression is time-dependant. Breakage of particles presumably takes time because as mentioned in Section 2.6.1.6 as one particle breaks this then causes an increase in the stress on the surrounding particles, which then in turn may also fracture.

Yamamuro and Lade (1993) confirmed this commenting that fracturing and rearranging of soil particles requires time and that with an increased strain rate the time factor was reduced. This resulted in less compression and increased strength with increased strain rates. De Souza (1958) also found that there was a greater extent of particle crushing when the stress was applied more slowly.

2.6.2 Measures of particle breakage

Several authors have suggested ways of measuring the amount of breakage occurring in an element of soil, most of these are based on empirical methods. Figure 2.22 shows diagrammatically how different authors represented the amount of breakage. Leslie (1963, 1975), Marsal (1967) and others have used a single sieve size to represent the amount of breakage. The difficulty that arises with this method is that it does not represent the breakage occurring across the full grain size distribution curve. Leslie (1963) considered the point where 100% of the original material was retained and used the percentage passing this sieve size after testing to represent the amount of breakage. Later he revised this to the sieve size where 90% of the original material was retained (Leslie, 1975). Marsal (1967) used the percentage increase at the point of maximum difference between the pre and post curves. Lee and Farhoomand (1967) (Figure 2.22) looked at the difference in particle size for a measure of breakage. They considered the size ratio D_{15i}/D_{15a}, where D_{15} is the diameter for which 15% of the specimen is finer. D_{15i} is from the initial grading curve and D_{15a} is from the after test grading curve. 15% passing was chosen because it was "the key size criterion used in the design of drains and filters" of dams.

As can be seen in Figure 2.22 breakage of soil particles is evident across a range of particle sizes. Hardin (1985) therefore proposed a method for calculating the relative breakage (B_r) of a specimen of soil for breakage that is significant to soil behaviour.

$$B_r = \frac{B_t}{B_p} \qquad \text{Equ. 2.7}$$

where B_t = the total breakage that occurred during the test and

B_p = the breakage potential of a given soil specimen, shown in Figure 2.23

Hardin considered that the distribution of silt size particles was less important to soil behaviour than the distribution of particles larger than silt size and therefore used the 0.074mm sieve, i.e. the largest silt size, as a lower limit.

Lade et al. (1996), analysed the different particle breakage factors. They found that there was a significant amount of scatter between the different methods, even though calculated from the same grain size distribution data. With the Marsal (1967) method, when particle crushing is extensive, there can be a significant shift in the gradation curves leaving only a few sieve sizes that correspond to both the pre- and post-test gradation curves. The D_{15i} / D_{15a} method proposed by Lee and Farhoomand (1967) uses only a single size sieve, which Lade et al. (1996) consider not to be a particularly controlled test as the D_{15a} grain size, which could be very small is in the denominator increasing the scatter in the results. Thus with their B_{10} breakage factor, which is also based on a single grain size, Lade et al. have used the inverse with the initial grading as the denominator. They commented that Hardin's (1985) relative breakage factor, which includes the change in grain size across the whole range of the distribution is therefore a fairly robust factor, insensitive to any small variation in measurements.

2.6.3 Single particle crushing

It is widely accepted that the failure of a spherical particle under compression is a tensile failure. Therefore with the use of the Weibull statistics on the fracture of brittle ceramics, a consistent definition of grain tensile strength can be calculated (Weibull, 1951) (Figure 2.24).

The characteristic tensile stress induced in a single particle, when crushed between two diametrically opposite flat platens may be defined as:

$$\sigma = \frac{F}{d^2} \qquad \text{Equ. 2.8}$$

where d =particle diameter and

F = force applied. (Jaeger, 1967; Shipway and Hutchings, 1993; and Lee, 1992).

This is also consistent with the Brazilian test for the definition of tensile strength of concrete.

For angular materials the load displacement plot is not a single smooth curve, but is made up of several smaller peaks before the final peak and loss of resistance to the load.

McDowell and Bolton (1998) interpreted the smaller peaks as fracturing of asperities (Figure 2.25). The force of each peak is considered to be in relation to the size of the asperity breakage and is therefore not related to the size of the main particle. At the final peak, McDowell and Bolton (after Lee, 1992) used the definition of tensile strength (σ) of a particle:

$$\sigma = \frac{F_f}{d^2} \qquad \text{Equ 2.9}$$

where F_f = force at failure, and

d = diameter of particle at failure.

From this the probability of survival $P_s(d)$ for any particular size of aggregate can be calculated by:

$$P_s(d) = \exp\left[-\left(\frac{\sigma}{\sigma_o}\right)^m\right] \qquad \text{Equ. 2.10}$$

where: $\sigma = F/d^2$ (Equ. 2.8),

σ_o= characteristic tensile strength and

m = Weibull modulus.

where the Weibull modulus (m) reduces with increased variability and the characteristic tensile strength (σ_o) for a particle size d is the strength at which 37% of the tested particles survived. McDowell (2001) shows that at least thirty particles must be tested to determine the characteristic tensile strength (σ_o) and Weibull's modulus (m) within reasonable limits (25% accuracy at 95% confidence).

Single particle survival curves can be plotted against the characteristic stress as seen in Figure 2.26, where the survival probability (P_{sc}) for each particle was calculated by positioning the tensile stresses at failure (σ_f) in ascending order and dividing by the total number of particles tested plus one as seen in Equation 2.11.

$$P_{sc} = \frac{N_{i(\sigma \geq \sigma c)}}{N_{total} + 1} \qquad \text{Equ. 2.11}$$

where: $N_{i(\sigma \geq \sigma c)}$ = the number of particles with a characteristic strength (σ) greater than the crushing stress (σ_c), and

N_{total} = the total number of particles tested.

Nakata et al. (1999) noted that it is important to understand the behaviour of a soil specimen in the context of the crushing characteristics of a single particle. They therefore examined the relationship between the single particle crushing characteristics

and the crushing behaviour of single particles embedded in a soil matrix. Two types of test were carried out, firstly the crushing of individual particles and secondly triaxial compression tests with marked particles.

Test one gave two definitions of crushing force, F_c = at the initial breakage (probably of an asperity) and F_f = at particle failure.

Test two describes an average characteristic tensile stress (σ_{sp}) acting on a single particle within a matrix as:

$$\sigma_{sp} = \frac{F_{sp}}{\bar{d}^2} = \sigma\left(\sqrt[3]{\frac{(1+e)\pi}{6}}\right)^2 \qquad \text{Equ. 2.12}$$

where: F_{sp} = single particle force,

$\bar{d}$ = mean particle diameter.

This shows that the characteristic tensile stress is not dependent on particle size but on void ratio and suggest that the characteristic tensile stress increases with void ratio, in line with Golightly (1990). The force on a single particle (F_{sp}) in a matrix (triaxial test) can then be calculated as (Nakata et al, 1999):

$$F_{sp} = \frac{\sigma}{N^{2/3}} \qquad \text{Equ. 2.13}$$

where: N = the number of particles in a cross section of the specimen, and

N = the volume of solids divided by the volume of a single particle.

The percentage of particles in the matrix likely to survive the characteristic tensile stress (σ_{sp}) at 37% can then approximately be determined from the particle survival curves, Figure 2.26.

2.6.4 Description of particle breakage

Nakata et al. (1999) used three different definitions of breakage; type 1, abrasion; type 2, breaking off of fragments; and type 3, fracturing of whole particles. Type 2 damage was assumed to happen at F_c (first point at which the load slipped) and type 3 at F_f (peak force at major splitting). This work was refined by Hyde and Nakata (2001) and Nakata et al. (2001a), who describe the breakage of particles in terms of 5 different types. These have been tabulated in Table 6.3 and outlined briefly below. Type I – no visible damage; Type II – single abrasion or breakage of asperity; Type III – more than one abrasion or asperity fracture; Type IV – major splitting of the grain into two or more particle; and Type V – further breakage of type IV sub particles. They noted that

it was not possible to remove all of the fragments of type V breakage, due to sub particles crumbling and they further commented that the description of breakage given to each particle relied heavily on visual observation and required a measure of judgement. This was especially the case at the boundary between different types of breakage.

To further investigate individual particle crushing, Nakata et al. (2001a) placed seeded particles in a one-dimensional compression test. The change in cross sectional area (R_a) of each seeded particle was calculated (using digital images and computer scanning software). It was found that R_a sometimes helped to clarify the breakage that was visually observed.

2.7 Shakedown theory

Collins and Boulbibane (2000) reviewed a model known as 'shakedown' commenting that pavements which operate at loads less than critical, i.e. less that the failure load, will eventually shake down to a steady state. The elastic response by definition cannot cause failure. Shakedown has typically been viewed from a pavement's perspective where the build up of plastic strains over many load cycles will eventually cause failure in the forms of sub-surface slip, rut formation or surface cracking. In the railway environment the ballast is loaded by the sleepers and failure is one of serviceability due to the non-uniform settlement of the sleepers into the ballast. It is therefore understood that this would be similar to the rutting failure mentioned above.

The analysis of long term behaviour of surfaces all use the concept of shakedown theory, with the basic assumption of an inhomogeneous elastic/plastic material. Collins and Boulbibane (2000) split the elastic/plastic strain cyclic into various possible responses (Figure 2.27). At first, where no permanent strains are induced due to the load being sufficiently small, the material is purely elastic. After this if the load exceeds the elastic load, then permanent plastic strains will be induced and the response to consecutive loads will be different. After a finite number of cycles, the build up of residual stresses and changing material properties can be such that the material's response is once again elastic and no further plastic strain occurs. It is at this point that Collins and Boulbibane say that the specimen is at 'shakedown'. At higher loads this will not happen but instead the specimen will either settle into a closed cycle of permanent strains - 'cyclic plasticity', or 'ratchetting' where the plastic strains increase indefinitely. The critical load, below which the sample shakes down and above which

the specimen fails is called the shakedown load. This parameter is defined by upper and lower bound limits.

Werkmeister et al. (2001) reviewed the 'shakedown' model in terms of unbound granular materials. They carried out drained cyclic load triaxial tests on two well graded aggregates with a maximum particle size of 32mm and a moisture content of 4%. The cell pressure was set at different levels between 70kPa and 280kPa, with a constant cyclic stress of between 35kPa and 700kPa set for each individual test. The rate of loading was 5Hz. They presented their permanent strain results in a new way with the rate of strain versus the accumulated strain. This can be seen in Figure 2.28, where Werkmeister et al. (2001) identified three types of permanent strain accumulation (A, B and C). Range A, is that of plastic shakedown, where as seen in Figure 2.28 the rate of strain decreases to almost nothing, leading to an asymptotic final permanent strain. In other words it has reached 'shakedown'. They commented that particle crushing probably did not occur, or was insignificant. Range C, is that of incremental collapse or ratcheting. In Figure 2.28 this is shown to reach a repeated increment of permanent plastic strain. This strain rate appears to depend on the load level. Werkmeister et al. observed that the closer the load level was to the (assumed) monotonic failure load then the decrease in the strain rate was reduced i.e. the specimen behaviour was more likely to fall within Range C. In Range C, particle abrasion and crushing was assumed to have occurred.

Range B, was termed intermediate response – plastic creep. This is because, as seen in Figure 2.28, initially there is a rapid reduction in the strain rate to a relatively low rate. They speculate that this is possibly tending to a constant strain rate. In Range B, they suspect a slight abrasion of the particles may occur. Werkmeister et al redefined the initial shakedown model to fit the granular response observed, as seen in Figure 2.29. There are three main features that are different from the original model presented by Collins and Boulbibane (2000). Firstly, in granular material there is no real ability to undergo tension, therefore the plastic recovery part of the hysteresis loop does not occur. Secondly, they never observed any form of purely elastic or elastic shakedown behaviour as identified in the original model (also not found by Janardhanam and Desai, 1983). Thirdly, due to the material's non-linearity, the hysteresis loop is unlikely to be symmetrical.

From the results of the test programme, Werkmeister et al. developed a model in terms of cell pressure and deviator stress (Figure 2.30) This was based on a sandy gravel

material at 4% moisture content. On this they overlaid the three regions; Region A – plastic shakedown, Region B – plastic creep, and Region C – incremental collapse.

When loading specimens of gabbro sand with up to 5 million load cycles Festag and Katzenbach (2001) found that the specimen would reach cyclic shakedown after a period, but after further cycling may undergo further plastic strain (Figure 2.17). They explained this as a local failure due to grain abrasion. Even after 4 million load cycles a final shakedown could not be verified. With quartz sand they observed a slow increase in the plastic strain but no sign of shakedown as see in the gabbro sand.

Hellawell (1997) comments that after tamping maintenance "it does not take many passing trains to shakedown the substructure." Unfortunately he did not put this in quantitative terms that could be compared to track performance after track maintenance using the Stoneblower.

2.8 Field testing

Brown (1996) makes the point that there are always questions raised about the effectiveness of such tests as the triaxial test, and whether the samples are representative of field conditions. For many years the static plate loading test has been used within pavement soil mechanics. However this also does not produce real conditions but allows pore pressures to dissipate, whereas a transient load is essentially an undrained event. However Sweere (1990) reviewed in-situ testing and concluded that the dynamic plate loading test was appropriate for assessing the resilient modulus of granular layers.

Recent work carried out by Ping and Yang (1998), compared resilient moduli calculated through the use of the repetitive rigid plate test in a test pit facility with that of laboratory tests. They carried out tests on five typical Florida subgrades at three different moisture contents. The results showed that the moisture content of the subgrade affected the resilient modulus, which is consistent with the results found in the laboratory triaxial tests (Section 2.4.1.4). They also concluded that the resilient modulus resulting from the laboratory triaxial tests could be used to predict the resilient deformation of the subgrade material.

2.8.1 Track settlement

Sato (1995), based on extensive work in Japan, expressed the settlement of freshly tamped track under train passage as:

$$y = \gamma(1 - e^{\alpha x}) + \beta x \qquad \text{Equ. 2.14}$$

where: y = settlement,

x = repeated number of loads or tonnage carried by the track,

α, β, γ = coefficients.

This equation is clearly based on experimental methods an unfortunately it does not give details regarding the units used. However the settlement is presumed to have been in millimetres; and the equation and corresponding graph, as seen in Figure 2.31, clearly show the behaviour of the newly tamped ballast bed. Sato explains the first term in this equation ($\gamma(1-e^{ax})$) as the initial rapid settlement, where the ballast consolidates. The second term (βx) expresses the linear settlement after this initial settlement, where there is lateral movement of the particles under the sleepers. He then goes on to say that the initial consolidation will depend on the work done on the ballast.

The long term settlement due to the passing of trains depends on the value of β. From this work he concluded that:

i) β for crushed stone is 1/6 – 1/7 of that of gravel.

ii) β increases in proportion to the square of the velocity of the repeated load.

iii) β in contaminated ballast is smaller than that of clean dry ballast.

iv) The standard deviation of β is proportional to its mean value. Therefore the growth of track irregularities is proportional to β.

In the prediction of permanent ballast settlement Ford (1995) used the following expression as detailed by Stewart and Selig (1982), Selig and Alva-Hurtado (1982), and Shenton, 1982). He found that as long as the cyclic stress was below, say, 70% of the failure strength as determined from the monotonic stress then a linear relationship exists between the axial strain at the Nth cycle and the log of the number of cycles.

$$\varepsilon = \varepsilon_1(1 + C \times \log(N)) \qquad \text{Equ 2.15}$$

where: ε = total permanent strain after N cycles,

ε_1 = permanent strain after first cycle, and

C = dimensionless constant controlling the rate of growth of deformation.

This 70% value would appear to be linked with the plastic shakedown load as described in Section 2.7.

Chrismer and Selig (1993) used computer modelling to predict the cumulative plastic strain (ε_p) in the ballast layer:

$$\varepsilon_p = \sum_{i=1}^{10} \varepsilon_1 k_w k_a k_f N^b \qquad \text{Equ. 2.16}$$

where: ε_1 = first load cycle plastic strain,

k_w, k_a, k_f = coefficients for wheel load, ballast durability, initial degree of ballast fouling,

N = equivalent number of load repetitions,

b = ballast material component.

2.8.2 Track stiffness

Sussmann & Selig (1999) looked at several ways to manipulate the track stiffness including increasing the sleeper length, altering the layer thickness, using asphalt layers and modification to the pads and fastenings. Using GEOTRACK (Li and Selig, 1995) they found no significant change in the track stiffness due to a change in sleeper length, as the bearing area of any sleeper is generally concentrated only below the rail seat. Decreasing sleeper spacing would however increase the track stiffness, as would increasing the sleeper stiffness by increasing its width and depth.

Li and Selig (1995) considered a high track modulus to give better track performance. In general a minimum of 28MPa is desirable as a lower track modulus may give rise to ballast or subgrade problems. However higher dynamic wheel loads are generated from stiff track, which suggests that the track modulus should not be too high either, this appears to be in agreement with Raymond (1985).

2.9 Summary

It is clear from the literature reviewed that there are two main areas that need to be focused on concerning the behaviour of granular materials for railway track maintenance. These are the basic understanding of the geo-mechanical behaviour under controlled testing in the laboratory and the field, and the analysis of the track quality data regarding the maintenance techniques used on the railways in the UK. It is believed that with an increase in depth and breadth of understanding in these two areas then the management and performance of railway track maintenance can be improved.

The following points were therefore considered to be areas where there was a limited knowledge/understanding and further research was necessary:

1) It is fairly well recognised under monotonic loading that the breakage of granular particles at high stresses causes the rate of dilation to be reduced, the peak stress to

occur at a lower stress and a higher axial strain, and a reduction of the calculated angle of shearing resistance. This in turn leads to a curved Mohr-Coulomb failure envelope. Although this phenomena is recognised there was still only a limited understanding in the available literature directly relating particle breakage to the volumetric strain behaviour.

2) There have been several proposals presented in the literature (not all have been included in Chapter 2) attempting to define the parameters that control plastic strain under repeated loading. These results would appear at best to be varied.
3) The understanding of the effect of moisture on the breakage of granular materials appears to be slightly confused. Very little has been reported on the effect of the moisture content on the long term accumulation of plastic strains under cyclic loading.
4) In the research undertaken by Key (1998) there were clear limitations concerning the volume change measurements using the radial LVDT's. As the current work uses the apparatus designed by Key it would be necessary for a better volume change measurement system to be developed.
5) Within the railway industry the performance of the stoneblower is still little understood with a large amount of scatter in the post maintenance performance.

The aims and objectives of the current work, detailed in Chapter 1, have therefore been based on the above five points.

Mechanical maintenance	4kg fines/tamp/sleeper
Wagon spillage (e.g. near quarries)	4kg fines/m^2/year
Air borne fines	0.8kg/m^2/year
Traffic loading	0.2kg/sleeper/million tons of traffic

Table 2.1 - Source of ballast contamination (Evans, 1992)

Stoneblower design category	Application
A*	Highest quality high speed track
A	Track speeds form 105 to 125 mph
B	Track speeds form 75 to 105 mph
C	Track speeds up to 75 mph
(D)	(Miscellaneous maintenance sites)

Table 2.2 - Stoneblower design categories (McMichael, 2001)

Quality band	Speed range mph	Level 35m filter				Line 35m filter				Level 70m filter			Line 70m filter		
		50 %	90 %	100 %	Max	50 %	90 %	100 %	Max.	50 %	90 %	100 %	50 %	90 %	100 %
1	10-20	5.2	7.4	8.3	8.3	3.0	5.0	5.6	9.3						
2	25-30	4.3	6.1	7.7	7.7	2.7	4.5	5.2	8.6						
3	35-40	4.1	5.8	7.2	7.2	2.5	4.1	4.7	7.9						
4	45-50	3.8	5.4	6.7	6.7	2.2	3.7	4.5	7.3						
5	55-60	3.5	5.0	6.3	6.3	2.0	3.3	4.2	7.0						
6	65-70	3.0	4.3	5.4	6.0	1.7	2.9	3.6	6.7						
7	75-80	2.7	3.8	4.8	5.7	1.5	2.5	3.1	6.3	3.7	5.7	6.3	3.0	5.2	5.7
8	85-95	2.2	3.2	4.0	5.3	1.3	2.1	2.7	6.0	3.3	5.1	5.6	2.6	4.5	5.0
9	100-110	1.9	2.7	3.4	5.0	1.1	1.8	2.3	5.7	2.9	4.5	5.0	2.2	3.8	4.3
10	115-125	1.7	2.4	3.0	4.7	1.0	1.6	2.0	5.0	2.4	4.0	4.4	1.8	3.2	3.7
11	130-140	1.5	2.1	2.6	4.4	0.8	1.4	1.8	4.7	2.0	3.5	3.8	1.5	2.7	3.1

Table 2.3 - Track quality bands – acceptable standard deviations in mm for eighth mile sections (British Railways Board, 1993)

Author	Specimen diameter (mm)	Max. stone size (mm)	D/d_{max}
Sweere (1990)	400	40	10
Pappin et al. (1992)	150	40	3.75
Salmon (1994)	150	20	6
Brown (1996)	280	40	7
Kolisoja (1997)	300	64	4.7
Key (1998)	236	50	4.7
Key (1998)	236	20	11.8
Indraratna et al. (1998)	300	52	5.7
Kohata & Sekine (1999)	300	63	4.7

Table 2.4 - D/d_{max} summary table

Author	Density (Mg/m3)	Void ratio	Comments
Indraratna et al (1998)	1.53		Latite basalt ballast
Indraratna (2001)	1.56	0.72	Large triaxial tests
Indraratna (2001)	1.67		Large cubical triaxial
Ishikawa and Sekine (2002)	1.55+1.61		2 diff gratings ballast
Kohata and Sekine (1999)	a) 1.57 b) 1.57 c) 1.76	0.637 0.650 0.711	Diabase ballast was densest
Janardhanam and Desai (1983)	1.49		Granite gneiss ballast
Stewart (1986)	1.58	0.66	Well graded railway ballast
Key (1998)	1.47		

Table 2.5 - Specimen densities from previous research

Seating errors caused by gaps closing between:	• Ram or internal load cell and top platen. • Platens and porous stones.
Alignment errors resulting from equipment and specimen nonconformity, specifically:	• Porous stones of nonuniform thickness. • Non-vertical / eccentricity of loading ram. • Non-horizontality of platen surfaces. • Tilt of specimen.
Bedding errors caused by surface irregularities and poor fit at the interfaces between the specimen and porous stone.	
Compliance errors which may occur because:	• The tie bars extend and cause relative displacement of the top of the cell with respect to the piston. • The internal load cell deflects. • The lubricant is compressed in systems using lubricated ends. • The porous paper is compressed.

Table 2.6 - Sources of error of strain in conventional deformation measurement (Scholey et al, 1995)

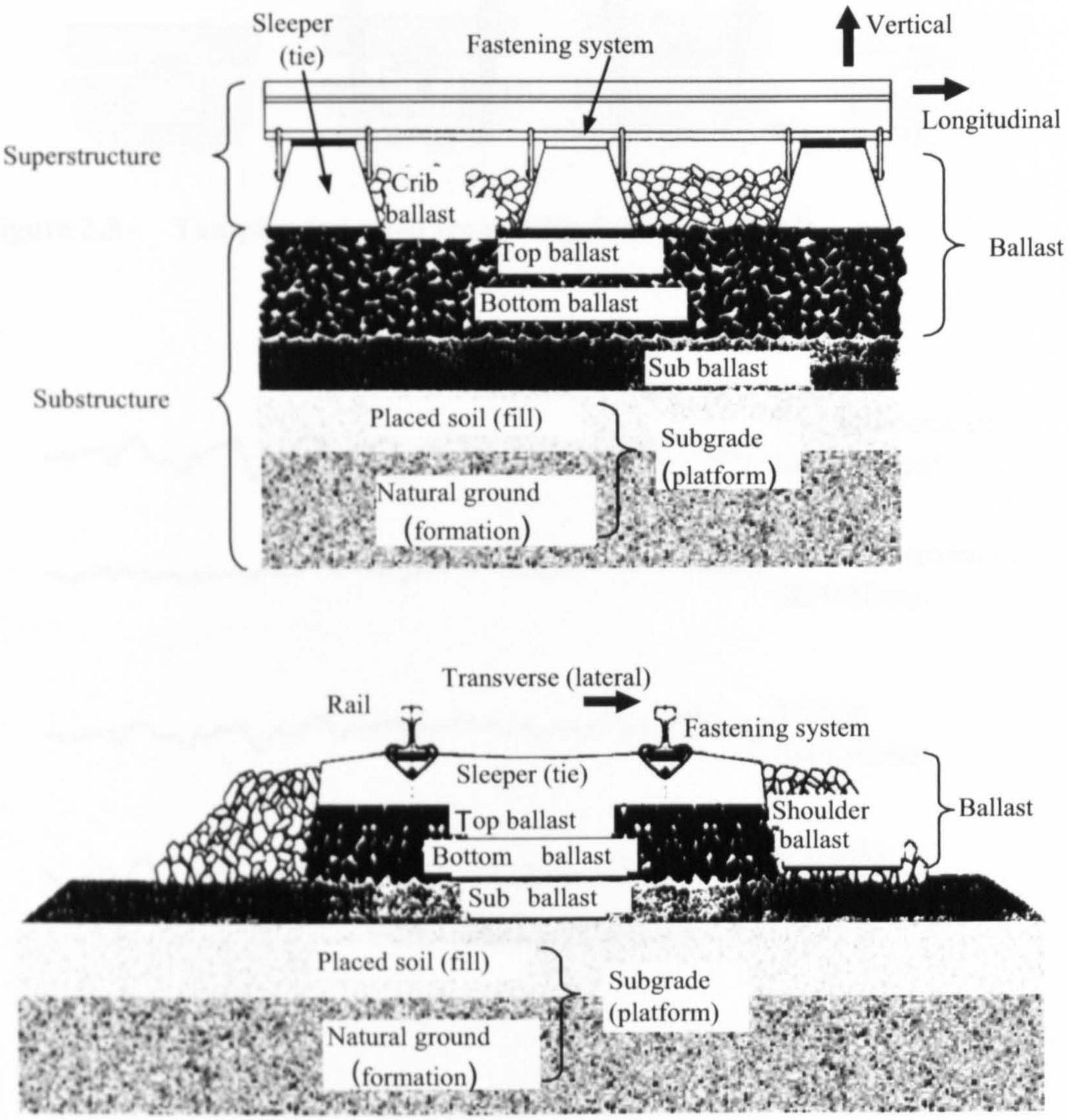

Figure 2.1 - Track structure and components (Selig and Waters, 1994)

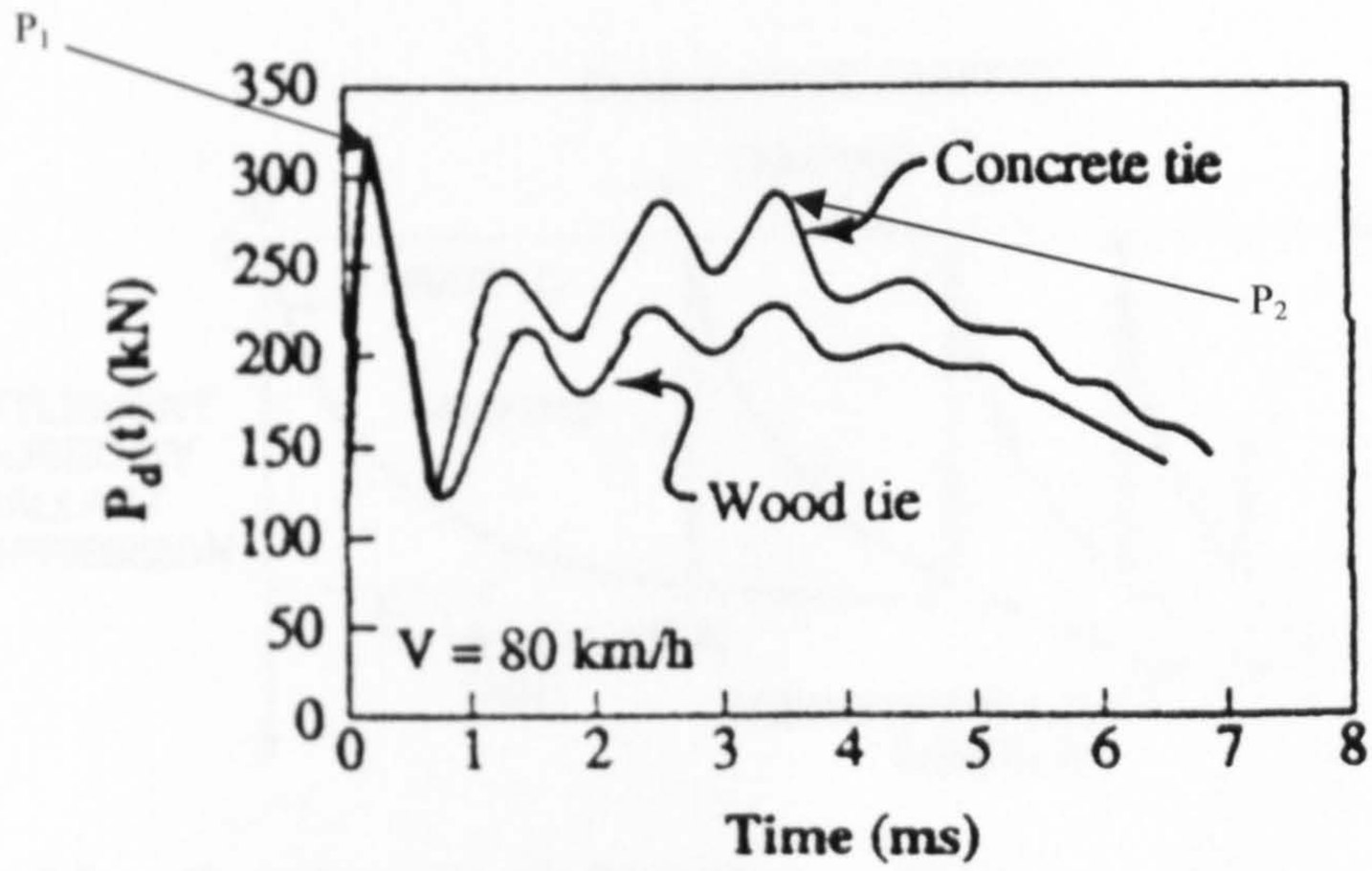

Figure 2.2 - Predicted dynamic wheel loads due to a dipped joint (Li & Selig, 1995)

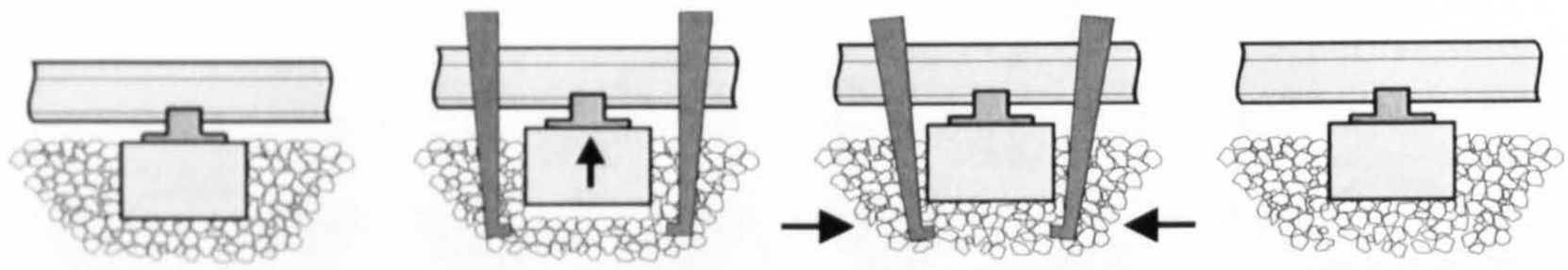

Figure 2.3 - Tamping (adapted from Selig & Waters, 1994)

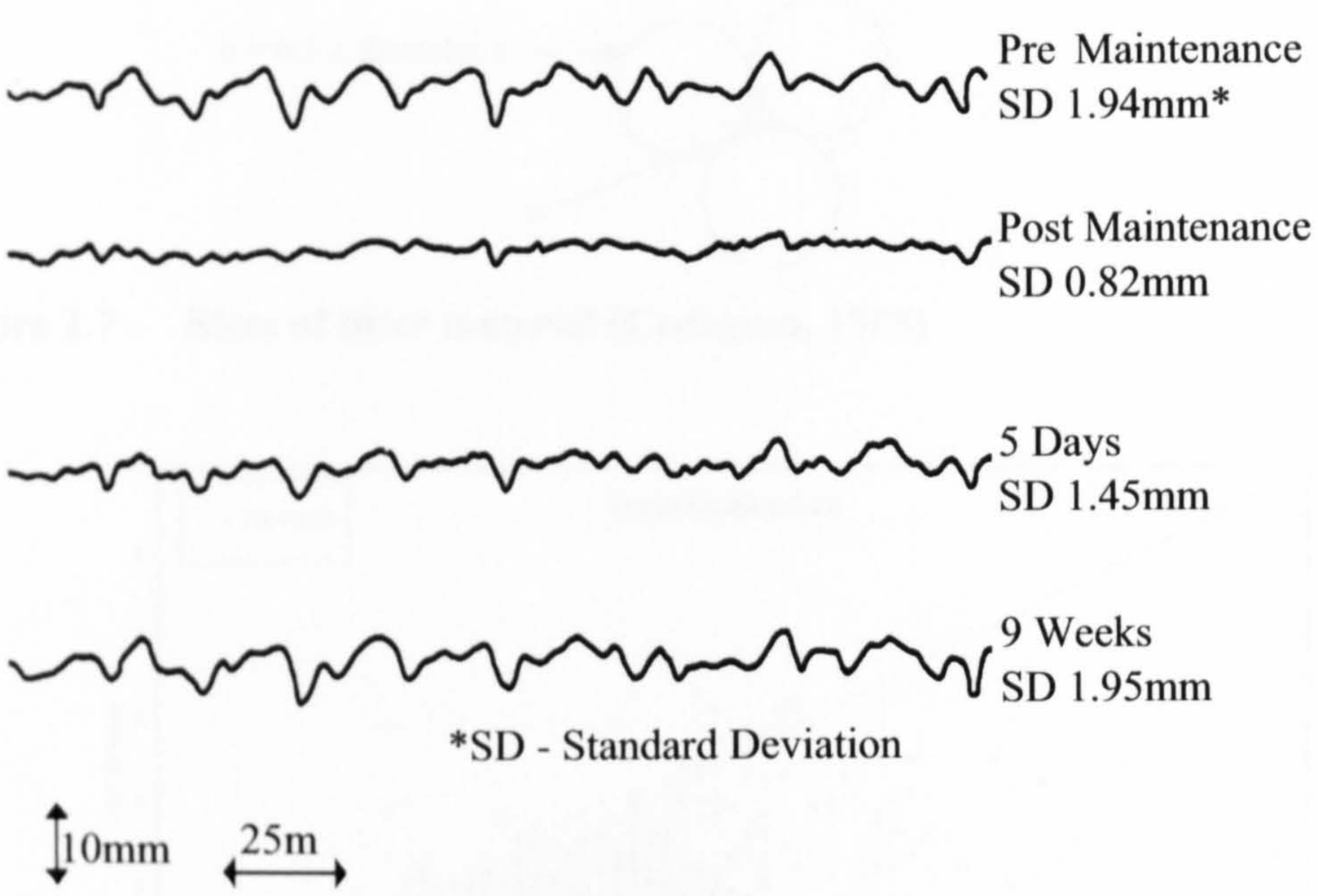

Figure 2.4 - Ballast memory (McMichael, 2000)

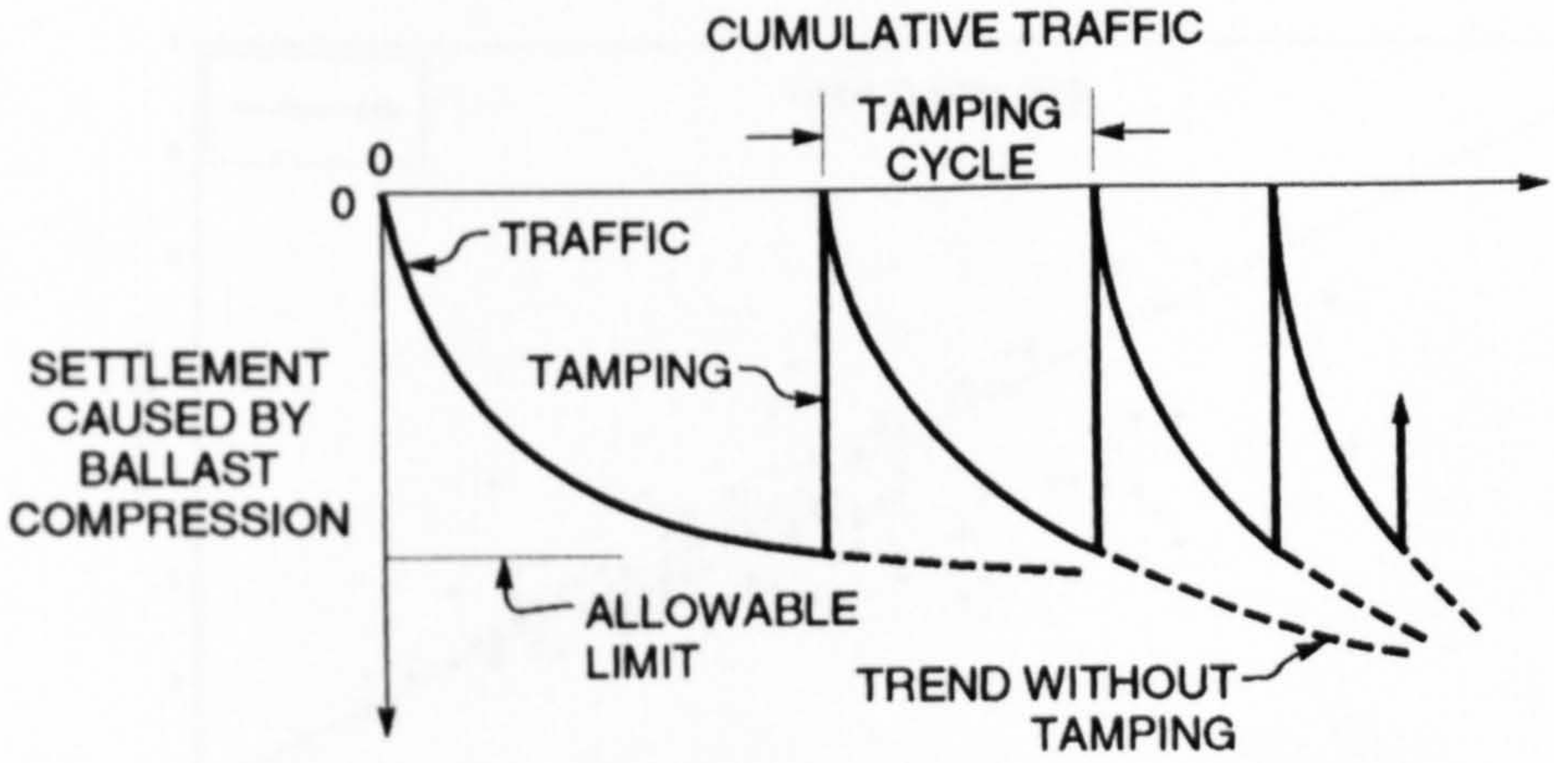

Figure 2.5 - Tamping cycle (Selig & Waters, 1994)

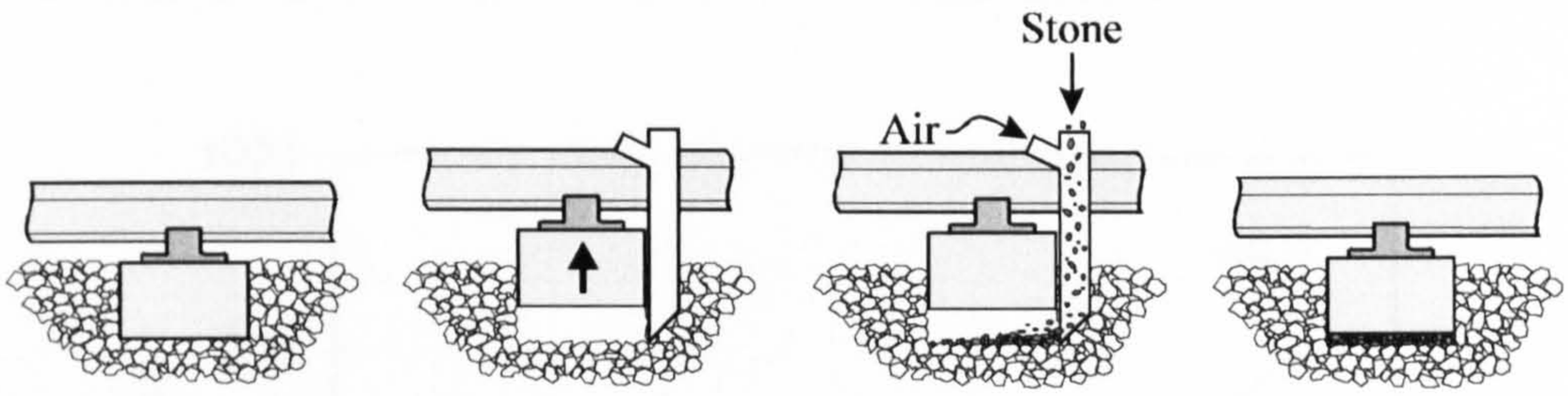

Figure 2.6 - Stoneblowing (adapted from Selig & Waters, 1994)

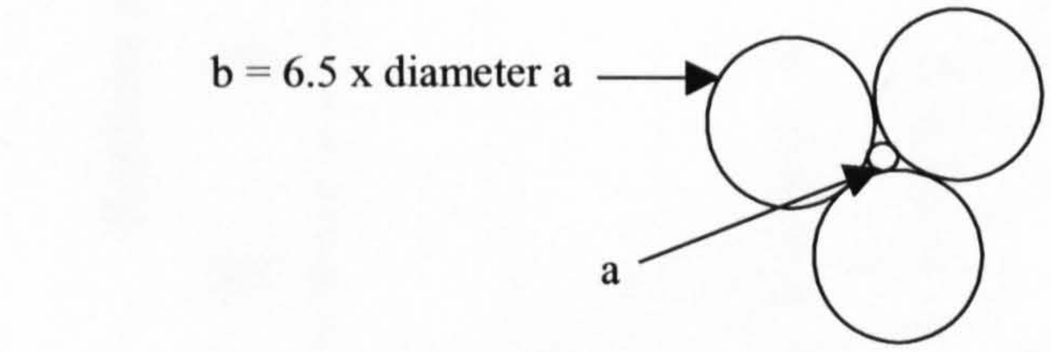

Figure 2.7 - Sizes of filter material (Cedegren, 1989)

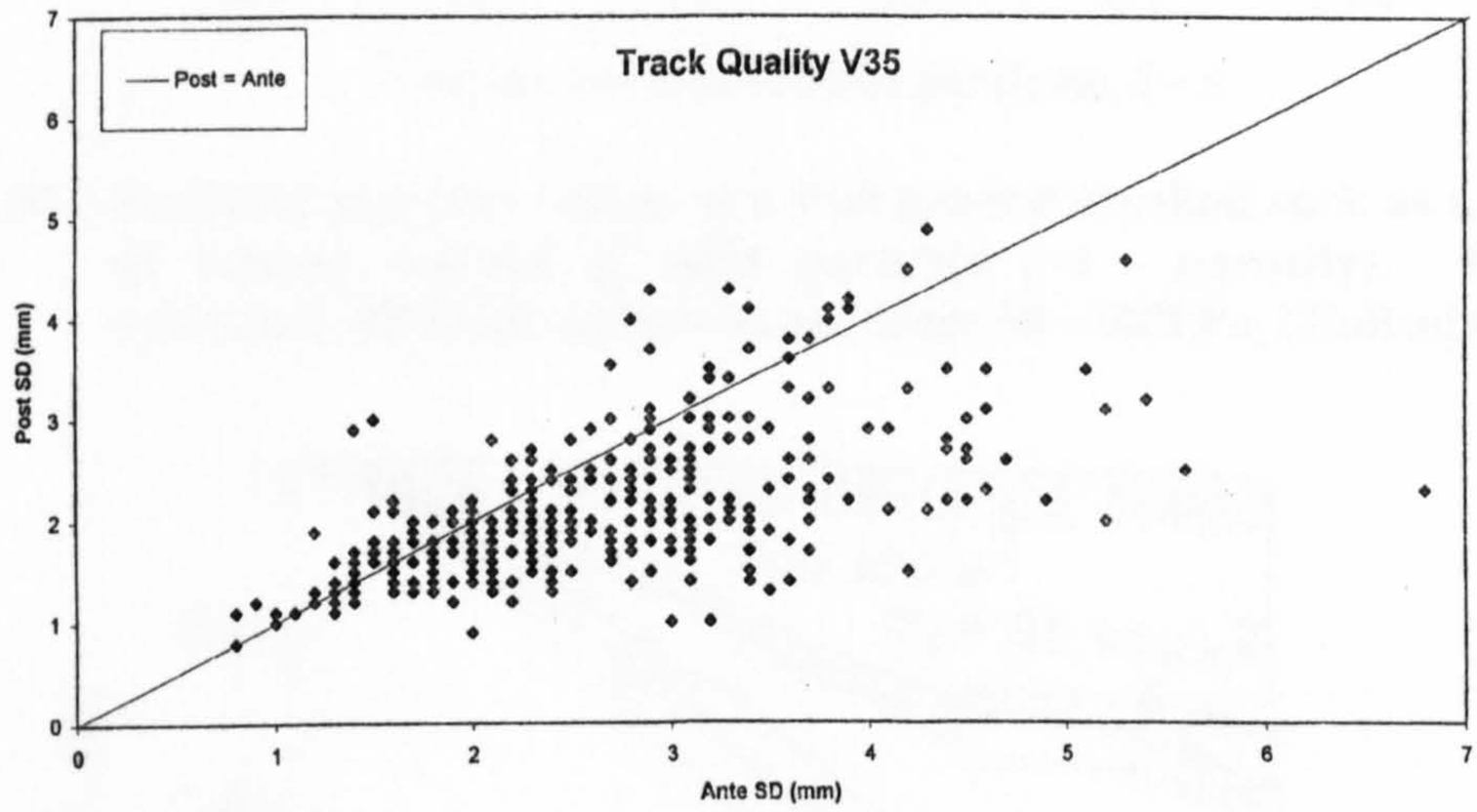

Figure 2.8 - Pre- and Post-maintenance track quality data (Baulk, 1999)

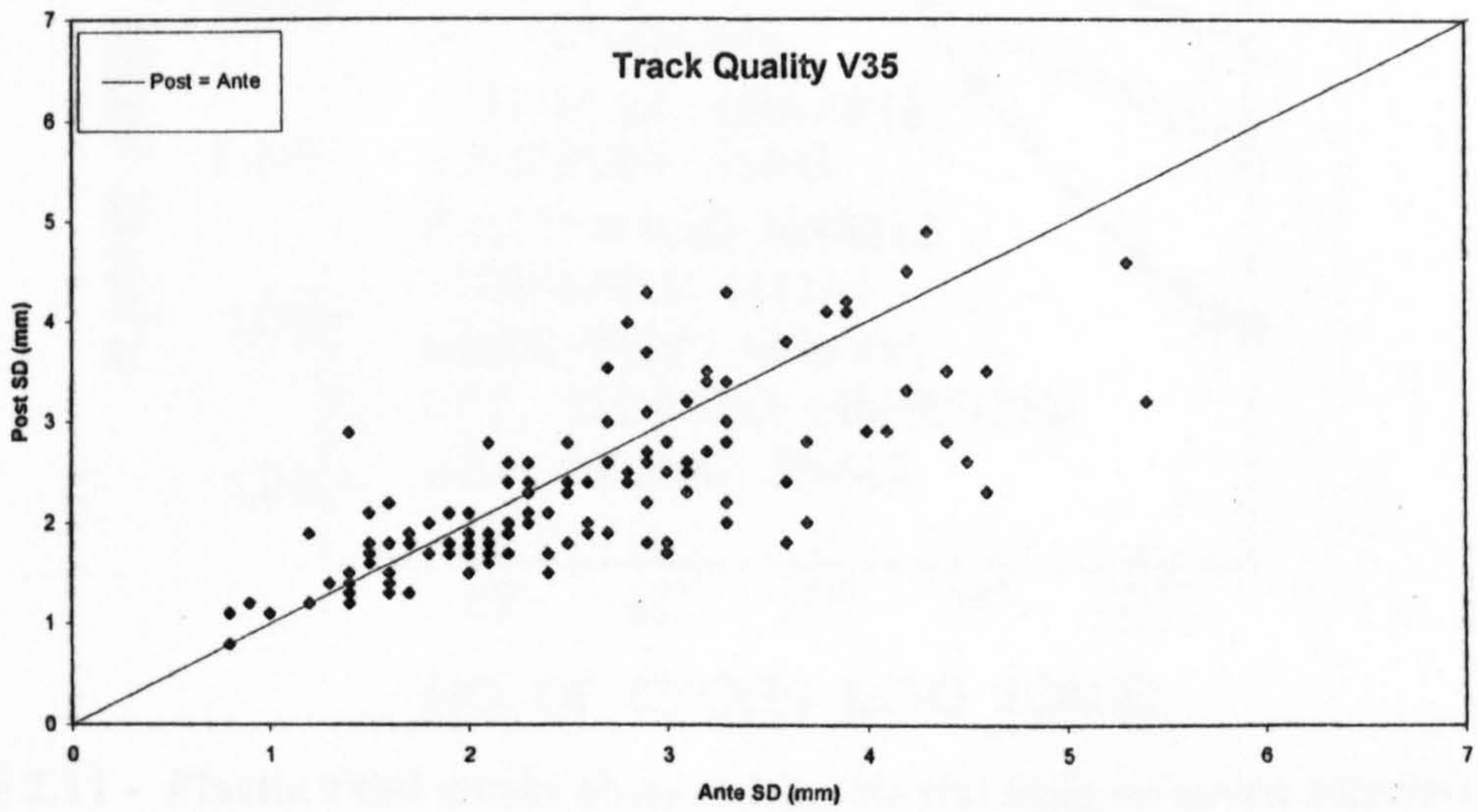

Figure 2.9 - Pre- and Post-maintenance track quality data - ramping in and out only (Baulk, 1999)

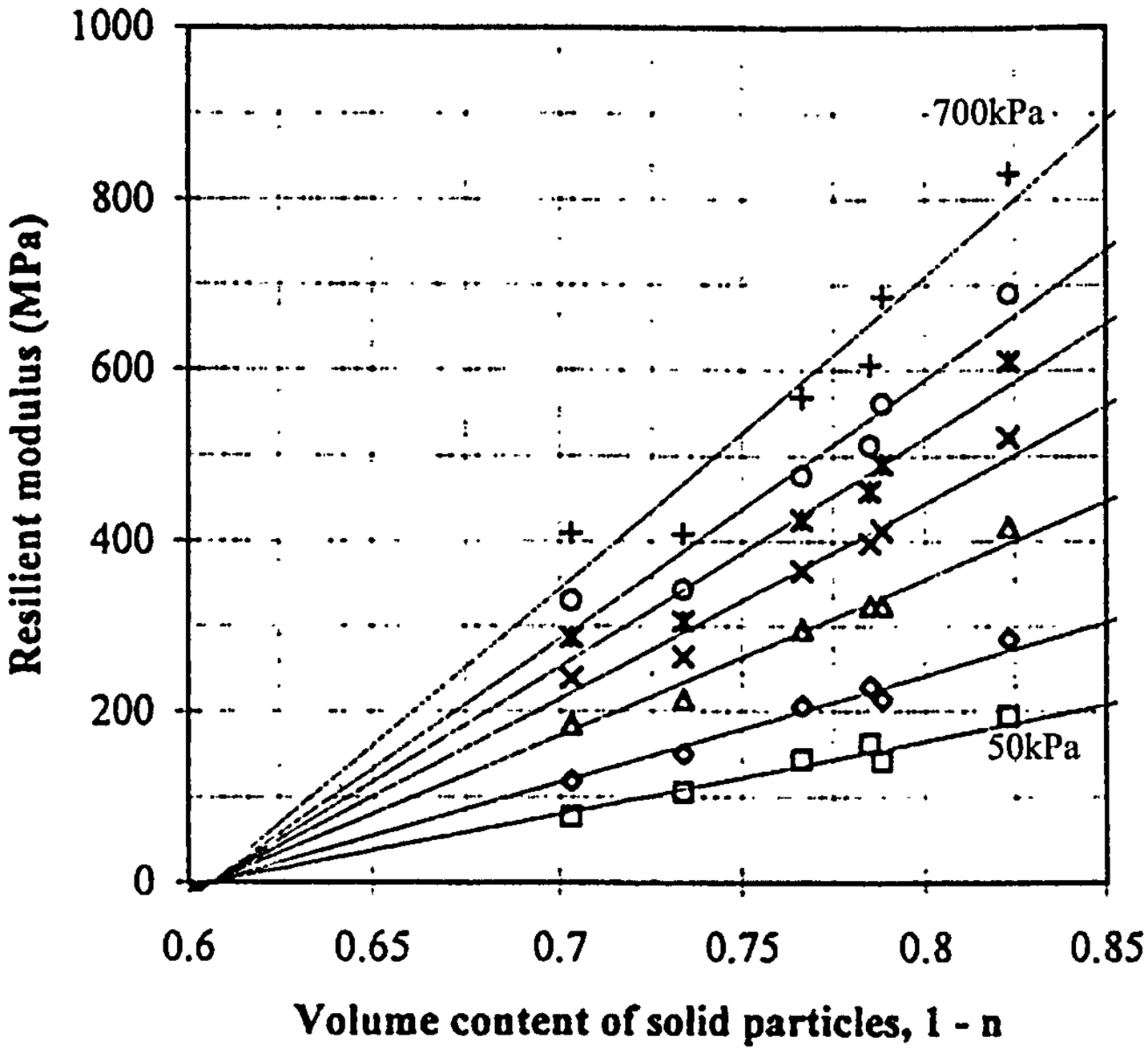

Figure 2.10 - Resilient modulus values of a well graded crushed rock as a function of volume content of solid particles (=1 - porosity). The lines represent different cell pressures from 50 –700kPa (Kolisoja, 1997)

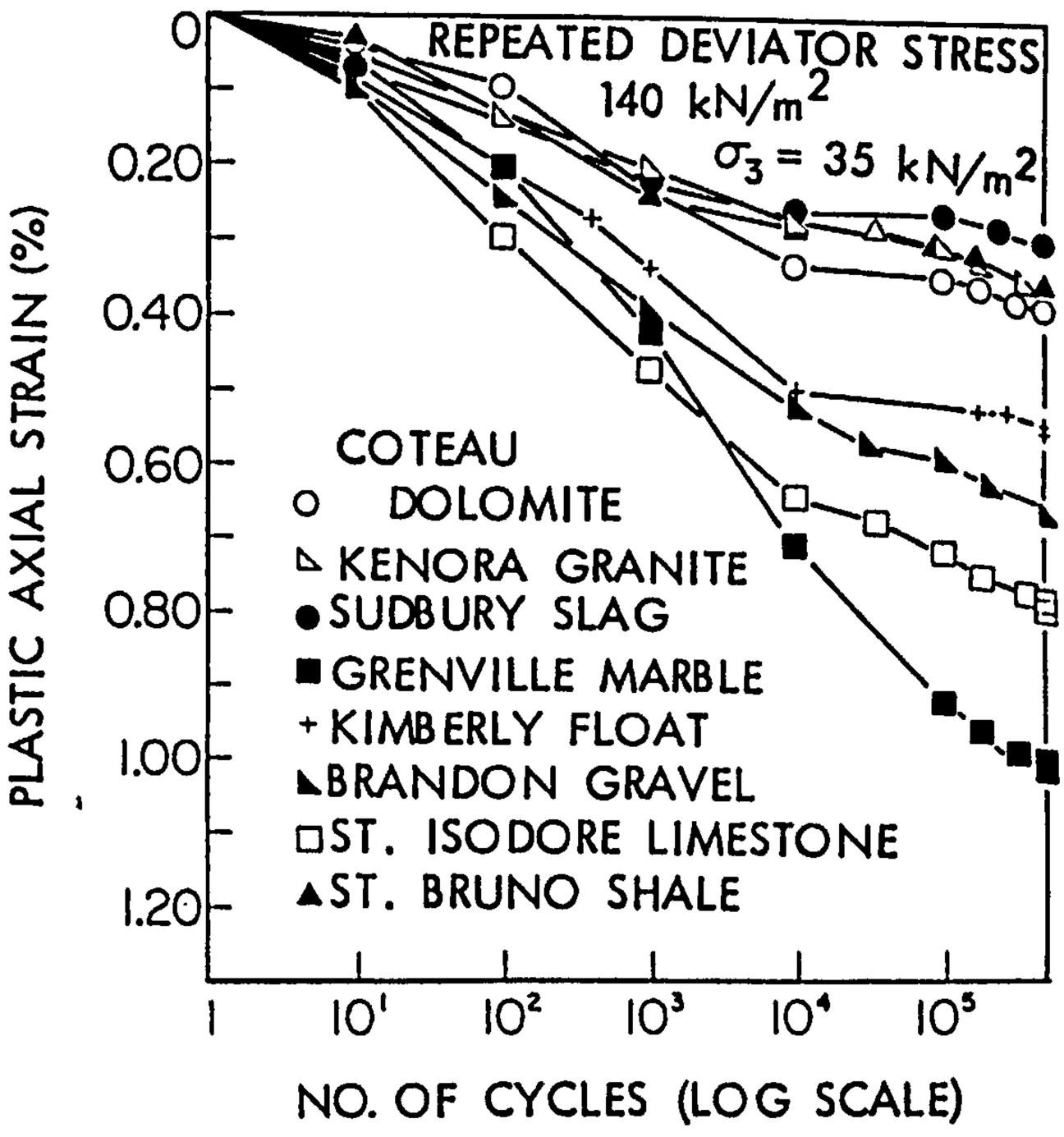

Figure 2.11 - Plastic axial strain observed in triaxial tests on seven selected ballasts (+control) (Raymond & Bathurst, 1994)

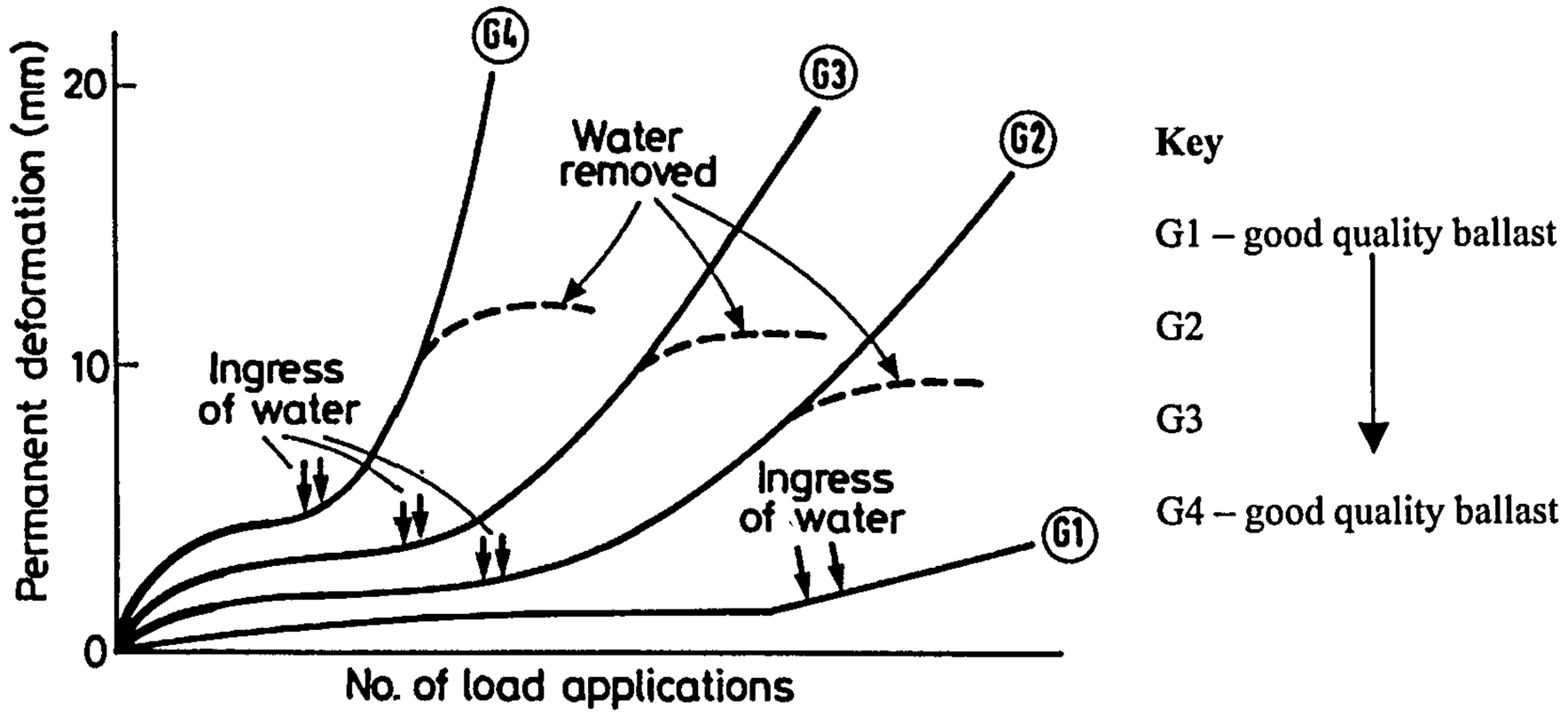

Figure 2.12 - Influence of water on permanent strain development in granular materials (Freeme and Servas, 1985)

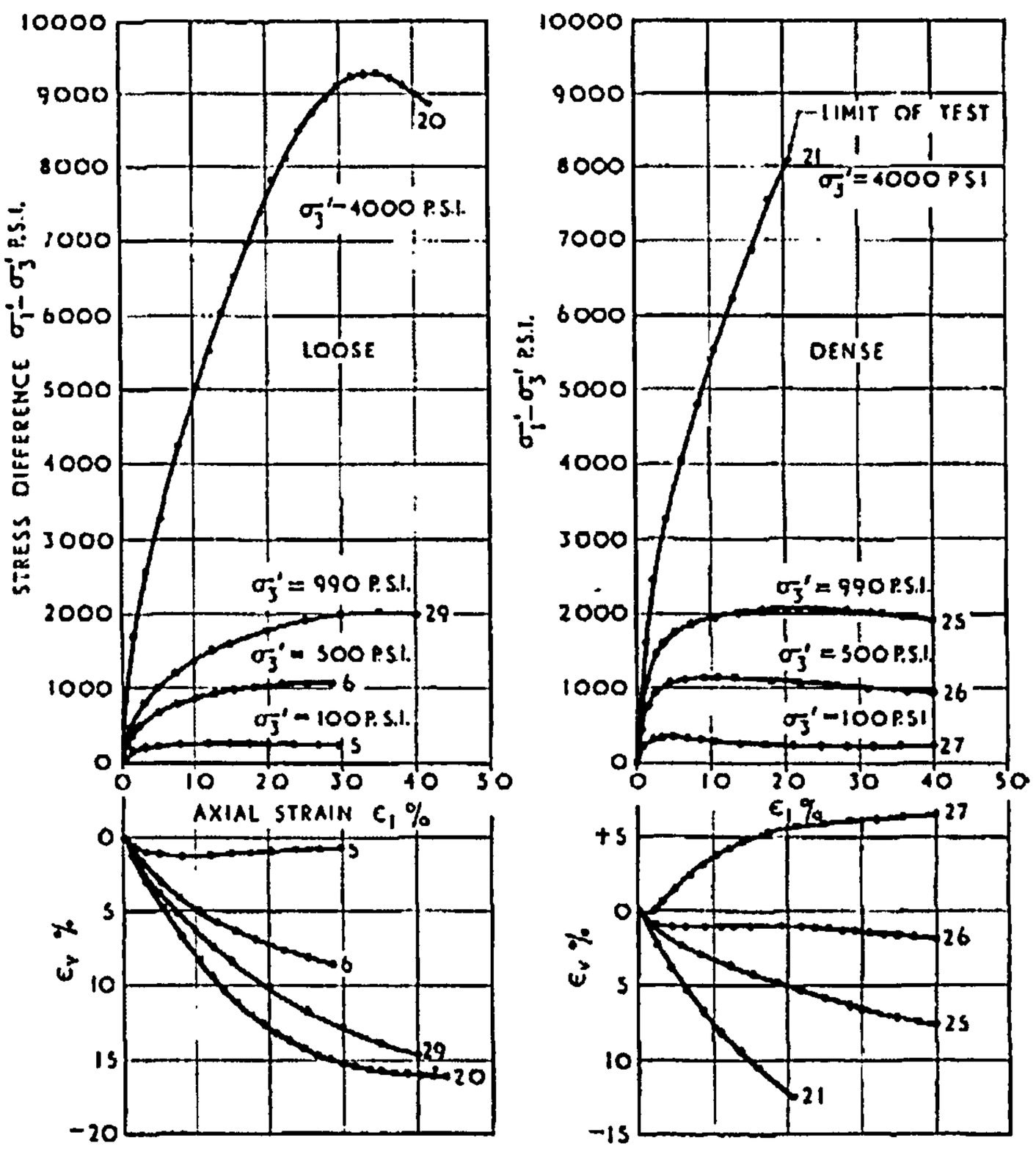

Figure 2.13 - Stress-strain plots for sand (Bishop, 1966)

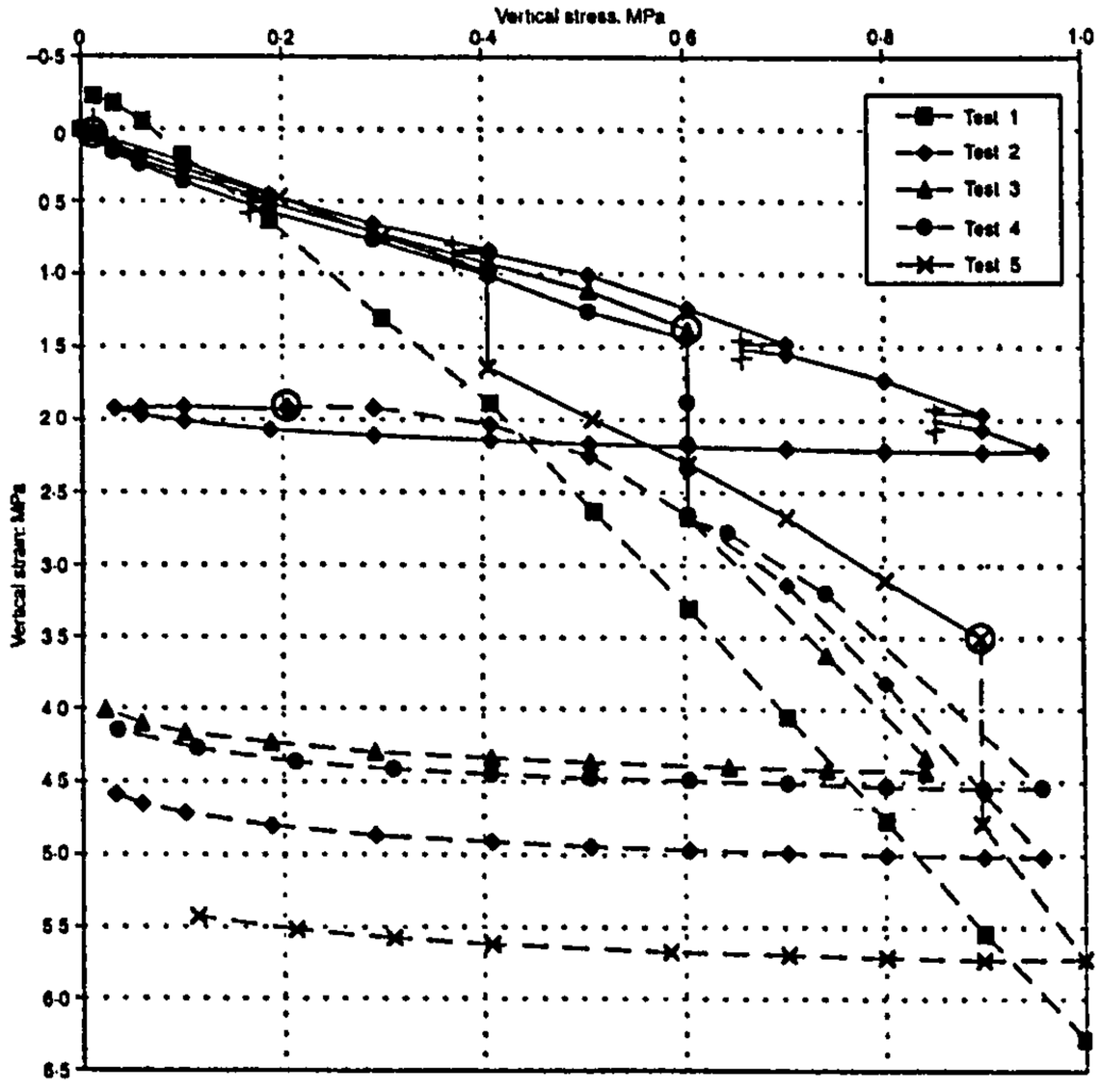

Figure 2.14 - Effect of moisture on axial displacement (Oldecop and Alonson, 2001)

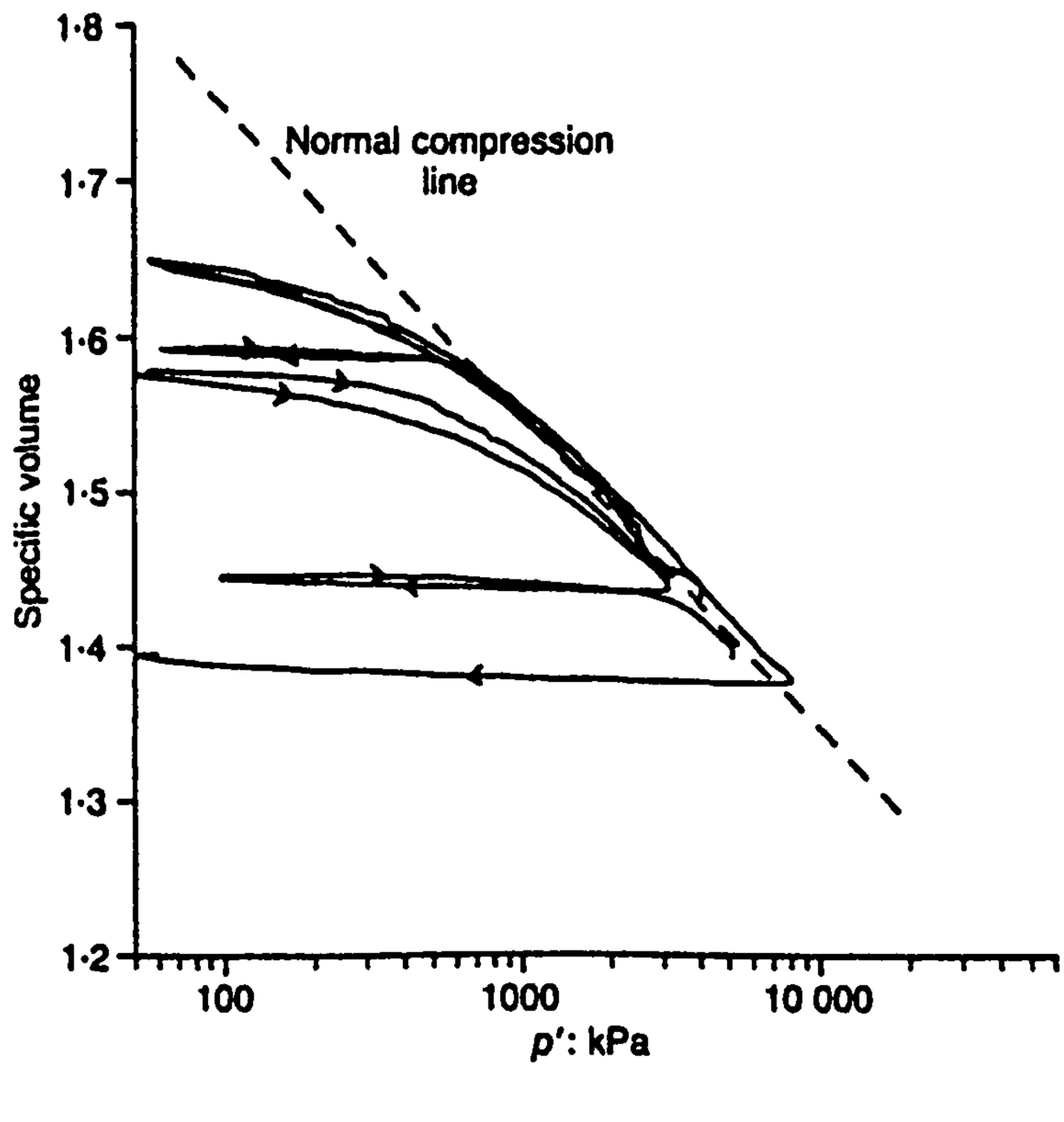

Figure 2.15 - Normal compression line (Coop and Lee 1993)

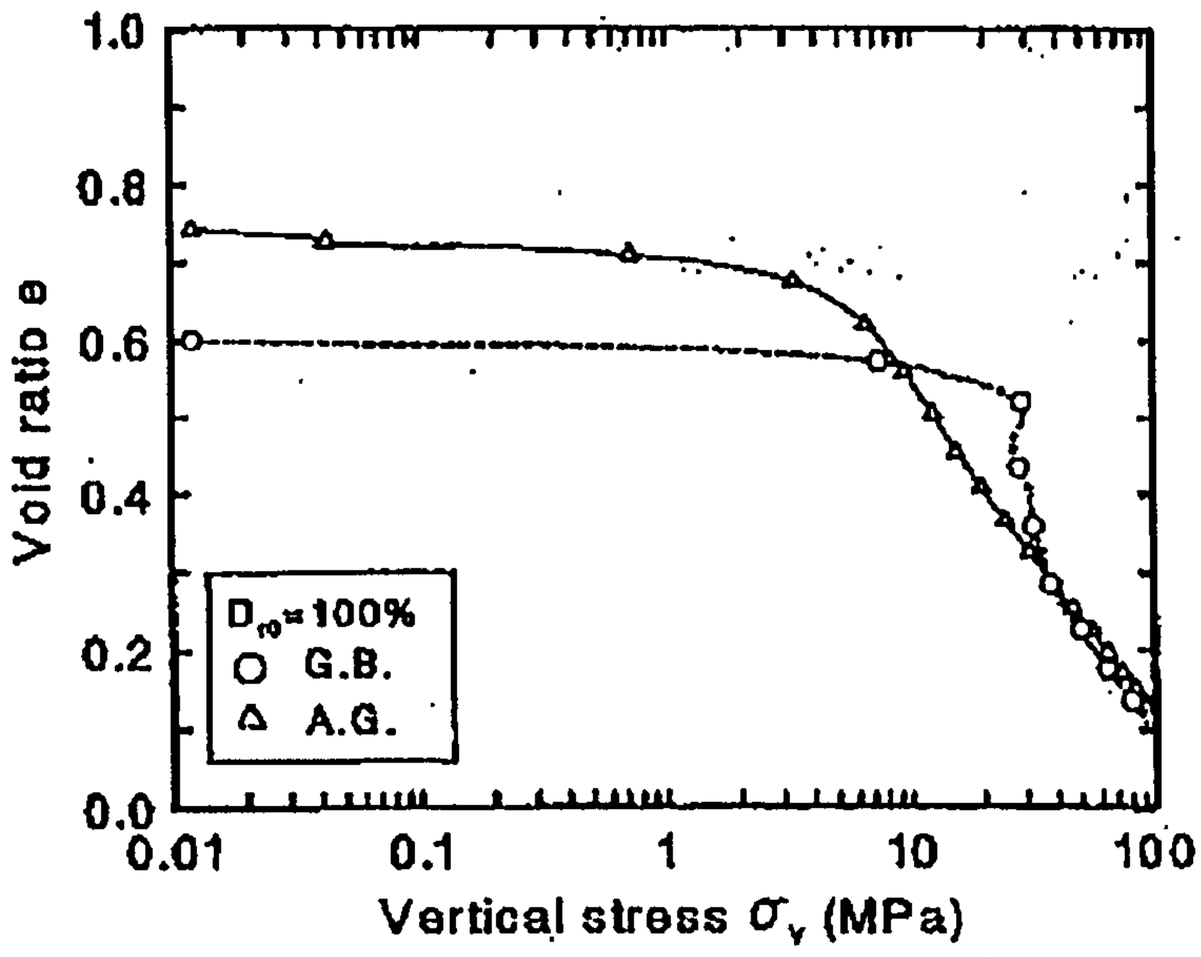

Figure 2.16 - Effect of particle angularity on the yielding point in e-logσv space (Nakata et al., 2001b)

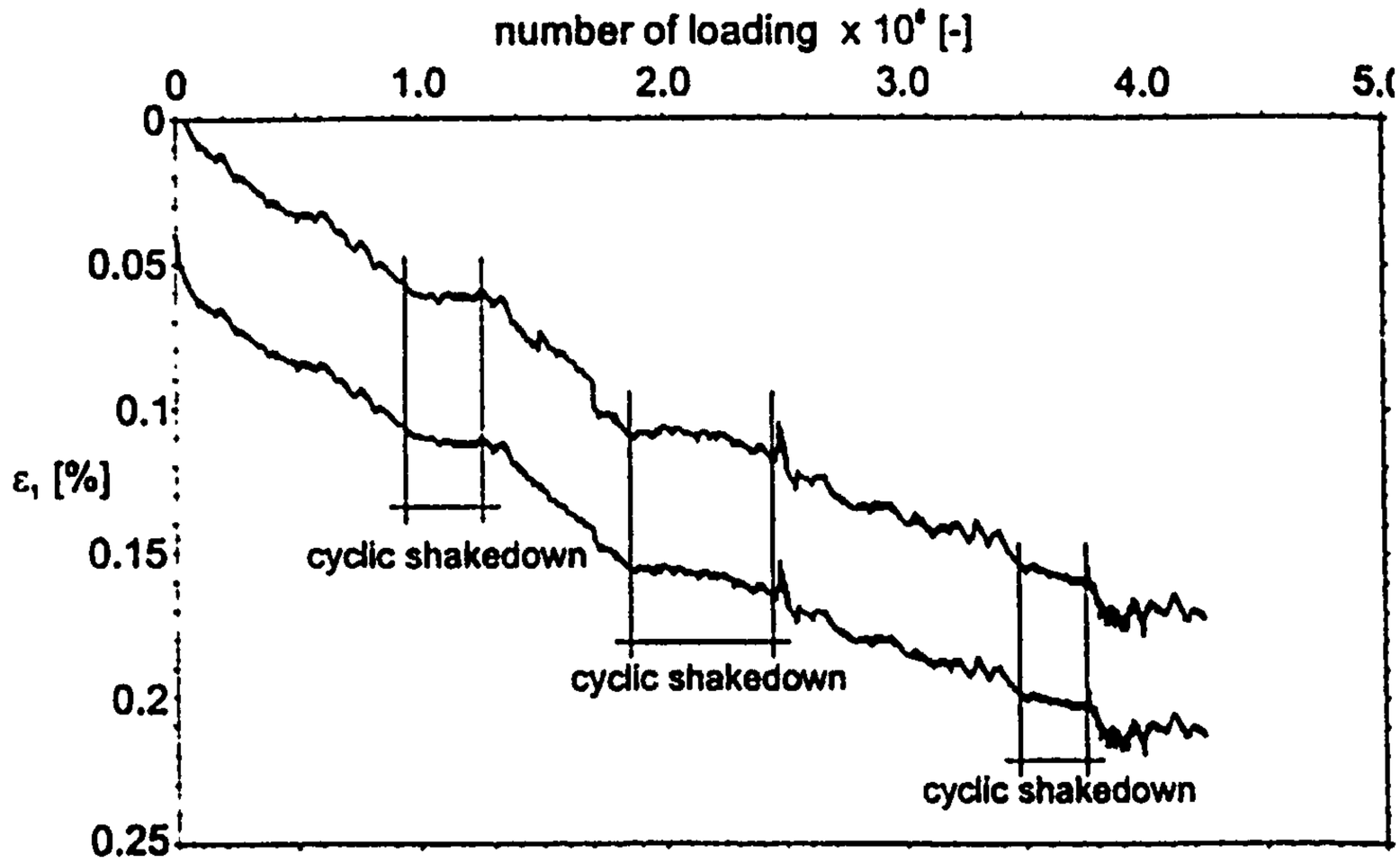

Figure 2.17 - Axial displacement of dense gabbro sand (Festag and Katzenbach, 2001)

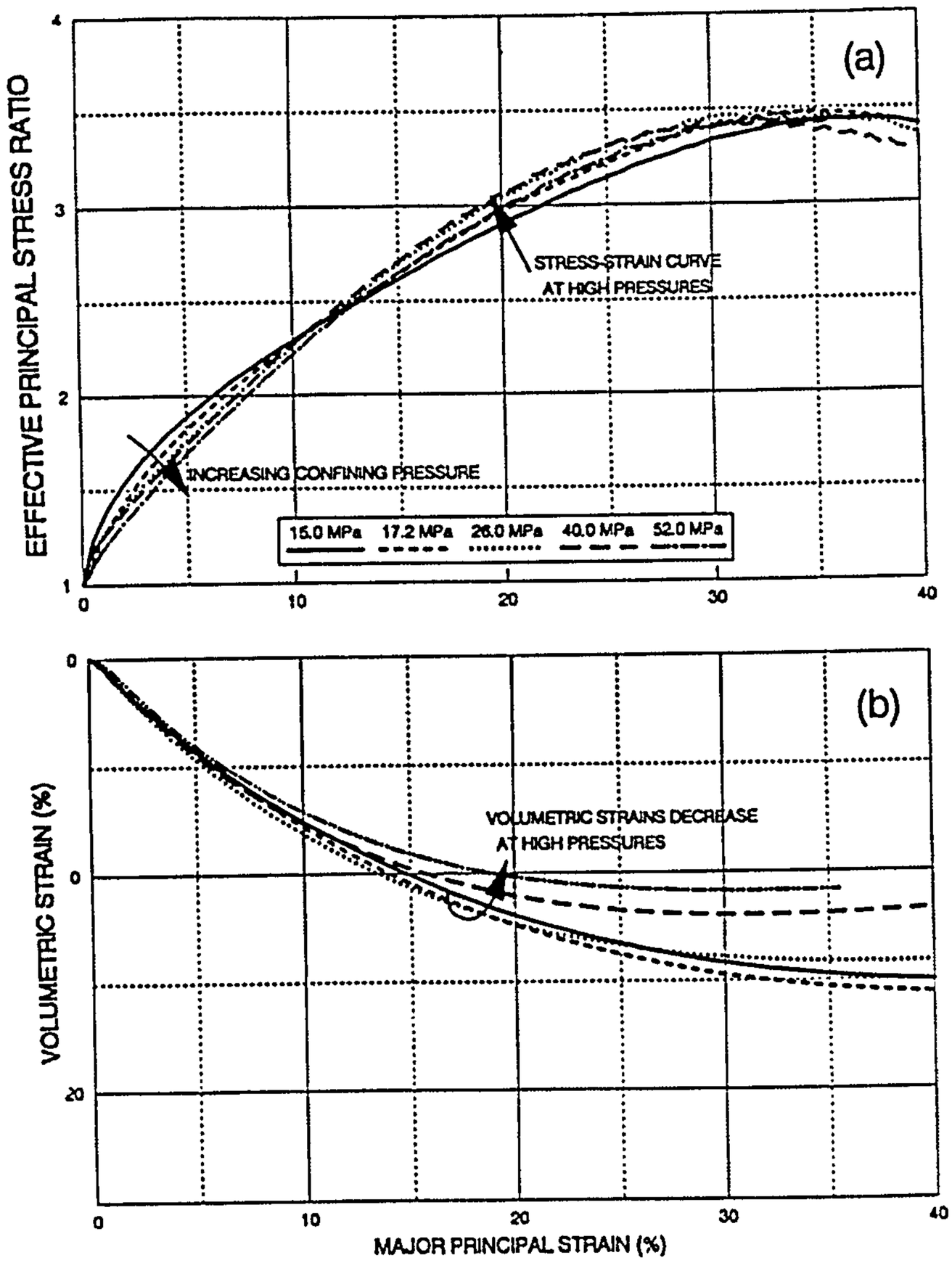

Figure 2.18 - Triaxial test results showing effect of breakage; a) stress strain, curves b) volumetric strain curves (Yamamoro and Lade, 1996)

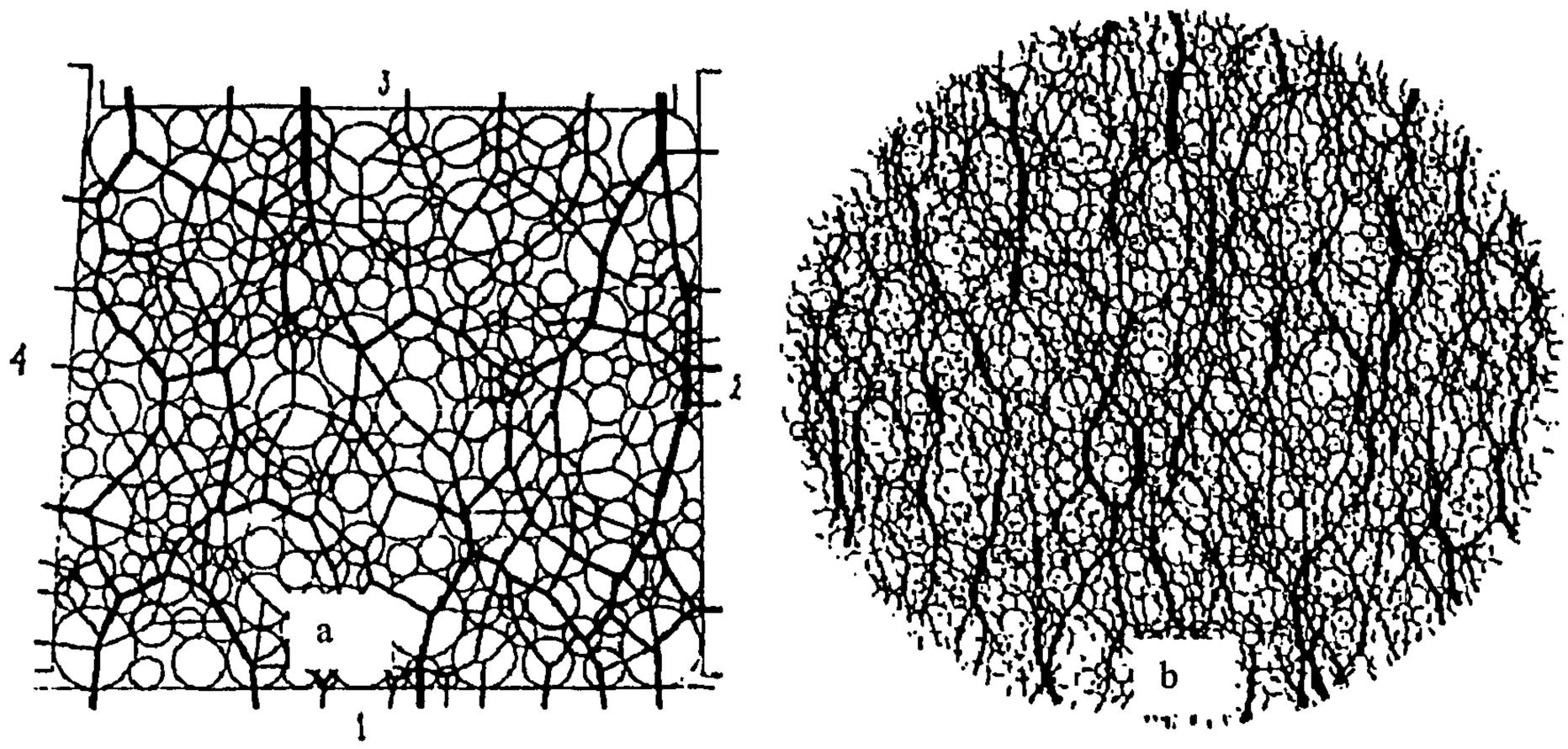

Figure 2.19 - Stress path through a matrix; a) Cundal and Strack (1979), b) Adams (1994)

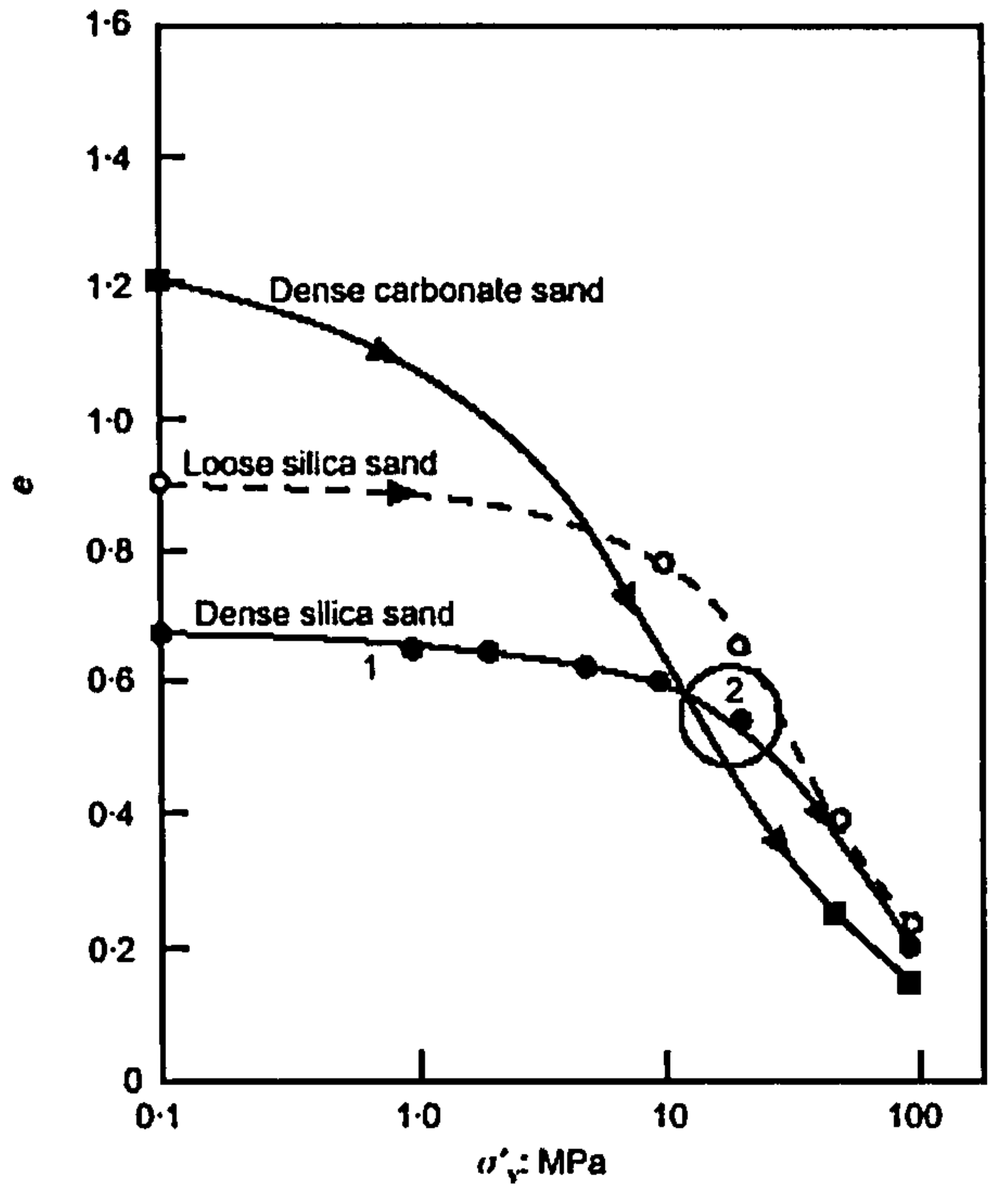

Figure 2.20 - One dimensional compression plots showing the yield points (Golightly, 1990)

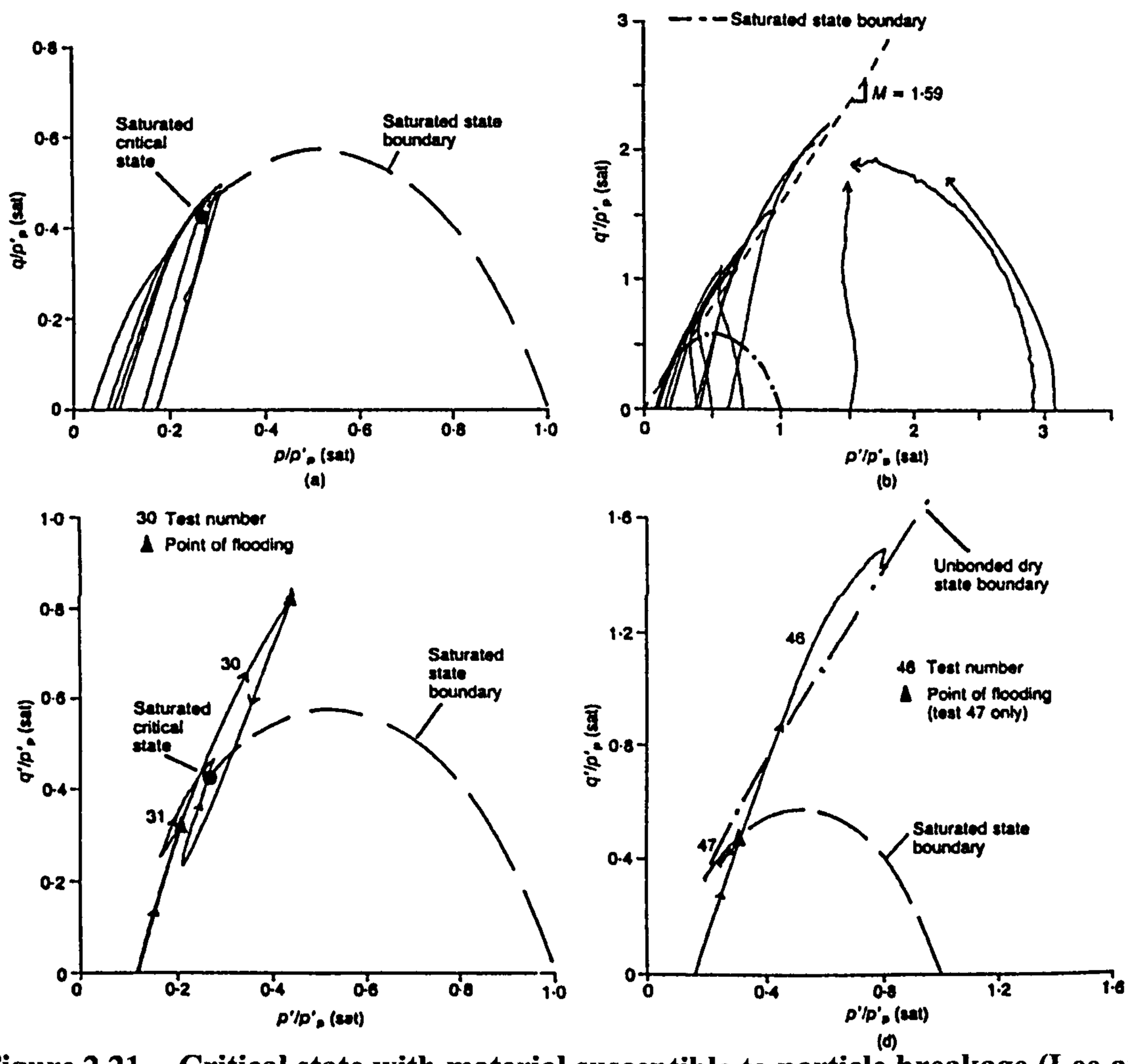

Figure 2.21 - Critical state with material susceptible to particle breakage (Lee and Coop, 1995)

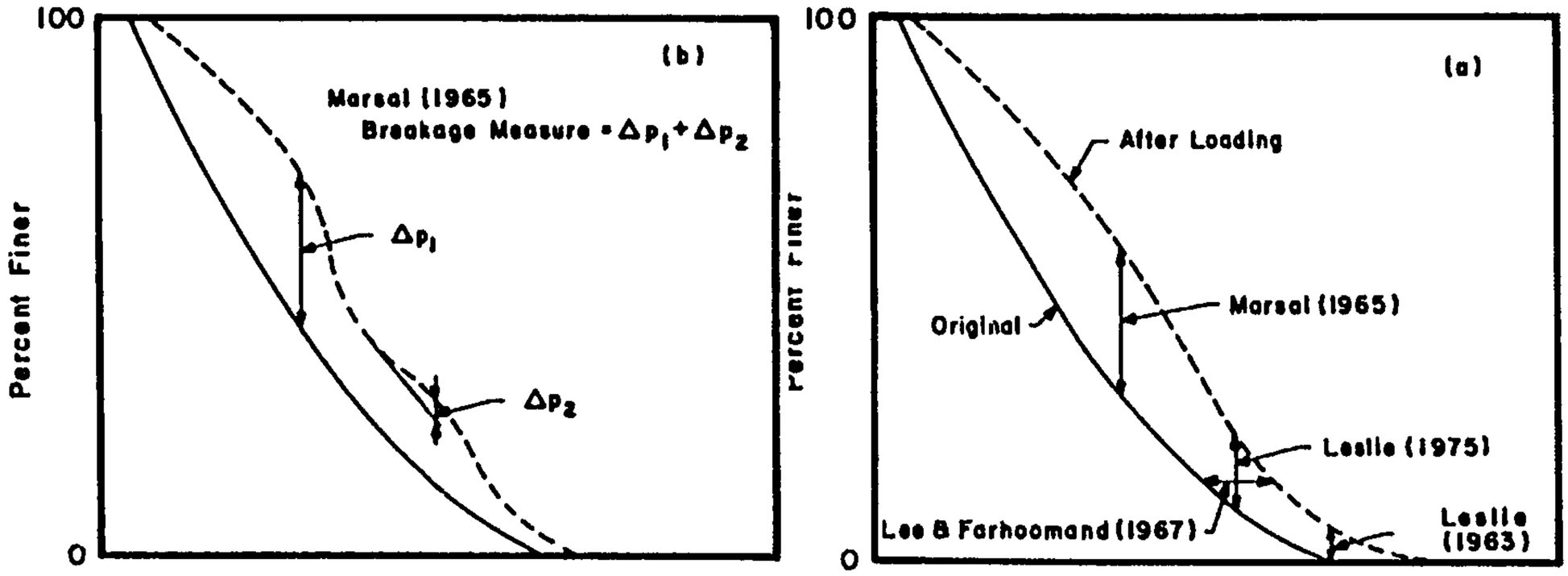

Figure 2.22 - Previous measures to determine the amount of breakage (Hardin, 1985)

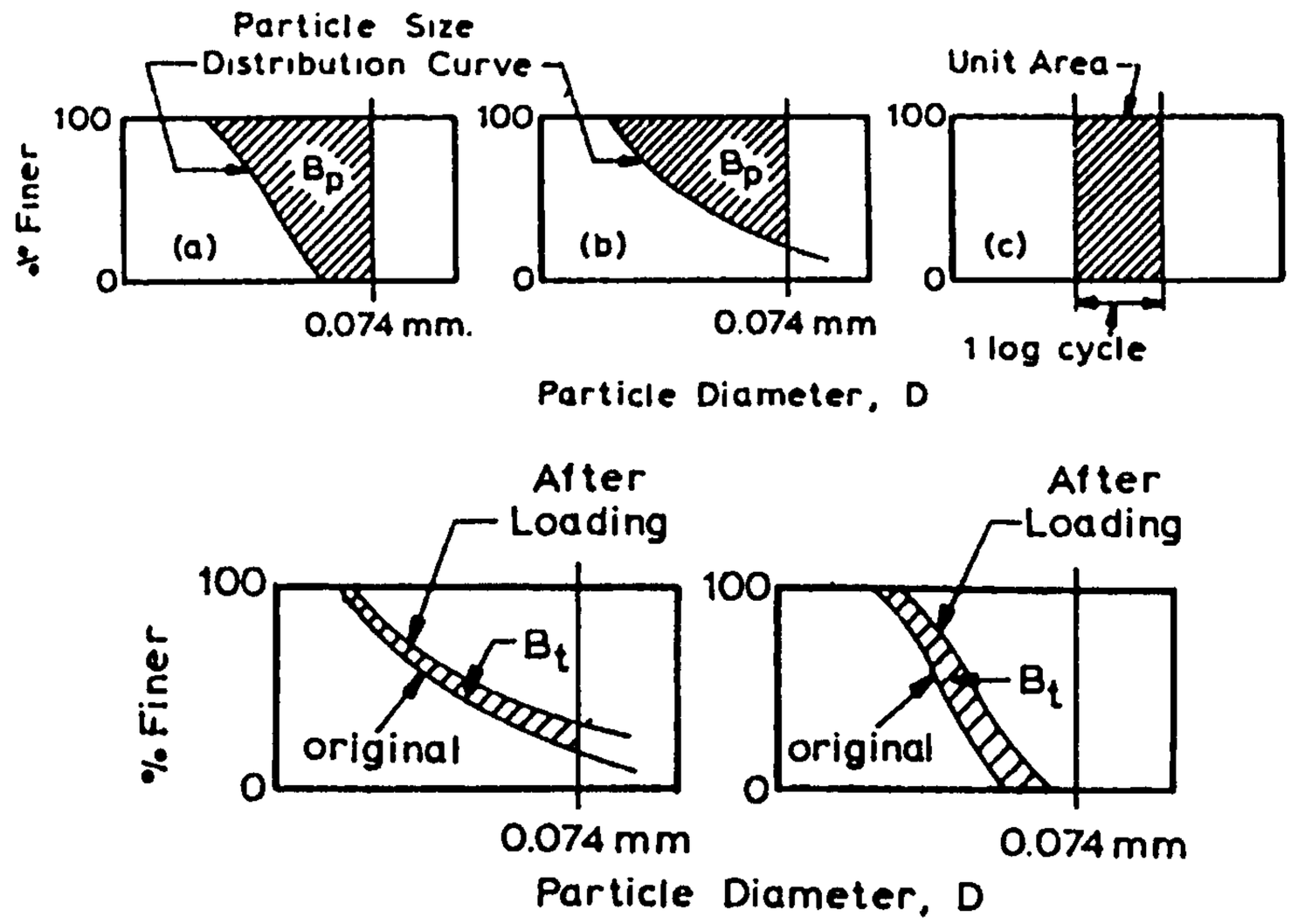

Figure 2.23 - Definition of breakage potential (Hardin, 1985)

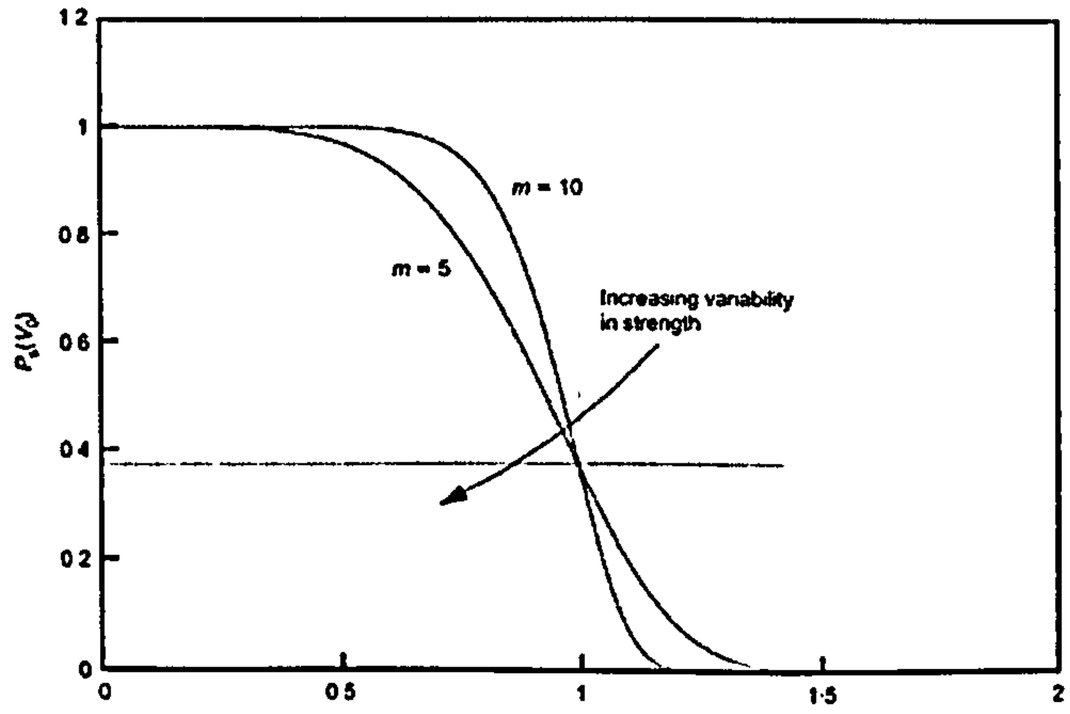

Figure 2.24 - Weibull distribution curves (Weibull, 1951)

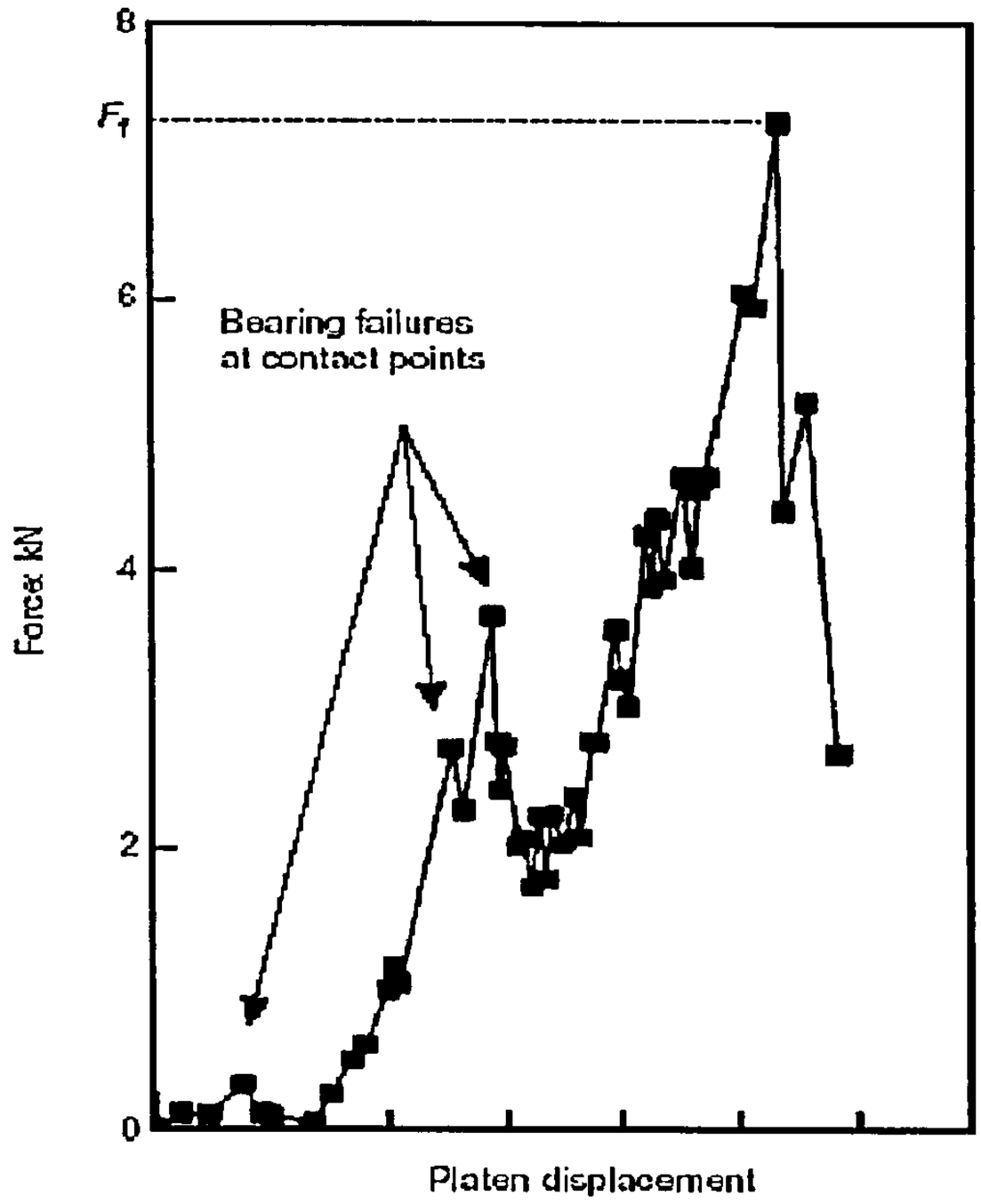

Figure 2.25 - Load displacement plots for a single particle crushing test (McDowell and Bolton, 1998)

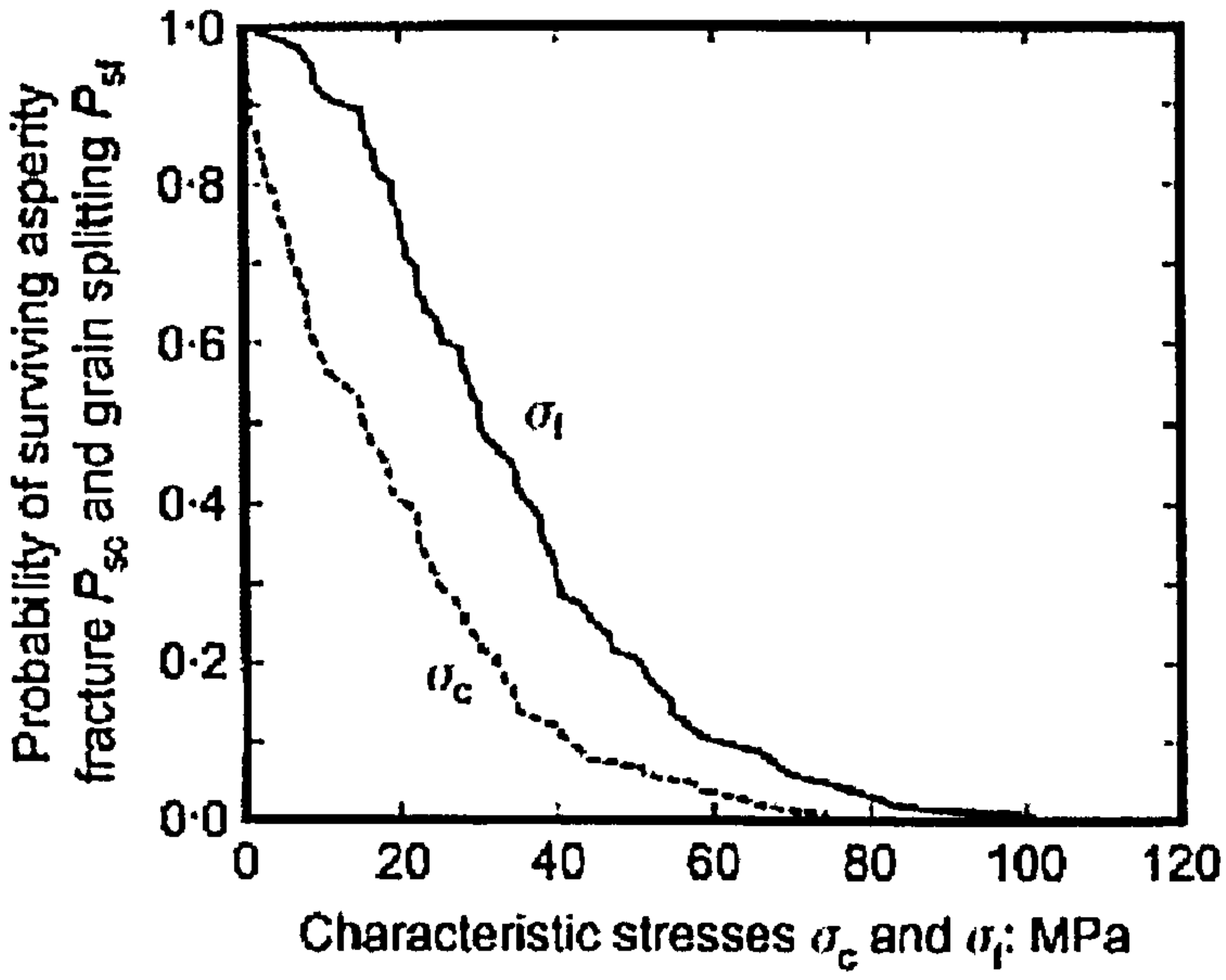

Figure 2.26 - Single particle survival curves for asperity failure and complete particle fracture (Nakata et al., 1999)

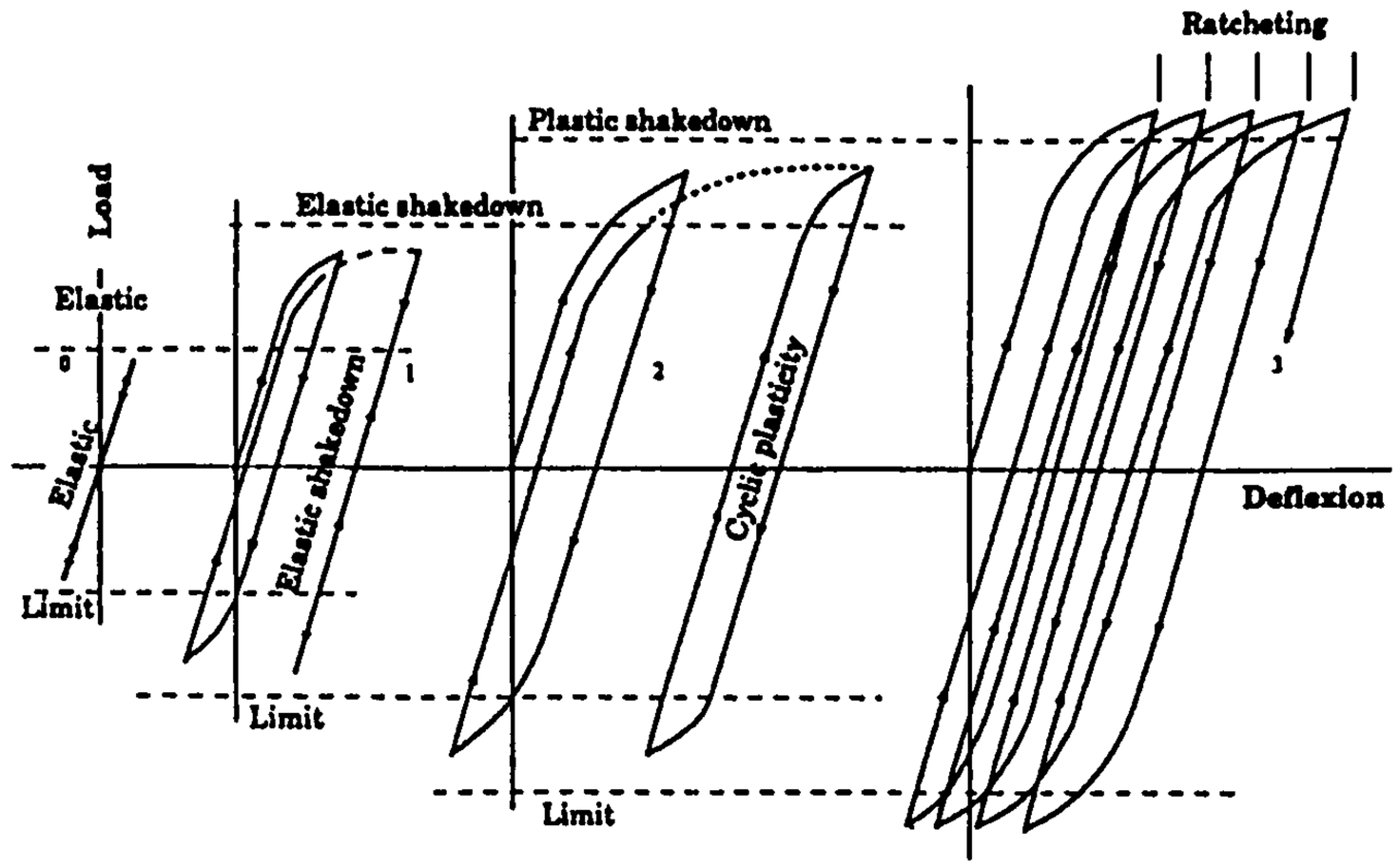

Figure 2.27 - Shakedown theory (Collins and Boulbibane, 2000)

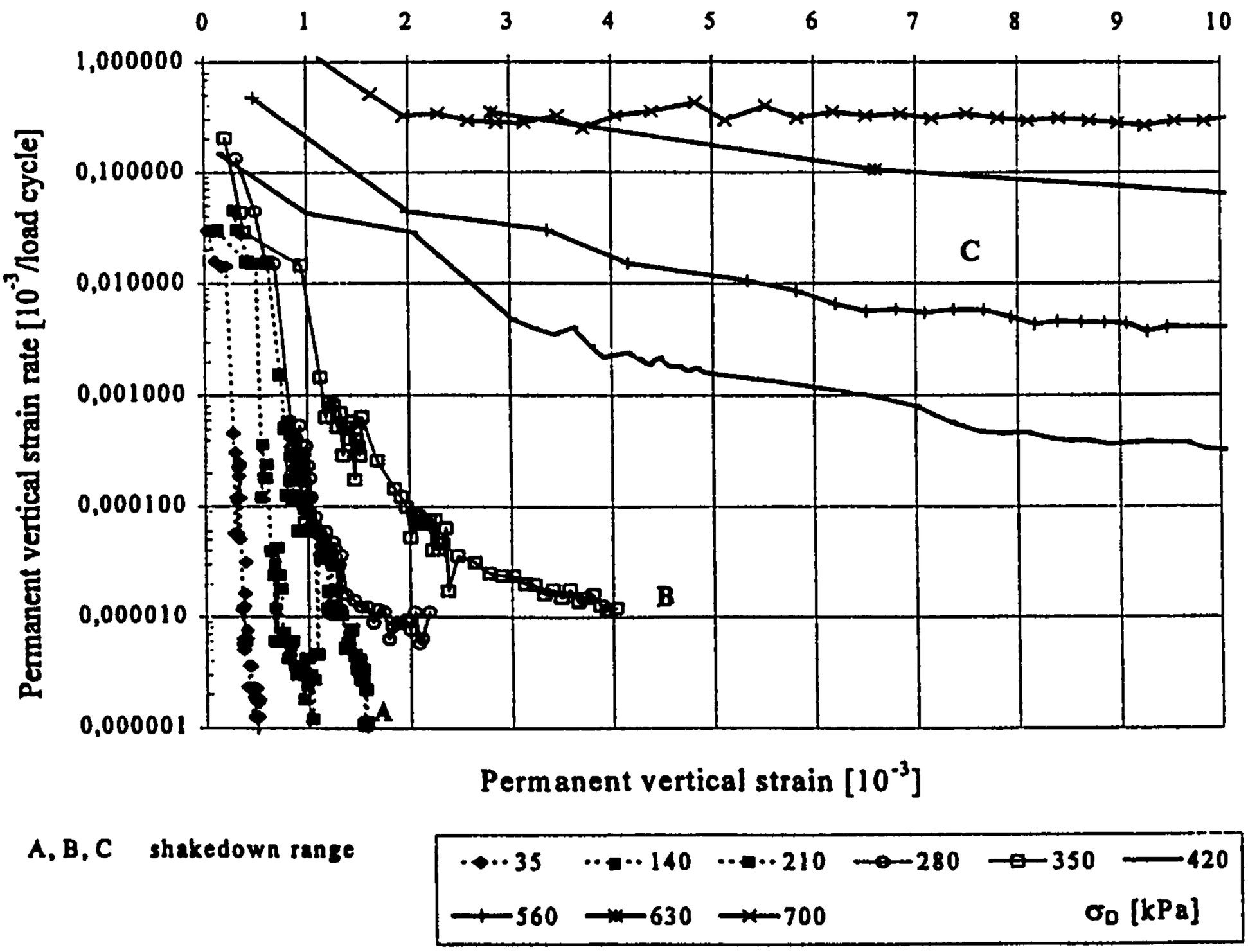

Figure 2.28 - Rate of strain accumulation (Werkmeister et al., 2001)

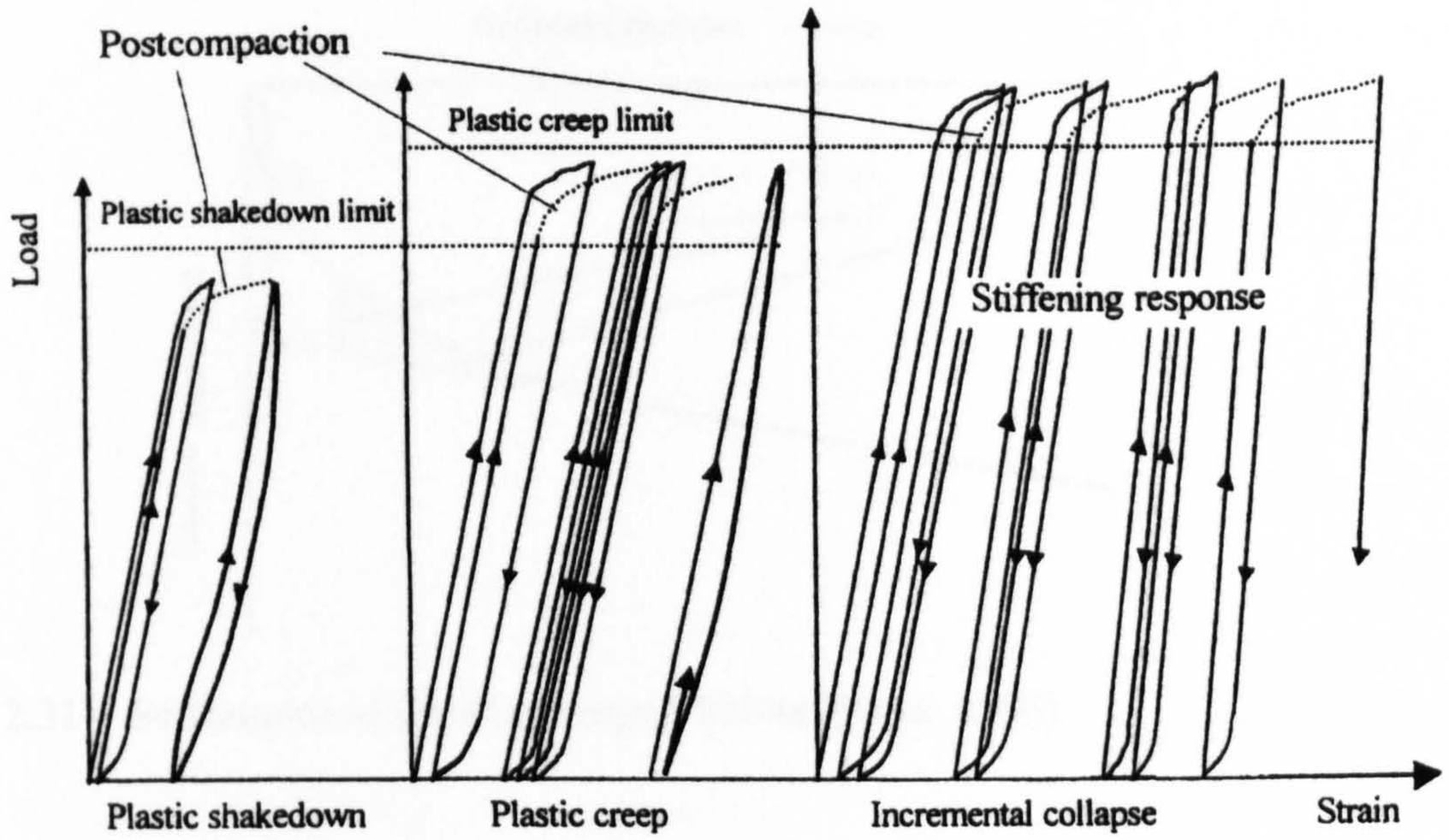

Figure 2.29 - Adapted Shakedown model (Werkmeister et al., 2001)

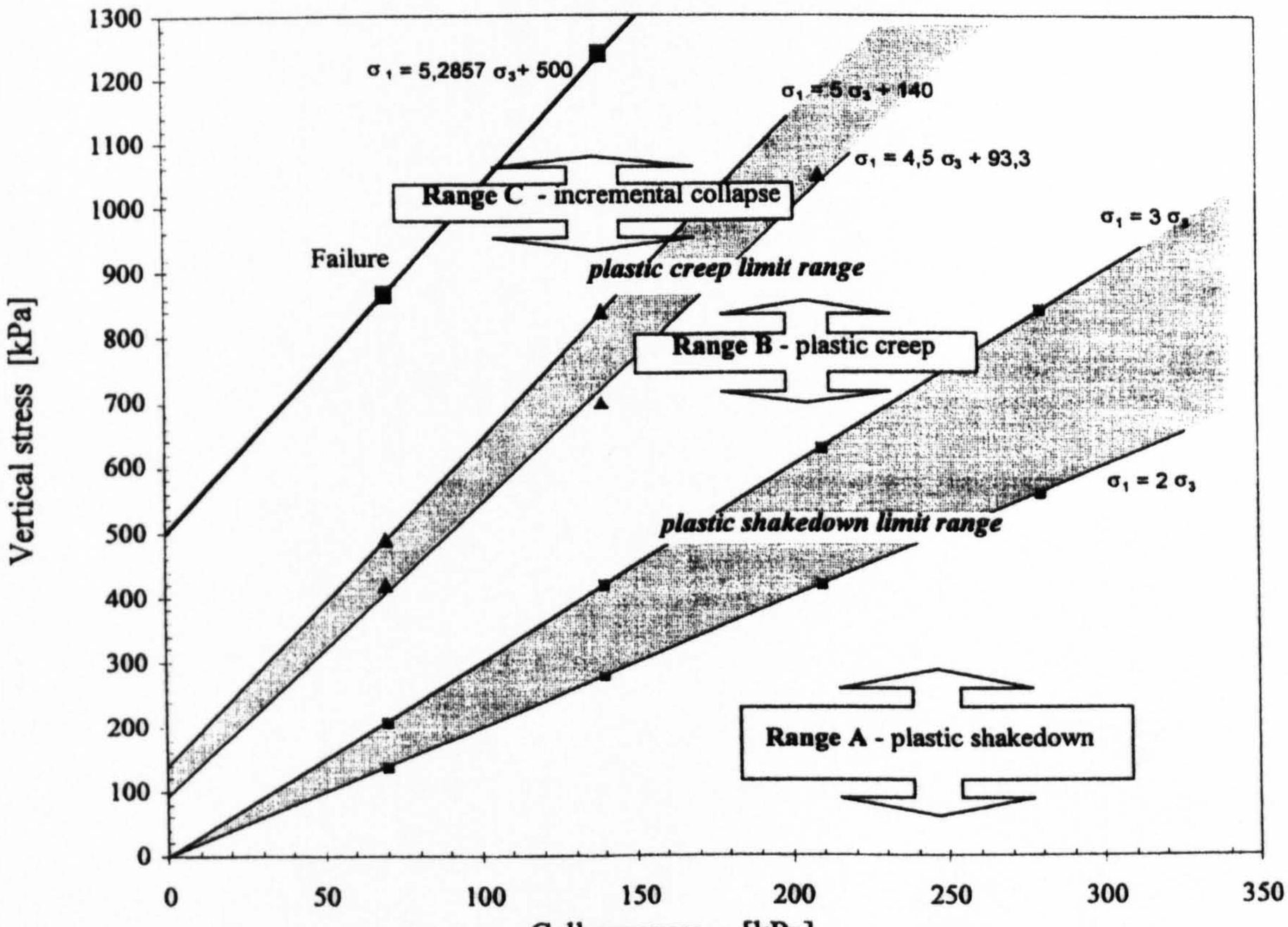

Figure 2.30 - Shakedown model space (Werkmeister et al., 2001)

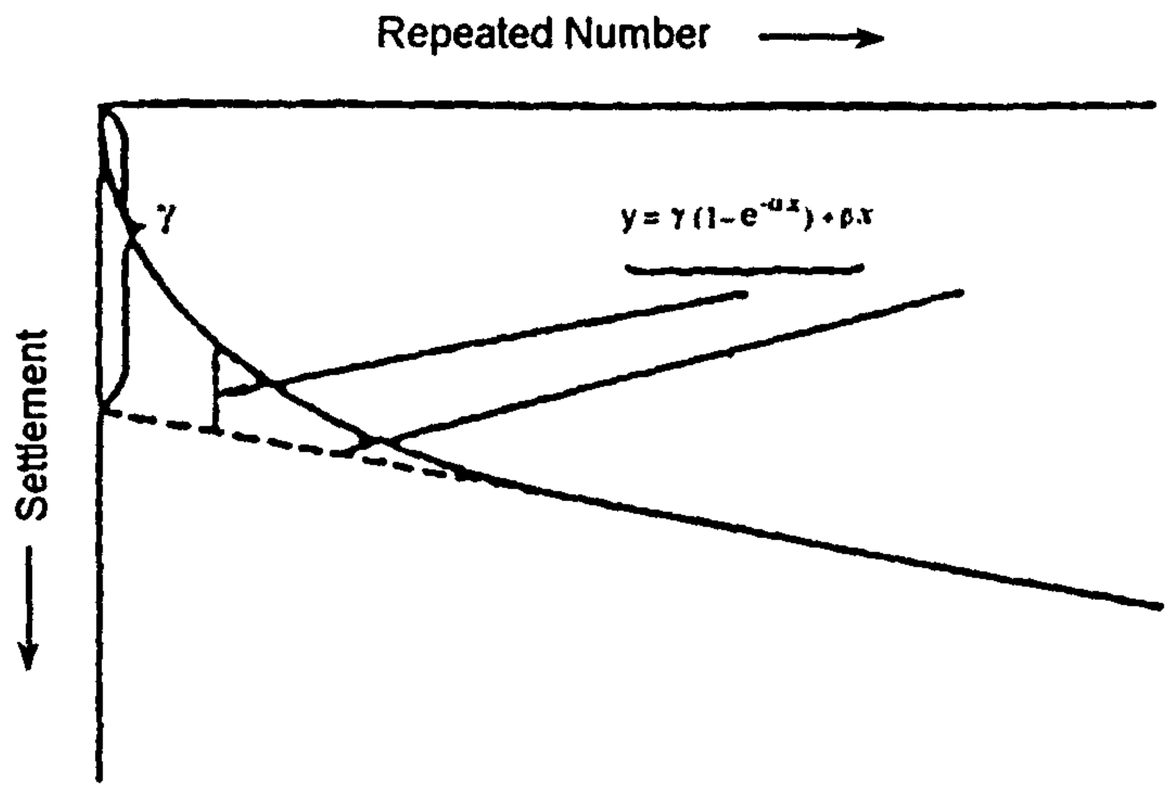

Figure 2.31 - Settlement of freshly tamped ballast (Sato, 1995)

CHAPTER 3

Materials, Apparatus and Test Procedures

3.1 Introduction

A programme of drained monotonic load triaxial tests and drained cyclic load triaxial tests has been carried out to investigate the deformation behaviour, volume change behaviour, resilient modulus, and breakage of coarse-grained granular materials specific to the railway track-bed environment. A series of single-particle crushing tests was also carried out to investigate the strength and breakage characteristics of individual particles. The understanding gained from this was then used in the interpretation of the particle breakage occurring during the triaxial tests.

In this chapter the materials, the development of the triaxial apparatus and the single-particle crushing test apparatus are reviewed. The testing procedure for the triaxial test and the single-particle crushing test are described and the programme for the test series is summarised including the materials, pressures and loadings used. Data acquisition and processing are discussed in Chapter 4 along with the calibrations and corrections applied.

3.2 Materials

The main materials used in this project were nominal sized 50mm ballast and 20mm stone, which were supplied from Railtrack stockpiles at Bardon quarry, Leicestershire (map reference, FK 445 128). Both materials were as supplied to railway infrastructure maintenance contractors using the stoneblower and should therefore have conformed to the Railtrack specifications. For consistency all the 50mm ballast was taken from one batch and all the 20mm stone was taken from another batch. After the material was delivered to the laboratory it was washed to remove dust and left to air dry.

Due to breakage of the material during testing, no material was reused and in the latter parts of the test programme the material was stored after each test should further testing be required. Standard analysis of each material gave the properties detailed below.

The 50mm ballast was passed through a 50mm sieve to remove any larger particles so as to increase the ratio of the specimen diameter to particle size. Approximately 50kg of material larger than 50mm was removed per tonne of material delivered to the

laboratory. It was believed that the relatively small number of large particles would have had little influence on the overall behaviour of the in-situ ballast, yet could have significantly affected the results of the triaxial tests. This was also discussed by Nobari and Duncan (1972) on work relevant to rockfill. The number of particles removed per test was approximately 6, which would equate to approximately 1.5kg and was therefore equal to 5% of the total specimen mass.

Sieve analysis was carried out according to BS 1377: Part 2:1990:9.3. Figure 3.1 shows the grading curve for the 50mm ballast together with the Railtrack specification for comparison. The specific gravity determined using the gas jar water displacement method according to BS 1377: Part 2:1990:8.2 gave an average specific gravity for the 50mm ballast of 2.67, the same as that determined by Key (1998).

In early tests two types of 20mm material were used. The first was that tested by Key (1998) and supplied by Bardon Quarry, Leicestershire. This Bardon stone is typically used in the stoneblower. However, some railway track maintenance contractors use Lanark Red Granite, supplied by Cloburn Quarry in Scotland. This stone is visually less dusty and apparently works better in the stoneblower causing less jams in the system (McMichael, 2001). Early in the test programme a decision was made to only use the Bardon stone. This decision will be discussed later in the triaxial test discussion chapter (Section 7.3.2)

The 20mm Bardon stone grading curve is also shown in Figure 3.1 together with the Railtrack specification for comparison. The specific gravity for the 20mm Bardon stone was 2.81, which was slightly less than 2.85 determined by Key (1998). For the Cloburn stone the specific gravity was 2.65, significantly less than the Bardon stone.

3.3 Triaxial apparatus

The triaxial apparatus used in this project was almost identical to that used by Key (1998). The main development was that of a new volume change unit described in Section 3.3.4.

Details of the triaxial cell are shown in Figure 3.2 and Plate 3.1. Only a brief overview of the apparatus is given below as full details of the apparatus development was given by Key (1998).

The cell had an internal diameter of 296mm and height of 605mm. A maximum specimen size of diameter 236mm and height 455mm was therefore chosen by Key to

allow for sufficient radial and vertical clearances during cell assembly and for instrumentation. The ratio of the specimen diameter to maximum particle size (D/d_{max}) was 4.7, for the 50mm ballast. It is generally recommended that D/d_{max} should be greater than 6, however Knutson and Thompson (1978) and Brown and O'Reilly (1991) have used ballast specimens of similar D/d_{max} ratios. This lower ratio meant that comparisons were valid with other research where there had been similar ratios used and within this project itself, although absolute values, in terms of the stress-strain characteristics of the specimens, needed to be treated with caution. The height to diameter ratio (H/D) was 2, which was equal to that recommended in the literature. The height to diameter ratio should be greater than or equal to 2 so that the friction between the specimen and the end platens, which encourages barrelling in the specimen, does not affect the overall specimen strength.

Most tests were conducted with both the top and bottom platens being of mild steel. However some tests had alternative platens to allow for effects such as wooden sleepers and soft subgrades to be investigated. In the current work this has been referred to as 'damping'.

3.3.1 Cell pressure and vacuum systems

During specimen set up a small vacuum was applied to the specimen to allow it to be self supporting during the assembly of the cell until a cell pressure could be applied. A diagram of the vacuum system has been combined with the cell pressure system in Figure 3.3.

Key (1998) used a single 700kPa rated air pressure regulator to regulate the air pressure and hence the cell fluid pressure. Incorporating a 240kPa regulator in series with the 700kPa regulator reduced the effects of fluctuating cell pressure conditions caused by the cyclic loading of the specimen. The second (lower rated) regulator was more sensitive to the fluctuations as the pressure difference across it was less.

There was no pore/back pressure system used in the tests as the material was tested dry.

3.3.2 Loading

The triaxial cell was mounted on a 100kN loading frame, on which two types of triaxial tests were carried out. A bottom up drive unit was used for monotonic load triaxial tests and a top down hydraulic ram was used for the cyclic load triaxial tests. The load was transmitted via the reaction frame through the loading piston, on which an internal load

cell was mounted, and then onto the top cap of the specimen via a ball and seat connection.

For drained monotonic load triaxial tests with dry granular materials the rate of loading was considered not to be critical as there would be no build up of pore pressures. Therefore a rate of loading of 0.22% strain/min was chosen as the highest compression rate available.

The drained cyclic load triaxial tests were designed to simulate the loading on an element of ballast beneath a railway sleeper. The cyclic load apparatus was set up as designed by Key (1998) and briefly described below.

A single chip 'Stamp' computer from Parallax Corporation controlled a solenoid valve within the hydraulic system. It was programmed to allow the test to run in two stages. The first stage cycled at a slow speed (0.16Hz) to allow for the larger deformations at the start of the test. The second stage cycled at a faster rate (0.5Hz) when the amount of deformation per cycle had reduced. The point at which the speed was changed was defined by the user and during this test programme was set at 50 cycles. After a preset number of cycles the control unit finished the test leaving a minimum load on the specimen. For the majority of tests this was after 100,000 cycles.

The hydraulic loading system used in the cyclic load tests is shown in Figure 3.4. The solenoid valve regulated the axial load applied and the system was allowed to cycle between preset maximum and minimum loads. The maximum load applied to the top platen was set at 11kN, which gives a stress of approximately 250kPa for a specimen of 236mm diameter. This is similar to the loads imposed on the railway track bed as detailed in Section 2.3.1.3. The minimum load was set at an arbitrary value of 0.6kN (15kPa) to represent the 'at rest' load of the superstructure (rails, sleepers and fastening systems). Furthermore, by setting a minimum load, the hydraulic ram did not lose contact with the loading piston and hence the occurrence of impact loading was prevented.

Using a solenoid valve, an approximate square loading wave was applied to the specimen (Figure 3.5). This did not simulate exactly the loading applied to the ballast under a sleeper and may cause greater ballast settlement than a sinusoidal wave as discussed in Section 2.4.2.5.

3.3.3 Instrumentation

Five variables were measured throughout each test. These were the axial displacement, the axial load, the radial displacement, the cell fluid volume change and the cell fluid pressure. Three radial transducers were used to measure the radial displacement; hence seven instruments were used in all.

The axial displacement was measured using a 50mm Linear Variable Displacement Transducer (LVDT). An external form of measurement was chosen over the preferred internal measuring devices due to the limited size of the triaxial cell and as large strains were involved, on specimen measurement was not so critical (Section 2.3.1.4.1).

A fatigue rated water resistant load cell with a normal working load range of 22.5kN and a maximum range of 50kN was used to measure the axial load.

The cell pressure was measured by a 100kPa pressure transducer mounted on a T-block at the inlet tap at the base of the triaxial cell (Figure 3.3). A 700kPa pressure transducer was also available for tests where the cell pressure exceeded 100kPa.

To measure the radial displacement, three $^{+}$/-12.5mm LVDT's (total range of 25mm) were mounted perpendicular to the specimen and at 120° around the specimen. The height of the LVDT's was fixed at the mid height of a specimen with 10% axial strain (Figure 3.2). The LVDT's reacted against targets that were fixed onto the specimen during the specimen preparation. The targets, 80mm by 80mm square, were made from 2mm aluminium sheeting and were curved to fit the specimen as can be seen in Plate 3.2.

By assuming the specimen remained a right-angled cylinder, Key (1998) calculated the volume change using the radial and axial measurements. However there were severe limitations with this method especially at larger strains (>0.3%) as the specimen bulged. Plate 3.2 shows a typical 20mm specimen with the white lines drawn on to highlight the bulging. These limitations could be one of the reasons behind Key's work not conforming to theoretical behaviour or to previous research, as his calculated volume changes were significantly greater than those observed by others (Alva Hurtado and Selig, 1981 and Indraratna et al, 1998).

Therefore a new volume change unit was designed that allowed both a large volume change (<2000ml) to be measured over the duration of the test and was still able to accurately measure the volume changes over individual cycles. The volume change unit was included in the apparatus from Series 2 (test T19) in the test programme.

3.3.4 Development of the new volume change unit

As the materials in the specimens were tested dry, the usual way of measuring the volume change by connecting the volume change unit to the pore fluid drainage valve could not be used. Based on the assumption that the change in the cell fluid volume was equal to the change in the specimen volume, a volume change unit was fitted on the cell fluid pressure line, as seen in the cell pressure system (Figure 3.3).

Initially a 1litre Imperial College type rolling diaphragm volume change unit was used; however, especially with cyclic loading, this unit suffered several difficulties including hysteresis and diaphragm jamming. Therefore a new type of unit was needed to allow direct volume change measurement.

Lade (1988) listed many desirable features of an automatic volume change unit including minimum hysteresis, ease of setting up / taking down, simplicity and low cost, conformation of electronic reading by a visual means, a linear relationship between the volume change and the measured response, and robustness and insensitivity to corrosive permeants, soil particles and the environment.

The design chosen satisfied most of the requirements and combined the air/water interface tank and the volume change unit into one cylinder. Details can be seen in Figure 3.6 and Plate 3.3. The cylinder was a transparent acrylic tube. A magnetic resonance transducer (Tempersonic® R series) supplied by RDP was fitted inside the cylinder. The 10mm diameter transducer had continuous measurement over the 500mm range, with an output range of 0-10 Volts. The manufacturer stated accuracy was 0.02% over the full scale of the transducer (i.e. 0.1mm).

The cylinder had a 70mm internal diameter and the unit an internal height of 600mm. A float was made up from three layers of low-density engineering plastic screwed together with a magnet on top. The volume of water in the cylinder was measured by the height of the magnet (float) at the air/water interface. The internal volume of the unit was 2300ml (excluding the volume of the transducer), although the actual measurable volume change was 1770ml, which was limited by the active length of the transducer. The internal area of the cylinder was 3849mm^2, which gives an estimated accuracy of the unit of 385mm^3 (3849 x 0.1) or approximately 0.4ml. Therefore with a specimen of 236mm in diameter and 440mm in height the estimated accuracy was equivalent to 0.002% volumetric strain where other potential errors were not included.

The volume change unit was designed to work up to pressures of at least 700kPa, and was tested at 40kPa, 90kPa and 700kPa. From the regression lines shown in Figure 3.7

it can be seen that the cell pressure has no influence on the calibration of the volume change unit. Complete calibration testing of the new volume change unit is detailed in Section 4.3.4.

From Figure 3.8 (taken from test T40) it can be seen that both methods of determining the volumetric strain (calculated and measured) showed the specimen was contracting at the start of the monotonic load test and then quickly started to dilate. As expected the calculated volumetric strains recorded a much greater change in the specimen volume, both in compression and dilation, than the measured volumetric strains due to the bulging of the specimen. By 6% axial strain the calculated volumetric strain showed approximately 3 times greater dilation than the measured volumetric strain. This was typical in most of the monotonic load tests. The corrected volumetric strain curve in Figure 3.8 will be discussed later.

Salman (1994) suggested from tests that he carried out on granular materials, with stone sizes up to 20mm, that the measured volumetric strains (using an Imperial college type volume change unit) and calculated strains (using the displacements of three radial LVDT's and the axial LVDT) were comparable up to 0.3% axial strain. In this project this has not been realised either with the 20mm stone or the 50mm stone specimens.

Although calibration and initial trials with the new volume change unit appeared to show a good, repeatable and accurate device, there was one problem that was noticed. The specimen in each test was left to consolidate, under the test cell pressure, for a period of time before the loading began. It was noted that during this consolidation period the float level in the volume change unit dropped, i.e. water flowed out of the volume change unit into the triaxial cell, indicating a possible (long-term) consolidation/creep effect in the specimen.

To try and understand what was causing this change in volume eight potential reasons were identified and, where feasible, were addressed. i) Specimen consolidation/creep, ii) apparatus leakage, iii) apparatus creep, iv) leakage of water into the specimen, v) membrane creep, vi) air pockets dissolving, vii) piston movement, and viii) measurement error.

Having investigated this problem it was clear that the volume change unit recorded some form of continuous drop in the water level throughout the period of a normal test, when left in a static condition, which in terms of volumetric strain would be recorded as compression of the specimen.

The volume change occurring when a 90kPa cell pressure was applied with a concrete dummy specimen is shown in (Figure 3.9). As would be expected there was an initial drop in the volume. This was followed by a continued creep effect, which was not expected. Although the errors were minimal for the short duration of the monotonic load tests, it was not possible to calculate the effects on the longer term cyclic load tests due to the large variation in the creep/consolidation effect recorded during the investigation. It was also unclear how this effect would have manifested itself under cyclic loading with the specimen rapidly changing size and shape and the direction of flow of the cell fluid constantly changing. However the errors that occur due to this limitation in apparatus appear to be small in comparison to the errors that are assumed to occur when calculating the specimen volume due to the bulging of the specimen. At the higher cell pressures where barrelling was not such an issue then this made the behaviour of the two systems more comparable with one another.

The effects of this 'loss' of volume on the measured volumetric strain, in a monotonic load test, can be seen in Figure 3.8 where an approximate correction made 0.2% difference in the measured volumetric strain. Compared to the difference with the calculated strain (6% to 8% higher) this was minimal. The investigation into the causes of this apparent compression was however inconclusive and no correction was applied to the data. However the measured strain was considered to be more accurate, reliable and repeatable than the calculated strains and was therefore used in the analysis.

3.4 Triaxial test procedure

For monotonic load and cyclic load tests the specimens were prepared in an identical way. This is outlined below and a full step-by-step procedure is included in Appendix A (Disk 1).

The triaxial base plate was bolted to a vibration table. A thin film of silicon grease was applied to the rim of the base pedestal and a membrane was fastened to the pedestal using an O-ring. The membranes were 0.75mm thick made of natural rubber and supplied by Precision Dippings. A split mould was put around the pedestal and the membrane was pulled up inside and drawn back over the top of the split mould. A disc of filter paper was laid on the pedestal to stop fines from going into the drainage pipe at the bottom of the specimen.

A thin layer of the test material was laid in the bottom of the mould so that no material got under the filter paper. The vibration table was switched on and the material slowly

added. The 50mm ballast was dropped from approximately 750mm above the top surface of the material. Each particle was passed through a template (Plate 3.4) and the size of the particle was recorded; this included the thin layer of material originally laid in the bottom of the mould. The 20mm stone was also slowly poured from approximately 750mm above the top surface of the material. The material was then levelled by hand and covered with a thin (1mm) steel plate. With the 50mm ballast specimens a 22.75kg surcharge was applied for 1 minute under vibration. With the 20mm stone specimens the surcharge was applied for 30 seconds, also under vibration.

In order to prepare two-layer specimens with densities similar to Key (1998) the following procedure was used (also summarised in Table 3.1). The desired height for the first layer was marked on the inside of the membrane. The material was added up to this height and surcharged under vibration for 30 seconds with a 10kg weight. The next layer of material was then added and surcharged for a further 30 seconds with the 22.75kg weight. For specimens where the second layer of material was only a single or double layer of 20mm stone then the first layer of material was surcharged as normal with a 22.75kg weight for 1 minute. The vibration table was turned off, a thin layer of 20mm stone was added and the steel top plate was laid on top. To create a level surface the 22.75kg weight was rotated clockwise and anticlockwise 10 times through 180° in the horizontal plane. After the surcharge had been removed the height of the specimen was checked at three points. If there was more than 3mm difference in any of these heights the specimen was discarded.

A thin layer of silicon grease was applied to the rim of the top cap before it was placed on top of the thin steel plate and the membrane was pulled up around the side. An internal vacuum of between 20-30kPa was applied to the specimen and the split mould removed. A second membrane was slid over the specimen and a second O-ring was placed around the pedestal to secure both membranes. Two further O-rings sealed the second membrane at the top of the specimen. The heights of the radial LVDT targets were marked on the outer membrane and the targets fixed onto the specimen using a silicon sealant (Plate 3.2).

After the targets were secured the base plate was released from the vibrating table. A large O-ring was greased and placed in a groove in the base plate to act as a seal between the base and the cell body. Using a hoist the cell body was lowered over the specimen. The position of the top cap in relation to the loading piston was checked to make sure they were aligned, after which the cell was secured by tightening the

diametrically opposite tie rods. The pore fluid tap on the base plate was closed and the vacuum line was disconnected from the base plate.

Once the cell had been raised into position in the loading frame and the radial LVDT's had been bolted into their mountings the cell was filled with water. When the cell was full it was slightly tilted from side to side to remove any trapped air. The cell fluid line between the cell and the volume change unit was then attached and the volume change unit was filled with water, flushing out any air trapped in the system. The vacuum on the specimen was released by opening the pore fluid valve at the base of the cell and the bleed valve at the top of the cell was closed. The hydraulic ram stabilising bar and frame reaction bar were placed in position and secured (Figure 3.2). The desired cell pressure was then applied and the specimen was left for a period of consolidation, which was normally 1 hour. The compression frame platen was manually raised until the load piston was just touching the hydraulic ram. The appropriate logging program, depending on the type of test, was selected and the filename and details were entered.

For monotonic load triaxial tests the logging was started on the computer and the driving motor on the compression frame was turned to 'cell up' position causing the specimen to be loaded under strain control. When one of the radial LVDT's had reached the end of its range then the test was stopped and the apparatus dismantled.

For the cyclic load triaxial tests the hydraulic system was attached to the hydraulic ram. The hydraulic shut off valve was opened and both the bypass valves on the hydraulic system were closed (Figure 3.4). The logging was started on the computer. The Stamp computer was reset and the automatic loading selected. After 50 load cycles the control unit was manually switched to the high-speed loading. With the majority of cyclic load tests a monotonic load test was carried out after the cyclic load test had finished. These were called post cyclic monotonic load tests.

Before starting the post cyclic monotonic load test it was necessary to make sure the hydraulic ram had been pushed back up inside its casing and the cell base manually raised until the loading piston was just in contact with the ram again. This was necessary to make sure that there was a solid reaction against the load piston as it was found that this was not the case in some early tests and the ram had been pushed back up during the test.

To dismantle the equipment at the end of the test the air pressure inlet valve at the top of the volume change unit and the cell fluid inlet valve at the base of the triaxial cell were closed. To release the pressure in the volume change unit the bleed valve was opened

and the water was drained off through the drainage valve at the base of the volume change unit. The cell pressure pipe was disconnected and the cell pressure valve opened to drain the cell, collecting the water in a bucket. Once the initial pressure had been released the bleed valve at the top of the triaxial cell was opened. When the cell was empty it was lifted back onto the vibration table using the hoist. The tie rods were loosened by unscrewing the diametrically opposite bars at the same time.

The cell body was lifted up over the top of the specimen using the hoist and the specimen was dismantled particle by particle. Each particle was assessed for the amount of breakage that had occurred as discussed in Section 6.3.1. Further to this the perceived original particle size was recorded. Each piece of the particle was then passed through the particle size template. Where breakage had occurred this could mean there were several 'new' particles.

3.5 Triaxial test programme

Over 80 triaxial specimens were tested during the course of this project. Those included in the analysis have been split into six series of triaxial tests, which have been summarised in Table 3.2. Details of the individual particle crushing tests are described in Section 3.6.

For each type of specimen there were usually three tests carried out, the monotonic load triaxial test, the cyclic load triaxial test and the post cyclic monotonic load triaxial test. Each test, that is each specimen prepared, was numbered in the chronological order that the tests were carried out. Cyclic load tests and post cyclic monotonic load tests have the same test number. This was because the post cyclic monotonic load tests were carried out on the same specimen after the cyclic load test had finished.

3.5.1 Series 1 – 20mm stone tests

Series 1 was scheduled to consist of a small number of tests to provide data on repeatability within the project itself and also to clarify that the tests were reproducible when compared with those of Key (1998) and others. Furthermore, Series 1 compared the basic soil characteristics between the two different types of 20mm stone used by the stoneblower. Test details for Series 1 are detailed in Table 3.3.

3.5.2 Series 2 – Characterisation tests

With the development of the new volume change unit and the work relating to particle breakage Series 2 included several tests using only one type of aggregate. This allowed a level of understanding to be developed that would give a benchmark to which the results of other series of tests could be compared. Test details for Series 2 are detailed in Table 3.4. During the development of the volume change unit, between Series 1 and Series 2, eight tests were carried out. The data from these tests could not easily be incorporated into the project and have therefore not been included in the analysis of the results or the discussions.

3.5.3 Series 3 – Development of breakage

Series 3 investigated the development of breakage of the material throughout the cyclic load test. This consisted of five extra tests, a 100, a 1000, a 10,000, a 1 million and a '2 million' load cycle test. During the first 1 million load cycle test, which was run over the Christmas break 2001, there was a power cut at around 800,000 cycles. It was decided to run a further 1 million load cycle test on the same specimen (T42), accumulating to over 1.7 million cycles. This test is referred to as the 2 million load cycle test. Although the test data was difficult to analyse, due to the power cut causing errors in the data, the specimen was dismantled and breakage analysis was carried out.

After each test the specimen was dismantled and the breakage assessed. For completeness, particle breakage data for the 100,000 load cycle test was used from Series 2. Tests included in Series 3 are detailed in Table 3.5.

3.5.4 Series 4 – Two-layer specimens

Series 4, detailed in Table 3.6, investigated the behaviour of layer specimens, building on the research of Key (1998). Specimens were prepared where half of the specimen was 20mm stone overlying half a specimen of 50mm ballast (called a 1-1 layer specimen – see Table 3.6). Furthermore specimens with a third stone overlying two thirds ballast (1-2 layer) and two thirds stone overlying a third ballast (2-1 layer) were also tested. With the understanding gained from these tests, specimens were also set up with single and double layers of stone overlying the ballast, more akin to the arrangement produced by the stoneblower maintenance.

3.5.5 Series 5 – Damped specimens

The effect of altering the modulus at the base and top plates was investigated in Series 5 (Table 3.7). This was achieved by simply inserting a 3mm thick disc of rubber at the base of the specimen to simulate a subgrade and a wooden disc (8mm thick MDF hardboard) was laid on top of the material at the top of the specimen under the top cap instead of the 1mm mild steel disc (see Section 3.4). This has been referred to as specimen damping.

3.5.6 Series 6 – Wetted ballast

Series 6 examined the behaviour of material that was wet when the specimen was set up and is detailed in Table 3.8. To ensure repeatability the ballast was soaked for 24 hours before the test and was allowed to drip dry for 5 minutes immediately before preparing the specimen.

3.6 Single-particle crushing test apparatus

Single-particle crushing tests have been carried out to gain deeper understanding of the breakage occurring during the triaxial tests.

It is widely accepted that the failure of a spherical particle under compression is a tensile failure, as mentioned in Section 2.6.4. The tensile strength of an individual particle is usually measured indirectly by compressing the particle between two flat plates until the particle fails. Failure is when the particle splits in several pieces as described by Jaeger (1967).

Figure 3.10 and Plate 3.5 show the particle crushing apparatus used in this work. It was adapted from an aggregate impact testing machine used to get the Aggregate Impact Value (BS 821). The apparatus had two hardened steel plates between which the particle was crushed and two guide posts to keep the upper plate horizontal. The apparatus was designed to fit inside the triaxial cell and the 100kN loading frame detailed in Section 3.3.2. The triaxial cell was used as this was a system that already had a reaction frame, and a way of measuring the load and axial displacement and it ensured that all the pieces of apparatus were aligned. The displacement, and hence the particle diameter at failure, was measured using the external axial LVDT. The load applied during the test was measured by the load cell (Section 3.3.3).

McDowell (2001) showed that it is necessary to crush 30 particles of similar size to calculate the mean strength and standard deviation in strength within prescribed

confidence limits. He showed that the characteristic strength could be determined to within 25% at a confidence of 95% with 30 tests.

3.7 Single-particle crushing test procedure

Four different sizes of materials were tested in the single-particle crushing apparatus, these were 37-50mm ballast, 28-37mm ballast, 20-28mm ballast and 20mm stone as supplied for the stoneblower. Thirty particles of each sized material were selected and tested in the apparatus described above and in the manner described below. Therefore a total of one hundred and twenty particles were tested.

The triaxial cell base was placed on the loading rig and the single-particle crushing apparatus lifted onto the base. The underside of the single-particle crushing apparatus had a groove cut out so that it always sat central on the triaxial base. The particle was placed in the centre of the bottom loading plate and the top plate was gently lowered until it rested on the particle. The triaxial cell body was lowered onto the base plate and secured, using the tie rods, to ensure that the loading piston and top plate piston were aligned and stayed aligned during the test. The axial LVDT was fastened in position. Once the computer logging had been started the knob on the loading rig was turned to the 'cell up' position. The test was left to run until the particle failed; this was determined with the help of the charts within the logging program and a certain amount of observational judgment to determine when the particle was deemed to have failed. The computer logging was stopped, apparatus dismantled and the particle removed.

The results of the individual particle-crushing tests are discussed in Section 6.2.

	20mm stone layer = 1/3rd or 2/3rds of specimen height	Single/double layer of 20mm stone
Bottom layer	30sec vibration with a 10kg weight	1min vibration with a 22.75kg weight
Top layer	20sec vibration with a 22.75kg weight	Rotate 22.75kg weight 10 times through 180° in the horizontal plane

Table 3.1 - Summary table of vibration time and weight of surcharge for two-layer specimens.

	Summary	Series characteristics / comments
Series 1	15 specimens (9 monotonic, 6 cyclic, 6 post cyclic monotonic load tests) - Repeatability, - Reproducibility, - Comparing Bardon stone and Cloburn stone, - General soil characterisation.	Volume change calculations based on the assumption of the specimen staying a right-angled cylinder.
Series 2	32 specimens (8 monotonic, 24 cyclic, 16 post cyclic monotonic load tests) - Repeatability/Reproducibility, - General soil characteristics, - Breakage characteristics in basic tests, - Development of the resilient modulus throughout the cyclic tests.	Volume change unit introduced to improve the accuracy of the volume change calculations. Quantification of particle breakage. Data logging system improved to recorded data in a way which would allow the calculation of the resilient modulus at defined points throughout the test.
Series 3	5 specimens (5 cyclic load tests) - To investigate particle breakage during the cyclic test.	50mm ballast only. Cyclic tests stopped after different number of load cycles and particle breakage assessed.
Series 4	18 specimens (9 monotonic, 9 cyclic, 8 post cyclic monotonic load tests) - To investigate the behaviour of layered specimens.	Monotonic and cyclic tests set up with different amounts of 20mm/50mm materials.
Series 5	3 specimens (3 cyclic load tests) - Specimens tested with different top/base materials (damped specimens).	A rubber mat was placed at the bottom of the specimen and a wooden disc on top of the specimen below the top cap.
Series 6	6 specimens (6 cyclic load tests) - The specimen material was wet before each test.	50mm ballast only. The ballast was soaked for 24hrs. before each test was prepared.

Table 3.2 - Summary of the triaxial test programme

Series 1: General specimen characterisation		
Test No.	Loading*	Comments
T1, T6	mono.	20mm Cloburn stone, 40kPa cell pressure
T11, T13	cyclic	
T8, T17, T18	mono.	20mm Cloburn stone, 90kPa cell pressure
T2	cyclic	
T5, T14	mono.	20mm Bardon stone, 40kPa cell pressure
T4, T15	cyclic	
T7, T16	mono.	20mm Bardon stone, 90kPa cell pressure
T9	cyclic	

Table 3.3 - Details of test specimens in Series 1

Series 2: Further specimen characterisation - including the new volume change unit and particle breakage assessment -		
Test No.	Loading*	Comments
T19, T72	mono.	20mm Bardon stone, 40kPa cell pressure
T20, T33, T54, T55, T56, T73, T74	cyclic	
T22	mono.	20mm Bardon stone, 90kPa cell pressure
T21, T34, T35	cyclic	
T63	mono.	20mm Bardon stone, 140kPa cell pressure
T59, T68	cyclic	
T76	cyclic	20mm Bardon stone, 240kPa cell pressure
T27	mono.	50mm Ballast, 40kPa cell pressure
T23, T24, T38, T57	cyclic	
T26, T40	mono.	50mm Ballast, 90kPa cell pressure
T25, T36, T37	cyclic	
T60	mono.	50mm Ballast, 140kPa cell pressure
T61, T62, T64	cyclic	
T77	cyclic	50mm Ballast, 240kPa cell pressure

* mono. = monotonic load test

Table 3.4 - Details of test specimens in Series 2

Series 3: Development of breakage in the cyclic tests		
Test No.	Loading	Comments
T65	cyclic	50mm Ballast, 140kPa cell pressure, 100 cycles
T66	cyclic	50mm Ballast, 140kPa cell pressure, 1000 cycles
T67	cyclic	50mm Ballast, 140kPa cell pressure, 10,000 cycles
T75	cyclic	50mm Ballast, 90kPa cell pressure, 1million cycles
T42	cyclic	50mm Ballast, 90kPa cell pressure, 2 million cycles

Table 3.5 - Details of test specimens in Series 3

Series 4: Layered specimens				
Test No.	Loading*	Cell pressure (kPa)	Comments	20mm stone 50mm ballast
T50	mono.	40	Single layer of 20mm Bardon stone overlying 50mm ballast	Single layer stone
T39, T48	cyclic	40		
T41	cyclic	90	Single layer of 20mm Bardon stone overlying 50mm ballast	Single layer stone
T52	mono.	40	Double layer of 20mm Bardon stone overlying 50mm ballast	Double layer stone
T51	cyclic	40		
T53	mono.	40	Top third 20mm Bardon stone overlying bottom two thirds 50mm ballast	1-2 layered
T46	cyclic	40		
T28, T29, T43, T44	mono.	40	Top half 20mm Bardon stone overlying bottom half 50mm ballast	1-1 layered
T31, T45	cyclic	40		
T30	mono.	90	Top half 20mm Bardon stone overlying bottom half 50mm ballast	1-1 layered
T32	cyclic	90		
T49	mono.	40	Top two thirds 20mm Bardon stone overlying bottom third 50mm ballast	2-1 layered
T47	cyclic	40		

* mono. = monotonic load test

Table 3.6 - Details of test specimens in Series 4

Series 5: Effects of specimen damping		
Test No.	Loading	Comments
T69	cyclic	50mm ballast, 140kPa cell pressure. Specimen includes rubber mat and wooden disc damping
T70	cyclic	Double layer 20mm Bardon stone overlying 50mm ballast, 140kPa cell pressure. Specimen includes rubber mat and wooden disc damping
T71	cyclic	20mm Bardon stone, 140kPa cell pressure. Specimen includes rubber mat and wooden disc damping

Table 3.7 - Details of test specimens in Series 5

Series 6: Effects of wet ballast		
Test No.	Loading*	Comments
T81	mono.	50mm wet ballast, 40kPa cell Pressure
T80	cyclic	
T82	mono.	50mm wet ballast, 90kPa cell Pressure
T83	cyclic	
T79	mono.	50mm wet ballast, 140kPa cell Pressure
T78	cyclic	

* mono. = monotonic load test

Table 3.8 - Details of test specimens in Series 6

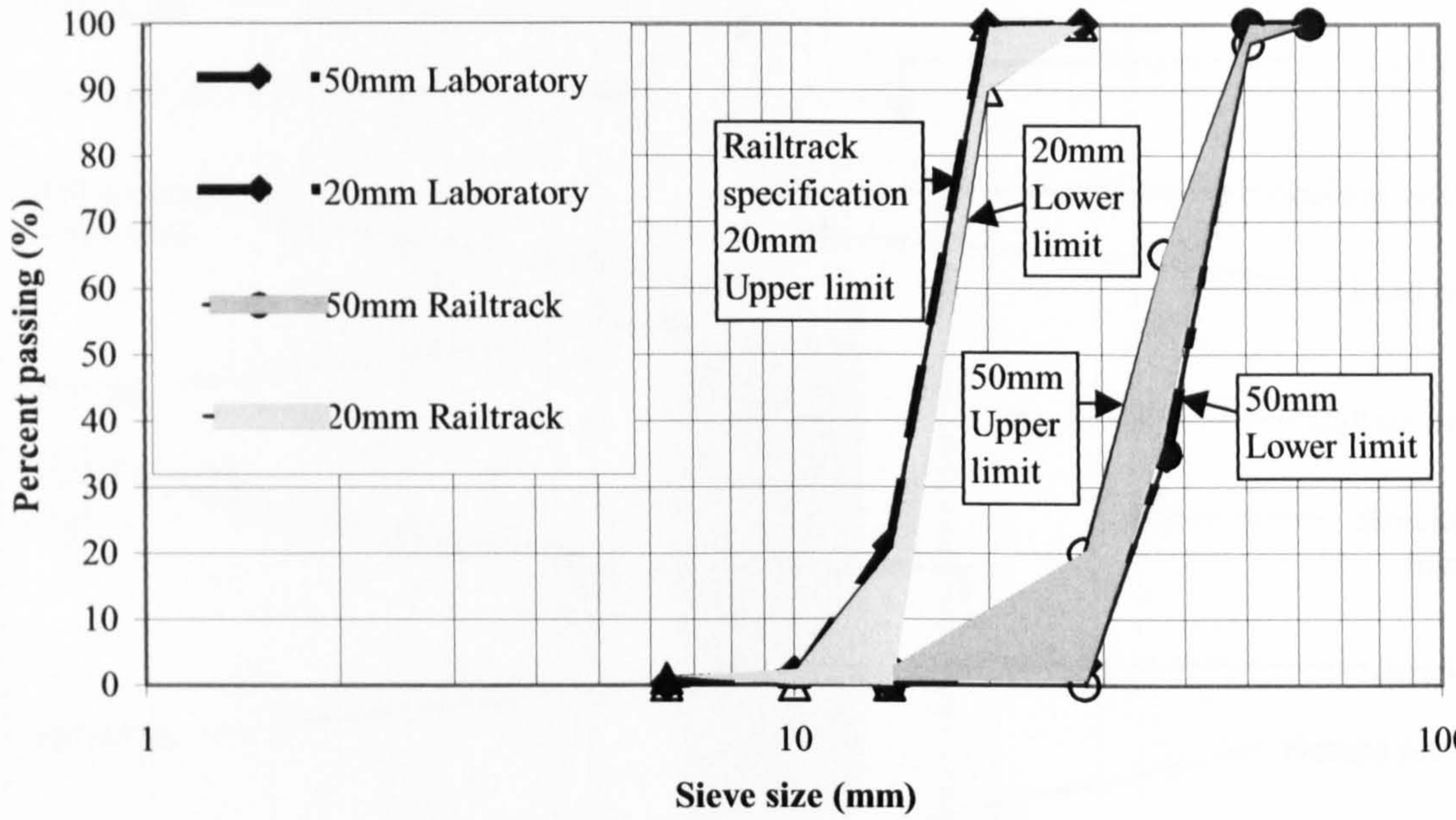

Figure 3.1 - Particle size distribution curves for the 50mm ballast and the 20mm stone from the Bardon quarry used in the triaxial tests and the respective Railtrack standards

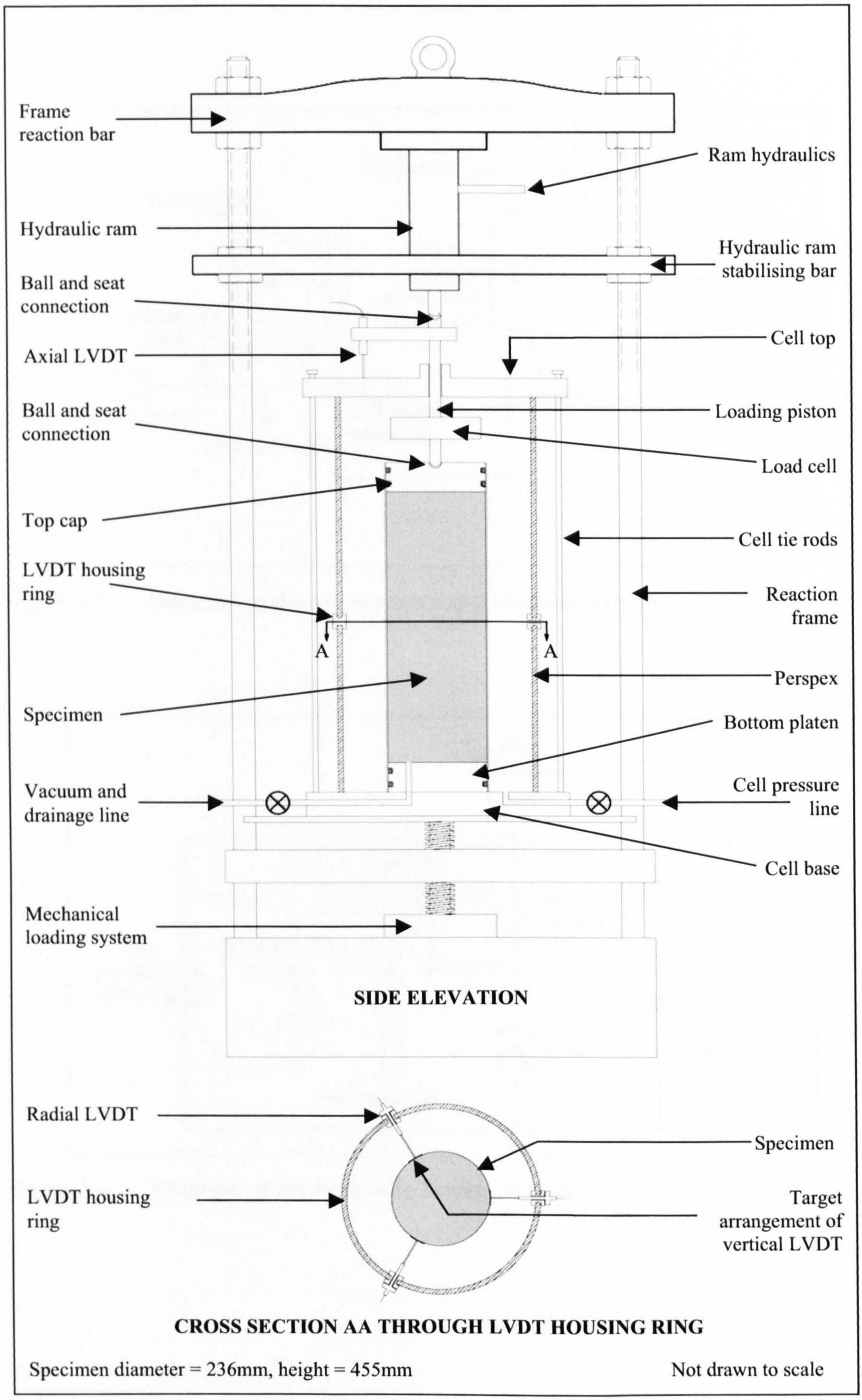

Figure 3.2 - Diagram of the triaxial cell (adapted from Key, 1998)

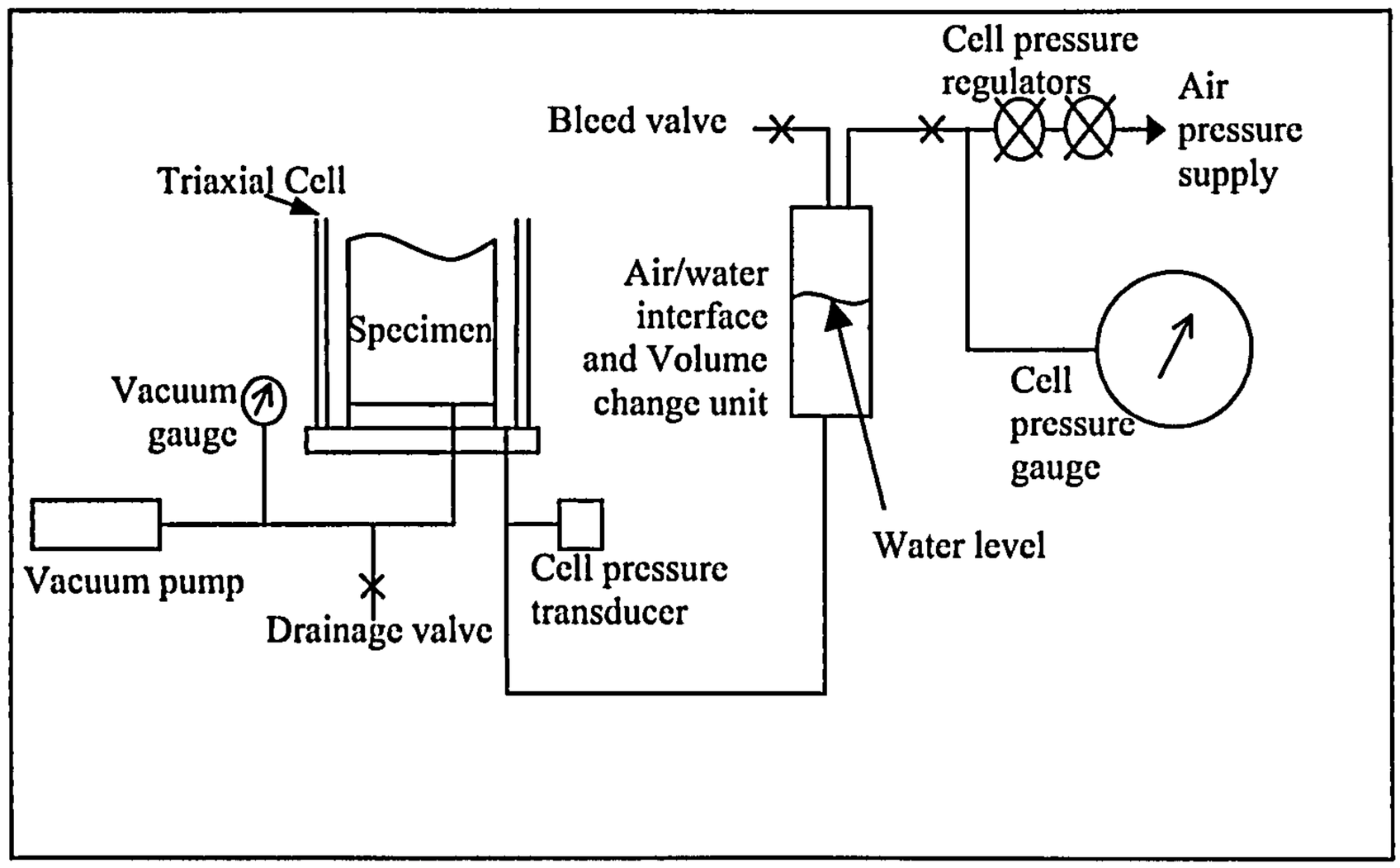

Figure 3.3 - Diagram of the cell pressure and vacuum systems

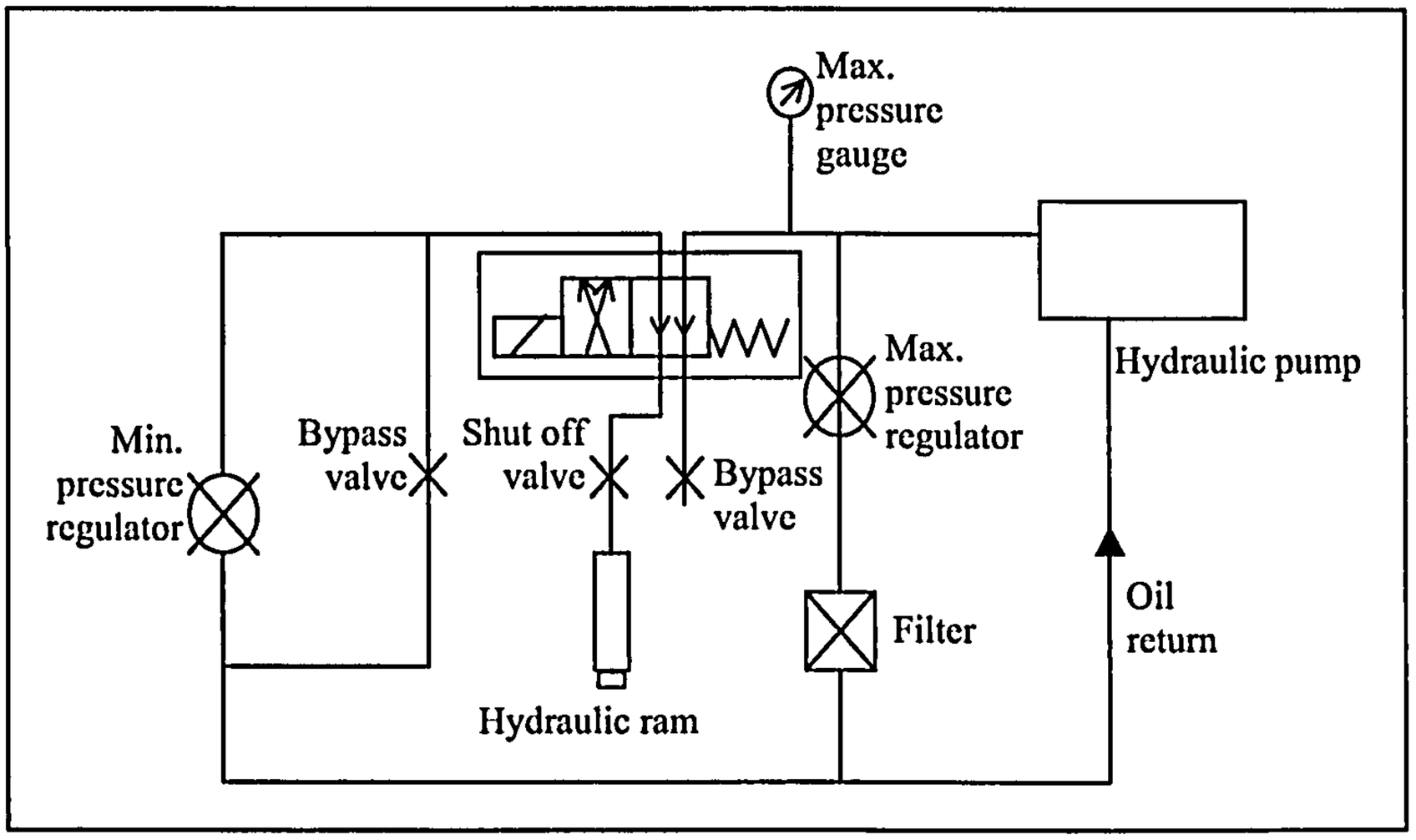

Figure 3.4 - Diagram of the hydraulic loading system

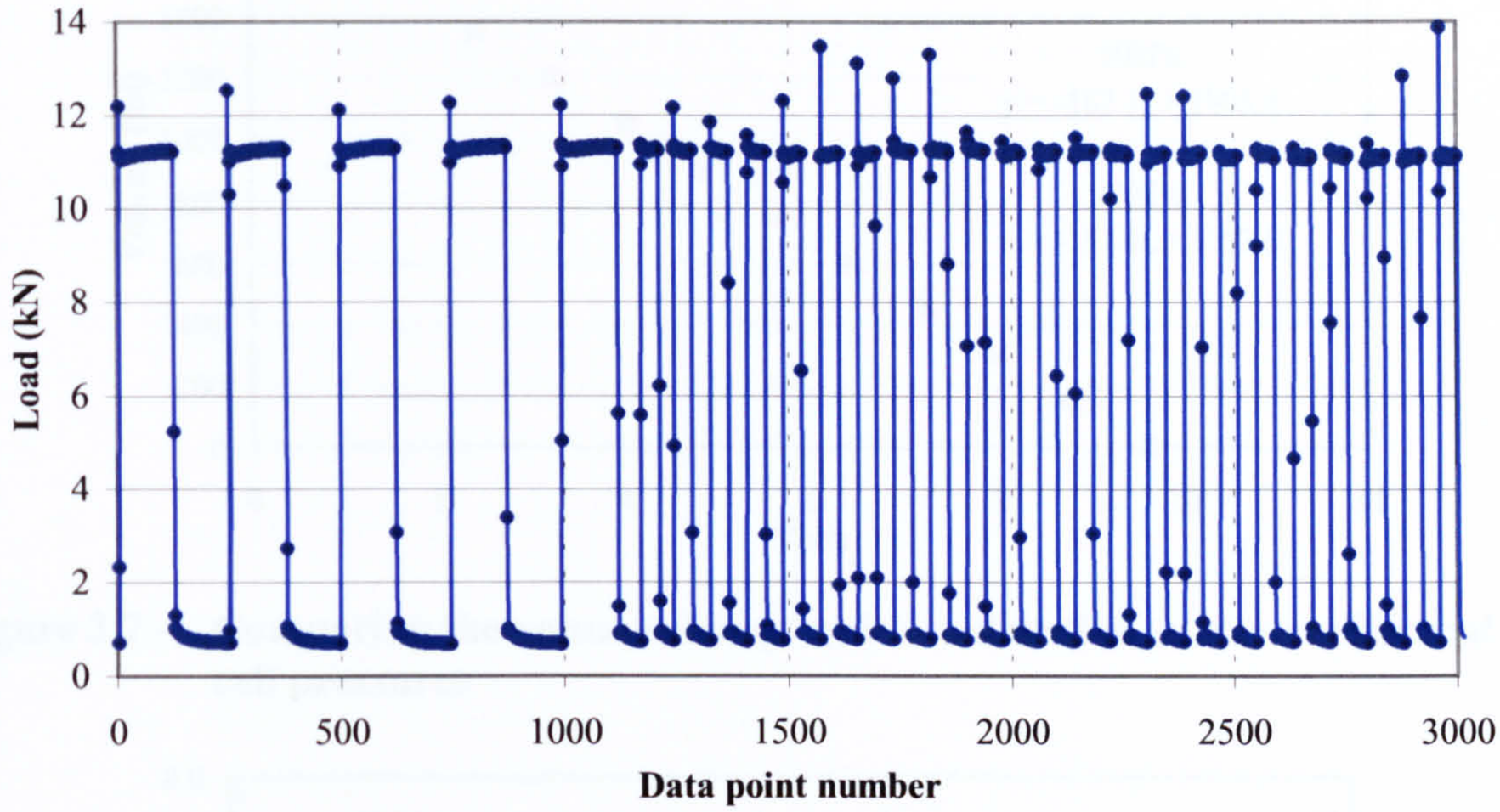

Figure 3.5 - Load waveform generated by the solenoid valve

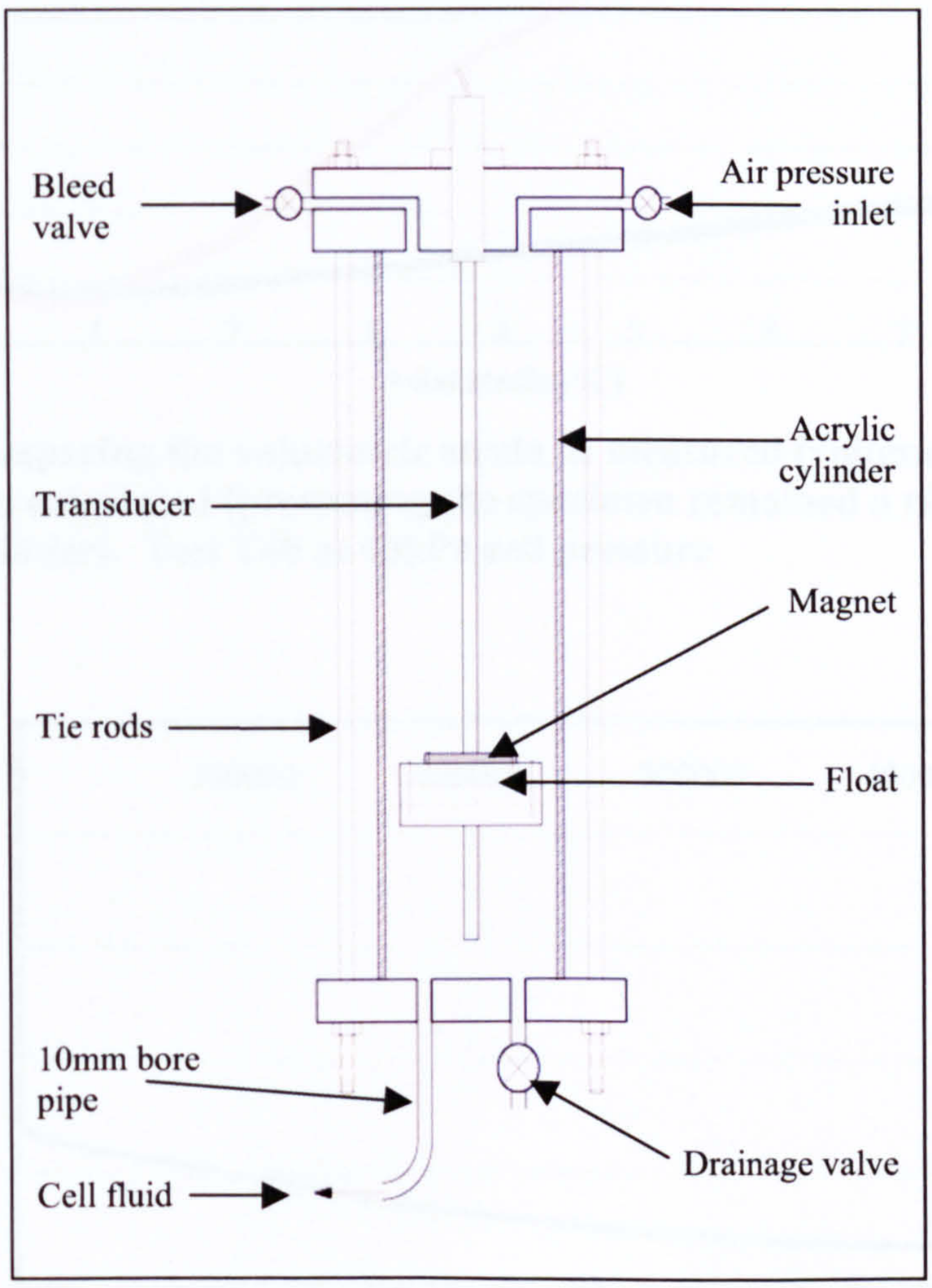

Figure 3.6 - Diagram of the volume change unit

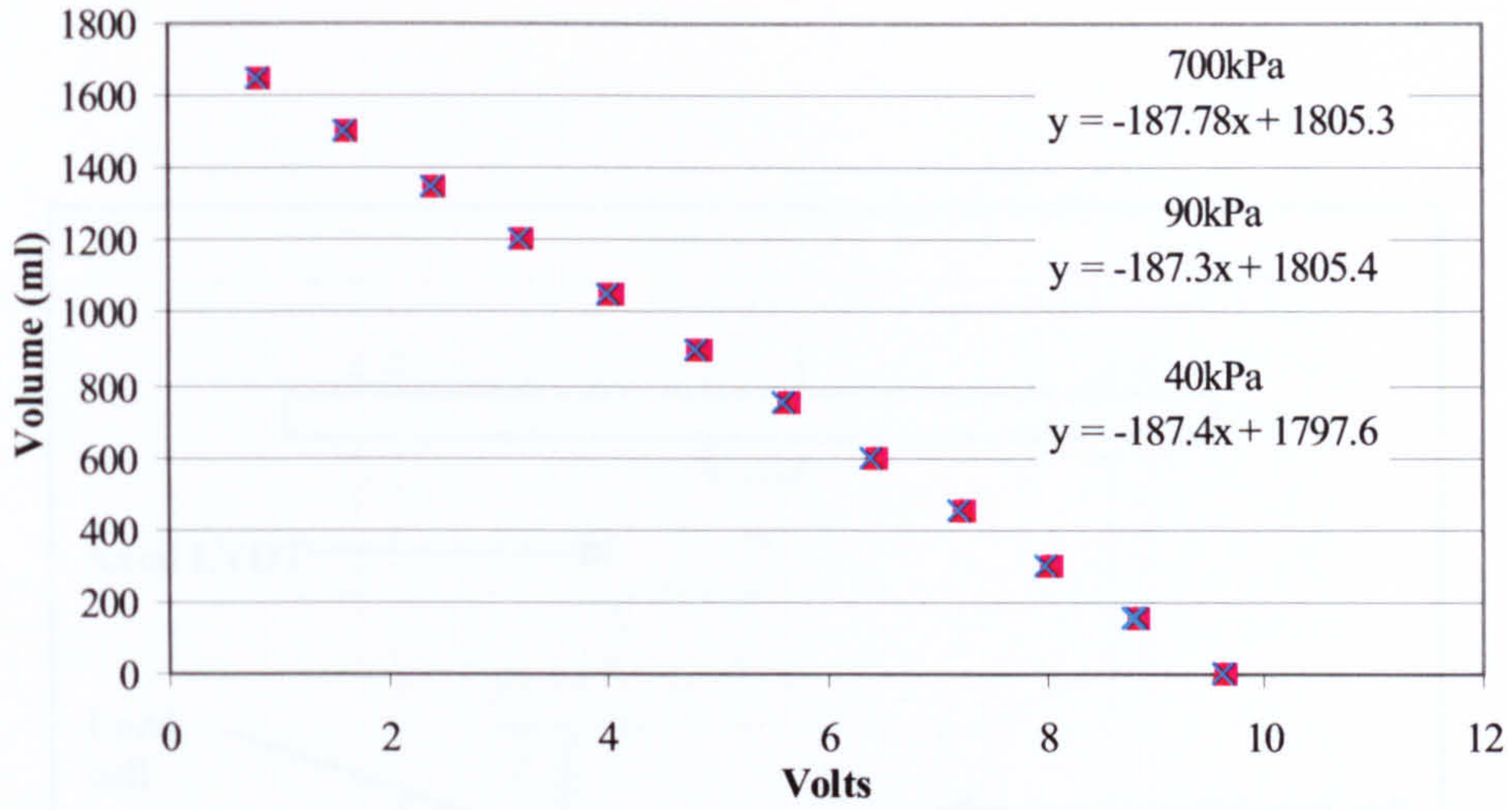

Figure 3.7 - Comparing the volume change unit's calibration curves at different cell pressures

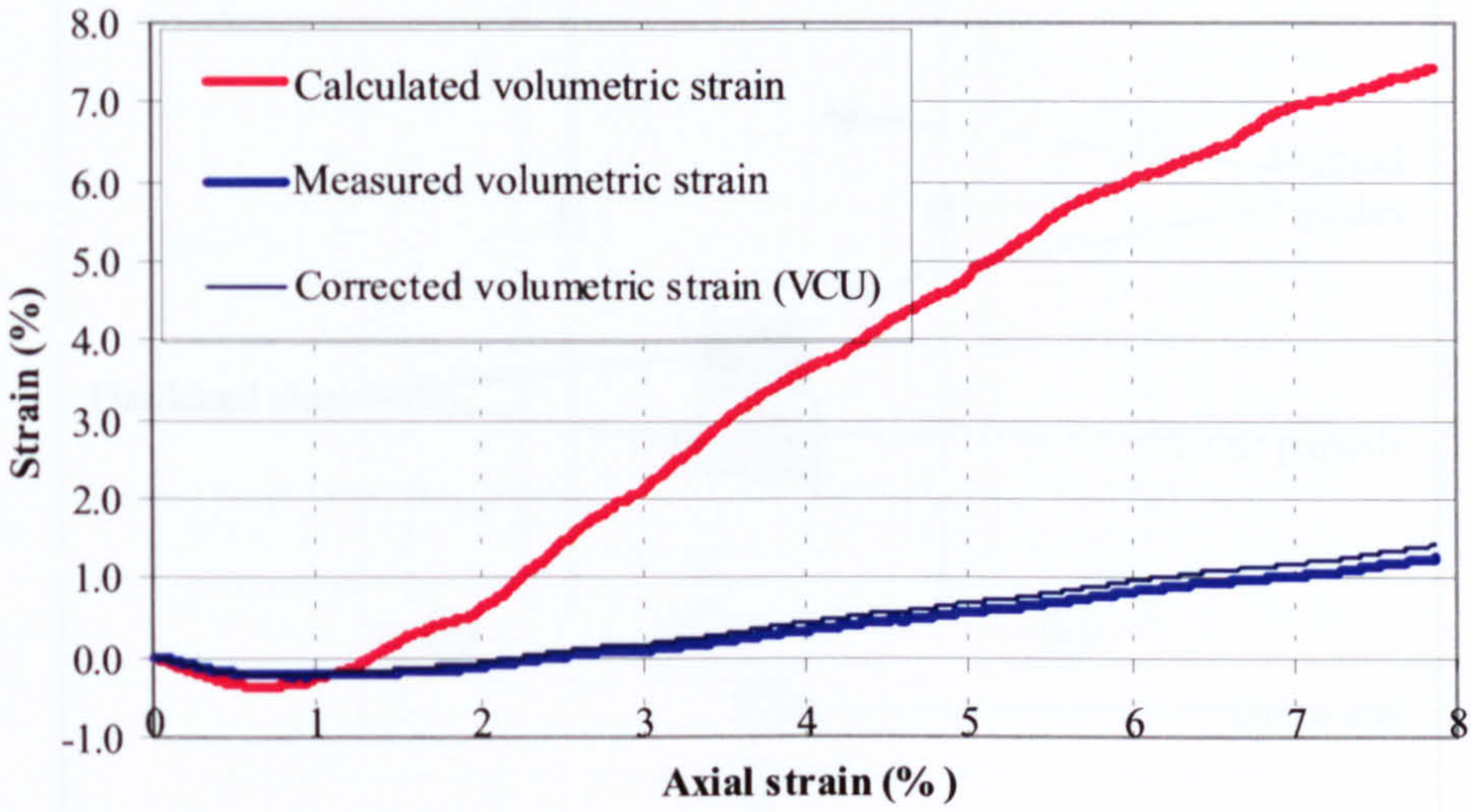

Figure 3.8 - Comparing the volumetric strain as measured (volume change unit) and calculated (presuming the specimen remained a right-angled cylinder). Test T40 at 40kPa cell pressure

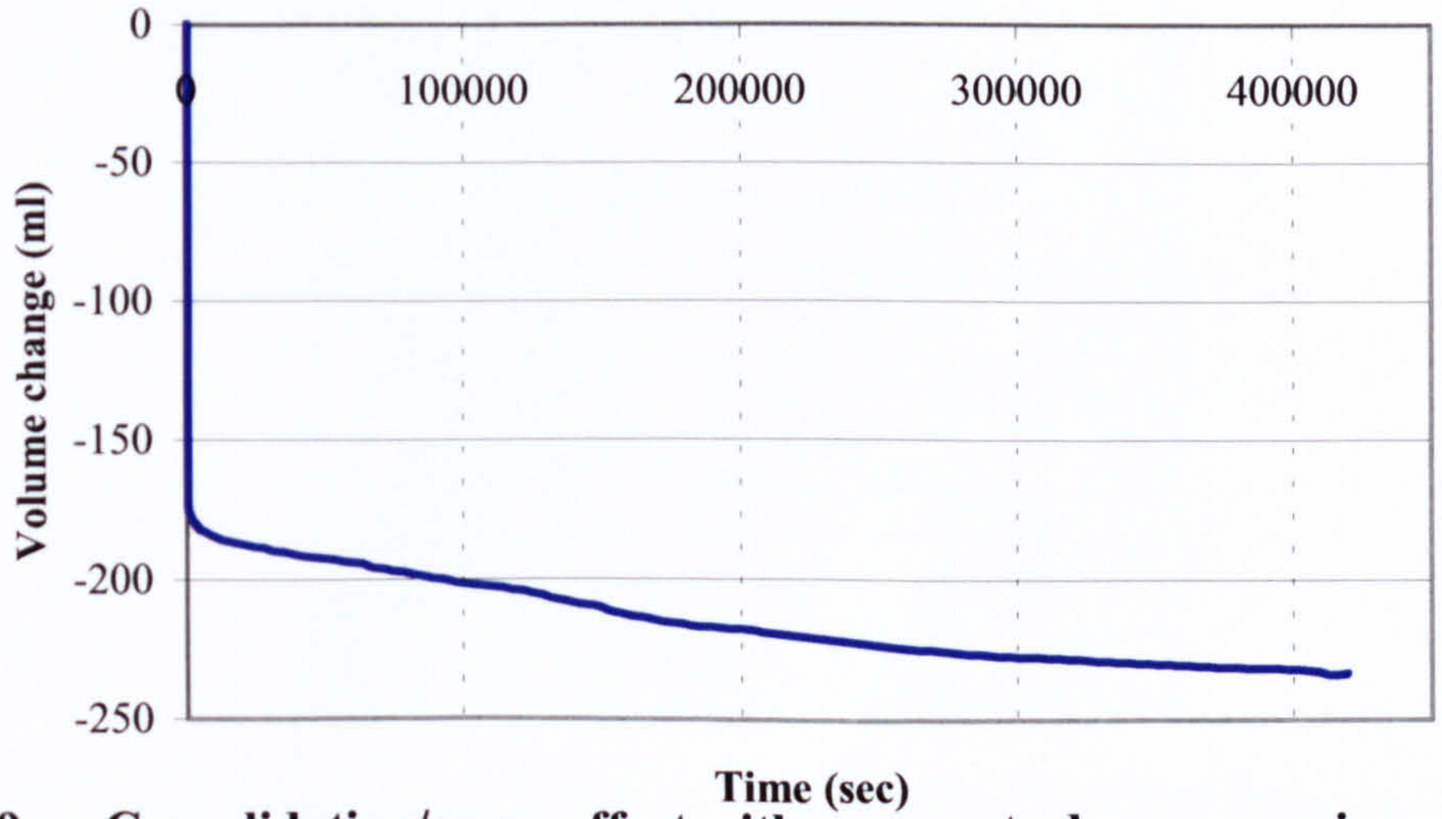

Figure 3.9 - Consolidation/creep effect with a concrete dummy specimen under a 90kPa cell pressure

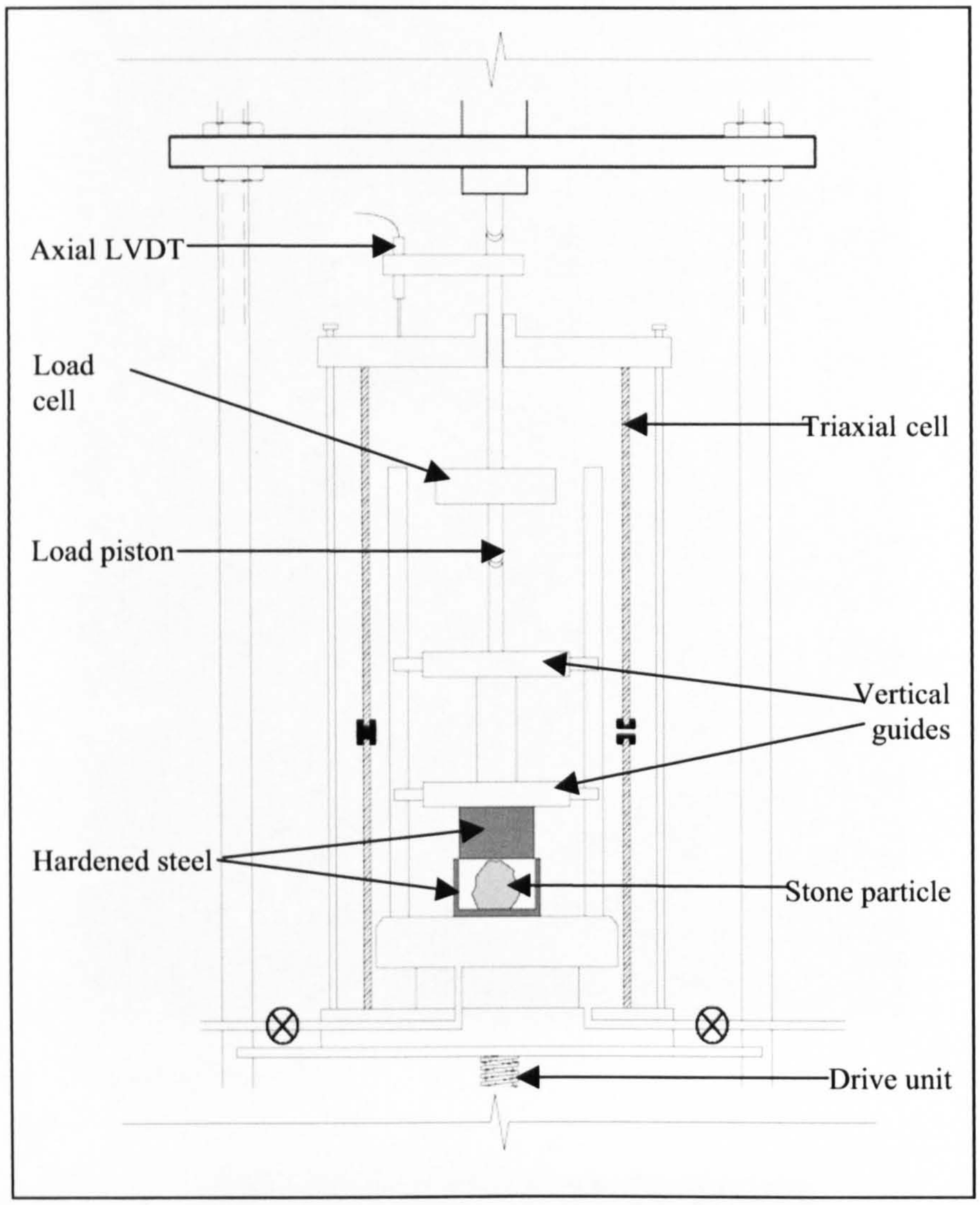

Figure 3.10 - Single-particle crushing apparatus

Plate 3.1 - The triaxial cell

Plate 3.2 - Showing a target on the side of the specimen and bulging failure after a monotonic load triaxial test

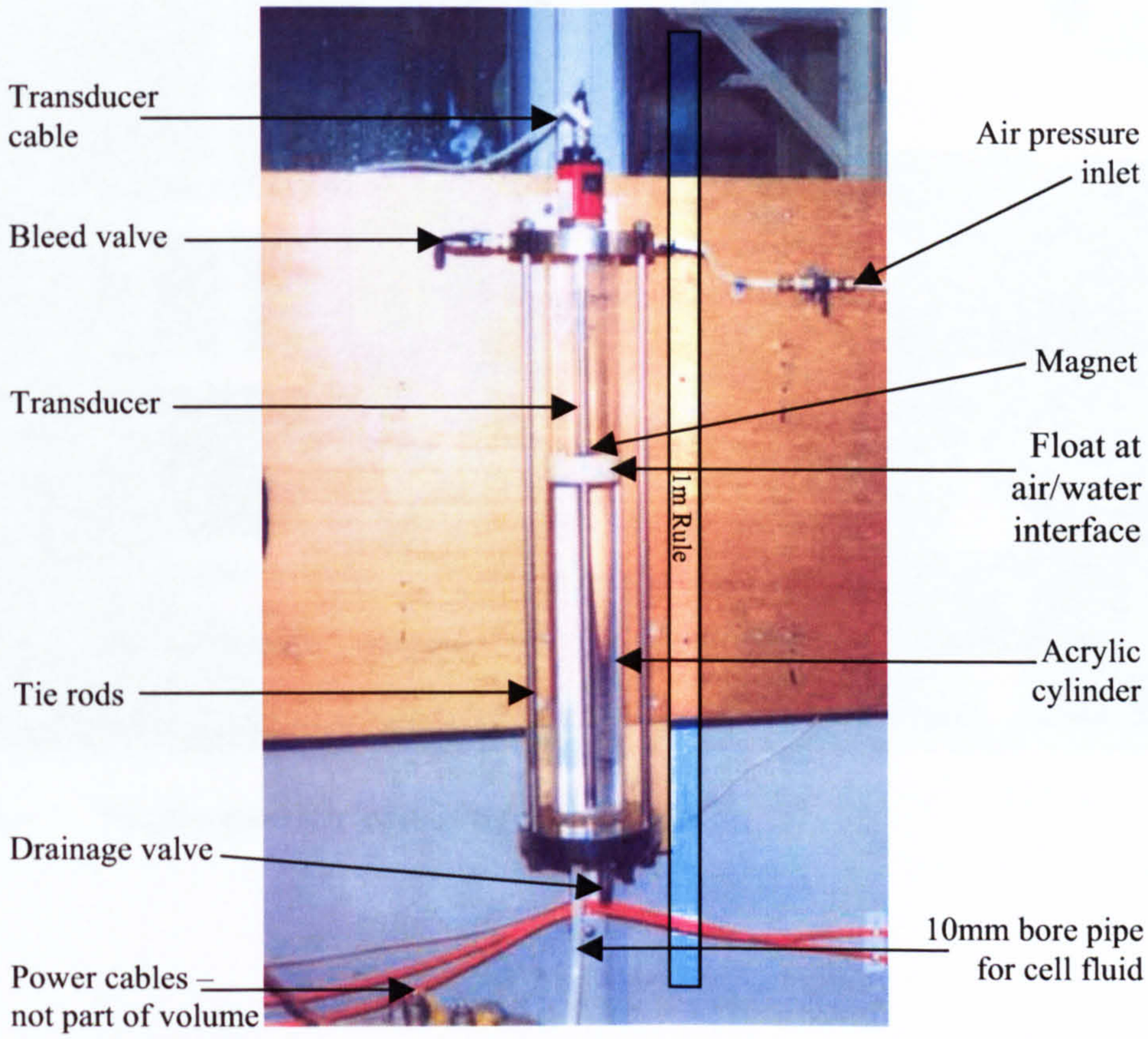

Plate 3.3 - Volume change unit

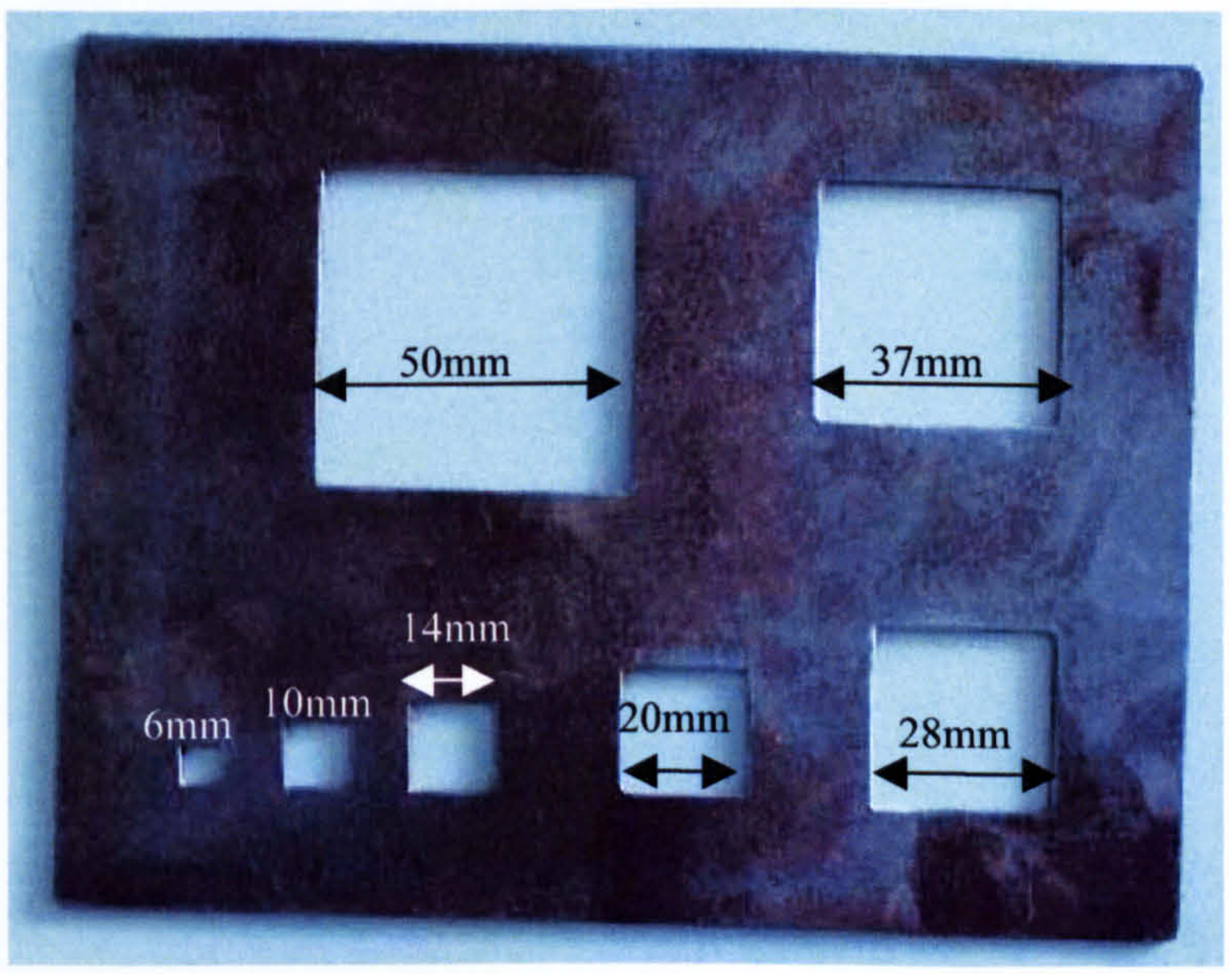

Plate 3.4 - Particle size template

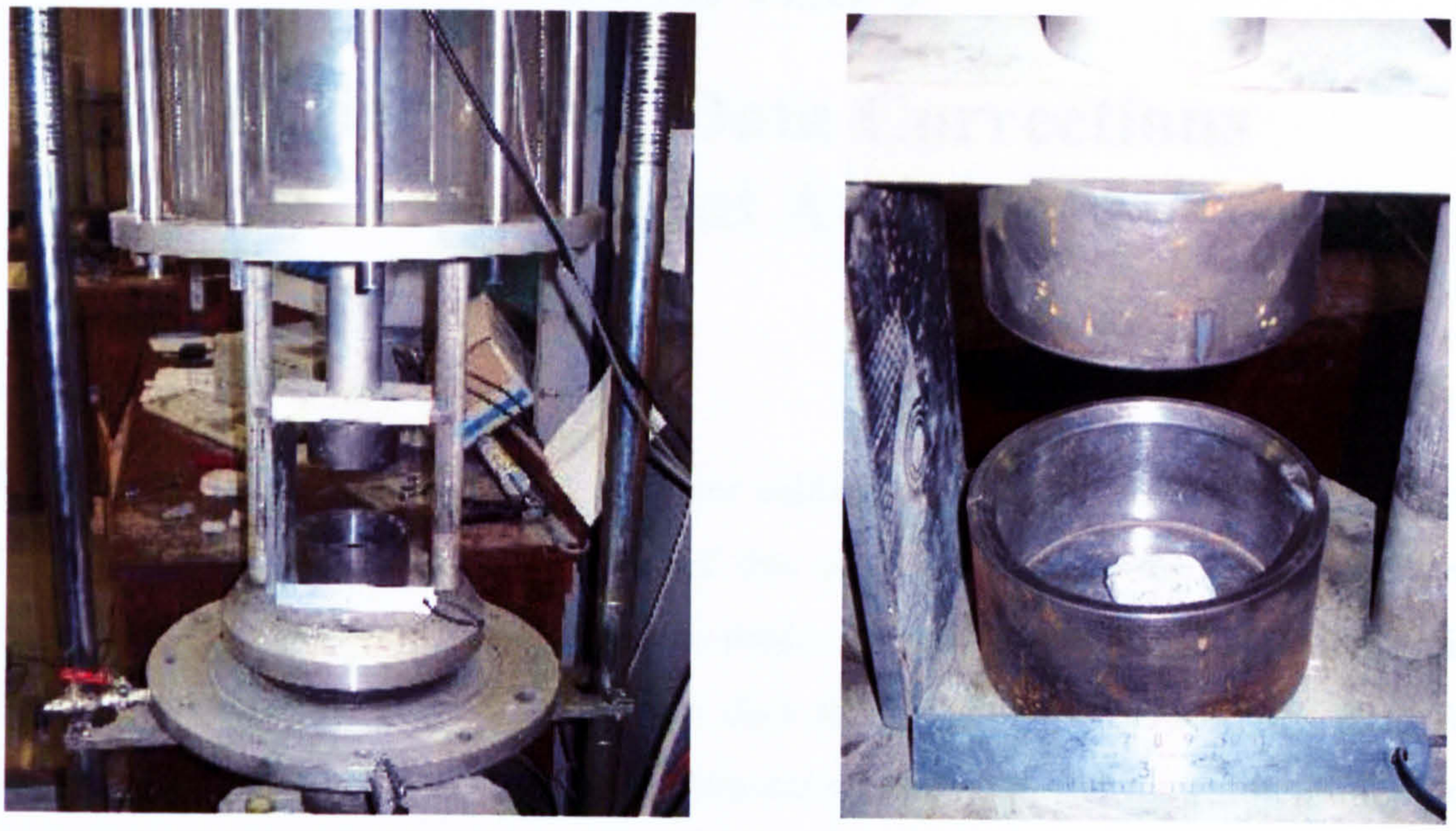

Plate 3.5 - Single-particle crushing apparatus

CHAPTER 4

Calibrations, Data Corrections and Initial Analysis

4.1 Introduction

The methods of data acquisition, transducer calibrations and the corrections applied to the data are covered in the early part of this chapter. During the analysis several procedures were followed and calculations made; these are described along with details of the initial analysis carried out on the data from each test. Procedures used for calculating the specimen stiffness in the monotonic load tests, and the resilient modulus in the cyclic load tests, and the method used to determine the peak and final stresses in the monotonic load tests and the strains in both the monotonic and cyclic load tests are also reviewed.

4.2 Data acquisition

The axial LVDT, the three radial LVDT's, the load cell and the pressure transducer were all connected to an amplifier, which had its own stabilised power supply and should therefore not have been affected by any fluctuations in the mains power supply. The magnetic resonance transducer had its own separate power supply. Strawberry Tree "Workbench" programs were used for data logging in all of the tests.

The Workbench program layout for the monotonic load triaxial tests and single-particle crushing tests can be found in Appendix B (Disk 1) . This was set up to record data from each transducer every second. The data was then processed using a piece of software written in Visual Basic for Applications program (VBA for Excel) as detailed in Appendix C (Disk 1).

It is considered usual, where the rate of strain increase decreases with time, i.e. a log type relationship, that the data be recorded in logarithmic time. From a practical point of view this reduced the size of the data files. However the data acquisition software had no provision for recording data on a logarithmic scale. To record the data for each cycle in the cyclic load triaxial test would create a data file of an unmanageable size. Therefore a system was developed within the Workbench environment that would allow data to be recorded on a 'logarithmic' scale. Using an iterative approach, data was

recorded approximately every $^1/_{40}^{th}$ of a second during the 1st cycle, 2nd cycle, 5th, 10th, 20th, 50th, …., 20,000th, 50,000th and the 100,000th cycle. The fastest rate of data acquisition of the system was limited to $^1/_{40}^{th}$ of a second. Data was also recorded with the same logging rate, to a separate file, for cycles 50 – 150, 950 – 1050, 9750 – 10,250 and 99,250 – 100,000. This second set of data allowed the average resilient modulus to be calculated at cycles 100, 1000, 10,000 and 100,000 over the aforementioned ranges. Both sets of data were again processed using software written in VBA for Excel. The Workbench screen layout and the VBA software are detailed in Appendix B and C (Disk 1) respectively.

Data acquisition within the Workbench program was synchronised with the load cycles throughout the test via a digital input from the control 'Stamp' unit as described in Section 3.3.2.

4.3 Calibration

For reliable results there needed to be confidence in the measuring equipment. Calibrations were therefore performed on each of the seven instruments to ensure that data recorded during each test was to an acceptable accuracy and was repeatable. Initially Key (1998) checked the calibration of the transducers every six weeks, and found that there was little variation with time. He therefore carried out full calibrations approximately every six months. This appeared to be sufficient and was therefore continued in this project. Calibration tests were carried out at the start, in the middle and at the end of the test programme. Due to the quick turn over between tests all of the instruments were left permanently connected to the power supply.

For reliable calibration the instrument should be cycled through its full range 3 times prior to the calibration. The first reading should be taken at an absolute zero value where no displacement, pressure or load is applied to the instrument. Then with at least ten incremental steps the instrument should be taken through its full range and back again with a further ten steps, recording the voltage at each incremental step. On this data linear regression analysis can be used to calculate the calibration factor, i.e. the gradient of the best-fit line and the coefficient of conformity (R^2).

As all of the LVDT's and the volume change unit were only used to measure the relative displacement and relative volume, the drift was calculated as the variation in the gradient of the calibration factor with time. The accuracy of each instrument (scatter in the reading) was calculated by dividing the reading with the maximum deviation from

the best-fit line by the full measuring range of the transducer (FS %). Table 4.1 lists each of the instruments used in the triaxial tests. Table 4.2 details the calculated calibration factors, accuracy, and the drift of each transducer. Details of the individual calibrations are described below, with a typical section taken from the calibration of the axial displacement transducer shown in Figure 4.1.

4.3.1 Linear variable displacement transducers (LVDT)

Two different types of LVDT were used in the research. The first type was a fixed armature LVDT with a 50mm range. This was used externally to measure the axial displacement of the specimen. The second type of transducer was a free armature submersible LVDT, of which there were 3, with a range of 25mm (+/-12.5mm). These were used to measure the on specimen radial displacement. All four LVDT's were calibrated against a Mitutoyo digital vernier accurate to 0.001mm.

It was found with both the axial and radial displacement transducers that the data was non-linear at the extremity of the transducer range (that is with the armature completely compressed). With linear regression analysis this gave a lowest R^2 value equal to 0.9961 for radial displacement transducer number 2. The accuracy of the regression was improved by limiting the radial displacement transducer calibration to a 20mm displacement rather than the full 25mm, giving an R^2 value equal to 0.9996. The accuracy of the radial transducers was calculated to be 0.5%, 0.75% and 0.68% expressed as a percentage over 20mm displacement of the transducer for radial transducers R1, R2 and R3 respectively.

Similarly for the axial displacement transducer an increase in accuracy was achieved, when calibrated over a 40mm displacement rather than the full 50mm. This led to an increase in the correlation factor from 0.9995 to 1 and an accuracy of 0.18%.

This type of correction was considered acceptable as the tests were usually stopped before these displacements were reached. Where these displacements had been passed during a test then the data was not used in the analysis.

The drift calculated for the radial displacement transducers was minimal at a maximum 0.06mm over 6 months. As this was considerably less than the accuracy of the transducers no calibration corrections were included in the analysis for the radial displacement transducers and an average calibration factor was used instead. The drift of the axial displacement transducer was minimal at less than 0.03mm over 6 months, which again was less than the accuracy of transducer. Therefore no calibration

correction was included in the analysis for the axial displacement transducer and an average calibration factor was used instead.

The average calibration factor was calculated from the three calibrations at the start, middle and end of the testing programme. The average calibration factor could be used without any perceivable loss in the accuracy of the data as the calibration factors, for each individual transducer, were similar and minimal drift was calculated.

4.3.2 Load cell

The load cell was calibrated against a 25kN proving ring. The accuracy of the load cell was 0.34% and the drift was calculated as minimal at 60N per 6 months. Therefore no calibration correction was included in the analysis for the load cell and the average calibration factor was used instead.

Towards the end of the test programme a further calibration was carried out on the load cell up to 40kN against a 100kN proving ring. This was necessary to check that the behaviour of the load cell was still linear at these higher loads as the loads applied during the monotonic load triaxial tests with a 140kPa cell pressure were passing the limits of the previous calibrations. The gradient of the regression line was only slightly different to the previous calibrations, to the third significant figure. Therefore no correction was applied to the calibration factor. The calibration curves for the load cell are shown in Figure 4.2.

4.3.3 Pressure transducer

A Budenburg air dead weight tester was used to calibrate the pressure transducer. The drift in the calibration factor was negligible at 0.16kPa per 6 months, so the average calibration factor was used.

4.3.4 Volume change unit

The volume change unit was calibrated against a GDS unit (with a step controlled motor) accurate to $1mm^3$. Due to the time required during this calibration and considering the accuracy of the GDS the volume change unit was calibrated on two fill/empty cycles using 12 incremental steps of 150ml to fill/empty the volume change unit. There was no perceivable drift in the calibrations of the volume change unit and the deviation of the maximum reading from the regression line was 14ml although it was typically less than 2ml equating to an accuracy of 0.7% over the range of the unit.

The calculated drift over a 6 month period was minimal so the average calibration factor was used.

4.4 Data correction

To improve the accuracy of the data, corrections were applied to the axial deformation, specimen cross sectional area and for bedding errors as explained in the following sections. The data from both the monotonic load and cyclic load tests was filtered, also explained below.

Corrections for the additional radial stress due to the effect of membrane restraint were derived using the correction curve and equation as suggested by Head (1992). These were found to be negligible with a correction of 0.21kPa at 6% axial strain, so the corrections were not incorporated in the analysis.

4.4.1 Axial deformation correction

As the axial strain was measured externally it was necessary to determine the effect of the deformation of the loading frame. The deformation of the loading frame was then subtracted from the total axial deformation measured, leaving the corrected specimen axial deformation.

To determine the effect of the deformation of the loading frame a concrete dummy specimen (assumed to have negligible deformation) was placed in the triaxial cell and tested under both monotonic loading and cyclic loading. Key (1998) calculated the correction value as 0.017mm/kN under both monotonic and cyclic loading and found that there was no perceptible drift in the correction value. Likewise in the current work the correction value for monotonic loading was also 0.017mm/kN, although a slightly higher value of 0.02mm/kN was calculated for the cyclic loading. For the load cell at full range that equates to 0.38mm and 0.45mm under monotonic and cyclic loading respectively, which in terms of resilient strains were significant. These corrections have therefore been included in the analysis.

4.4.2 Specimen cross sectional area correction

The varying cross sectional area of the specimen as it barrels (Section 3.3.3) was taken into account when calculating the deviator stress by using Equation 4.1.

$$q = \frac{F}{A_0} \times \left(\frac{1-\varepsilon_a}{1-\varepsilon_v} \right) \qquad \text{Equ. 4.1}$$

Where q = deviator stress (kPa),

F = piston load (kN),

A_0 = original area (m^2),

ε_a & ε_v = axial and volumetric strains.

4.4.3 Alignment correction (bedding errors)

Due to the nature of the test procedure and the size of the specimen it was difficult to achieve good alignment between the top cap and the loading piston as shown in Figure 4.3. Figure 4.4 shows a stress-strain graph with significant bedding errors, where the deviator stress formed a plateau as the axial strain increased. This was seen in varying degrees in the monotonic load triaxial tests. In some cases this plateau region lasted up to 1% axial strain (4.5mm), which although appearing to be large was less than half the depth of the ball and seat connection in the top cap (11mm). It was noted that this behaviour was usually accompanied by an increase in radial strain of one or two of the radial transducers and a decrease in radial strain of the other radial transducers. The plateau region in the stress-strain curve occurred as the top cap and the loading piston were aligned causing the specimen to move sideways. This error was corrected by removing the data in the plateau region and back calculating the initial gradient of the remaining stress-strain graph to a corrected origin. This was done by calculating the regression line (best-fit) through the initial straight portion of the stress-strain curve. The straight portion of the stress-strain curve was initially defined by eye and was only accepted once the coefficient of correlation (R^2) was better than or equal to 0.99. There was usually a minimum of 20 data points used in the derivation of the best-fit line. The new origin was defined as the point on the regression line where the deviator stress was equal to zero. The stress-strain curve was then back calculated to this point (Figure 4.5).

Although originally this behaviour was not considered to effect the post cyclic monotonic load tests as the load piston and the top cap were already aligned and in contact after the cyclic load test. It would appear, as seen in Figure 4.6 that some form of error did occur giving a lower stiffness over the initial part of the test. It was therefore necessary to carry out similar back analysis so as to calculate a more precise and repeatable stiffness value for the post cyclic monotonic load tests.

4.4.4 First load cycle correction

It was observed that the axial strains occurring during cyclic load tests were inconsistent between similarly prepared tests. It would appear that like the monotonic load triaxial

tests there were bedding errors occurring during the first cycle causing these discrepancies. When the axial strains of the first cycles were removed then the overall strains between similarly prepared tests were more consistent. Figure 4.7 shows the uncorrected axial strains compared with the corrected axial strains for three cyclic load tests carried out at 140kPa cell pressure within 14 days of each other. The minimum strain after the first cycle was 0.13%, the maximum was 2.5%, and the average was 0.92%. For consistency in analysis the axial strains for each cyclic load test were corrected by subtracting the measurements of the first cycle.

4.4.5 Smoothed data – cyclic load tests

The continuous movement of all the transducers during each cycle in a cyclic test meant that the data recorded during the cyclic load tests was not easy to analyse or compare with other tests. This can be seen in Figure 4.8a, which was taken from a section of a volumetric strain graph. The data was therefore smoothed to allow the general behaviour of the specimen throughout the test to be more easily reviewed and for better comparison between the different tests. In each cyclic load test a smoothed line was calculated through the trough of each load cycle (at unload). The data for the complete test with the smoothed curve can be seen in Figure 4.8b. The data for the trough of each load cycle was calculated by averaging the stresses (and strains) over the last ten data points (0.25 sec) before the specimen was reloaded. This smoothing process was carried out on all of the parameters, that is the axial strain, three radial strains, two volumetric strains (recorded with the volume change unit and calculated assuming the specimen remained a right-angle cylinder), two deviator stresses calculated using the two volumetric strains, the normal effective stress, the void ratio and the specific volume.

4.4.6 Filtered data – monotonic load tests

Key (1998) commented that his monotonic load test results were not showing smooth curves like those of other authors; likewise in this project the stress-strain curves had spikes, possibly representing 'stick-slip' phenomena or aggregate breakage. Kohata et al (1999) also showed this behaviour in his work. It was therefore presumed that where this 'stick-slip' phenomena had not been shown it was because the data had been filtered, or some form of smooth curve had been fitted. A smooth curve was not fitted to the data in this research, because the 'stick-slip' behaviour was considered to be important in the analysis of the results. It was decided however that a form of filtering

would be applied. A nine point averaging filter was applied to both the axial strain and the deviator stress. This filter length was chosen because during a monotonic load test the data was recorded every second, yet the specimen was only loaded at 0.016mm/sec (or per data reading). However the accuracy of the transducer was only 0.15mm, which meant that nine readings occurred within the range of the accuracy of the transducer (0.15/0.016 = 9.4 seconds, one data reading per second). The axial displacement transducer accuracy of 0.15mm was as calculated at the time the decision was made, and not 0.18mm as calculated after further calibrations and as shown in Table 4.2. Figure 4.9a shows a portion of the unfiltered stress-strain curve from test T27. Figure 4.9b shows the filtered curve. From this it can be seen that the extremities of the 'stick-slip' behaviour have been limited. It was therefore argued that this filtering process 'cleaned up' the data although some of the details of 'stick-slip' behaviour may have been lost.

4.5 Initial analysis

In this section an overview of the whole process of the initial analysis of the data will be described, including the calibrations, corrections and processes described earlier in this chapter. The data from each test was run through a Visual Basic for Applications macro (VBA in Excel) (Section 4.2). To run the macro a specimen text file for each specimen was created containing all the information about that specific specimen and test, as seen in Figure 4.10. This text file contained information on the mass of the specimen, the height of the specimen, the cell pressure and the type of test that was run, plus any further comments that were made regarding the test. It was also possible to input data regarding the post cyclic specimen, for specimens where a post cyclic monotonic load test was carried out. A flow diagram of the process is shown in Figure 4.11. After opening the relevant files the macro calculated the density, the void ratio and the porosity of the specimen. The macro was pre-programmed with the value of the specific gravity due to the material size entered in the text file. If, in the case of the layered specimens, the macro was not programmed with a value of specific gravity then it would prompt the user to enter a value during the running of the program. The macro then applied the calibrations, that is the average calibration factor for each transducer, to the raw data and corrected the displacements. Corrections for the apparent 'compression' of the specimen however, were not included as discussed in Section 3.3.4.

After the calibrations and corrections had been applied to the raw data the axial, radial and volumetric strains were calculated as were the deviator stress (with the cross-sectional area correction), the normal effective stress, the void ratio and the specific volume. The volume strains were calculated both directly from the volume change unit measurements and also by using the radial and axial strains, assuming the specimen remained a right-angled cylinder throughout the test. Using the two different volumetric strains, two deviator stresses were calculated to allow a comparison to be made between the two methods. For each recorded data point the normal effective stress, the void ratio and the specific volume were all calculated. For the cyclic load tests the data was smoothed (Section 4.4.5) and for the monotonic load tests the axial strains and deviator stresses were filtered (Section 4.4.6).

For each test a selection of graphs were plotted. For the monotonic load tests these were deviator stress versus axial strain (q vs. ε_a), radial and volumetric strains versus axial strain (ε_r, ε_v vs. ε_a), and void ratio versus axial strain (e vs. ε_a) (see Figure 4.12). Further graphs included the stress path (q vs. p'), the specific volume (v vs. ε_a) and the cell pressure throughout the test. Similarly for the cyclic load tests the axial strain versus number of cycles (ε_a vs N), deviator stress versus axial strain (q vs. ε_a), radial and volumetric strains versus axial strain (ε_r, ε_v vs. ε_a), and the volumetric strain versus the number of cycles (ε_v vs. N) with a repeat graph on a log scale (see Figure 4.13). Further graphs again included the stress path, the void ratio, the specific volume and the cell pressure throughout the test.

After the macro was applied to the results of each test the first load cycle correction for a cyclic load test was carried out and, if necessary, for the monotonic load test any bedding errors were corrected.

For each cyclic load test the average resilient modulus at 100, 1000, 10,000 and 100,000 cycles was calculated with the use of the macro. The average resilient modulus at cycle 100 was calculated as the average resilient modulus, for cycles 50 to 150, where the resilient modulus for each individual cycle was calculated as the change in stress divided by the change of strain on the unloading of the specimen as shown in Equation 4.2.

$$M_r = \frac{\Delta q}{\Delta \varepsilon_a} \qquad \text{Equ. 4.2}$$

This process was also used to calculate the average resilient modulus at cycles 1000, 10,000 and 100,000 over the ranges specified in Section 4.2.

For the post cyclic monotonic load tests the density was calculated using the original mass and the volume of the specimen at the end of the cyclic load test. The data was then analysed in the same way as a normal monotonic load test.

4.6 Specimen Characterisation

4.6.1 Specimen stiffness – monotonic load tests

The stiffness of the specimen was recorded using two different methods. The first was the tangent modulus, E_t, which was calculated by linear regression analysis (best fit line) through the initial straight portion of the curve, i.e. the tangent of the curve through / at the origin (Figure 4.14). For consistency a coefficient of correlation (R^2) better than 0.99 was required. There was usually a minimum of 20 data points used in the derivation of the best-fit line.

The second method was the Young's modulus taken at a deviator stress of 250kPa. 250kPa is a significant stress as this was the peak deviator stress used in the cyclic load tests. Although not strictly a secant modulus, the Young's modulus in this project is defined as the secant modulus, E_s, which is also shown in Figure 4.14.

4.6.2 Average peak deviator stress

The peak deviator stress in the monotonic load tests was not easily defined due to constant fluctuation in the deviator stress as discussed in Section 4.4.6. Therefore the peak deviator stress had to be an averaged value taking into account the data values recorded close to the strain at which the peak stresses occurred. In this project it was decided that the peak stress was to be interpreted 'by eye' and the average peak stress was then calculated as the average stress over the 0.5% strain centred about the specific point. The same process was also used to derive any stresses that have been quoted in this project. However the peak stress was not always reached in all of the tests and therefore, in such tests, the average peak stress was calculated as the average peak stress over the final 0.25% axial strain of the test.

For the post cyclic monotonic load tests the same process was used as described above, except where there was a specific peak during the early stage of the test. The peak stress at this point was the peak stress used in the analysis. No ultimate stress was reached due to the bulging of the specimen and the limits of the radial transducers.

4.6.3 Angle of shearing resistance

For each individual test the angle of shearing resistance (φ') was calculated using the Mohr-Coulomb failure criteria as defined in Equation 4.3.

$$\sin\varphi' = \left(\frac{\sigma_1 - \sigma_3}{\sigma_1 + \sigma_3}\right) \qquad \text{Equ. 4.3}$$

where: σ_1 and σ_3 = principal stresses.

This assumes a c' value equal to 0, i.e. no cohesion, which is perfectly acceptable with granular material. The Mohr-Coulomb failure envelope was used to determine the angle of shearing resistance for the material as a whole across a range of different cell pressures.

Type of instrument	No. of instruments	Measuring range	Manufacturer's claimed accuracy	Parameter measured
Fixed armature LVDT (S/N HS 50/7069)	1	0-50mm 40mm used range	0.5% F.S. Manufacturer - MPE	Specimen axial deformation
Free armature immersible LVDT (D5/500W/72)	3	+/- 12.5mm 20mm used range	0.5% F.S. Manufacturer - RDP	Specimen radial deformation
Immersible fatigue rated load cell (S/N 491338)	1	0-22.5kN (normal) (0-50kN maximum)	0.1% F.S. (hysterysis) 0.1% F.S. (non linearity) Manufacturer - RDP	Applied axial load
Pressure transducer (S/N 790495)	1	0-100kPa	0.1% F.S. Manufacturer - CE	Cell pressure
Magnetic resonance transducer (Temposonics R Series, Analog)	1	0-500mm (0-1650ml)	0.02% F.S. Manufacturer - RDP	Cell fluid volume change

% F.S.= % Full scale of instrument

Table 4.1 List of instruments used in the tests

Type of Instrument	Average calibration factor	Recorded accuracy (% F.S.)	Coefficient of correlation (R^2)	Average drift
Axial LVDT	200.9mV/mm	0.18	1	minimal @ 0.03mm/6 months
Radial LVDT 1 (No. 3195)	79.4mV/mm	0.50	1	minimal @ 0.05mm/6 months
Radial LVDT 2 (No. 3197)	78.3mV/mm	0.75	0.9996 - 1	minimal @ 0.06mm/6 months
Radial LVDT 3 (No. 3196)	76.8mV/mm	0.68	0.9999 - 1	minimal @ 0.06mm/6 months
Load cell	324.3mV/kN	0.34	1	minimal @ 60N/6 months
Pressure transducer	91.3mV/kPa	0.24	0.9999 - 1	minimal @ 0.16kPa/6 months
Volume change unit*	187.1V/ml	0.70	1	negligible

*Note the magnetic resonance transducer is only part of the volume change unit

% F.S.= % Full scale of instrument

Table 4.2 - Instrument calibrations, accuracies and drifts

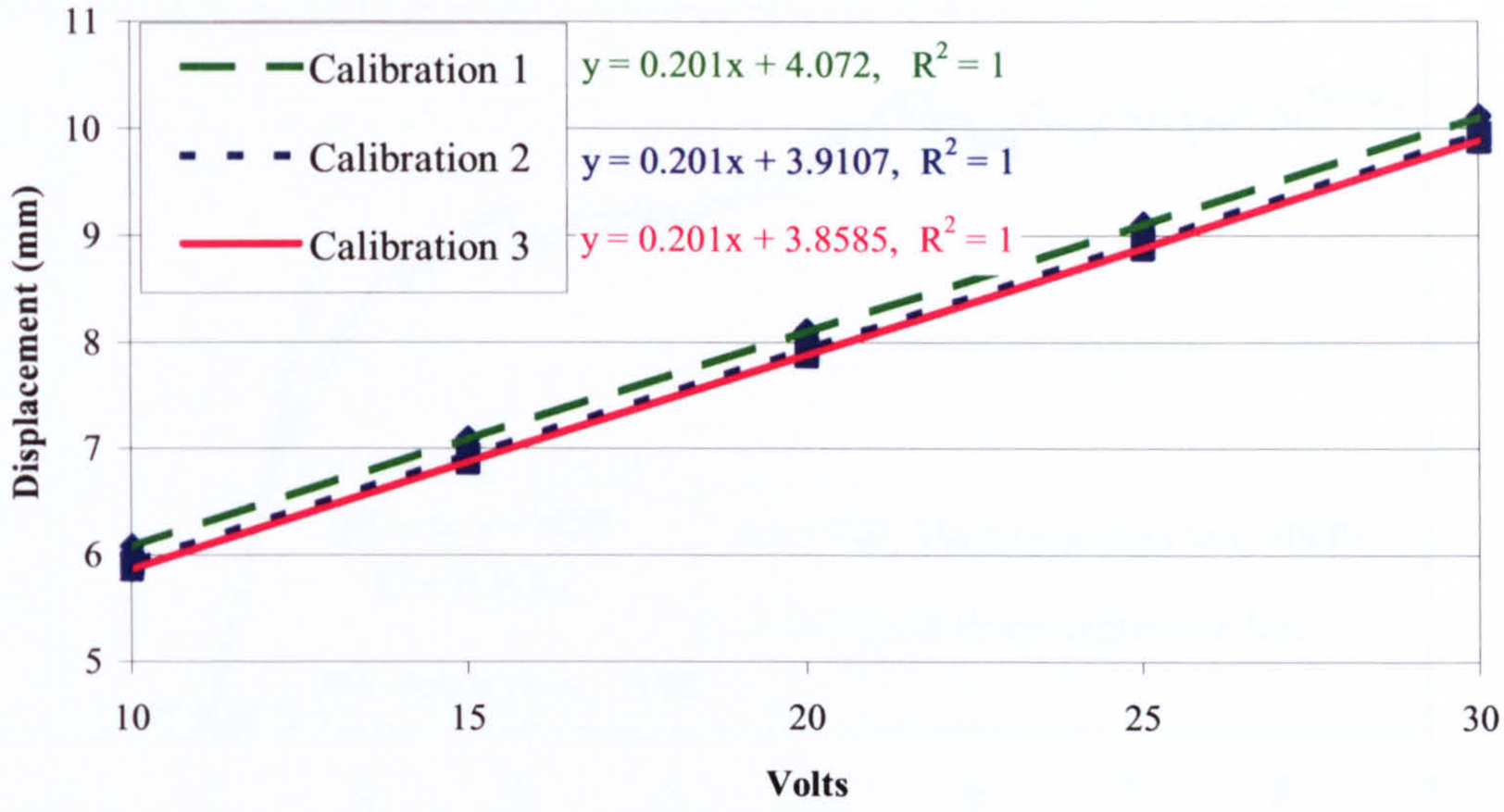

Figure 4.1 - Calibrations curves; section from the axial displacement calibration

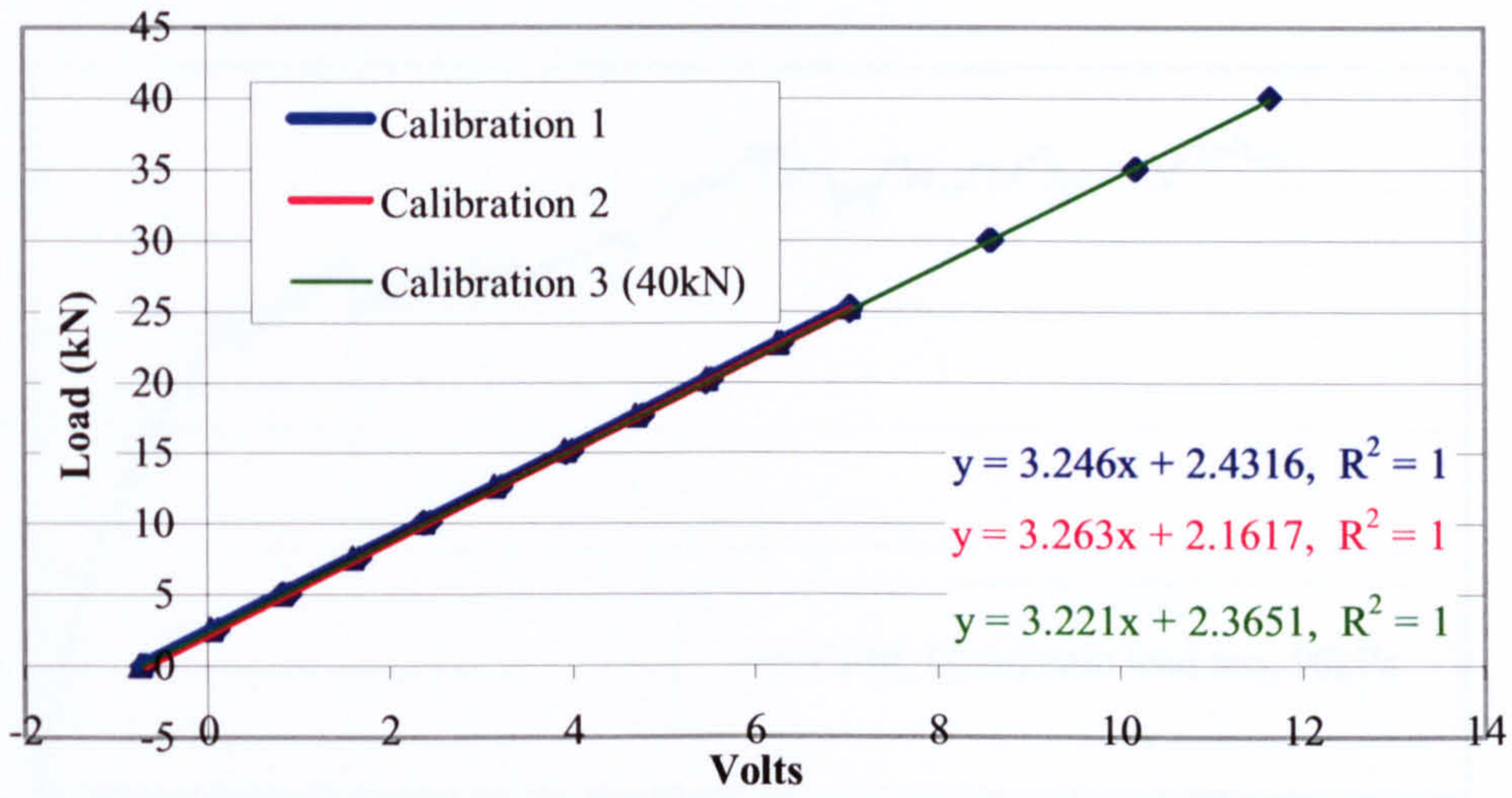

Figure 4.2 - Calibrations curves; full calibration for the load cell

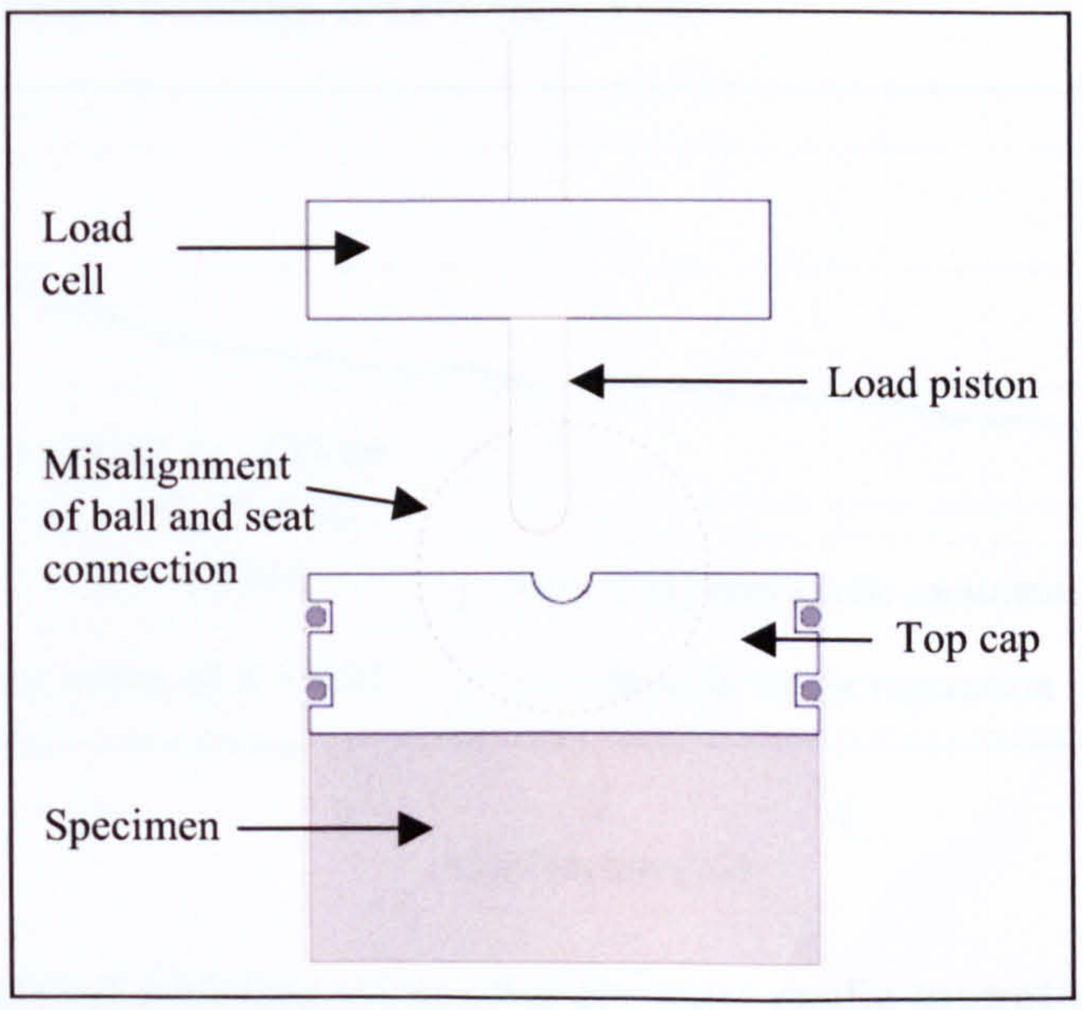

Figure 4.3 - Misalignment of the top cap

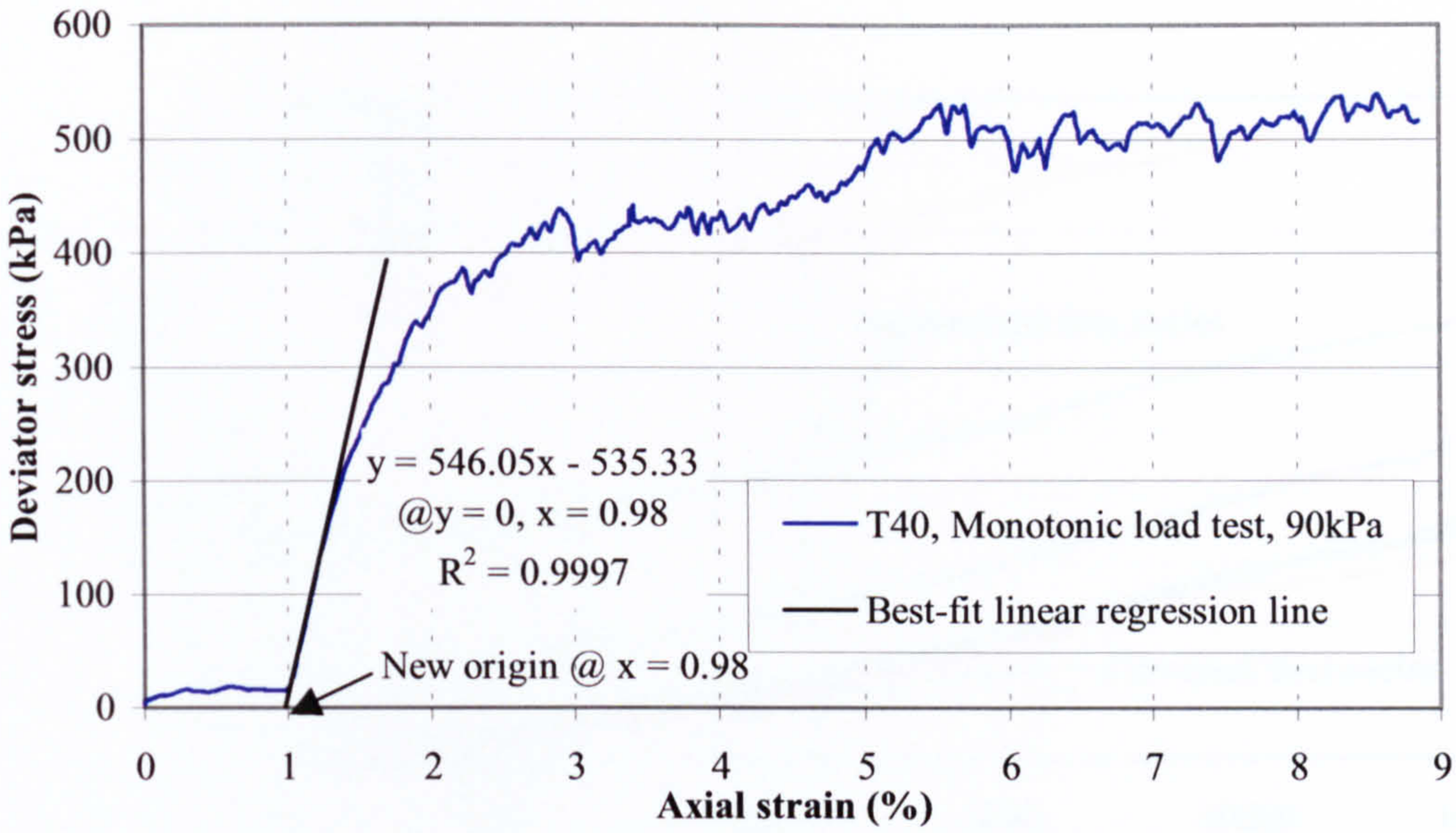

Figure 4.4 - Top cap alignment bedding errors (test T40)

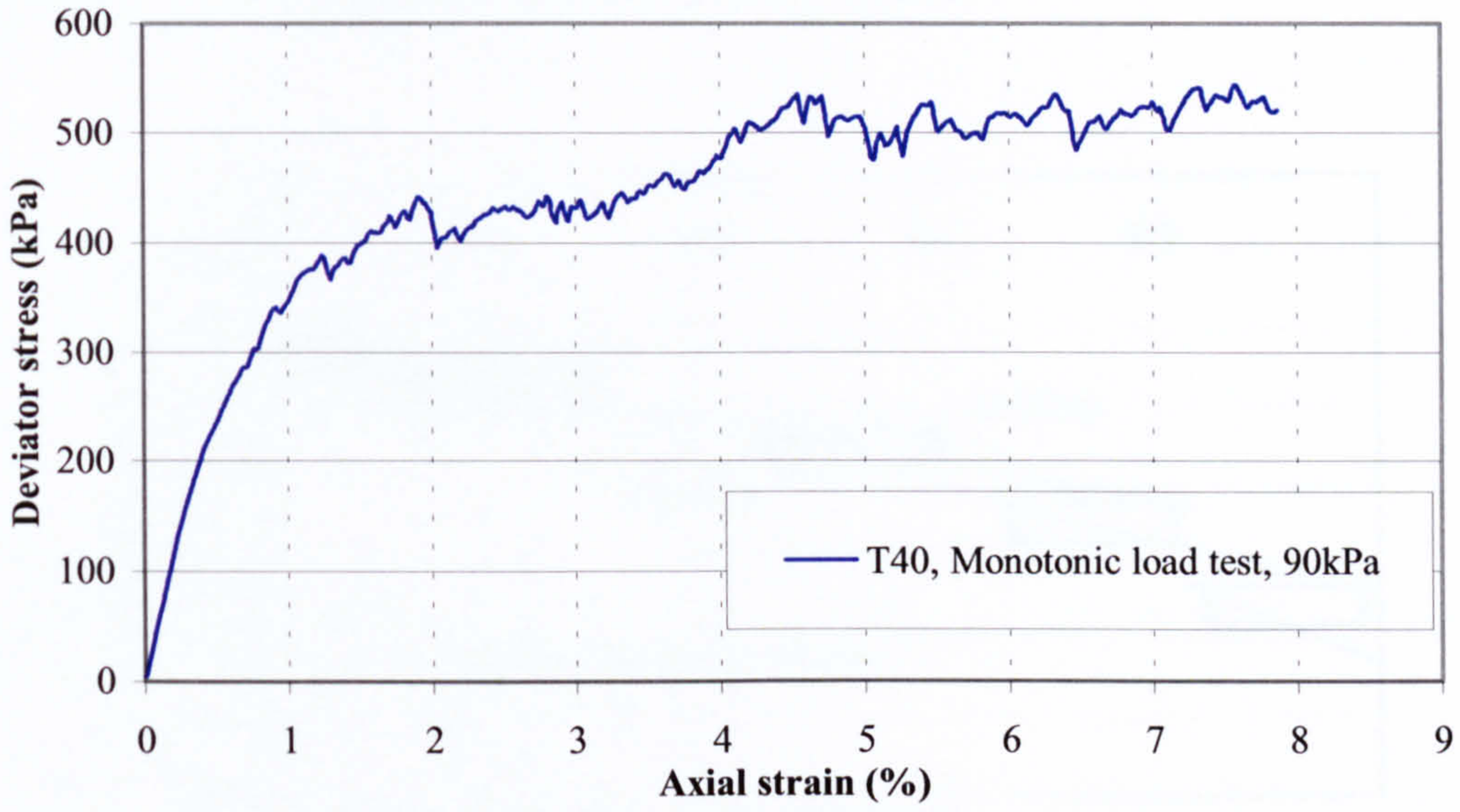

Figure 4.5 - Corrected bedding errors (test T40)

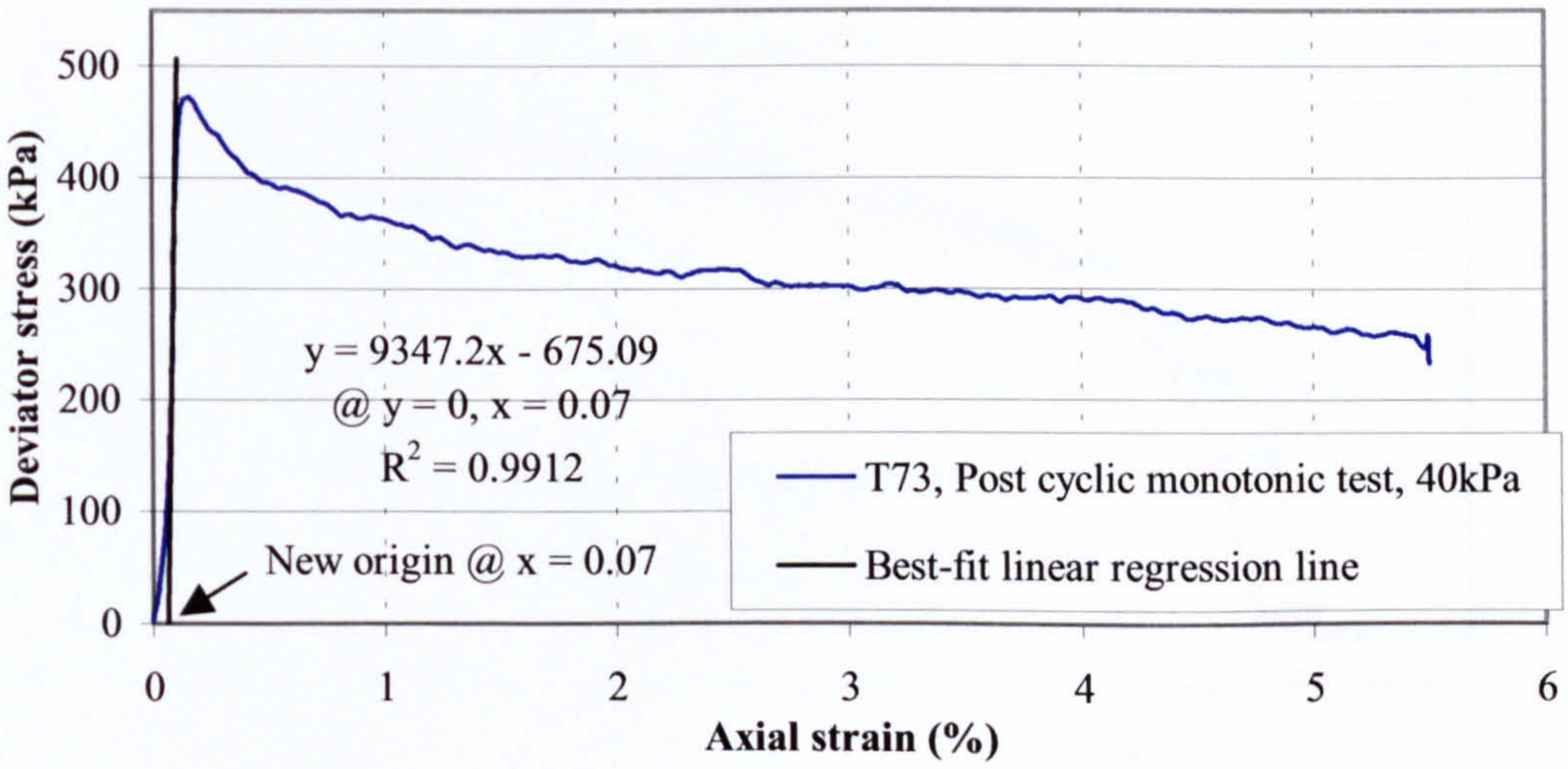

Figure 4.6 - Corrected bedding errors for the post cyclic monotonic load test (T73)

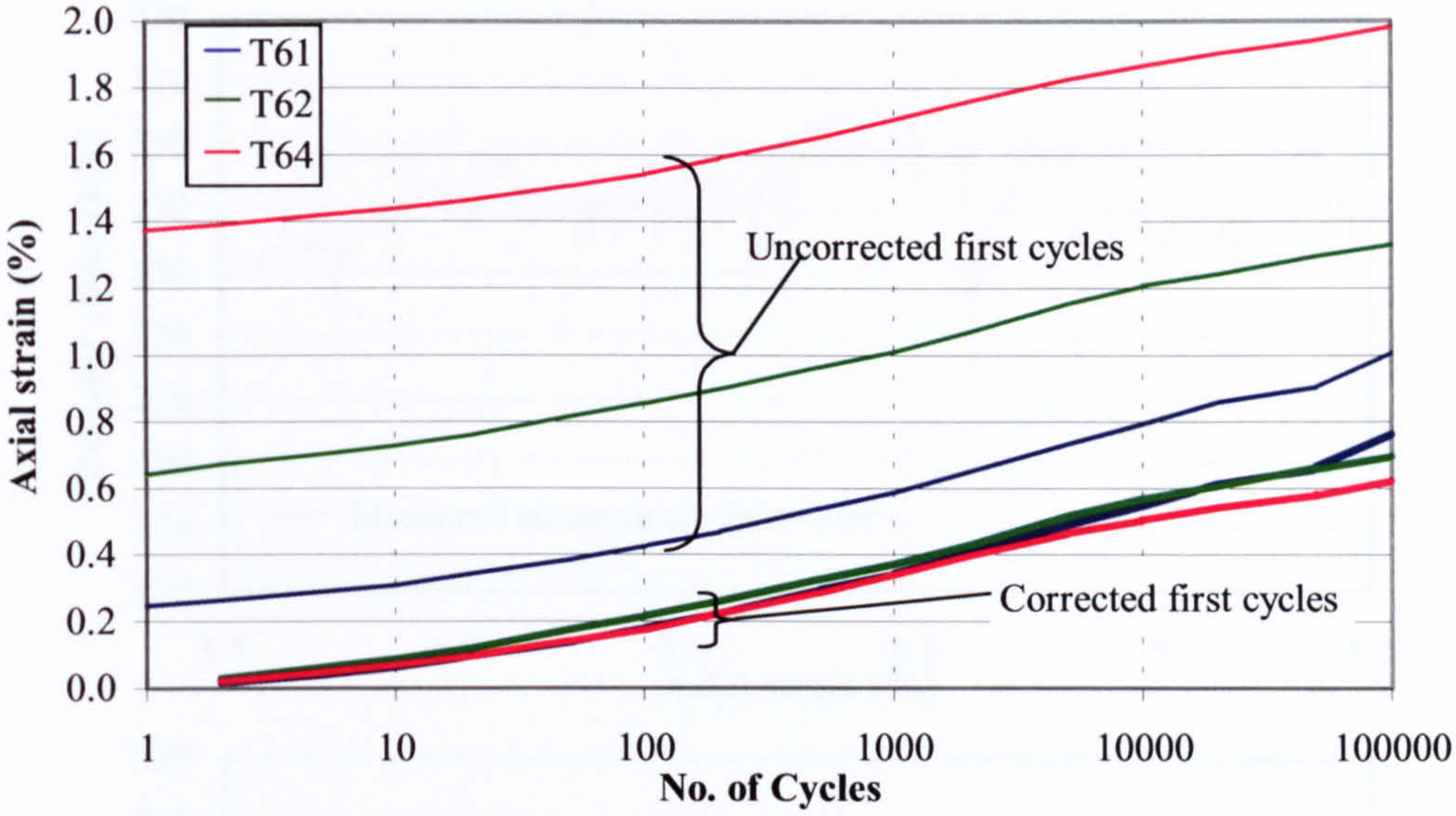

Figure 4.7 - First load cycle axial strain correction

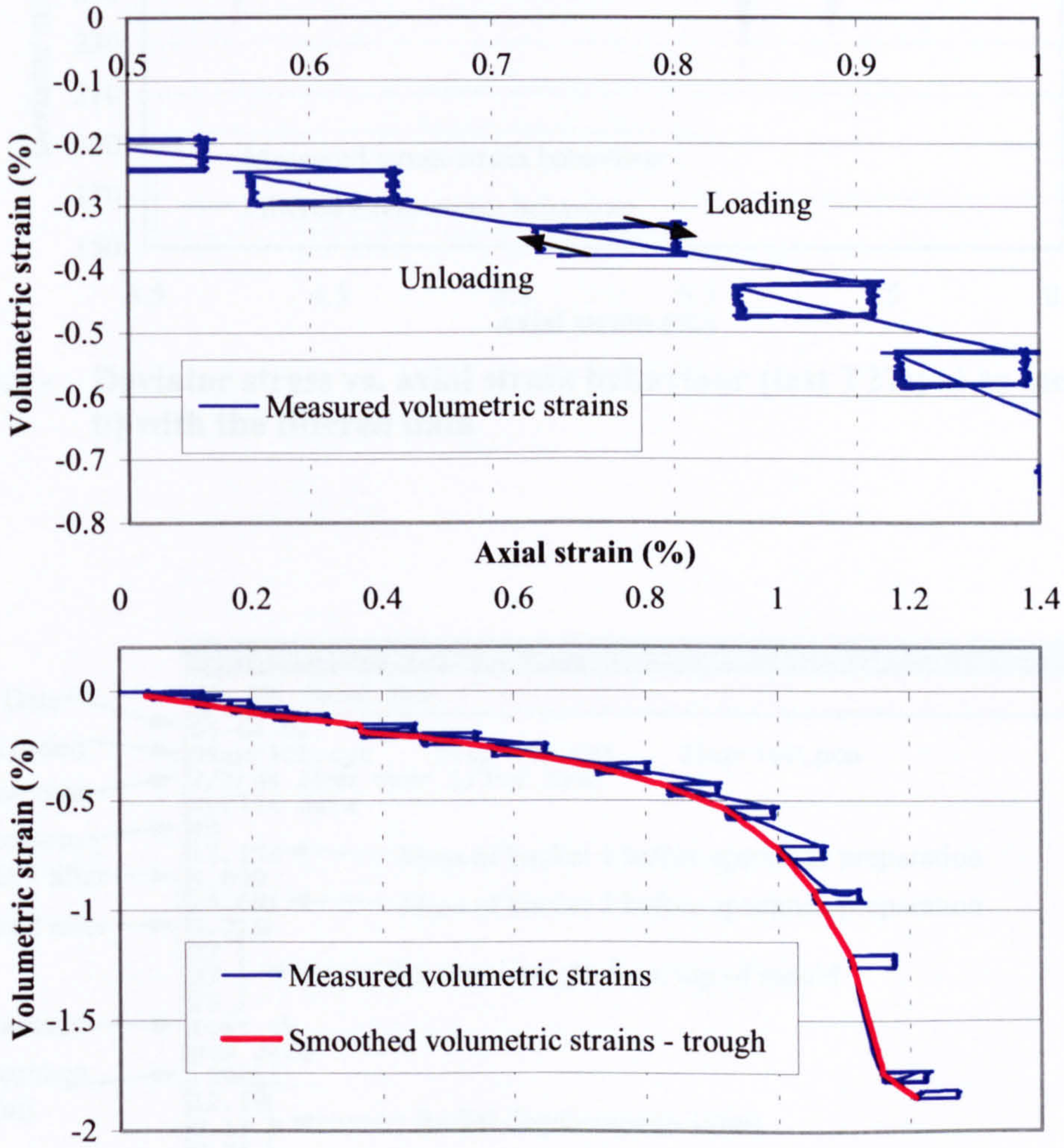

Figure 4.8 - Volumetric strain data (test T36); a) as measured, b) data smoothed

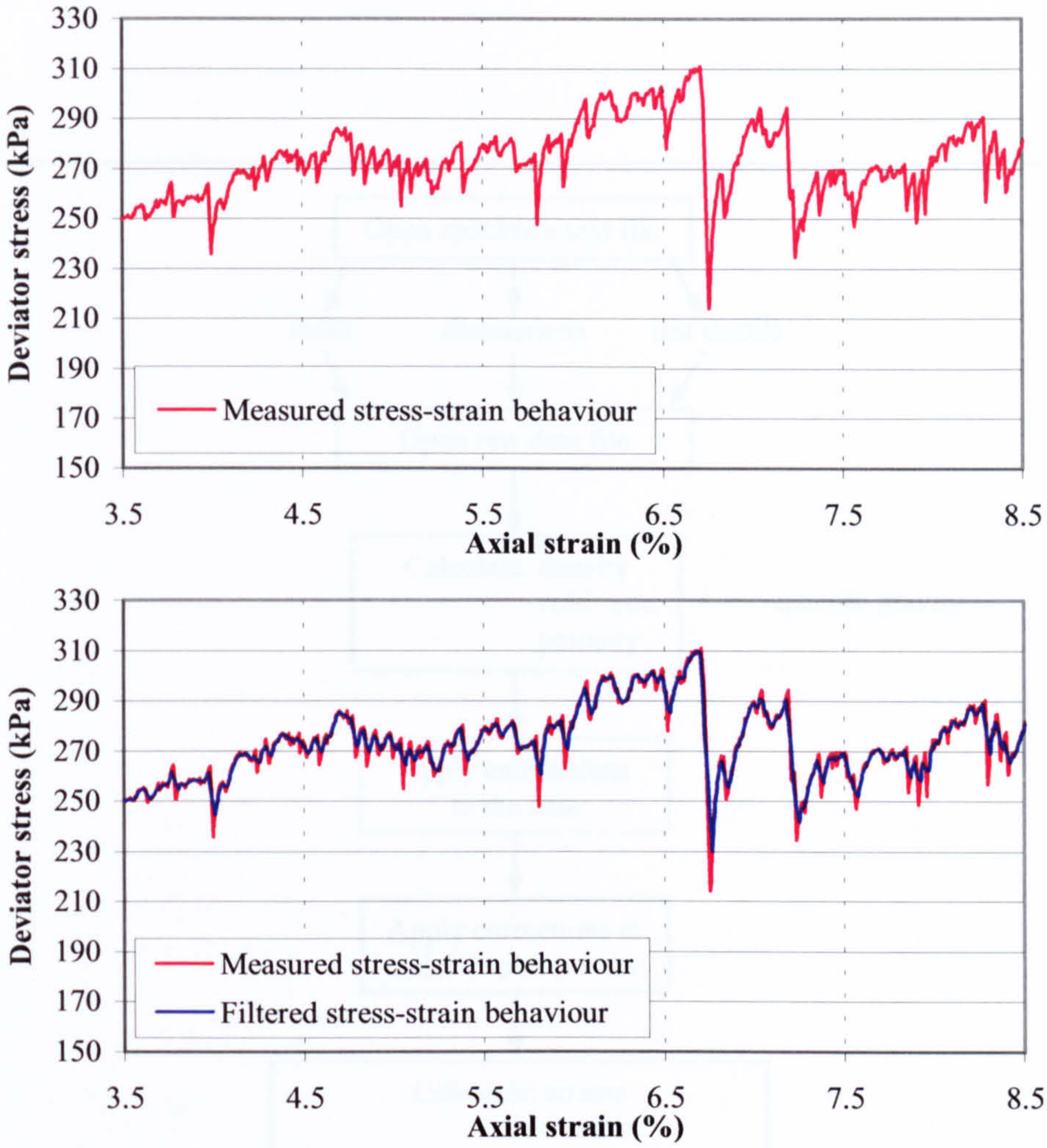

Figure 4.9 - Deviator stress vs. axial strain behaviour (test T27); a) as measured, b) with the filtered data

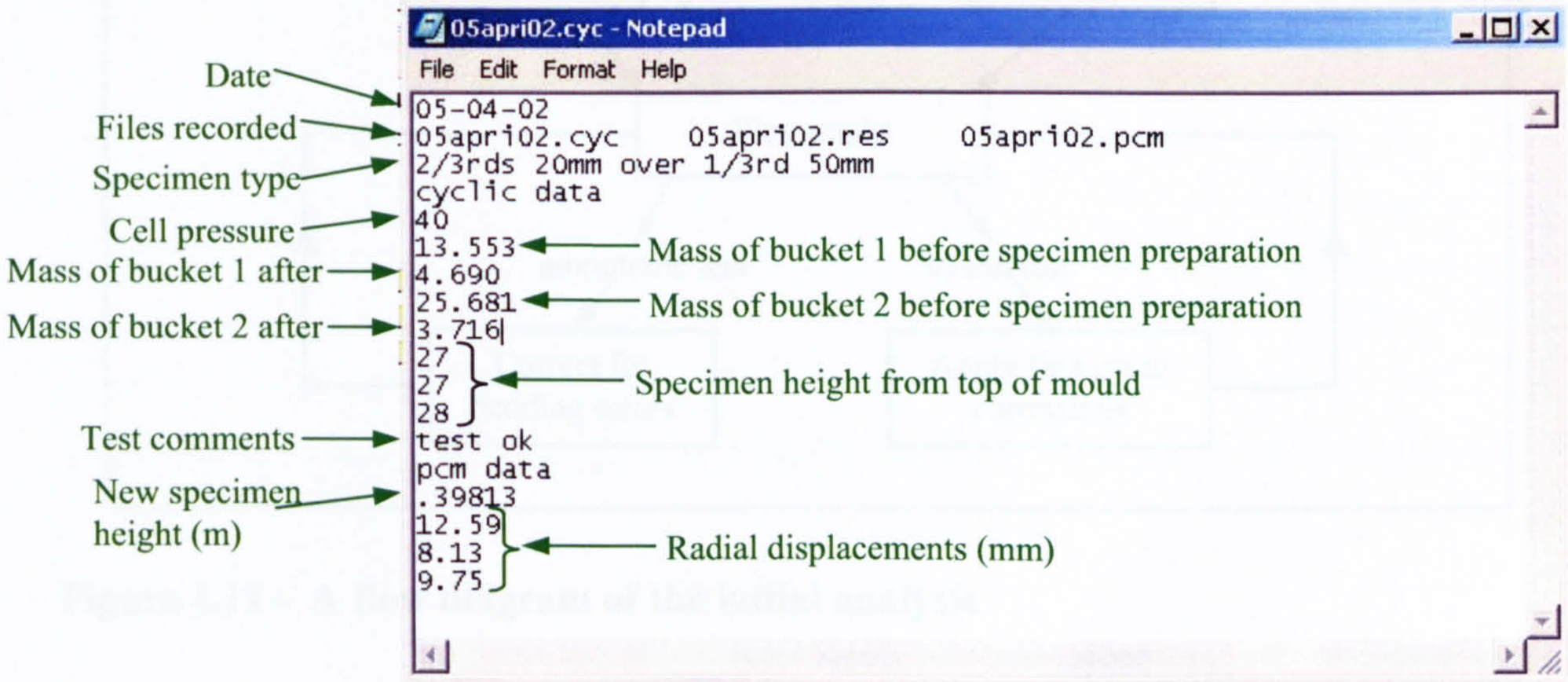

Figure 4.10 - Specimen text file (test T47)

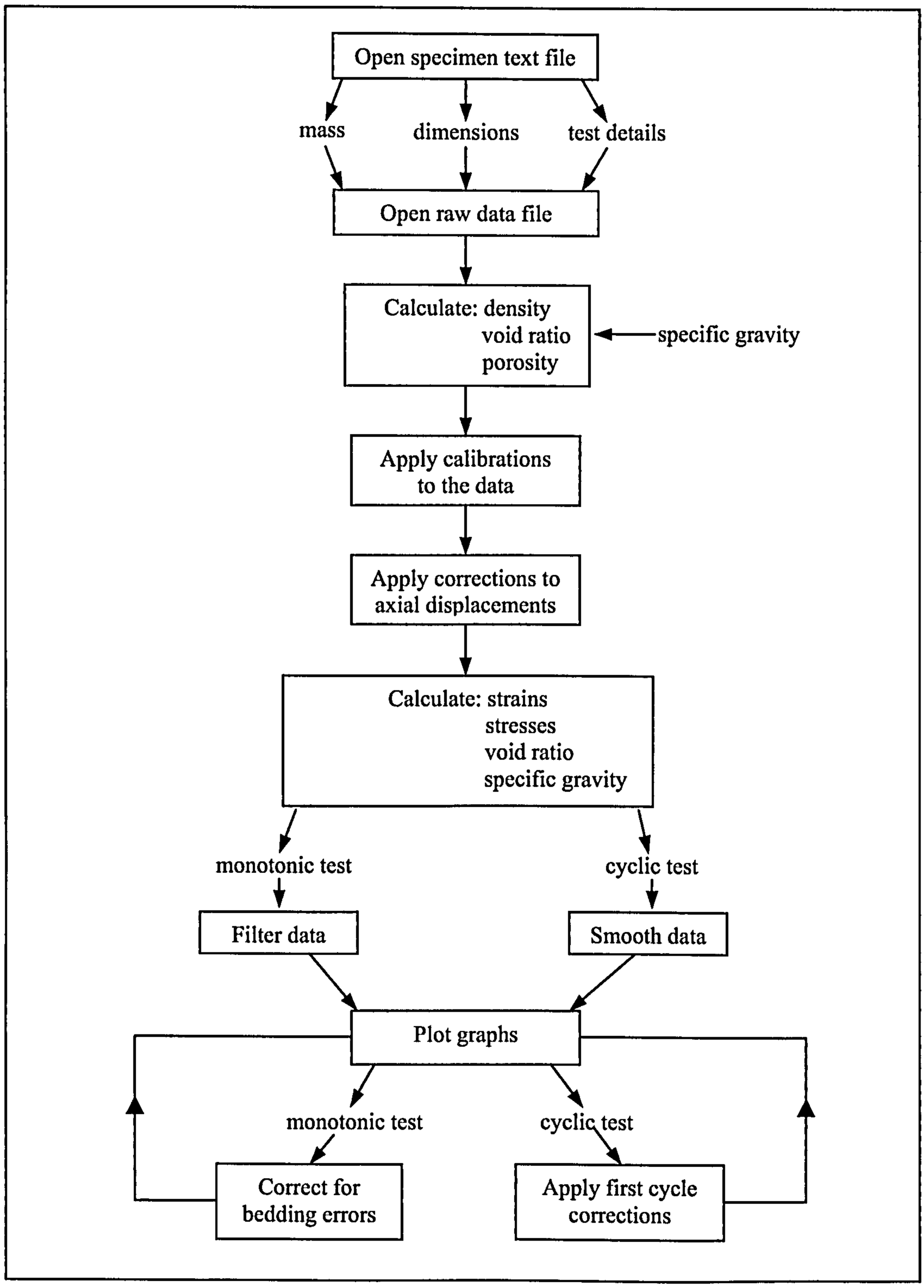

Figure 4.11 - A flow diagram of the initial analysis

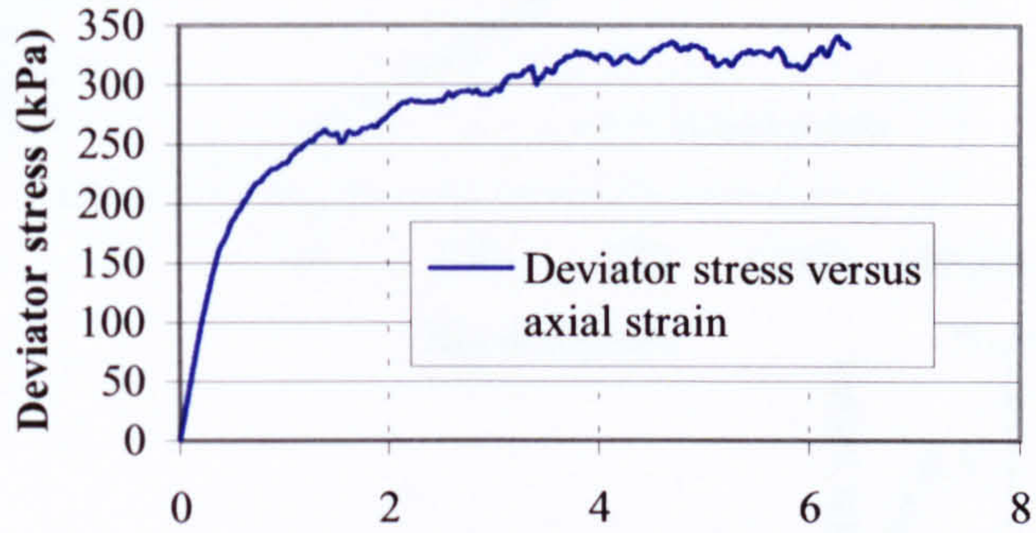

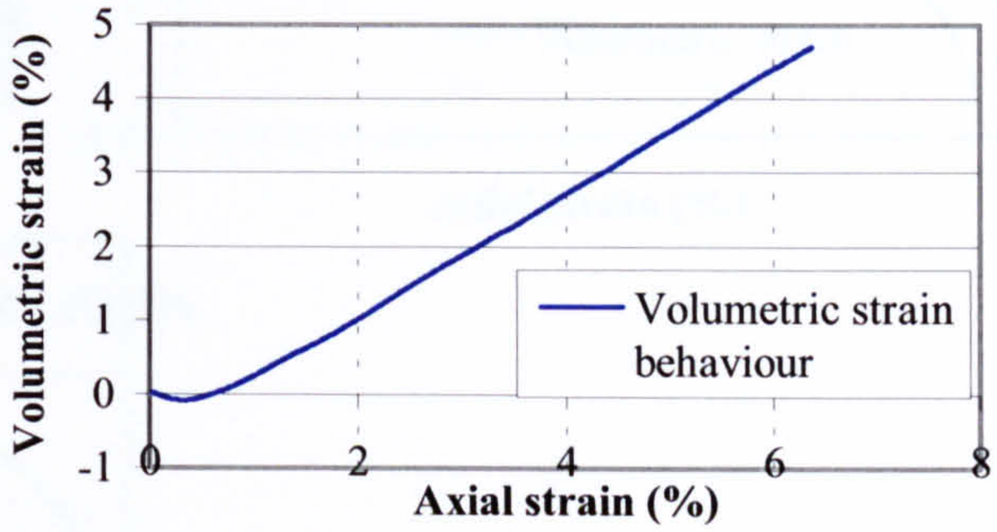

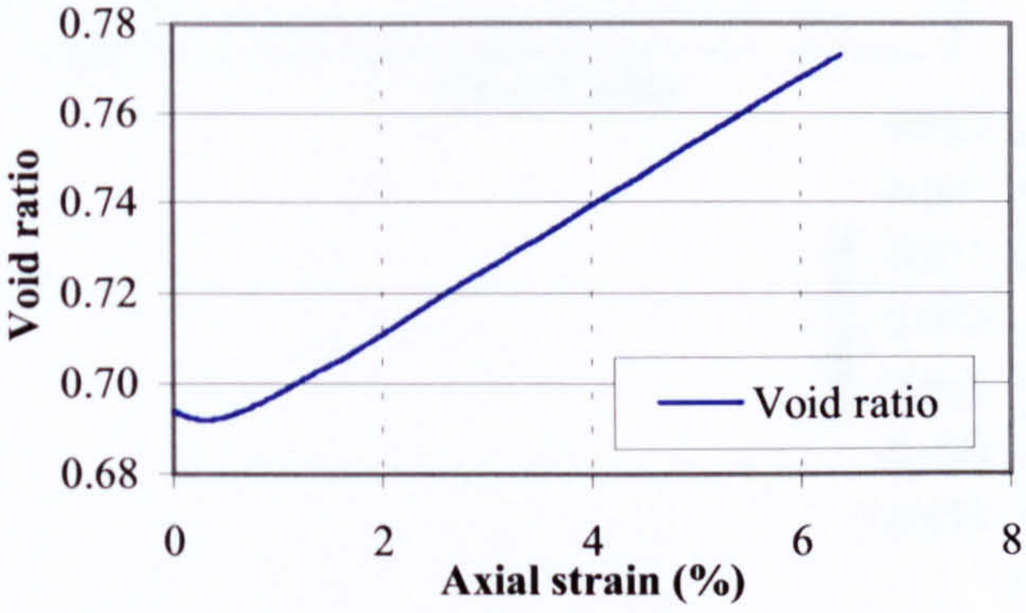

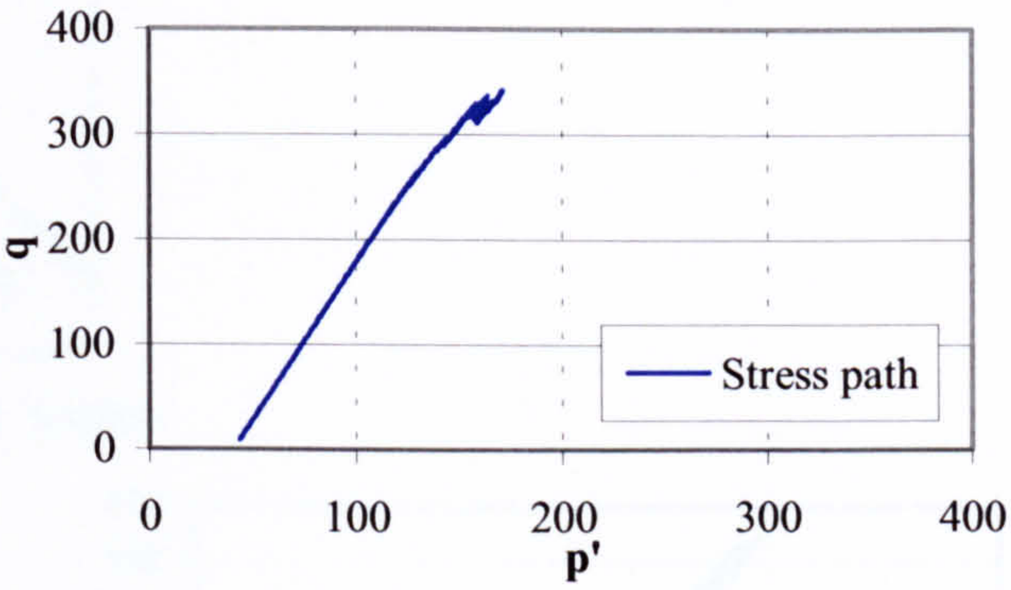

Figure 4.12 - Selection of graphs used in the analysis of the monotonic load tests (test T44)

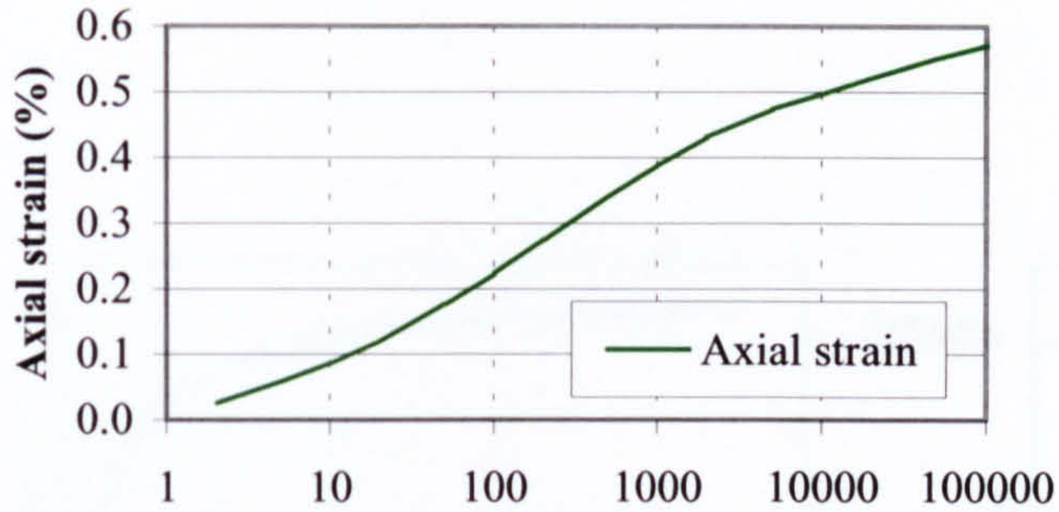

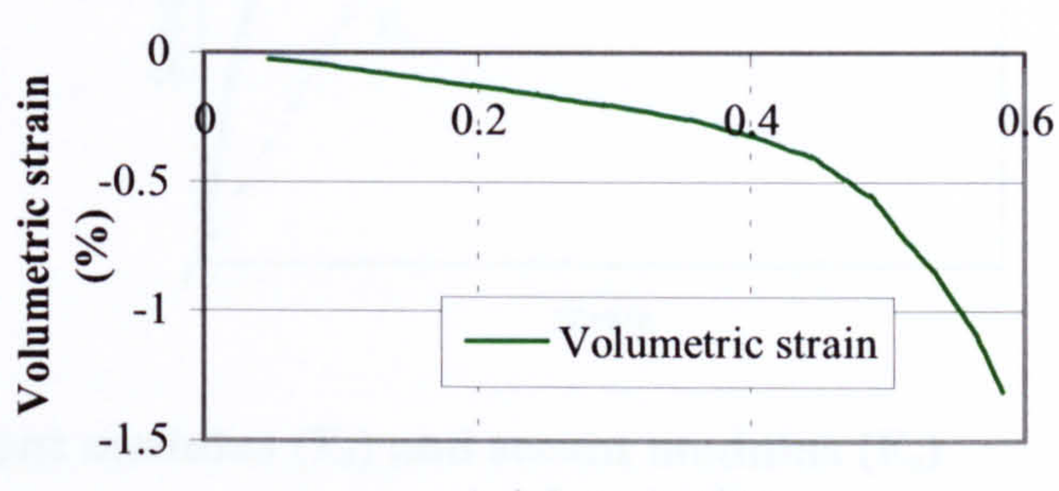

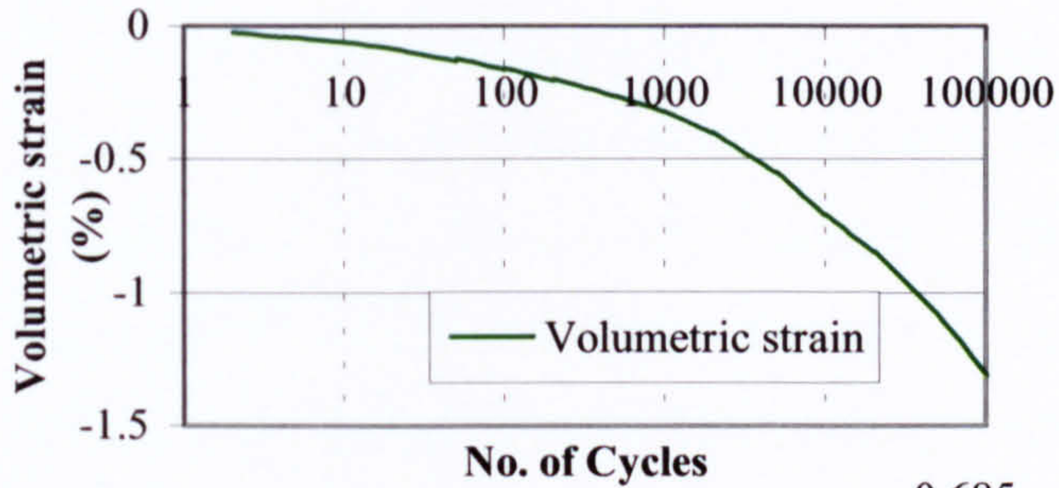

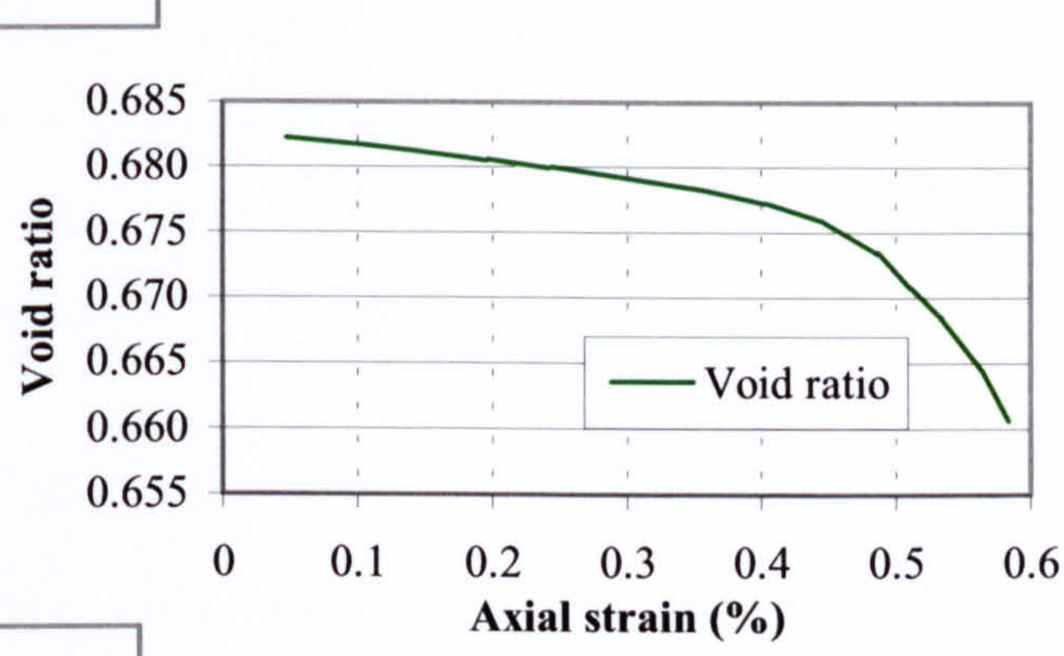

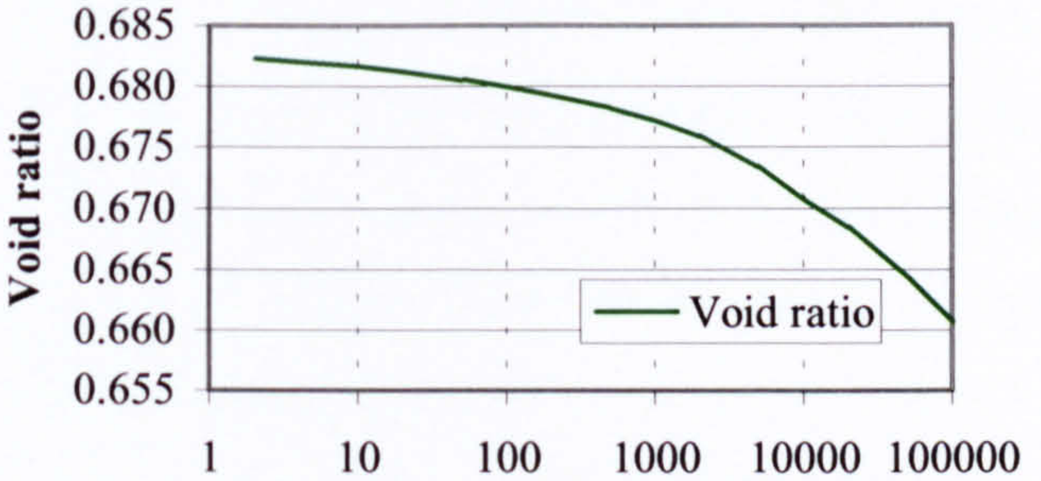

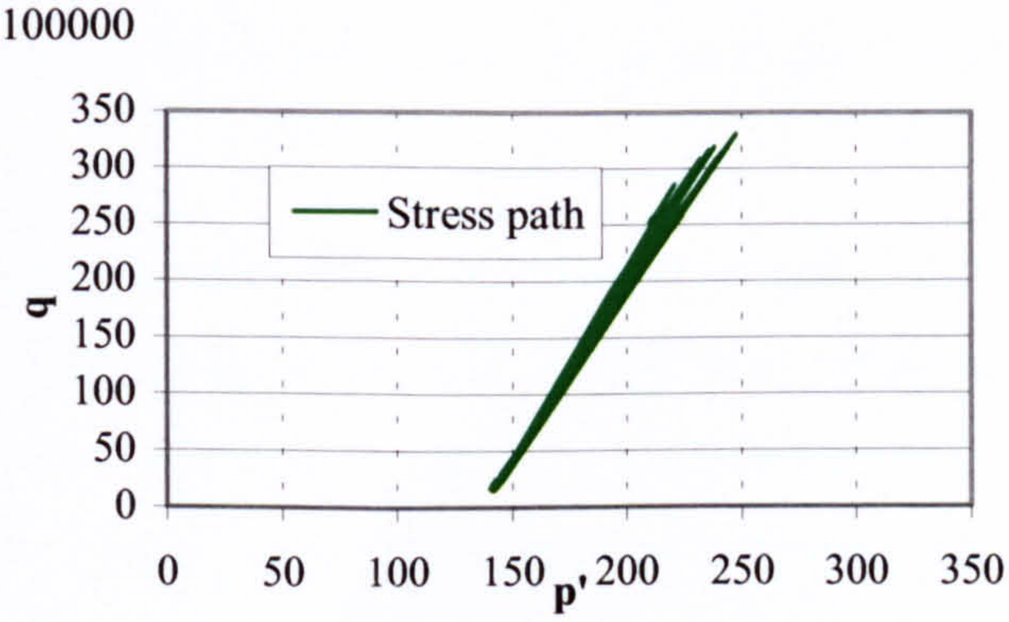

Figure 4.13 - Selection of graphs used in the analysis of the cyclic load test (T68)

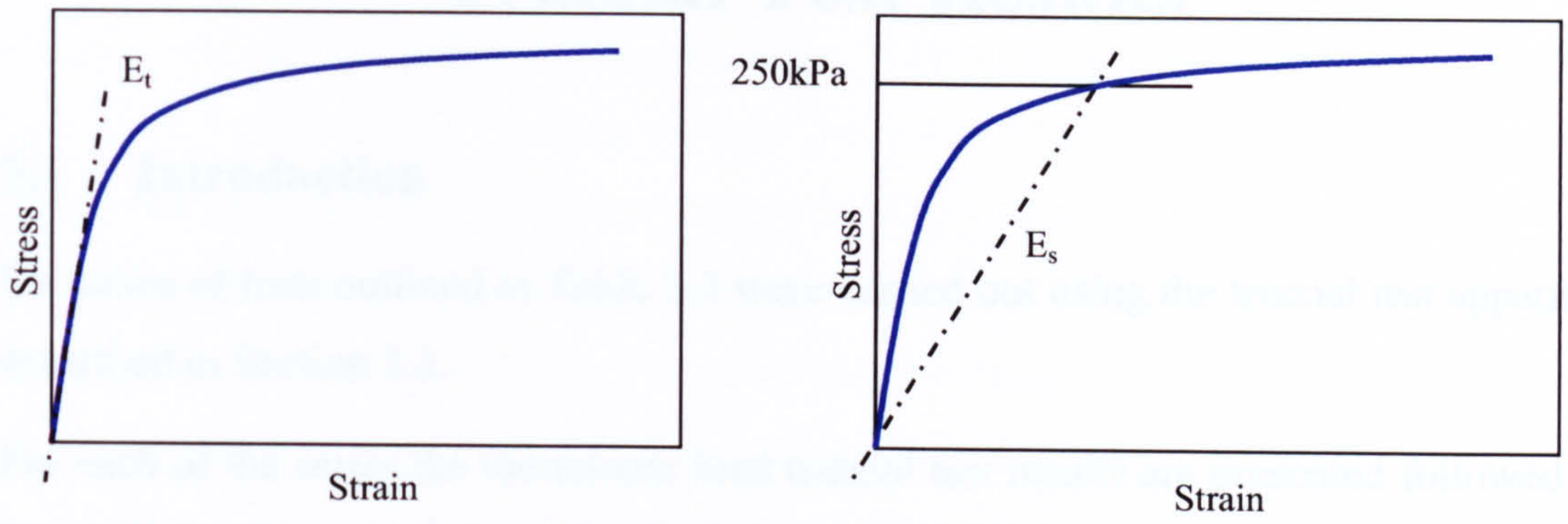

Figure 4.14 - Definitions of the tangent modulus (E_t) and secant modulus (E_s)

CHAPTER 5

Triaxial Test Results

5.1 Introduction

Six series of tests outlined in Table 3.2 were carried out using the triaxial test apparatus described in Section 3.3.

For each of the series the monotonic load triaxial test results are presented followed by the cyclic load test results and finally the post cyclic monotonic load triaxial test results. Each set of results is split into the following two sections, (i) stress-strain behaviour or axial strain behaviour for monotonic or cyclic load tests and (ii) volumetric strain behaviour. After these have been considered for each loading type the shear strength characteristics (c' and φ') are reported. The resilient modulus results calculated throughout the cyclic load tests are reviewed separately towards the end of this chapter (Section 5.8). Analysis of particle breakage occurring in the triaxial tests is reported in Chapter 6 along with the results from the single particle crushing tests. A discussion for all of the laboratory work, followed by the conclusions drawn from this are presented in Chapter 7. All the results from all the tests have been included on Disk 2.

5.2 Series 1 – 20mm stone specimens

Tables 5.1 and 5.2 outline details of the triaxial test conditions and specimen details tested in Series 1 for the monotonic, cyclic and post cyclic monotonic load tests. The results from each test are also given in these tables along with a comments column for any specific points regarding the test. The objectives of Series 1 were to assess the general characteristics of the materials, and to compare the 20mm Bardon stone and the 20mm Cloburn stone so as to decide whether to include the Cloburn stone in the rest of the test programme.

Towards the end of Series 1 the importance of measuring the volume change more accurately was realised; furthermore a vast amount of data on particle breakage occurring during the tests had up to this point not been recorded. Therefore Series 1 was curtailed to allow a reliable volume change unit and a way of gathering and recording particle breakage data to be developed. Series 1 therefore focused entirely on the difference in behaviour between the two 20mm aggregates (Table 3.3).

5.2.1 Specimen preparation

Fifteen 20mm stone specimens were prepared and tested during Series 1. Seven were with Bardon stone and eight with Cloburn stone. Table 5.3 gives details of the densities of the material recorded for each test series where relevant and also the details taken from Key's (1998) work. It can be seen for Series 1 that the average density of the 20mm Bardon stone was close to that found by Key, although the range was larger. The Cloburn stone specimens had an average density significantly less than the Bardon stone, with the range of densities being considerably larger.

The average of the void ratios given in Table 5.1, were only slightly higher for the Bardon stone than the Cloburn stone. As the particle shape and the grading for the two aggregates were similar it was anticipated that their void ratios would also have been similar. The similarity between the void ratios implies that there was consistency in the specimen preparation between the two different materials.

5.2.2 Monotonic load triaxial tests

Nine monotonic load tests have been carried out in Series 1, four using Bardon stone specimens and five using Cloburn stone specimens.

5.2.2.1 Deviator stress-strain behaviour

Figure 5.1 shows the deviator stress versus axial strain graphs for two similar Bardon stone and two similar Cloburn stone specimens with a cell pressure of 40kPa. The overall stress-strain behaviour between the two Bardon stone tests was similar although specimen T14 had a higher tangent modulus, E_t, which was the modulus of the tangent at zero percent strain (defined in Section 4.6.1). The modulus values from all the tests in Series 1 can be found in Table 5.1. The secant modulus, E_s was also higher for specimen T14 than specimen T5. E_s was the modulus value taken at 250kPa stress, which was the maximum cyclic stress (defined in Section 4.6.1). The average peak deviator stresses, as defined in Section 4.6.2, for the two tests were similar at approximately 375kPa and occurred in both tests at axial strains of 5.5% - 6%.

For the Cloburn stone tests, specimen T1, although having had a significantly higher initial modulus, E_t, had an E_s value $1/3^{rd}$ that of specimen T6. This implies that it would have had a much lower resistance to plastic straining were it in a cyclic load test.

It can be seen from Figure 5.1 that the Cloburn stone specimens were initially stiffer than the Bardon stone specimens. However, after about 0.2% - 0.3% axial strain the Cloburn stone specimens appear to have yielded and deformed at a lower average peak

deviator stress than the Bardon stone specimens. This is seen in Table 5.1, where the E_s values for the Cloburn stone (6MPa and 17MPa) were notably lower than the Bardon stone (20MPa and 31MPa). The overall compressive strengths of the Bardon stone specimens were on average some 90kPa higher than those of the Cloburn stone specimens.

Figure 5.2 shows the stress-strain behaviour of the monotonic load tests of the Bardon and Cloburn stone specimens with an applied cell pressure of 90kPa. The behaviour of the two materials was similar in terms of E_t and E_s and the average peak deviator stress. The stress-strain behaviour seen in Figures 5.1 and 5.2 show typical behaviour of a loose to medium dense specimen, with the stiffness and compressive strength increasing with an increase in cell pressure. The Cloburn stone specimens appeared to be more variable than the Bardon stone specimens at both 40kPa and 90kPa cell pressure.

5.2.2.2 Volumetric strain behaviour

Figure 5.3 shows the volumetric strain versus axial strain for the Bardon stone and Cloburn stone specimens tested at 40kPa cell pressure. The volumetric strain was calculated by using the axial and radial displacements and assuming that the specimen deformed as a right-angled cylinder. Although there was variability in the stress-strain behaviour in Figure 5.1, the volumetric strain behaviour at 40kPa in Figure 5.3 was remarkably similar. The volumetric strain curves show the specimens to have behaved as a dense granular material. After a slight period of volumetric compression they began to dilate. Typically one would have expected the rate of volumetric strain to reduce with axial strain as the specimens approach critical state. However, in these tests the specimens were still dilating at a constant rate at the end of the test ($\approx$ 6% axial strain).

Figure 5.4 compares the volumetric strain behaviour of the Cloburn stone and Bardon stone specimens at 90kPa cell pressure. Generally the Bardon stone underwent slightly more volumetric compression than the Cloburn stone and less overall dilation. At 90kPa cell pressure the volumetric strain behaviour was a lot more varied than at 40kPa cell pressure. This was surprising as one would normally expect better consistency with higher cell pressures as was noted by Yamamuro and Lade (1993).

5.2.3 Cyclic load triaxial tests

Six cyclic load tests were carried out in Series 1, three with Bardon stone specimens and three with Cloburn stone specimens (Table 5.2).

5.2.3.1 Axial strain behaviour

Figure 5.5 shows the axial strains occurring under cyclic loading of Bardon stone and Cloburn stone specimens at 40kPa cell pressure and a Bardon stone specimen at 90kPa cell pressure. There was good repeatability between each of the similarly prepared tests. The rate of strain in the Bardon stone tests started to level off after 1000 load cycles and the total axial strain reached 3.2% to 3.4% after 100,000 load cycles. After 100 load cycles the strains occurring in the Cloburn stone specimens diverged significantly from the Bardon stone specimens, to such a degree that by 100,000 load cycles the strains in the Cloburn specimens were approximately double those of the Bardon specimens. With the 90kPa cell pressure tests on the Bardon stone specimens the rate of strain started to reduce after 1000 load cycles and the final axial strain after 100,000 load cycles was 0.7%, about a fifth of that seen in the 40kPa cell pressure tests.

5.2.3.2 Volumetric strain behaviour

Figure 5.6 shows the volumetric strains occurring in the Bardon stone and Cloburn stone specimens during cyclic load tests at 40kPa and 90kPa cell pressures. Although the axial strain behaviour for the two Bardon stone specimens was similar (Figure 5.5) the volumetric strain behaviour was different with test T4 undergoing some 50% extra dilation than test T15. The majority of the extra straining appears to have occurred during the first 1000 load cycles, after which the curves are parallel. The observed dilation behaviour for the Bardon and Cloburn stone specimens at 40kPa cell pressure would suggest that the specimens were like a dense granular material. Where little further axial strain (Figure 5.5) or volumetric strain occurred this would suggest that the test had reached some form of stability or shakedown as described by Collins and Boulbibane (2000) in Section 2.7.

In Figure 5.6 it was clear that the Cloburn stone specimens underwent more than twice the amount of volumetric strain than the Bardon stone specimens. Unlike the Bardon stone the Cloburn stone specimens continued to show a high rate of dilation up to 10,000 load cycles before starting to level off.

The Bardon stone specimen at 90kPa cell pressure showed slight contraction throughout the duration of the test as seen in Figure 5.6.

5.2.4 Post cyclic monotonic load triaxial tests

After each cyclic load test a post cyclic monotonic load test was carried out on the specimen as described in the testing procedure (Section 3.4). Table 5.1 gives the details of each post cyclic monotonic load test in Series 1.

5.2.4.1 Deviator stress-strain behaviour

Figure 5.7 shows the stress-strain behaviour of all of the post cyclic monotonic load tests at 40kPa and 90kPa cell pressure in Series 1. As with the initial monotonic load tests at 40kPa cell pressure the Cloburn stone specimens gave lower peak deviator stress values than the equivalent Bardon stone specimens (Figure 5.1). Although this was not seen in the monotonic load tests at 90kPa cell pressure (Figure 5.2), it was observed in the 90kPa cell pressure post cyclic monotonic load tests. With the 40kPa cell pressure tests there was a very obvious peak in the deviator stress before 0.5% axial strain; this peak was not so obvious in the tests with a 90kPa cell pressure.

When comparing the initial monotonic and post cyclic monotonic load tests of the Bardon stone and Cloburn stone specimens in Figures 5.8 and 5.9 it was clear that the deviator stresses with the Bardon stone at 40kPa and also at 90kPa cell pressure were approaching similar ultimate values respectively. This trend, however, was not so clear with the Cloburn stone specimens, although it was expected that this was due to variability of specimens rather than characteristic behaviour. It was clear that the specimens in the post cyclic monotonic load tests had E_t values that were considerably higher than those specimens that had not undergone cyclic loading (Table 5.1).

5.2.4.2 Volumetric strain behaviour

The volumetric strain behaviour for the post cyclic monotonic load tests for both the Bardon stone and Cloburn stone specimens in Series 1 are shown in Figure 5.10. In some of the tests the specimen may have undergone very slight compression before dilating, suggesting a very dense granular material, thus complimenting the deviator stress versus axial strain behaviour.

5.2.5 Shear strength parameters c' and φ'

Table 5.7 presents the shear strength parameters; the cohesion intercept, c' and the angle of shearing resistance, φ', determined using the Mohr-Coulomb failure criteria for the monotonic load triaxial tests in Series 1 (Section 4.6.3). The failure envelopes for the Bardon stone and Cloburn stone specimens in the initial monotonic load tests are shown in Figure 5.11. From this and from Table 5.7 it can be seen that the materials behaved

slightly differently. The Cloburn stone specimens at 40kPa and 90kPa cell pressure had very similar angles of shearing resistance, φ', at 51° and had an intercept value c' = 0 (Figure 5.11(a)). The Bardon stone specimens however had a higher φ' value at 40kPa than at 90kPa cell pressure, possibly suggesting a slight curve in the failure envelope (Figure 5.11(b)).

From Table 5.7 the angle of shearing resistance increased between the monotonic and post cyclic monotonic load tests when using the peak deviator stresses and assuming no cohesion (c' = 0). However, when the envelope was not forced through zero then in the post cyclic monotonic load tests c' increased dramatically as φ' reduced significantly as seen for the Bardon stone in Figure 5.11(c).

5.2.6 Series 1 - summary

Figures 5.1 and 5.2 clearly showed that under monotonic load conditions there was little overall difference between the Bardon stone and the Cloburn stone specimens, although under cyclic loading it became very clear that the Cloburn stone specimens were a lot more susceptible to straining (Figure 5.5). The decision not to include the Cloburn stone in further tests, however, was based on the results from the monotonic load tests alone.

During preliminary testing with the 50mm ballast specimens (not reported in Series 1 analysis), the ballast particles were liable to undergo alterations in terms of scratching, rounding, asperity breakage, fragment crushing and whole particle breakage. It was considered that the breakage of the material would have a marked influence on the strength, stiffness and overall volume change of the specimen. Therefore it was necessary to determine a way of recording such breakage. This method and the analysis of the breakage behaviour used in Series 2 onwards has been described in Chapter 6.

5.3 Series 2 – material characterisation

Series 2 consists of forty-seven triaxial tests carried out on thirty-two different specimens. The objectives of Series 2 were as follows:

- to consider the repeatability and reproducibility of the tests;
- to gain a comprehensive understanding into the general soil characteristics;
- to investigate the development of the resilient modulus in the cyclic load tests; and
- to gain an understanding into the influence of the particle breakage on the volumetric behaviour.

As discussed in Section 3.3.3 and 3.3.4, the volumetric behaviour of the specimens was assessed using two methods. Firstly by calculating the volume change using the radial and axial displacement transducers and assuming a right angled cylinder, and secondly by measuring the volume change using the volume change unit. However as the volume change unit was considered more refined, the volume change of the specimens in Series 2 to 6 has been interpreted using only the measured volume change.

Hereafter the 20mm Bardon stone will be referred to as the stone and the 50mm Bardon ballast as the ballast. A full list of the tests included in Series 2 is given in Tables 5.4 and 5.5.

5.3.1 Specimen preparation

Seventeen tests in Series 2 were prepared with stone and fifteen with ballast with the specimen properties detailed in Table 3.4. The average density for the stone specimens was calculated as 1.67Mg/m^3, the same as that quoted by Key (1998). The range was slightly smaller than that quoted by Key and significantly smaller than that found in Series 1. The average density of the ballast specimens value was the same as that quoted by Key, although the range was slightly larger.

5.3.2 Monotonic load tests

Eight monotonic tests were carried out as part of Series 2, four with stone specimens and four with ballast specimens (Table 5.4).

5.3.2.1 Deviator stress-strain behaviour

Figure 5.12 shows the deviator stress versus axial strain graphs for the monotonic load tests on stone specimens. When comparing the 40kPa cell pressure tests to similar tests in Series 1, Figure 5.1, it is clear to see that the average peak deviator stresses in Series 2 were approximately 50kPa lower, 325kPa compared with 375kPa. The majority of this was due to the different correction applied to the deviator stress in Series 1, which used the calculated volume change, whereas in Series 2 it used the measured volume change.

It can be seen from Figure 5.12 that as the cell pressure increased the deviator stress also increased as would be expected, although it would appear that the amount of increase in the average peak deviator stress (as defined in Section 4.6.2) decreased with each increment in cell pressure. In terms of stiffness (Table 5.4) it was clear to see that both E_t and E_s increased as the cell pressure increased, as was also expected.

Figure 5.13 shows the stress-strain behaviour for ballast specimens with cell pressures of 40kPa, 90kPa and 140kPa. Although it was not understood why test T26 behaved so differently over the first 2% axial strain, it clearly showed that the specimen behaviour could vary considerably due to the natural variation in size and shape of the particles making up the specimen.

The main parameters that may cause a difference in the behaviour of two similar specimens include the initial density, the cell pressure, the rate of loading, and any leakage. In cyclic load tests this would also include variation of the minimum and maximum deviator stresses applied to the specimen. Typically during the initial analysis (as described in Section 4.5) these parameters would be checked, where there were discrepancies in the results then a more thorough check was carried out and comments made in Tables 5.4 and 5.5. As the specimens were prepared and the tests carried out with appropriate rigor this would imply, where there were no discrepancies, the differences were a natural variation in the material/specimen.

Again with an increase in the cell pressure there was an increase in the stiffness of the specimens (E_t and E_s, Table 5.4). Between 40kPa and 90kPa cell pressure there was a significant increase in the average peak deviator stress yet between 90kPa and 140kPa there was only a small increase. Table 5.4 shows that although the stone and ballast specimens had similar E_t values at 40kPa cell pressure; at 90kPa and 140kPa cell pressures the E_t values for the stone specimens increased significantly more than with the ballast specimens.

When comparing the behaviour of the two materials (c.f. Figure 5.12 and 5.13) it was noticeable that there was a slight difference in the way the specimens behaved under applied load. In the ballast tests the stress-strain curve had much greater variations in deviator stress. This may have been due to stick-slip phenomena, breakage of the ballast or possibly a combination of both.

5.3.2.2 Volumetric strain behaviour

The two monotonic load tests on stone specimens with a 40kPa cell pressure showed similar volumetric strain behaviour in Figure 5.14. With an increase in cell pressure there was slightly more initial compression and less overall dilation. As mentioned in Series 1, this behaviour would normally be associated with a dense material.

The patterns for the volumetric strain behaviour of the ballast specimens are very similar to those described above for the stone specimens. Figure 5.15 shows the

volumetric strain results for the monotonic load tests with ballast specimens The volumetric strain behaviour of test T26 confirms the stress-strain behaviour seen in Figure 5.13 and would suggest that T26 was an anomaly. Whether this was due to the slight leakage could not be confirmed (Table 5.4).

Comparing the volumetric strains of the stone and the ballast specimens at 40kPa cell pressure (Figures 5.14 and 5.15) the compressive strains of the ballast specimen were slightly greater than those recorded for the stone specimen although the amount of dilation in the ballast specimen at 6% axial strain was only about 60% of that in the stone specimen. A similar pattern was also noted in the 90kPa and 140kPa cell pressure tests.

5.3.3 Cyclic load tests

Twenty-four cyclic load tests have been included in the analysis in this section, thirteen of which were on stone specimens and eleven on ballast specimens (see Table 5.5). Tests T20 and T55 were not included in the analysis due to faults in the data acquisition.

5.3.3.1 Axial strain behaviour

Figure 5.16 shows the axial strains occurring in the cyclic load triaxial tests over 100,000 load cycles on stone specimens with a 40kPa cell pressure. From this it was clear that even after the first load cycle corrections have been made (Section 4.4.4) there was still a large variation in the strains occurring, which after 100,000 load cycles varied between 2.5% and 4.1%.

Figure 5.17 shows the average line for similarly prepared stone specimens at different cell pressures, with the error bars showing $^{+}$/- two standard errors of the mean ($2SE(\overline{X})$), calculated as:

$$SE(\overline{X}) = \frac{s}{\sqrt{n}} \qquad \text{Equ. 5.1}$$

where: s = standard deviation of the specimens, and

n = number of specimens

A similarly prepared specimen is 95% probable to fall somewhere in the range of the error bars. Figure 5.17 clearly shows that the results were statistically viable and that the observed trends were valid.

Figure 5.17 compares the axial strains occurring in the cyclic load tests on stone specimens at different cell pressures. With each increase in cell pressure the amount of

axial strain occurring in the specimen reduced, with the majority of the straining in each test occurring within the first 1000 load cycles.

With the ballast specimens a similar pattern emerged (Figure 5.18) although the axial strains occurring at 40kPa cell pressure after 100,000 load cycles were noticeably less than with the stone specimens. The range of strains occurring in the ballast tests at 40kPa cell pressure was between 2.1% and 3%. At 90kPa and 140kPa cell pressure the opposite was seen with the strains in the ballast specimens being slightly kigher than those of the stone specimens. At 240kPa cell pressure there was no noticeable difference in the behaviour between the stone and the ballast specimens.

5.3.3.2 Volumetric strain behaviour

As with the axial strains there was a lot of scatter in the volumetric strain data especially in the stone specimens at 40kPa cell pressure (Figure 5.19). Typically the specimen dilated over the first 1000 load cycles before starting to compress. Figure 5.20 shows that with a cell pressure of 90kPa or greater then there was an immediate compression of the specimen (unlike at 40kPa cell pressure).

The same patterns were evident with the ballast as with the stone specimens. At 40kPa cell pressure the overall volumetric strain for the ballast specimens showed a little dilation before compressing to values slightly below those of the stone specimens. This can be seen in Figure 5.21.

At 90kPa cell pressure the volumetric strains showed very slight compression similar to the stone specimens. Slightly less compression is shown with the higher cell pressures (140kPa and 240kPa) than the 90kPa cell pressure tests.

It is clear from Figures 5.20 and 5.21 that although the trends observed at the different cell pressures were generally repeatable, the absolute volumetric strain behaviour could vary considerably.

5.3.4 Post cyclic monotonic load tests

Post cyclic monotonic load tests were carried out on fifteen of the specimens after 100,000 load cycles (Table 5.4). They were, however, not carried out on certain specimens to allow the ballast breakage behaviour due to the cyclic loading alone to be assessed.

5.3.4.1 Deviator stress-strain behaviour

Figure 5.22 shows the deviator stress versus axial strain behaviour of the stone in post cyclic monotonic load tests. The specimens were very stiff at the start of the test with E_t values typically of 700MPa in the 40kPa cell pressure tests with an average peak deviator stress of around 400kPa occurring within the first 0.2% axial strain. The 240kPa cell pressure test was stopped before the load cell reached its maximum working load, unfortunately this was before the peak deviator stress was reached. However, the E_t value was calculated as 1725MPa, over 400MPa higher than test T68 with a cell pressure of 140kPa.

As would be expected, the overall compressive strength of the stone specimens increased with an increase in cell pressure as seen in Figure 5.22. However, the E_t values given in Table 5.4, for the stone specimens at 90kPa and 140kPa cell pressure, were similar to each other at around 1000MPa.

In Figure 5.23 both the monotonic load tests and the post cyclic monotonic load tests for the stone specimens are plotted. It would appear that the ultimate stresses in the monotonic load tests were similar to those in the post cyclic monotonic load tests, as was observed in Series 1 (Section 5.2.4.1). This was also observed for the ballast specimens as seen in Figure 5.24, although the error bars have been removed to avoid confusion.

The stress-strain behaviour of the ballast specimens is shown in Figure 5.24.

The E_t values for the ballast specimens at each of the cell pressures were similar at approximately 500kPa (Table 5.4), which were significantly lower than those recorded in the stone tests.

5.3.4.2 Volumetric strain behaviour

Figure 5.25 shows the volumetric strain behaviour in the post cyclic monotonic load test for the stone specimens. The initial amount of compression was significantly reduced compared to the normal monotonic load tests to almost negligible amounts (-0.01% or less). Although the amount of dilation occurring was comparable to that seen in the monotonic load tests (Figure 5.14). Similar results for the ballast tests are seen in Figure 5.26, where the overall amounts of dilation for ballast were slightly less in the post cyclic compared to the monotonic load tests (Figure 5.15).

5.3.5 Strength parameters c' and φ'

The strength parameters; cohesion, c', and angle of shearing resistance, φ', determined using the Mohr-Coulomb failure criteria for Series 2 are given in Tables 5.8 for the monotonic and post cyclic monotonic load tests. The Mohr-Coulomb failure envelopes for the stone and ballast specimens in the monotonic load triaxial tests are shown in Figures 5.27 and 5.28.

With the stone specimens tested at 40kPa cell pressure under monotonic loading, the specimens had an angle of shearing resistance 3° higher than the 90kPa and 140kPa specimens. With the ballast specimens this decrease in shear strength was more marked, by 90kPa cell pressure the angle of shear resistance had dropped by 4°-6° compared to the specimens tested at 40kPa cell pressure and a further 5° by 140kPa cell pressure. That made a total drop of approximately 10° between the 40kPa tests and the 140kPa tests. The effect of this can be seen in Figure 5.29 where an approximate curved failure envelope was fitted to the ballast specimen tests results.

It is clear from Table 5.8 that the stone specimens overall had a greater resistance to shearing than the ballast specimens. With an increase in cell pressure the difference in the value of the angle of shearing resistance between the stone and the ballast specimens also increased. This again implies that the stone specimens resisted the higher loads better than the ballast, possibly due to breakage occurring in the ballast specimens.

The general patterns discussed above were also present in the post cyclic monotonic load tests. The angle of shearing resistance at 40kPa cell pressure with both the stone and ballast specimens was significantly higher in the post cyclic monotonic load tests than in the monotonic load tests (3°-7°). At 90kPa and 140kPa cell pressure the difference in the angle of shear strength between the monotonic and post cyclic monotonic load test was relatively small at 0°-2°. This naturally affects the failure envelope by increasing the intercept value and decreasing the angle of shearing resistance.

5.3.6 Series 2 – summary

The results of a large number of triaxial tests with three different cell pressures of 40kPa, 90kPa, and 140kPa have been presented. The objectives of Series 2 were:

- to further the understanding of the deviator stress-strain, axial strain and volumetric strain behaviour in the monotonic, cyclic and post cyclic monotonic load triaxial tests using the measured volumetric strains and the knowledge of the breakage behaviour;

- to gain an appreciation of the development of the stiffness of the material throughout the cyclic tests and;
- to check the repeatability and reproducibility of the tests.

With an increase in cell pressure in the monotonic load tests there was an increase in the stiffness of the specimen and the average peak deviator stress; there was also an increase in the initial compression and a decrease in the dilation of the specimens. The main difference in the stone and ballast behaviour was the occurrence of sudden decreases in the deviator stress due to slipping of interlocked particles or particle breakage.

In the cyclic load tests, as the cell pressure increased there was a reduction in the amount of axial strain and an increase in the amount of compression. The ballast specimens underwent less axial strain at 40kPa cell pressure than the stone specimens although slightly more at 90kPa and 140kPa cell pressure. There was slightly less dilation in the ballast specimens at 40kPa cell pressure and the volumetric strains were similar at cell pressures of 90kPa and 140kPa.

With the post cyclic monotonic load tests at a 40kPa cell pressure the specimens were stiffer than in the initial monotonic load tests and had an initial peak in the deviator stress. This was unexpected behaviour as during the cyclic load test the specimens dilated slightly and therefore had a higher void ratio. It would therefore be anticipated that the specimen would have had a lower E_t value. At 90kPa and 140kPa cell pressure the specimens compressed during the cyclic load tests, therefore an increase in initial stiffness was expected.

As mentioned previously the breakage behaviour was not included in the above results but is included in Chapter 6 along with the single particle crushing test results and discussion. The resilient modulus calculated throughout the cyclic load tests are considered together at the end of this chapter, Section 5.8.1 and the repeatability and reproducibility of the tests are discussed in detail in Section 7.2.

5.4 Series 3 – breakage accumulation under cyclic loading

Series 3 consisted of five cyclic load tests on ballast specimens, a 100, 1000, 10,000, a 1 million, and a 2 million load cycle test as described in Section 3.5.3. As the main emphasis of Series 3 was looking at the development of particle breakage throughout the cyclic load test only a limited stress-strain, volumetric strain analysis is discussed

below. Details of the resilient moduli are reviewed in Section 5.8.2 and the particle breakage behaviour is included in Chapter 6.3. There are two sections to this analysis, firstly the cyclic load tests with less than 100,000 load cycles tested at 140kPa cell pressure and secondly those with more than 100,000 load cycles tested at 90kPa cell pressure.

5.4.1 Specimen preparation

Table 5.6 gives details of the specimens tested in Series 3. The densities of these specimens were similar to the average density of the specimens recorded in Series 2, i.e. 1.48Mg/m^3.

5.4.2 Axial strain behaviour

The axial strain behaviour for the 100, 1000, and 10,000 cyclic load tests with a 140kPa cell pressure is plotted in Figure 5.30, along with the average 100,000 load cycle curve from the ballast tests in Series 2. Specimen T65, the 100 load cycle test, had a very similar axial strain to that of the average curve in Series 2. The other two specimens T66 and T67 seem to have had higher axial strains than those in Series 2 to such an extent that they did not fall within the 95% confidence limits. Having considered possible reasons for these differences (cf. Section 5.3.2.1) it was concluded that once again the differences were due to natural material/test variation. The relative axial strains were still less than in a test with a cell pressure of 90kPa (cf. Figure 5.31). Figure 5.31 shows the axial strain behaviour of the 1 million load cycle test (T75), the first part of the 2 million load cycle test (T42), and the average curve from Series 2 with a 90kPa cell pressure. Again it is clear to see that the tests had comparable axial strain behaviour with those of Series 2.

5.4.3 Volumetric strain behaviour

The volumetric strain behaviour of the 140kPa cell pressure tests in Series 3 was very comparable to that in Series 2, as shown in Figure 5.32. Figure 5.33 shows the volumetric strain behaviour of the 90kPa cell pressure tests in Series 3, which again was similar to that in tests in Series 2. It was unclear what happened in test T75 to cause the volumetric behaviour to suddenly change from contraction to dilation at around 200,000-500,000 load cycles. However as can be seen in Figure 5.33 there was also a slight increase in the rate of axial strain after 500,000 load cycles. This would suggest

that some change in the specimen structure caused the specimen to suddenly start dilating leading to a collapse of the specimen under the cyclic loading.

5.5 Series 4 – layered specimens

Tests in Series 4 as detailed in Section 3.5.4, were used to investigate the behaviour of layered specimens based on the understanding developed in Series 2 of the individual material behaviour and building on the work of Key (1998). In total there were twenty-six triaxial tests carried out in Series 4, with the specimen and test details given in Tables 5.4 and 5.5. Typically one monotonic and one cyclic load test at 40kPa cell pressure was carried out on each type of layered specimen.

Table 5.9 describes the nomenclature along with a simple diagram for each of the layered specimens. Each test name described the amount of stone overlying the ballast. For example, single layer, meant a specimen with a single layer of stone overlying the ballast and a 1-2 layer, meant a specimen with the top one-third stone overlying the bottom two-thirds ballast (etc). The resilient moduli of the specimens are reviewed in Section 5.8.3 and the breakage details in Section 6.3.

5.5.1 Specimen preparation

The specimen preparation was hard to control as the exact height of the ballast in the bottom of the specimen mould was difficult to determine and the variation in the size of the voids between the particles due to the individual ballast particle shapes allowed the stone to infiltrate to some degree. As can be seen in Table 5.5 the range of densities for the layered specimens was more varied than for the stone only or ballast only specimens. With the 1-1 layer specimens the range of densities was 0.04Mg/m^3, with the average density equal to 1.61Mg/m^3. In comparison to the stone or ballast only specimens the densities were slightly higher than the average density of the two materials combined (1.58Mg/m^3). This would suggest that the stone made up slightly more than half of the total specimen mass possibly due to the smaller stone infilling the void spaces at the top of the ballast layer.

5.5.2 Monotonic load tests

As seen in Table 5.4 nine monotonic load tests were carried out as part of Series 4. These were a single layer specimen, a double layer specimen, a 1-2 layer specimen, five 1-1 layer specimens, and a 2-1 layer specimen. All tests were carried out with a 40kPa

cell pressure apart from one (test T30, a 1-1 layer specimen), which was tested with a 90kPa cell pressure.

5.5.2.1 Deviator stress-strain behaviour

Figure 5.34 shows the deviator stress versus axial strain behaviour of the 1-1 layer specimens with 40kPa and 90kPa cell pressures. From this it can be seen that the general behaviour of the 1-1 layer specimens was more typical of the stone only specimens, rather than the ballast specimens, from Series 2; especially at 90kPa cell pressure. The stick-slip phenomena behaviour observed for the ballast specimens in Series 2 was much reduced with the 1-1 layer specimens.

The limited effect of a small layer of stone underneath the top cap overlying the ballast can be seen in Figure 5.35, where the behaviour of the thin layered specimens was similar to the stone only and ballast only specimens. It was thought that the 50kPa difference in average peak deviator stress between the single layer and double layer specimens was due to material/test variability. The 1-2 layer and 2-1 layer specimens behaved in a similar manner as seen in Figure 5.36, with the average peak deviator stresses being slightly higher than those of the stone only specimens.

In Series 4 the range of E_t values was 36MPa to 76MPa, and the range of average peak deviator stresses was from 290kPa to 365kPa. When comparing the variability seen in Series 4 with the variability seen in the stone only or ballast only tests at 40kPa cell pressure there would appear to be little difference in the behaviour of any of these specimens.

5.5.2.2 Volumetric strain behaviour

Figure 5.37 shows the volumetric strain behaviour of three repeated 1-1 layer specimens at 40kPa and one at 90kPa cell pressure. The shapes of the volumetric strain curves were almost identical to one another (in the 40kPa cell pressure tests), giving confidence in the equipment and the results. In general the volumetric strain behaviour of the 1-1 layer specimens at both 40kPa and 90kPa cell pressure was about halfway between the strains from the stone only and ballast only specimens (Figure 5.38).

The volumetric strain behaviour of the specimens with a thin layer of stone overlying the ballast can be seen in Figure 5.39. This may explain the difference in the stress-strain behaviour of the two specimens (Figure 5.35). The volumetric strain behaviour of the single layer specimen showed slightly more initial compression and slightly less dilation than the specimen with the double layer of stone. Comparing this behaviour

with that of the stone only or ballast only specimens revealed that the volumetric strains of both of the thin layered specimens were more comparable to the ballast only specimens than the stone only specimens.

The volumetric strain behaviour of the 1-2 layer specimen and the 2-1 layer specimen in Figure 5.40 was very similar, as was seen with the stress-strain behaviour. The behaviour of both specimens was more comparable to the behaviour of the stone only specimens and not the ballast only specimens.

Although the stress-strain behaviour of the specimens was similar, Figure 5.41 reveals that the volumetric strain of the single and double layer stone specimens was appreciably less than the other tests which had a significant amount of stone overlying the ballast. The volumetric strain behaviour of the single and double layer specimens was similar to the ballast only specimens, whilst the other tests were closer to the behaviour of the stone only specimens.

5.5.3 Cyclic load tests

There were nine cyclic load tests in Series 4 comprising of differing thicknesses of stone overlying the ballast layer, as detailed in Table 5.5.

5.5.3.1 Axial strain behaviour

Figure 5.42 shows the axial strain behaviour for the 1-1 layer specimens with 40kPa cell pressure and 90kPa cell pressures. When comparing the 1-1 layer specimen behaviour at 40kPa cell pressure with the stone only and ballast only specimens, test T31 specimen behaved as a typical stone only specimen and test T45 specimen gave similar results to the ballast only specimens. Having checked the specimen set up there was still no apparent reason for this difference.

At 90kPa cell pressure the axial strains of the 1-1 layer specimen (T32) was in between those of the stone only and ballast only specimens as seen in Figure 5.42.

In the tests with a single layer of stone overlying the ballast, Figure 5.43, the two 40kPa cell pressure tests (T39 and T48) were comparable and showed significantly more displacement than the 90kPa cell pressure test (T41). The behaviour of the stone only and ballast only specimens is also shown on Figure 5.43. The behaviour of the single layered specimens at 40kPa cell pressure would seem to be closer to the behaviour of the ballast specimens, as was seen with the monotonic load tests. The 90kPa cell pressure test, specimen (T41), also followed the behaviour of the ballast specimen.

Figure 5.44 includes the double layer specimen (T51) at 40kPa cell pressure, which although initially followed a similar curve to the single layer specimen it soon (within 20-30 load cycles) diverged to higher strains. This could tie in with the lower deviator stress in the double layer specimen seen in the monotonic load test.

With the 1-2 layer and 2-1 layer specimens at 40kPa cell pressure (test T46 and T47 respectively), shown in Figure 5.45, there was a significant difference in their behaviour. The 2-1 layer specimen ($2/3^{rds}$ stone) deformed according to the stone only tests and the 1-2 layer specimen ($2/3^{rds}$ ballast) deformed similarly to the ballast only specimen. This would appear to make sense although the degree of difference was surprising, especially as the E_s values of the 1-2 layer and 2-1 layer specimens when loaded monotonically were not significantly different. However test T47, the 2-1 layer specimen, had a very large strain recorded on the first load cycle of 3% axial strain (taken out with the first load cycle correction, Section 4.4.4) compared with only 0.34% axial strain in test T46, the 1-2 layer specimen. This may have had an influence on the long term behaviour of the specimen.

5.5.3.2 Volumetric strain behaviour

The results of the 1-1 layer specimens tested at 40kPa cell pressure, in Figure 5.46, show that the volumetric strains between the two like tests were very similar with an increase in the amount of compression in the 90kPa cell pressure test. It was seen that at 40kPa cell pressure the volumetric strains were in between those recorded for the stone only and ballast only specimens. At 90kPa the 1-1 layer specimen contracts more than either the stone only or the ballast only specimens.

The volumetric strain behaviour of the specimens with a single layer and a double layer of stone overlying the ballast can be seen in Figure 5.47. Their behaviour was very much akin to that of the ballast only specimen even though the strains of the double layer specimen were higher than in the single layered specimens (Figure 5.44).

The volumetric strains of the 2-1 layer specimens (Figure 5.48) showed slightly greater dilation than in the 1-2 layer specimen. The volumetric strain for the 1-2 layer specimen was very much in line with the lower end of the stone specimens (towards that of the ballast specimens). The 2-1 layer specimen tested in this project had a slightly greater dilation than the most dilatant stone only specimen.

5.5.4 Post cyclic monotonic load tests

Eight post cyclic monotonic load tests were carried out in Series 4. These have been detailed in Table 5.4.

5.5.4.1 Deviator stress-strain behaviour

The behaviour of the 1-1 layer specimens as seen in Figure 5.49 was similar. The ultimate stresses at both 40kPa and 90kPa cell pressure were similar to those seen in the initial monotonic load tests, as was also seen for the monotonic load tests in Series 2, Figures 5.23 and 5.24.

The post cyclic monotonic load behaviours of the single and double layer specimens were remarkably similar as seen in Figure 5.50. The ultimate stresses (from test T51) were similar to the ultimate stresses in the initial monotonic load test (T52). This would suggest that there was a slight anomaly with test T50 that had a lower deviator stress than the single layer specimen. It was interesting to note that in the post cyclic monotonic load tests there were much greater sudden stress changes (stick-slip phenomena) than seen in any other monotonic load or post cyclic monotonic load tests.

The 1-2 layer specimen (T46) and 2-1 layer specimen (T47) had similar E_t values although the peak and average ultimate deviator stresses of the 2-1 layer specimen were about 50kPa less than those of the 1-2 layer specimen (Figure 5.51). The behaviour of the monotonic load 1-2 layer specimen however was comparable to the behaviour seen with the stone only and ballast only specimens in Series 2 (Figures 5.12 and 5.13). This suggests that, compared to the 1-2 layer specimen, the greater displacement and dilation in the 2-1 layer specimen during the cyclic load test (seen in Figures 5.45) lowered the strength of the 2-1 layer specimen in the post cyclic monotonic load test.

5.5.4.2 Volumetric strain behaviour

Figure 5.52 shows the volumetric strain behaviour for the post cyclic monotonic load tests in Series 4, which shows very slight compression of the specimens before they started to dilate as was seen in Series 2 (Figures 5.25 and 5.26). As seen in the monotonic load tests the rate of dilation generally increases with an increase in the thickness of the stone overlying the ballast.

5.5.5 Strength parameters c' and φ'

Table 5.10 shows the strength parameters for all the monotonic load tests in Series 4. The angle of shearing resistance of the layered specimens at 40kPa cell pressure was

typically 2°-3° higher than those of stone only and ballast only specimens. At 90kPa the angle of shearing resistance for the 1-1 layer specimen was similar to the stone only specimens in Series 2.

At 40kPa cell pressure in the post cyclic monotonic load tests (Table 5.11) the angle of shearing resistance for the layered specimens was similar to both the stone only and ballast only specimens. However, the angle of shearing resistance at 90kPa cell pressure in the 1-1 layer specimen was significantly higher (6°) than the stone only and ballast only specimens.

5.6 Series 5 – damped specimens

Three cyclic load triaxial tests were carried out in Series 5, as detailed in Section 3.5.5. The results from these tests were used to add breadth to the analysis by trying to simulate, to a slightly better degree, the railway environment within the triaxial test. This was done by inserting a wooden disc (MDF board) in-between the top cap and the specimen and also by adding a thick rubber disc at the base of the specimen, both in the same test specimen. Henceforth the MDF disc and the rubber disc will collectively be referred to as dampers in a damped specimen.

It was postulated that with the damping (MDF and rubber) there would be greater elastic strain occurring in each load cycle as the wood and rubber had lower Young's moduli than the normal metal top cap/base plate; this would potentially lead to reduced plastic strain. Furthermore, the damping would absorb some of the initial impact of each load cycle, reducing the rate of loading applied to the stone, which would reduce the amount of breakage occurring, hence less plastic deformation. The axial strain behaviour is discussed below; the stiffness of the specimen in terms of resilient modulus is discussed in Section 5.8.4 and the breakage behaviour in Chapter 6.3. Although the 140kPa cell pressure used in tests would be higher than the lateral stresses expected in the railway environment, this confining pressure was used as the test results were more consistent with the higher cell pressures and it was therefore expected that this would give a clearer picture of the effect on strain, stiffness and breakage.

5.6.1 Specimen behaviour

Table 5.5 shows the specimen details for three tests; one stone only, one ballast only and one double layer specimen in Series 5. For each specimen the densities were within the ranges of densities of similarly prepared specimens in Series 2 and Series 4.

5.6.1.1 Axial strain behaviour

Figure 5.53 shows the axial strain behaviour for specimens T69 and T71 compared with the ballast and the stone only specimens. Test T70, the double layered specimen, could not be included in the analysis, as the first 4 load cycles were not recorded due to an error at the start of loading. It was possible, however, to observe that the specimen deformed 0.78% axial strain between load cycles 4 and 100,000, which would make it comparable to test T69, the ballast only specimen with damping. From Figure 5.53 it can be seen that the ballast specimen with damping had similar deformation to the stone specimen with damping up to around 200 load cycles after which it diverged to higher axial strains. A similar pattern was also seen with the ballast only and stone only specimens without damping (from Series 2), where the ballast specimen results diverged from the stone specimen results at around 1000 load cycles to higher axial strains. Contrary to initial thinking outlined above, the specimens with damping had higher plastic strains than those without.

5.6.1.2 Volumetric strain behaviour

Figure 5.54 shows the volumetric strain behaviour for tests T69 and T71. Typically the behaviour was very similar, although it was not clear what caused the strains to suddenly alter in T71. When comparing the volumetric strain behaviour of these tests in Series 5 with that of the ballast only and stone only specimens in Series 2 one could see that the general behaviour was similar, with the damped specimens showing slightly more compression.

5.7 Series 6 – wetted ballast

Testing in Series 6 was carried out towards the end of the test programme. The tests were carried out by a different operator under the laboratory supervision of the author. Six specimens of wet ballast were tested under monotonic load and cyclic load conditions as detailed in Section 3.5.6.

5.7.1 Specimen preparation

The specimens were prepared in the usual way (Section 3.4), although the material had been soaked in water for 24hrs before specimen preparation. The specimen densities were similar to those in Series 2, Tables 5.4 and 5.5, except specimen T81, which had a higher density.

5.7.2 Monotonic load tests

Three monotonic load tests were conducted at 40kPa, 90kPa and 140kPa cell pressure. The deviator stress versus axial strain behaviour is plotted in Figure 5.55, showing the typical patterns as seen in Series 2 of an increase in the peak deviator stress with confining pressure. It is clear to see that the overall stress-strain behaviour between the wet and dry ballast specimens is similar at each of the confining pressures, although at 90kPa and 140kPa the compressive strength of the wet specimens was slightly lower. At 40kPa and 140kPa cell pressure the initial stiffness of the specimens (E_t) are greater than those of the dry specimens (cf. Table 5.4). It was also observed that at 90kPa and 140kPa the stick-slip phenomena was slightly reduced.

The volumetric strain behaviour of the wet ballast, Figure 5.56, shows a similar pattern to the dry ballast (Series 2). An increase in the confining pressure resulted in an increase in the compression and a reduction in the dilation of the specimen. The volumetric strain curve for the specimen tested at 140kPa cell pressure (test T79) was not included in the discussions due to inconsistencies in the volume change data. It is possible that there was a loose connection or some other fault in the volume change unit, causing the data to be defective. The wet ballast specimen at 90kPa cell pressure (test T82) had a similar volumetric strain curve to that of the dry specimen at 140kPa cell pressure, even though their stress-strain curves were distinctly different. Test T81, which had the higher density, behaved in the pattern as would be expected from Series 2 results.

5.7.3 Cyclic load tests

The cyclic load triaxial tests in Series 6 are shown in Figure 5.57, compared to similar dry tests of Series 2. At 40kPa cell pressure the amount of axial strain in the wet ballast specimen was twice that of the dry specimen. This pattern was also seen with the 90kPa cell pressure tests. At 140kPa cell pressure the axial strain in the wet specimen was three times that of the dry specimen.

The patterns seen with the volumetric strain behaviour in Figure 5.58 were not so clear to identify. At 40kPa cell pressure the wet specimen dilated slightly more than the dry specimen and at 90kPa and 140kPa the wet specimens contracted more than the dry specimens.

5.8 Resilient modulus

The average resilient modulus for each of the four intervals recorded during the cyclic load test, was calculated as described in Section 4.5. Each series of tests is addressed separately, looking at the development of the resilient modulus of the specimen throughout the cyclic load test and the effect of the confining pressure on the resilient modulus. Series 1 has not been included in this section, as the necessary data was not recorded during the tests.

5.8.1 Resilient modulus in Series 2 – characterisation tests

The resilient moduli for tests carried out in Series 2 are tabulated in Table 5.5. Figure 5.59 shows the development of resilient modulus versus the number of load cycles in the 20mm stone tests for each of the cell pressures (40kPa – 240kPa). It is clear from this that as the number of load cycles increased so did the resilient modulus of the specimen. Typically the rate of increase in modulus decreased with an increase in load cycles. As would be expected the resilient modulus of the specimen also increased with an increase in the cell pressure. However the exact pattern was curious, as the increase in the resilient modulus was only slight between 90kPa and 140kPa cell pressure, yet by 240kPa cell pressure the resilient modulus had significantly increased.

At 40kPa cell pressure all of the tests had very similar resilient modulus values apart from test T33, which had a higher resilient modulus. There was a range of strains occurring in the five different tests on stone only specimens at 40kPa cell pressure in Series 2, Figure 5.16, of which test T33 was a test that was very close to the mean of those five tests. It was therefore surprising that test T33 should be the one with dissimilar modulus. This unexpected behaviour was also observed in the 140kPa cell pressure tests, where the strains occurring in tests T59 and T68 were very similar, as seen by the small standard error bars in Figure 5.17, yet the values of the resilient modulus calculated for the two tests were significantly different.

Figure 5.60 shows a similar plot for the ballast specimens. This confirms many of the observations mentioned above. i) That the resilient modulus increased with number of load cycles, ii) the resilient modulus increased with an increase in cell pressure, iii) that there was a marked increase in modulus between 140kPa and 240kPa cell pressure. Furthermore, for the ballast, the rate of increase in resilient modulus appeared to be less in the final stages of the test than in the stone test results. Test T77, at 240kPa cell pressure, was stopped after 20,000 load cycles due to a ruptured membrane.

It is clear to see from Figures 5.59 and 5.60 that the stone specimens were considerably stiffer than the ballast specimens. From Figure 5.61, which compares the behaviour of the ballast and the stone at 100, 1000, 10,000 and 100,000 cycles, a clear relationship was detected. The stone specimens were three times stiffer than the ballast specimens when a cyclic load of between 15kPa and 250kPa was repeatedly applied to the specimen. Although this maybe a reality, it may also be the size effect due to the differing D/d_{max} ratio of the two specimens, 4.7 for the 50mm ballast and nearly 12 for the 20mm stone. Further testing is required to ascertain what the cause of this significant difference is between the two sizes of stone.

An alternative way of looking at this data is shown in Figure 5.62. This graph shows for both the stone and ballast specimens the development of the resilient modulus versus the confining stress for load cycles 100, 1000, 10,000, and 100,000.

In Figure 5.63 the resilient modulus was normalised with respect to the cell pressure, σ_3, for the ballast tests. The 40kPa cell pressure tests had the highest normalised resilient modulus values, which implied that the specimen was stiffer at lower cell pressures than at higher pressures. It was postulated that with greater breakage occurring at the higher cell pressures then the modulus would be reduced. However, as will be demonstrated in Chapter 6, the amount of breakage is little affected by the cell pressure in the cyclic load tests (Table 6.5). Furthermore this pattern was also observed, although not so well defined, in the stone tests where little if any breakage was observed.

When the resilient modulus is normalised with respect to the bulk stress ($\theta = \sigma_1+\sigma_2+\sigma_3$, where σ_1 is at the loaded stress state) then the development of the resilient modulus (normalised) with the number of load cycles, irrespective of the cell pressure, is a lot more consistent as seen for the ballast specimens in Figure 5.64. This trend was also seen in the 20m stone tests, apart from the 240kPa cell pressure test. Comparing the normalised stone only and ballast only resilient modulus in Figure 5.65 shows again a clear pattern. However the correlation was not as good as was seen in Figure 5.61 (R^2 = 0.642 compared to 0.976).

5.8.2 Resilient modulus in Series 3 – development of breakage

Series 3 consisted of two test subdivisions. The first one was those tests carried out with 1 million and 2 million load cycles, at 90kPa cell pressure. The resilient modulus versus the number of load cycles for these tests is plotted in Figure 5.66. The third curve on this graph is the average resilient modulus for the ballast specimens tested at

90kPa cell pressure in Series 2. This shows good repeatability between the two test series. After 500,000 load cycles the resilient modulus reduced to values similar and below that calculated at 100 load cycles. As explained in Section 3.5.3 the test procedure for test T42 was unusual due to a power cut at around 800,000 load cycles. The test was restarted after a period where only the nominal axial stress of 15kPa was left on the specimen, and was run for a further 1 million load cycles. It was unclear why there was such a high resilient modulus calculated at the start of the second phase of loading, although it could possibly mean the tests are not comparable. However it is noticeable that there was a similar drop off in the resilient modulus value in both tests after 200,000-500,000 load cycles.

The second subdivision in Series 3 was for those tests that were carried out at 140kPa and were investigating the breakage of material in the early stages of the cyclic load test (Figure 5.67). Typically the values of resilient modulus calculated for these three tests were comparable with similar tests in Series 2, although the resilient modulus of test T66 was slightly higher than the other tests. Again when the resilient modulus was normalised with respect to the bulk stress for the tests carried out at 90kPa and 140kPa cell pressure in Series 3, then the development of the resilient modulus with load cycles was consistent irrespective of cell pressure (Figure 5.68).

5.8.3 Resilient modulus in Series 4 – two-layer specimens

The majority of tests in Series 4 were carried out with a 40kPa cell pressure. The resilient modulus versus number of load cycles graph (Figure 5.69) shows the results of tests carried out in Series 4 compared with the average resilient modulus for stone and ballast specimens from Series 2. This shows that where there was a small layer of stone overlying the ballast the resilient modulus was slightly lower at the start of the test than a typical ballast specimen. By 100,000 load cycles the values of the resilient moduli were similar to the ballast specimens. However, where there was a significant amount of stone overlying the ballast then the resilient moduli calculated were in-between those of the stone and the ballast.

This pattern was also noted with the 90kPa cell pressure tests with the single layer specimen having a slightly lower resilient modulus than the ballast specimen, and the 1-1 layer specimen being in between that of the ballast and the stone.

5.8.4 Resilient modulus in Series 5 – damped specimens

Tests in Series 5 had a disc of MDF in between the top of the specimen and top cap and a rubber mat between the bottom of the specimen and the base pedestal (damping). The modulus of both the MDF disc and the rubber mat was tested. This equated to a correction of up to a maximum of 0.25MPa, which in terms of the overall modulus of the specimens was insignificant.

It is clear from Figure 5.70 that the resilient modulus was significantly reduced in all of the tests with damping compared to the conventional tests in Series 2. There was little difference between the double layer damped specimen and the ballast only damped specimen. This would appear to be in accordance with the results from Series 4 (Section 5.8.3).

5.8.5 Resilient modulus in Series 6 – wet specimens

In Series 6 where the ballast was wetted before the tests it was seen that the wet specimens had a significantly lower resilient modulus than a similarly prepared dry specimen (Figure 5.71). It was also noticeable that the values of the resilient modulus for the different cell pressures in the wet tests were very similar to one another compared to those in the dry tests.

	Test details						Deviator stress (kPa)				Modulus (MPa)		Volumetric strain (%)			
	Specimen No.	Specimen details	Load -ing*	Cell pressure (kPa)	Dry density (Mg/m^3)	Void ratio	Peak	Finish	@ 4% strain (3% pcm.)	@ 6% strain	E_t	E_s	@ 1% strain	@ 4% strain (3% pcm.)	@ 6% strain	Comments
Monotonic	T1	Cloburn stone	mono.	40	1.59	0.662	-	260	240	-	122	6	1.03	8.20	-	approximate height
	T6	Cloburn stone	mono.	40	1.66	0.597	-	309	304	311	64	17	0.89	8.83	14.03	-
	T8	Cloburn stone	mono.	90	1.63	0.629	-	665	616	-	86	73	0.46	6.49	-	-
	T17	Cloburn stone	mono.	90	1.57	0.683	-	620	630	620	123	70	0.96	9.12	14.84	slight pre loading from reaction bar
	T18	Cloburn stone	mono.	90	1.58	0.672	-	580	538	-	61	41	-0.52	4.43	9.25	lose of vacuum as the top cap was realigned
	T5	Bardon stone	mono.	40	1.70	0.649	-	380	325	380	33	19	0.29	8.21	13.40	-
	T14	Bardon stone	mono.	40	1.68	0.670	-	365	363	365	51	31	0.87	8.03	12.60	-
	T7	Bardon stone	mono.	90	1.70	0.657	-	698	655	-	78	69	0.10	4.86	-	slight ingress of water, possibly after test had finished
	T16	Bardon stone	mono.	90	1.64	0.709	-	670	610	660	88	72	0.27	5.55	9.36	-
	T10	ballast	mono.	40	1.47	0.818	-	254	268	-	68	25	0.22	4.05	-	-
	T12	ballast	mono.	90	1.50	0.777	-	637	541	630	106	88	0.22	4.05	6.30	-
Post cyclic monotonic	T11	Cloburn stone	pcm.	40	1.50	0.767	351	-	-	-	432	435	-	-	-	-
	T13	Cloburn stone	pcm.	40	1.42	0.863	367	-	-	-	442	432	3.47	-	-	-
	T2	Cloburn stone	pcm.	90	1.50	0.879	-	490	480	-	220	206	2.17	7.31	-	-
	T4	Bardon stone	pcm.	40	1.60	0.759	435	-	326	-	1283	1226	3.00	8.58	-	slight hydraulic problems at start of test
	T15	Bardon stone	pcm.	40	1.64	0.718	428	-	333	-	870	868	2.66	7.62	-	-
	T9	Bardon stone	pcm.	90	1.72	0.631	-	723	653	-	1567	1550	1.50	5.80	13.00	-
	T3	Ballast	pcm.	40	1.40	0.909	432	-	367	-	328	329	1.04	-	-	-

*mono. = monotonic load test, pcm. = post cyclic monotonic load test

Table 5.1 - Test details and results for monotonic and post cyclic monotonic load triaxial tests in Series 1

	Test details					Axial strain (%)			Volumetric strain (%)		
	Specimen No.	Specimen details	Cell pressure (kPa)	Dry density (Mg/m^3)	Void ratio	1st cycle	100 cycles (corrected)	100,000 cycles (corrected)	100 cycles (corrected)	100,000 cycles (corrected)	Comments
Cyclic	T11	Cloburn stone	40	1.64	0.613	0.40	2.4	6.80	2.90	8.80	-
	T13	Cloburn stone	40	1.57	0.690	1.21	2.46	5.92	4.00	9.39	-
	T2	Cloburn stone	90	1.50	0.763	-	-	-	-	-	axial lvdt not attached until cycle 23
	T4	Bardon stone	40	1.67	0.685	0.33	2.05	3.43	3.00	3.85	-
	T15	Bardon stone	40	1.66	0.691	2.50	1.75	3.18	1.60	2.54	-
	T9	Bardon stone	90	1.71	0.644	0.27	0.28	0.69	-0.16	-0.56	specimen drainage valve closed for first 800 cycles
	T3	Ballast	40	1.43	0.865	0.87	2.13	4.32	1.30	1.27	-

Table 5.2 - Test details and results for cyclic load triaxial tests in Series 1

	Specimen	Dry density (Mg/m^3)				
		Minimum density	Maximum density	Average density	Range of densities	Void ratio
Key (1998)	20mm Bardon	1.65	1.68	1.67	0.04	-
	50mm Bardon	1.45	1.48	1.47	0.02	-
Series 1	20mm Bardon	1.64	1.71	1.68	0.07	0.672
	20mm Cloburn	1.5	1.66	1.59	0.16	0.664
Series 2	20mm Bardon	1.66	1.68	1.67	0.02	0.679
	50mm Bardon	1.44	1.5	1.48	0.06	0.806

Table 5.3 - Densities of specimens tested in Series 1 and Series 2 compared with those tested by Key (1998)

	Test details						Deviator stress (kPa)				Modulus (MPa)		Volumetric strain (%)			
	Specimen No.	Specimen details*	Cell pressure (kPa)	Density (Mg/m^3)	Void ratio	Particles in	Peak	Finish	@ 4% strain (3% pcm.)	@ 6% strain	E_t	E_s	@ 1% strain	@ 4% strain (3% pcm.)	@ 6% strain	Comments**
Monotonic load tests	T19	stone	40	1.67	0.681	-	-	320	311	-	33	13	0.10	2.70	-	-
	T72	stone	40	1.68	0.668	-	-	308	302	314	83	14	0.29	3.20	5.40	very slight leak at base – effVC.
	T22	stone	90	1.67	0.680	-	-	577	580	620	193	93	0.04	1.86	3.51	-
	T63	stone	140	1.68	0.674	-	-	883	740	807	228	96	-0.25	1.00	2.30	-
	T27	ballast	40	1.45	0.838	346	-	300	260	284	55	21	0.00	1.70	2.80	-
	T26	ballast	90	1.49	0.792	431	-	435	413	470	67	21	-0.46	0.00	0.70	slight leak internal down one side – effVC.
	T40	ballast	90	1.47	0.812	336	-	525	481	511	55	45	-0.23	0.33	0.84	-
	T60	ballast	140	1.47	0.817	379	-	573	552	562	81	74	-0.28	-0.14	-0.18	-
	T50	single layer	40	1.46	0.825	336	290	270	235	280	36	5	-0.13	1.20	2.30	-
	T52	double layer	40	1.52	0.733	385	340	330	310	-	46	27	0.07	1.60	-	slight leak to atmosphere – effVC.
	T53	1:2 layer	40	1.57	0.736	268	365	365	345	-	72	34	0.40	2.60	-	poss. drainage valve problem
	T28	1:1 layer	40	1.63	0.683	186	310	300	280	310	71	9.8	0.28	2.40	4.10	-
	T29	1:1 layer	40	1.60	0.714	203	-	350	345	350	60	19	0.18	2.50	4.40	-
	T43	1:1 layer	40	1.59	0.726	158	-	-	-	-	76	8	-	-	-	slight leak to atmosphere. No volume change unit
	T44	1:1 layer	40	1.62	0.694	178	330	330	320	320	48	21	0.24	2.70	4.40	slight leak to atmosphere– effVC.
	T30	1:1 layer	90	1.58	0.731	193	665	600	580	640	85	68	-0.17	1.30	2.50	slight leak to atmosphere– effVC.
	T49	2:1 layer	40	1.63	0.702	115	340	335	330	335	44	20	0.22	3.00	4.90	-
	T81	wet ballast	40	1.53	0.747	380	-	260	280	-	86	18	0.20	2.00	-	very dense
	T82	wet ballast	90	1.47	0.812	379	-	410	390	390	43	30	-0.39	-0.20	-0.40	-
	T79	wet ballast	140	1.48	0.809	370	-	520	470	510	120	93	-	-	-	error with the volume change unit readings
	T58	ballast	90	1.49	0.891	395	-	-	-	-	-	-	-	-	-	control test – no load applied
Post cyclic monotonic load tests	T33	stone	40	1.59	0.772	-	400	300	300	-	550	-	1.40	3.70	-	-
	T54	stone	40	1.60	0.753	-	375	-	280	-	634	-	1.50	3.80	-	-
	T55	stone	40	1.55	0.810	-	390	-	285	-	726	-	1.40	3.60	-	Significant leak at bottom – effVC.
	T56	stone	40	1.63	0.728	-	420	-	320	-	750	-	1.40	3.90	-	-
	T73	stone	40	1.60	0.758	-	470	-	300	-	934	-	1.50	3.90	-	-
	T74	stone	40	1.59	0.769	-	415	275	275	-	678	-	1.50	3.90	-	-
	T35	stone	90	1.69	0.667	-	-	-	567	585	918	-	0.73	2.30	4.80	-
	T59	stone	140	1.68	0.677	-	-	844	809	860	1048	-	0.29	1.40	3.60	-
	T68	stone	140	1.69	0.660	-	-	863	780	868	1387	-	0.34	1.40	3.50	slight leak during pcm – see above, no radial trans.
	T76	stone	240	1.71	0.639	-	-	-	-	-	1725	-	-	-	-	test stopped due to too high axial loads
	T24	ballast	40	1.50	0.805	-	465	-	330	280	500	-	1.20	2.60	4.20	-
	T57	ballast	40	1.46	0.830	-	420	-	330	330	544	-	1.00	2.60	-	-
	T25	ballast	90	1.47	0.820	-	495	-	425	463	650	-	0.36	1.10	2.00	slight internal leak – effVC.
	T61	ballast	140	1.48	0.799	-	-	571	538	567	490	-	0.15	0.40	1.20	big leak in pcm. – effVC.
	T62	ballast	140	1.53	0.749	-	-	700	653	715	605	-	0.14	0.50	1.50	very slight leak into sample – see above
	T39	single layer	40	1.47	0.819	-	440	340	330	330	507	-	0.80	3.00	4.50	-
	T48	single layer	40	1.48	0.799	-	440	330	370	-	465	-	0.90	2.40	-	twisted top cap
	T51	double layer	40	1.48	0.803	-	460	325	340	350	530	-	1.00	2.60	4.70	-
	T46	1:1 layer	40	1.54	0.761	-	420	370	325	-	815	-	1.10	2.90	-	-
	T31	1:1 layer	40	1.52	0.801	-	413	-	-	-	552	-	1.30	-	-	-
	T45	1:1 layer	40	1.60	0.713	-	455	300	330	-	920	-	1.40	3.70	-	-
	T47	2:1 layer	40	1.50	0.839	-	345	-	270	-	510	-	1.30	3.40	-	-
	T32	1:1 layer	90	1.63	0.685	-	655	655	590	655	860	-	0.50	1.70	3.60	-

*A nomenclature for the layered specimens in Series 3 is given in Table 5.8
pcm. = post cyclic monotonic load test
**effVC. = could possibly effect the volume change unit reading

Table 5.4 - Test details and results for monotonic and post cyclic monotonic load triaxial tests in Series 2, 4 and 6

Test details						Axial strain (%)			Volumetric strain (%)		Average resilient modulus				
Specimen No.	Specimen details	Cell pressure (kPa)	Density (Mg/m^3)	Void ratio	Particles in	1st cycle	100 cycles corrected	100,000 cycles corrected	100 cycles corrected	100,000 cycles corrected	@ 100 Cycles	@ 1000 Cycles	@ 10,000 Cycles	@ 100,000 Cycles	Comments effVC. = possibly effect the volume change unit reading
T20	stone	40	1.67	0.683	-	-	-	-	-	-	-	-	-	-	test void
T33	stone	40	1.66	0.691	-	2.24	1.95	3.35	0.10	-0.45	324	427	625	616	-
T54	stone	40	1.66	0.688	-	2.50	2.30	4.10	0.60	0.66	269	355	412	465	-
T55	stone	40	1.68	0.678	-	-	-	-	-	-	281	353	477	520	data acquisition error & significant leak effVC.
T56	stone	40	1.67	0.679	-	0.70	1.40	2.50	0.40	-0.11	320	384	477	503	-
T73	stone	40	1.68	0.674	-	0.90	2.00	3.90	0.48	0.17	289	398	462	539	big leak effVC.
T74	stone	40	1.67	0.681	-	1.20	1.90	3.91	0.67	-1.60	296	385	442	530	v.s.leak to sample effVC.
T21	stone	90	1.66	0.698	-	-	-	-	-	-	-	-	-	-	s.leak to atmosphere effVC. & data acquisition problem
T34	stone	90	1.66	0.698	-	-	-	-	-	-	512	595	671	795	large leak effVC. + error after 20,000 cycles
T35	stone	90	1.67	0.678	-	1.00	0.53	1.00	-0.20	-1.69	502	636	681	723	-
T59	stone	140	1.67	0.687	-	0.13	0.22	0.52	-0.16	-1.26	491	544	568	667	v.s.leak to specimen. effVC.
T68	stone	140	1.67	0.682	-	0.30	0.22	0.57	-0.16	-1.31	635	820	906	959	no radial transducers
T76	stone	240	1.68	0.675	-	0.05	0.13	0.38	-0.12	-1.46	1327	1533	1596	1949	-
T23	ballast	40	1.44	0.845	333	-	-	-	-	-	-	-	-	-	tilting top cap - stopped test
T24	ballast	40	1.49	0.796	365	-	1.2	3.00	0.16	-0.84	211	259	313	298	1, 10, 100...100,000 cycles not recorded
T38	ballast	40	1.48	0.799	366	0.70	0.86	2.10	-0.04	-0.97	215	252	284	313	-
T57	ballast	40	1.49	0.790	378	1.70	1.0	2.10	0.01	0.40	197	221	272	264	possibly slight leak. effVC.
T25	ballast	90	1.47	0.820	381	1.15	0.72	1.72	-0.30	-1.80	275	317	347	356	v.slight leak into specimen. effVC.
T36	ballast	90	1.49	0.791	403	1.30	0.46	1.21	-0.21	-0.85	301	326	354	378	-
T37	ballast	90	1.49	0.794	398	0.78	0.39	1.13	-0.14	-0.16	300	326	368	369	v.slight leak - few ml. effVC.
T61	ballast	140	1.47	0.814	355	0.2	0.18	0.76	-0.14	-0.25	353	379	398	385	slight leak cyclic. effVC., big leak in pcm
T62	ballast	140	1.50	0.774	386	0.60	0.22	0.69	-0.17	-1.66	360	367	357	386	v. slight leak into specimen. effVC.
T64	ballast	140	1.49	0.790	389	1.40	0.17	0.62	-0.15	-1.17	350	386	410	432	-
T77	ballast	240	1.49	0.792	360	0.05	0.12	-	-0.13	-	548	601	693	-	failed after 20,000 cycles
T39	single layer	40	1.49	0.790	372	1.50	1.10	2.62	-0.03	-0.82	200	225	292	315	-
T48	single layer	40	1.50	0.782	344	2.20	0.86	2.64	-0.05	-1.30	213	212	242	262	-
T41	single layer	90	1.49	0.789	324	0.60	0.47	1.20	-0.32	-1.99	282	300	321	345	-
T51	double layer	40	1.48	0.805	353	2.80	1.50	3.60	-0.03	-0.94	186	236	256	299	-
T46	1:2 layer	40	1.57	0.727	216	0.34	1.10	2.20	0.21	-0.56	251	298	305	370	-
T31	1:1 layer	40	1.62	0.695	207	1.26	2.00	3.70	4.80	-0.55	255	298	355	385	-
T45	1:1 layer	40	1.62	0.689	177	1.70	0.80	1.75	0.15	-0.57	305	308	373	366	-
T47	2:1 layer	40	1.63	0.701	121	3.00	2.30	5.00	0.73	0.40	234	297	293	394	-
T32	1:1 layer	90	1.60	0.712	161	1.30	0.35-	0.98	-0.28	-2.25	368	411	466	493	-
T69	ballast, damping	140	1.46	0.825	344	0.63	0.27	0.94	-0.22	-1.53	213	217	227	259	-
T70	double layer stone, damping	140	1.48	0.820	350	-	-	-	-	-	-	243	255	275	first 4 cycles not recorded - manual error
T71	stone, damping	140	1.66	0.692	-	0.22	0.31	0.72	-0.21	-1.15	328	370	391	435	-
T80	wet ballast	40	1.49	0.794	370	1.60	1.75	4.90	0.20	-1.00	182	212	251	219	-
T83	wet ballast	90	1.47	0.815	351	0.43	0.44	1.90	-0.20	-2.00	230	262	305	-	-
T78	wet ballast	140	1.45	0.837	345	0.42	0.51	2.40	-0.35	-2.50	281	268	282	246	-

Table 5.5 - Test details and results for cyclic load triaxial tests in Series 2, 4, 5 & 6

Test details						Axial strain (%)				Volumetric strain (%)			Average resilient modulus							
Specimen No.	Specimen details	Cell pressure (kPa)	Density (Mg/m^3)	Void ratio	Particles in	1st cycle	100 cycles (corrected)	100,000 cycles (corrected)	1 million cycles (corrected)	100 cycles (corrected)	100,000 cycles (corrected)	1 million cycles (corrected)	100 cycles	1000 cycles	10,000 cycles	100,000 cycles	500,000 cycles	1 million cycles	1.8 million cycles	Comments
T65	ballast	140	1.48	0.807	365	0.30	0.19	-	-	-0.17	-	-	357	-	-	-	-	-	-	-
T66	ballast	140	1.49	0.796	338	0.30	0.24	-	-	-0.21	-	-	370	431	-	-	-	-	-	-
T67	ballast	140	1.49	0.790	347	0.34	0.27	-	-	-0.24	-	-	342	376	391	-	-	-	-	-
T75	ballast	90	1.49	0.791	367	0.07	0.48	1.80	1.35	-0.20	-1.30	-1.30	318	335	361	403	385	316	-	-
T42	ballast	90	1.49	0.798	330	0.95	0.30	0.98	1.20	-0.20	-1.25	-2.00	273	295	327	373	385	258	233	-

Table 5.6 - Test details and results for cyclic load triaxial tests in Series 3

		Cell pressure (kPa)	Specimen numbers	Individual angles of shearing resistance $\varphi'^{(o)}$		Angle of shearing resistance $\varphi'^{(o)}$ and intercept c'	
						intercept c' = 0	
Monotonic	Clobum stone	40kPa	T1, T6	50 - 53	52	-	φ' = 51 c' = 0
		90kPa	T8, T17, T18	49 - 52	51		
	Bardon stone	40kPa	T5, T14	55 - 56	55	φ' = 53 c' = 0	φ' = 50 c' = 19
		90kPa	T7, T16	52 - 53	52		
Post cyclic monotonic	Clobum stone	40kPa	T11, T13	55		φ' = 54 c' = 0	φ' = 35 c' = 65
		90kPa	T2	47			
	Bardon stone	40kPa	T4, T15	57 – 58		φ' = 57 c' = 0	φ' = 48 c' = 39
		90kPa	T9	53			

Table 5.7 - Shear strength parameters for the initial monotonic and post cyclic monotonic load triaxial tests in Series 1

		Cell pressure (kPa)	Specimen numbers	Individual angles of shearing resistance $\varphi'^{(o)}$	Angle of shearing resistance $\varphi'^{(o)}$ and intercept c'	
					intercept c' = 0	
Monotonic	Stone	40	T19, T72	53	φ' = 51	φ' = 48 c' = 16
		90	T22	51		
		140	T63	51		
	Ballast	40	T27	52	φ' = 46	φ' = 39 c' = 39
		90	T26, T40	46 - 48		
		140	T60	42		
Post cyclic monotonic	Stone	40	T33, T54, T55, T56, T73, T74	56 – 59	φ'= 56	φ'= 44 c'= 49
		90	T35	50		
		140	T59, T68	49		
	Ballast	40	T24, T57	57 - 59	φ'= 46	φ'= 35 c'= 84
		90	T25	46		
		140	T61, T62	42 - 46		

Table 5.8 - Shear strength parameters for the initial monotonic and post cyclic monotonic load triaxial tests in Series 2

Code	Connotation	20mm stone 50mm ballast
single	A single layer of stone under the top cap overlying the ballast specimen	 Single layer stone
double	A double layer of stone under the top cap overlying the ballast specimen	 Double layer stone
1-2 layer	The top third of the specimen is stone, overlying the bottom two thirds of ballast	 1-2 layer
1-1 layer	The top half of the specimen is stone, overlying the bottom half of ballast	 1-1 layer
2-1 layer	The top two thirds of the specimen is stone, overlying the bottom one third of ballast	 2-1 layer

Table 5.9 - Nomenclature of tests in Series 4

Specimen number	Specimen code	Cell pressure (kPa)	Individual test angle of shear resistance $\varphi'^{(o)}$	Angle of shear resistance $\varphi'^{(o)}$ and intercept c'	
				intercept c' = 0	
T27	ballast only	40	52	φ' = 46 (including the 140kPa cell pressure test)	φ' = 39 c' = 39 (including the 140kPa cell pressure test)
T26, T40	ballast only	90	46 - 48		
T50	single	40	52	-	-
T52	double	40	54	-	-
T53	1-2 layer	40	55	-	-
T28, T29, T43, T44	1-1 layer	40	53 - 54	φ' = 53	φ' = 50 c' = 13
T30	1-1 layer	90	52		
T49	2-1 layer	40	54	-	-
T19, T72	stone only	40	53	φ' = 51 (including the 140kPa cell pressure test)	φ' = 48 c' = 16 (including the 140kPa cell pressure test)
T22	stone only	90	51		

Table 5.10 - Shear strength parameters for the initial monotonic load triaxial tests in Series 4 including the results from Series 2

Specimen number	Specimen code	Cell pressure (kPa)	Individual test angle of shear resistance $\varphi'^{(o)}$	Angle of shear resistance $\varphi'^{(o)}$ and intercept	
				Intercept c' = 0	
T24, T57	ballast only	40	57 – 59	$\varphi' = 46$ (including the 140kPa cell pressure test)	$\varphi' = 35$, $c' = 84$ (including the 140kPa cell pressure test)
T25	ballast only	90	46		
T39, T48 ,	single	40	58	-	-
T51	double	40	59	-	-
T46	1-2 layer	40	57	-	-
T31, T45	1-1 layer	40	58	$\varphi' = 52$	$\varphi' = 50$, $c' = 12$
T32	1-1 layer	90	52		
T47	2-1 layer	40	54	-	-
T33, T54, T55, T56, T73, T74	stone only	40	56 - 59	$\varphi' = 46$ (including the 140kPa cell pressure test)	$\varphi' = 35$, $c' = 84$ (including the 140kPa cell pressure test)
T35	stone only	90	46		

Table 5.11 - Shear strength parameters for the post cyclic monotonic load triaxial tests in Series 4 including the results from Series 2

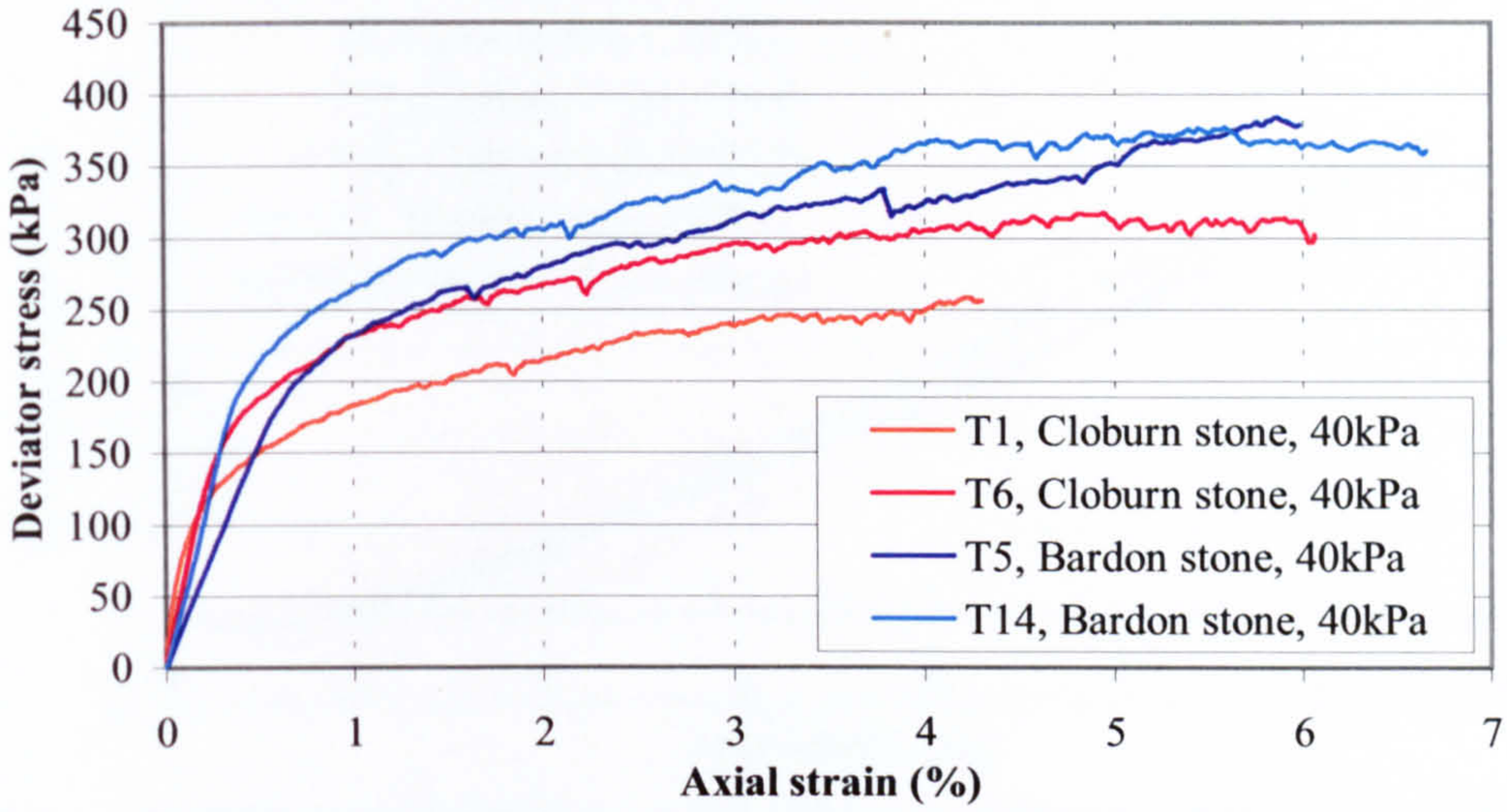

Figure 5.1 - Stress-strain behaviour of Bardon and Cloburn stone specimens in monotonic load triaxial tests at 40kPa cell pressure (Series 1)

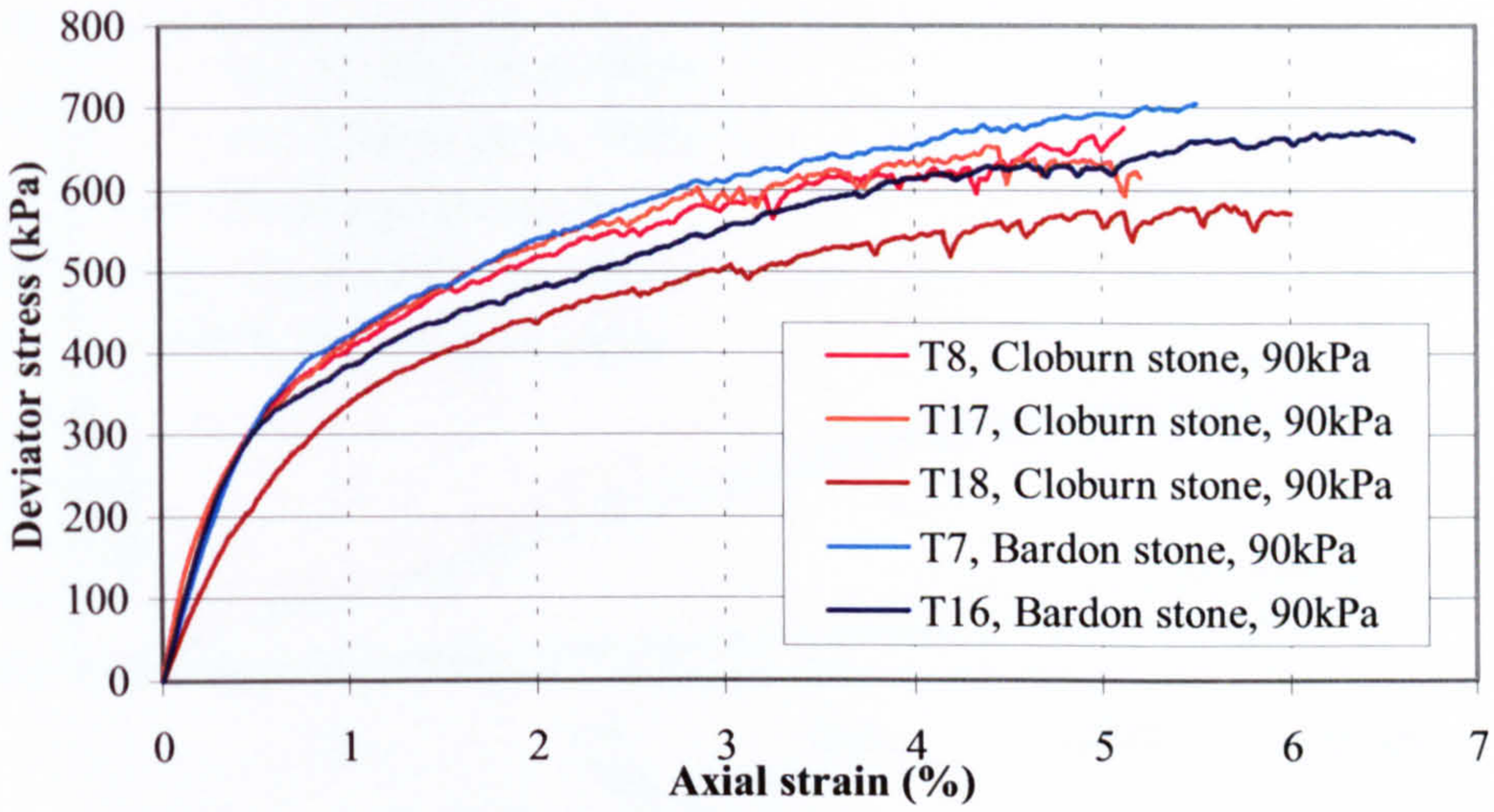

Figure 5.2 - Stress-strain behaviour of Bardon and Cloburn stone specimens in monotonic load triaxial tests at 90kPa cell pressure (Series 1)

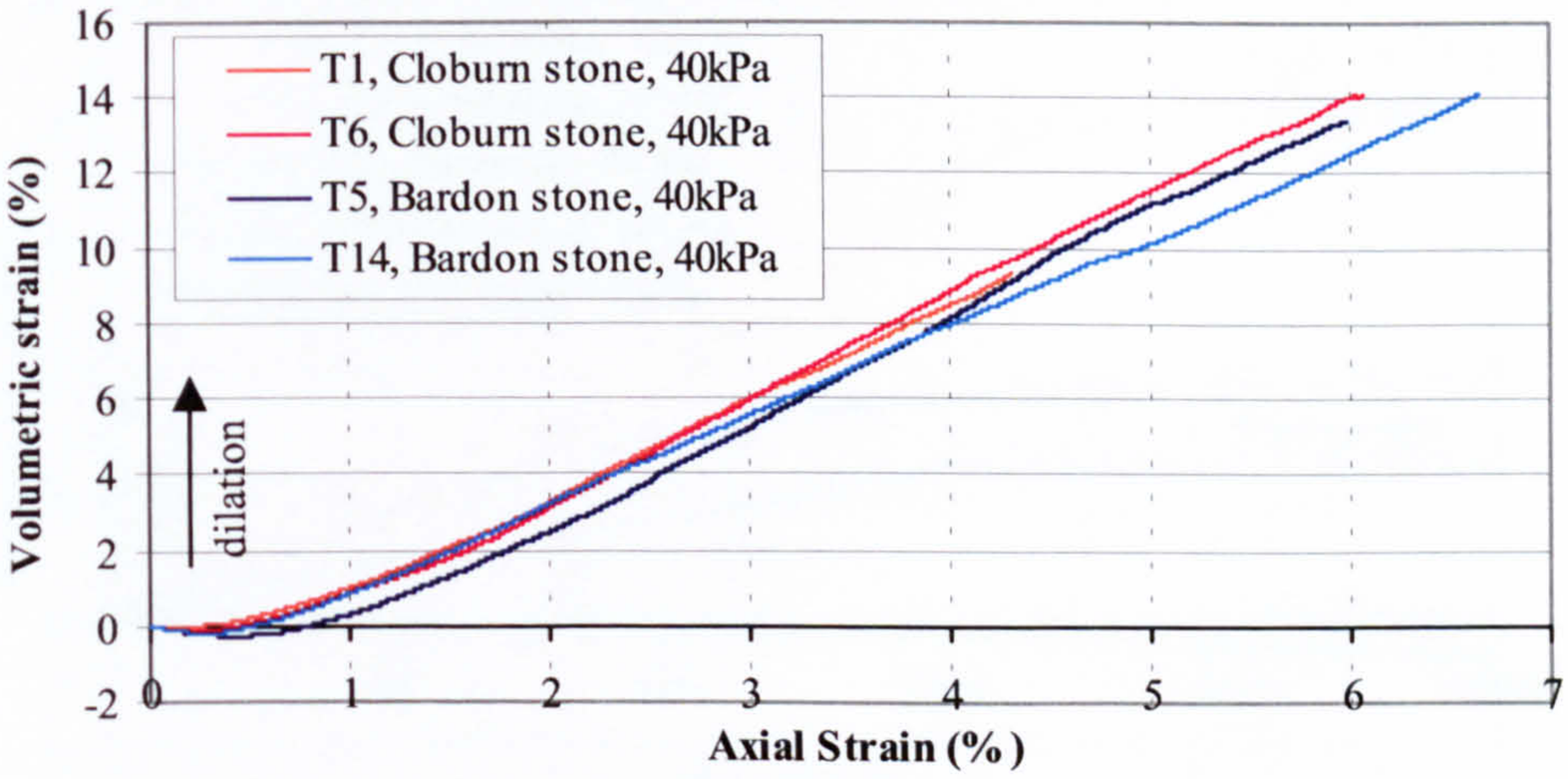

Figure 5.3 - Volumetric strain vs. axial strain behaviour of Bardon and Cloburn stone specimens in monotonic load triaxial tests at 40kPa cell pressure (Series 1)

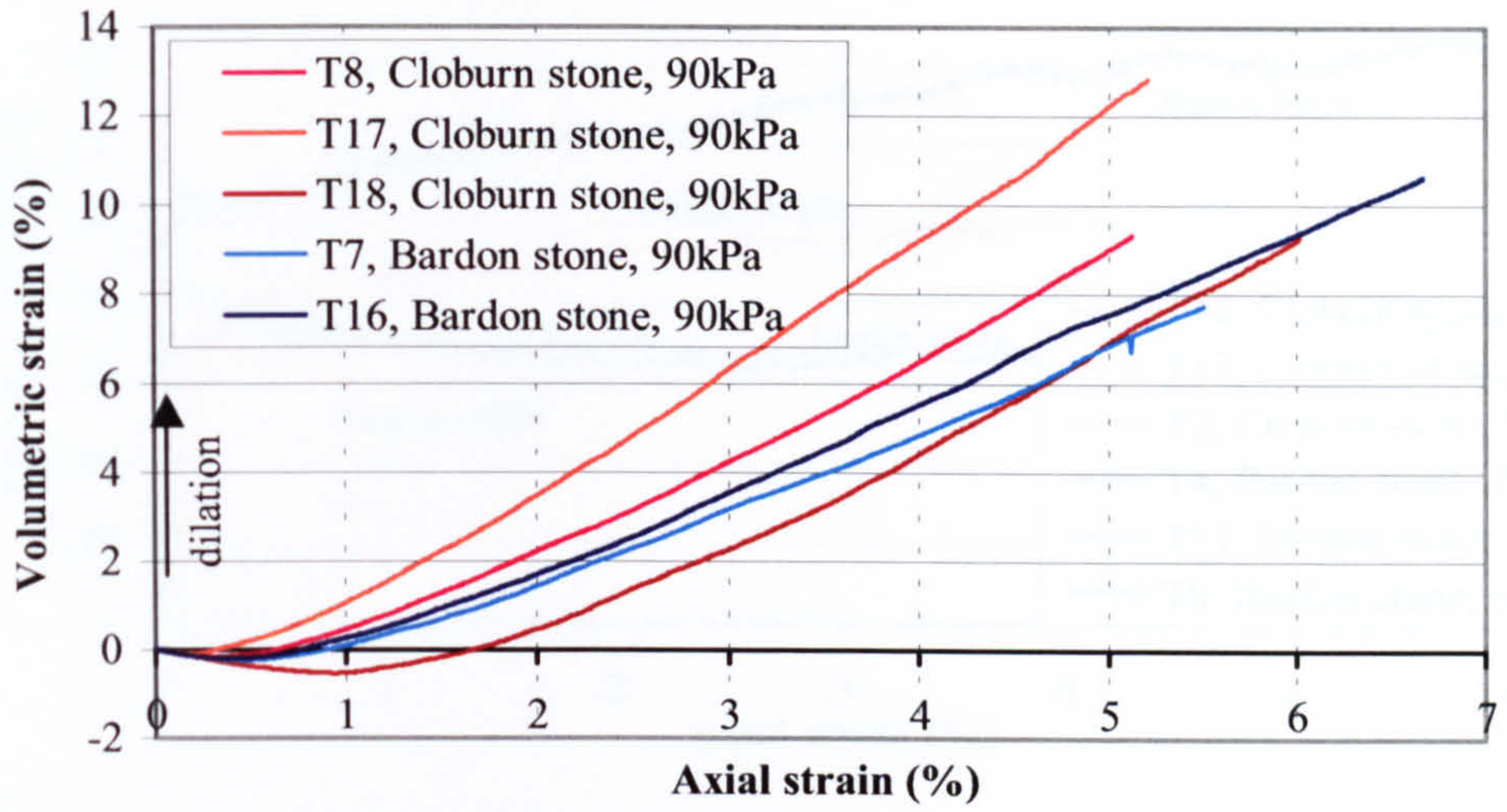

Figure 5.4 - Volumetric strain vs. axial strain behaviour of Bardon and Cloburn stone specimens in monotonic load triaxial tests at 90kPa cell pressure (Series 1)

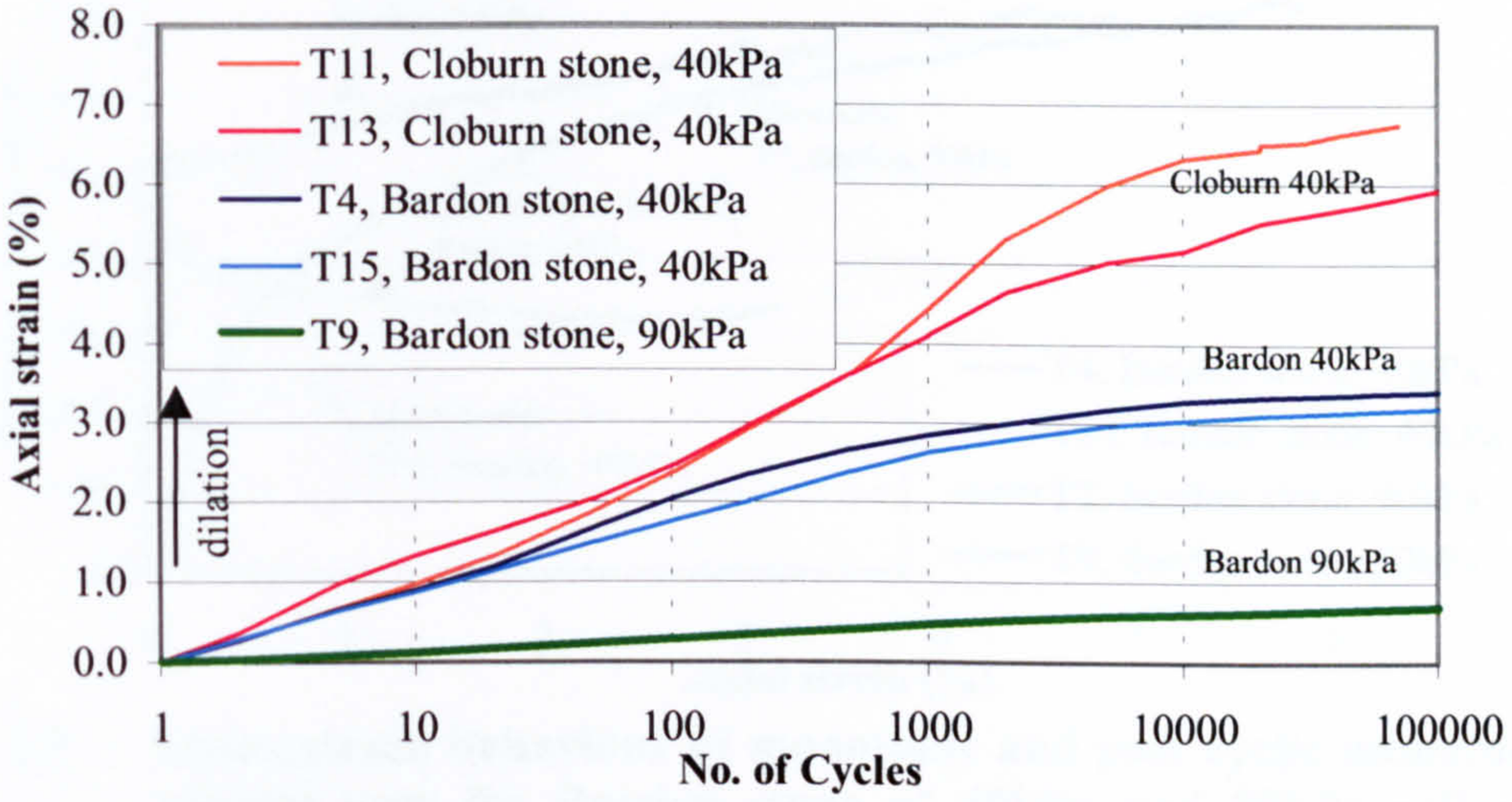

Figure 5.5 - Axial strain behaviour of Bardon and Cloburn stone specimens in cyclic load triaxial tests at 40kPa cell pressure and a Bardon stone specimen at 90kPa cell pressure (Series 1)

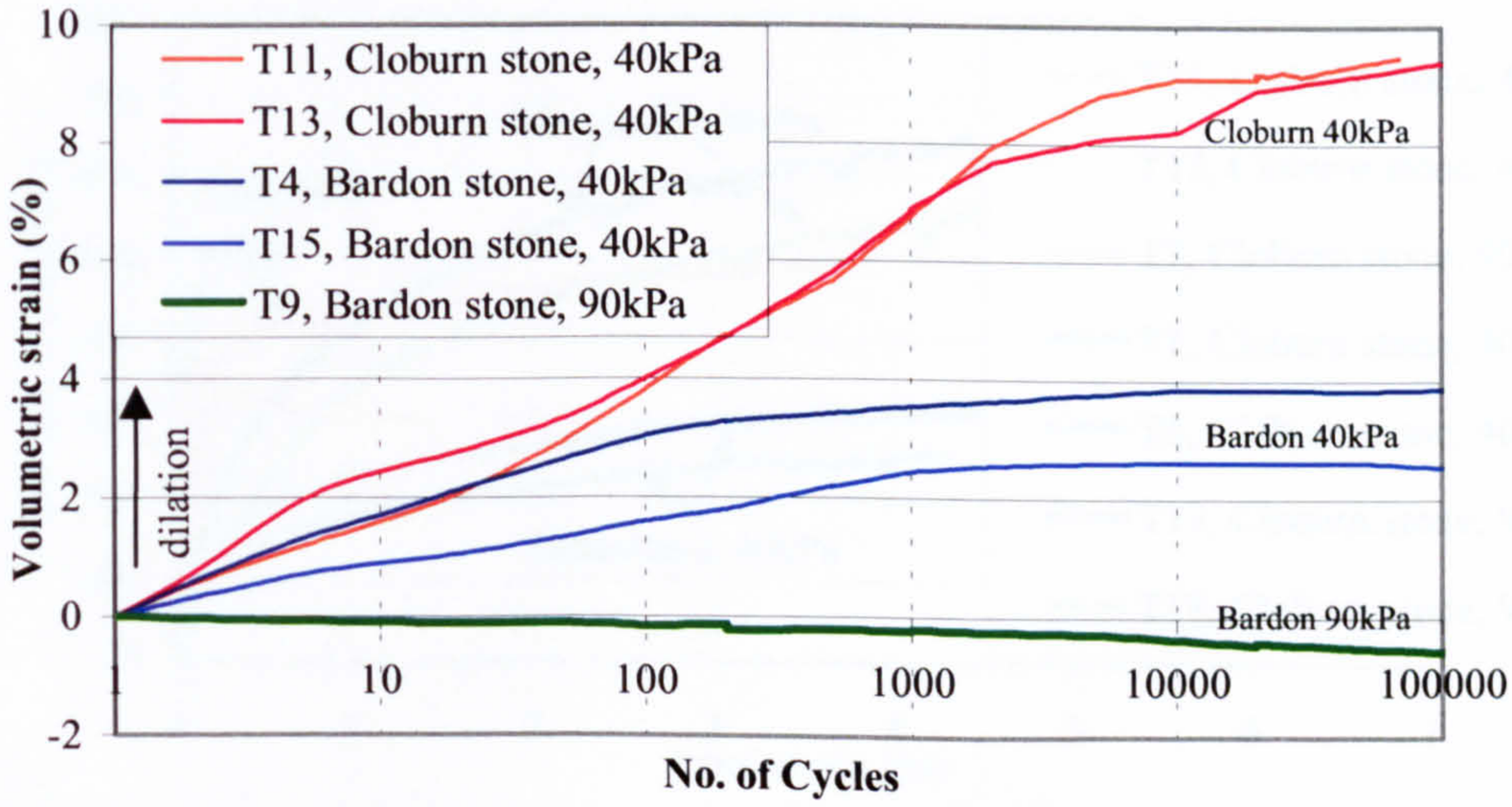

Figure 5.6 - Volumetric strain behaviour of Bardon and Cloburn stone specimens in cyclic load triaxial tests at 40kPa cell pressure and a Bardon stone specimen at 90kPa cell pressure (Series 1)

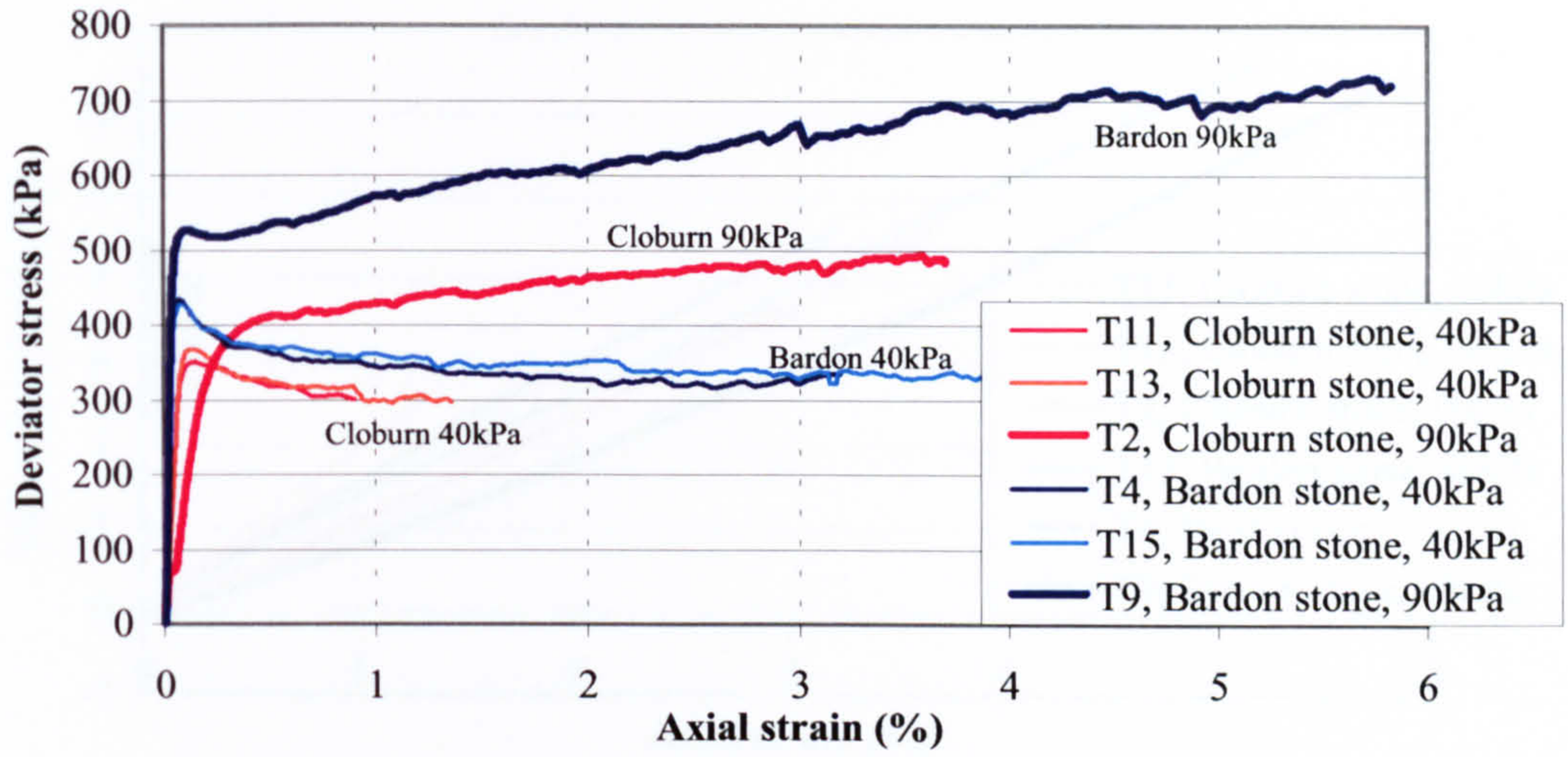

Figure 5.7 - Stress-strain behaviour of all the post cyclic monotonic load triaxial tests at 40kPa and 90kPa cell pressure (Series 1)

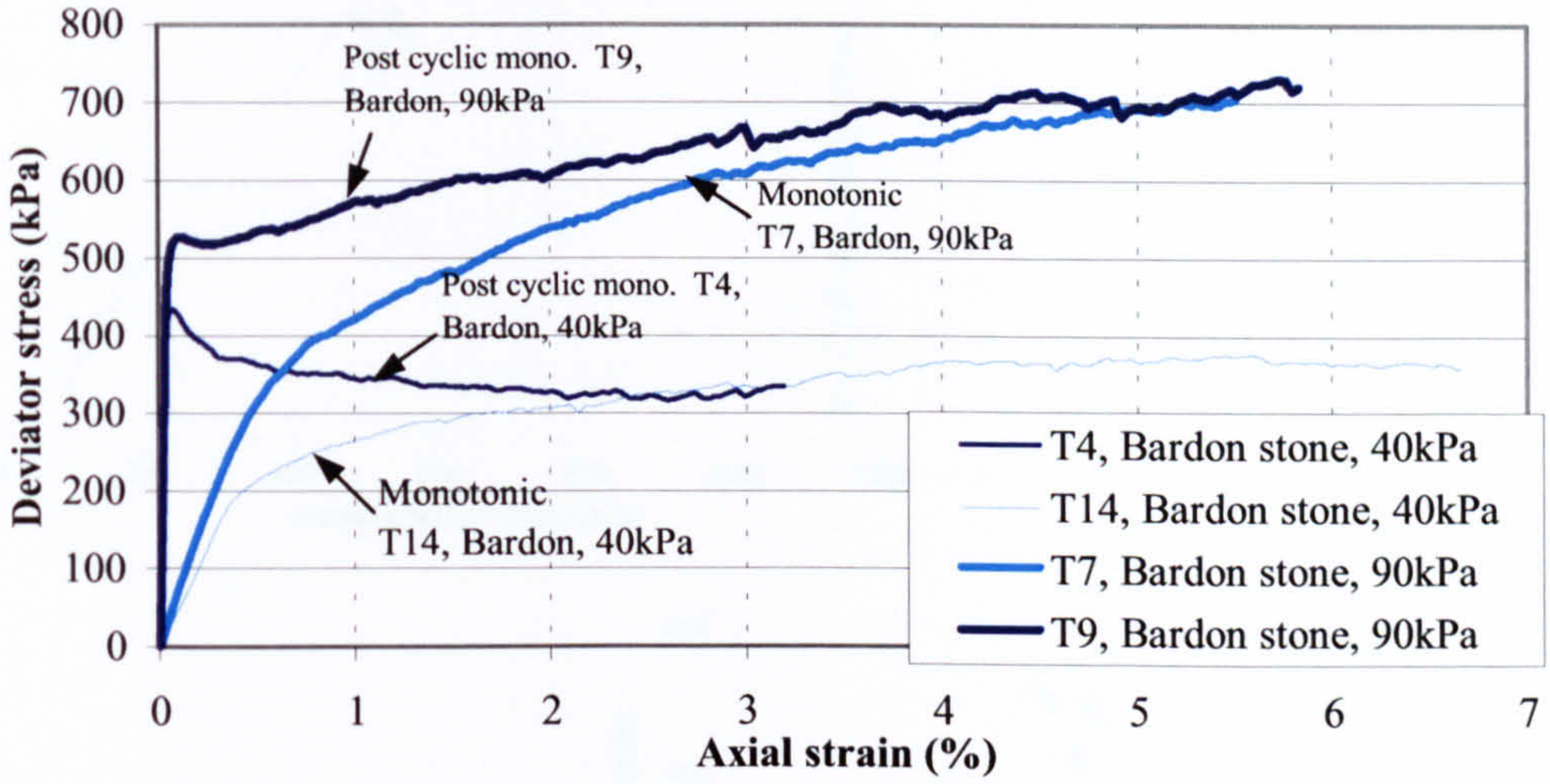

Figure 5.8 - Stress-strain behaviour of monotonic and post cyclic monotonic load triaxial tests for Bardon stone at 40kPa and 90kPa cell pressure (Series 1)

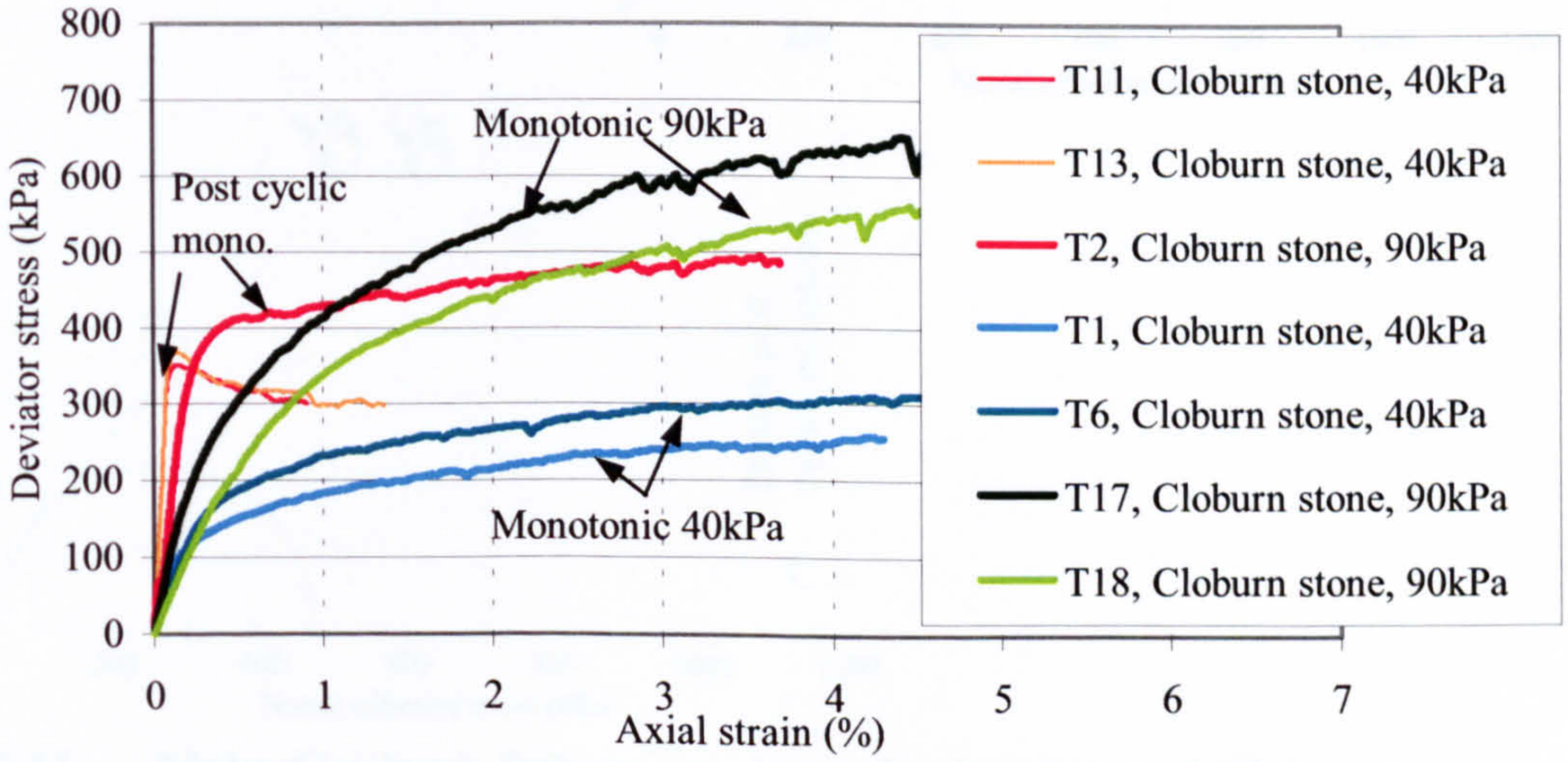

Figure 5.9 - Stress-strain behaviour of monotonic and post cyclic monotonic load triaxial tests for Cloburn stone at 40kPa and 90kPa cell pressure (Series 1)

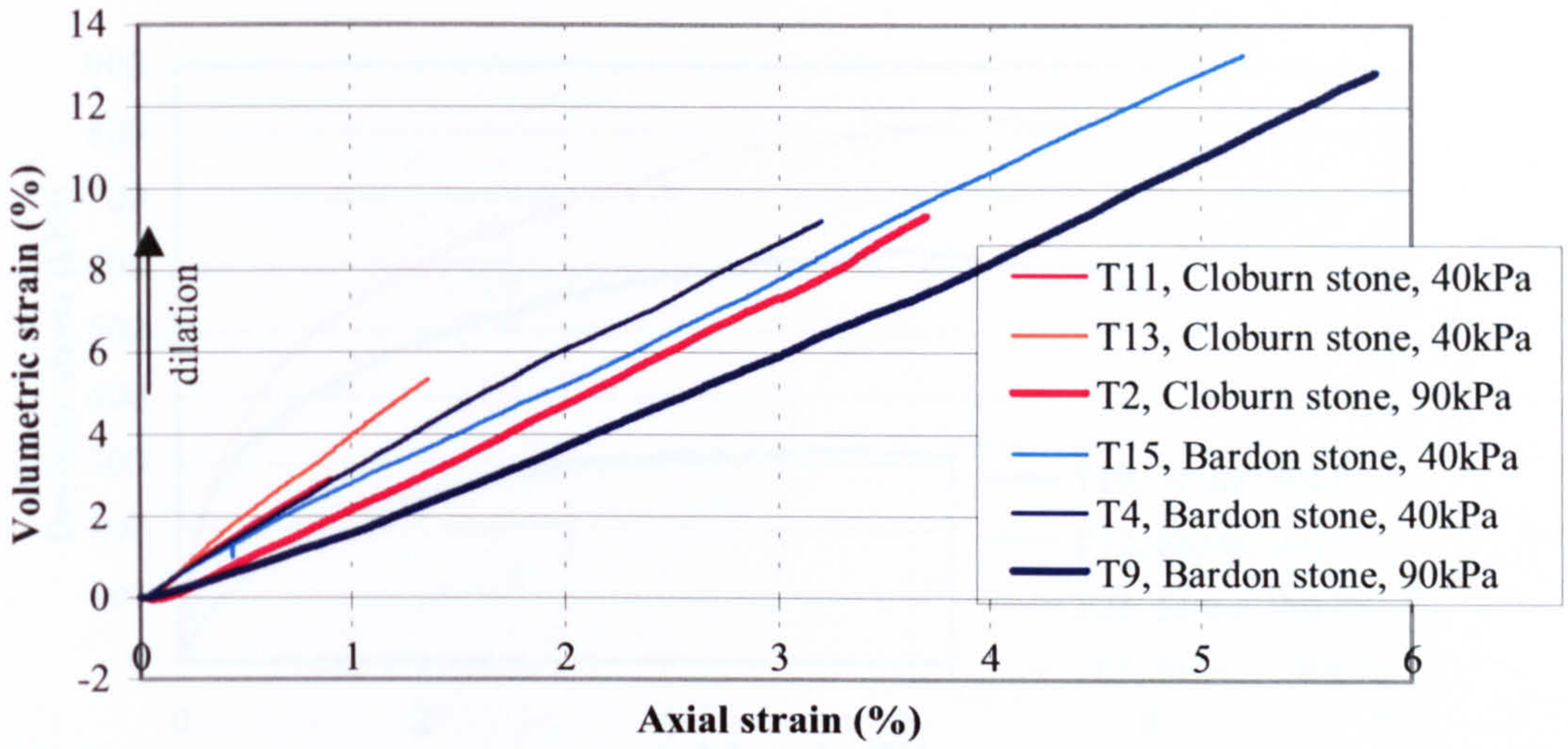

Figure 5.10 - Volumetric strain behaviour of all the post cyclic monotonic load triaxial tests at 40kPa and 90kPa cell pressure (Series 1)

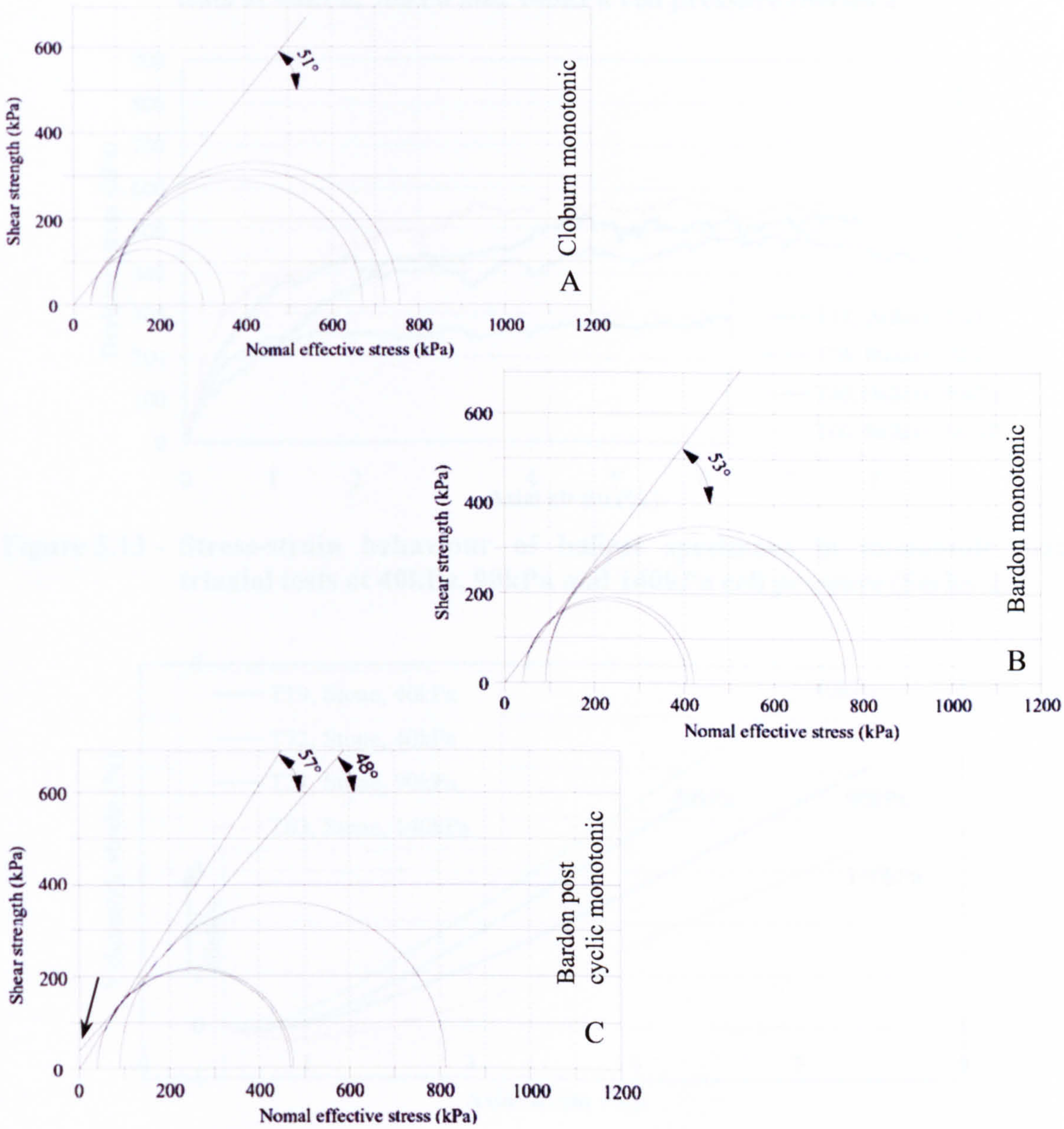

Figure 5.11 - Mohr-Coulomb failure envelopes for Bardon and Cloburn stone in monotonic load triaxial tests (Series 1)
a) Cloburn stone (monotonic), b) Bardon stone (monotonic), and c) Bardon stone (post cyclic monotonic)

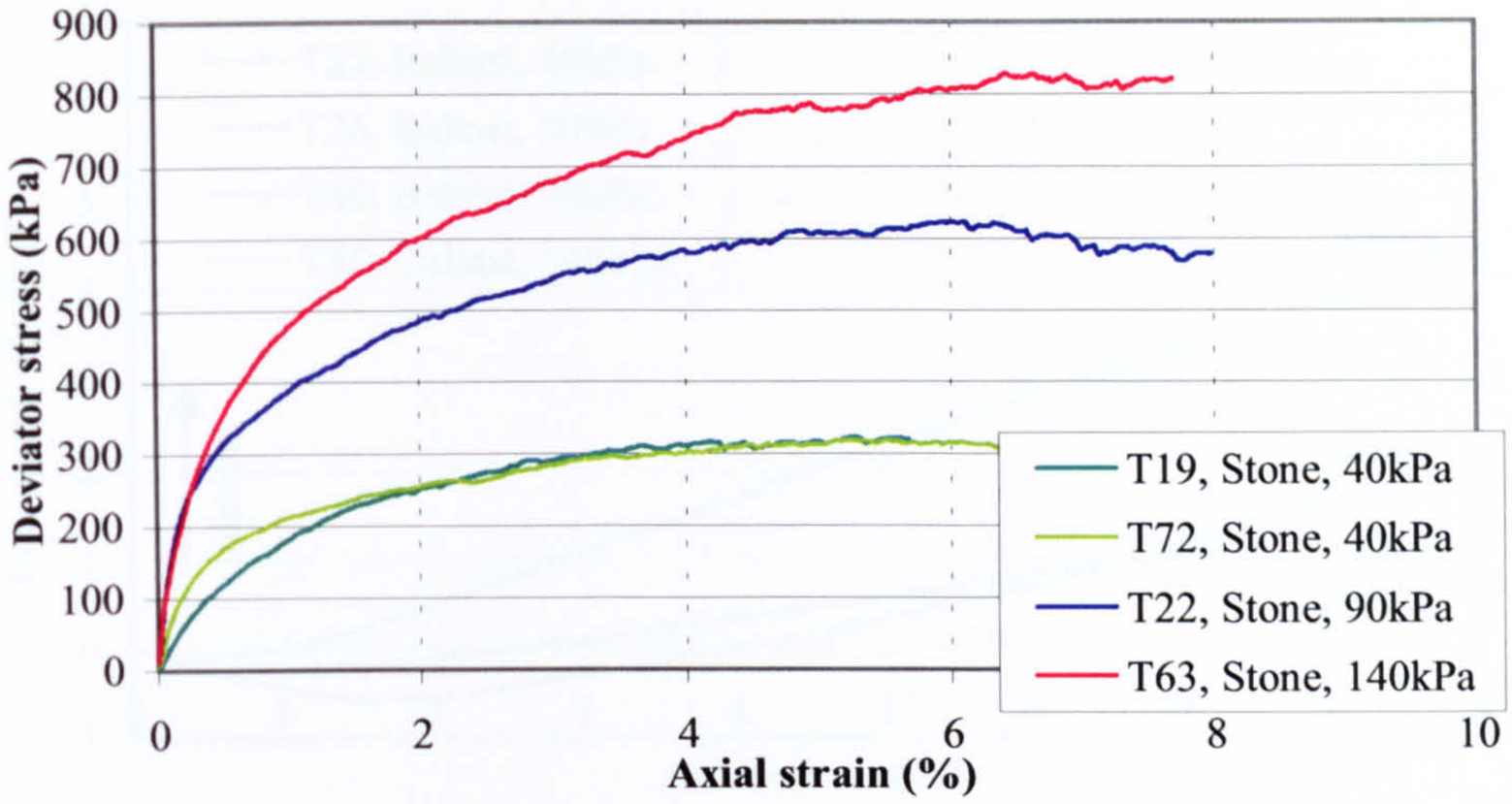

Figure 5.12 - Stress-strain behaviour of stone specimens in monotonic load triaxial tests at 40kPa, 90kPa and 140kPa cell pressure (Series 2)

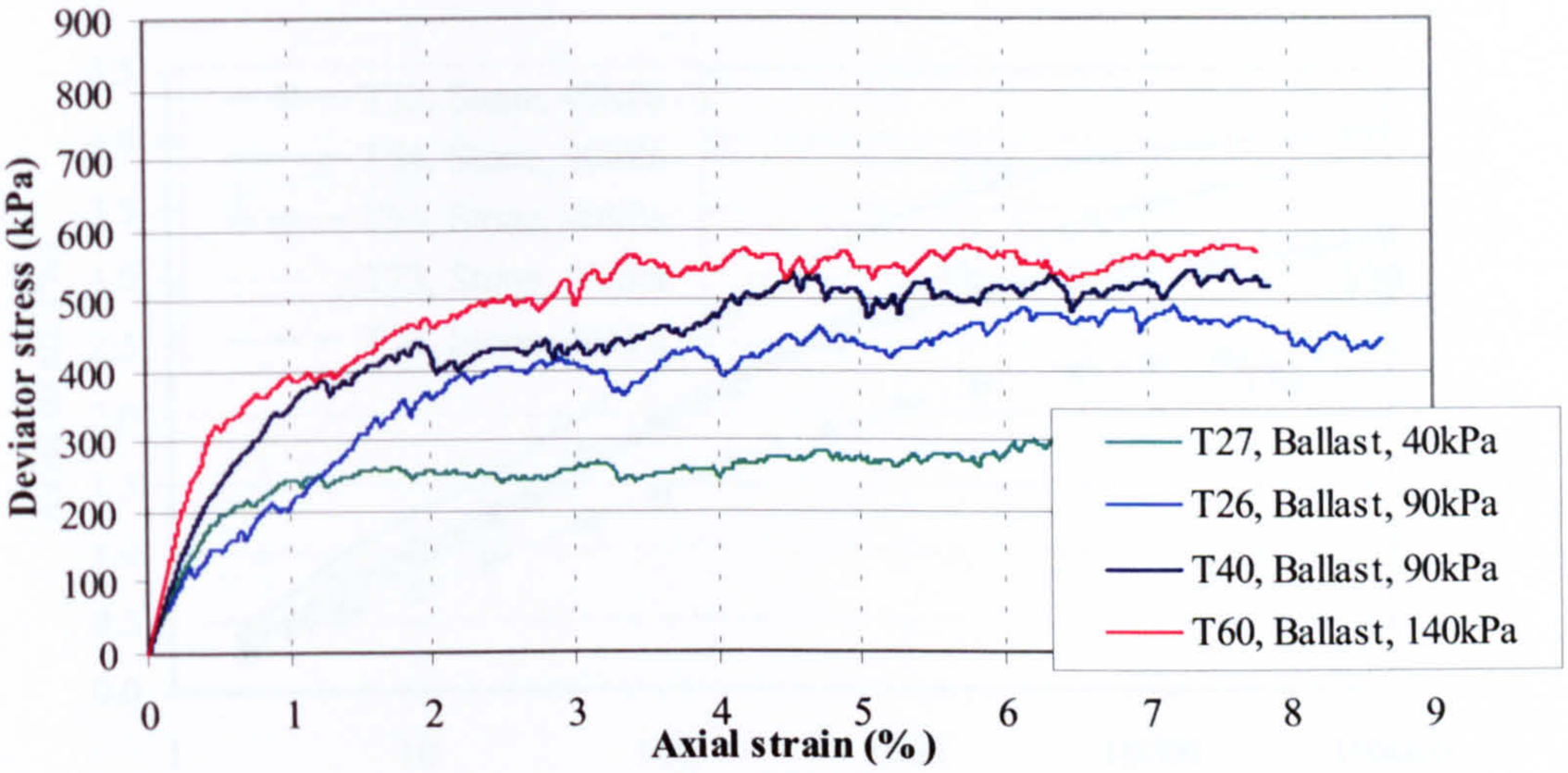

Figure 5.13 - Stress-strain behaviour of ballast specimens in monotonic load triaxial tests at 40kPa, 90kPa and 140kPa cell pressure (Series 2)

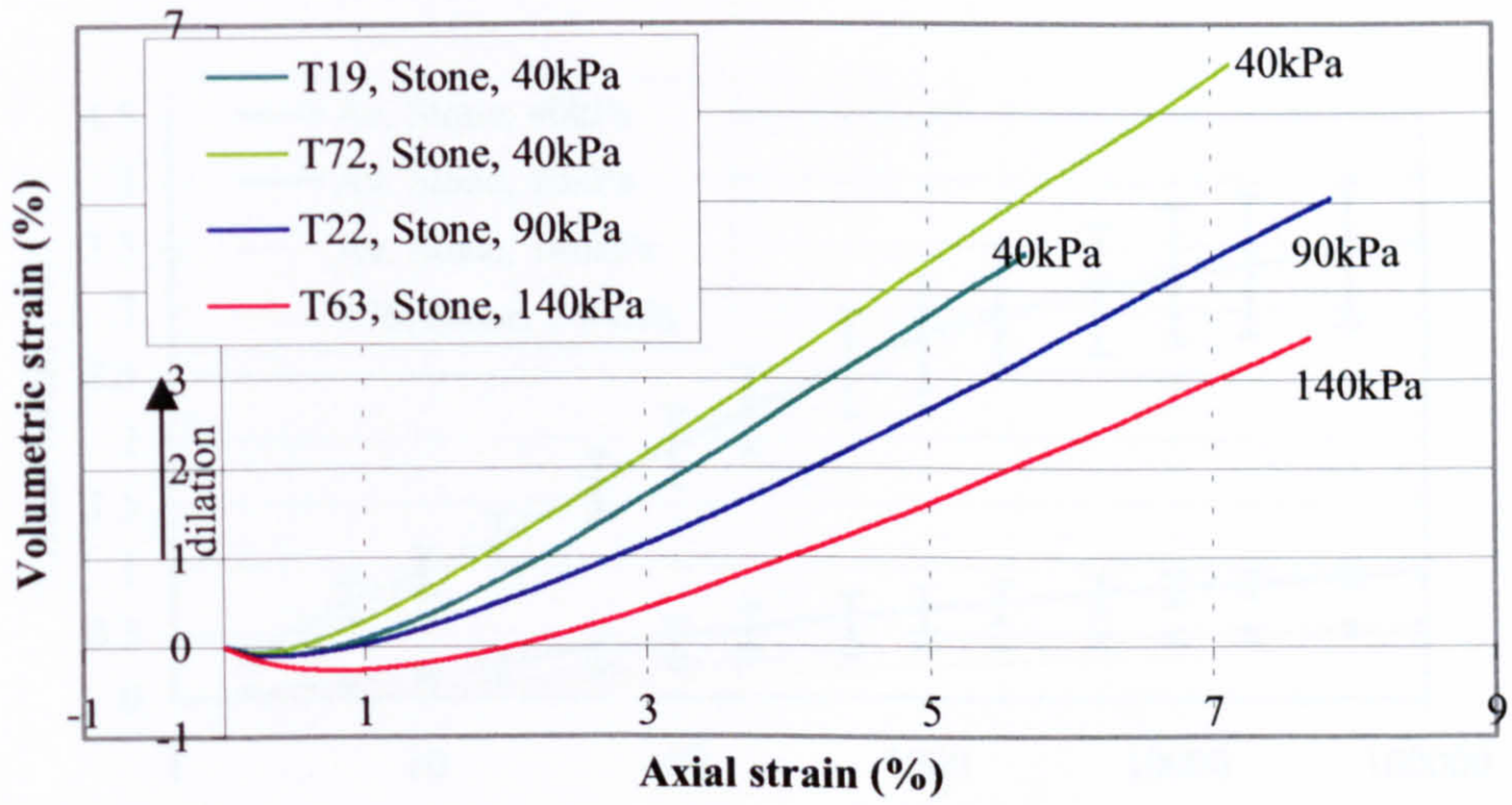

Figure 5.14 - Volumetric strain behaviour of stone specimens monotonic load tests at 40kPa, 90kPa and 140kPa cell pressure (Series 2)

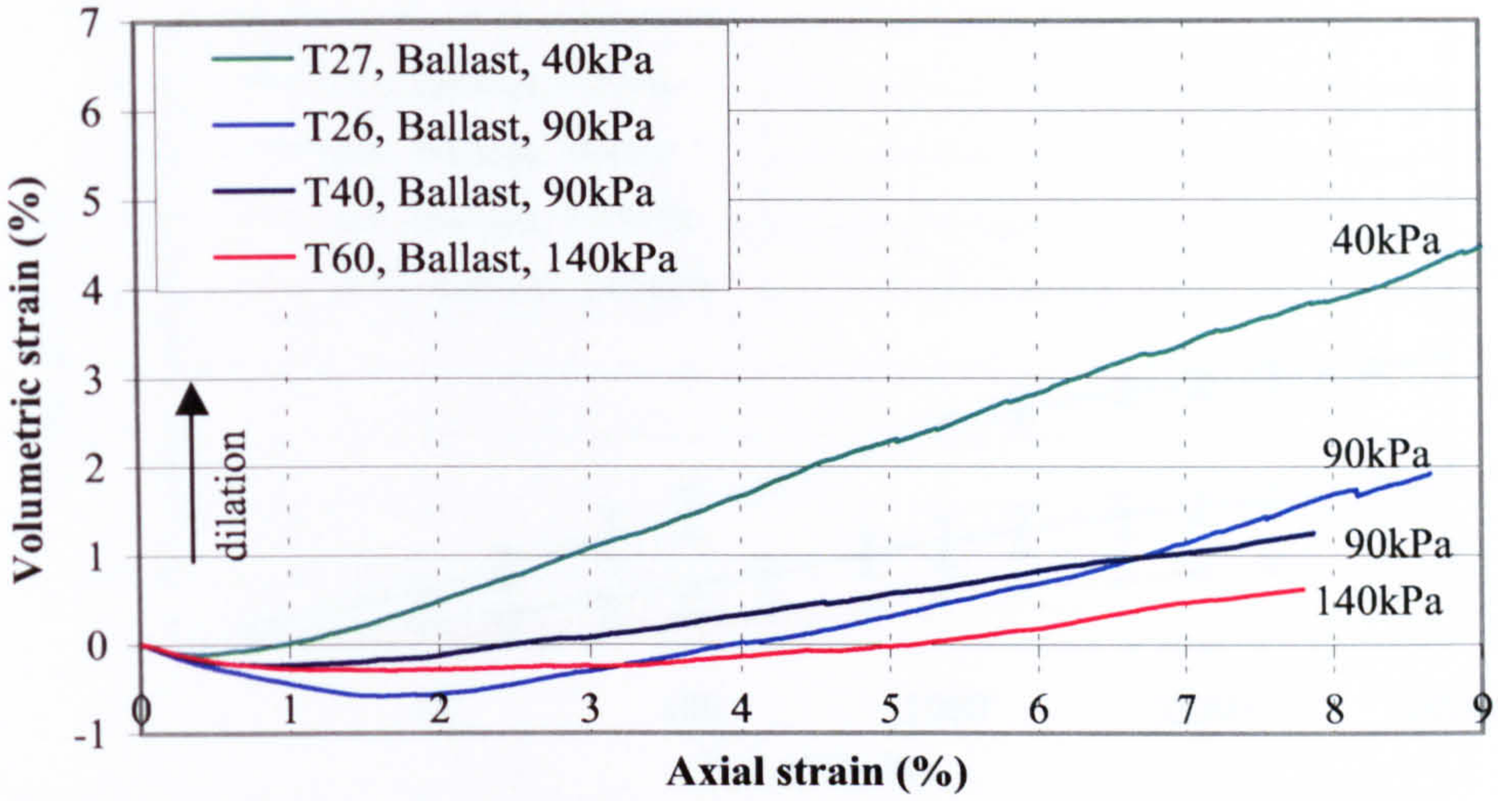

Figure 5.15 - Volumetric strain behaviour of ballast specimens in monotonic load triaxial tests at 40kPa, 90kPa and 140kPa cell pressure (Series 2)

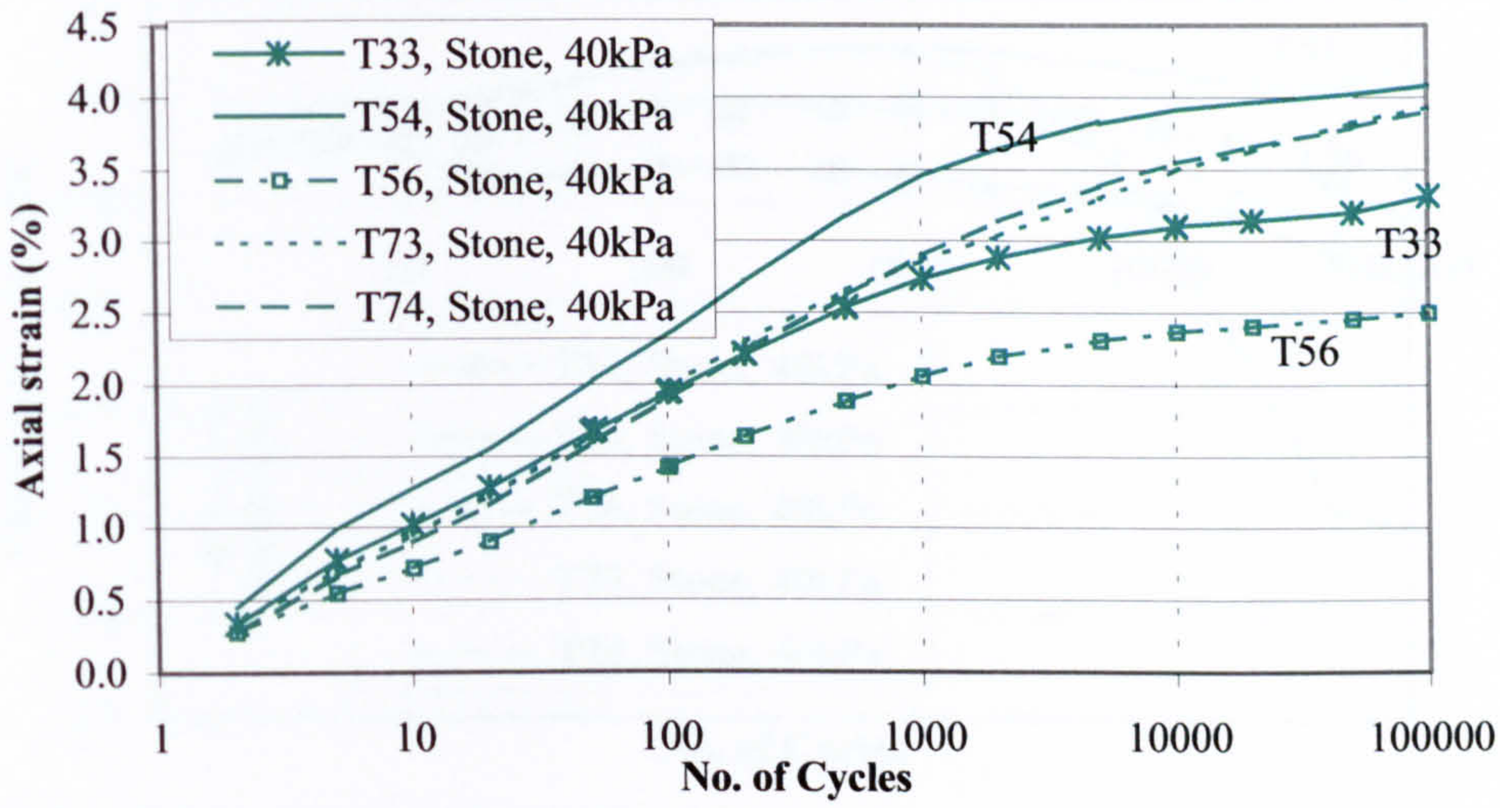

Figure 5.16 - Axial strain behaviour of stone specimens in cyclic load triaxial tests at 40kPa cell pressure (Series 2)

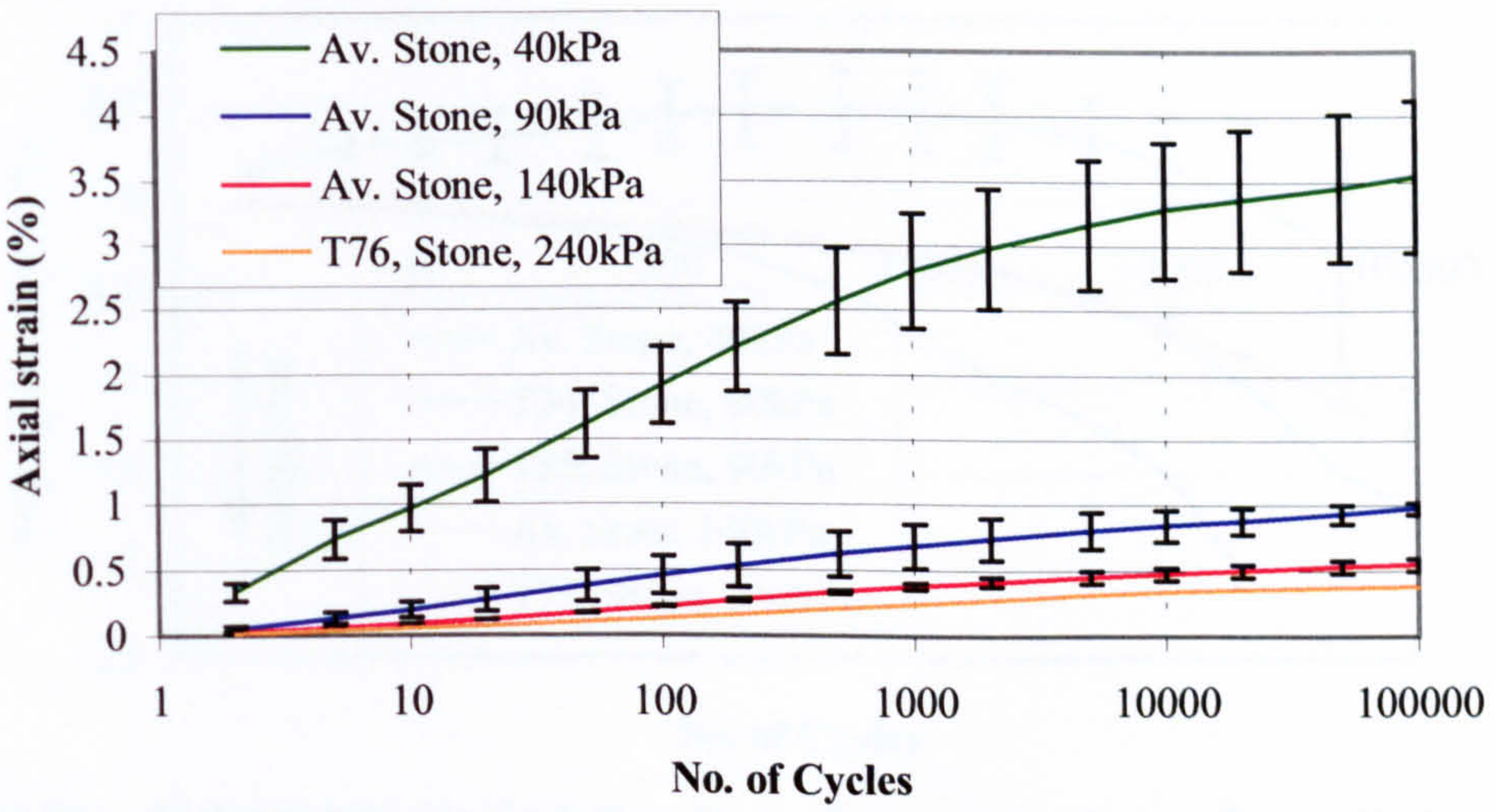

Figure 5.17 - Axial strain behaviour of stone specimens in cyclic load triaxial tests at 40kPa, 90kP, 140kPa and 240kPa cell pressure (Series 2)

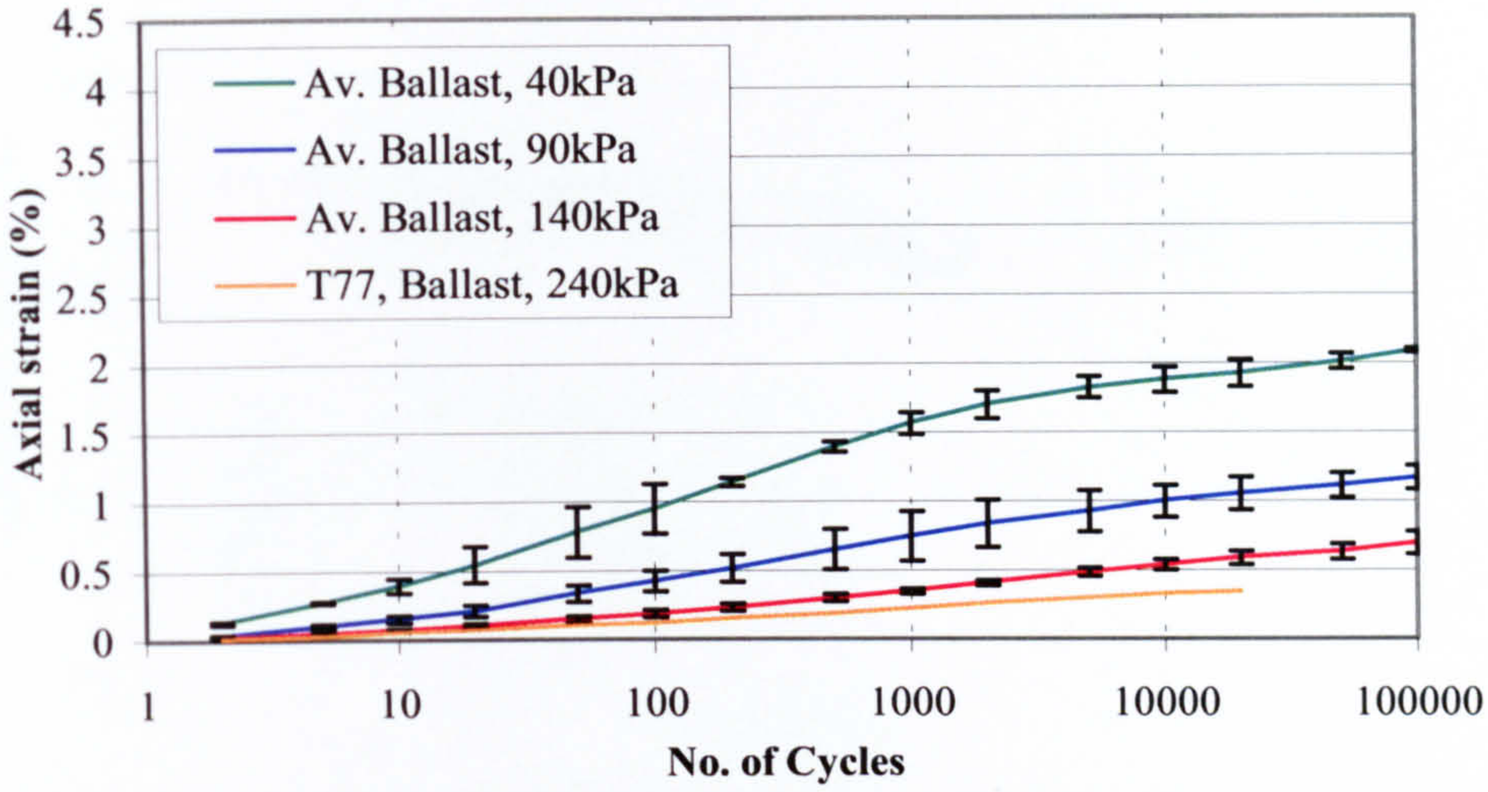

Figure 5.18 - Axial strain behaviour of ballast specimens in cyclic load triaxial tests at 40kPa, 90kPa, 140kPa and 240kPa cell pressure (Series 2)

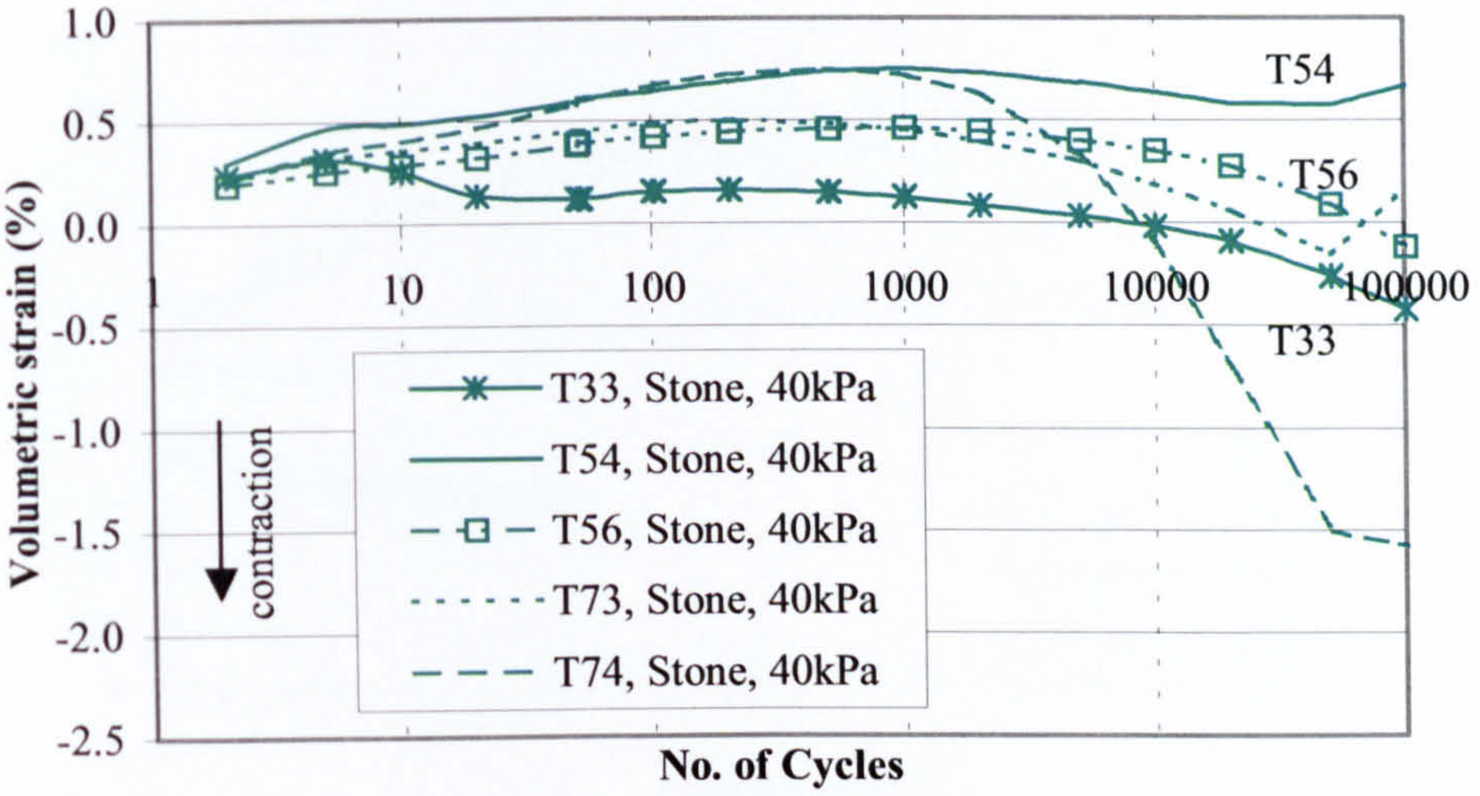

Figure 5.19 - Volumetric strain behaviour of stone specimens in cyclic load triaxial tests at 40kPa cell pressure (Series 2)

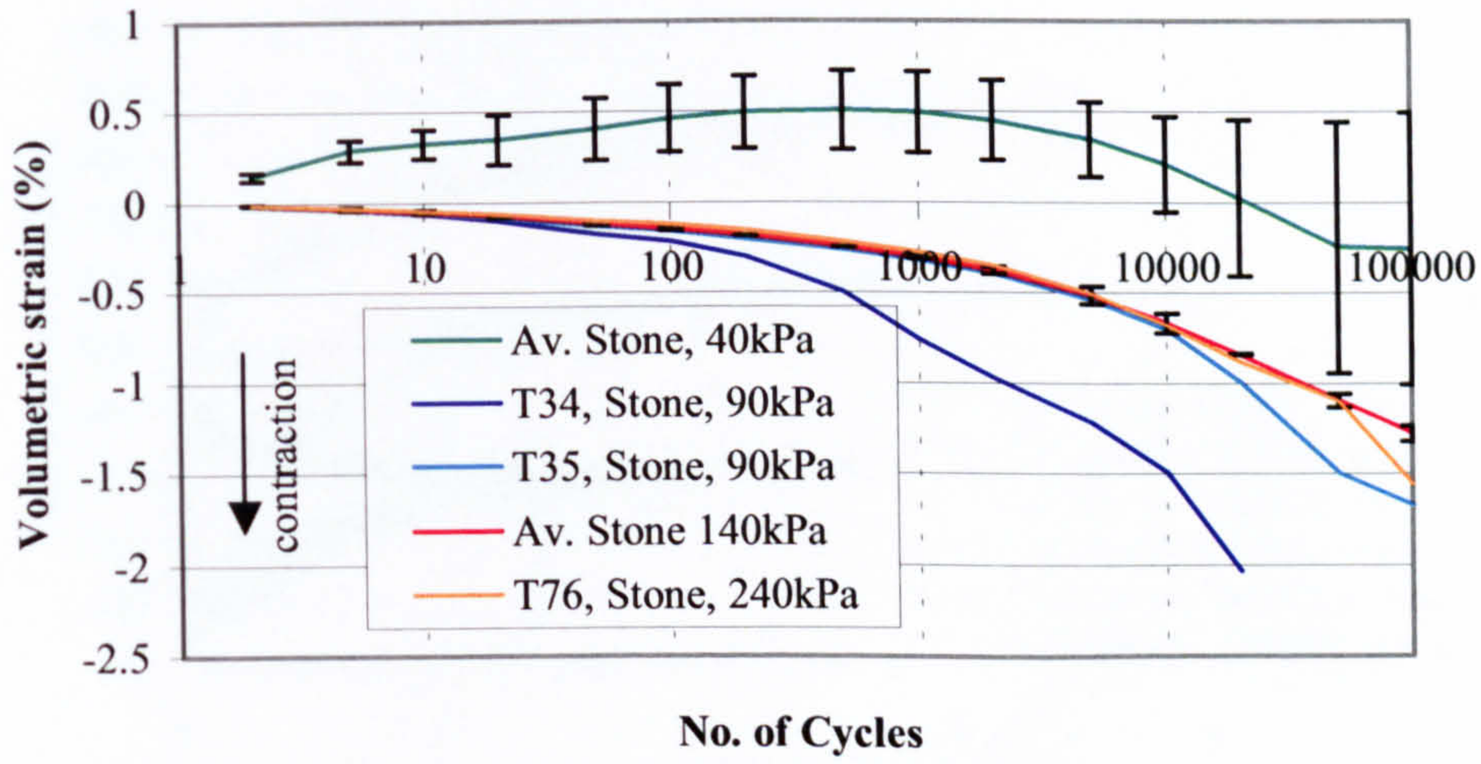

Figure 5.20 - Volumetric strain behaviour of stone specimens in cyclic load triaxial tests at 40kPa, 90kPa, 140kPa and 240kPa cell pressure (Series 2)

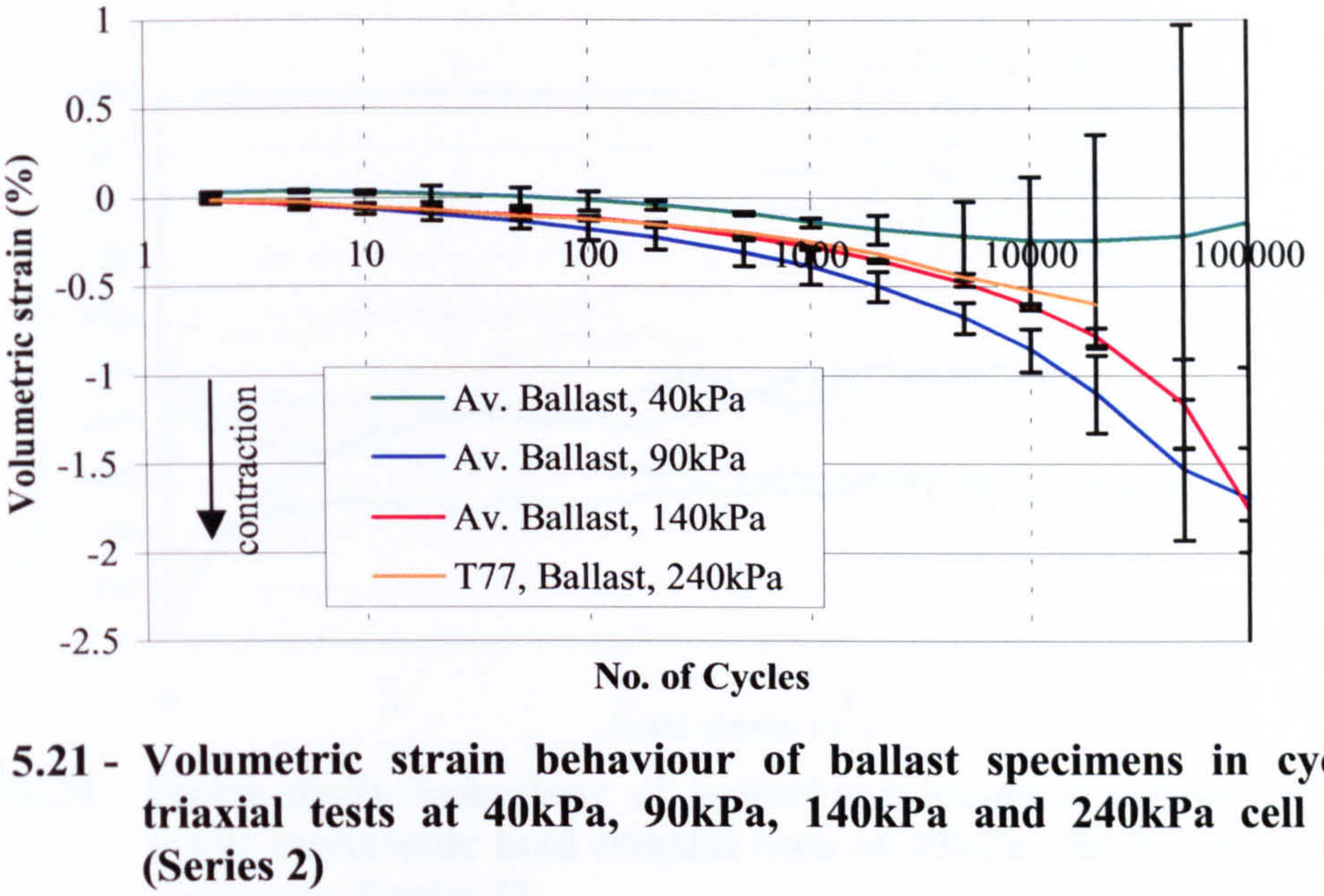

Figure 5.21 - Volumetric strain behaviour of ballast specimens in cyclic load triaxial tests at 40kPa, 90kPa, 140kPa and 240kPa cell pressure (Series 2)

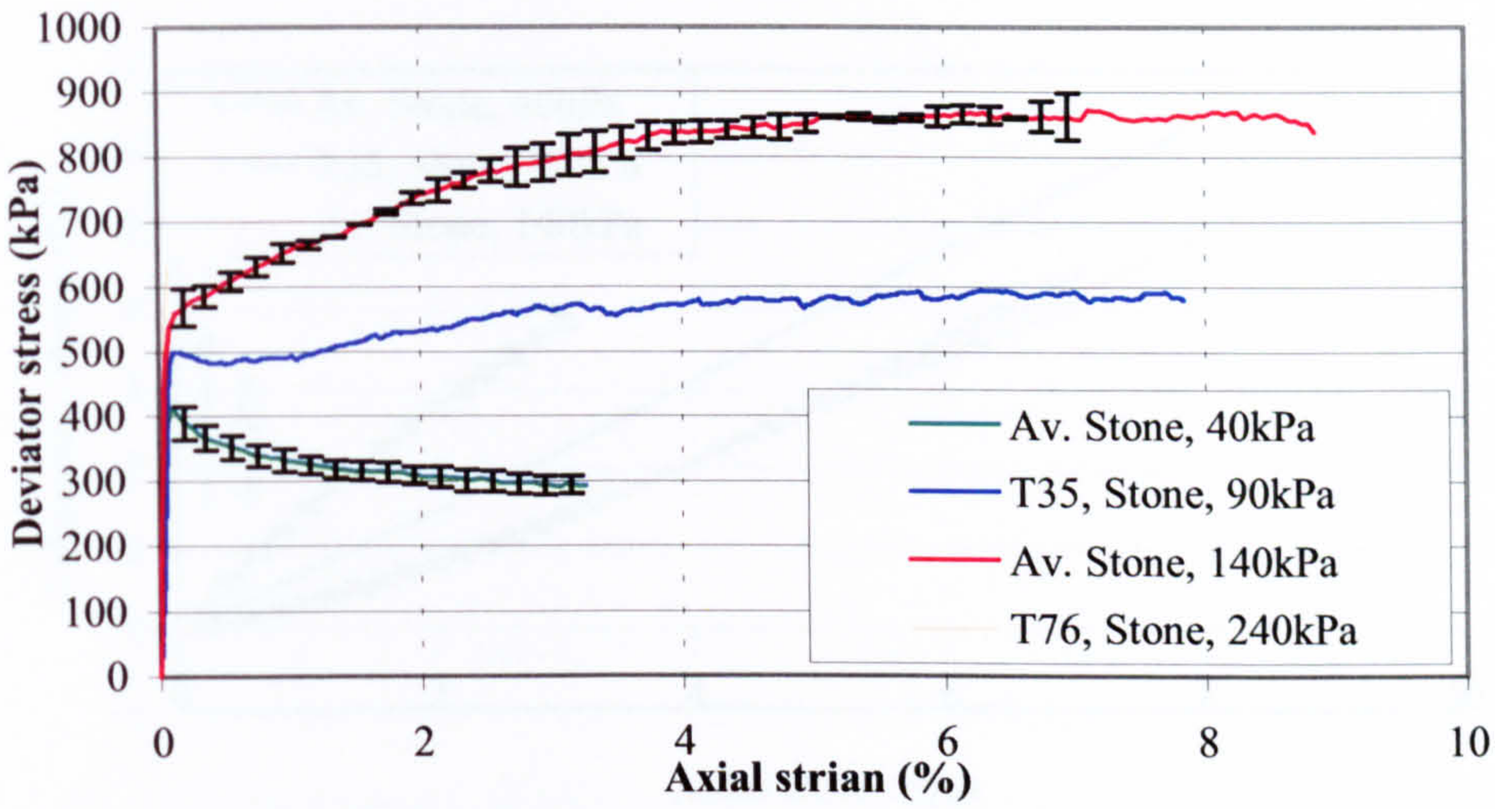

Figure 5.22 – Stress-strain behaviour of stone specimens in post cyclic monotonic load triaxial tests at 40kPa, 90kPa and 140kPa cell pressure (Series 2)

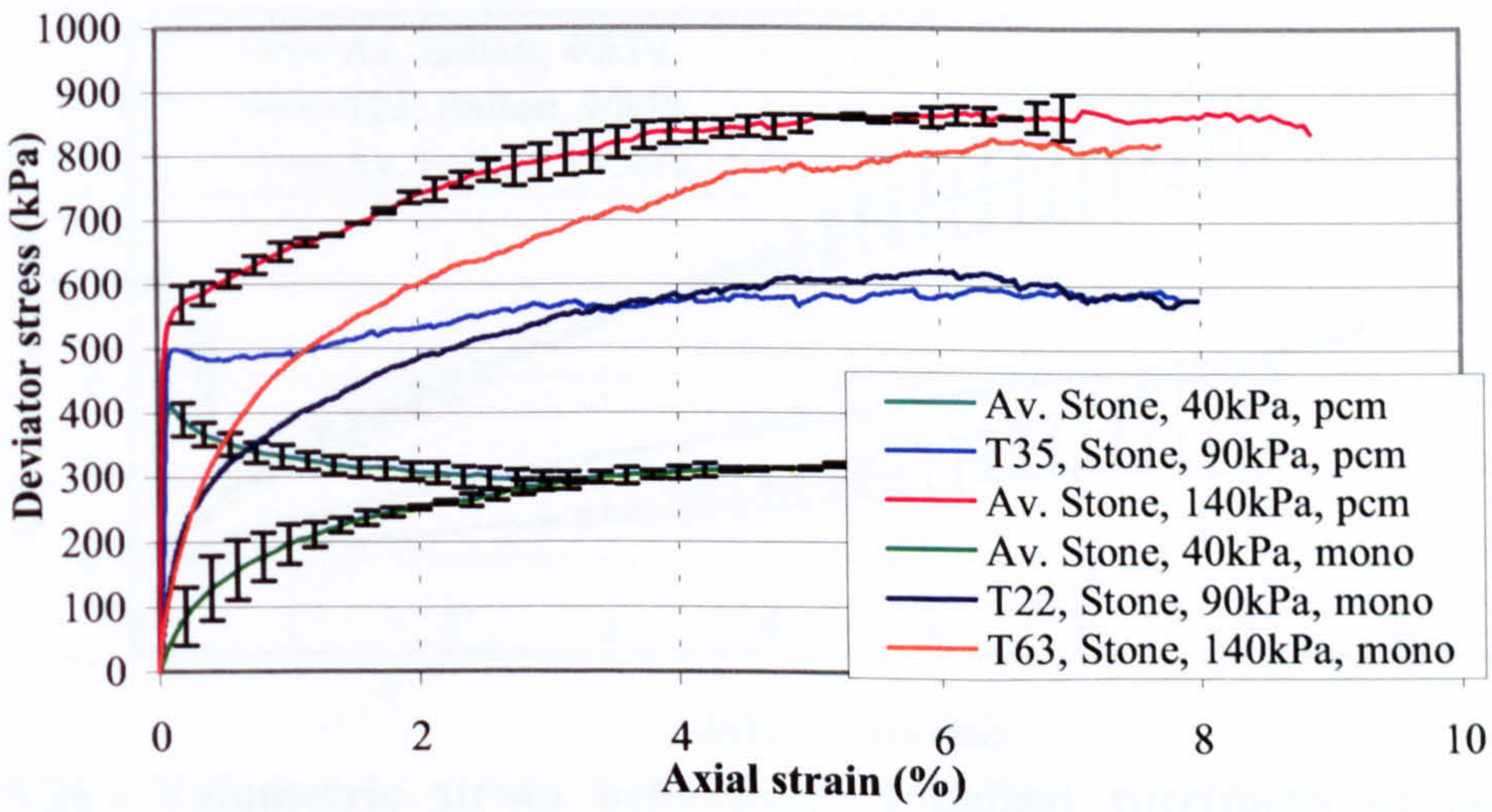

Figure 5.23 - Stress-strain behaviour of stone specimens in monotonic and post cyclic monotonic load triaxial tests at 40kPa, 90kPa and 140kPa cell pressures (Series 2)

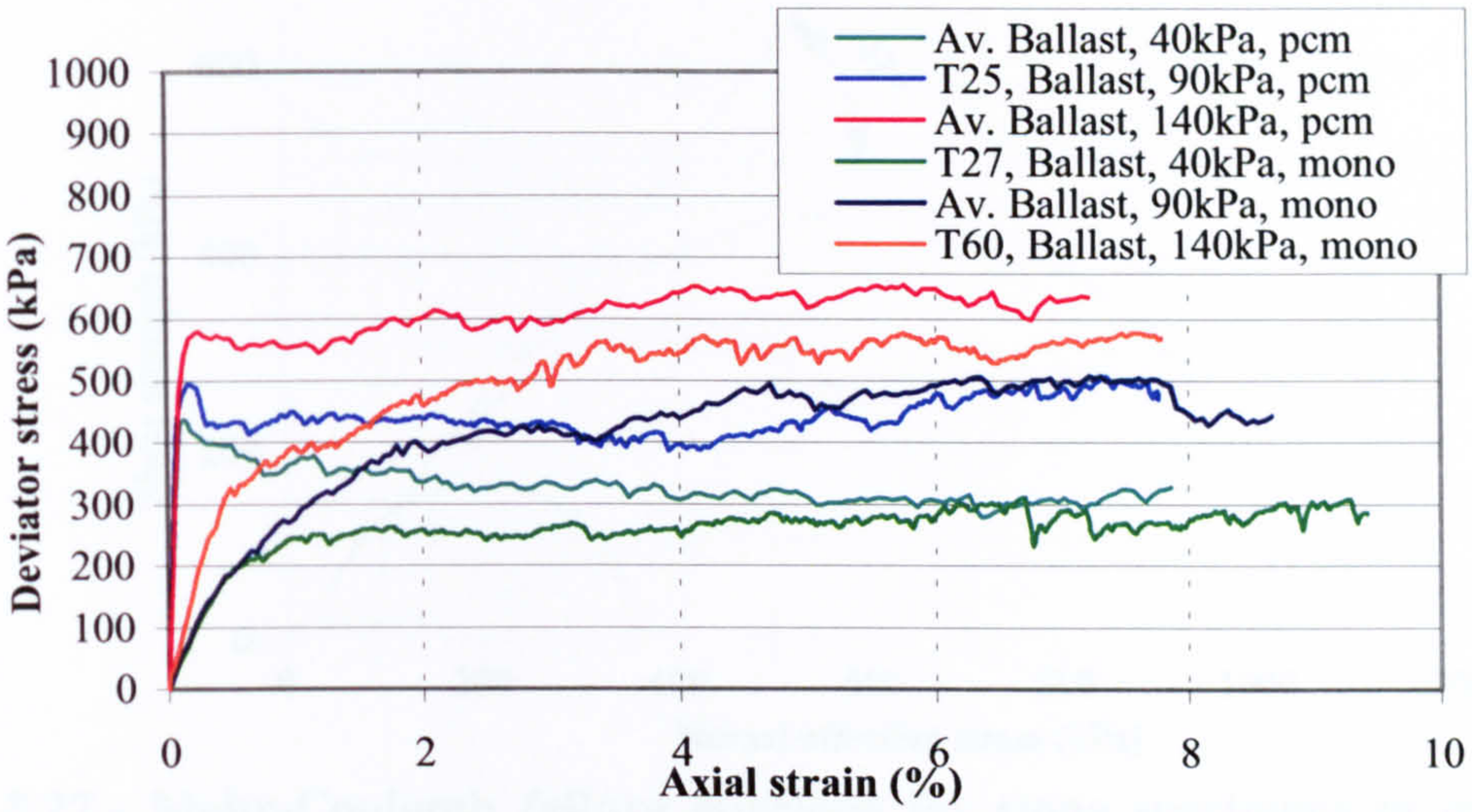

Figure 5.24 - Stress-strain behaviour of ballast specimens in monotonic and post cyclic monotonic load triaxial tests at 40kPa, 90kPa and 140kPa cell pressures (Series 2)

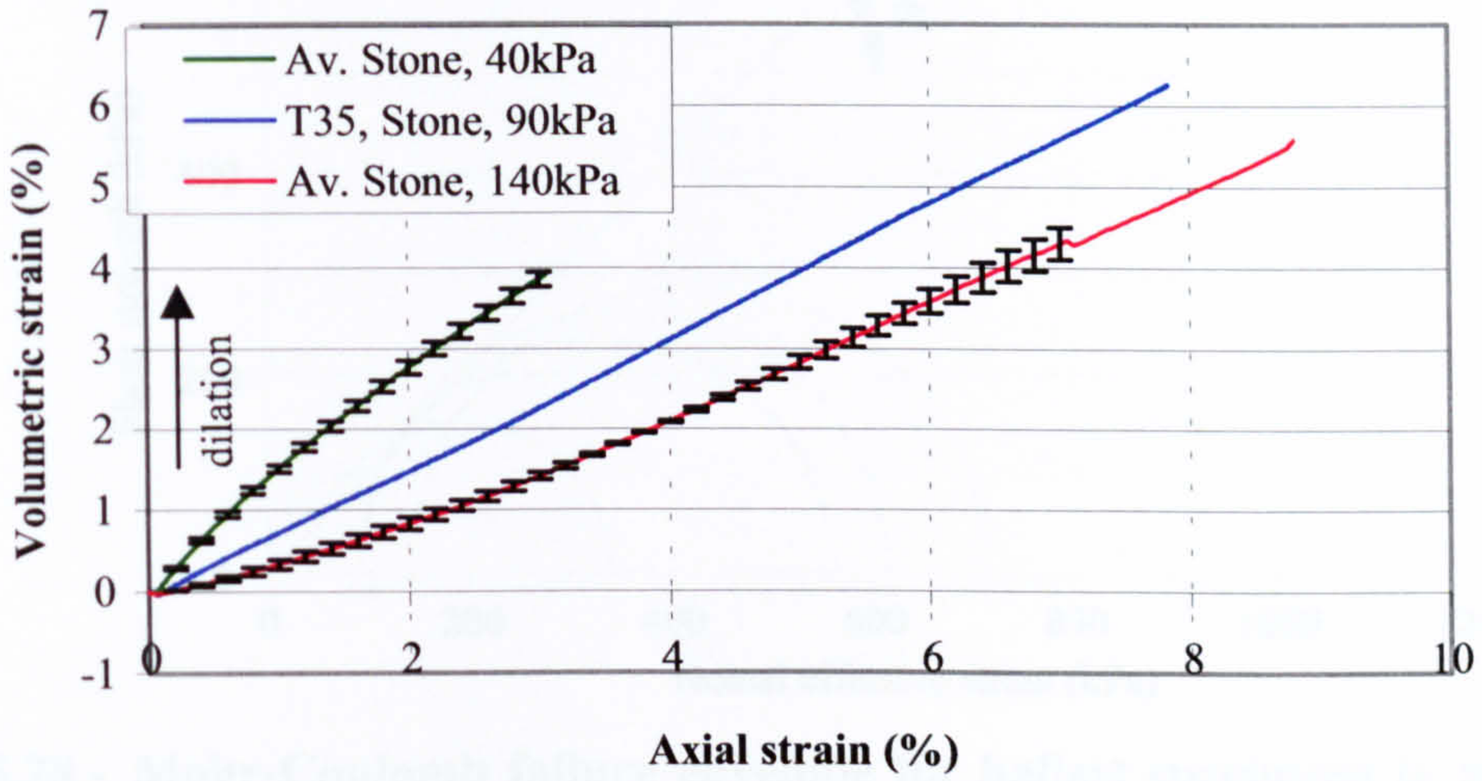

Figure 5.25 - Volumetric strain behaviour of stone specimens in post cyclic monotonic load triaxial tests at 40kPa, 90kPa and 140kPa cell pressure (Series 2)

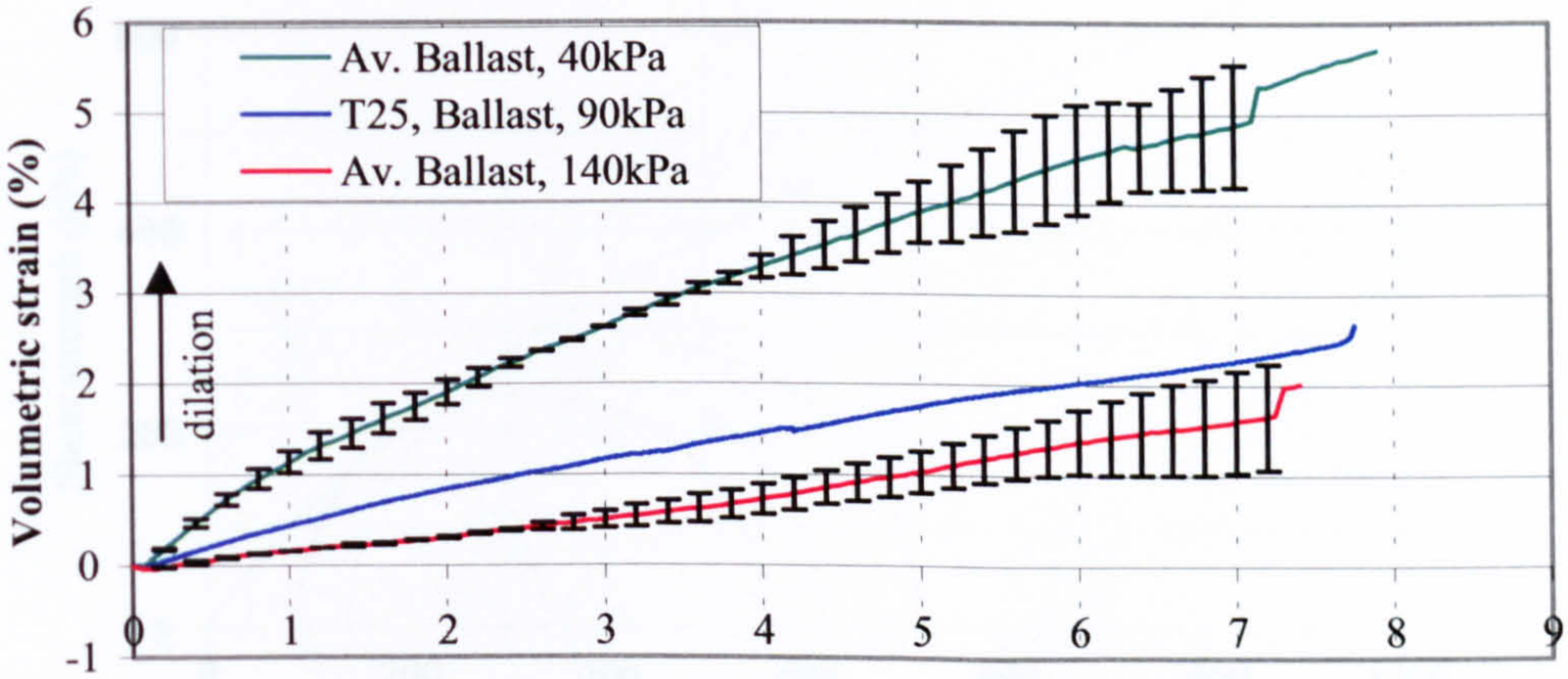

Figure 5.26 - Volumetric strain behaviour of ballast specimens in post cyclic monotonic load triaxial tests at 40kPa, 90kPa and 140kPa cell pressure (Series 2)

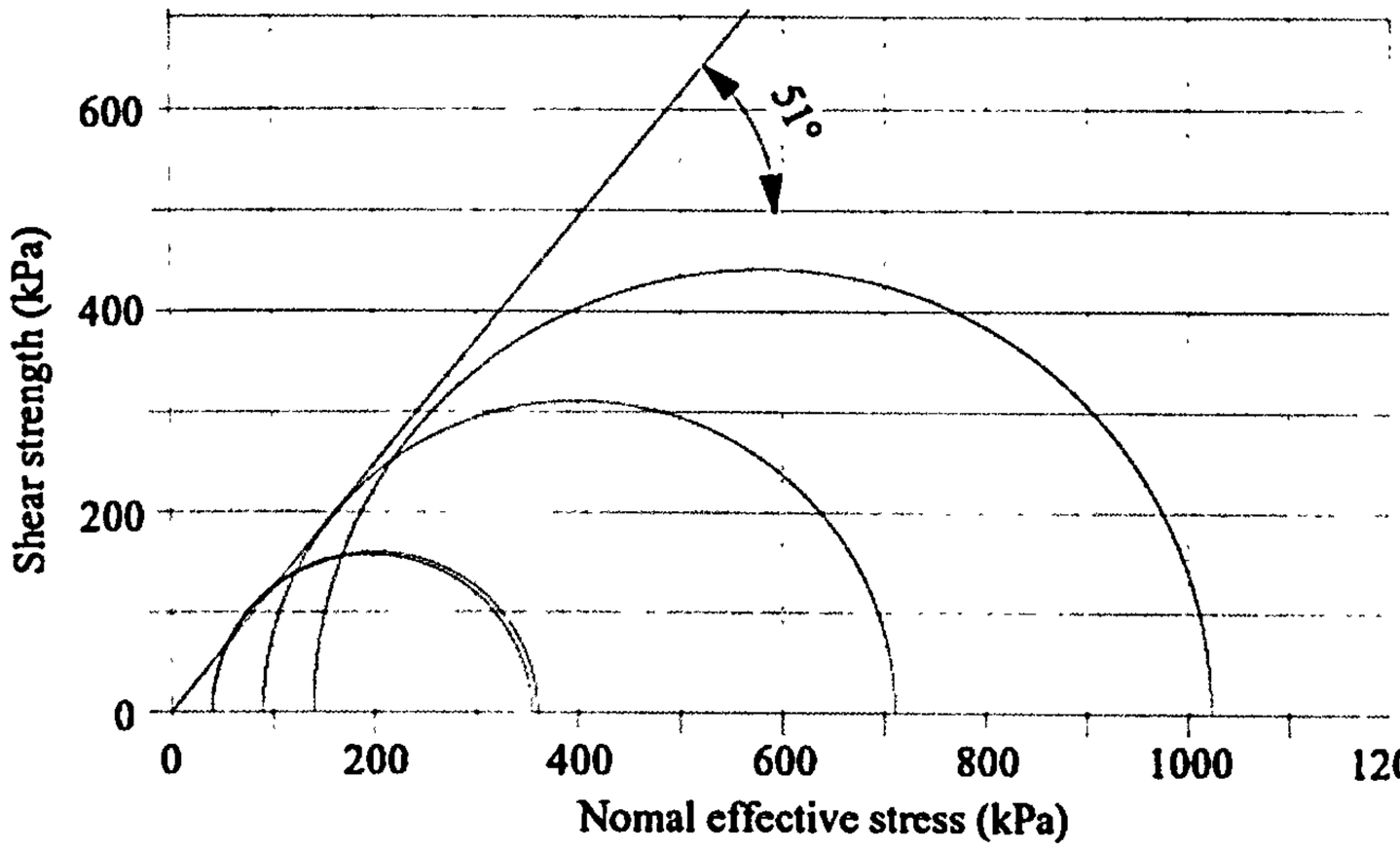

Figure 5.27 - Mohr-Coulomb failure envelope for stone specimens in monotonic load triaxial tests (Series 2)

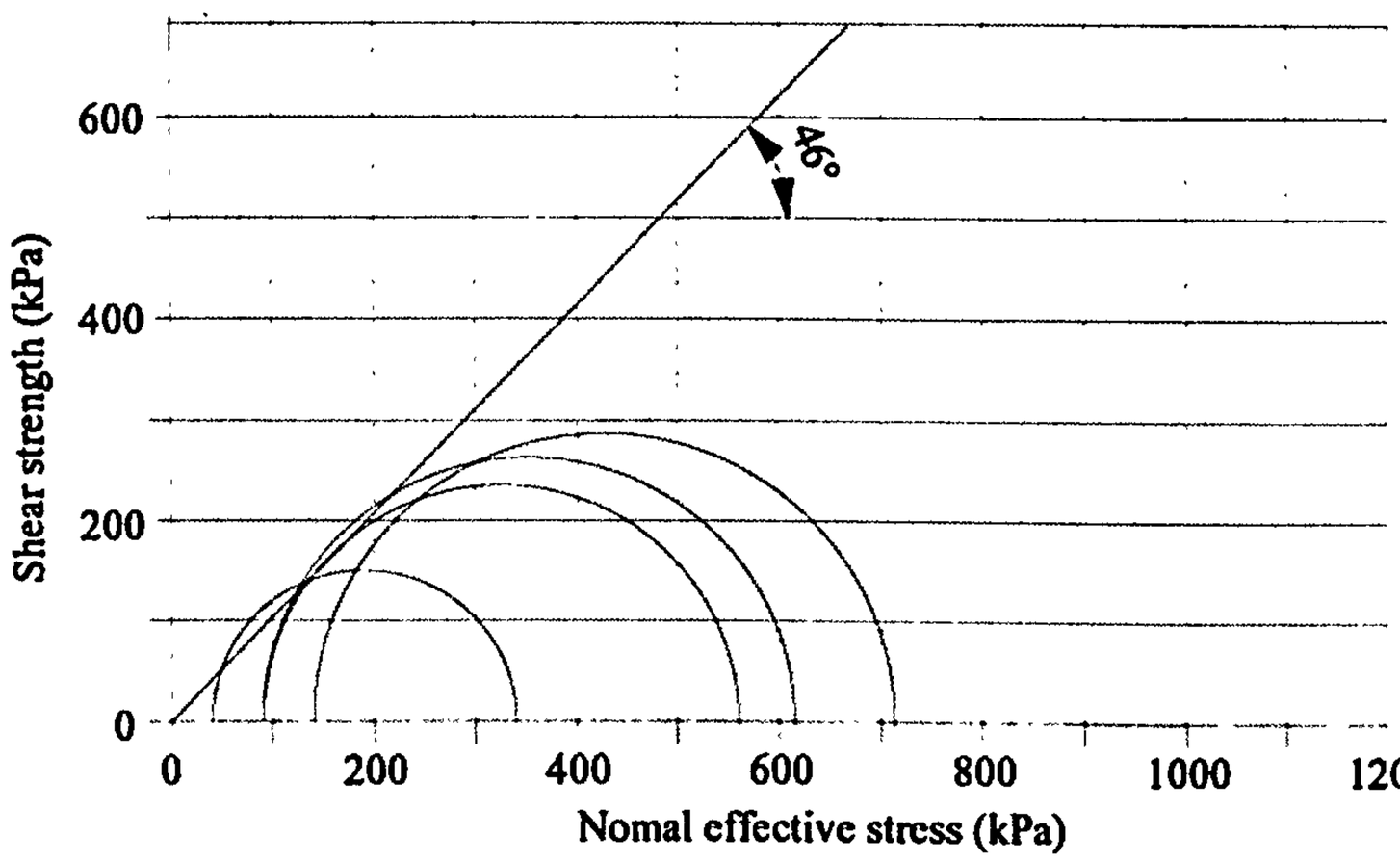

Figure 5.28 - Mohr-Coulomb failure envelope for ballast specimens in monotonic load triaxial tests (Series 2)

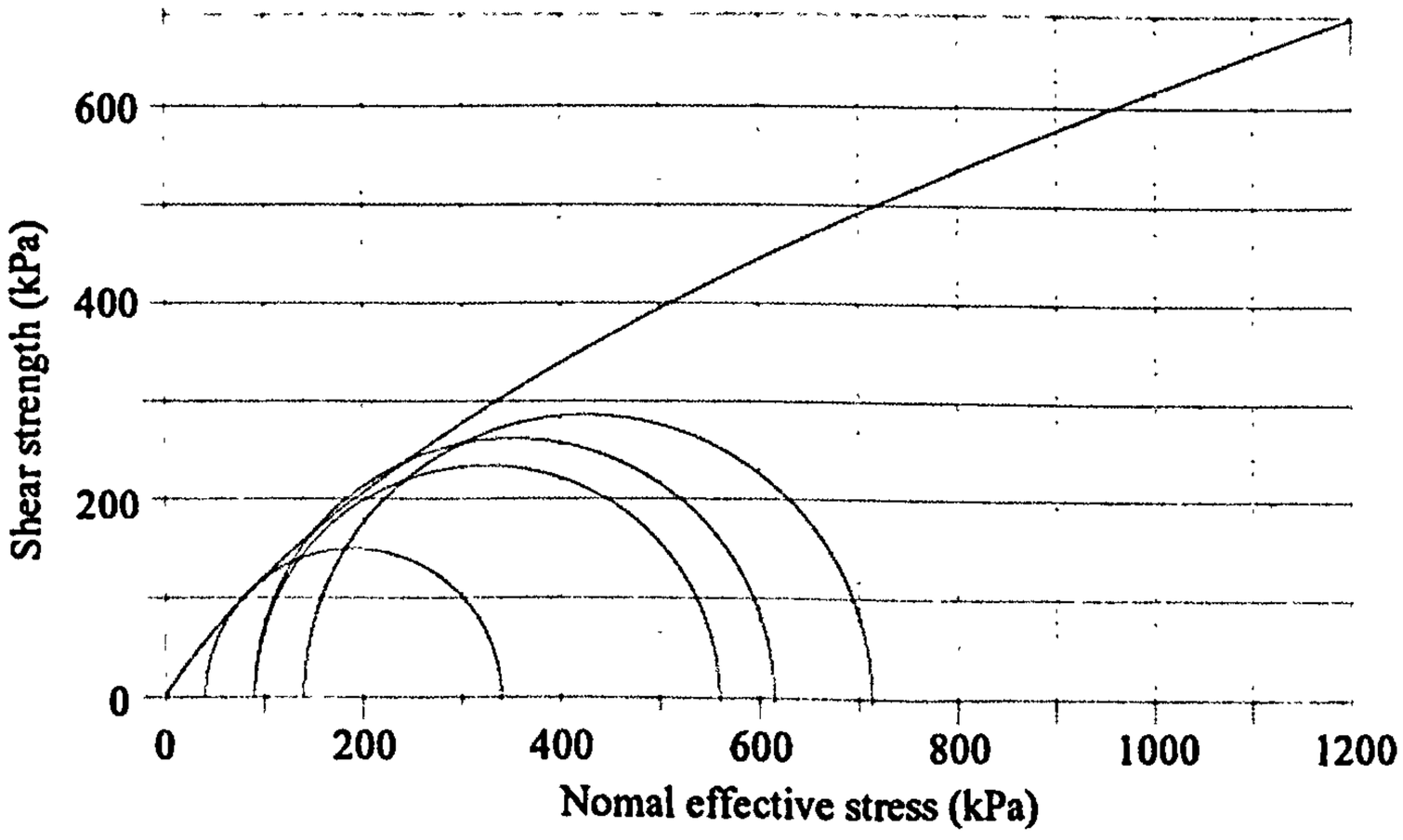

Figure 5.29 - An approximate curved Mohr-Coulomb failure envelope for ballast specimens in monotonic load triaxial tests (Series 2)

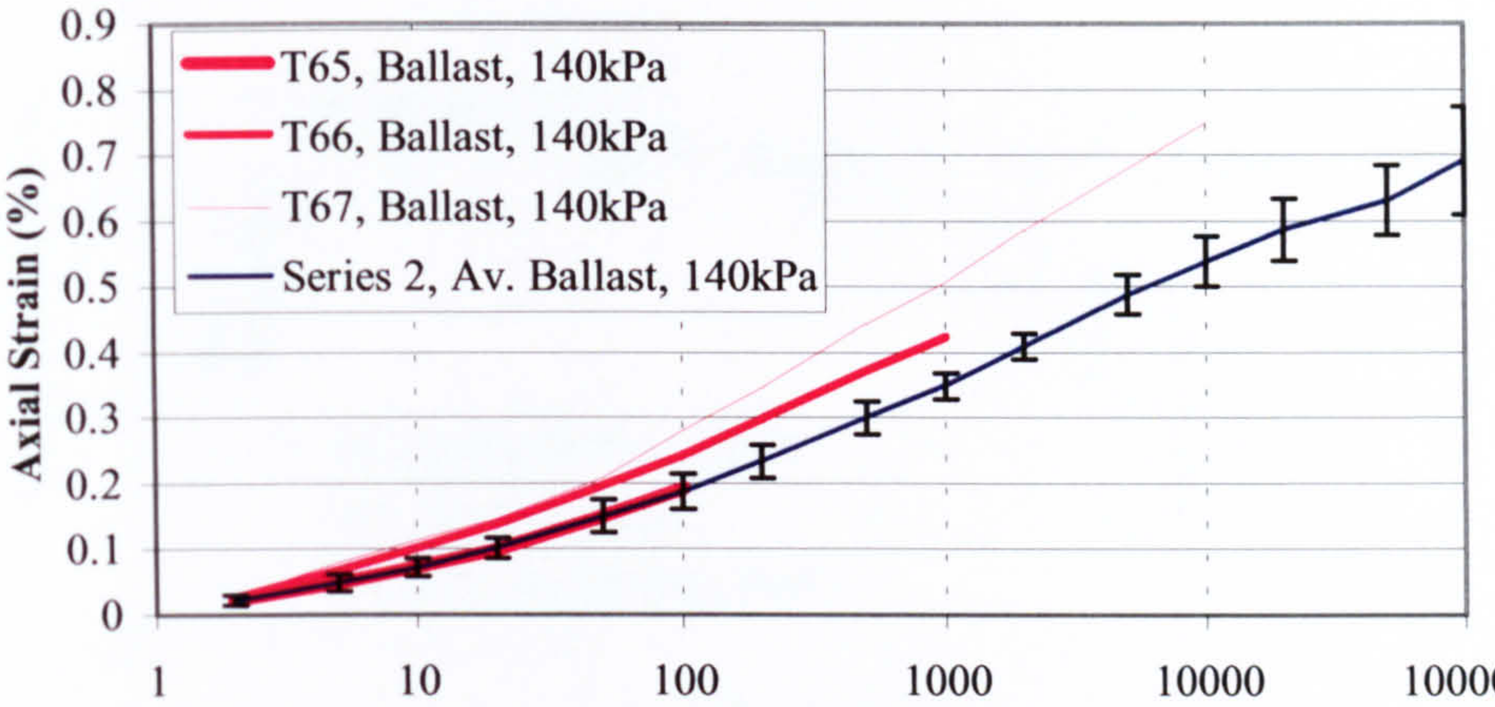

Figure 5.30 - Axial strain behaviour of ballast specimens in cyclic load triaxial tests at 140kPa cell pressure (Series 3)

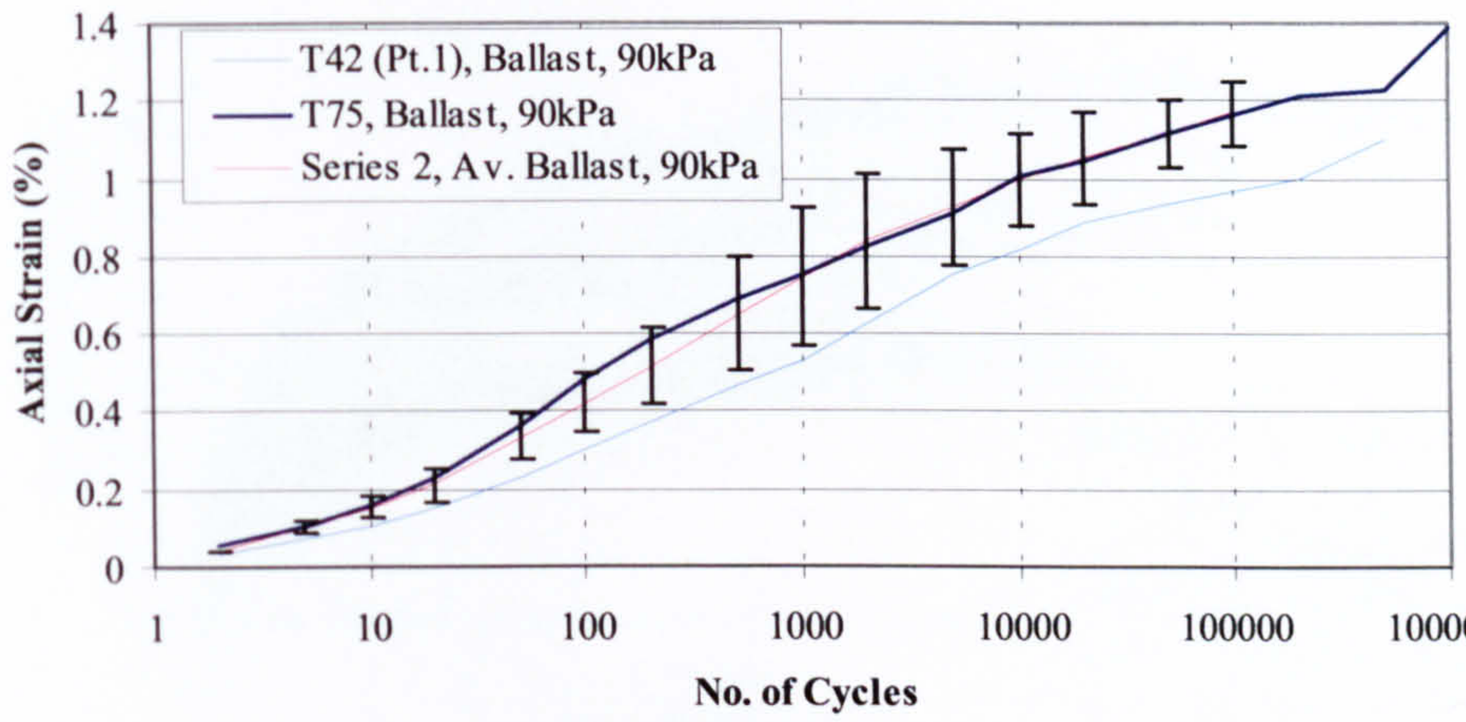

Figure 5.31 - Axial strain behaviour of ballast specimens in cyclic load triaxial tests at 90kPa cell pressure (Series 3)

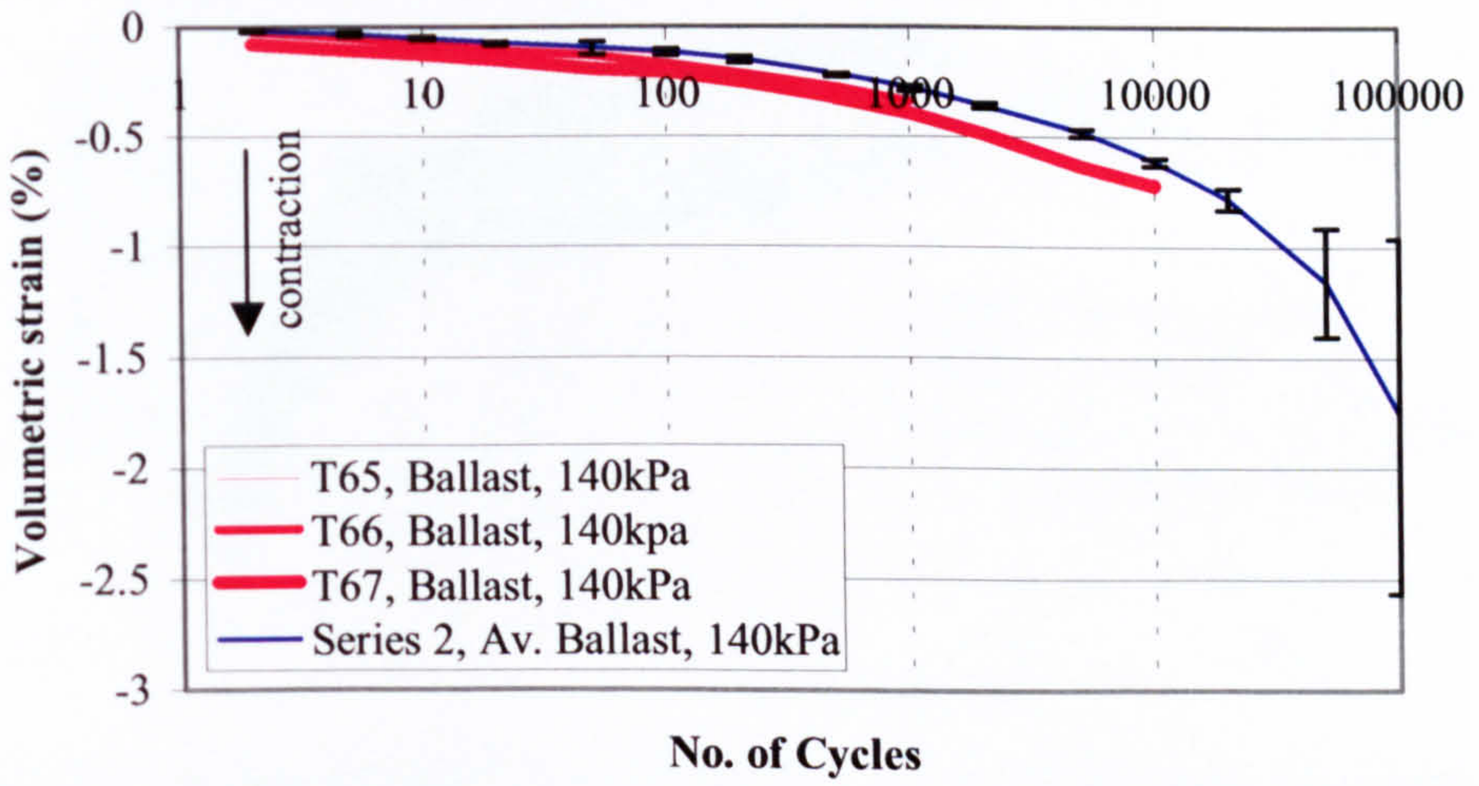

Figure 5.32 - Volumetric strain behaviour of ballast specimens in cyclic load triaxial tests at 140kPa cell pressure (Series 3)

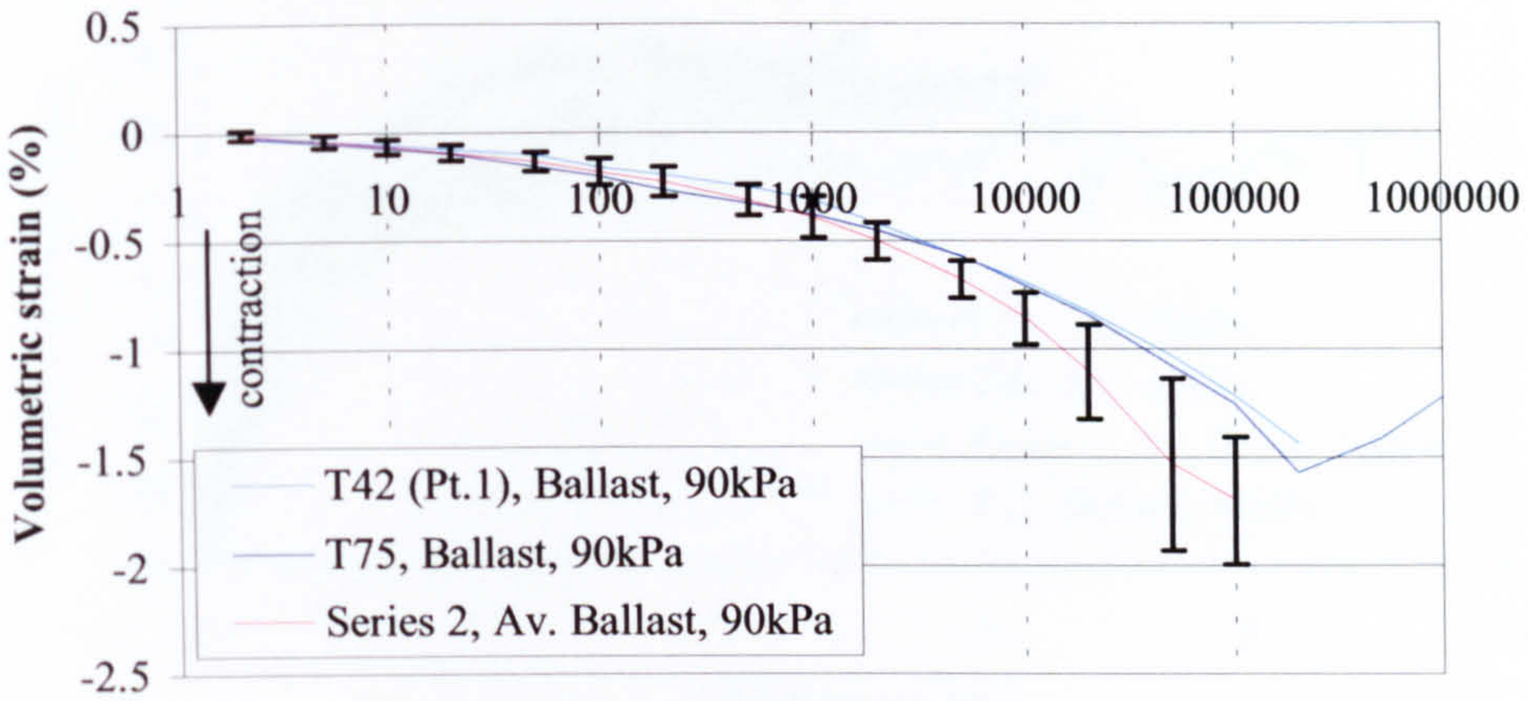

Figure 5.33 – Volumetric strain behaviour of ballast specimens in cyclic load triaxial tests at 90kPa cell pressure (Series 3)

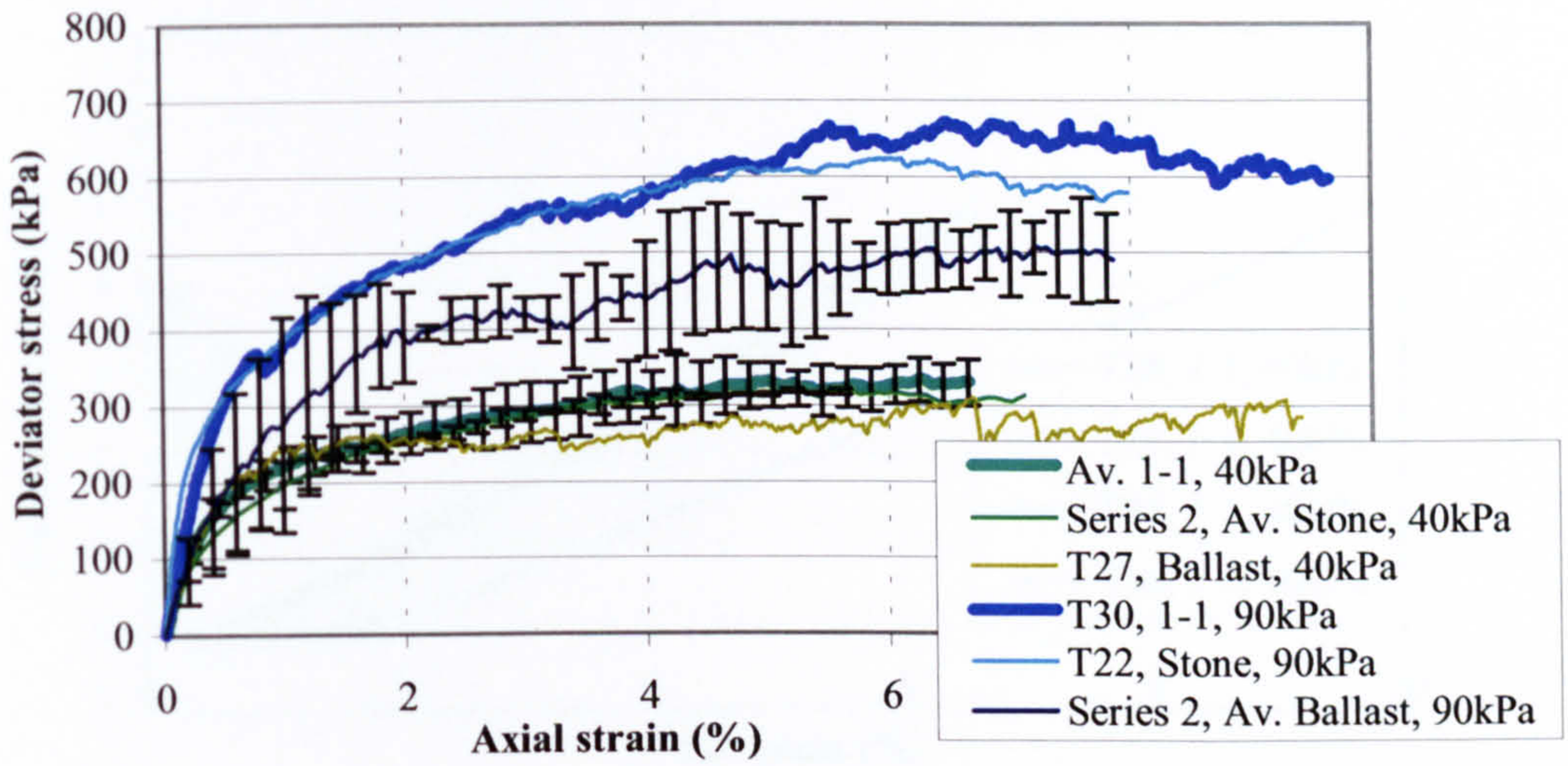

Figure 5.34 - Stress-strain behaviour of 1-1 layer (Series 4) and stone only and ballast only specimens (Series 2) at 40kPa and 90kPa cell pressure

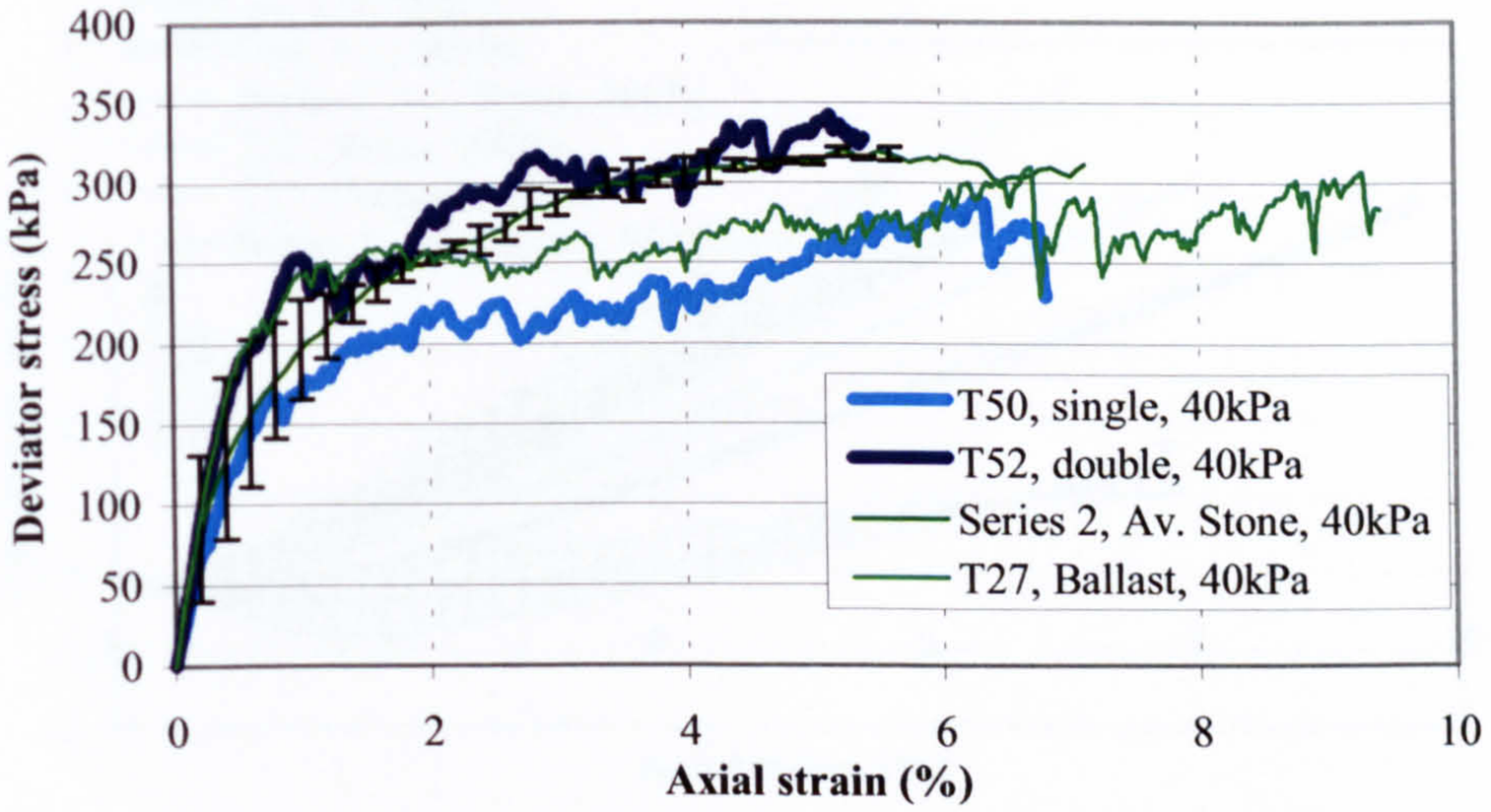

Figure 5.35 - Stress-strain behaviour of a thin layer of stone overlying the ballast (Series 4) and stone only and ballast only specimens (Series 2) at 40kPa and 90kPa cell pressure

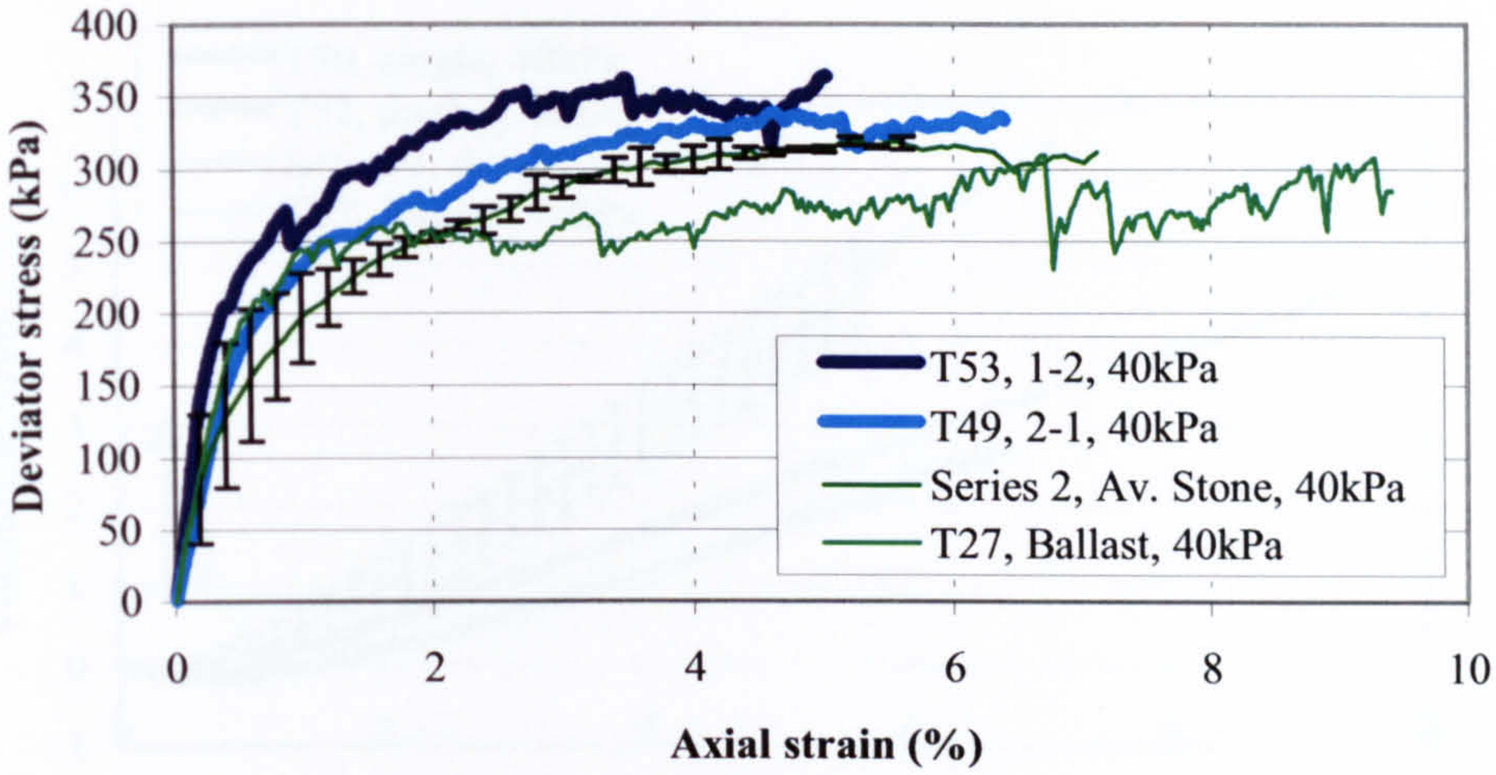

Figure 5.36 - Stress-strain behaviour for 1-2 layer and 2-1 layer (Series 4) and stone only and ballast only specimens (Series 2) at 40kPa cell pressure

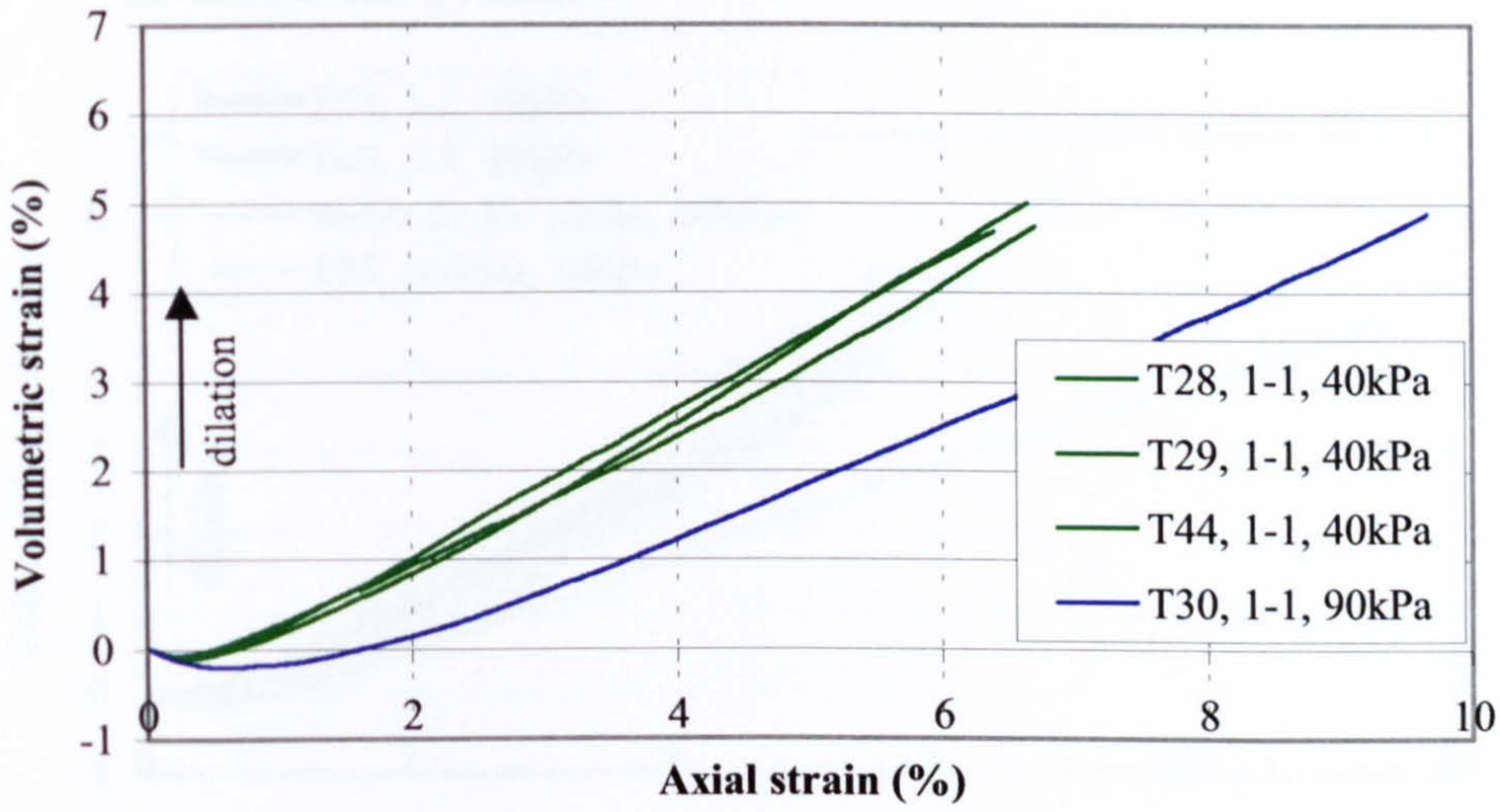

Figure 5.37 - Volumetric strain behaviour of 1-1 layer specimens in monotonic load triaxial tests at 40kPa and 90kPa cell pressure (Series 4)

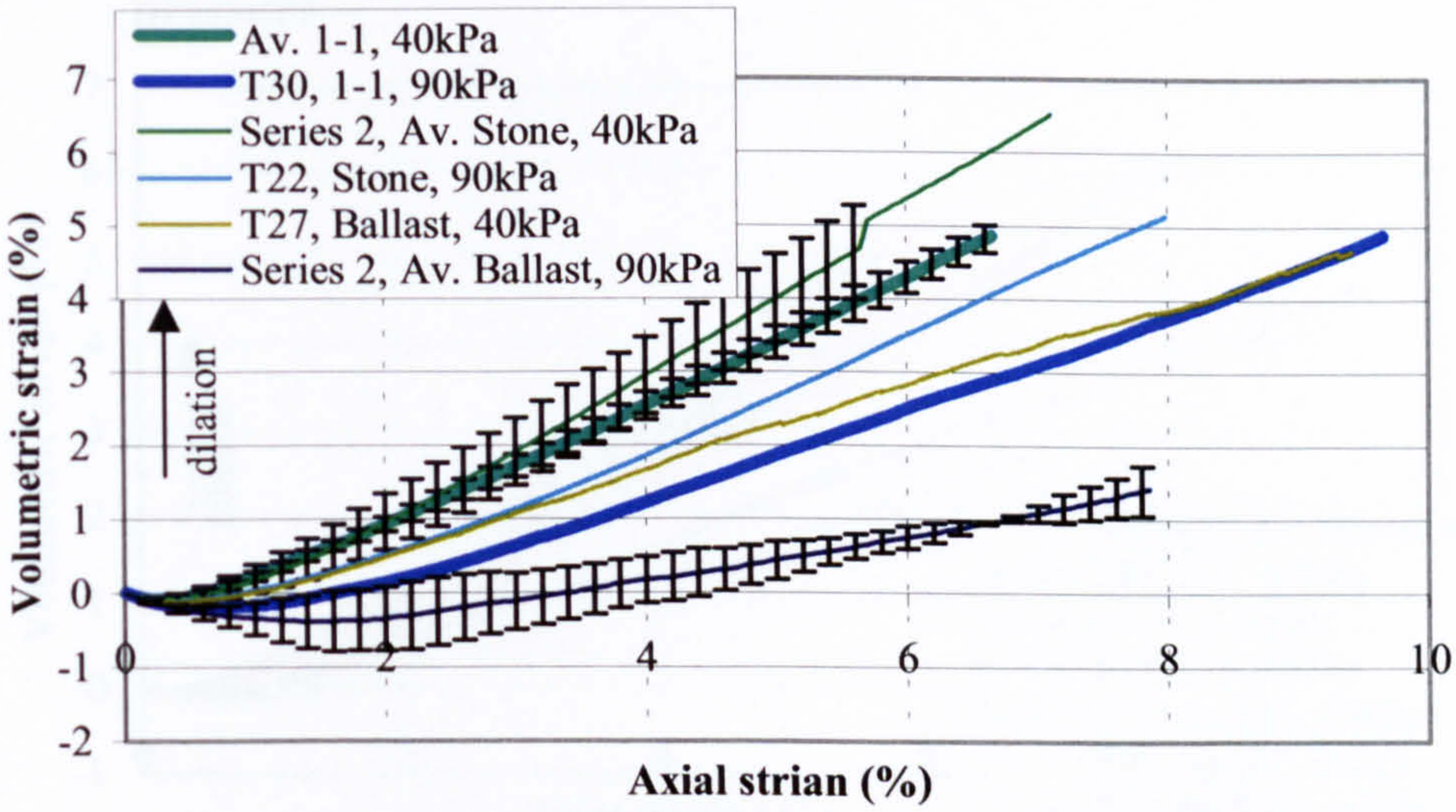

Figure 5.38 - Volumetric strain behaviour of 1-1 layer (Series 4) and stone only and ballast only specimens (Series 2) at 40kPa and 90kPa cell pressure

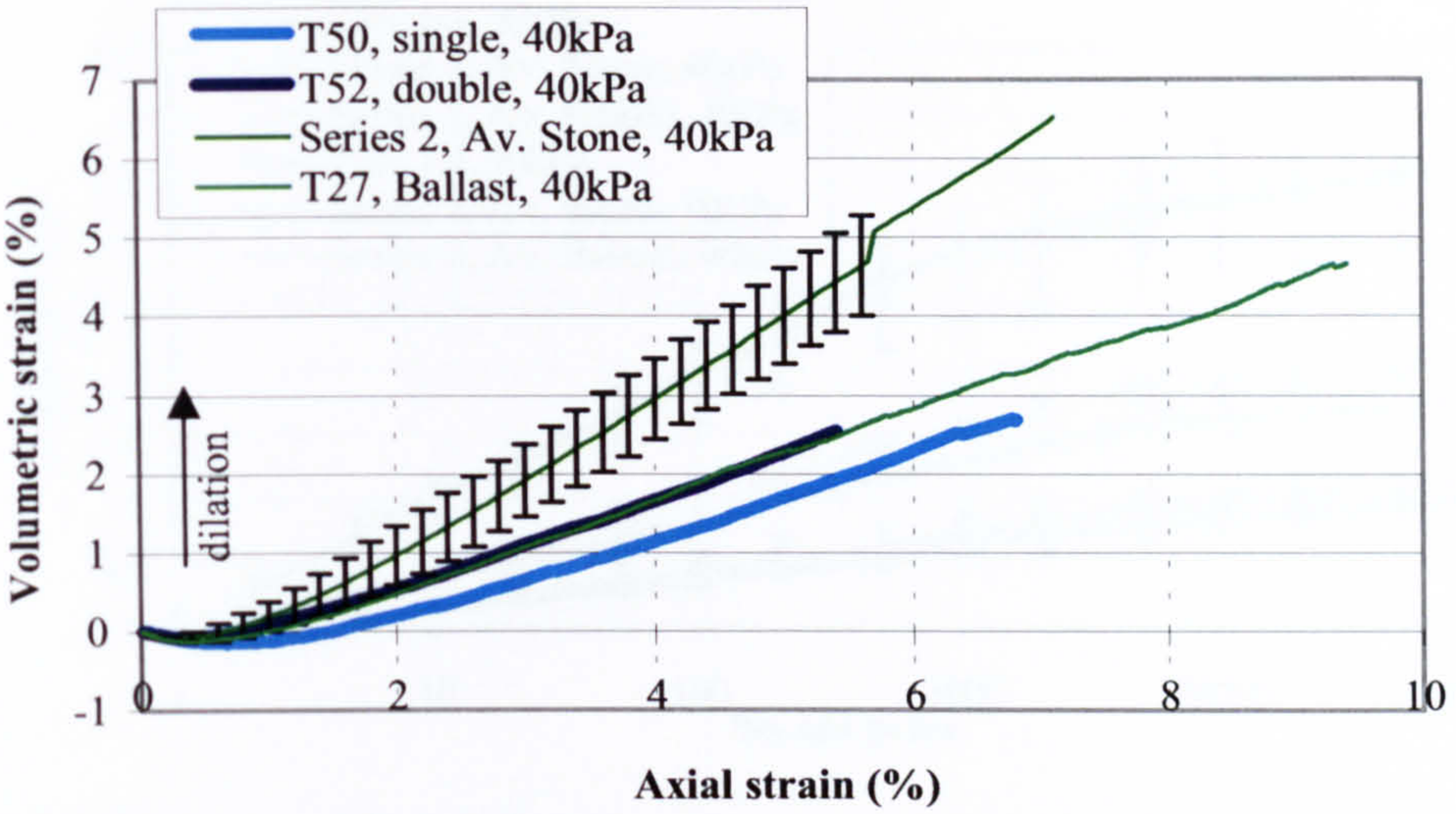

Figure 5.39 - Volumetric strain behaviour for a thin layer of stone overlying the ballast (Series 4) and stone only and ballast only specimens (Series 2) at 40kPa cell pressure

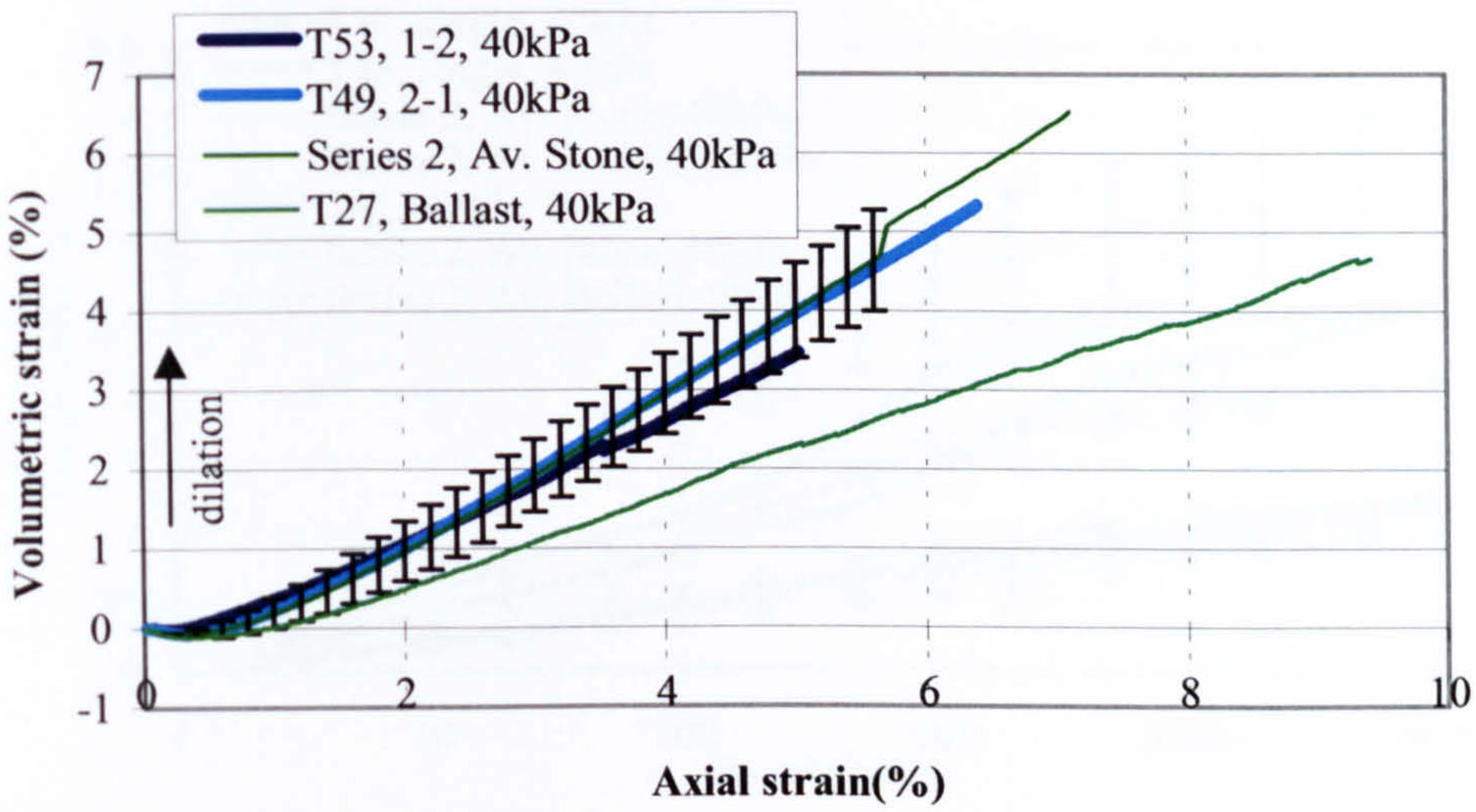

Figure 5.40 - Volumetric strain behaviour of 1-2 layer, 2-1 layer (Series 4) and stone only and ballast only specimens (Series 2) at 40kPa cell pressure

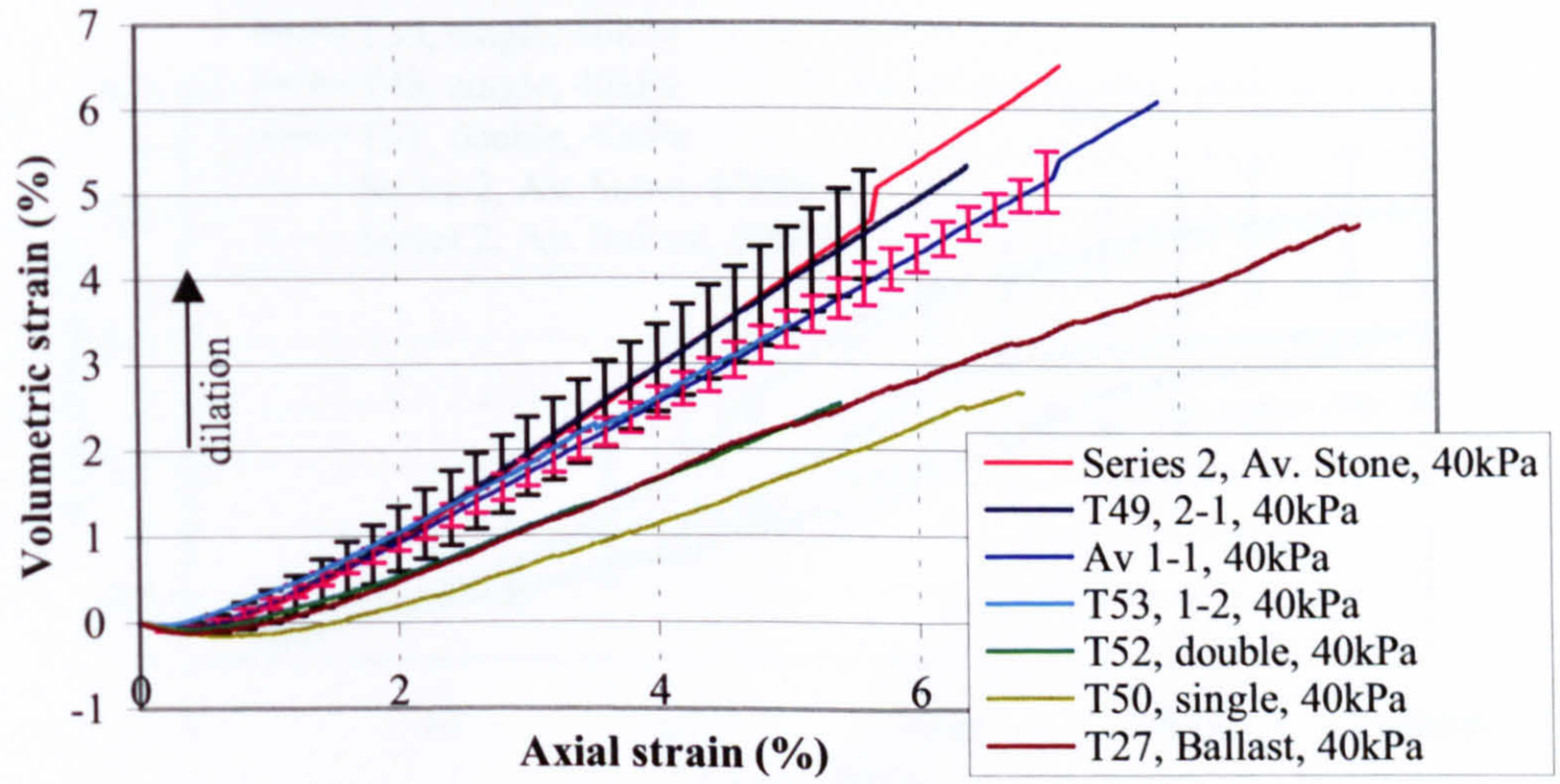

Figure 5.41 - Volumetric strain behaviour for all the layer specimens (Series 4) and stone only and ballast only specimens (Series 2) at 40kPa cell pressure

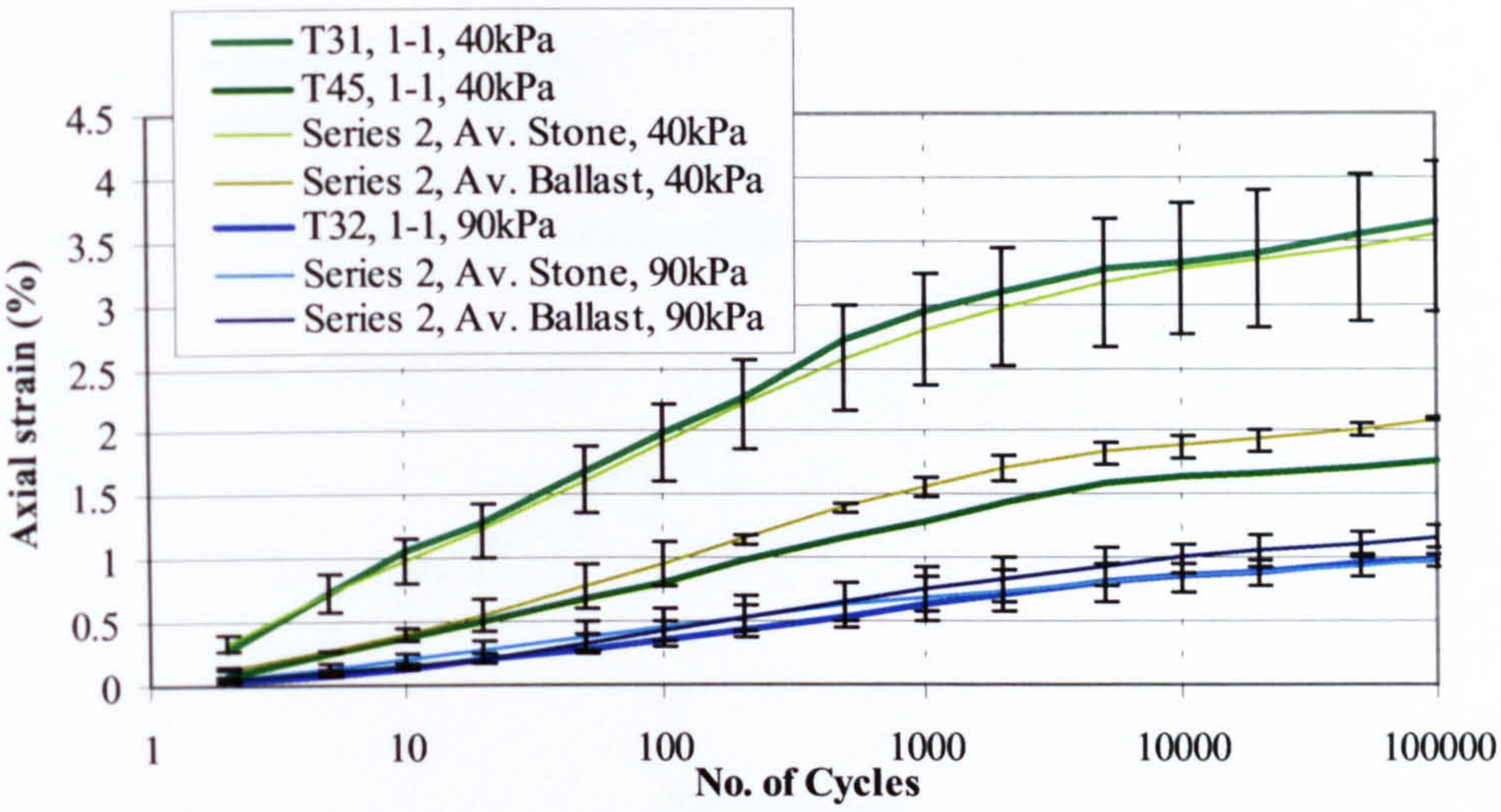

Figure 5.42 - Axial strain behaviour of 1-1 layer (Series 4) and stone only and ballast only specimens (Series 2) specimens in cyclic load triaxial tests at 40kPa and 90kPa cell pressure

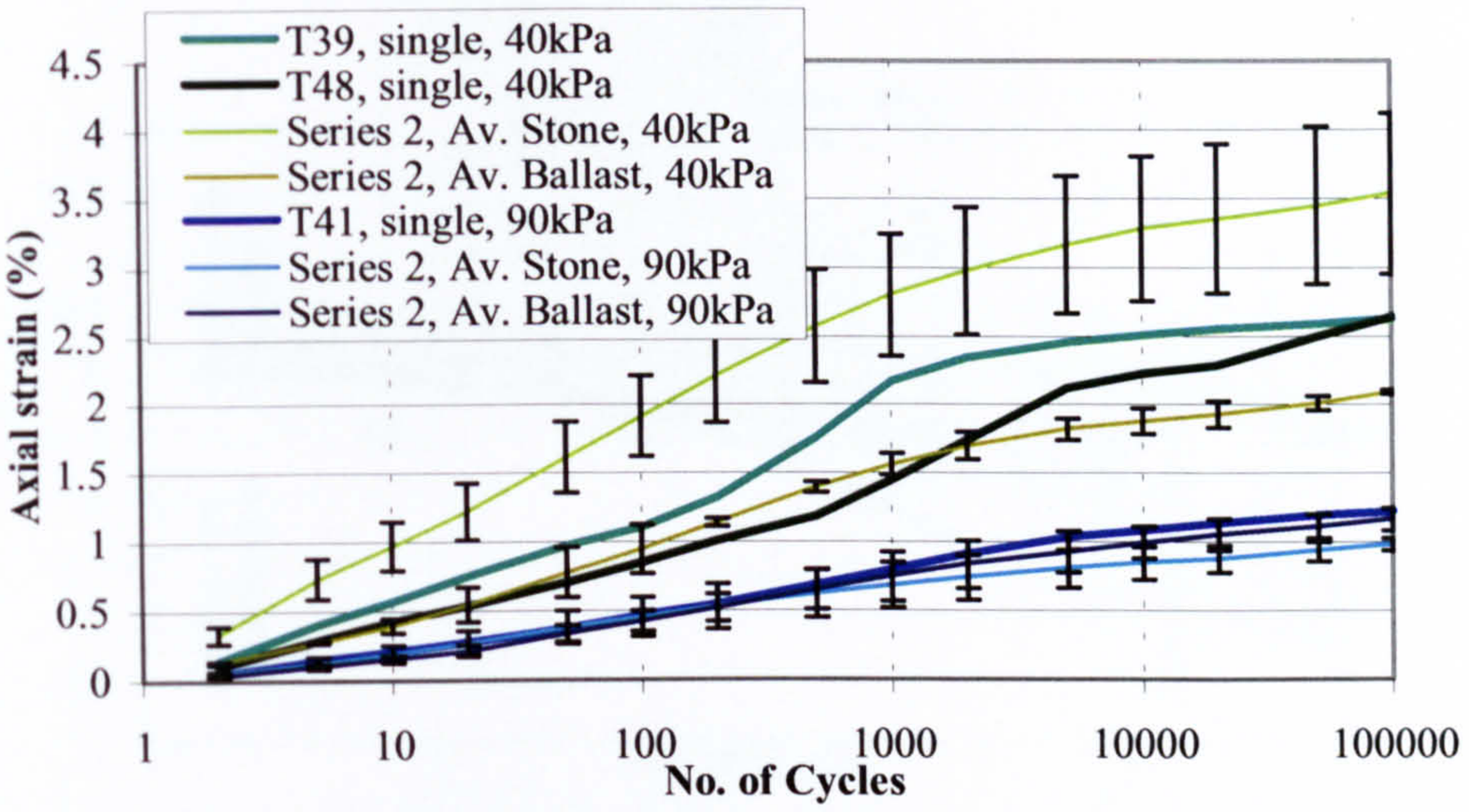

Figure 5.43 - Axial strain behaviour for single layer of stone overlying the ballast (Series 4) and stone only and ballast only specimens (Series 2) in cyclic load triaxial tests at 40kPa and 90kPa cell pressure

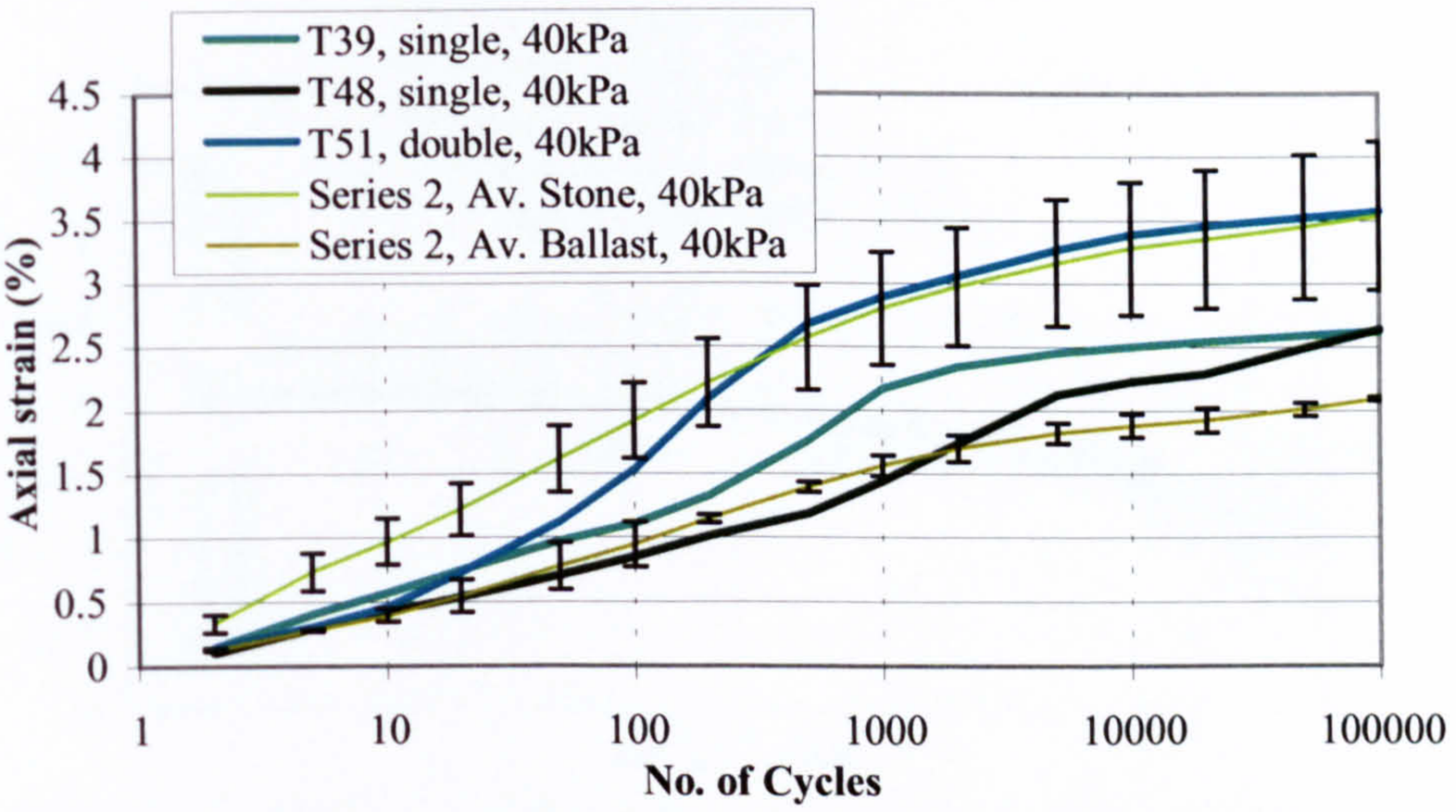

Figure 5.44 - Axial strain behaviour for thin layers of stone overlying the ballast (Series 4) and stone only and ballast only specimens (Series 2) in cyclic load triaxial tests at 40kPa cell pressure

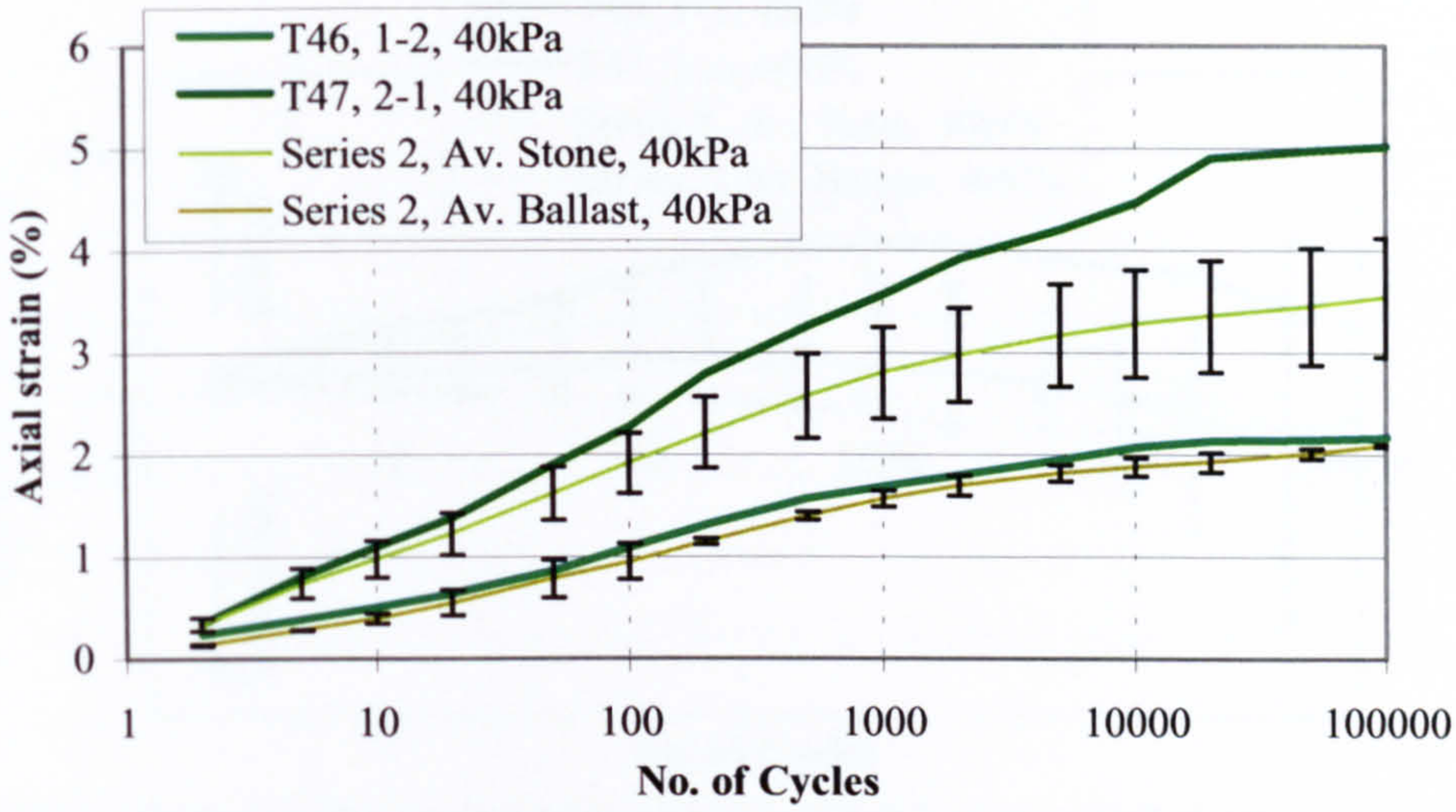

Figure 5.45 - Axial strain behaviour of 1-2 layer and 2-1 layer (Series 4) and stone only and ballast only specimens (Series 2) in cyclic load triaxial tests at 40kPa cell pressure

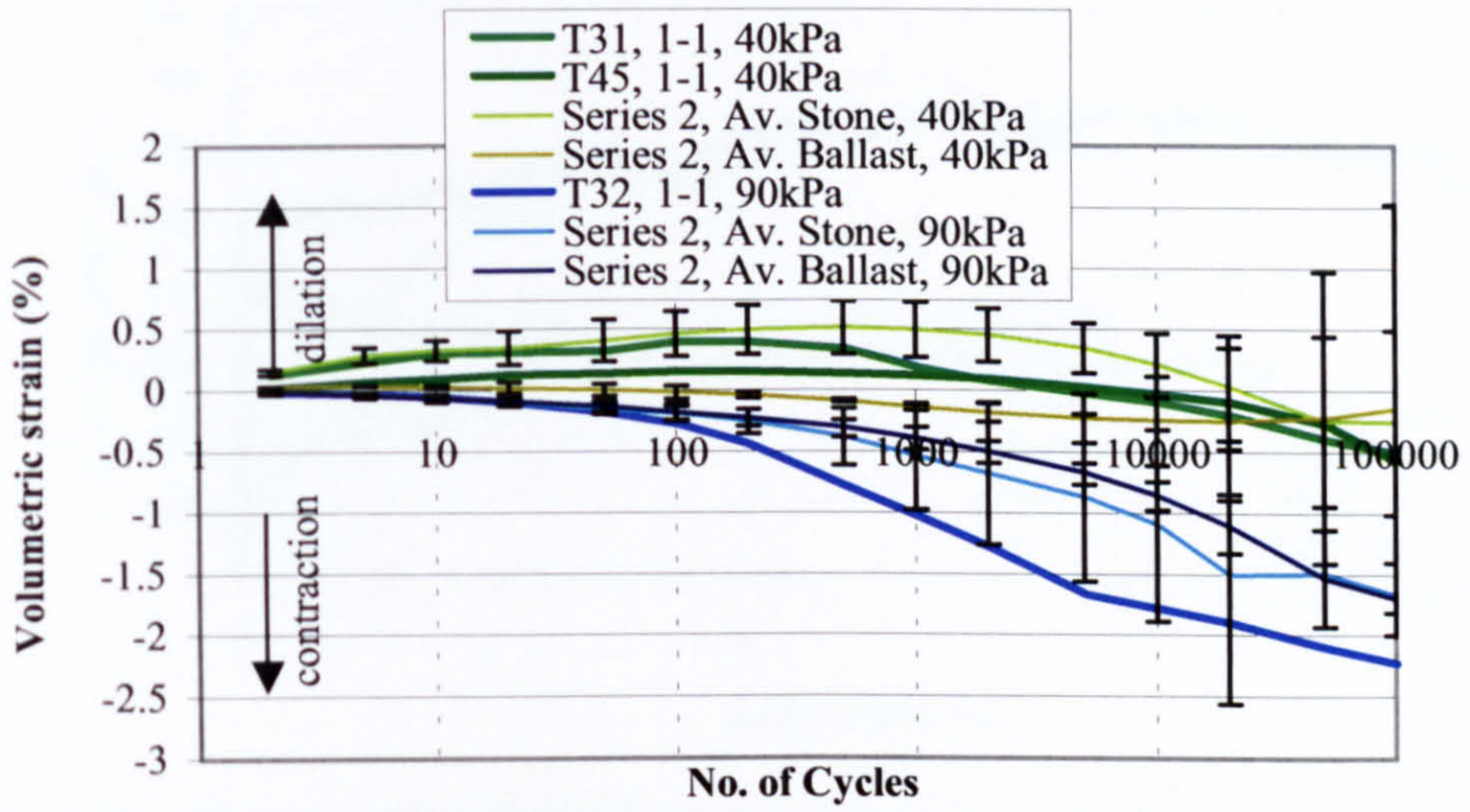

Figure 5.46 - Volumetric strain behaviour of 1-1 layer (Series 4) and stone only and ballast only specimens (Series 2) in cyclic load triaxial tests at 40kPa and 90kPa cell pressure (Series 4)

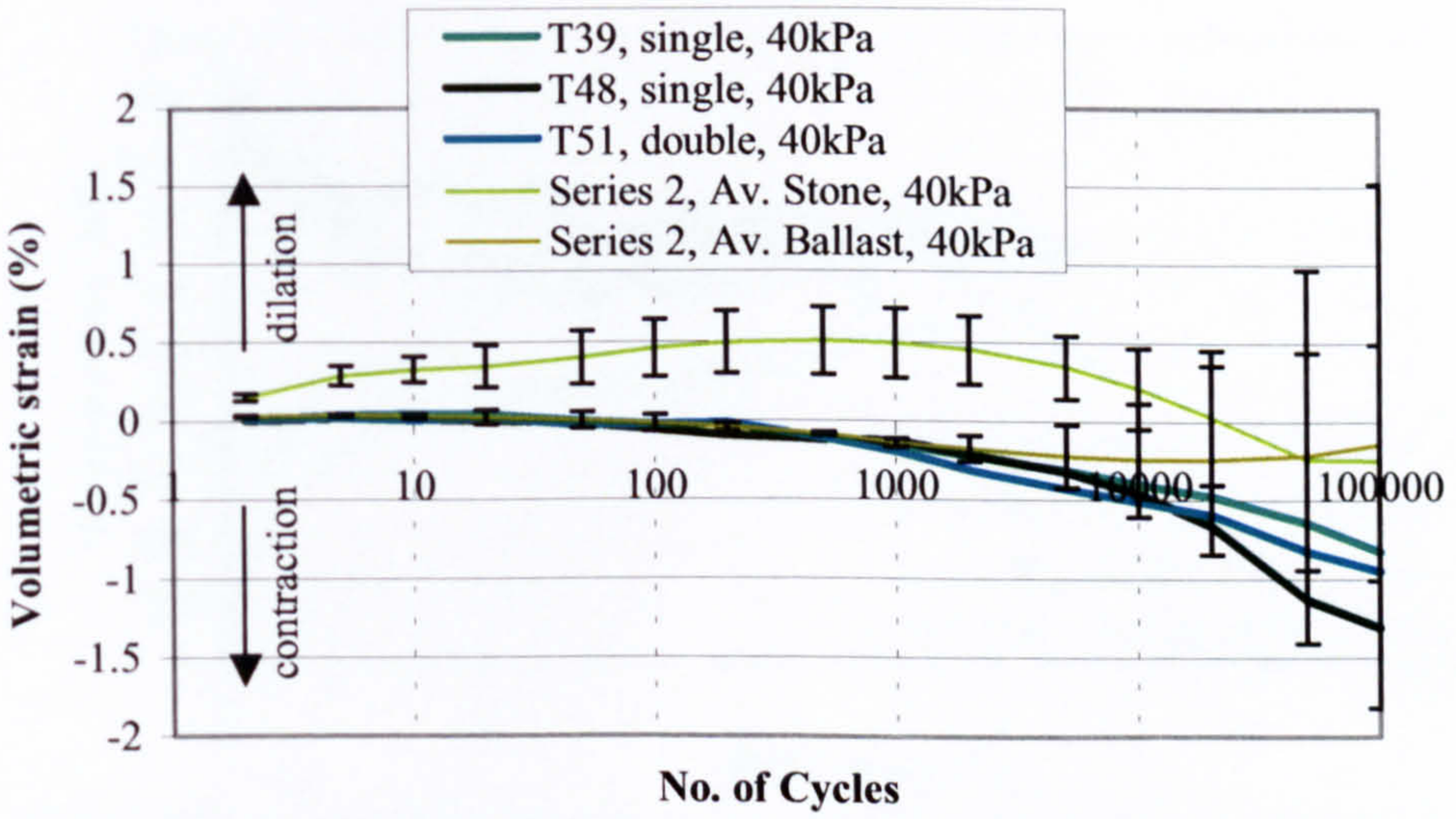

Figure 5.47 - Volumetric strain behaviour for a thin layer of stone overlying the ballast (Series 4) and stone only and ballast only specimens (Series 2) in cyclic load triaxial tests at 40kPa cell pressure (Series 4)

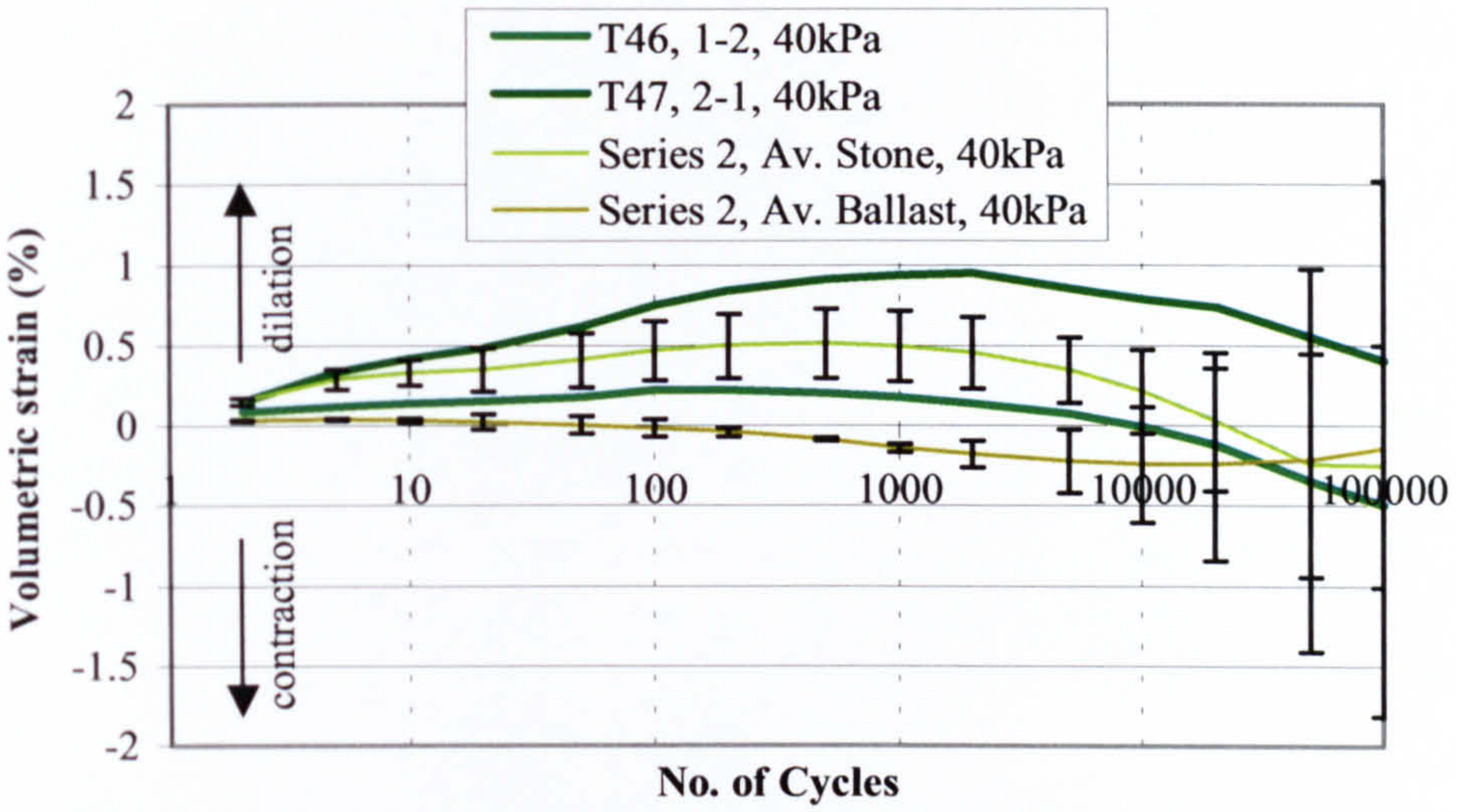

Figure 5.48 - Volumetric strain behaviour of 1-2 layer and 2-1 layer (Series 4) and stone only and ballast only specimens (Series 2) at 40kPa cell pressure in cyclic load triaxial tests (Series 4)

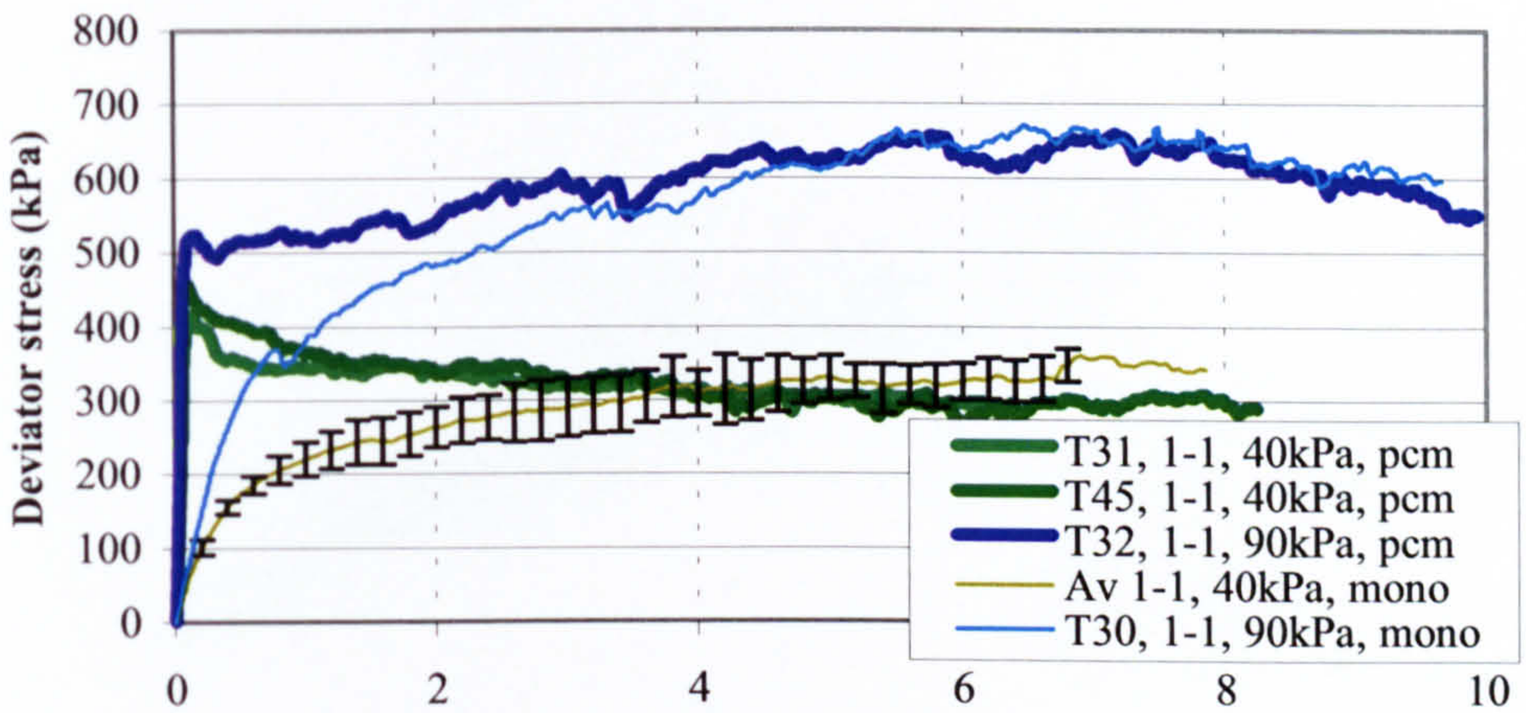

Figure 5.49 - Stress-strain behaviour of 1-1 layer specimens in monotonic load tests and post cyclic monotonic load tests at 40kPa and 90kPa cell pressure

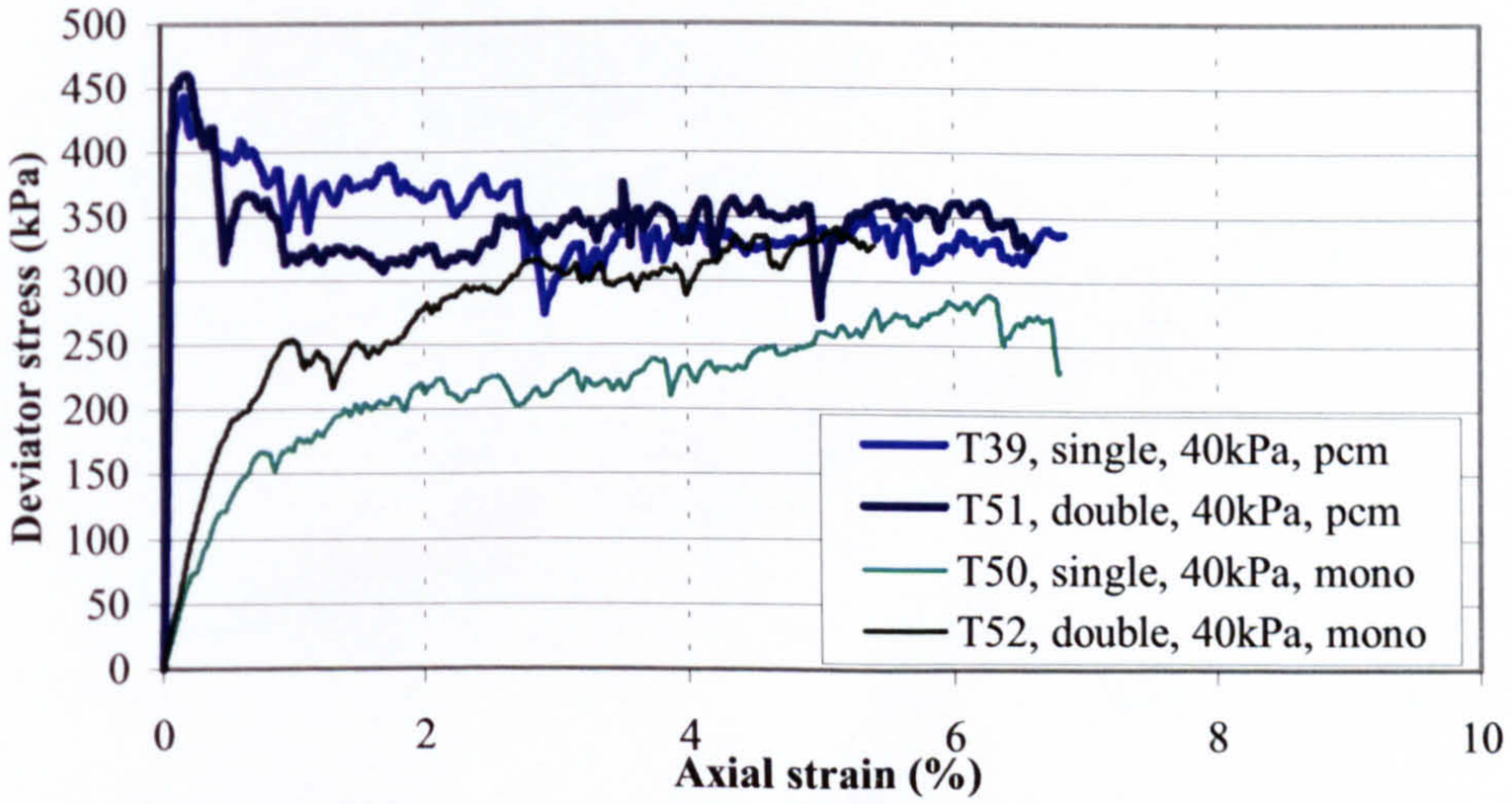

Figure 5.50 - Stress-strain behaviour for thin layer of stone specimens overlying the ballast in monotonic and post cyclic monotonic load triaxial tests at 40kPa cell pressure (Series 4)

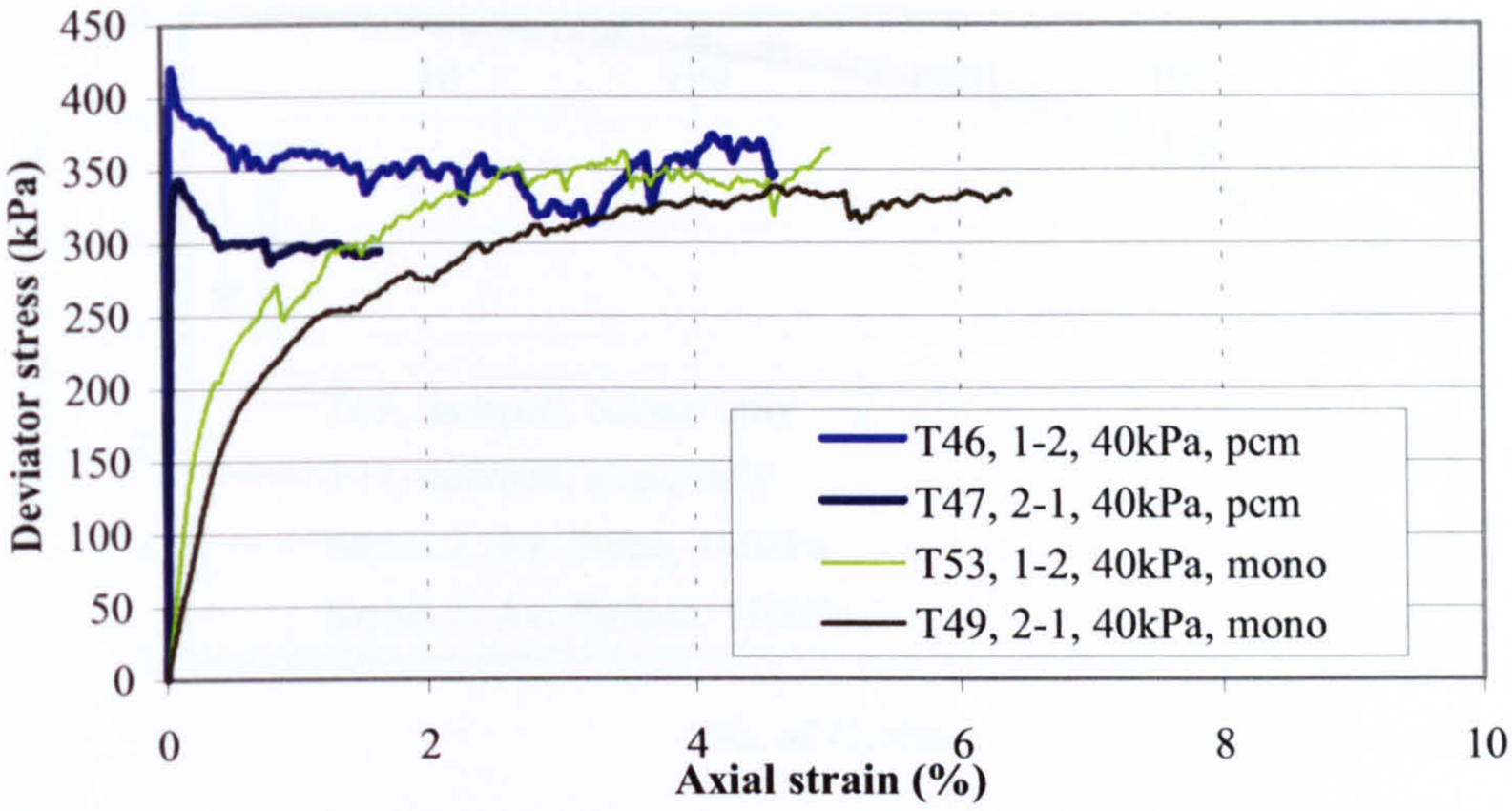

Figure 5.51 - Stress-strain behaviour of 1-1 layer and 2-1 layer specimens in monotonic and post cyclic monotonic load triaxial tests at 40kPa cell pressure (Series 4)

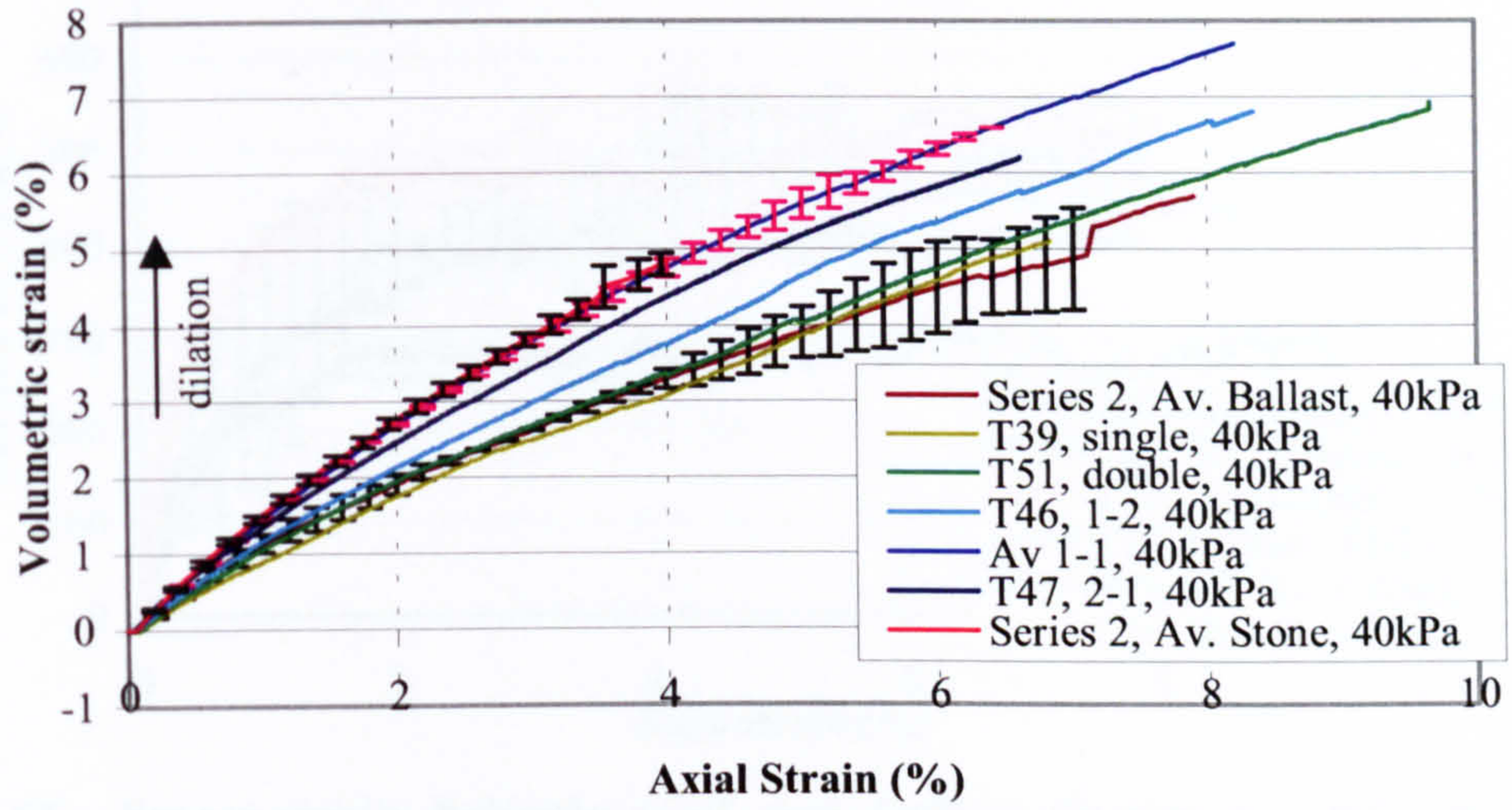

Figure 5.52 - Volumetric strain behaviour for all the layered (Series 4) and stone only and ballast only specimens (Series 2) in post cyclic monotonic load triaxial tests at 40kPa cell pressure

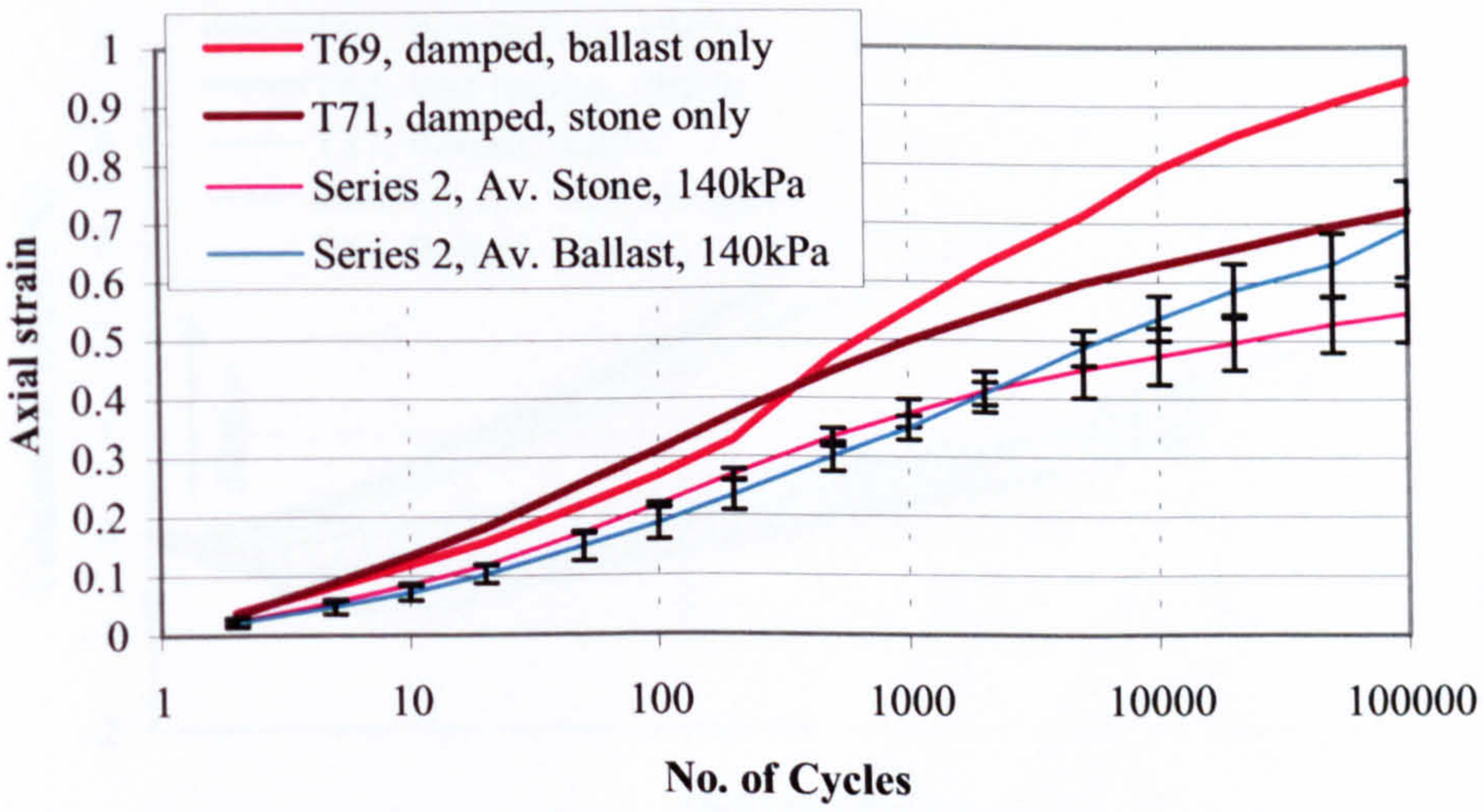

Figure 5.53 - Axial strain behaviour of damped ballast (Series 5) and stone only and ballast only specimens (Series 2) in cyclic load triaxial tests at 140kPa cell pressure

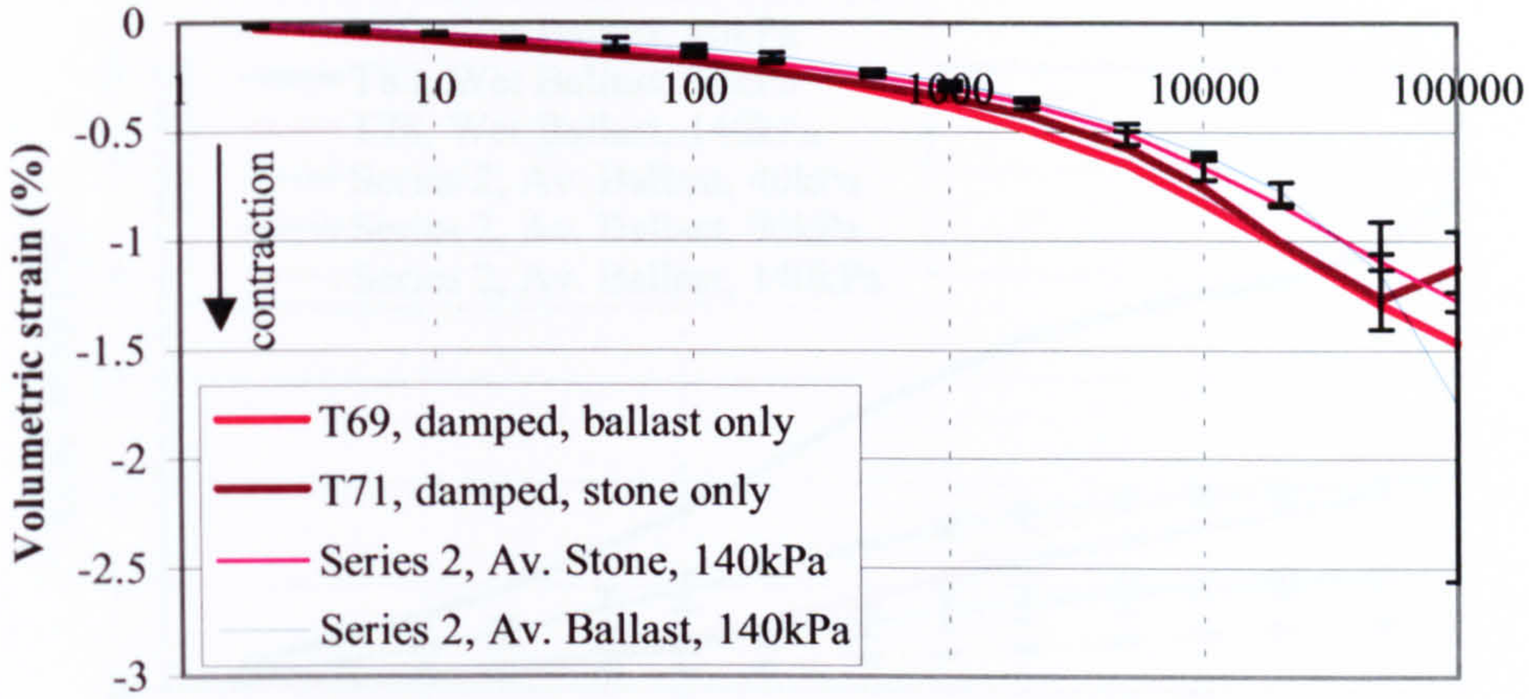

Figure 5.54 - Volumetric strain behaviour of damped ballast (Series 5) and stone only and ballast only specimens (Series 2) in cyclic load triaxial tests at 140kPa cell pressure

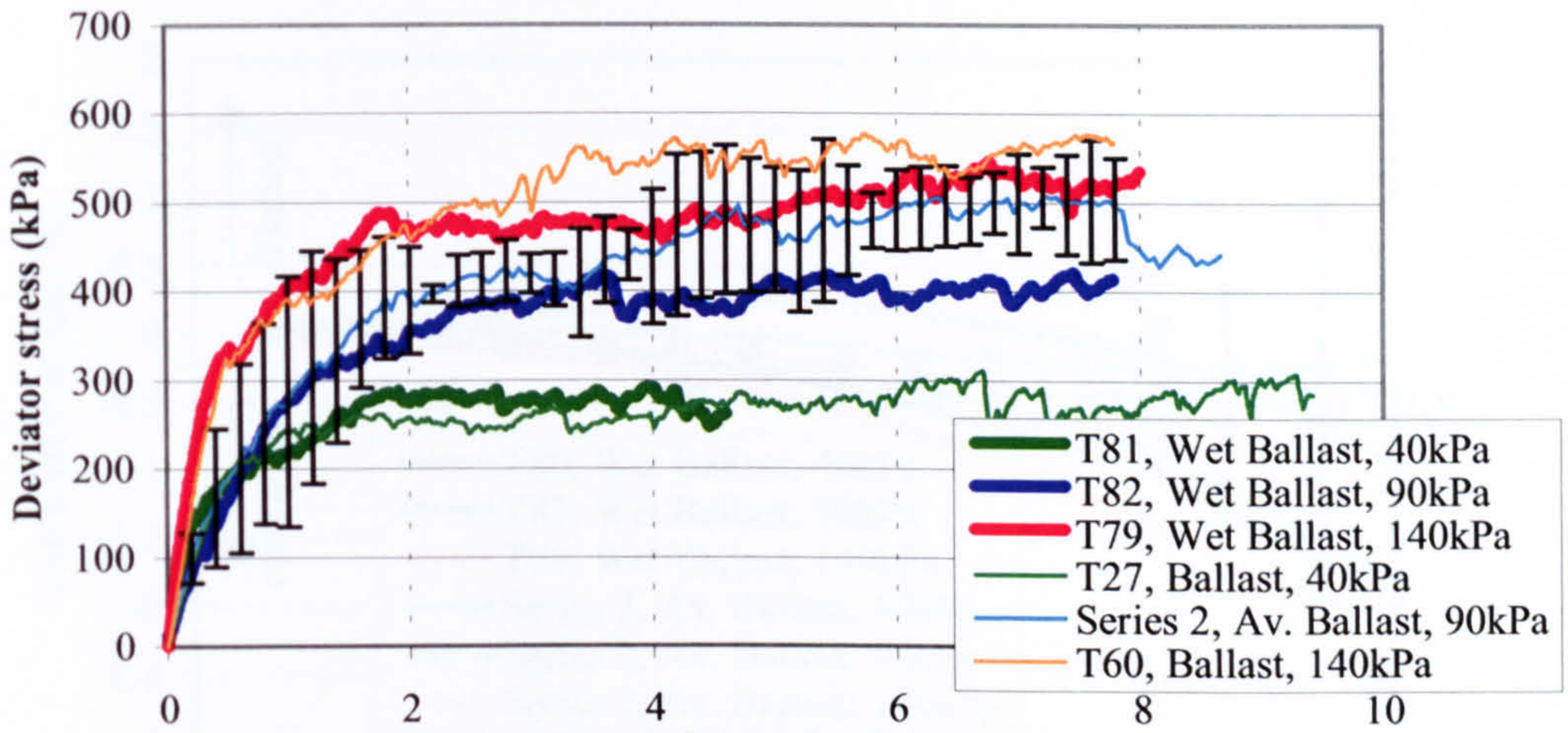

Figure 5.55 - Stress-strain behaviour of wet ballast (Series 6) and dry ballast specimens (Series 2) in monotonic load triaxial tests at 40kPa, 90kPa and 140kPa cell pressure

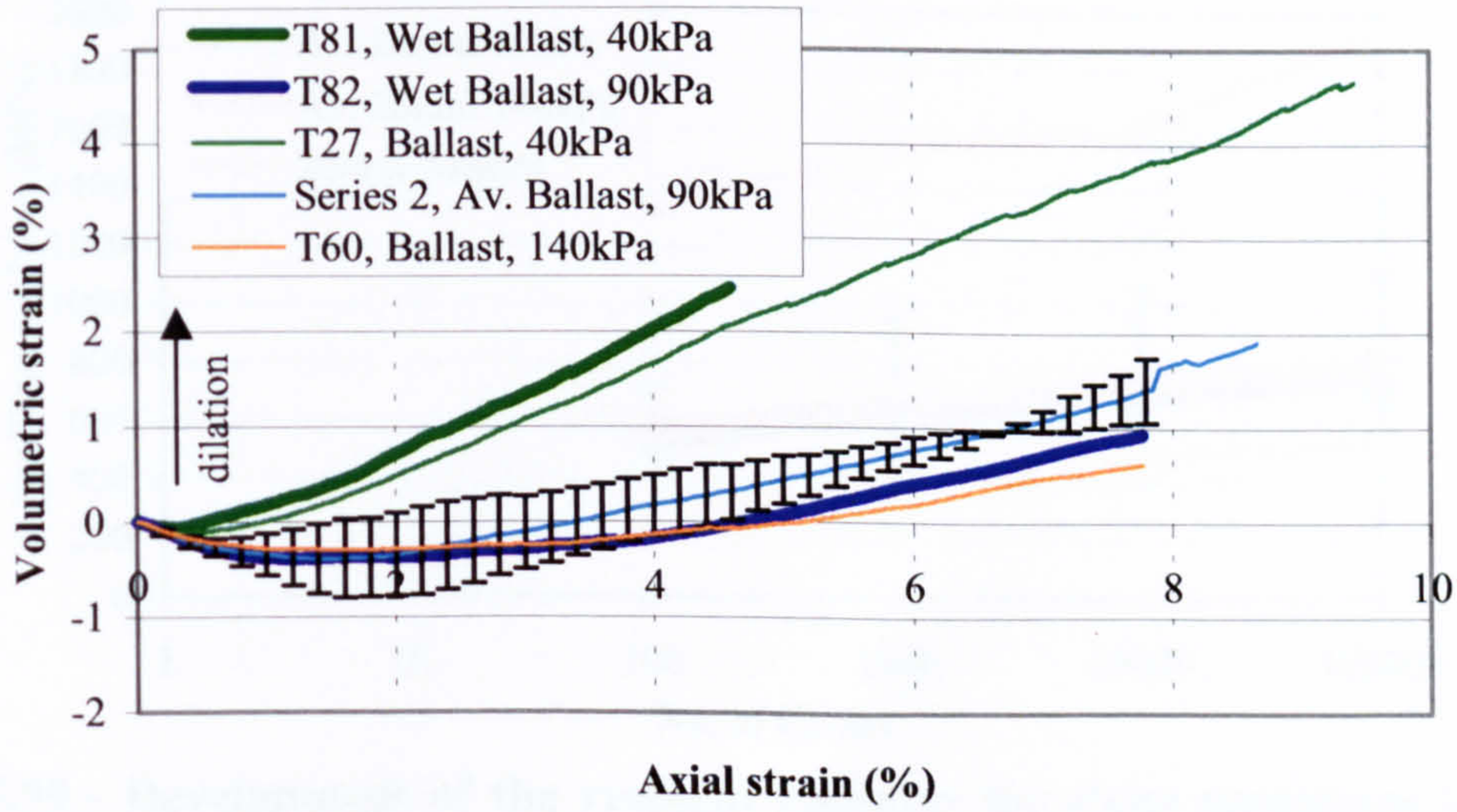

Figure 5.56 - Volumetric strain behaviour of wet ballast (Series 6) and dry ballast specimens (Series 2) in monotonic load triaxial tests at 40kPa, 90kPa and 140kPa cell pressure

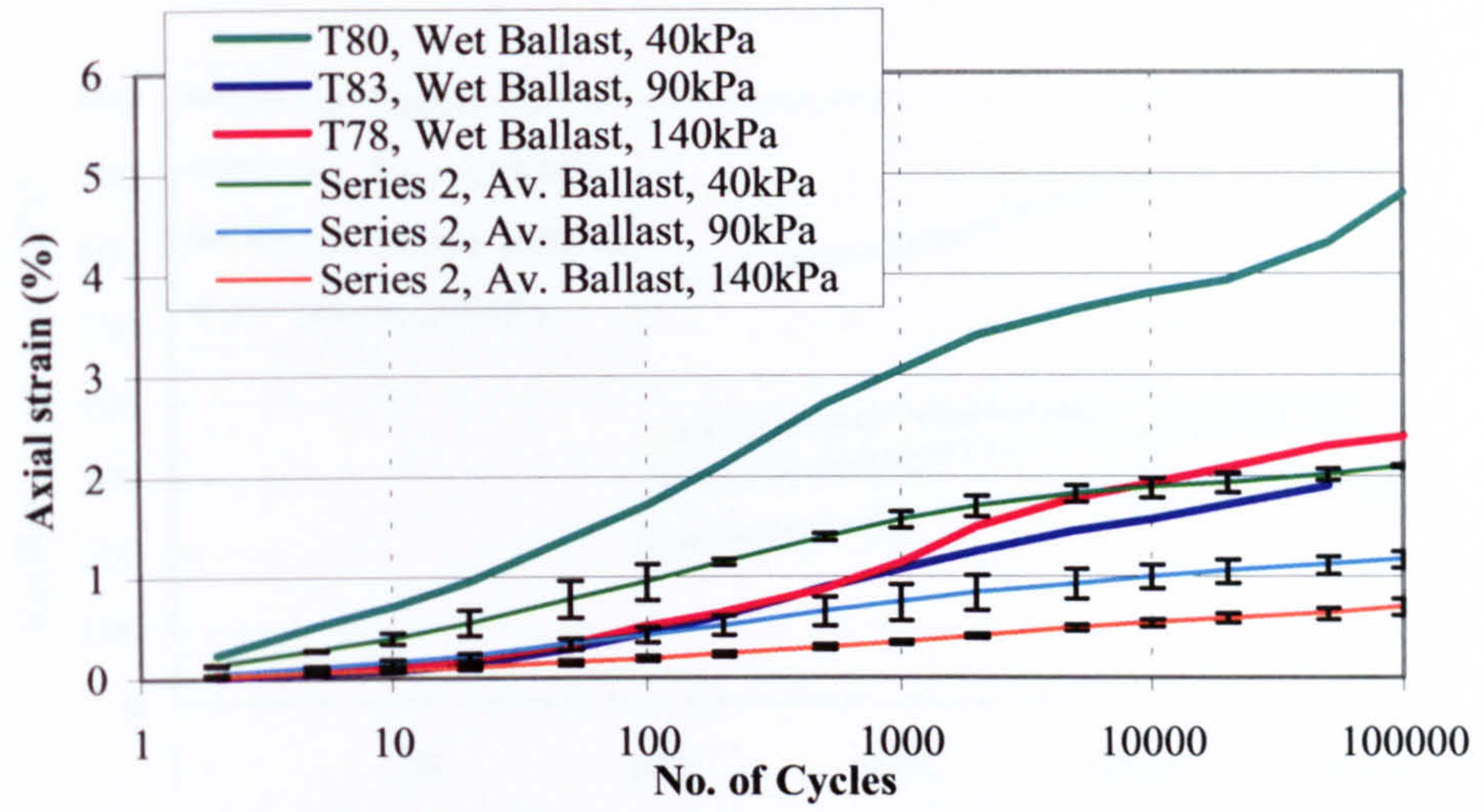

Figure 5.57 - Axial strain behaviour of wet ballast (Series 6) and dry ballast specimens (Series 2) in cyclic load triaxial tests at 40kPa, 90kPa and 140kPa cell pressure

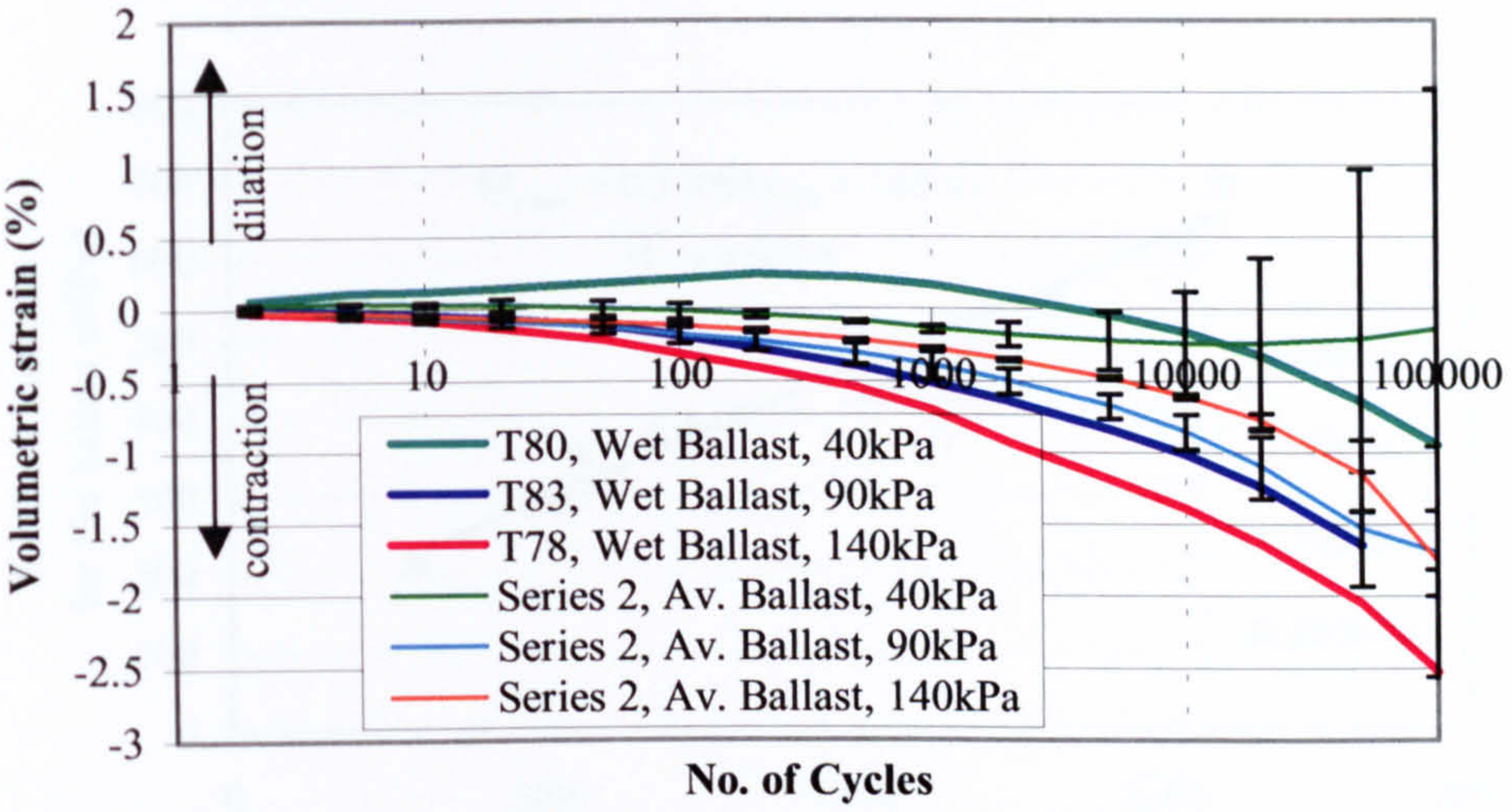

Figure 5.58 - Volumetric strain behaviour of wet ballast (Series 6) and dry ballast specimens (Series 2) in cyclic load triaxial tests at 40kPa, 90kPa and 140kPa cell pressure

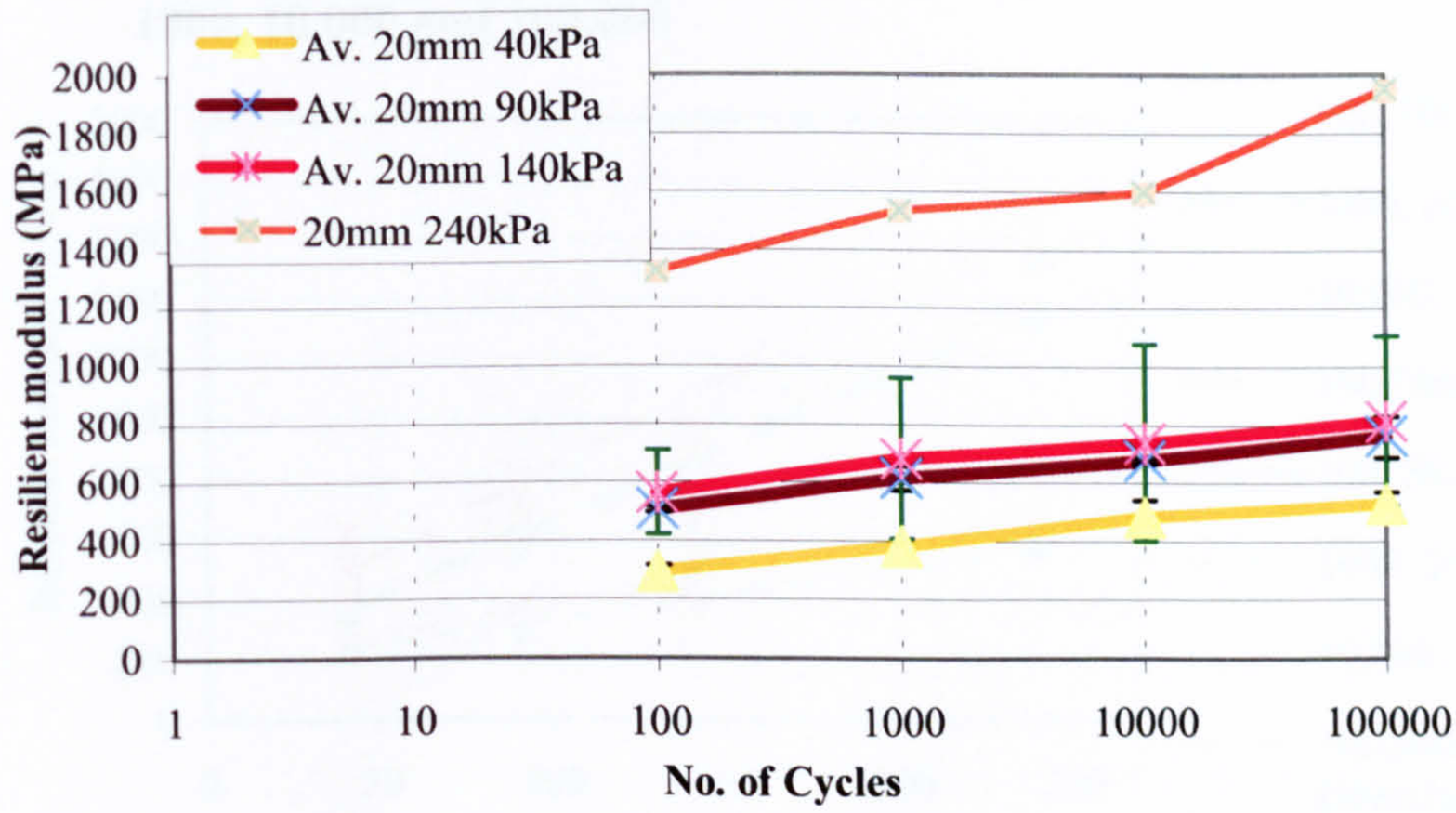

Figure 5.59 - Development of the resilient modulus for stone specimens in cyclic load triaxial tests at 40kPa, 90kPa, 140kPa and 240kPa cell pressure (Series 2)

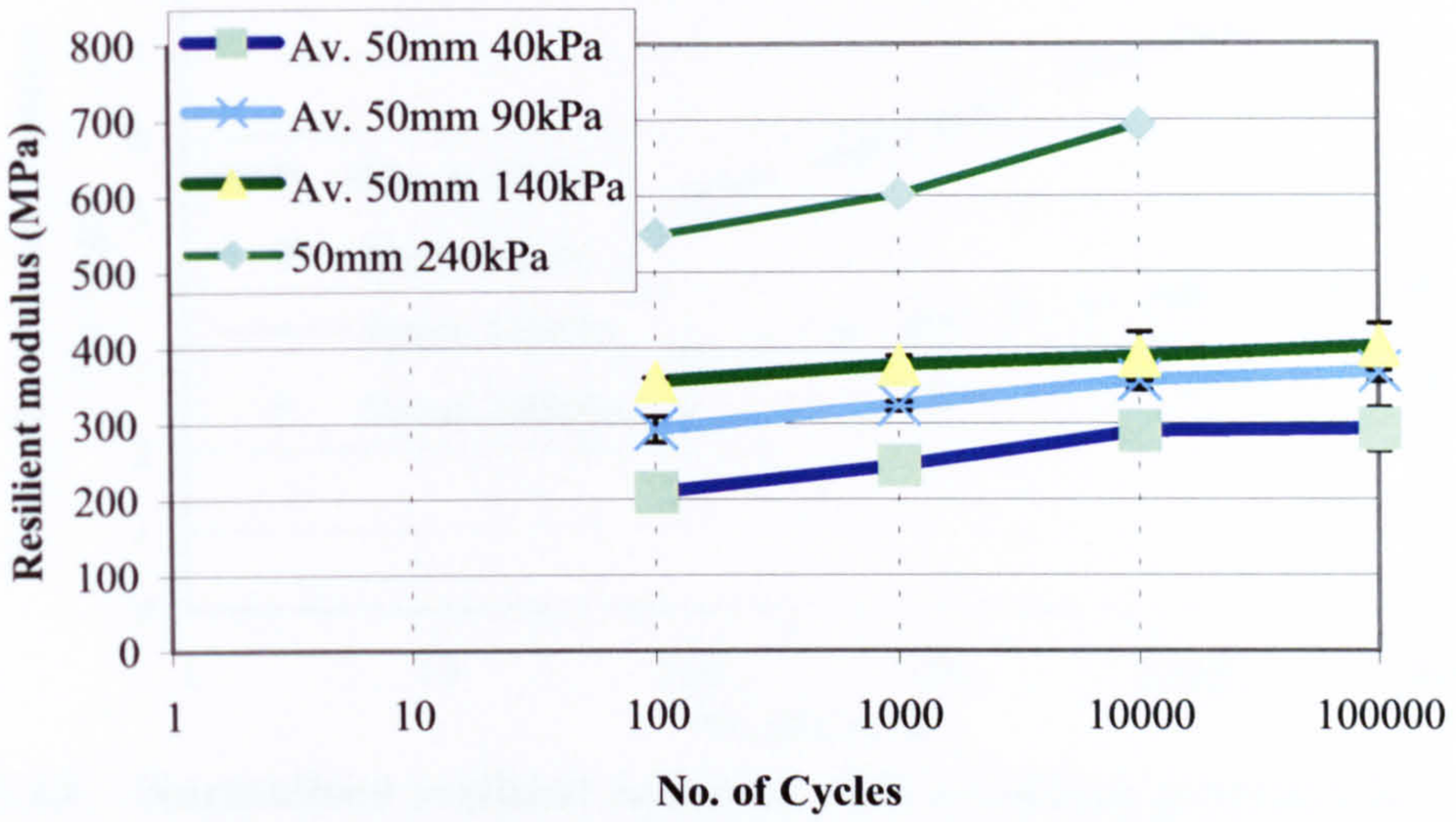

Figure 5.60 - Development of the resilient modulus for ballast specimens in cyclic load triaxial tests at 40kPa, 90kPa, 140kPa and 240kPa cell pressure (Series 2)

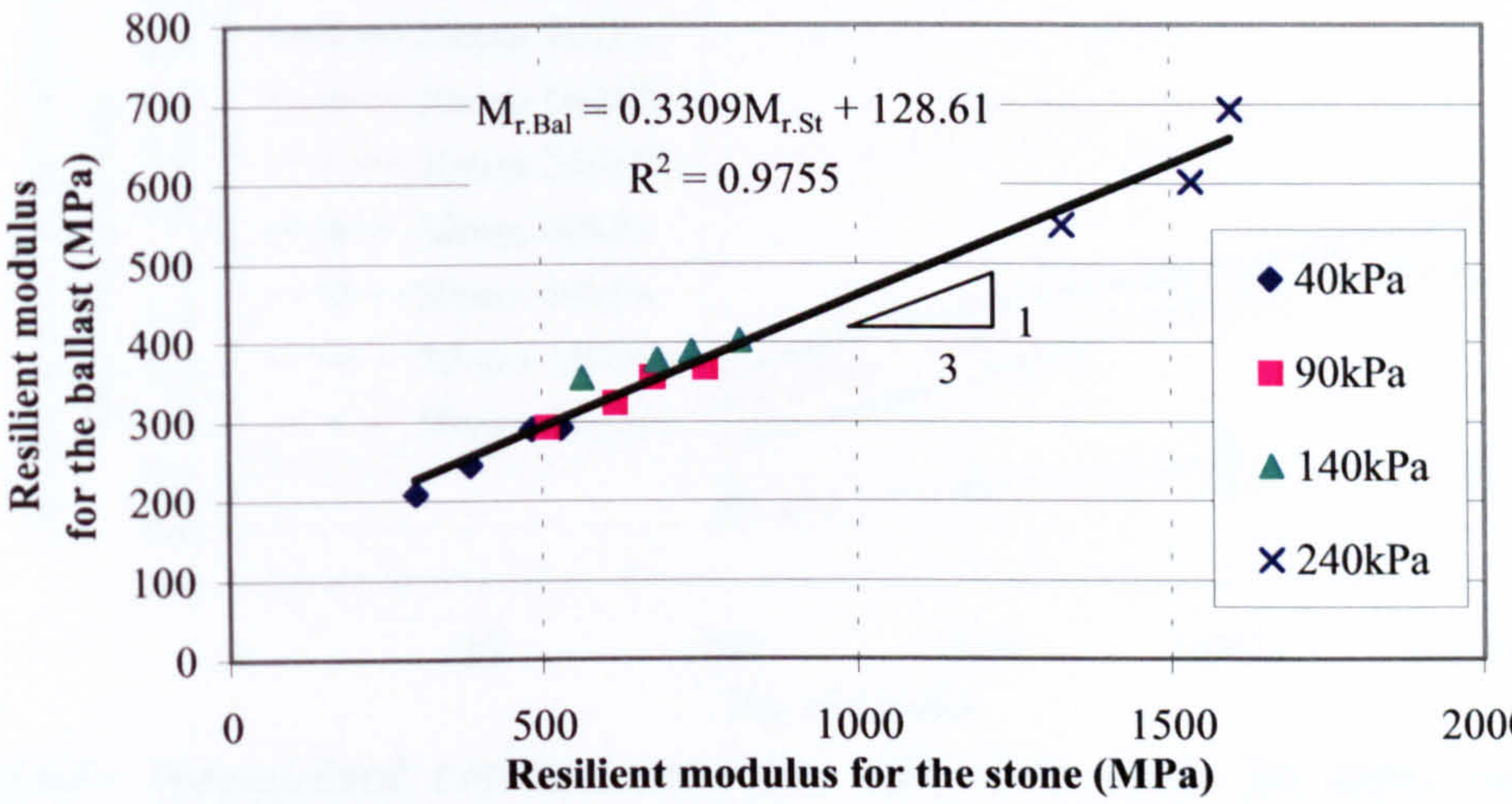

Figure 5.61 - Comparing the development of the resilient modulus for the stone and ballast specimens in cyclic load triaxial tests (Series 2) at 100, 1000, 10,000 and 100,000

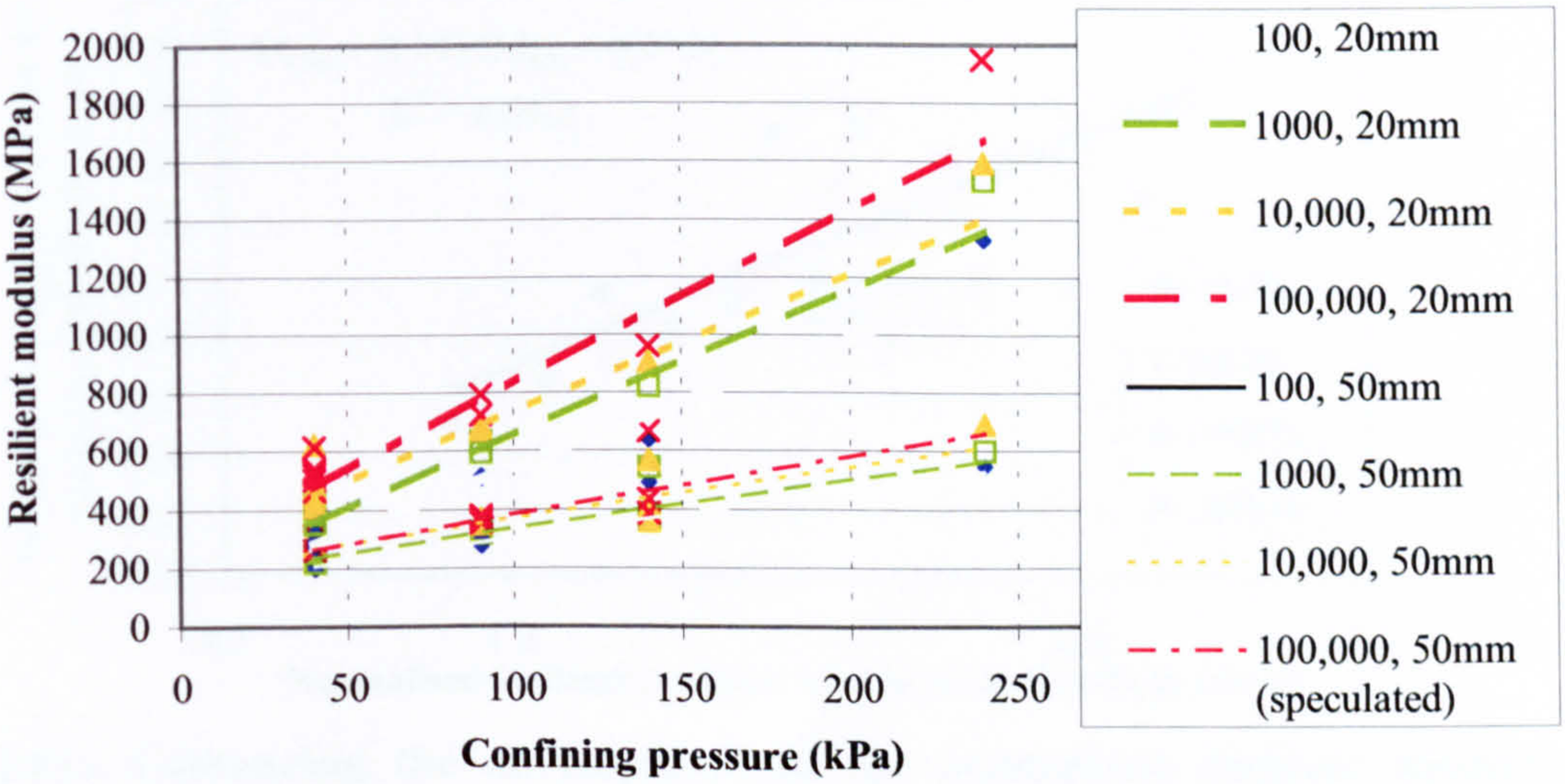

Figure 5.62 - Resilient modulus vs. confining pressure for the stone and ballast specimens in cyclic load triaxial tests at 40kPa, 90kPa, 140kPa and 240kPa cell pressure (Series 2)

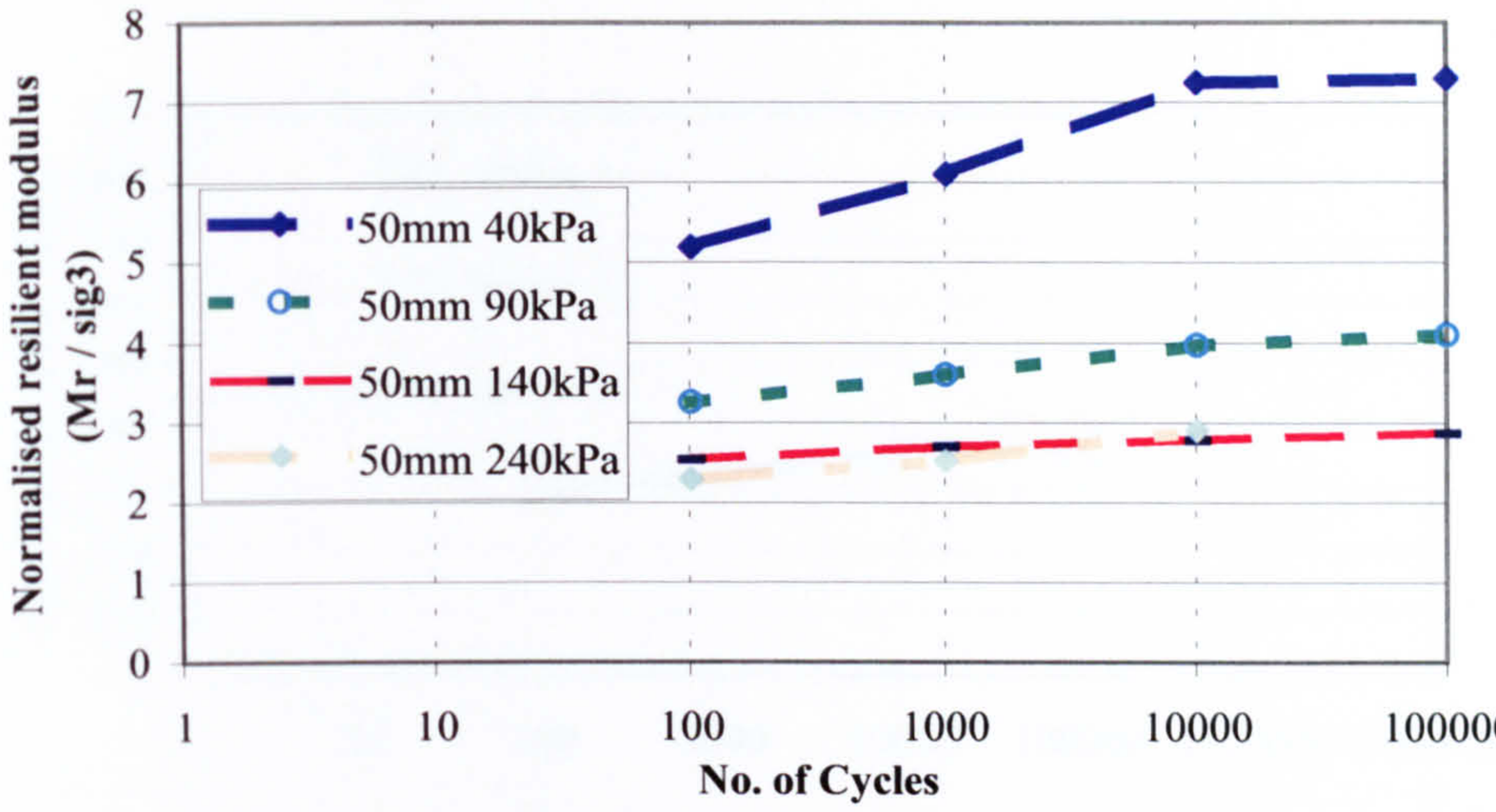

Figure 5.63 - Normalised resilient modulus with confining pressure for the ballast specimen in cyclic load triaxial tests at 40kPa, 90kPa, 140kPa and 240kPa cell pressure (Series 2)

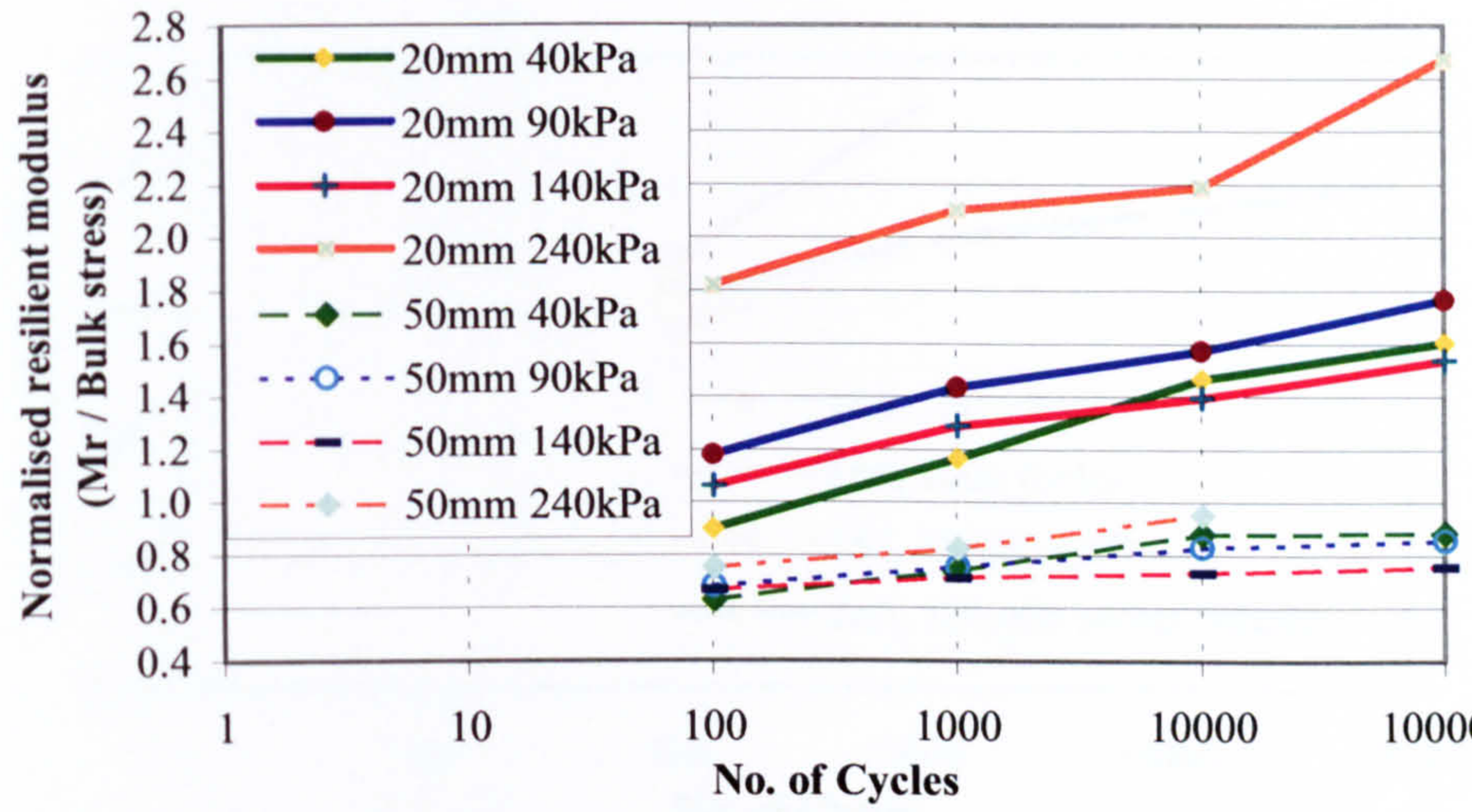

Figure 5.64 - Normalised resilient modulus with bulk stress for stone and ballast specimens in cyclic load triaxial tests at 40kPa, 90kPa, 140kPa and 240kPa cell pressure (Series 2)

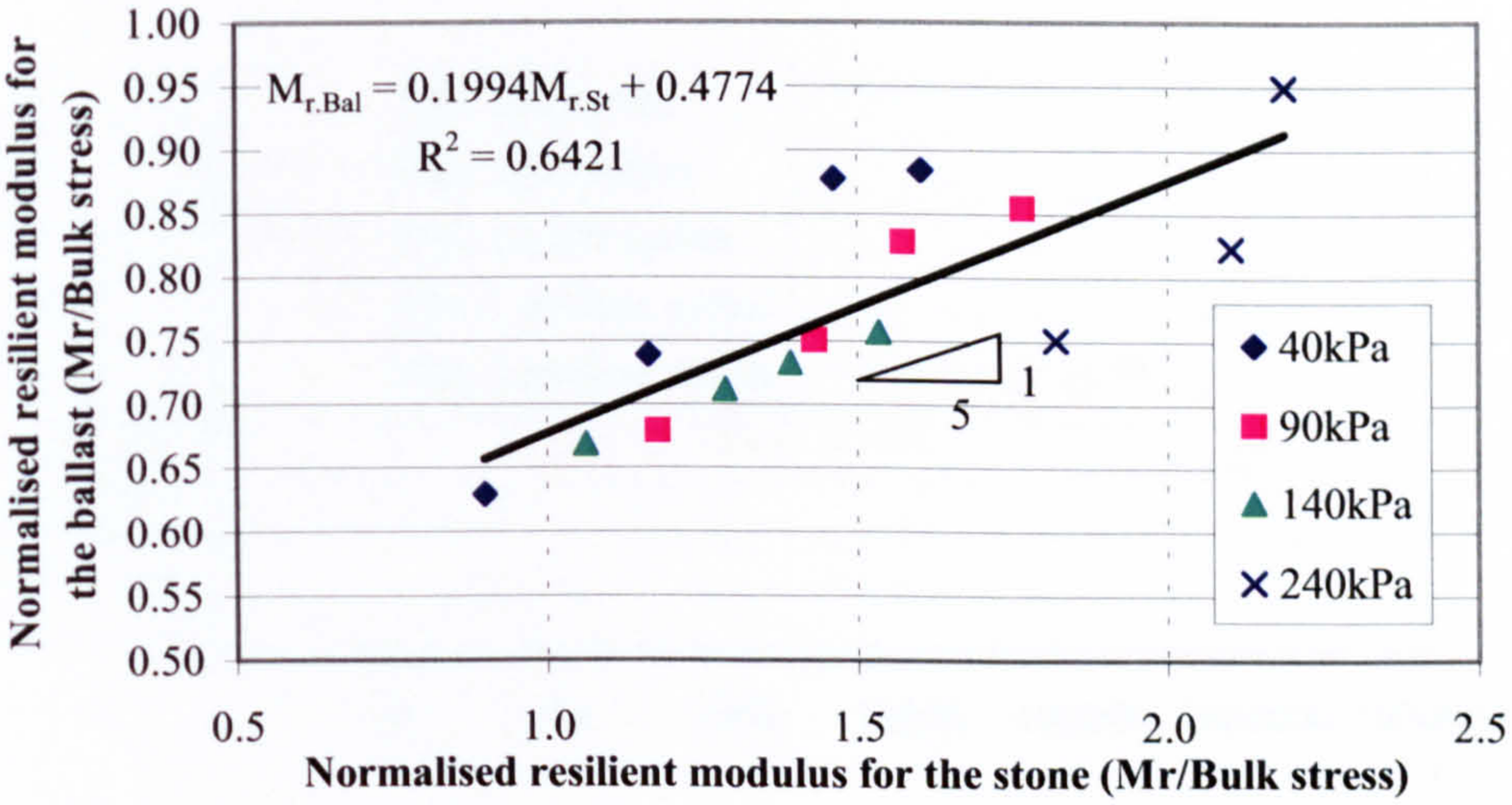

Figure 5.65 - Comparing the development of the normalised resilient modulus (with bulk stress) for the stone and ballast specimens in cyclic load triaxial tests (Series 2)

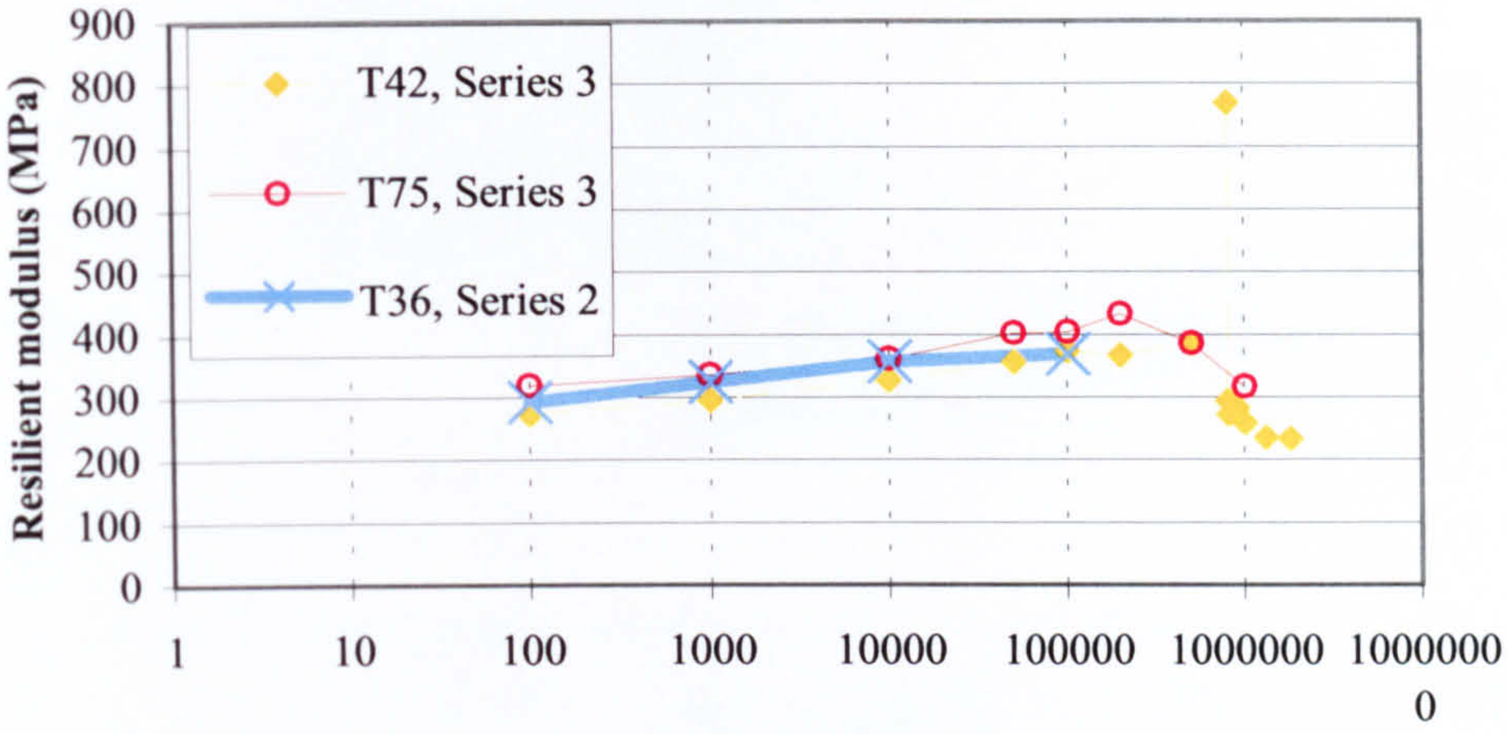

Figure 5.66 - Development of the resilient modulus for stone specimens in cyclic load triaxial tests at 90kPa cell pressure (Series 3)

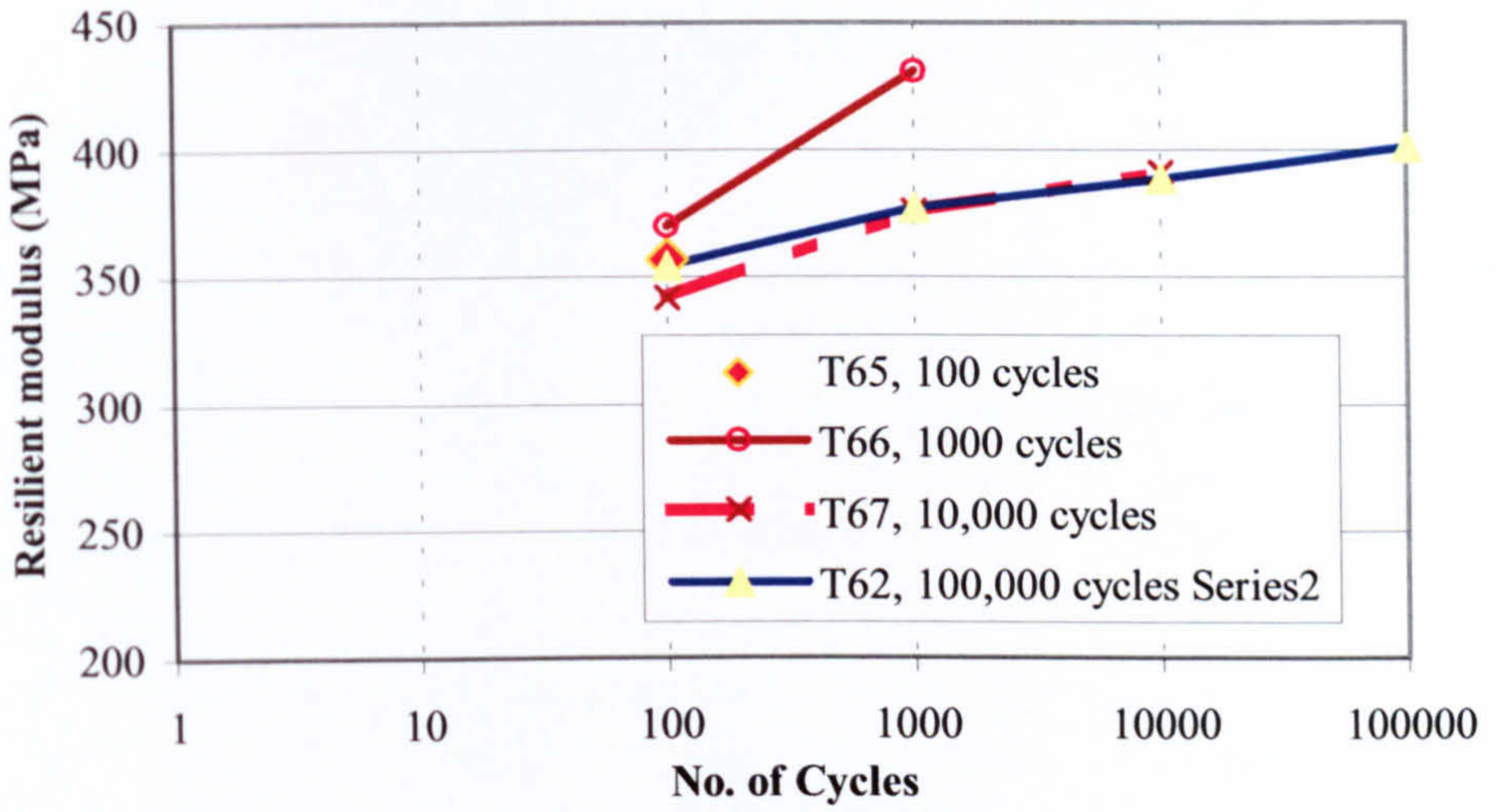

Figure 5.67 - Development of the resilient modulus for stone specimens in cyclic load triaxial tests at 140kPa cell pressure (Series 3)

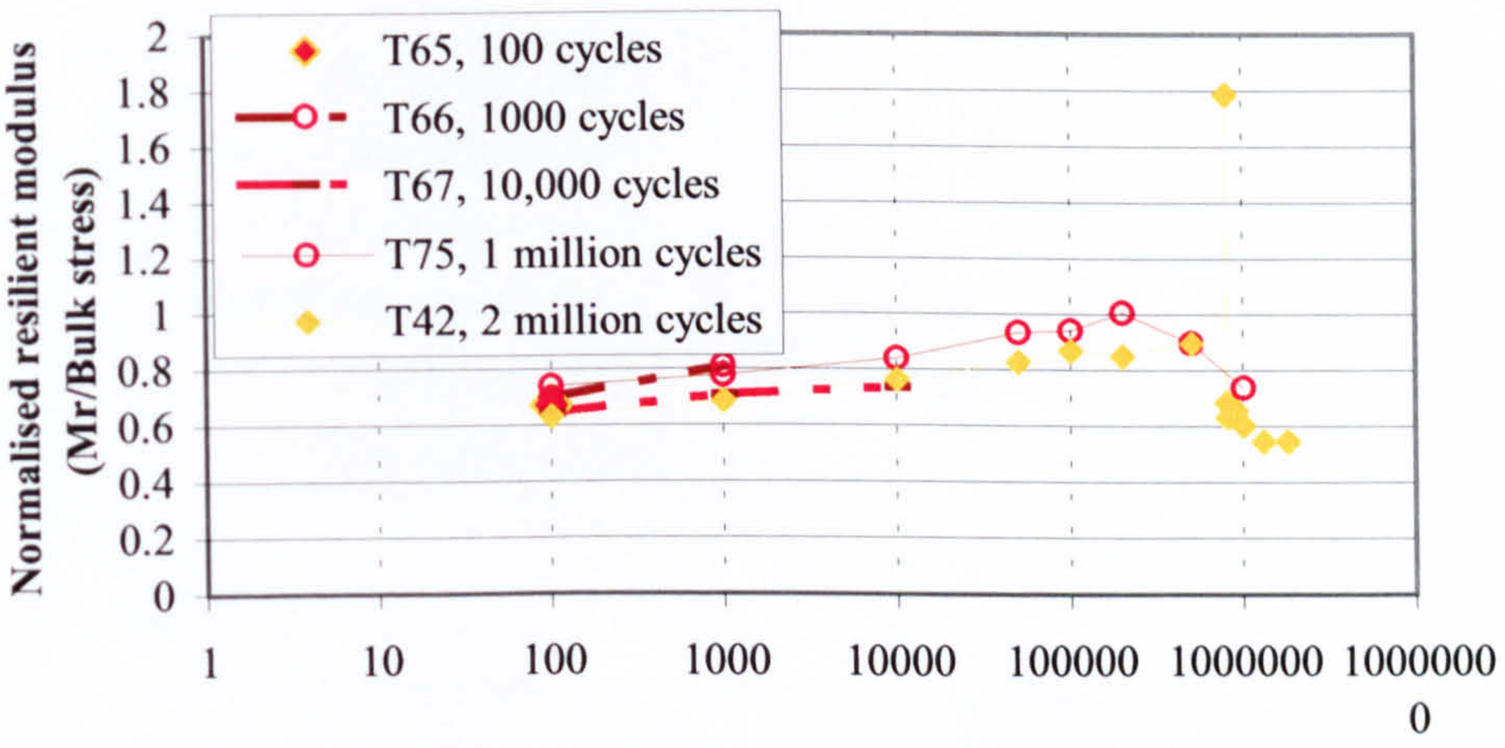

Figure 5.68 - Development of the normalised resilient modulus with bulk stress for stone specimens in cyclic load triaxial tests at 140kPa cell pressure (Series 3)

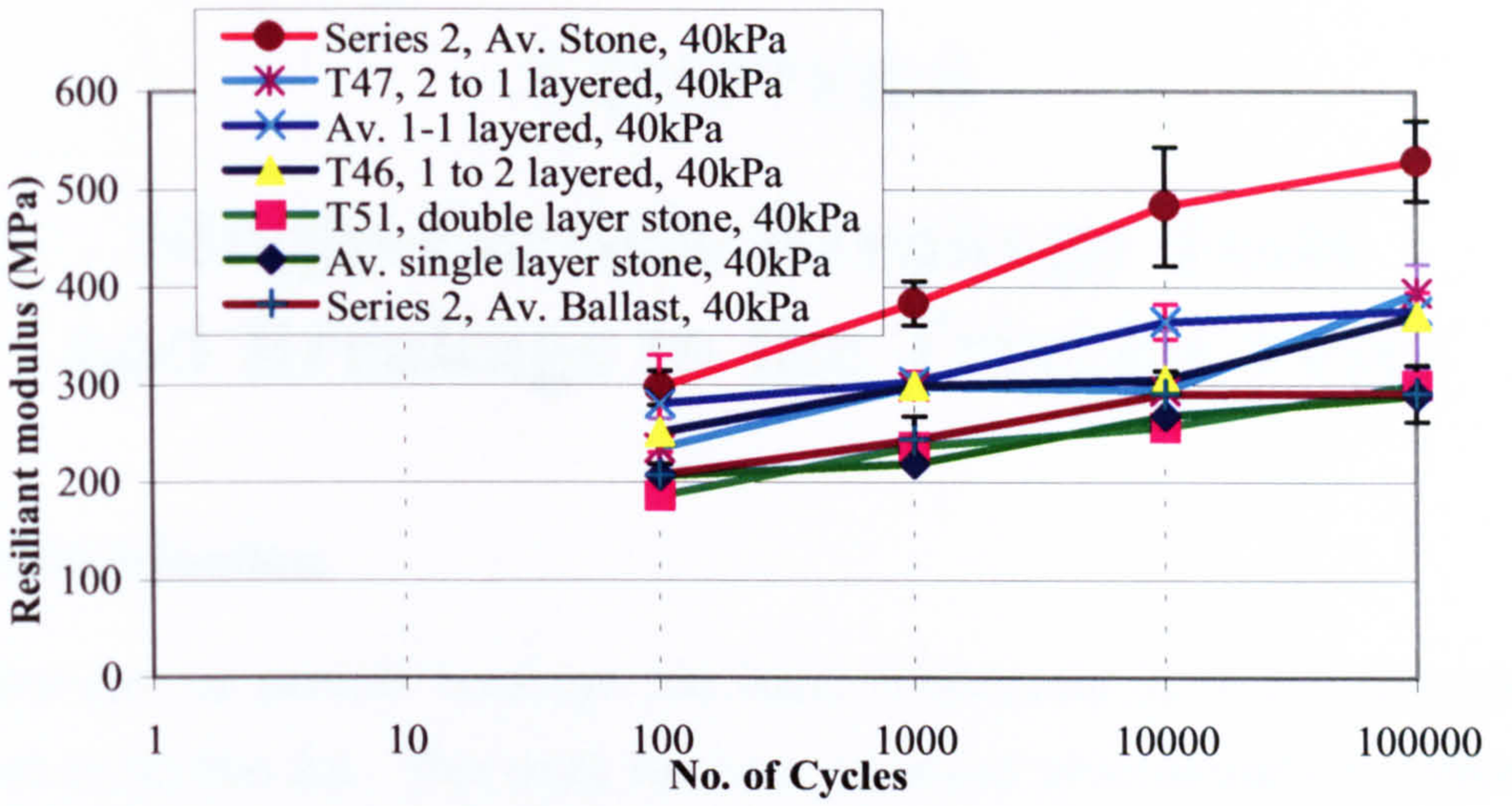

Figure 5.69 - Development of the resilient modulus for the layered (Series 4) and stone only and ballast only specimens (Series 2) in cyclic load triaxial tests at 40kPa cell pressure

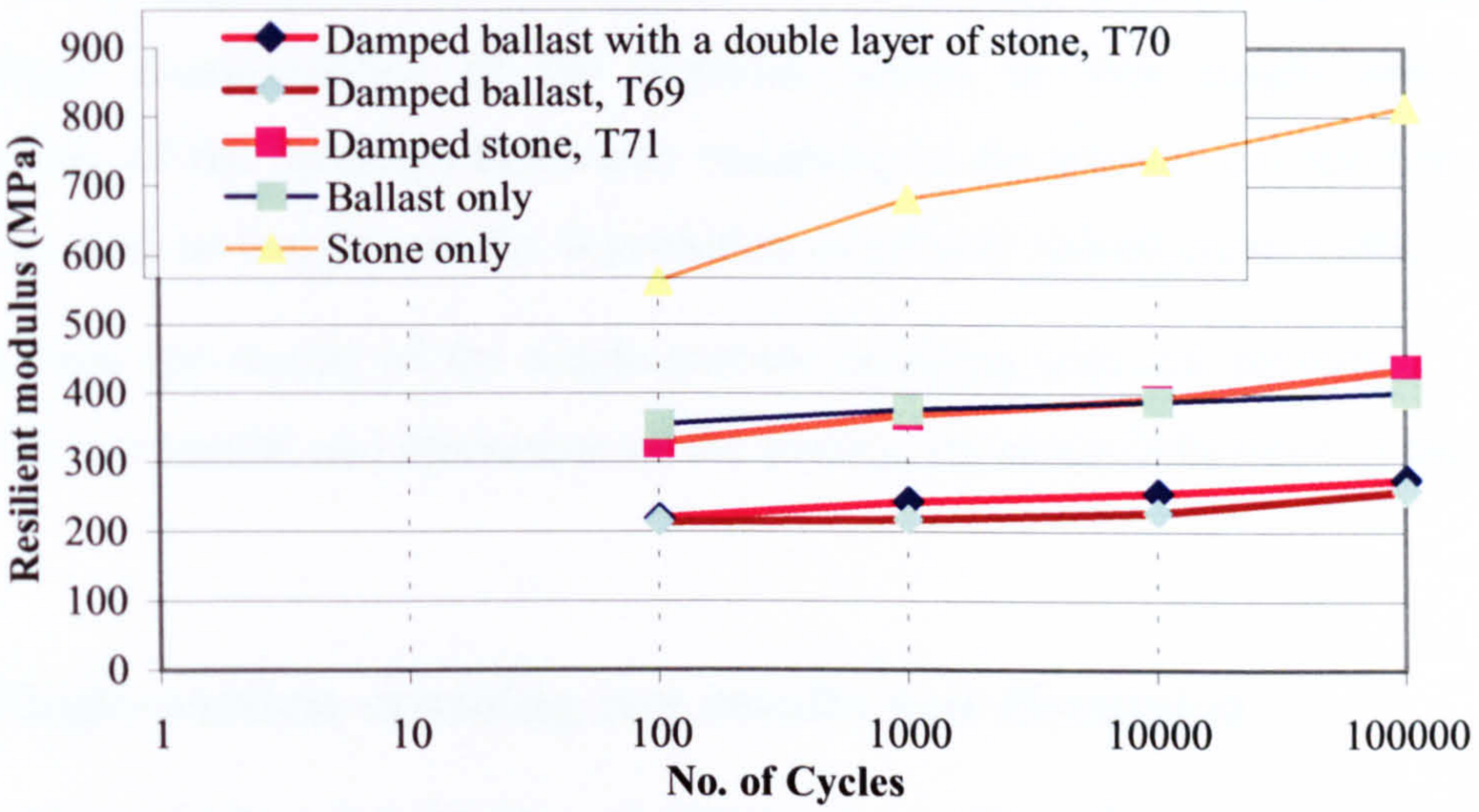

Figure 5.70 - Development of the resilient modulus for the damped (Series 5) and stone only and ballast only specimens (Series 2) in cyclic load triaxial tests at 140kPa cell pressure

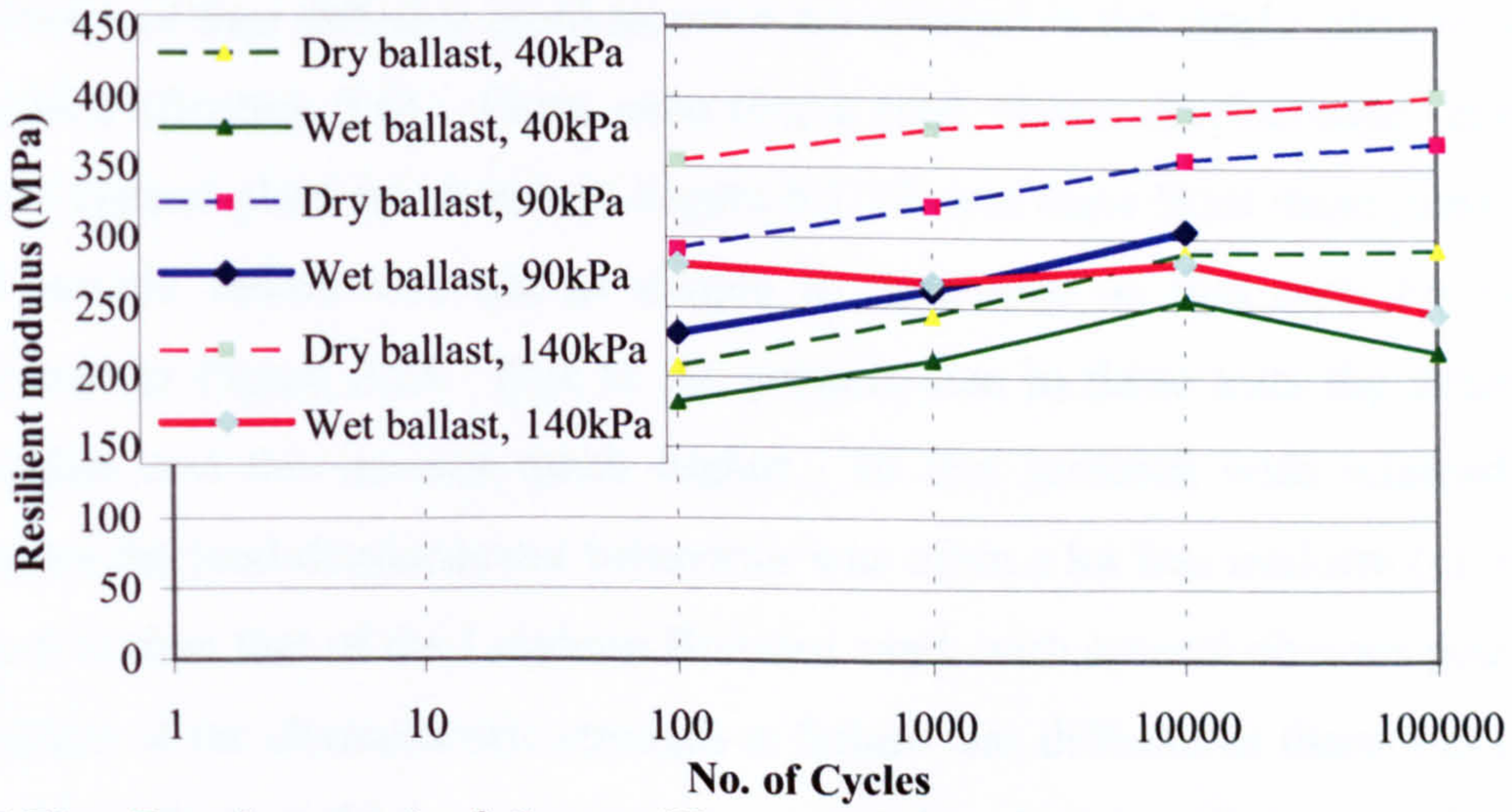

Figure 5.71 - Development of the resilient modulus for the wetted (Series 6) and dry specimens (Series 2) in cyclic load triaxial tests at 40kPa, 90kPa, and 140kPa cell pressure

CHAPTER 6

Single-Particle Breakage Tests and Breakage in the Triaxial Tests

6.1 Introduction

The behaviour of particle breakage has been investigated by many researchers as discussed in Section 2.6. This work has been advanced more recently by Nakata et al (1999) and McDowell and Bolton (1998) who have started to consider the relationships between particle breakage and the behaviour of the material in engineering situations. The aim of the single-particle crushing tests was to develop a deeper understanding of the breakage characteristics of the material, which in turn would enhance the understanding of the breakage behaviour occurring in the triaxial test specimens, and furthermore give an insight into the degradation of railway ballast under traffic loading.

In this section the results of the single-particle crushing tests are presented. This is followed by the results and discussion of the particle breakage behaviour in the triaxial tests.

6.2 Single-particle crushing test results and discussion

As discussed in Section 3.6, McDowell (2001) shows that at least thirty particles must be tested to determine the characteristic tensile strength (σ_o) and Weibull's modulus (m) within reasonable limits (25% accuracy at 95% confidence). Therefore in this research thirty particles of four different sized stones were crushed in the single-particle crushing test apparatus (Section 3.6). From each test a load versus displacement graph was drawn, two typical plots are shown in Figure 6.1. It was clear from these plots that the point of particle failure was not as simple to determine as that seen for Leighton Buzzard sand in Figure 2.25. Due to the particle size in these tests the strains were much smaller and the stresses much higher. In this research with relatively large particle sizes the load-displacement behaviour was often a lot less uniform (cf. test T28 in Figure 6.1) than that of the Leighton Buzzard sand, with several obvious peaks. The determination of the characteristic strength at failure was difficult as there was often no obvious peak that could be recognised as causing major splitting, defined as a catastrophic failure and a reduction of load to near zero.

From the graphs the load and displacement at the breakage of the first asperity and at particle fracture were recorded and the tensile stress for the first asperity breakage (σ_a) and for particle fracture (σ_f) were calculated:

$$\sigma_a = \frac{F_a}{d_a^{\,2}} \quad \& \quad \sigma_f = \frac{F_f}{d_f^{\,2}} \qquad \text{Equ 6.1}$$

where: F_a = force at first asperity failure,

F_f = force at particle fracture, and

d_a^2 = particle diameter at first asperity failure, and

d_f^2 = particle diameter at particle fracture

The particle diameter at failure (or fracture) is taken as the distance between the two platens at failure (or fracture), as defined by Jaeger (1967). As the point of fracture in the tests were not always clear, a technique was necessary for the consistent analysis of the graphs and the determination of the force at fracture (F_f). The method used in this project to determine F_f was to take the first major peak at which the load was reduced by more than 50%. Once this failure had occurred it was assumed that the load was being transferred by more than one piece of the original particle. Hence, loading thereafter was not a true representation of the particle strength. A limitation of the calculated tensile stress of the asperity failure is that only the size of the particle was known and not the size of the asperity that was broken off.

As discussed in Section 2.6.4 the probability of survival $P_s(d)$ for any particular size of aggregate can be calculated by:

$$P_s(d) = \exp\left[-\left(\frac{\sigma}{\sigma_o}\right)^m\right] \qquad \text{Equ. 6.2}$$

where: $\sigma = F/d^2$ (Equ. 6.1),

σ_o= characteristic tensile strength and

m = Weibull modulus

where the Weibull modulus (m) reduces with increased variability and the characteristic tensile strength (σ_o) for a particle size d is the strength at which 37% of the tested particles survived.

Thirty 20mm stone, thirty 20-28mm ballast, thirty 28-37mm ballast and thirty 37-50mm ballast particles were crushed to determine characteristic tensile strength (σ_o) and Weibull's modulus (m) for each particle size. The stone particles were as used by the

stoneblower and the ballast particles were randomly selected from the Railtrack specification ballast (Railway Board, 2000) used in the triaxial test programme.

The survival probabilities, for each size of particle, were calculated by positioning the tensile stresses at failure (σ_a and σ_f) in ascending order. The mean survival probability was then calculated by dividing the position number by the total number plus one. i.e. 30/31 (97%) is the survival probability of 29 particles surviving the value of σ_a (or σ_f) of the particle with the lowest σ_a (or σ_f). The probability of survival curves are shown in Figures 6.2 and 6.3. It would normally be expected that the larger the particle the lower the tensile stress at failure and the lower the value of characteristic tensile strength (σ_o, at 37% probability of survival). From Figure 6.2 it can be seen that the curves for the asperity breakages for all the different sized stones were similar. This implies that the actual force at asperity failure was larger for the larger specimens where d is greater (see Equation 6.1). In Figure 6.3 the tensile strength typically decreased with particle size. However it was interesting to note that the different sized ballasts had characteristic tensile strengths very close to one another when compared with the characteristic tensile strength of the 20mm stone. Figure 6.4 compares the probability of survival curves for the asperity failure and the complete particle fracture curves. The differences in strength can be clearly seen.

Equation 6.2 can be rewritten as:

$$\ln\left(\ln\left(\frac{1}{P_s}\right)\right) = m\ln\sigma - m\ln\sigma_o \qquad \text{Equ. 6.3}$$

from which the graph $\ln(\ln(1/P_s))$ versus $\ln\sigma$ is drawn, showing the Weibull distribution of strength. The Weibull modulus is determined by the gradient of the line and the characteristic tensile strength σ_o can be calculated by equating $\ln(\ln(1/P_s))$ to zero. Figures 6.5 and 6.6 show the Weibull distribution of strengths for the asperity failure and particle fracture for the four nominal stone sizes. The values of m (Table 6.1), taken as the gradient of the best-fit lines, were all very low. This shows that there was a large variability in the strength of the particles tested. This is particularly surprising for the 20mm stone particles at fracture, as one would have expected a slightly higher value of m, because the stones were generally more alike in size and shape than the larger sized ballasts. It was also noted that there was greater variability in m for the asperity fracture than the particle failure tensile strengths. This was presumably because the

sizes of the first asperity fracture varied significantly depending on the shape and orientation of the original particle in respect to the crushing plates (see Figure 3.10).

Figure 6.6 also includes the best-fit lines from McDowell et al. (2003). They tested thirty particles of 10-14mm Mountsorrel ballast and thirty 37.5-50mm Mountsorrel ballast. From these curves the value of m was determined as was the characteristic tensile strength for each of the nominal sizes at particle failure. The values of m and σ_o are compared for each of the curves in Table 6.1.

From Figure 6.6 (and Table 6.1) one can see that the 20mm Bardon stone had a slightly lower particle fracture characteristic tensile strength than the 10-14mm Mountsorrel ballast as would be expected. However the 37.5-50mm Mountsorrel had a significantly higher particle fracture characteristic tensile strength than that seen for the 37-50mm Bardon ballast.

The reason for the discrepancies in the observed results when compared with those of McDowell was unclear. However, there were three factors which could have had a significant influence over the test results. Firstly the apparatus used in the two projects was different. McDowell et al. (2003) used a large Zwick testing machine, which was assumed to have a much stiffer reaction frame than the converted 100kN loading frame used in this project. Hence with a stiffer reaction frame the loading regime, especially as asperities fractured off the particle, would have been slightly different. The effect of this difference in apparatus could not be determined. Comparisons of similar stone is needed in both machines to check the validity of comparing results between these two, and other, machines. Secondly the cup in which the particle was placed in this research was not transparent (see Plate 3.5) and therefore the point at which the particle failed could not be observed. This led to the problem already mentioned above of not being certain of when the particle had failed catastrophically. Although it was considered to have had little significance on the overall results this may have caused an increase in the variability (i.e. a decrease in m). It would be better to remove the cup wall in future testing. This would not reduce the safety of the testing device as the crushing apparatus was set up inside the triaxial cell. Thirdly, in the discussion on the probabilistic approach to sand particle crushing in the triaxial test McDowell (2001) pointed out that when applying Weibull's statistics the particles should have a similar shape and loading regime. Although the ballast particles were all passed through the particle size template (Plate 3.4) the overall shape varied (within each nominal size), thus the loading regime could well have been significantly different. This could be a possible explanation for

the lack of clearly observed size effect between the different sized ballast particles. The 20mm stones were all of relatively similar geometry.

Furthermore, as McDowell et al. (2003) pointed out, the process by which the particles are produced at the quarry could mask the true size effect. The larger particles which have been through the grinding processes have already proved themselves to be stronger than the total sample of large particles produced up to that point in the process. They could therefore be considered statistically strong, hence masking the true size effect on the Weibull distribution curves. However from these results it was clear that the size effect was still apparent, especially with the 20mm Bardon stone.

6.3 Particle breakage behaviour in the triaxial tests

As detailed in Section 3.4 the specimens for the triaxial test were prepared by adding the ballast one particle at a time through the particle size template to determine how many particles of each specific size went into the specimen. On dismantling the specimen each particle was removed one by one, including all its component pieces. The original size of the whole particle was assessed and a breakage score (B_s) given. Each piece of the original particle was then passed through the particle size template and the information recorded in a table. After every particle had been removed and analysed a total breakage score (B_{TBS}) was calculated for the whole specimen.

6.3.1 Particle breakage score

Each particle was given a breakage score (B_s) between one and ten. This was determined by following through the flow diagram (Figure 6.7) and tabulating the results as follows. A particle with all its constituent parts was removed from the specimen, the largest piece was assigned a breakage rating between 1 and 5 (Figure 6.7); this depended primarily on the size of the breakage mass and breakage face in comparison to the size of the whole particle. However well defined this was always open to subjectivity. Table 6.2 therefore gives the guidelines used to determine the breakage ratings with photographs of typical breakage ratings 1 to 5 shown in Plate 6.1.

If the largest breakage was rated at 1- / 1+ then for a single breakage the maximum breakage score (B_s) was 1. If there were a multiple of rating '1' breakages then the breakage score (B_s) equalled the square root of the number of breakages, this was rounded to the nearest whole number. The 1- / 1+ allowed the researcher the flexibility

of upgrading the breakage score (B_s) if it was felt appropriate. The maximum breakage score (B_s) for a multiple of rating '1' breakages was 3.

If the largest breakage was rated at '2' then for a single breakage the maximum breakage score (B_s) was 2. If there were a multiple of rating '2' breakages then the breakage score (B_s) equalled the square root of the number of breakages multiplied by 2 (that is multiplied by the breakage rating), this was rounded to the nearest whole number. The maximum breakage score (B_s) for a multiple of rating '2' breakages was 4. Where there was a multiple of rating '2' and '1' breakages then B_s equalled the square root of the number of rating '2' breakages multiplied by 2 plus the square root of the number of rating '1' breakages divided by 2 (that is divided by the breakage rating). The maximum breakage score (B_s) for a multiple of rating '2' and '1' breakages was 5.

This procedure was also used in each of the cases where the largest breakage was rated at '3', '4' and '5'. The equations used to calculate the individual particle breakage score (B_s) are all given in the guidance footnotes in Figure 6.7. From footnote 5b it can be seen that the influence of the smaller breakages e.g. ratings '2' and '1' become virtually insignificant. After assigning a breakage score, each component part of the particle was passed through the particle size template, and the sizes were tallied on a separate sheet (for the whole specimen).

As Nakata et al (2001) pointed out the definition of the different types of breakage occurring in their work relied largely on visual observations and required a measure of judgment. In this work the breakage score (B_s) was completely dependent on visual observations and a measure of judgment was always necessary. Where the breakage was only of large parts it was easy to remove all of the constituent parts. However, where there was further smaller breakage all the constituent parts could not always be found and removed as they would either crumble on removal or would have already separated from the main particle and moved elsewhere in the specimen.

With the extent of data available there were several routes that could have been taken in looking at the breakage of the particles. In this analysis the main three ideas that have been followed have been those of the change in the gradation curves (by particle size) before and after testing, the total breakage score for each specimen and the probability of breakage occurring during the tests. These three criteria have been considered for the triaxial test Series 2 to 6 in the following sections.

6.3.2 Gradation of specimens

During preparation and dismantling of the specimen the gradation of stone sizes was recorded (Section 3.4). This allowed the change in the gradation due to different load regimes and specimen preparations to be assessed.

Figure 6.8 shows the pre-test particle size distribution curves for those tests where the whole specimen was prepared with ballast only, taken from Series 2, 3, 5 and 6. the grey shaded area represents the UK railway specification for ballast (British Railway Board, 1993). It is clear that there was a scattering in the particle size distribution curves before the tests even commenced. This made direct comparison between pre- and post-test particle size distribution curves more difficult. However the particle size distribution analysis does give a quick overview into the specimen makeup before and after testing.

The particle size distribution curves for each test were plotted and the following trends were observed. Control test (T58), a ballast specimen set up and allowed to 'consolidate' at 90kPa cell pressure, after which it was dismantled without any further stress being applied, showed no difference between the pre- and post-test particle size distribution curves (Figure 6.9). This was as would have been expected as there was very little breakage greater than a '1' recorded for specimen T58.

In Series 2 (Table 3.4), two monotonic load tests, where particle breakage was assessed, were carried out with confining pressures of 90kPa and 140kPa. It can be seen in Figure 6.10 that as the cell pressure increased there was an increase in the difference between the pre- and post-test particle size distribution curves and that the post-test results were outside the railway standards (shown by the grey shaded area). In the cyclic load tests this development of breakage with increased cell pressure did not occur (Figure 6.11), with the pre- and post-test particle size distribution curves remaining close together. This difference in behaviour was clearly due to the applied vertical stress. In the cyclic load tests the deviator stress was limited to 250kPa yet in the monotonic load tests with a cell pressure of 90kPa the deviator stress reached 500kPa and at 140kPa cell pressure nearly 600kPa. Therefore it was concluded that an increase in deviator stress caused more breakage.

Figure 6.12 shows that as the number of load cycles increased in the cyclic load tests, in Series 3, so did the amount of breakage. However between 1 million and 2 million load cycles there was little further breakage (Figure 6.13). Figures 6.12 and 6.13 could not be compared as the cell pressures were different.

In Series 4 the general pattern was that as the amount of stone overlying the ballast increased the amount of breakage decreased, taking the grading of the specimens further outside the railway standards. This is shown in Figure 6.14 for 40kPa cell pressure cyclic load tests. This pattern was also observed in the monotonic load tests.

Figure 6.15 shows the particle size distribution curves before and after the tests in Series 5. These tests had a rubber mat at the base of the specimen and a wooden disc at the top of the specimen (damping). When compared to the ballast only specimen (without damping) the breakage was reduced. Adding a double layer of stone between the ballast and the wooden disc further reduced the amount of breakage. This would have been expected from the results in Series 4.

Figure 6.16 compares the results from the cyclic load tests of wet and dry specimens at 140kPa cell pressure in Series 6. It was clear to see that the difference between the pre- and post-test particle size distribution curves was significantly greater for the wet specimens than the dry specimens. This was also repeated at 40kPa and 90kPa cell pressures for the cyclic load tests. This pattern was however not observed in the monotonic load tests. Figure 6.17 shows the particle size distribution curves for the 90kPa cell pressure monotonic load tests. There was no obvious difference in breakage behaviour between the wet and dry specimens.

6.3.3 Probability of breakage

The amount of breakage occurring in a specimen can be analysed statistically by looking at the probability of breakage of a stone within that specimen. McDowell et al. (1996) introduced the concept of probability into this field of work. They commented that the likelihood of breakage increased with applied stress, but reduced with co-ordination number and with reduction in particle size. The co-ordination number is the number of contacts the particle has with its neighbouring particles.

In this research the approach taken was similar to that of Nakata et al. (2001), where the probability of any one stone within the specimen surviving a particular degree of breakage was calculated. Nakata et al. used a scale of one to five to determine the extent of breakage occurring to each particle in their one-dimensional compression tests. Type I damage was used to define a particle with no visual damage. Type II was a single abrasion or asperity breakage. Type III was defined as more than one abrasion or asperity breakage. Type IV damage consisted of a major splitting of the particle. Type V damage was where there had been further breakage in the sub particles of a Type IV

breakage. The definitions used by Nakata et al. have been tabulated in Table 6.3, alongside the equivalent breakage scores (B_s) as used in this research.

Table 6.4 shows the probability of breakage of each stone size for the control specimen (test T58). From this, one can see that it was highly probable (93% likely) that the 28mm particles would survive a breakage of B_s equal to 2 or more. In other words it was 7% likely that a 28mm particle will receive breakage of B_s equal to 2 or more. For the 37mm particles it was slightly higher at 97% and there was almost no damage of B_s equal to 2 or more for the 50mm particles (99% of particles were likely to survive a breakage score of 2 or more).

From test T58 it was clear that a significant amount of small breakage was occurring during the preparation of the specimen (B_s below 2). Out of the overall 383 particles with a breakage score of 0-1 (Table 6.4), 223 particles had a breakage score of 0, i.e. only 56% of particles were likely to survive a breakage score of 1 and 41% of particle were likely to undergo breakage of $B_s = 1$. It was therefore decided that the analysis would concentrate on particle break of B_s greater than or equal to 2.

Figure 6.18 shows the overall results of the control test T58 (taken from Table 6.4) alongside the results from the monotonic load tests in Series 2. It can be seen that as the cell pressure increased the probability of surviving breakage decreased, i.e. the likelihood of breakage increased. The amount of breakage occurring in the cyclic load tests at different cell pressures, seen in Figure 6.19, was similar for B_s greater than or equal to 4. The main difference between the tests at different cell pressures was the amount of small asperity breakage occurring in the 140kPa cell pressure test due to the increase in the bulk stress, although there was no overall increase in deviator stress. The probability of particle breakage was greater in the monotonic load tests than in the cyclic load tests, with a further increase in the cyclic load followed by post cyclic monotonic load tests.

Figure 6.20 shows the development of breakage in the cyclic load tests in Series 3. As previously seen there was little significant breakage (B_s of 4 or more) occurring in any of these tests. With a score of B_s equal to 2 or 3 the probability of surviving decreases with an increase in the number of load repetitions. By 1 million and 2 million load cycles, seen in Figure 6.21, the probability of surviving some of the higher breakage scores was slightly reduced, with a significant reduction in the probability of surviving a breakage score of 2 or 3. The discrepancy of the 2 million load cycle test at the lower B_s values was thought to be due to some of the smaller breakages not being recorded

properly as this was one of the early tests to have been analysed in this way and the methodology was still being developed.

At 40kPa cell pressure, as the amount of stone overlying the ballast increased, so generally did the probability of ballast survival, i.e. less breakage as seen in Figure 6.22. This was as noted in Series 4 with the particle size distribution analysis (Figures 6.14). However as can be seen in Figures 6.23 (monotonic load tests) and 6.24 (post cyclic monotonic load test), at 40kPa cell pressure the ballast in the 1-1 layer specimens had a higher probability of survival than in the ballast only specimens. This is opposite to that seen in the 90kPa cell pressure tests, where the ballast in the 1-1 layer specimens had a lower probability of survival than in the ballast only specimens.

At the start of Series 5 it was postulated that in the specimens with damping (with the rubber mat underneath and the wooden disc above) there would be less breakage due to a decrease in resilient modulus. This was strengthened further with the particle size distribution analysis. However, as can be seen in Figure 6.25, the breakage behaviour was not as expected and instead of the probability of survival increasing it actually decreased with the damping. This therefore offers an alternative explanation compared to that of the particle size distribution analysis.

Figure 6.26 (for the cyclic load tests) and Figure 6.27 (for the monotonic load tests) compare the probability of survival results in Series 6 between the wet and dry specimens. The trend which was already identified in the particle size distribution analysis was confirmed; in the cyclic load tests there was an increase in breakage in the wet ballast compared to the dry ballast specimens (Figure 6.16), and in the monotonic load tests the amounts of breakage in the wet and dry tests were similar (Figure 6.17).

6.3.4 Total breakage score

The total breakage score (B_{TBS}) was developed to allow each specimen to be given a unique breakage score. B_{TBS} was calculated by adding together the sum of the percentage of breakages of each score multiplied by the score, as seen in Equation 6.4 below;

$$B_{TBS} = \sum_{i=2}^{i=10} (x_{B_s=i} \times i) \qquad \text{Equ. 6.4}$$

where: x = percentage of particles with a breakage score (B_s) of i.

The total breakage score, B_{TBS}, did not include breakage of $B_s = 1$ for the reasons given in Section 6.3.3. Table 6.5 gives the total breakage score (B_{TBS}) for all the tests with

50mm ballast. It shows that for Series 2, 3 and 6 the total breakage score clarified further that which had already been discerned in Sections 6.3.2 and 6.3.3 above. This is that:

i) In Series 2 monotonic load tests the amount of breakage increased with an increase in σ_3, yet in the cyclic load tests σ_3 had no effect on the amount of breakage.

ii) In Series 3 the amount of breakage increased as the number of load cycles increased, up to a certain point, after which there was little further breakage.

iii) In Series 6 more breakage occurred in the wet cyclic load tests than the dry cyclic load tests of Series 2. Yet in the monotonic load tests there was little difference in the breakage behaviour between the wet and dry materials.

For Series 4, Figure 6.28 reveals the unique relationship between the increase in the percentage of stone overlying the ballast and the decrease in total breakage score, B_{TBS}, with monotonic loading and a 40kPa cell pressure. For Series 5 the total breakage score showed there to be greater breakage in the test specimens with damping, in line with the probability of survival analysis rather than the particle size distribution analysis. This is not surprising as B_{TBS} was derived from the probability of survival analysis data.

6.4 Particle breakage behaviour - discussion

From the discussion in Section 2.6.1, one would expect the amount of breakage to increase with an increase in particle size and also with the applied stress, and one would expect the amount of breakage to decrease with an increase in the co-ordination number (McDowell and Bolton, 1998). In Figure 6.3 it can be seen that the behaviour of the ballasts in the single-particle crushing tests were similar, with the 28-37mm ballast having a very similar characteristic tensile strength to the 37-50mm ballast and the 20-28mm ballast having a slightly higher characteristic tensile strength. This was possible due to the selection/grading process of the material at the quarry, as discussed in Section 6.2. It was postulated, therefore, that during the triaxial tests the 28-37mm and the 37-50mm ballast would have a similar occurrence of breakage, and the 20-28mm ballast would have slightly less breakage in any one specimen.

Figure 6.29 shows the probability of each sized aggregate undergoing breakage of different severities for monotonic load triaxial tests at 90kPa and 140kPa cell pressures (tests T40 and T60 respectively). This shows that for the 90kPa cell pressure test the probability of breakage slightly increased with an increase in the particle size. However

there was no such pattern in the 140kPa cell pressure test, where the 20mm-28mm and 37mm-50mm ballasts had similar probability of breakage.

It is important to recognise at this stage the effect that one or two particles may have had on the probability of breakage data. Typically there are between 350-390 particles in a ballast only specimen (Table 5.4, 5.5 and 5.6). Therefore three to four particles will have an effect on the probability of breakage of 1% on the whole specimen, i.e. to two significant figures. So where there is a difference in breakage probability of 0.01 or more then there have been three or more breakages extra. However there may only be sixty 20-28mm ballast particles in the specimen, therefore one 20-28mm particle will have an effect on the probability of breakage of 1.6%, and 6 particles an effect of 10%, i.e. to one significant figure. In practice, when taking down the test specimens, six particles of a Type II breakage or less would have little overall significance, yet even a couple of particles of Type IV breakage or more are significant, as reflected in Equation 6.4. Therefore the results for the 90kPa and 140kPa cell pressure tests are significant. This does not affect the results, as seen from the previous Section 6.3, because the analysis in it was undertaken for the whole specimen and not for the specific stone sizes.

In a post cyclic monotonic load test at 40kPa cell pressure (test T57), as seen in Table 6.6, it was found that with Type II breakage the probability of breakage increased with an increase in particle size. However with Type III breakage and greater there was a similar probability of breakage across each of the particle sizes. In the 140kPa cell pressure tests (tests T61 and T62, in Table 6.7) both tests confirmed that the 20-28mm sized particles were least likely to break, as postulated.

In Series 3 it was typical for smaller breakages, of Type II or III, to increase with particle size, yet breakage of Type IV or more to decrease with particle size. In Series 4 and 5 the 20-28mm particle size ballast was less likely to break, although the pattern was not so clear. In Series 6, with the wet ballast, the 28-37mm particles had the highest likelihood of survival.

From the discussion above it was clear that the data did not confirm or refute the statement of McDowell and Bolton (1998) that the amount of breakage would increase with particle size. However it was clear that there was little overall difference in the crushing behaviour of the different sized particles used in this research. This was also found with the characteristic tensile strengths of the different sized particles in the single-particle crushing test data (Section 6.2).

Nakata et al (2001) looked into the force on a single particle embedded in a soil matrix. Using a simplified approach they calculated the force acting on a single particle (F_{sp}) in a soil matrix and the characteristic particle stress (σ_{sp}), Equations 6.5 and 6.6 below:

$$F_{sp} = \sigma \left(\sqrt[3]{\frac{(1+e)\pi}{6}} \right)^2 \bar{d}^2 \qquad \text{Equ. 6.5}$$

$$\text{and } \sigma_{sp} = \frac{F_{sp}}{\bar{d}^2} = \sigma \left(\sqrt[3]{\frac{(1+e)\pi}{6}} \right)^2 \qquad \text{Equ. 6.6}$$

where: σ = the principal stress, and

$\bar{d}^2$ = the mean particle diameter squared.

These equations are in-accordance with Jaeger (1967), Lee (1992), McDowell and Bolton (1998) and others as discussed in Section 2.6.4. They suggest the characteristic particle stress is dependent on the void ratio and not on the particle size. The characteristic particle stresses for different triaxial tests carried out in this project have been included in Table 6.8 for the cyclic load tests and Table 6.9 for the monotonic load tests.

From Table 6.8 the calculated characteristic particle stresses (σ_{sp}) in the cyclic load tests varied between 277kPa (40kPa cell pressure - dry) and 376kPa (140kPa cell pressure - dry). This was surprising as the total breakage scores (B_{TBS}) in Table 6.5 for the normal ballast cyclic load tests were not too different. However this understanding did not appear to take into account wet or dry material as σ_{sp} for like tests of dry and wet materials are similar, yet the total breakage scores (B_{TBS}) for the wet ballast cyclic load tests were some three times higher than the dry ballast tests.

In the monotonic load tests, whose results are reported in Table 6.9 it was clear that as the cell pressure increased, there was a significant increase in the calculated characteristic particle stress; this correlates well with the increase in the total breakage scores (B_{TBS}) in Table 6.5 for the monotonic load tests.

Material / size (mm)	McDowell et al. (2003)		Current work					
	$m_{(f)}$	$\sigma_{0\,(f)}$ (MPa)	m_a	m_f	σ_a (MPa)	σ_f (MPa)	min. σ (aspertity failure MPa)	min. σ (particle fracture MPa)
20mm Bardon stone	-	-	1.4	2.3	5.7	32.1	1.11	9.08
20-28mm Bardon ballast	-	-	1.8	1.6	6.5	14.5	1.29	3.16
28-37mm Bardon ballast	-	-	1.3	2.3	4.5	11	0.416	2.27
37-50mm Bardon ballast	-	-	1.5	1.9	6.9	12.7	0.895	3.04
All Bardon ballast	-	-	1.5	1.7	6.0	17.7	-	-
10-14mm Mountsorrel stone	2.7	33.4	-	-	-	-	-	-
37.5-50mm Mountsorrel ballast	3.4	20.7	-	-	-	-	-	-

Table 6.1 - Comparing the m and σ_0 values from the current work with those of McDowell et al (2003)

Breakage rating	Approximate mass of breakage as a percentage of the original particle	Approximate surface area of the breakage
1- / 1+	<5%	$3mm^2$
2	6-15%	$10mm^2$
3- / 3+	16-30%	$15mm^2$
4	31-40%	-
5	41-50%	-

Table 6.2 - Guidelines for determining the breakage rating for a particle

Nakata et al 2001	Damage type	Current work – breakage score (B_s)
Type I	no visible damage	0 - 1
Type II	single abrasion or asperity breakage	2 - 3
Type III	more than one abrasion or asperity breakage	4 - 6
Type IV	major splitting of grain into two or more particles	7 - 8
Type V	further breakage of Type IV sub-particles	9 - 10

Table 6.3 - Comparing breakage scores descriptions in the current work with those used by Nakata et al. (2001a) and Hyde and Nakata (2001)

	No. of particles			
Breakage score (B_s)	28mm	37mm	50mm	Overall
0 to 1	62	202	117	383
2 to 3	5	7	1	13
4 to 6	0	0	0	0
7 to 8	0	0	0	0
9 to 10	0	0	0	0
Total	67	209	118	396
Probability of surviving Type II	0.925	0.967	0.992	0.967
Probability of surviving Type III	1	1	1	1
Probability of surviving Type IV	1	1	1	1
Probability of surviving Type V	1	1	1	1

Table 6.4 - Breakage scores (B_s) and the probability of breakage taken from the control test T58

		Test details and cell pressure (kPa)	Specimen no.	Total breakage score B_{TBS}
Consolidated only		90	T58	7
Series 2	Monotonic	40	T27	104
		90	T26, T40	(124, 112) 118
		140	T60	228
	Cyclic only	40	T38	35
		90	T36, T37	(27, 28) 28
		140	T64	44
	Post cyclic monotonic	40	T24, T57	(117, 117) 117
		90	T25	148
		140	T61, T62	(241, 254) 248
Series 3	Cyclic only	90, 2 million cycles	T42	78
		90, 1 million cycles	T75	80
		140, 100 cycles	T65	20
		140, 1000 cycles	T66	20
		140, 10,000 cycles	T67	40
Series 4	Monotonic	40, single layer 20mm	T50	75
		40, double layer 20mm	T52	75
		40, 1:2 layer	T53	55
		40, 1:1 layer	T28, T29, T43, T44	(50, 40, 37, 52) 45
		40, 2:1 layer	T49	51
		90, 1:1 layer	T30	169
	Cyclic only	90, single layer 20mm	T41	26
	Post cyclic monotonic	40, single layer 20mm	T39, T48	(87, 108) 97
		40, double layer 20mm	T51	129
		40, 1:2 layer	T46	118
		40, 1:1 layer	T31, T45	(57, 99) 78
		40, 2:1 layer	T47	57
		90, 1:1 layer	T32	206
Series 5	Cyclic only	140, ballast with damping	T69	67
		140, double layer 20mm, with damping	T70	58
Series 6	Monotonic	40, wet ballast	T81	94
		90, wet ballast	T82	158
		140, wet ballast	T79	196
	Cyclic only	40, wet ballast	T80	111
		90, wet ballast	T83	87
		140, wet ballast	T78	101

Table 6.5 - Total breakage scores (B_{TBS})

	No. of particles			
Breakage score (B_s)	28mm	37mm	50mm	Overall
0 to 1	50	124	81	259
2 to 3	10	36	31	78
4 to 6	5	16	10	31
7 to 8	1	1	4	6
9 to 10	2	1	3	6
Total	68	178	129	380
Probability of surviving Type II	0.735	0.697	0.628	0.682
Probability of surviving Type III	0.882	0.899	0.868	0.887
Probability of surviving Type IV	0.956	0.989	0.946	0.968
Probability of surviving Type V	0.971	0.994	0.977	0.984

Table 6.6 - Breakage scores (B_s) and the probability of breakage taken from test T57, a post cyclic monotonic load test at 40kPa cell pressure

	No. of particles test T61				No. of particles test T62			
Breakage score (B_s)	28mm	37mm	50mm	Overall	28mm	37mm	50mm	Overall
0 to 1	27	81	54	164	42	82	45	171
2 to 3	12	51	34	98	16	54	37	109
4 to 6	7	32	15	54	14	32	19	66
7 to 8	2	10	7	19	0	10	5	15
9 to 10	0	19	6	25	1	16	16	33
Total	48	193	116	360	73	194	122	394
Probability of surviving Type II	0.563	0.420	0.466	0.456	0.575	0.423	0.369	0.434
Probability of surviving Type III	0.813	0.684	0.759	0.728	0.795	0.701	0.672	0.711
Probability of surviving Type IV	0.958	0.850	0.888	0.878	0.986	0.866	0.828	0.878
Probability of surviving Type V	1.000	0.902	0.948	0.931	0.986	0.918	0.869	0.916

Table 6.7 - Breakage scores (B_s) and the probability of breakage taken from tests T61 and T62, post cyclic monotonic load tests at 140kPa cell pressure

Specimen No.	Specimen details	Cell pressure (kPa)	Calculated characteristic force on a single particle (F_{sp}) (kN)	Calculated characteristic particle stress on a single particle (σ_{sp}) (kPa)
T23	ballast	40	0.388	283.40
T24	ballast	40	0.381	278.36
T38	ballast	40	0.381	278.67
T57	ballast	40	0.380	277.74
T25	ballast	90	0.451	329.25
T36	ballast	90	0.446	325.74
T37	ballast	90	0.446	326.11
T61	ballast	140	0.516	376.84
T62	ballast	140	0.508	371.28
T64	ballast	140	0.511	373.51
T77	ballast	250	0.656	479.21
T80	wet ballast	40	0.381	278.15
T83	wet ballast	90	0.450	328.65
T78	wet ballast	140	0.520	380.02
T65	ballast	140	0.515	375.87
T66	ballast	140	0.512	374.34
T67	ballast	140	0.511	373.51
T75	ballast	90	0.446	325.74
T42	ballast	90	0.447	326.59

Table 6.8 - The calculated characteristic particle stress on a single particle (σ_{sp}) for cyclic load triaxial tests from Series 2, 3, 5 and 6.

Specimen No.	Specimen details	Cell pressure (kPa)	Calculated characteristic force on a single particle (F_{sp}) (kN)	Calculated characteristic particle stress on a single particle (σ_{sp}) (kPa)
T27	ballast	40	0.453	331.41
T26	ballast	90	0.734	536.71
T40	ballast	90	0.812	593.80
T60	ballast	140	0.944	689.69
T81	wet ballast	40	0.412	301.53
T82	wet ballast	90	0.660	482.77
T79	wet ballast	140	0.871	636.55
T58*	ballast	90	0.122	89.406

* specimen not loaded axially – consolidated only

Table 6.9 - The calculated characteristic particle stress on a single particle (σ_{sp}) for monotonic load triaxial tests from Series 2 and 6.

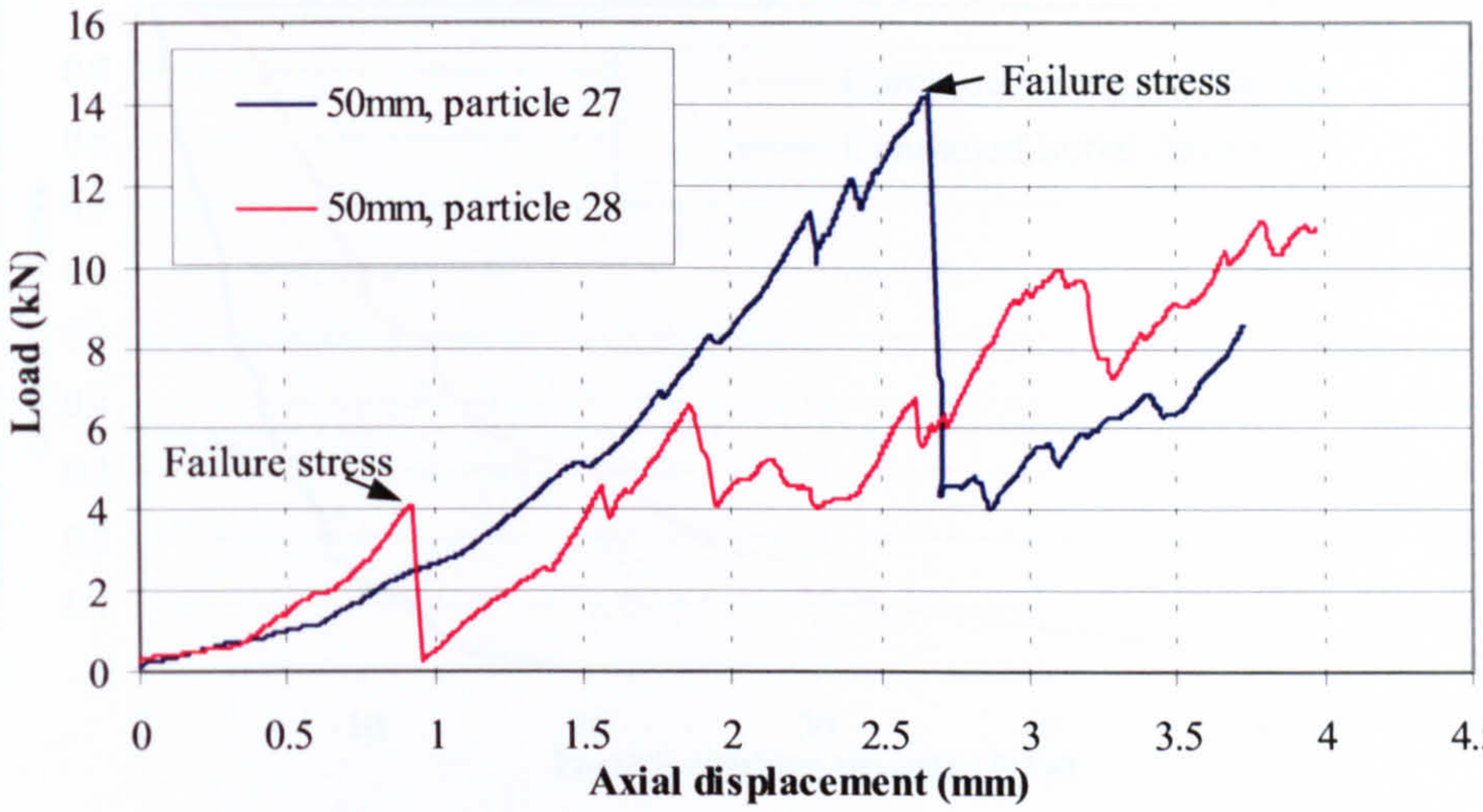

Figure 6.1 – Typical load vs. displacement graphs from the single-particle crushing tests

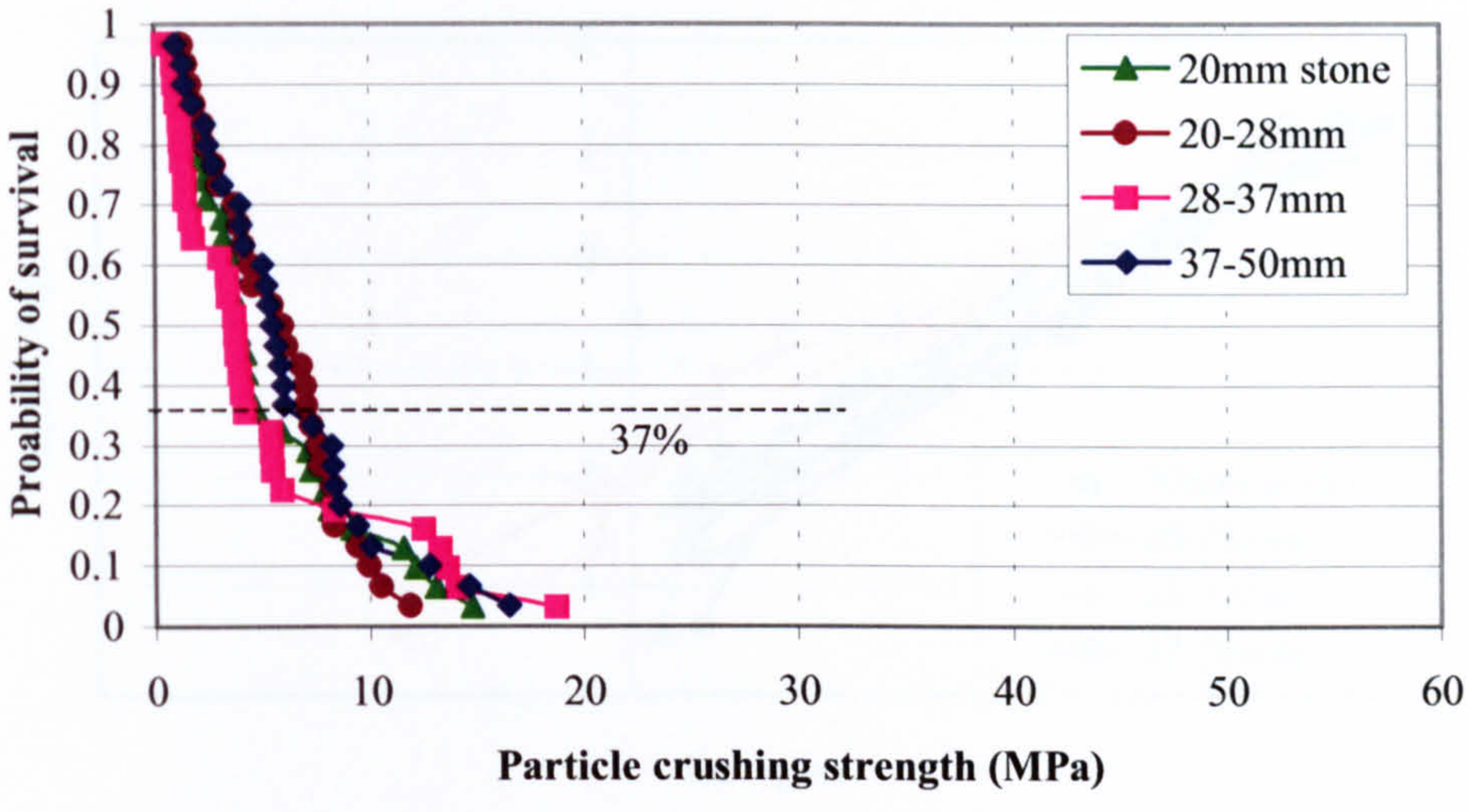

Figure 6.2 – Probability of survival curves for initial asperity failure (σ_a)

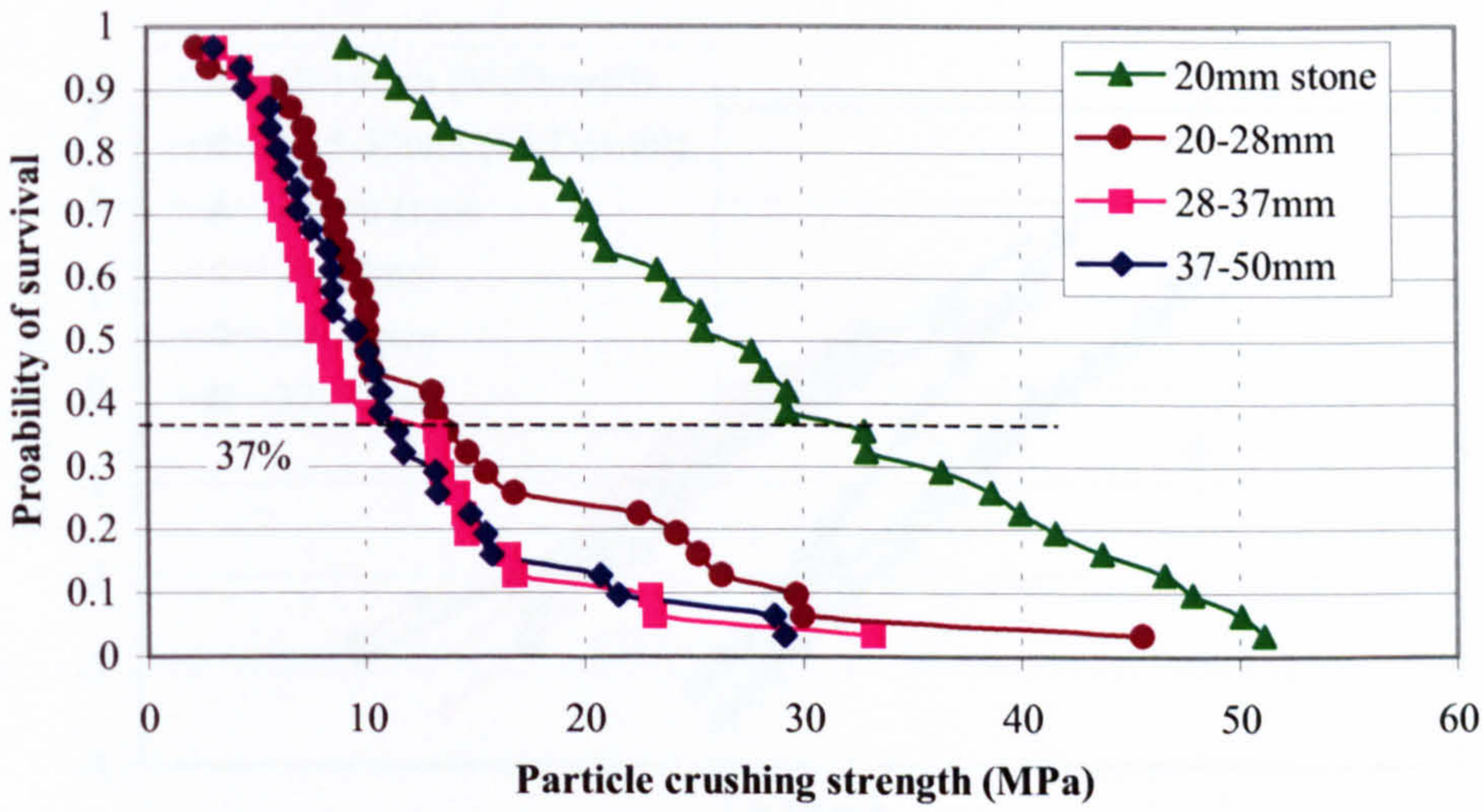

Figure 6.3 – Probability of survival curves for complete particle fracture (σ_f)

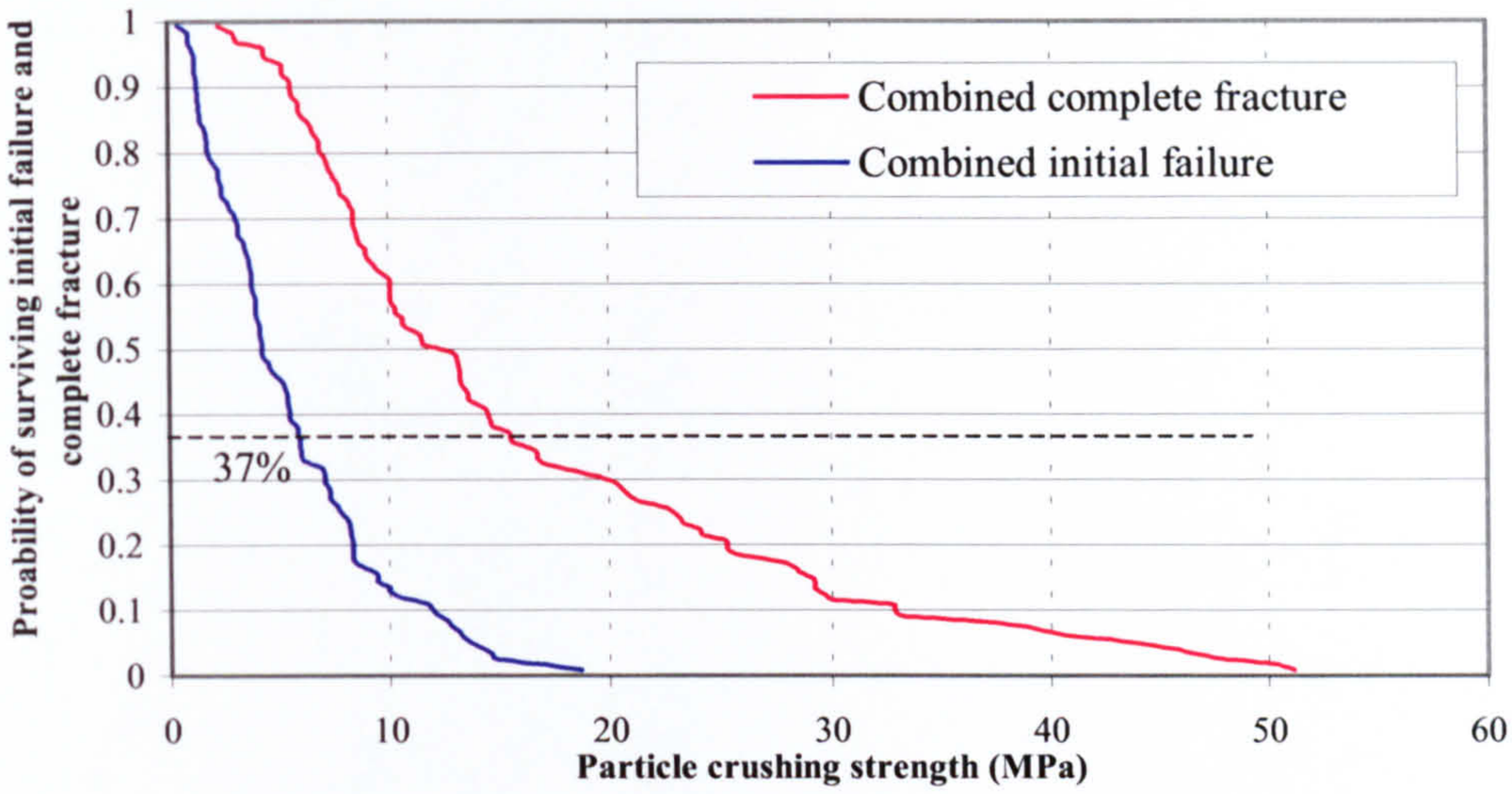

Figure 6.4 – Comparing the probability of survival curves for initial asperity failure (σ_a) and complete particle fracture (σ_f)

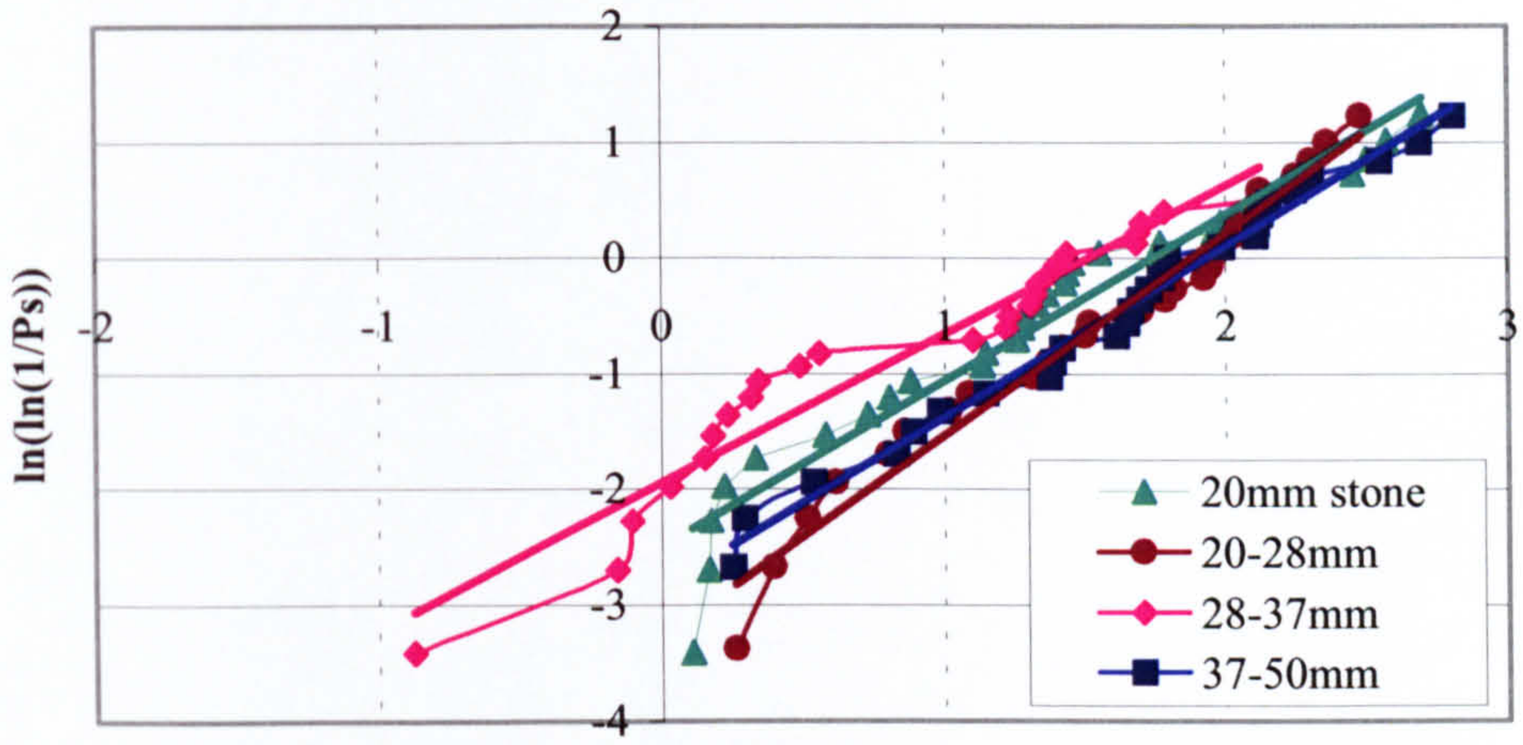

Figure 6.5 – Distribution of strength curves for initial asperity failure (σ_a)

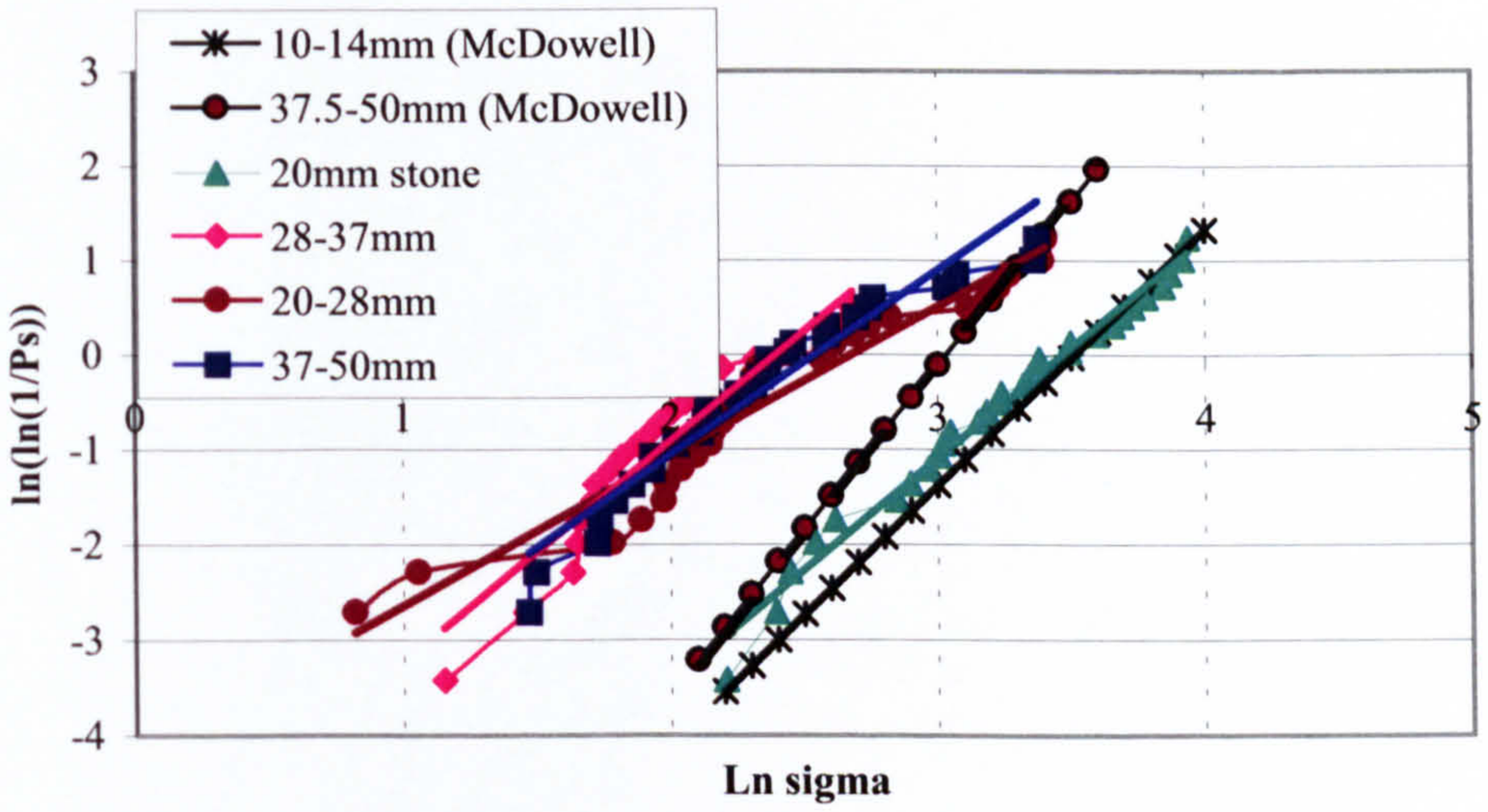

Figure 6.6 – Distribution of strength curves for complete particle fracture (σ_f) including those of McDowell (2003)

Using Plate 6.1 and Table 6.2 and the guidance footnotes [1a through to 5b] at the bottom of the page follow through the flow diagram to obtain a particle breakage score (B_s)

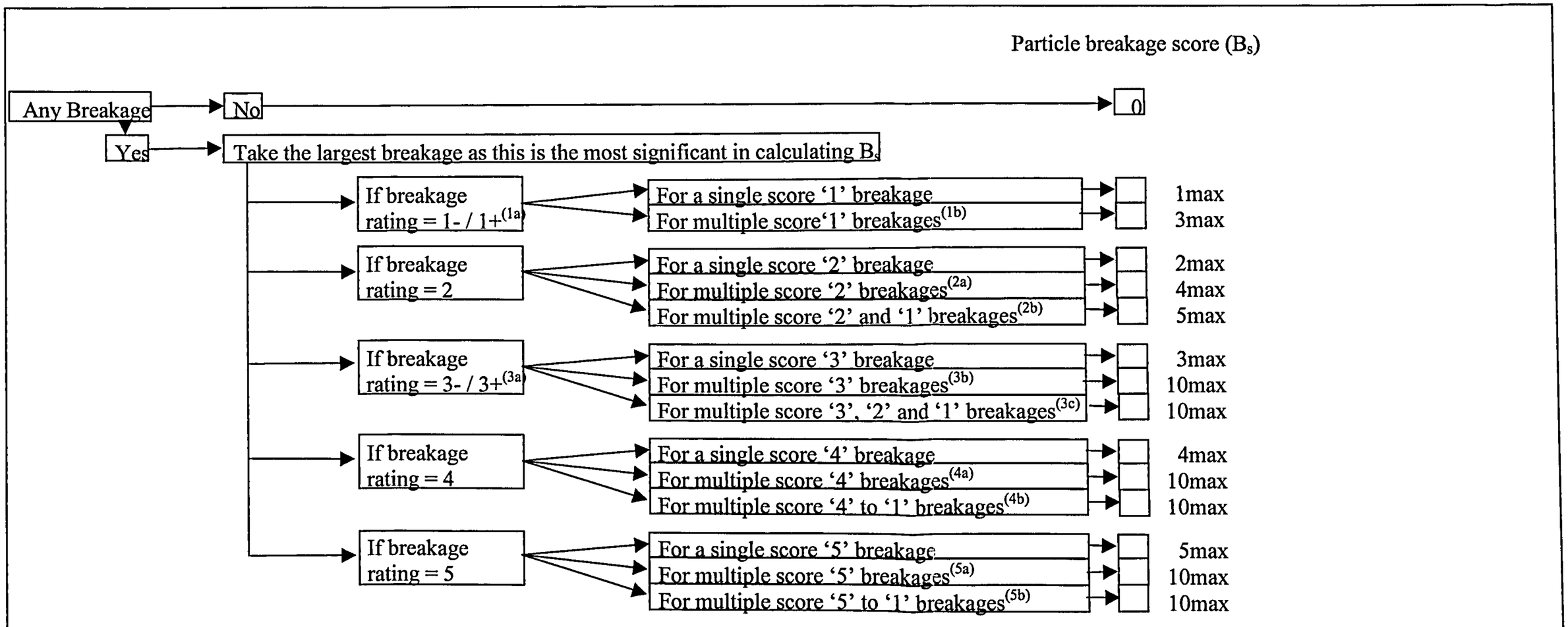

(1a) 1-/1+ allows the researcher to be flexible in the rounding up/down in 1b below

(1b) If there are multiple breakages of rating '1' then $B_s = \sqrt{(N_{b1})}$, where N_{b1} is the number of breakages of rating '1'.

(2a) If there are multiple breakages of rating '2' then $B_s = 2*\sqrt{(N_{b2})}$, where N_{b2} is the number of breakages of rating '2'.

(2b) If there are multiple breakages of rating '2' and '1' then $B_s = 2*\sqrt{(N_{b2})} + \sqrt{(N_{b1})}/2$.

(3a) 3-/13 allows the researcher to be flexible in the rounding up/down in 3b and 3c below, and also in 4a – 5b should they feel it is necessary.

(3a) If there are multiple breakages of rating '3' then $B_s = 3*\sqrt{(N_{b3})}$.

(3c) If there are multiple breakages of rating '3', '2' and '1' then $B_s = 3*\sqrt{(N_{b3})} + 2*\sqrt{(N_{b2})}/3 + \sqrt{(N_{b1})}/3$.

(4a) If there are multiple breakages of rating '4' then $B_s = 4*\sqrt{(N_{b4})}$.

(4b) If there are multiple breakages of rating '4', '3', '2' and '1' then $B_s = 4*\sqrt{(N_{b4})} + 3*\sqrt{(N_{b3})}/4 + 2*\sqrt{(N_{b2})}/4 + \sqrt{(N_{b1})}/4$.

(5a) If there are multiple breakages of rating '5' then $B_s = 5*\sqrt{(N_{b5})}$, although this would be unusual as a breakage rating of '5' means that the particle has broken in half.

(5b) If there are multiple breakages of rating '5', '4', '3', '2' and '1' then $B_s = 5*\sqrt{(N_{b5})} + 4*\sqrt{(N_{b4})}/5 + 3*\sqrt{(N_{b3})}/5 + 2*\sqrt{(N_{b2})}/5 + \sqrt{(N_{b1})}/5$

Figure 6.7 – Particle crushing analysis – guidance on calculating the particle breakage score (B_s).

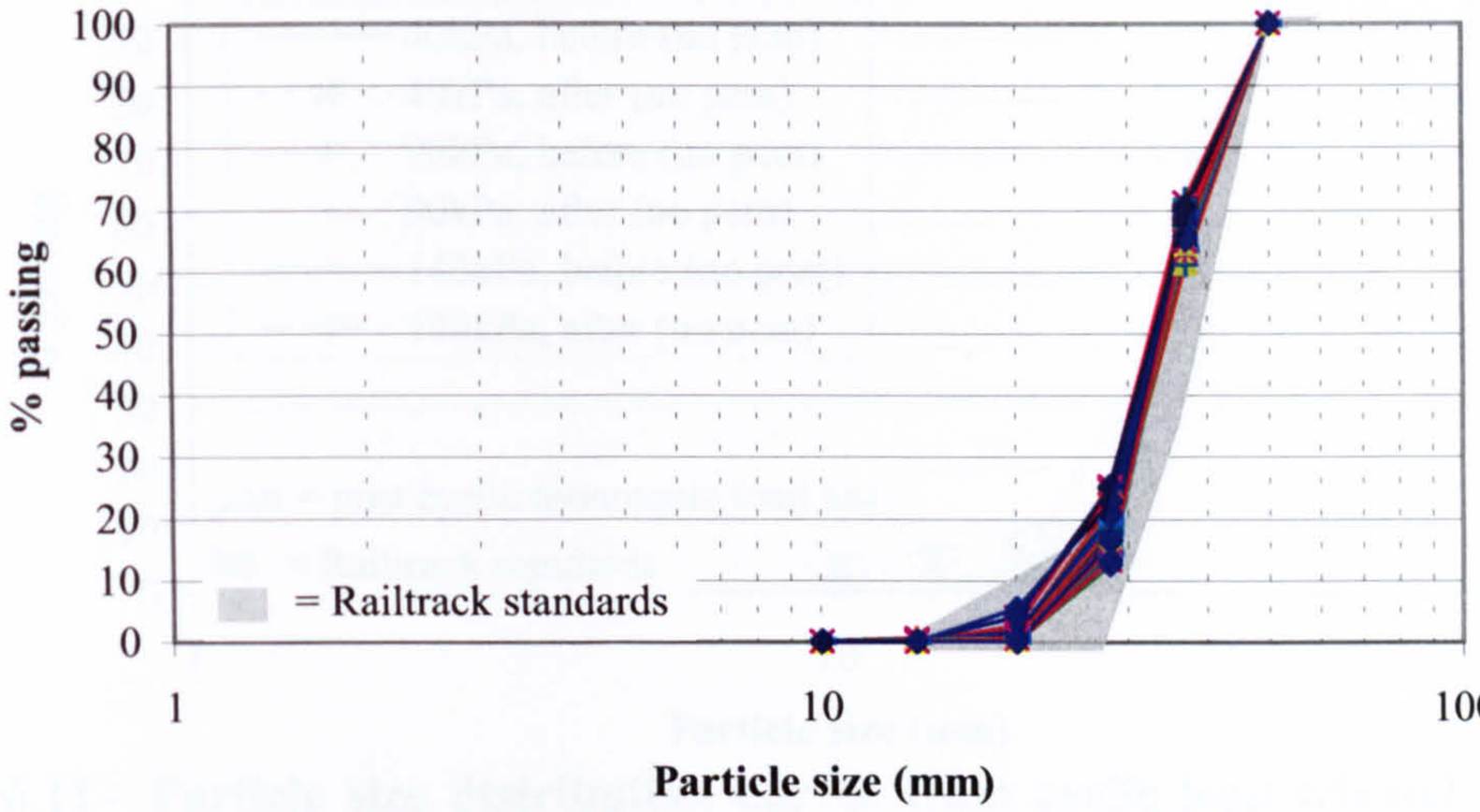

Figure 6.8 – The range of particle distribution curves for the prepared specimens (before testing) from all the ballast tests in Series 2, 3, 5 and 6

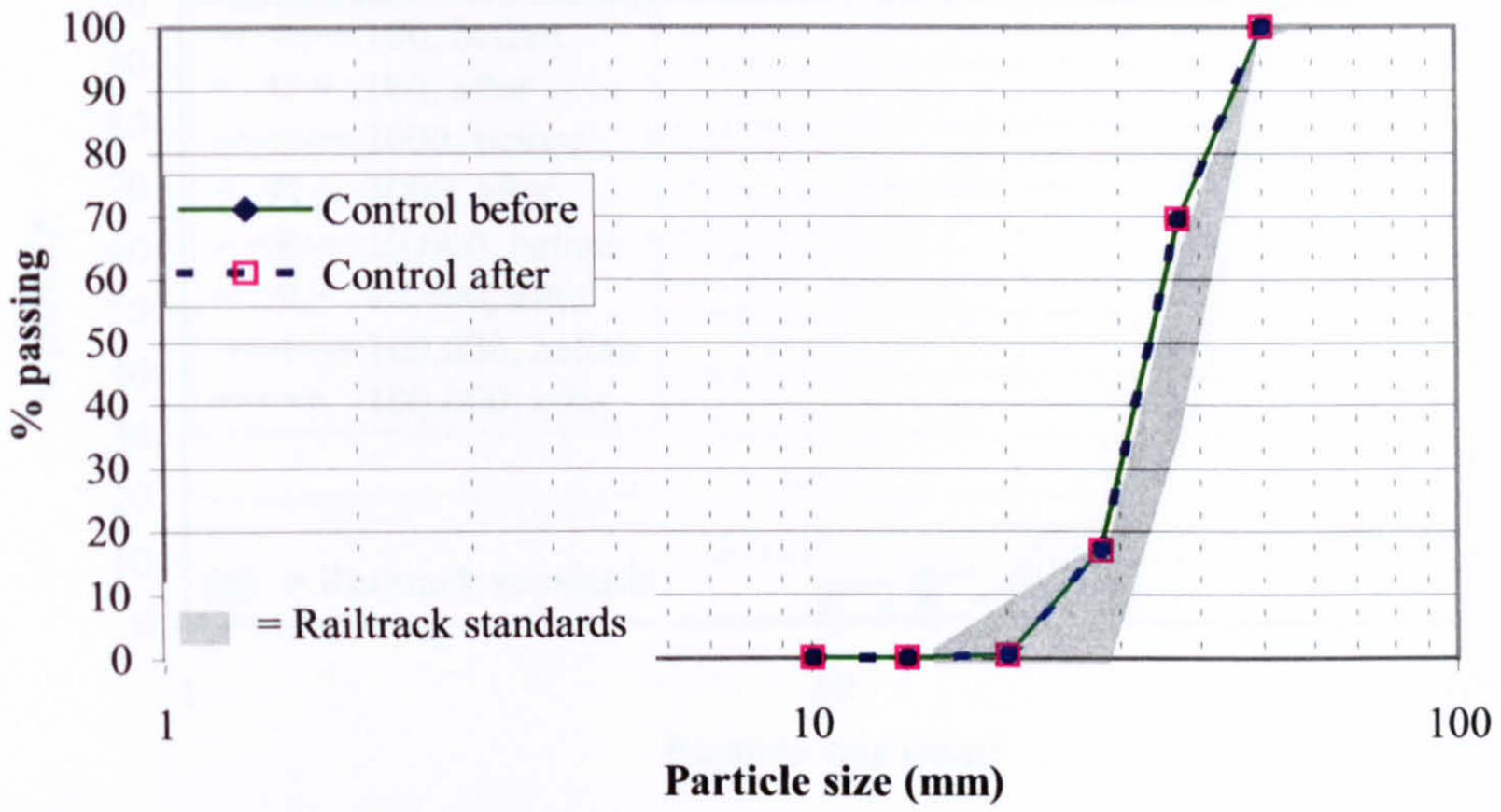

Figure 6.9 – Particle size distribution curves from the control test (T58) – before and after consolidation

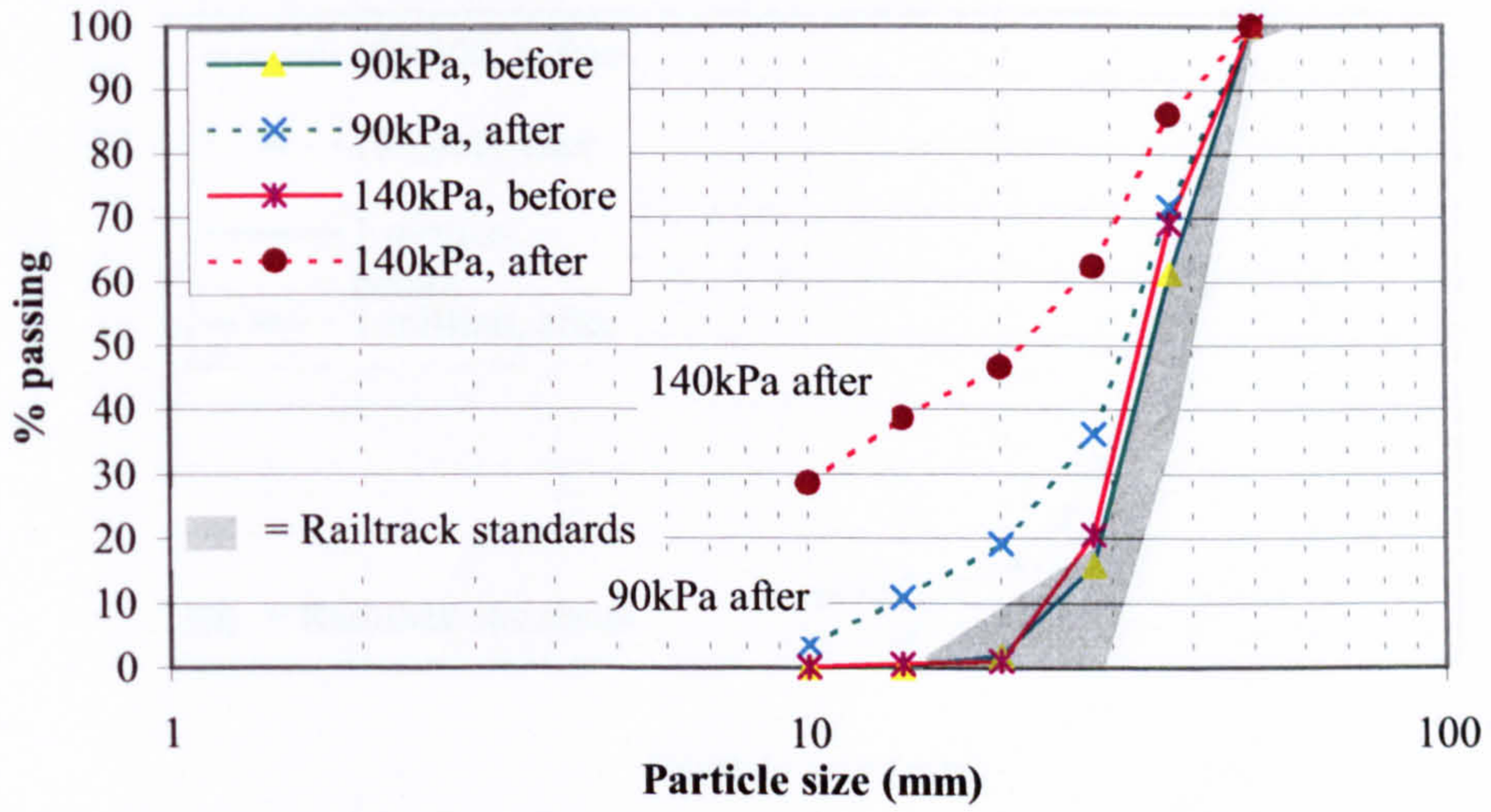

Figure 6.10 –Particle size distribution curves from monotonic load triaxial tests T40 and T60 at 90kPa and 140kPa cell pressure respectively – before and after loading (Series 2)

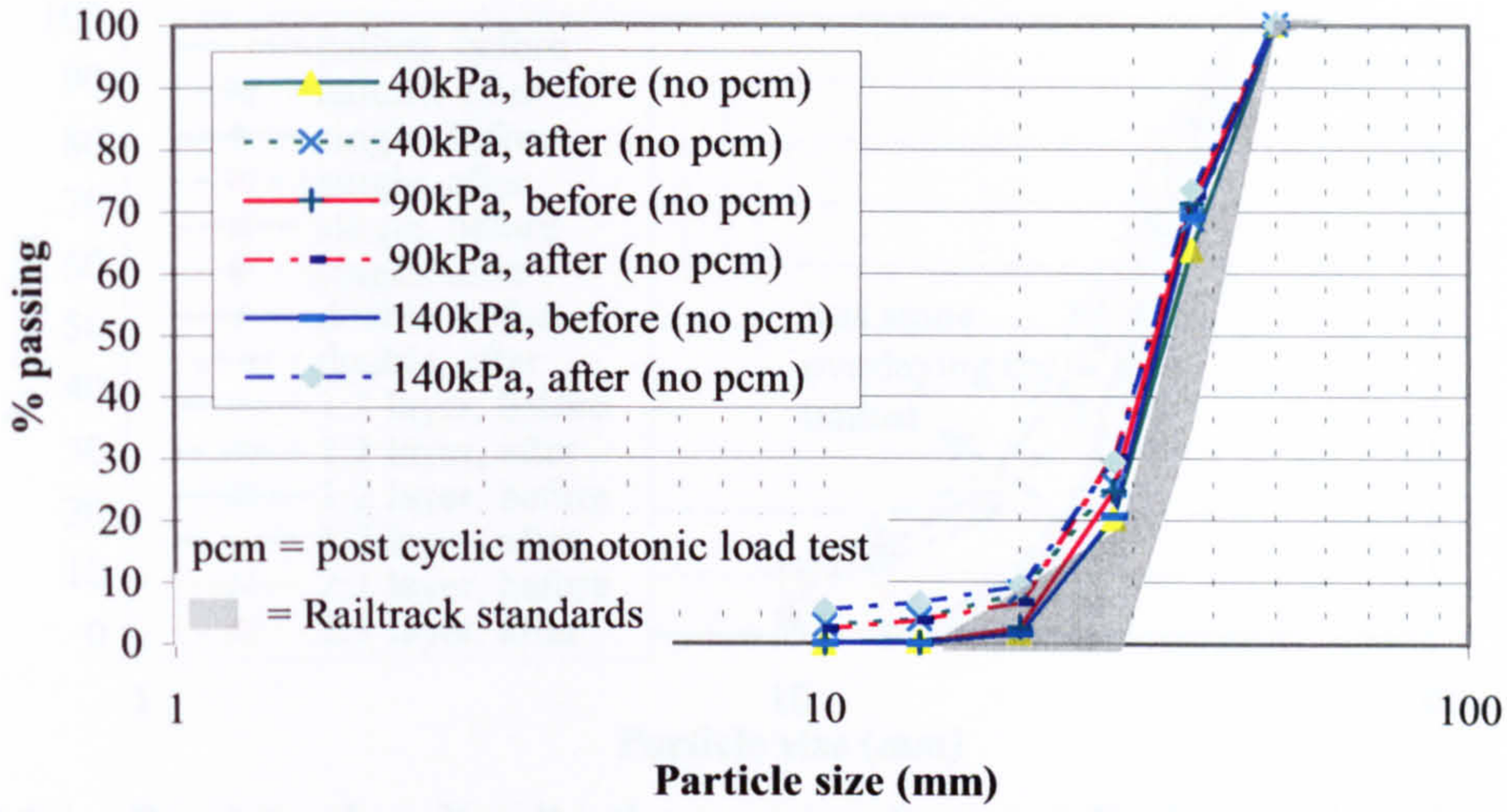

Figure 6.11 – Particle size distribution curves from cyclic load triaxial tests T38, T36 and T64 at 40kPa, 90kPa and 140kPa cell pressure respectively – before and after loading (Series 2)

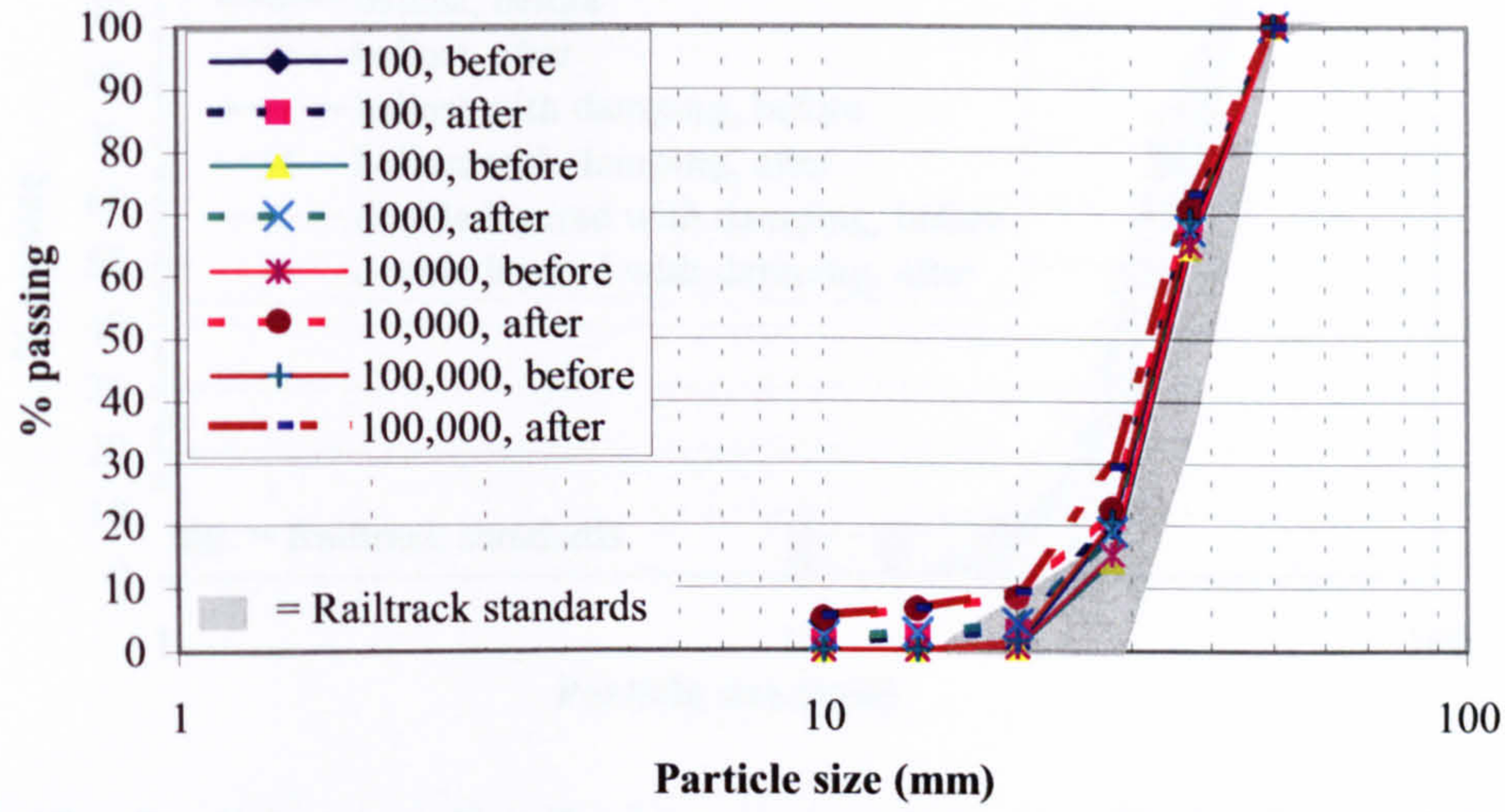

Figure 6.12 – Particle size distribution curves from cyclic load triaxial tests at 140kPa cell pressure in Series 3 – before and after loading (Series 3)

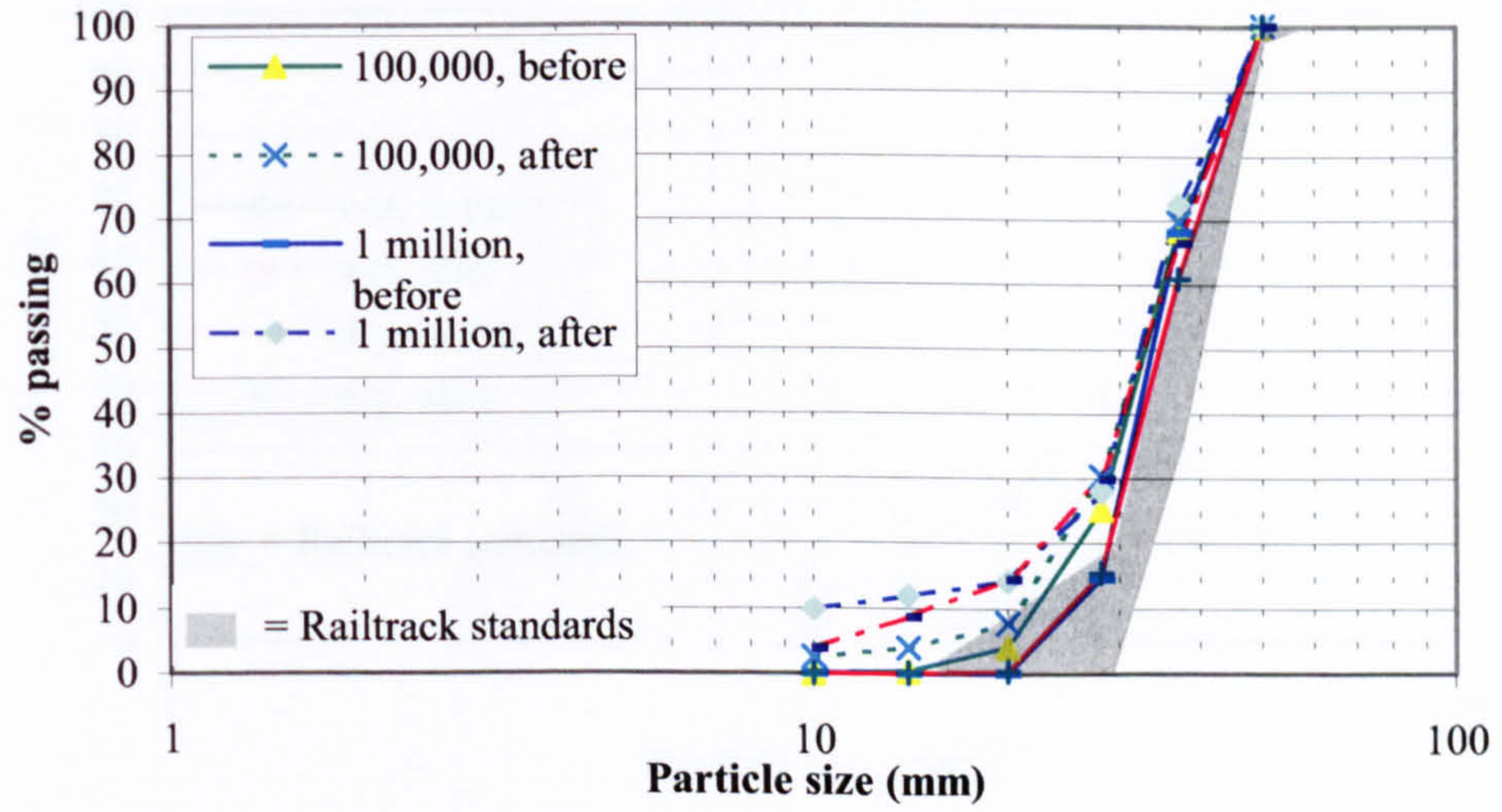

Figure 6.13 – Particle size distribution curves from cyclic load triaxial tests at 90kPa cell pressure– before and after loading (Series 3)

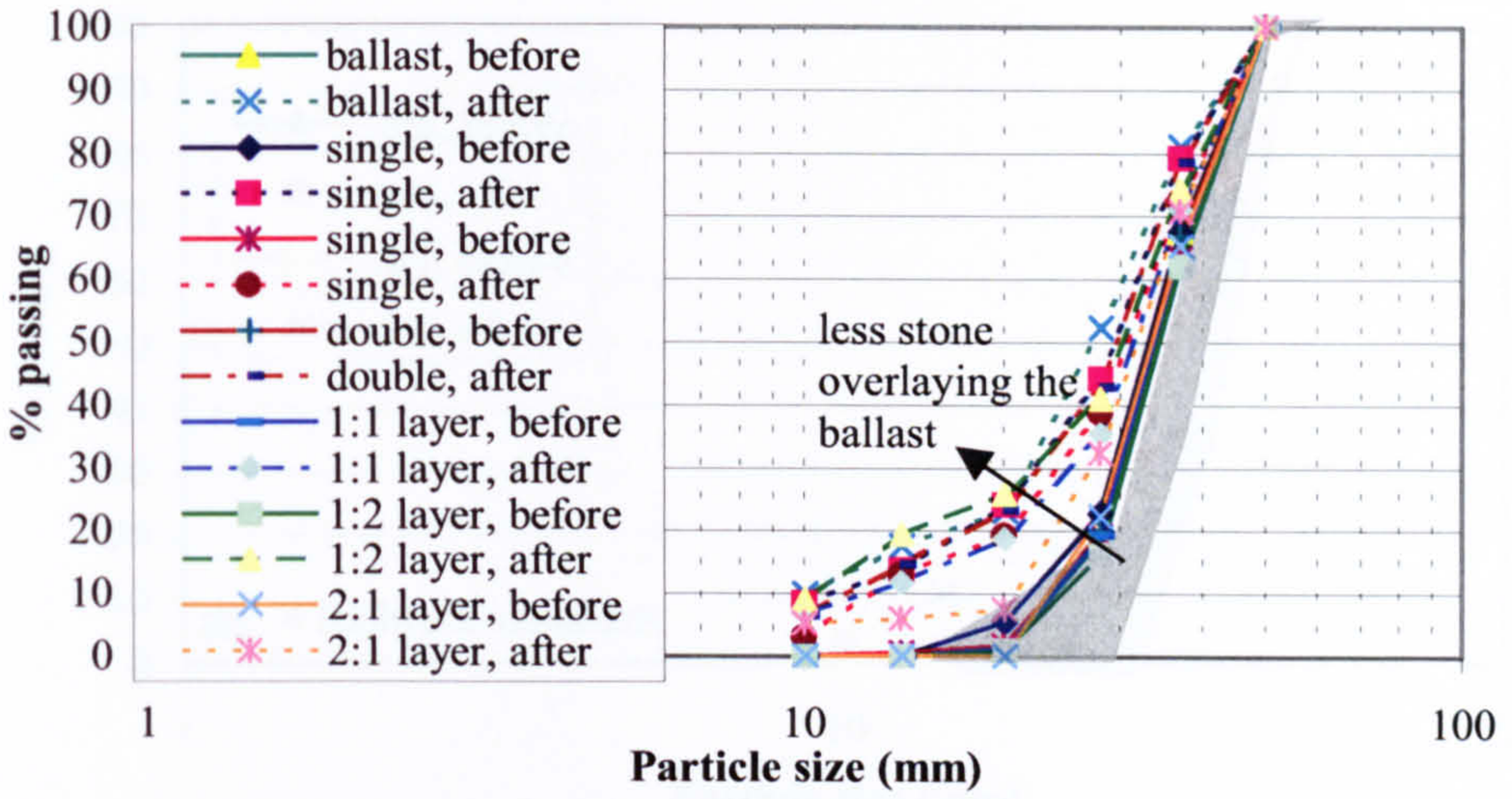

Figure 6.14 – Particle size distribution curves from cyclic load triaxial tests with layered specimens (Series 4) – before and after loading at 40kPa cell pressure

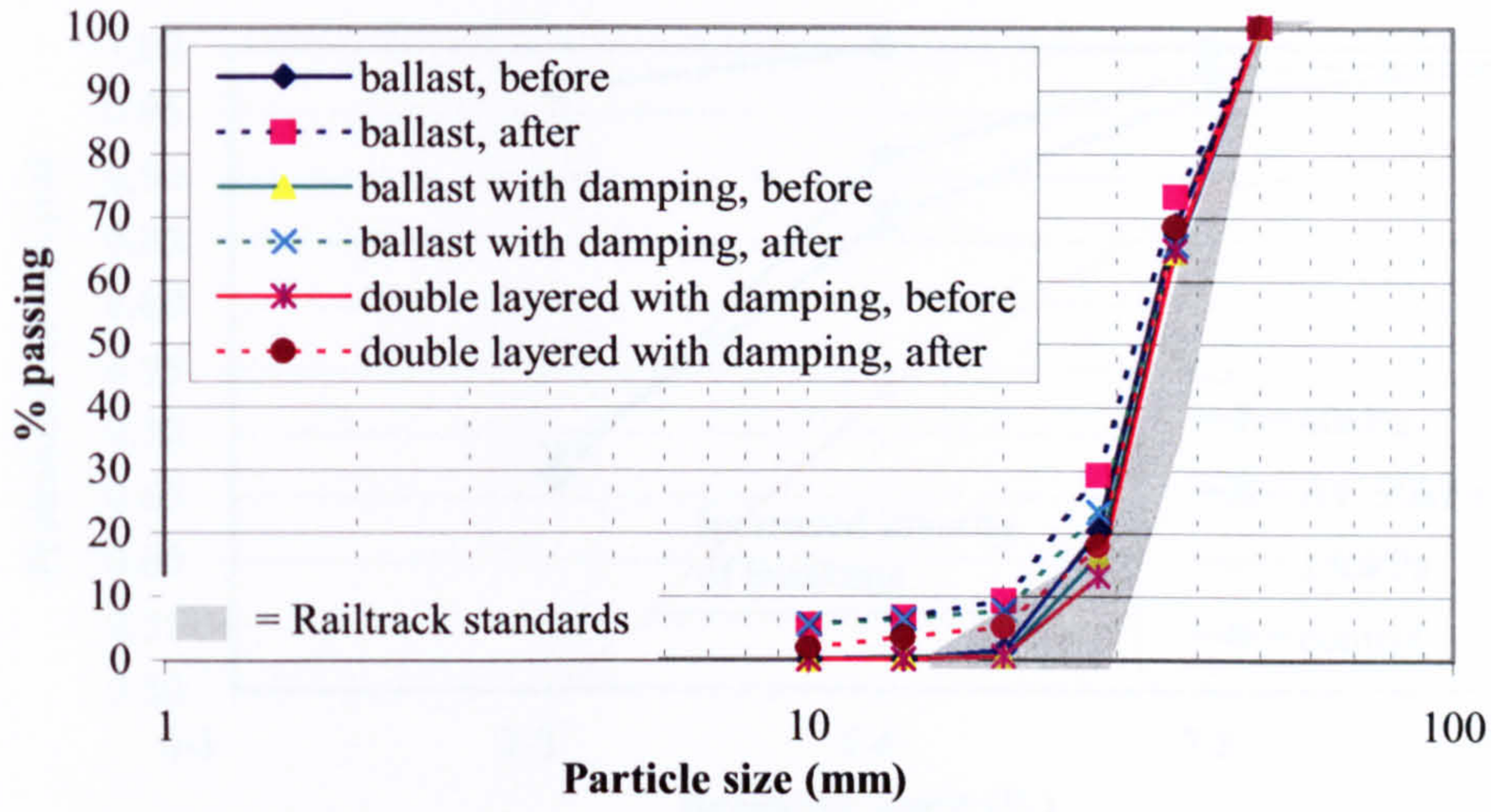

Figure 6.15 – Particle size distribution curves from cyclic load triaxial tests on specimens with damping (Series 5) – before and after loading at 140kPa cell pressure

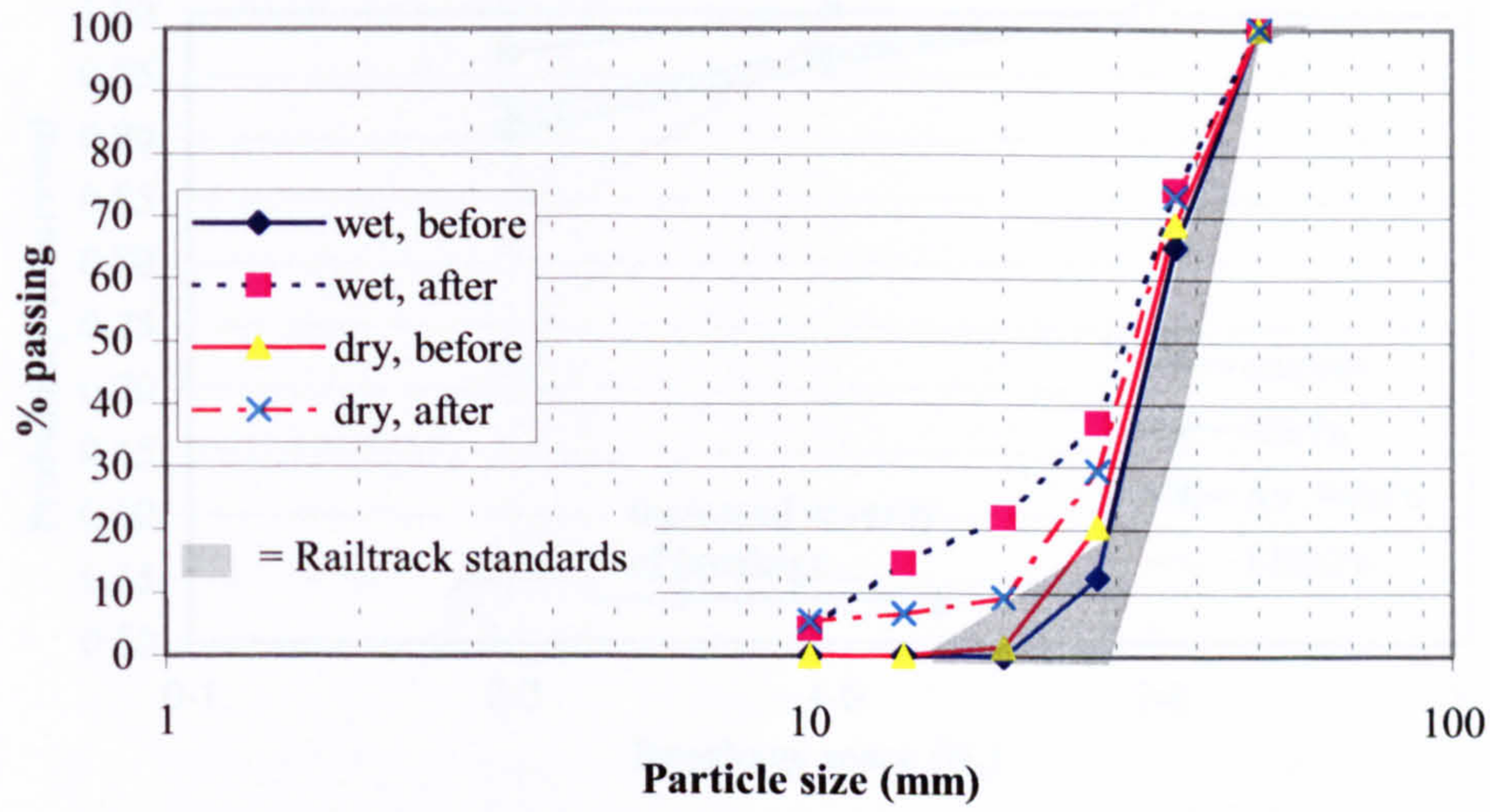

Figure 6.16 – Particle size distribution curves for wetted (Series 6) and dry specimens (Series 2) in cyclic load triaxial tests – before and after loading at 140kPa cell pressure

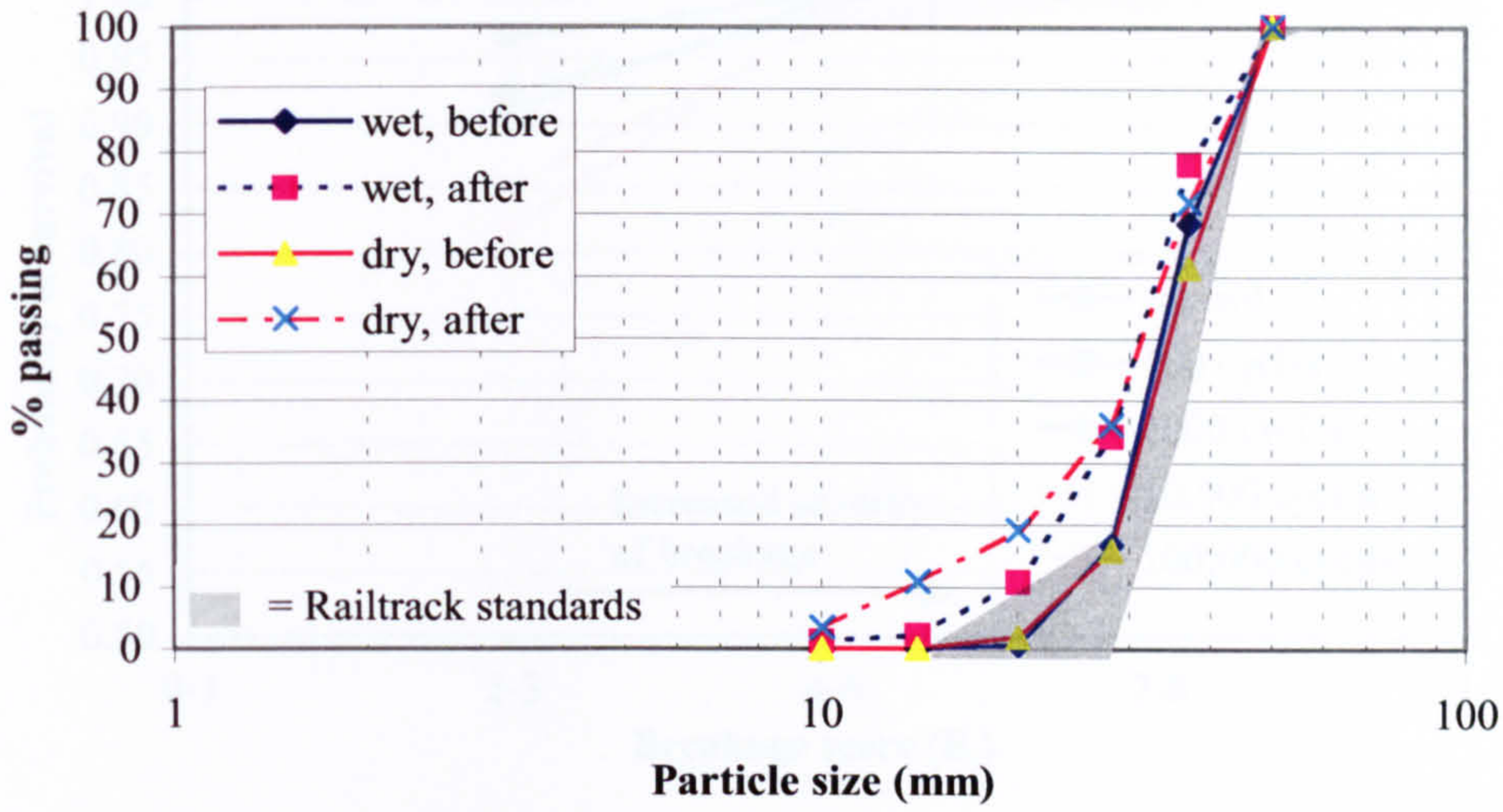

Figure 6.17 – Particle size distribution curves for wetted (Series 6) and dry specimens (Series 2) in monotonic load triaxial tests– before and after loading at 90kPa cell pressure

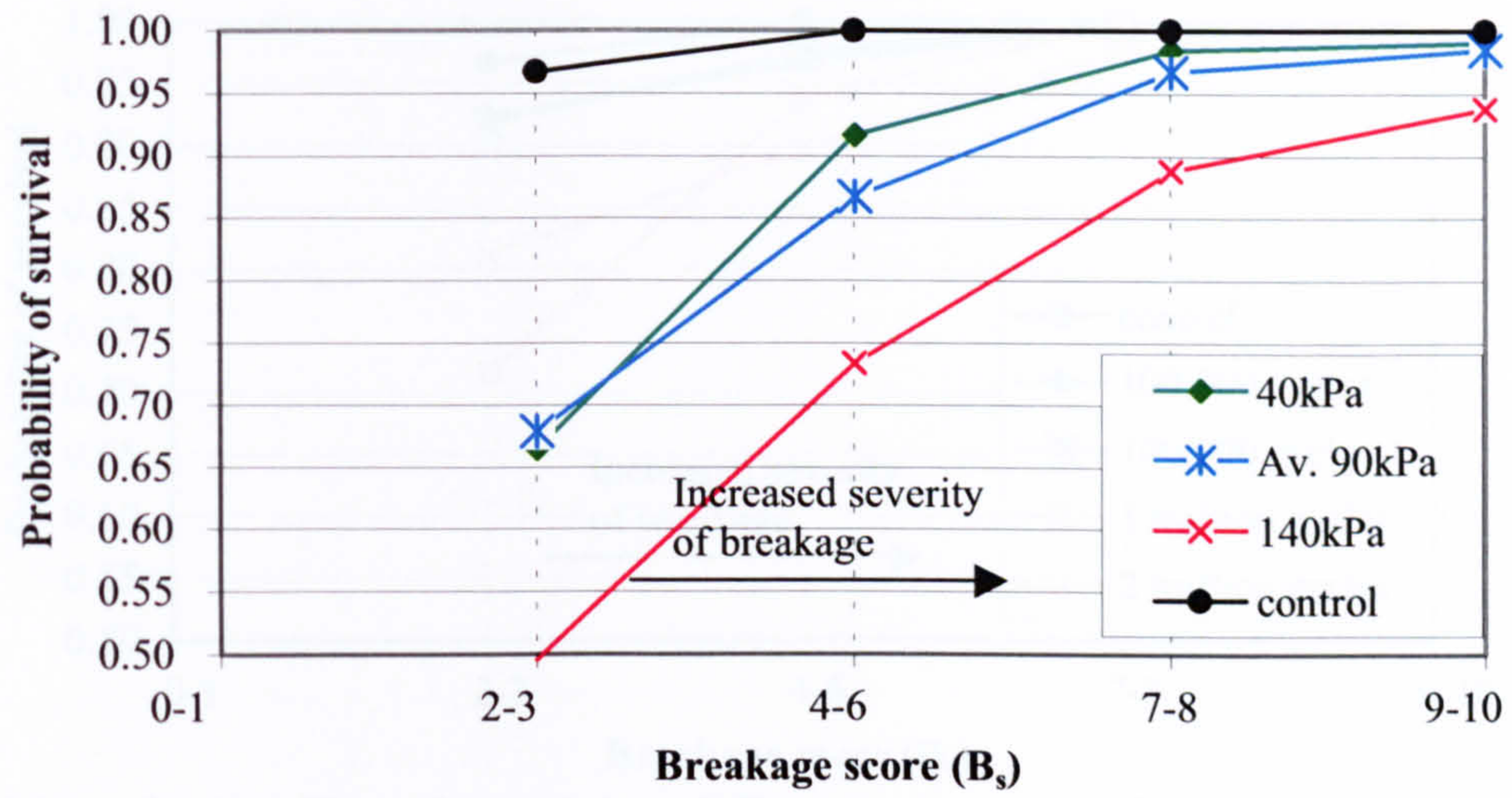

Figure 6.18 – Probability of surviving different amounts of breakage in the control test (T58) and the monotonic load triaxial tests (Series 2)

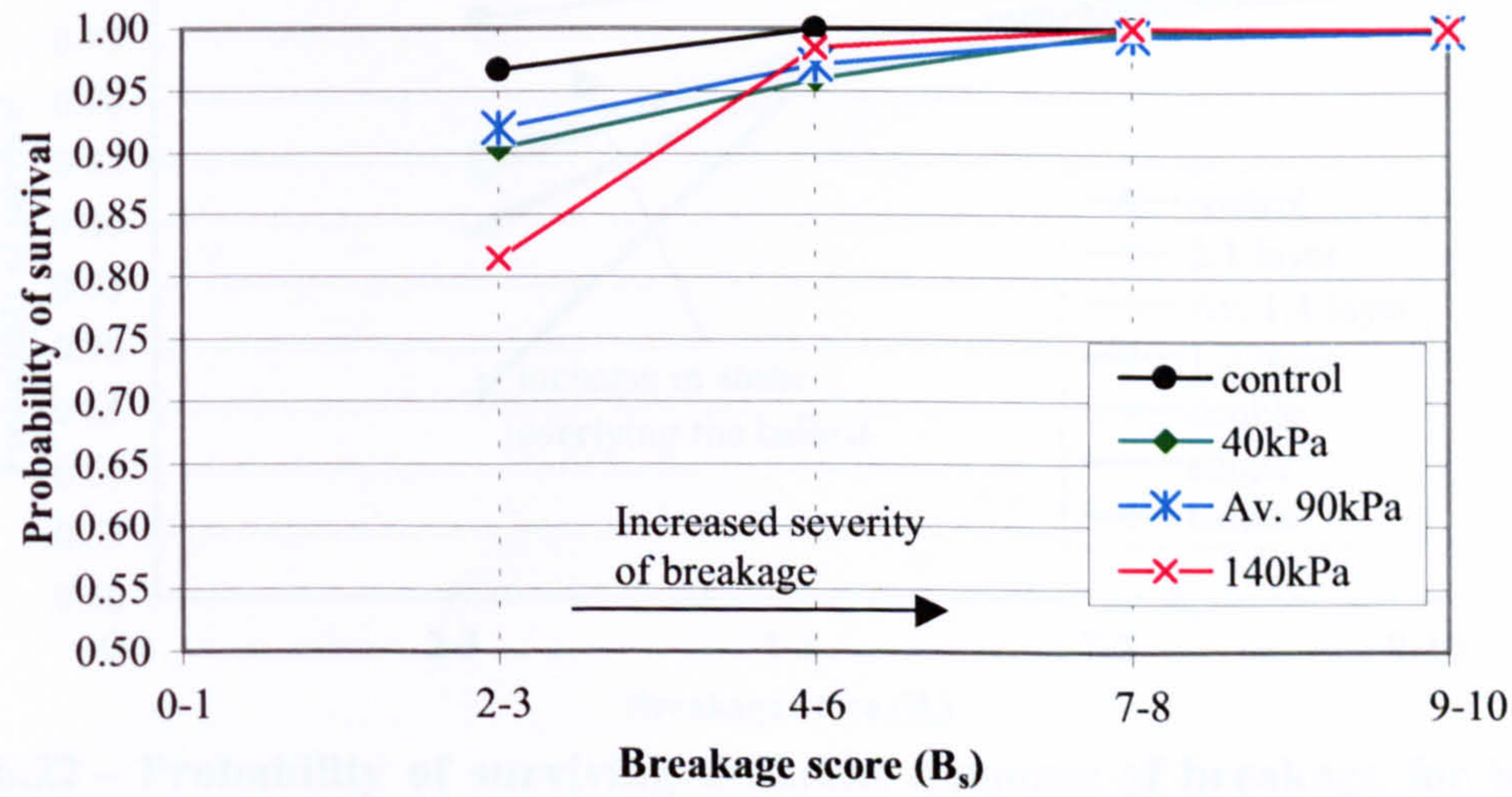

Figure 6.19 – Probability of surviving different amounts of breakage in the cyclic load triaxial tests (Series 2) and the control test

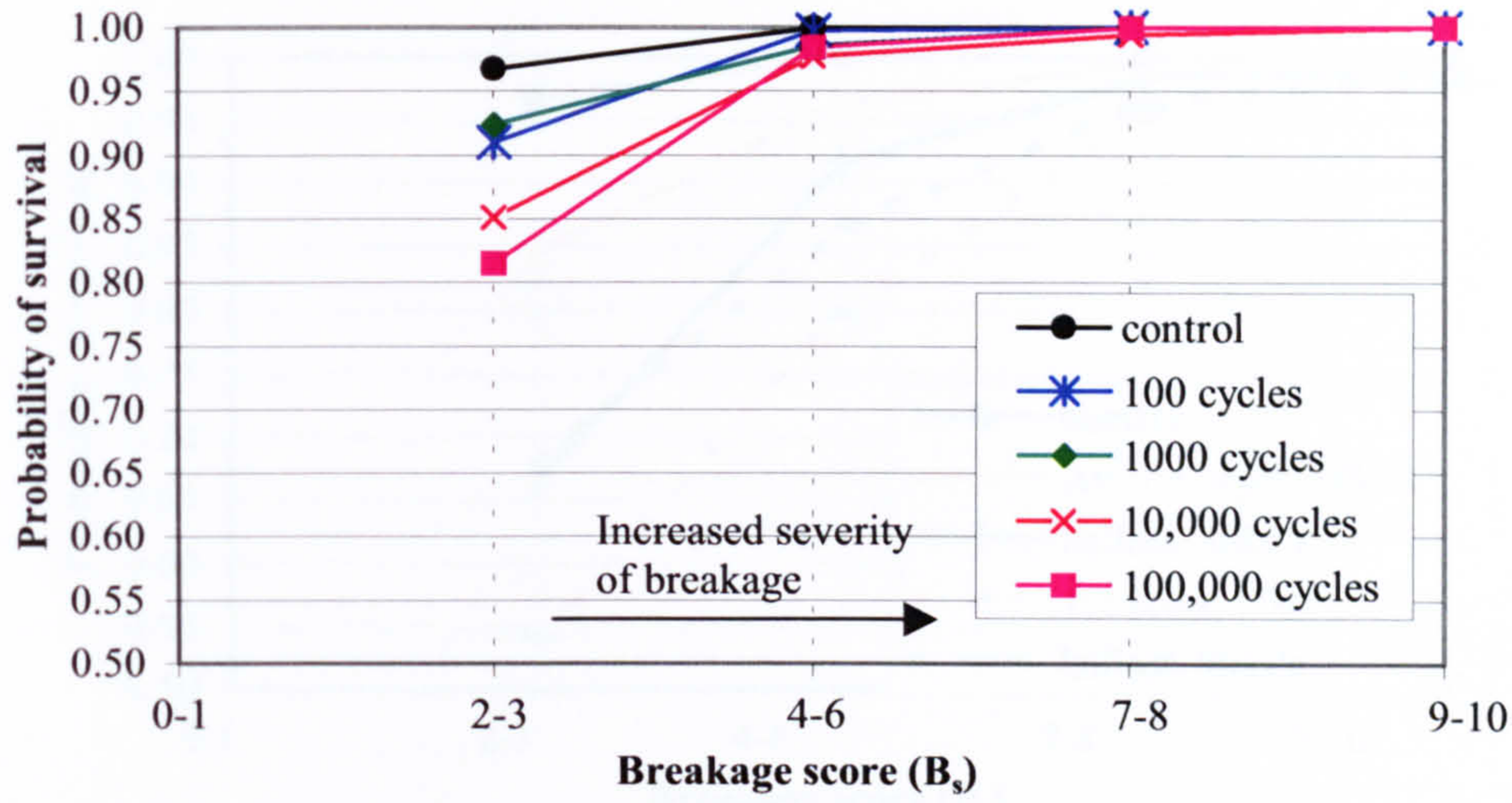

Figure 6.20 – Probability of surviving different amounts of breakage in the cyclic load triaxial tests (Series 3) at 140kPa cell pressure

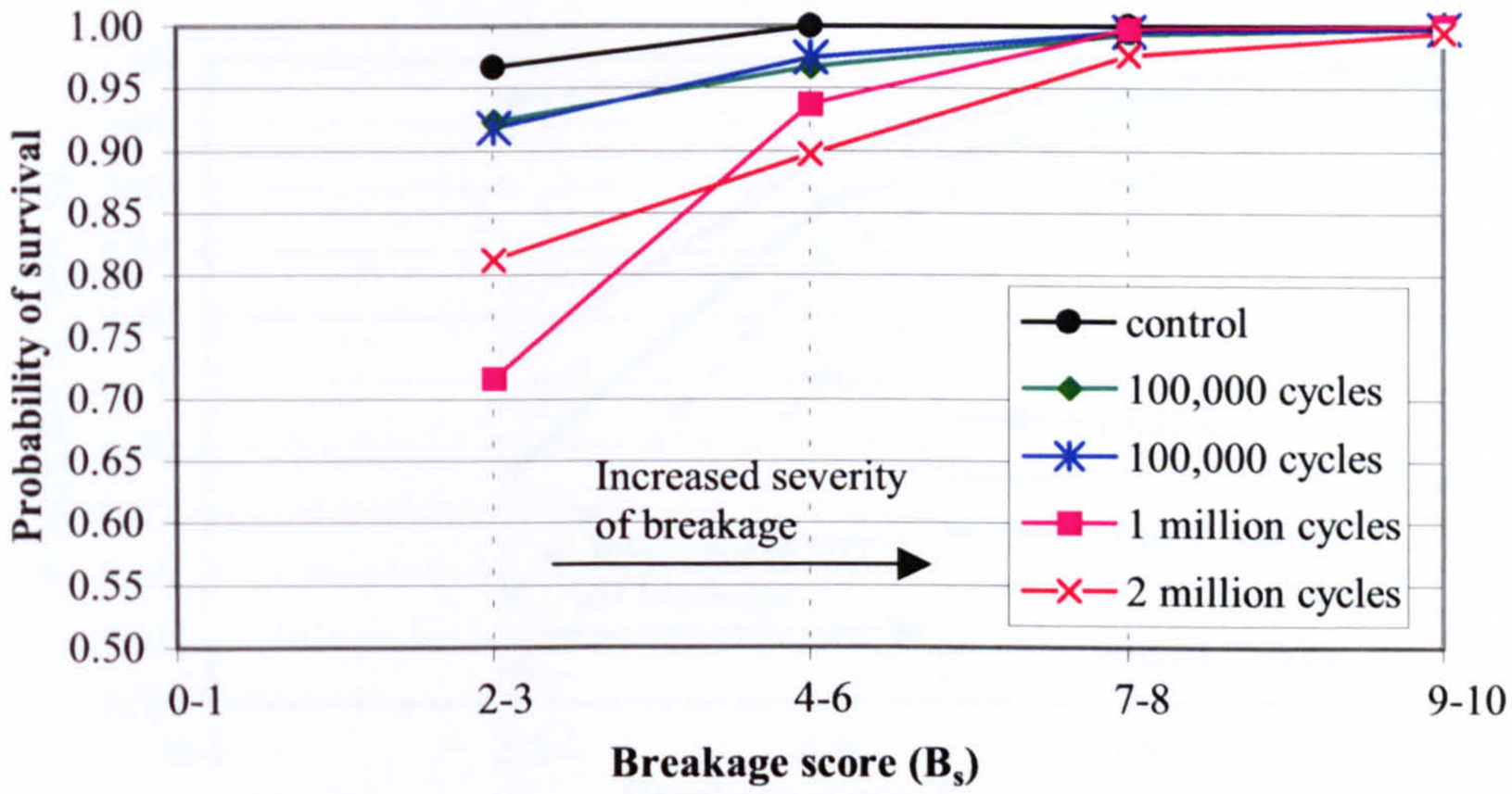

Figure 6.21 – Probability of surviving different amounts of breakage in the cyclic load triaxial tests (Series 3) at 90kPa cell pressure

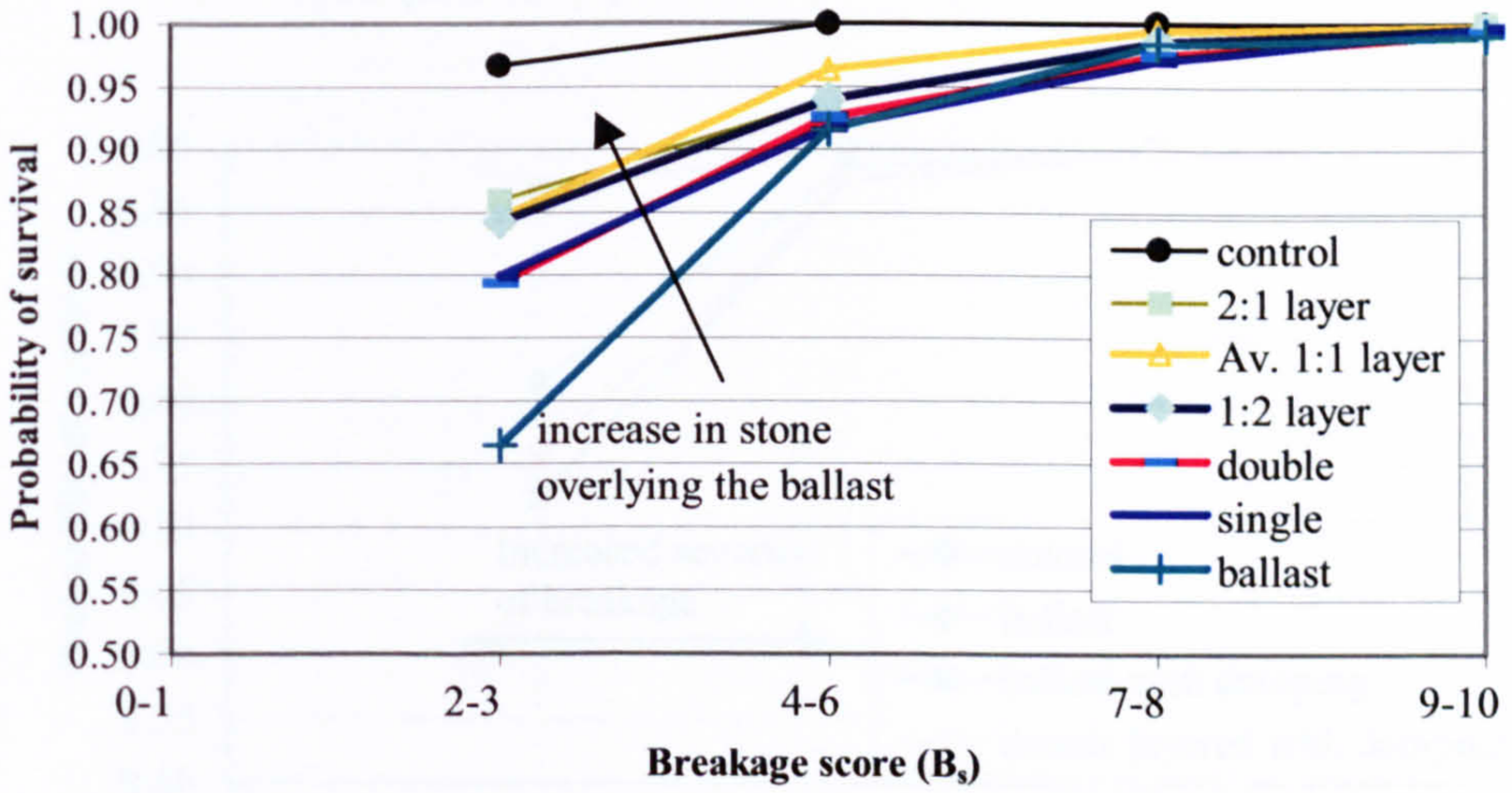

Figure 6.22 – Probability of surviving different amounts of breakage for layered specimens in monotonic load triaxial tests at 40kPa cell pressure (Series 4)

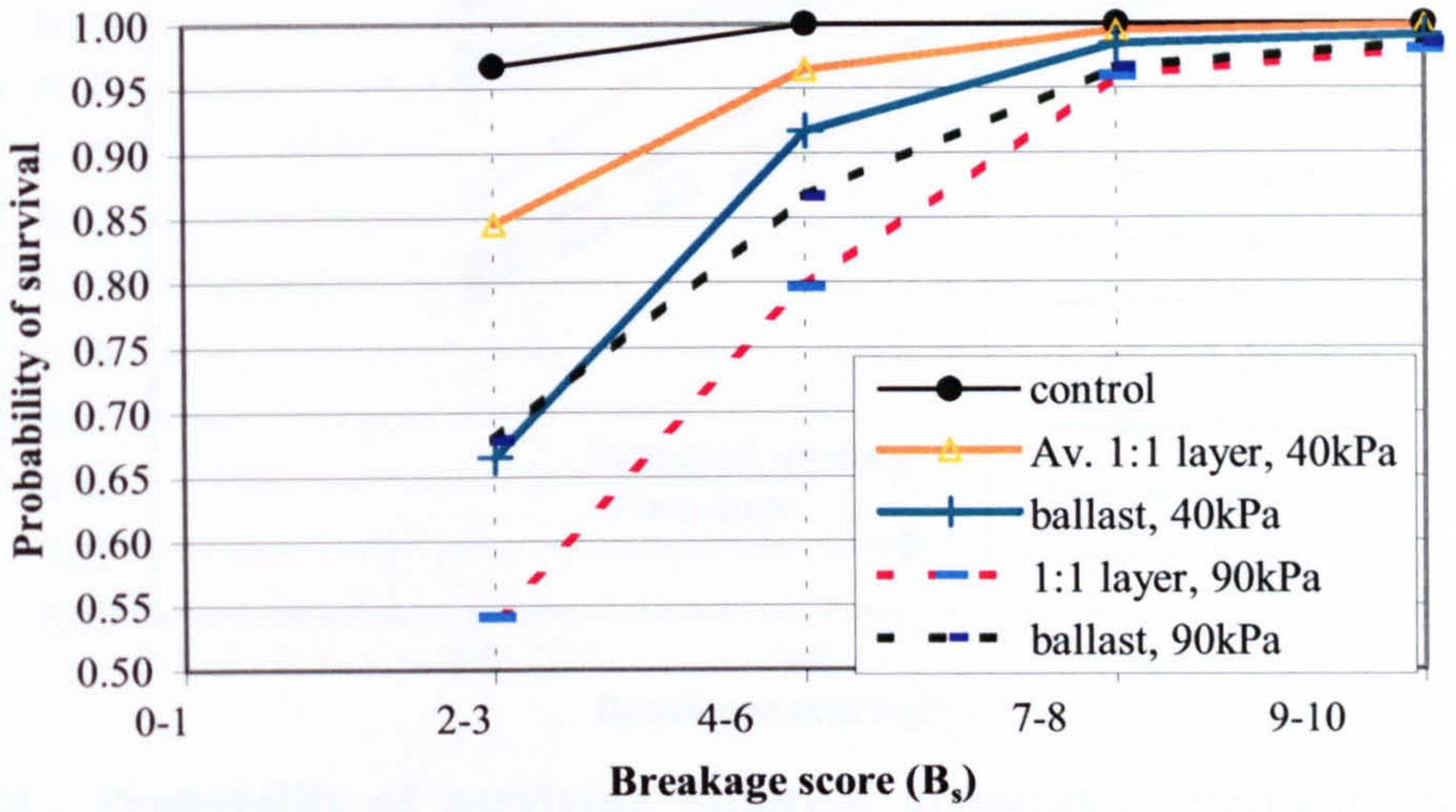

Figure 6.23 – Probability of surviving different amounts of breakage for layered specimens in monotonic load triaxial tests at 40kPa and 90kPa cell pressure (Series 4)

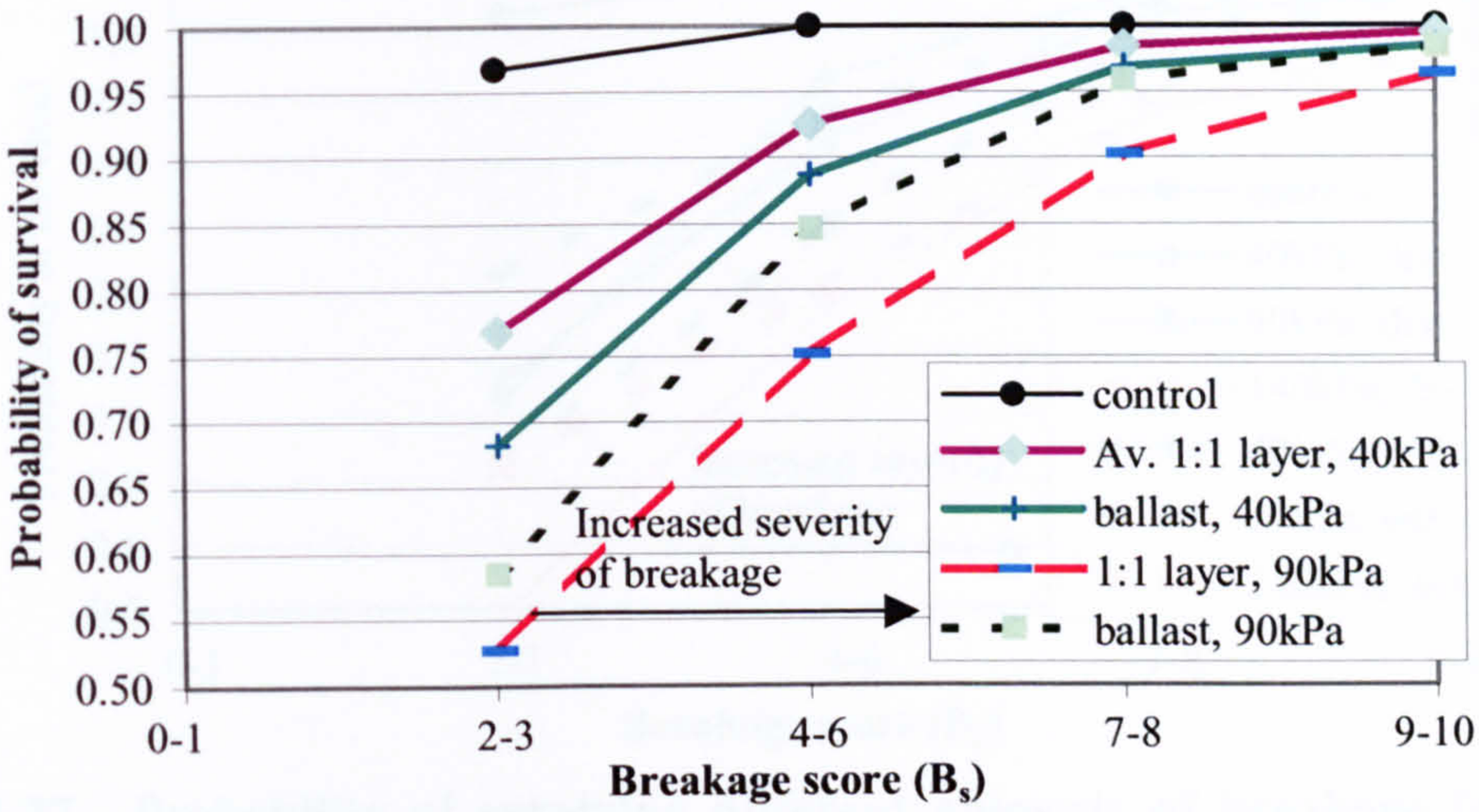

Figure 6.24 – Probability of surviving different amounts of breakage for 1:1 layer specimens in post cyclic monotonic load triaxial tests at 40kPa and 90kPa cell pressure (Series 4)

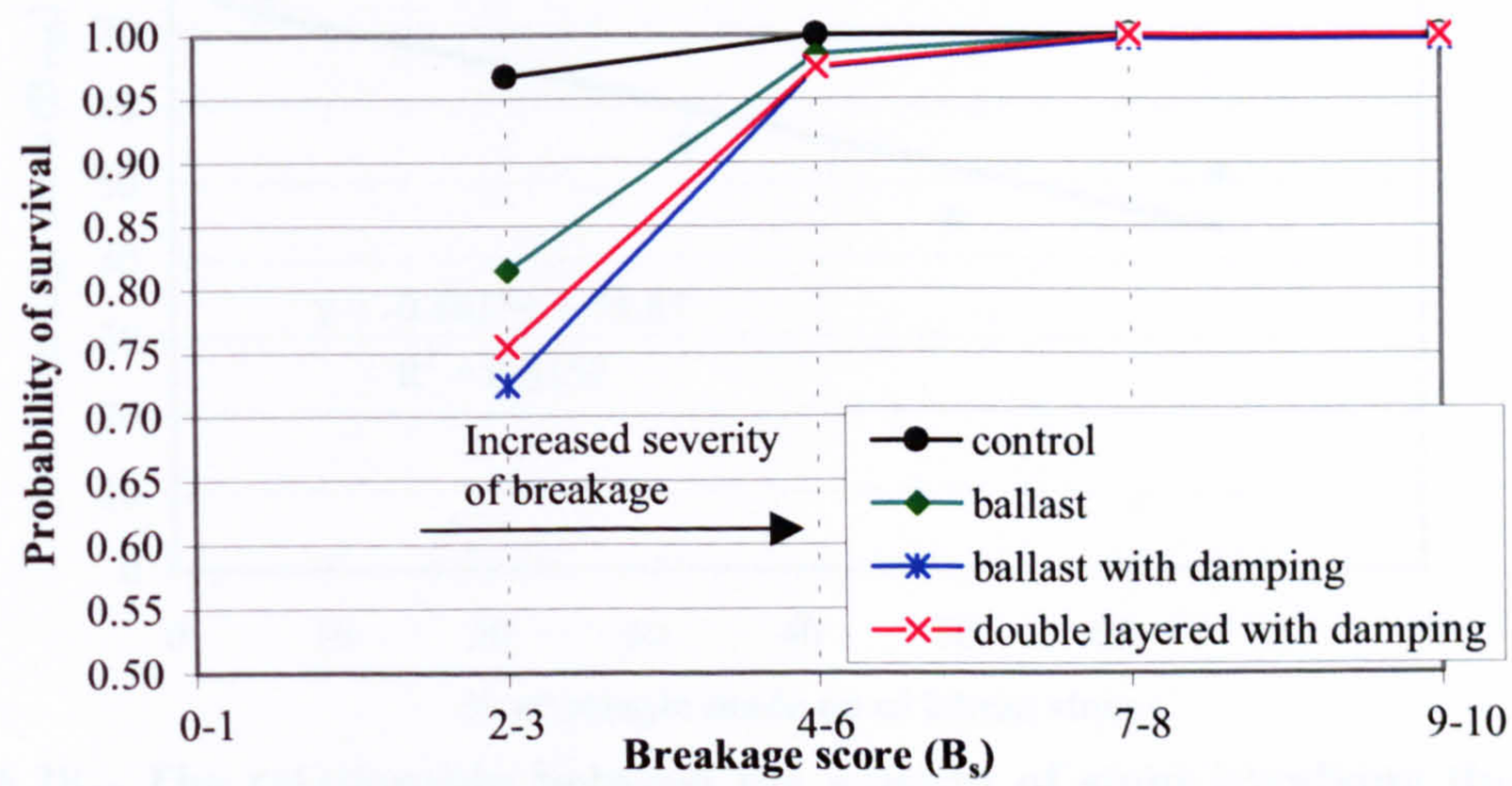

Figure 6.25 – Probability of surviving different amounts of breakage for specimens with damping under cyclic loading at 140kPa cell pressure (Series 5)

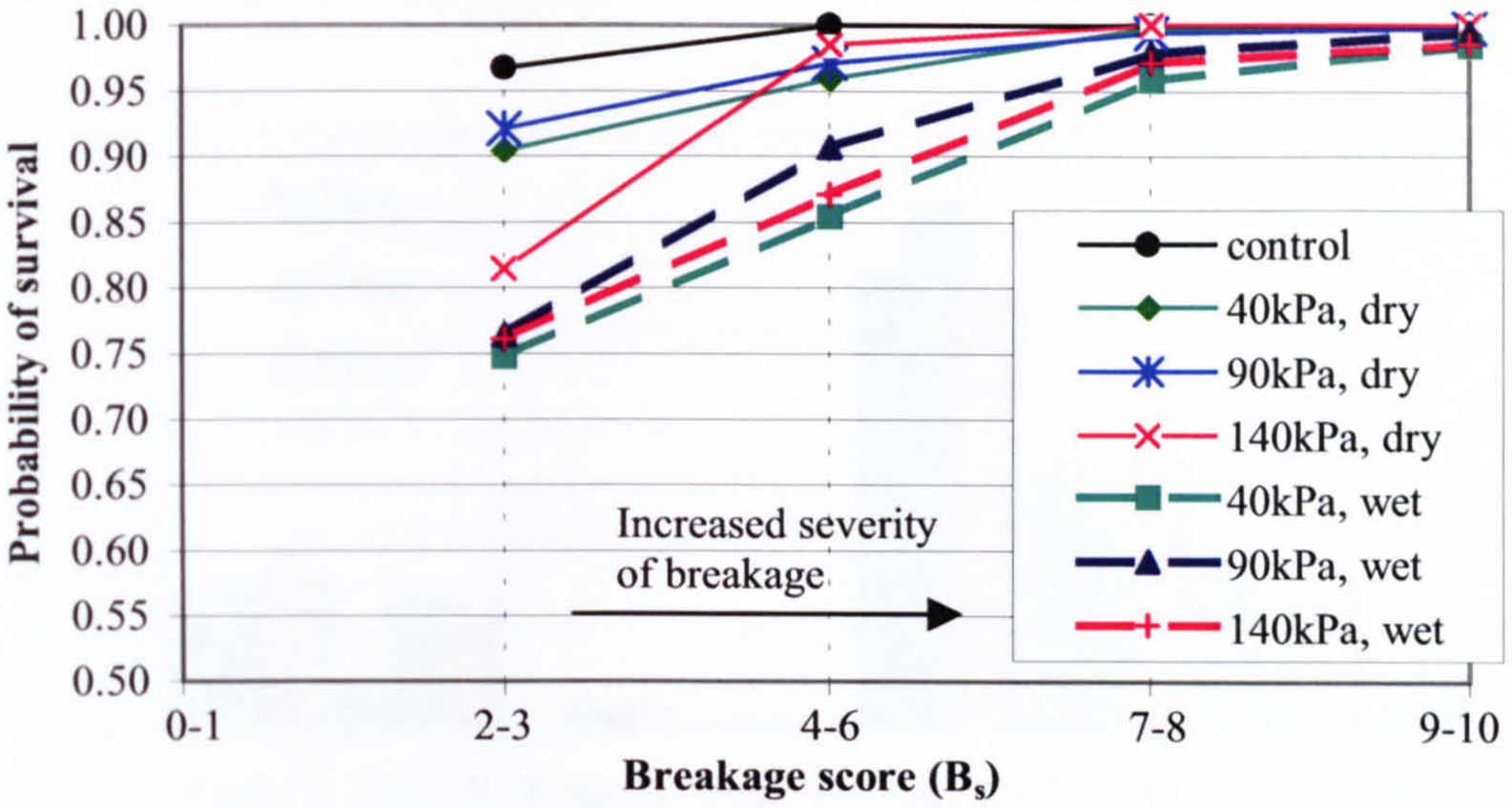

Figure 6.26 – Probability of surviving different amounts of breakage for wetted (Series 6) and dry ballast specimens (Series 2) in cyclic load triaxial tests

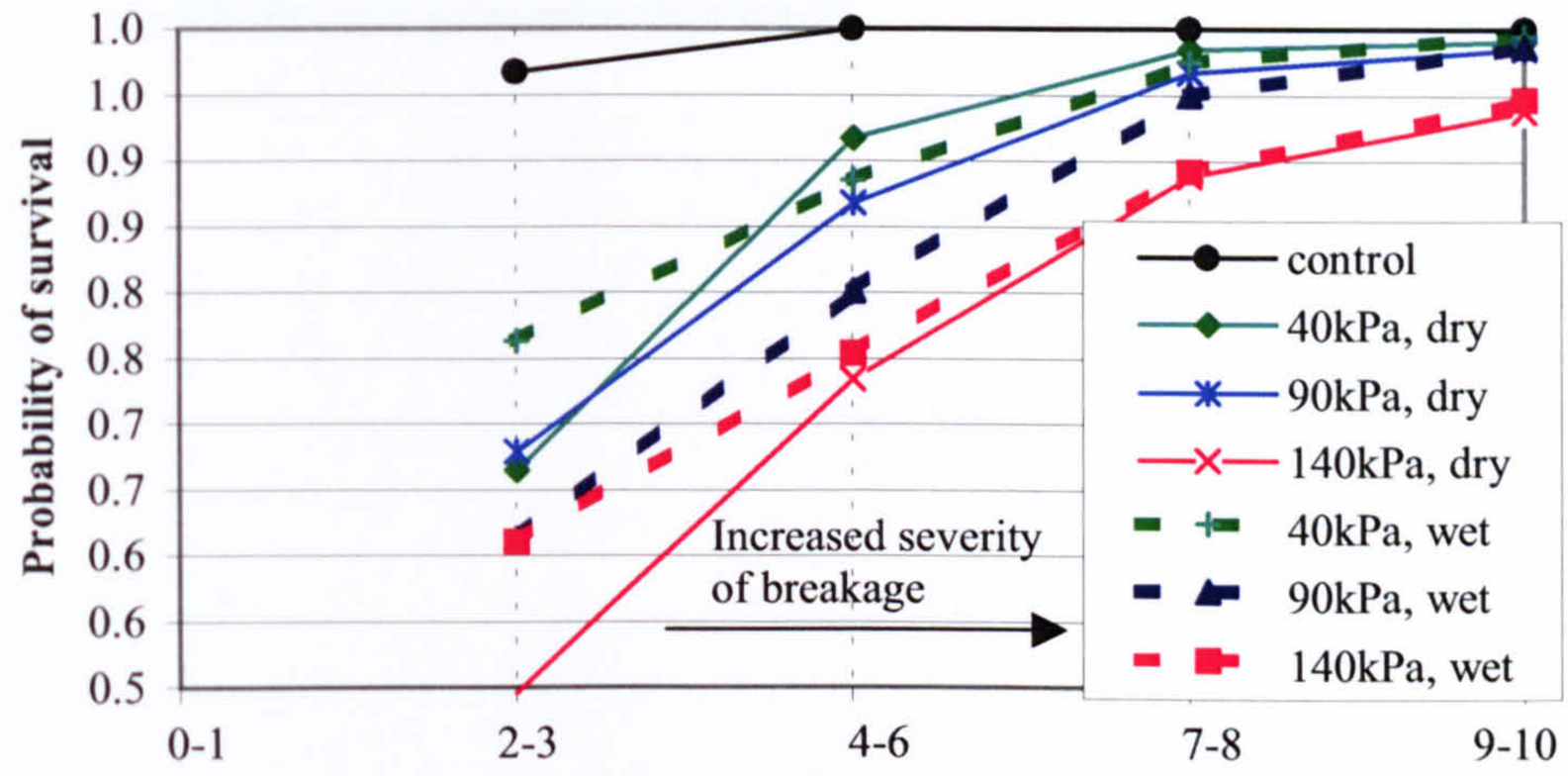

Figure 6.27 – Probability of surviving different amounts of breakage for wetted (Series 6) and dry ballast specimens (Series 2) in monotonic load triaxial tests

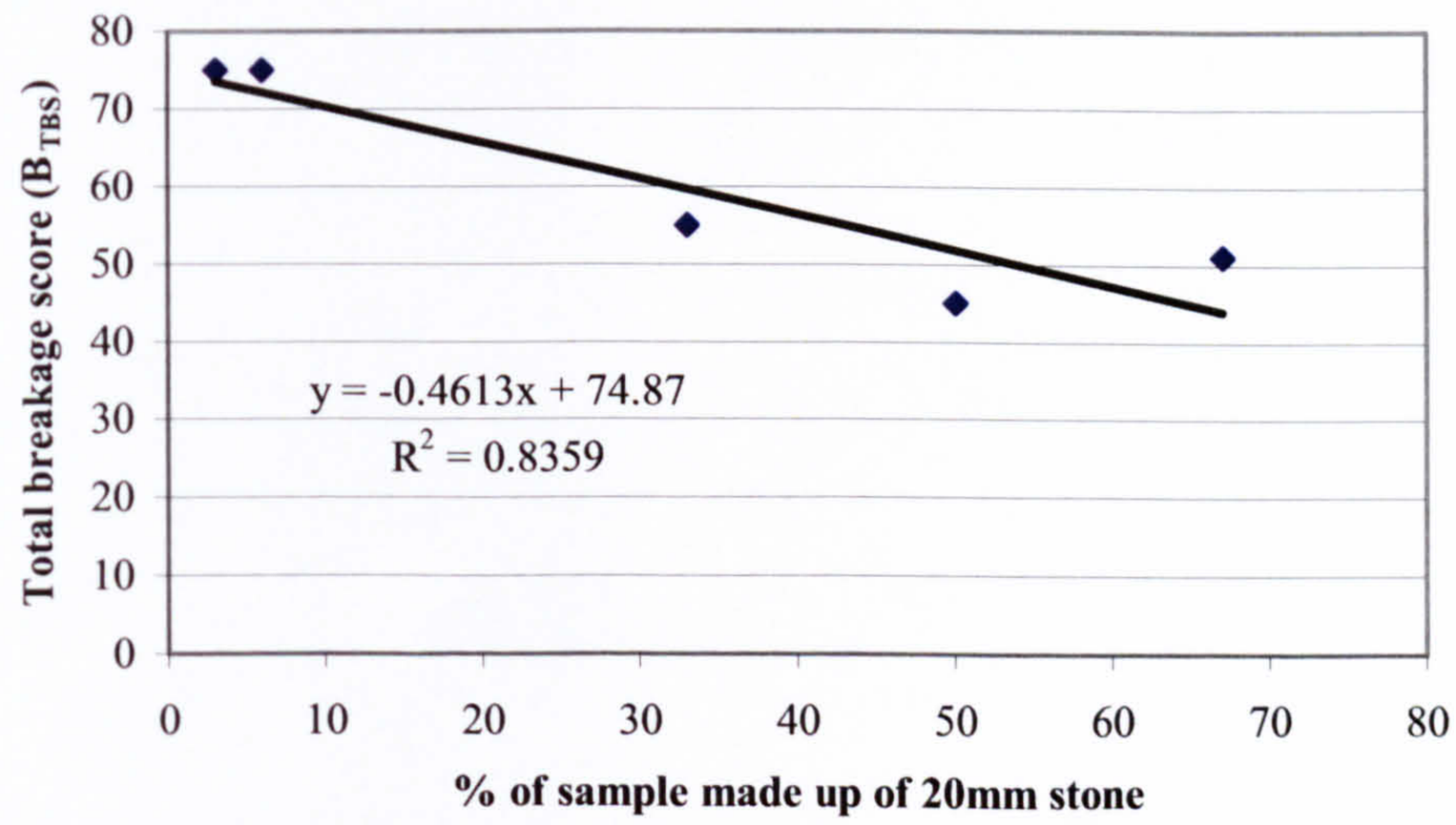

Figure 6.28 – The relationship between the amount of stone overlying the ballast and the amount of breakage occurring in monotonic load triaxial tests at 40kPa cell pressure

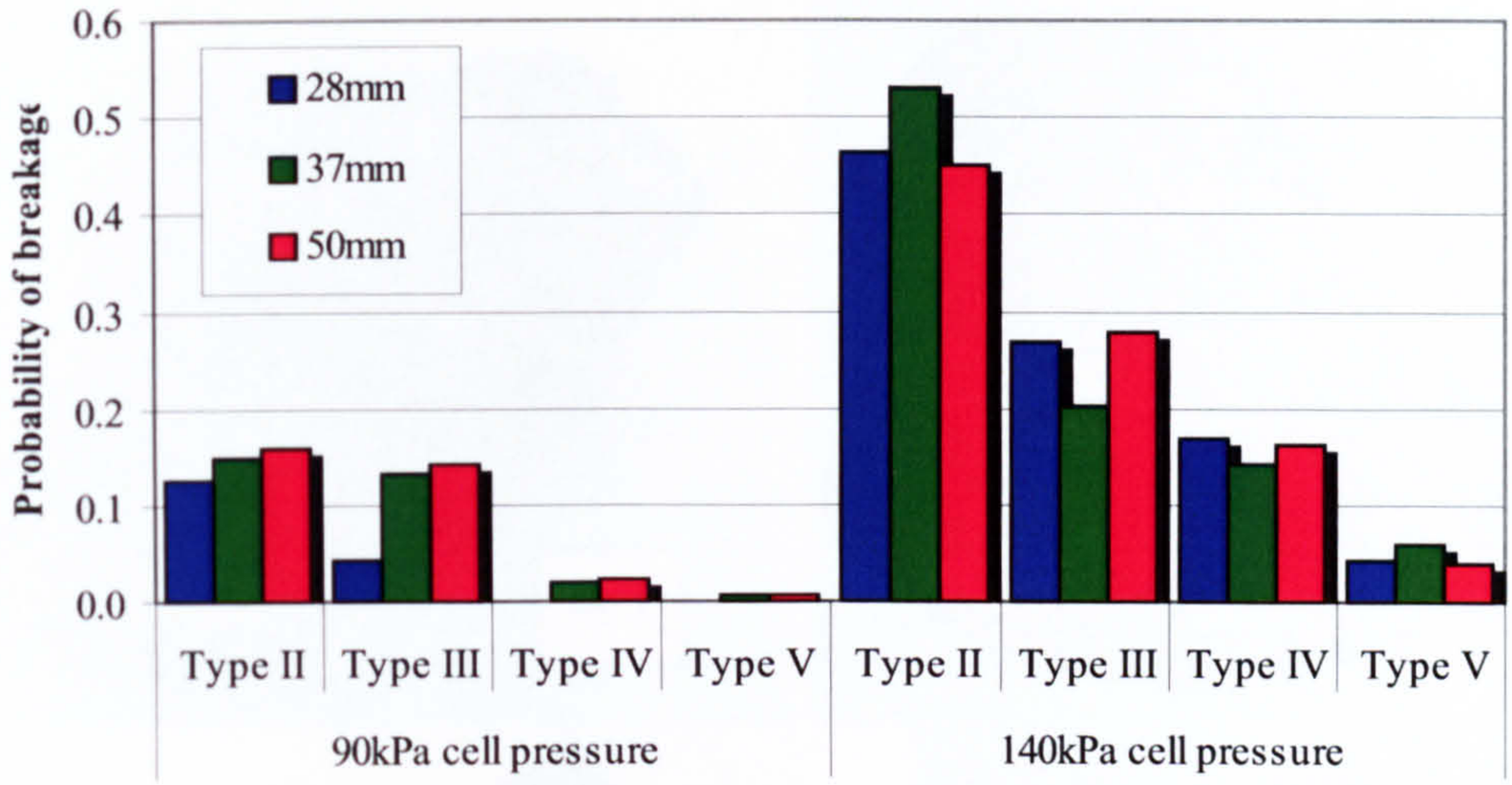

Figure 6.29 – Particle size effects on the probability of breakage of different degrees of breakage in monotonic load triaxial tests at 90kPa and 140kPa cell pressure (Series 2)

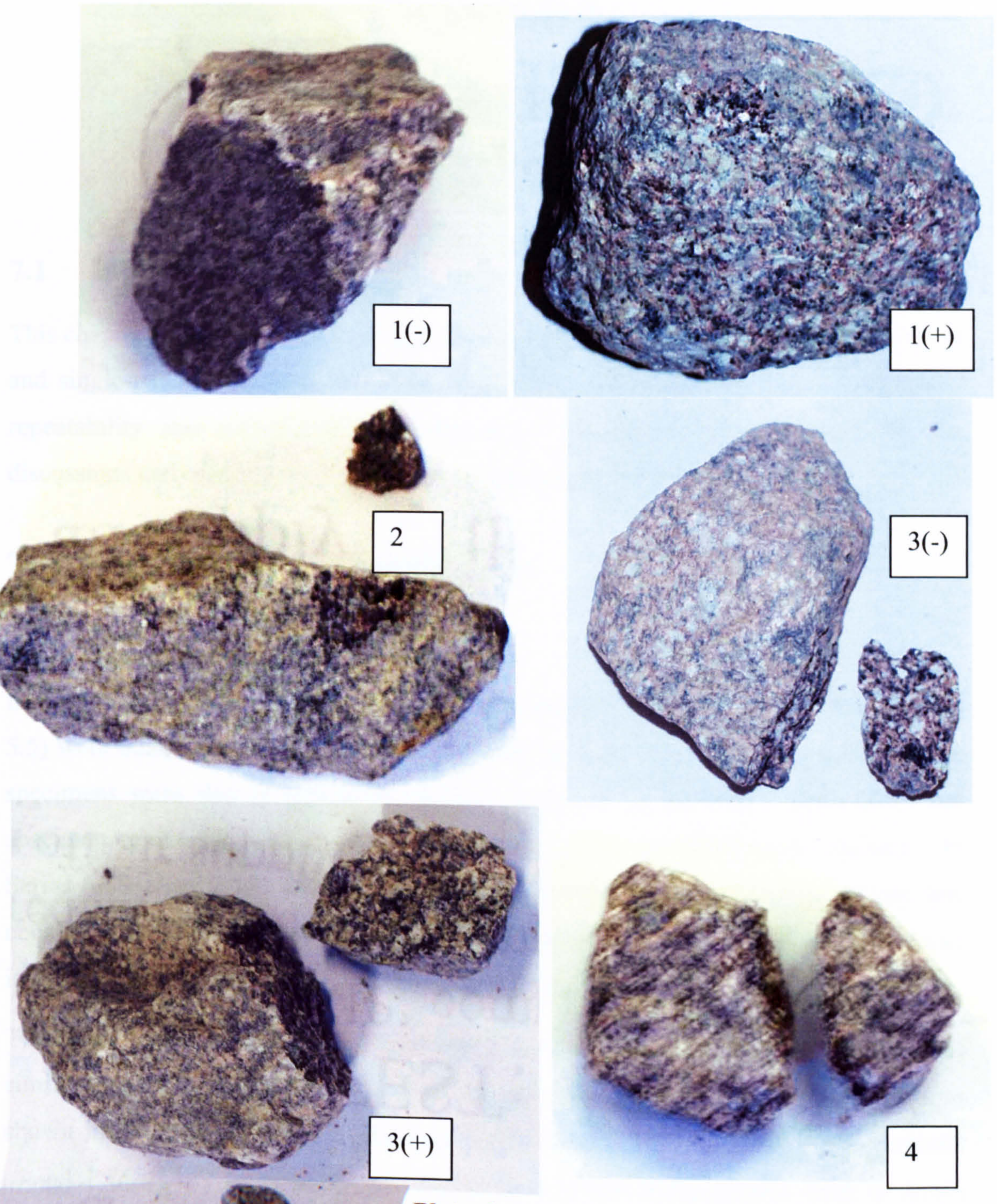

Plate 6.1. – *Photographs showing typical breakage ratings 1-5 (see Figure 6.7)*

CHAPTER 7

Discussion and Conclusions of Laboratory Test Results

7.1 Introduction

This chapter gathers together the results and trends established from the triaxial test data and single-particle crushing data reported in the previous two chapters. Initially the repeatability and reproducibility of the tests will be reviewed followed by the discussions and conclusions drawn from the laboratory test results.

7.2 Repeatability and reproducibility

7.2.1 Specimen preparation

In general the densities of the 20mm stone specimens tested in Series 2 (Tables 5.4 and 5.5) were much more repeatable than they were in Series 1; the densities of the ballast specimens were also as repeatable as those found by Key (1998). This shows that specimen production was a repeatable process, which developed with practice. In Series 6 (Section 5.7.1) the densities of the wet ballast specimens were slightly less consistent than those of Series 2. This may be attributed to the wetness having had an influence on the compaction of the ballast during the specimen preparation.

The overall densities of the ballast specimens were slightly lower than most densities of similar material tested by others, except for that of Janardhanam and Desai (1983), as shown in Table 2.5. It was noted from Table 2.5 that their densities were typically around 1.56Mg/m^3, some 0.1Mg/m^3 higher than in either the present work or Key's (1998). It is probable that the range of densities reported is a reflection of the different mineralogies, gradings and sizes of stone used in the specimens from the different investigations.

The effects of density on monotonic load tests is well documented with an increased density giving a higher stiffness and strength. In this research, although the specimens were prepared in a similar manner, there was still a small variation in the densities due to the natural material variability. There was no clear pattern shown in either the stiffness or the strength of the specimens when considering their densities, suggesting

that the small variations in specimen density did not have measurable influence on the test results.

7.2.2 Triaxial test repeatability

The 20mm Bardon stone, cyclic load triaxial test with a cell pressure of 40kPa (Figure 5.16 and 5.19) was used to check repeatability of the laboratory work throughout the test programme. However, during the test programme several other tests were also repeated.

In the cyclic load tests in Series 2 it was clear that there was a large variation in terms of axial strain between similarly prepared stone specimens tested at 40kPa (Figure 5.16). However, when comparing the 40kPa cell pressure tests to those at 90kPa and 140kPa in Figure 5.17, it was clear that the variation was not so significant to bring into doubt the findings from the tests, as the error bars did not overlap. A similar test is 95% likely to fall between the error bars. Therefore although there was natural variation between the 40kPa tests their behaviour was still clearly different to the tests with different cell pressures. The differences were therefore interpreted as natural specimen variability. This pattern was also observed with the ballast tests. It can be seen from Figure 5.17 and 5.18 that the variation in the axial strains was much less at the higher pressures. Yamamuro and Lade (1993) carried out tests on sands and also found that the consistency in the test results increased at higher cell pressures. This was thought to be because at the lower cell pressures the individual particles were a lot freer to move and rotate within the specimen than at higher cell pressures.

The axial strains in the ballast at 40kPa cell pressure were lower than those in the stone only tests, yet at 90kPa and 140kPa cell pressures the two materials exhibited similar strains. This would appear to be a reflection of the stone specimens' behaviour at 40kPa cell pressure where the axial strains were significantly higher than the specimens tested at 90kPa cell pressure. Further research is therefore necessary to investigate the influence of the cell pressures between 40kPa and 90kPa on the axial strain behaviour of the stone specimens in cyclic load tests.

Variations in the stone specimens' behaviour was also seen with the volumetric strain curves at 40kPa cell pressure (Figures 5.19 and 5.20). In the higher cell pressure tests (90kPa and 140kPa cell pressure) the variation was greatest towards the end of the tests. This may have been a limitation of the new volume change unit, as discussed in Section 3.3.4.

Good repeatability of the Bardon stone monotonic load tests at 40kPa and 90kPa cell pressure, as seen in Figures 5.1 and 5.2, further added to the confidence in the repeatability of the tests.

Although it was not understood why test T26 in Figure 5.13 behaved so differently over the first 2% axial strain, it clearly showed that the specimens were open to a large amount of variability due to the natural variation in size and shape of the particles making up the specimen.

In summary, within the constraints of the natural material/specimen variability, the monotonic load tests had good repeatability in both the stress-strain and volumetric strain behaviour. In the cyclic load tests the axial strains were repeatable and although the volumetric strains showed repeatable trends the absolute values at large numbers of load cycles were not consistent. The issues identified here need to be addressed and resolved in future work.

7.2.3 Comparison with Key's work

Tests in Series 1 may be compared with Key's (1998) in that both used the calculated volume change instead of the measured volume change. However, Figure 7.1 shows significant differences between the stone tests at 40kPa cell pressure. The average peak deviator stresses in the monotonic load tests in this project were significantly higher than those calculated by Key although the calculated volumetric strains were similar. In the ballast tests the difference in behaviour was not so marked as in the stone tests.

As would be expected from the above discussions, and as reported in Table 7.1, the angles of shearing resistance calculated for the tests in this project were considerably higher than those of Key (1998). The angle of shearing resistance for the stone specimens in this project at 40kPa and 90kPa cell pressure were on average 2°-3° higher than Key's, likewise for the ballast specimens.

In the cyclic load tests with 40kPa cell pressure the axial strains in the current work were higher than Key's (Figure 7.2), although lower in the 90kPa cell pressure tests, with comparable volumetric strains at both cell pressures.

No reasons for the differences were apparent, as the specimens were prepared in the same way using the same material with similar densities. Furthermore the test procedure in the current work followed a similar routine to that of Key. Due to the differences in the test results the two pieces of research could not be combined with any confidence.

7.3 Laboratory test results discussion

Initially the measure of particle breakage is briefly discussed in Section 7.3.1, followed by each of the series thereafter. After Series 6 has been discussed further general patterns trends and observations from the tests are highlighted, a new model of volume change behaviour is proposed, and the theory of Shakedown discussed.

7.3.1 Measures of particle breakage

Several ways of measuring particle breakage have been discussed in the literature review (Section 2.6.3), the majority of which are based on the change in the particle size distribution curve based on mass. The difficulty with many of the early measures is that they do not represent the breakage across the full particle size distribution curve and are limited to the change in mass at one or two grain sizes. Hardin (1985) took a slightly different approach by looking at the relative breakage, which was the ratio of total breakage to the potential for breakage (Figure 2.23).

Figure 7.3 compares the relative breakage values (B_r) as determined by Hardin with those of the total breakage scores used in this work (B_{TBS}) (Section 6.3.4). It can be seen that there was a good correlation between the two forms of breakage analysis with an R^2 value of 0.95 and a small y intercept of -0.87 for the tests in Series 2 to 5. The small y intercept value shows the results correlate well as zero B_{TBS} should equal zero B_r. This shows that the B_{TBS} value, as with Hardin's B_r, reflects the breakage across the full particle size distribution curve.

The second line on the graph shows the correlation for five out of six tests in Series 6 (tests T79-T83). From this a different correlation was observed also with a very high level of correlation ($R^2 = 0.90$) and again with a low y intercept value of 0.90. The first test in Series 6 was test T78. This was dismantled by both the author and a second operator together (see Section 5.7). The results from this test (T78) were in good agreement with the results from Series 2 to 5, Figure 7.3. Subsequently the second operator carried out a further five tests (T79-T83) (Lau, 2003). It is clear from this that the determination of B_{TBS} was very much dependent on the interpretation of the operator. The method used to calculate B_{TBS} therefore needs to refined so that it will not be so reliant on the judgment of the operator.

7.3.2 Series 1 – comparing the Bardon and Cloburn 20mm stone

The aims of Series 1 were to establish the degree of repeatability and reproducibility in the tests and to compare the Cloburn and Bardon 20mm stones. Details of the tests are given in Tables 5.1 and 5.2.

In the monotonic load tests at 40kPa cell pressure the Bardon specimens showed slightly greater compressive strength than the Cloburn specimens (Figure 5.3), although at 90kPa cell pressure the compressive strengths of the different stones were similar (Figure 5.4). In both the 40kPa and the 90kPa cell pressure tests the Cloburn had an initial stiffness (E_t) slightly greater than the Bardon stone (Table 5.1). This would suggest that the Cloburn stone initially had a higher angle of inter-particle friction, although once this was mobilised then the specimen became weaker.

The typical stress-strain behaviour of the specimens seen in Series 1 (Figures 5.1 and 5.2) was that of a loose to medium dense granular material and one would have expected the specimen to be close to critical state. The volumetric strain behaviour of the specimens could however be interpreted as a dense granular material, with the specimens far from critical state due to their high rate of dilation. Likewise, Bishop (1966) found that with sands at high pressures the stress-strain behaviour of a dense specimen approached that of a loose material. From this he concluded that the dilatancy was suppressed due to particle crushing, where the peak occurred at a lower peak principal stress and at a larger axial strain. Bishop also demonstrated that axial strains of up to 25% were reached before the peak stress could be recorded (Figure 2.13), and Hall and Gordon (1963) quoted strains of between 15%-20% were required before failure was reached.

With the cyclic load tests the behaviour of the two materials was significantly different, with the Cloburn stone undergoing twice as much axial strain as the Bardon stone. This was confirmed by the good repeatability between the like tests as shown in Figures 5.5 and 5.6. During cyclic loading, the specimens underwent a large amount of dilation; this would imply that the specimens were dense. However, as was shown in Series 2 (Figures 5.14 and 5.15), the amount of dilation deduced was significantly reduced with the introduction of the new volume change unit.

In the 40kPa cell pressure tests there was an apparent stability reached at 10,000 – 20,000 load cycles with the Bardon stone specimens, both in terms of axial and volumetric strain. However this was not observed with the Cloburn stone specimens at 100,000 load cycles with a 40kPa cell pressure. Possibly the initial angle of internal

friction in the Cloburn stone, as discussed earlier in this section, was reduced to a mobilised angle of friction within the early stages of the test. With the lower mobilised angle of friction the specimens were less able to resist the repeated application of the deviator stress.

In the initial monotonic load tests the stiffness (E_t) was greater for the Cloburn stone specimens, this was not the case in the post cyclic monotonic load tests. At both 40kPa and 90kPa cell pressure the stiffness of the Bardon stone specimens was significantly greater. The average peak deviator stresses at 40kPa and 90kPa cell pressures were also higher with the Bardon stone specimens. This would again support the understanding of a reduced mobilised angle of friction in the Cloburn specimens.

At 40kPa cell pressure a clear peak was formed on the post cyclic monotonic load test's stress-strain graph (Figure 5.7) – relating to a very dense granular material. This was particularly surprising as the density of the specimen (using the calculated volume changes) reduced during the cyclic load tests. With the volumetric strain behaviour in the post cyclic monotonic load tests there was virtually no compression of the specimens before they started to dilate, again suggesting a very dense material. In the 90kPa cell pressure tests a clear peak was not formed and the deviator stress continued to increase up to the end of the test. The initial stiffness (E_t) of all the post cyclic monotonic load specimens were significantly higher than the initial stiffnesses (E_t) in the initial monotonic load tests as shown in Table 5.1.

Critical state soil mechanics theory states that two specimens of the same material will have similar ultimate deviator stresses irrespective of the initial density. This behaviour can be seen with the monotonic and post cyclic monotonic load tests in Figures 5.8 and 5.9.

A decision was made, based on the monotonic load tests alone, to use only the Bardon 20mm stone in further testing (Series 2 to 6). This was before the cyclic load test results were analysed. In the monotonic load tests the difference in behaviour between the two materials was not considered to be significant in relation to this work and little further knowledge would be gained by testing the two materials along side each other in the following test series. Furthermore, to keep the tests as comparable to Key's (1998) as possible it was decided to keep the number of variables to a minimum. However, it was clear from the cyclic load tests (Figures 5.5 and 5.6) that there was a significant difference in behaviour between the two materials under cyclic load conditions.

7.3.3 Series 2 – stone and ballast specimens

Tests in Series 2 were carried out to deepen the basic understanding of the general material characteristics. Innovation in this series included the use of the new volume change unit and the assessment of breakage of the 50mm ballast particles, which added a further depth of understanding to the research. No assessment was made of the breakage occurring in the 20mm stone as there was only very limited breakage observed and therefore the effects of the breakage were considered to be insignificant.

In Series 2 a similar pattern emerged to that already seen in Series 1. In summary, the stress-strain behaviour of the specimens in the monotonic load tests in both the stone (20mm Bardon stone) and the ballast showed behaviour typical of loose granular material (Figures 5.12 and 5.13), yet the volumetric strains showed typical dense material behaviour (Figures 5.14 and 5.15). In light of other research (Bishop, 1966 and Indraratna et al., 1998) it was assumed that the specimens were behaving as dense materials and that a peak stress may have developed with further axial straining. Typically the initial stiffness of the specimens (E_t) increased as the cell pressure increased, as did the average peak deviator stress. With each increase in cell pressure the amount of initial compression increased and the amount of overall dilation at failure decreased. Both trends were as would be expected.

From the monotonic load tests on the stone specimens it would appear that with each increase in cell pressure the increase in average peak deviator stress was reduced (Figure 5.12). This was even more defined in the ballast specimens, where there was only a small increase in the average peak deviator stress seen between the 90kPa and the 140kPa cell pressure tests (Figure 5.13). This therefore implied a curved Mohr-Coulomb failure envelope or a curved failure surface in q-p' stress space as plotted in Figure 7.4.

The curvature of the Mohr-Coulomb failure envelope is well covered in literature (Section 2.6.1.9). Bishop (1966) comments that curvature of the failure envelope is most marked for soils where:

i) the specimens were initially dense or heavily compacted,

ii) the particle grading was uniform, and

iii) for heavily over consolidated undisturbed specimens.

He further commented that the curvature of the failure envelope in specimens of granular material was linked with the crushing of particles, which meant a reduction in the rate of volumetric dilation and a reduction of φ' at failure.

This ties in well with the breakage analysis for the ballast in the current work. There was a slight increase in breakage seen between the 40kPa and 90kPa cell pressure tests, yet a significantly larger increase in the amount of breakage seen between the 90kPa and 140kPa cell pressure tests (Figure 6.19 and Table 6.5). From this it was concluded that a significant yield point in the strength of the ballast particles was reached somewhere between the 90kPa and 140kPa cell pressure tests. That was with an average peak deviator stress of between 500kPa and 600kPa. From the single-particle crushing tests it was found that asperities started to break at stresses of approximately 480kPa and as discussed in Section 6.4 it would be expected that this value would be lower in a matrix due to the different inter-particle stress paths and loading when compared to the flat horizontal plates between which the individual particles were crushed.

The difference between the behaviour of the stone and ballast specimens is apparent in Figures 5.12 and 5.13, with the stress-strain curve of the ballast being much rougher than the stone. This behaviour could be interpreted as stick/slip phenomena, where particles that were interlocked were suddenly released, and/or particle breakage occurred. It would appear from Figure 5.13 that the 90kPa and 140kPa cell pressure stress-strain curves were rougher than the 40kPa cell pressure curve, especially at the lower strains, possibly due to extra breakage occurring in these tests. It would appear that this exaggerated roughness started to occur at a deviator stress of around 300kPa and above.

It was interesting to note that the stone and ballast specimens at 40kPa cell pressure had similar initial tangent stiffnesses (E_t), yet at 90kPa and 140kPa cell pressure E_t for the ballast specimens was significantly lower than the stone specimens (Table 5.4). In the ballast specimens only a slight increase in E_t was seen with each increase in cell pressure, which was thought to have been due to asperity breakage.

From the cyclic load tests on stone at 40kPa cell pressure, it was clear that the volumetric strains were initially dilative, Figure 5.19, although after 1000 load cycles the specimen often began to compress ending with little overall volumetric strain. This pattern of volumetric strain behaviour suggested that initially the sample was relatively dense and after a slight volumetric expansion, with cyclic loading, particle rearrangement occurred and the specimen compacted. With the ballast specimens at 40kPa cell pressure there was only a slight dilation of the specimens before they started to compact (Figure 5.21). This was suspected to have been due to the extra particle

breakage occurring in the ballast compared with the stone specimens. This explanation however did not hold true at 90kPa, 140kPa or 240kPa cell pressures where the volumetric strains in the ballast are similar in both the stone and ballast specimens.

The resilient modulus calculated throughout the cyclic load tests showed that typically the modulus of the specimen increased at a decreasing rate with the number of load cycles (Figures 5.59 and 5.60), again suggesting that the specimens had reached a form of stability. An exception was the 240kPa cell pressure tests for both the stone and ballast specimens. From the axial strain (Figure 5.17 and 5.18) and the volumetric strain graphs (Figure 5.20 and 5.21) there was nothing to explain this difference in behaviour.

In the cyclic load tests the resilient modulus of the stone specimens was some 3 times greater than the ballast specimens; although there was no evidence of extra stiffness in the monotonic load tests between the stone and the ballast specimens, especially in the 40kPa cell pressure tests. One would have expected that specimens with a higher modulus would give lower axial strains; however as seen in the 240kPa cell pressure tests in Figures 5.17 and 5.18 the observed strains were only slightly less than in the 140kPa cell pressure tests even though the moduli of the specimens at 240kPa cell pressure were significantly higher.

The resilient modulus of the specimen at 40kPa, 90kPa and 140kPa cell pressure increased at a decreasing rate with the number of load cycles. This is in line with the findings of Shenton (1975). In other research Hicks and Monismith (1971) and Kalcheff and Hicks (1973) found that the specimens stabilised after 100 load cycles, Tutumluer et al. (1998) after 1000 load cycles and Brown (1974) reported stabilisation after 10,000 load cycles, albeit in different materials. Key (1998) suggested that the resilient modulus had stabilised after 40,000 load cycles.

With the volumetric strains it was interesting to observe, for both the stone and ballast specimens, excluding the 40kPa cell pressure tests, that the amount of compression was less with each increase in cell pressure (Figures 5.20 and 5.21). This would therefore tie into the resilient modulus data where a stiffer specimen would undergo less volumetric strain.

As already discussed in Section 6.3.2 there was little discernable difference in the breakage characteristics of the cyclic load tests at different cell pressures in Series 2.

In terms of shear strength (Table 5.7) the stone specimens showed a good correlation between each of the cell pressures, with an angle of shearing resistance of 51°. With the ballast specimens φ' reduced by 10° with an increase in the cell pressure from 40kPa to 140kPa. This was thought to be due to particle breakage occurring in the ballast specimens and the associated reduction in dilation. With the increased breakage and the reduced dilation the peak stresses and the angle of shearing resistance were reduced.

Thompson and Smith (1990) reported that the shear strength of an 'unconditioned' material was not representative of the strength of an in-service compacted material, where conditioning is taken as the cycling of moving vehicles (or the cyclic load triaxial test before the post cyclic monotonic load test). They found increases in strength of 34-217% between a monotonic load test which was 'unconditioned' and a monotonic load test which had been 'conditioned' (e.g. a post cyclic monotonic load test). This effect was also seen in the current work with cell pressures of 40kPa where the shear strengths increase by approximately 80% between the initial monotonic and the post cyclic monotonic load tests. However in the higher cell pressure tests (90kPa and 140kPa) there was no peak in deviator stress. It is thought that this may be a consequence of particle breakage and will be further addressed as part of the volumetric strain model developed in Section 7.5.

From testing in Series 2 the basic understanding has been advanced in five different ways:

i) During cyclic loading the specimens were generally compressing and not dilating as was observed using the calculated volumetric strains seen in Series 1 (Figures 5.6 and 5.20) and in Key's (1998) work.

ii) There was no correlation observed between the resilient modulus and the amount of axial strain.

iii) The characteristic strength of the particles determined by the single particle-crushing test (Section 6.4) was considered too high, possibly due to the differences in particle orientation in relation to the applied load in a matrix and the single-particle crushing tests.

iv) With higher confidence in the volume change measurements it was seen that the typical loose / dense behaviour of the materials tested did not altogether conform to critical state soil mechanics.

v) The reason for the non-compliance to critical state behaviour was deemed to be principally due to particle breakage. However, that leaves a question over the

20mm stone specimens where similar behaviour was also observed but the amount of breakage was significantly less.

7.3.4 Series 3 – effects of the number of load cycles

The cyclic load tests in Series 3 were terminated after different numbers of load applications to assess the amounts of breakage occurring at different stages of the test. The axial strain and volumetric strain behaviour was as expected from the results of Series 2 at both 90kPa and 140kPa cell pressure. Although there was only a limited amount of breakage in the cyclic load tests it can be seen from Figures 6.20 and 6.21 and Table 6.5 that as the number of load cycles increased so did the amount of breakage. This increase in breakage may only have occurred up to a certain point, after which it was postulated that the amount of breakage would be minimal as the specimen had reached a point where the load being transferred though the specimen and that carried by each individual particle was less than the tensile strength of the particles – hence no further breakage would occur.

The resilient modulus in the 90kPa cell pressure tests, as seen in Figure 5.66, increased rapidly during the first few load cycles and continued to rise up to at least 10,000 load cycles with the ballast specimens. However it was clear from Figure 5.66 that there may have been a threshold number of load cycles, at approximately 500,000 load cycles, after which the resilient modulus reduced. It would appear that this loss in stiffness was related to an increase in the amount of breakage (Figure 6.21). This is apparent in Table 6.5, where the total breakage score for the 1 million and 2 million load cycle tests were clearly higher than the tests with fewer load cycles. It can therefore be deduced that individual ballast particles could possibly have failed due to fatigue. Festag and Katzenbach (2001) reported that under continued cyclic loading a material that appears to have reached steady state, or shakedown, could become unstable. They concluded that local failure, i.e. abrasion and breakage occur due to fatigue.

It would therefore appear that the main conclusion from Series 3 is that breakage continued to slowly occur with the application of load cycles, and after a period of loading an increase in breakage occurred due to fatigue failure of the ballast particles resulting in an increase in strain and a reduction in stiffness.

7.3.5 Series 4 – layered specimens

Key (1998) carried out tests on three types of layered specimens, i) where the stone and ballast were of equal thickness at 40kPa, 60kPa and 90kPa cell pressure; ii) where approximately three quarters of the specimen was of stone overlying the ballast at 40kPa cell pressure; and iii) where approximately one quarter of the specimen was of stone overlying the ballast at 40kPa cell pressure. In this project there were similarly prepared specimens to Key's and further thin-layered specimens with a single layer and a double layer of stone overlying the ballast. Building on Key's work this research had the added benefit of the volume change unit, the breakage behaviour analysis and the more detailed analysis of the stiffness behaviour of the specimens.

The general characteristics described for Series 2 were again seen in the tests results for the layered specimens. In the monotonic load tests at 40kPa (Figures 5.34 to 5.36) this was that the stress-strain graph showed the behaviour of a typical loose specimen and the volumetric strain graphs the behaviour of a dense specimen. Typically the average peak deviator stress was alike for all the layered specimens between 290kPa and 365kPa similar to the average peak deviator stress for the stone only and ballast only specimens in Series 2. There was no correlation observed between the average peak deviator stress and the amount of stone overlying the ballast. Although the values of the average peak deviator stress for the layered specimens were similar, it was clear that the layered specimens were a lot more prone to variation than the stone only and ballast only specimens.

The stiffnesses of all the layered specimens were within the range of stiffnesses seen for the stone only specimens in Series 2, and there was no observed correlation between the specimen stiffness and the percentage of stone overlying the ballast.

An increase in dilation and a decrease in breakage were recorded with an increase in the amount of stone overlying the ballast in the monotonic load tests (Figures 5.41 and 6.28). This again supports the theory that breakage reduced the amount of dilation occurring in the specimen.

In the cyclic load tests the layered specimens showed similar axial strain behaviour to that of the stone only and ballast only specimens, again with a greater variability seen in the layered specimens (Figures 5.42 to 5.46). The volumetric strain behaviour in the layered specimens showed, although not so clearly, that there was an increase in the amount of dilation with an increase in the amount of stone overlying the ballast. Due to a lack of data, no trend in the cyclic load tests between the amount of particle breakage

and the amount of stone overlying the ballast could be identified, as for the monotonic load tests. However it is possible, as long as there is enough lateral restraint from the surrounding ballast (Key, 1998), that an increased depth of stone may be beneficial to railway track maintenance.

Limited migration of the 20mm stone into the ballast was observed in the layered specimens, confirming earlier research (e.g. Chrismer, 1991 and Key, 1998) dispelling the fears that the smaller stone would block the voids. This also complies with the theory proposed by Cedegren (1989, Section 2.2.4.2), where for a small stone to pass through the larger stones it has to be 1/6.5 the size of the larger stones. This was far from the case with the 20mm stone and the 50mm ballast.

7.3.6 Series 5 – cyclic load tests on specimens with dampers

In Series 5 a damper was added to the specimens in the form of a rubber base mat and a disk of wood between the material and the top cap. It was clear from Figure 5.53 that damping of the specimens increased the amount of axial strain occurring over 100,000 load cycles compared to those specimens without the damping (Series 2). The resilient modulus for the damped specimens was significantly lower than for the specimens without the damping (Figure 5.70). A tenuous link was observed between the reduction of stiffness in the specimen and the increase in the amount of axial strain occurring.

It was apparent that alongside the decrease in stiffness there was also an increase in the amount of breakage occurring in the damped specimens (Figure 6.25). This was contradictory to the expected behaviour proposed in Section 5.6, possibly due to the rearrangement of particles throughout the test allowing particular particle weaknesses to be exploited. In these tests the dampers were inserted at the top and bottom of the specimen to simulate the railway environment to a slightly better degree. The results suggested that using large scale triaxial equipment without simulating the boundary parameters at the top and bottom of the specimen may give artificially low permanent strain measurements and also a reduced amount of breakages.

7.3.7 Series 6 – wetted specimens

With the wetted specimens in the monotonic load tests the stress-strain behaviour was very similar to that of the dry specimens in Series 2 (Figure 5.55), possibly even with slightly higher initial stiffnesses (E_t) (Table 5.4). Although it was difficult to be confident due to the limited number of tests it would seem that the volumetric strain behaviour of the wet and dry specimens was similar. The amount of breakage occurring

in the wetted specimens was also similar to that of the dry specimens (Figure 6.27 and Table 6.5).

In a fairly conclusive piece of work by Oldecop and Alonso (2001) described in Section 2.5 it was clear that the behaviour of rockfill material, under oedometer test conditions, was very much dependent on the water content. They presented a clear argument that the collapse behaviour in rockfill could be due to the reduction of strength in the rock upon wetting. This confirmed what Hardin (1985) concluded, that water greatly increased the crushability, or possibly decreased the particle hardness of the material. Oldecop and Alonso proposed that there were three boundary conditions where the moisture content did not effect the behaviour of the specimen i) where the stress level was below the clastic yield stress; ii) at very dry states where the moisture content was less than some value defined by the material; and iii) where the water content was greater than the full saturation of the rock pores. The rock pores are the voids within the individual particles.

In the tests carried out as part of Series 6, where the ballast was soaked for 24 hours and allowed to drip dry for 5 minutes before specimen preparation, the moisture content was approximately 1.7% to 1.8%. The maximum deviator stress at 40kPa cell pressure for the dry specimens (Series 2) and the wet specimens was 300kPa and 280kPa respectively. The maximum deviator stress at 90kPa cell pressure for the dry and the wet specimens was 525kPa and 410kPa respectively. The maximum deviator stress at 140kPa cell pressure for the dry and the wet specimens was 573kPa and 520kPa respectively. Although there was possibly a slight reduction in the shear strength of the ballast between the dry and wet tests it was possible that these differences were only reflecting test variability (see Figure 5.55) and not representing the effect of moisture content. It is possible that there was no effect of moisture content on the behaviour of the ballast as the stresses may have been below the critical stress (clastic yield stress) as discussed above. The clastic yield strength as determined by McDowell and Bolton (1998) is the value of the macroscopic stress which causes the maximum rate of grain fracture under increasing stress, for particles loaded in this configuration.

At these relatively low stresses, in tests with cell pressures up to 140kPa, the moisture content would therefore appear to have had limited effect on the stress-strain behaviour for the wet or dry material.

However, in the cyclic load tests the axial strains of the wet ballast specimens were some 100 to 200% higher than the dry specimens (Figure 5.57). In terms of volumetric

strain the pattern was not so clear, with the wet specimen at 40kPa cell pressure showing an increase in the amount of dilation compared to the dry specimen; and the wet specimens at the higher cell pressures showing an increase in the amount of compression compared to the dry specimens (Figure 5.58). With ballast soaked in water for 2 hours before testing, Key (1998) found an increase in plastic strain of approximately 70% when compared with the dry tests. Thom and Brown (1988) also reported an increase in the plastic strains with an increase in the moisture content with granular materials with high void ratios.

The increase in axial strains in the wet specimens was accompanied by a decrease in the resilient modulus, as seen in Figure 5.71, and an increase in the amount of breakage (Figure 6.26 and Table 6.5). A decrease in the resilient modulus with wetted materials was also noted by Thom and Brown (1988), Hicks and Monismith (1971) Dawson Gomes Correia (1996), Ping and Yang (1998), and Khogali and Zeghal (2000). Key (1998), Pappin et al. (1992) and Kolisoja (1997), however, found the resilient modulus was not affected by the presence of water. It may be that some of these fall into the three boundary regions where the moisture content did not influence the specimen behaviour as suggested by Oldecop and Alonso (2001) and described in Section 2.5.

It would appear that there were two mechanisms at work here. Firstly, as seen in the monotonic load tests, there was limited effect of the increased moisture content on the material behaviour. Secondly, in the cyclic load tests, the increase in moisture content had a definite effect on the material behaviour. It was therefore deduced that under the repeated stresses the moisture in the rock pores might possibly have caused pulsing pore pressures within the particles themselves as the micro-cracks flexed under loading. The particles were therefore broken up under this high impact pore pressure, which led to a decrease in the resilient modulus and an increase in the plastic strains. A third effect of moisture content on the increased plastic strain and decrease in resilient modulus may have been the effect of lubrication between the particles caused by the moisture as suggested by Thom and Brown (1988).

7.4 Further discussion on specimen behaviour

7.4.1 Effect of specimen end restraint in triaxial tests

Stress non-uniformities in the specimen, commonly known as dead zones, which are caused by the frictional resistance of the end platens and the membrane at the top and bottom extremities of the specimen, are know to hinder the lateral spreading of the

specimen as stated by Dawson and Gillett (1998). The effect of this on particle breakage is unclear, however there could be two opposing effects. i) With the restricted movement there will be less breakage occurring as the stiffer specimen appears to have less breakage (comparing Series 2 with Series 5), or, ii) with the restrictive movement there is more breakage occurring due to the load being applied, either repeatedly in the cyclic load test or with increasing stress in the monotonic load test, through the same column of particles. It is more likely that the former is true as it is widely recognised that the dead zones limit the amount of strain. If there was more breakage occurring as with the latter explanation, then one would expect more straining to have occurred. It is possible however, that the dampers used in Series 5 reduced the effect of the dead zones thus allowing the amount of strain to increase. In Series 5 the specimens with damping also had a greater amount of breakage, again supporting the former arguments where with the restricted movement (no dampers) there was less breakage.

7.4.2 Effects of particle size and distribution

During the dismantling of the tests it was clear that there had been virtually no particle breakage occurring with the 20mm stone, yet significant breakage occurred in the ballast specimens. This could be as a combined effect from several of the different parameters that influence the behaviour of the specimen, including particle size, grading, and shape. With the smaller stone the stress was assumed to pass through many more particles, decreasing the stress on individual particles.

Hardin (1985) states that the potential for a particle to break increases with the particle size. This is supported by the literature based on triaxial and oedometer testing (Section 2.6.1.2). However it would appear not to be that simple as found by Sammis et al. (1987) and McDowell and Bolton (1998). They found that there were two opposing effects of particle survival; these were the particle size versus the co-ordination number. Nakata et al. (2001a) found that with well graded sands, smaller particles underwent more severe damage than the larger ones. This was understood to be due to a lower co-ordination number for the smaller particles in a well graded material. Therefore although individually the smaller particles were stronger than the larger particles, in a matrix their probability for survival was lower.

Figure 6.29 shows for uniform specimens a slight trend where the probability of particle breakage increased with particle size, with monotonic load tests at 90kPa cell pressure. Yet at 140kPa no trend was identifiable in the data. The lack of identifiable trends was also noted in the breakage behaviour of the post cyclic monotonic load tests at 40kPa

cell pressure. In those tests, the number of abrasions and asperity breakages (Type II) (see Table 6.3), increased with particle size. Yet for more severe breakage (Type III or higher) a similar probability of breakage was observed across each of the particle sizes at 40kPa cell pressure. Whereas at 140kPa cell pressure the smaller sized particles were least likely to break.

It is possible that with the uniform material the smaller particles may not be included in the load path, but are 'at rest' in the voids between the larger particles. As the specimen becomes gradually more well graded throughout the test, for example in Figure 6.10, the effects described by Sammis et al. (1987) and McDowell and Bolton (1998) may be experienced. That is that with a more well graded specimen the smaller stones will be included in the load path and with a lower co-ordination number undergo greater particle breakage.

7.4.3 Effect of the rate of loading

Gaskin et al (1978) and Sato (1995) both suggested that the peak acceleration in the load cycle was a dominant factor in ballast settlement (i.e. the load waveform). It is postulated from the current work that this may actually be an effect due to increased particle breakage under the increased acceleration of loading. The load waveform used in the cyclic load tests would return very high accelerations of load onto the specimens. Possibly where the accelerations are less, say with a sinusoidal waveform (more akin to the railway environment) the breakage may also be less and hence the plastic deformation will be less and the resilient modulus higher. This effect may be more critical in the wet tests where any pore pressures within the particles would not be able to dissipate. This however would appear to be opposite to the findings of Yamamuro and Lade (1993) who found that fracturing and rearranging of soil particles required time and that with an increased strain rate the time factor was reduced. They found that increased strain rates in the specimen resulted in less compression and increased strength.

7.5 Volumetric strain behaviour model

It was clear from previous research (e.g. Key, 1998; Indraratna, 1993; and Indraratna, 2001) that with large granular materials (nominal 37mm-50mm railway ballast) what is considered to be normal critical state behaviour was not observed. This is where a loose specimen will compress and a dense specimen after initial compression will dilate. Furthermore in a dense material a peak stress will be reached and occur at the same

axial strain as the maximum rate of dilation (Atkinson, 1993). It would appear that the peak stresses in the above mentioned research (Key's and Indraratna's) did not coincide with the maximum rate of dilation. Similar patterns have been identified in the current work (Figures 5.12 to 5.15). In Section 7.3.3 it was taken that the behaviour of the ballast in the current work was behaving as a dense granular material as seen with the volumetric strain behaviour, where dilation was observed (Figure 5.15), and not as a loose granular material as was initially interpreted from the stress-strain graphs, where no clear peak was observed (Figures 5.12 and 5.13). It was therefore assumed that the stress would reduce with further straining, and peak stresses would be identifiable. It was also thought that the peak stresses might have actually been reached in the majority of the tests.

7.5.1 Premise behind the proposed volume strain behaviour model

There are thought to be two opposing actions that are occurring in the volumetric strain behaviour seen in these tests; that is the volumetric strain due to particle rearrangement during the shearing process ($\Delta V_{\varepsilon,s}$) and the volumetric strain due to particle breakage ($\Delta V_{\varepsilon,b}$). The total or observed volumetric strain behaviour ($\Delta V_{\varepsilon,total}$) can therefore be expressed as:

$$\Delta V_{\varepsilon,total} = \Delta V_{\varepsilon,s} + \Delta V_{\varepsilon,b} \qquad \text{Equ 7.1}$$

The volumetric strain due to particle breakage is contractive, taken as negative.

At present there is no method of directly quantifying or measuring either of the two components of the total volumetric strain. However the following observations have been made. A dense granular material, under shearing, is expected to undergo a slight initial contraction before dilation occurs, with the amount of dilation decreasing with increased confining pressure (e.g. Bishop, 1966). The behaviour of three monotonic load tests at 40kPa, 90kPa and 140kPa cell pressure are sketched in Figure 7.5(a). These are based on the ballast behaviour in the present work (Figure 5.13). The total observed volumetric strain behaviour ($\Delta V_{\varepsilon,total}$) is shown diagrammatically in Figure 7.5(b). The breakage volumetric strain behaviour ($\Delta V_{\varepsilon,b}$) could be similar to that proposed in Figure 7.5(c). This shows a slow initial increase in the amount of breakage, the rate of which increases with increased cell pressure (stage 1). Towards the end of the test the volumetric strain due to breakage levels off to an asymptotic strain with no further breakage occurring (stage 3). Although stage 3 is shown to occur at the same strain for each of the different cell pressures, this may not actually be the case. The

point at which critical state was reached was when the volumetric strain due to the change in particle arrangement (dilation, $\Delta V_{\varepsilon,s}$) and the volumetric strain due to breakage (compression, $\Delta V_{\varepsilon,b}$) both reached equilibrium, as was also described by Chandler (1985).

With higher cell pressures higher stresses are reached, the effect of this on the volumetric strain curve for breakage is seen in the central part of the volumetric strain curve (stage 2, Figure 7.5(c)), where there is a sudden increase in the volumetric strain behaviour associated with an increase in the amount of particle breakage. The point at which this occurs will be called the 'threshold of breakage' as defined on the stress-strain curves in Figure 7.5(a) and is presumed to be a lower stress limit for the onset of particle breakage occurs. At lower pressures this 'threshold of breakage' stress is not reached and only slight breakage occurs, hence the specimen does not exhibit stage 2 behaviour.

Possible curves for the volumetric strain behaviour due to shearing alone ($\Delta V_{\varepsilon,s}$) may look akin to those drawn Figure 7.5(d).

The shearing volumetric strain behaviour ($\Delta V_{\varepsilon,s}$) is not known. However using some simple assumptions an approximate volumetric strain due to breakage ($\Delta V_{\varepsilon,b}$) can be calculated as described in the following sections.

7.5.2 Approximation of the volume change due to breakage

A large amount of data for each test specimen was collected from the triaxial tests. The details and methods of which are described in Chapters 3 and 4. In summary this data included the number and size of particles included in the original specimen, the number and size of complete particles taken out of the specimen (which should be equal to the number and size of particles in the original specimen), a breakage score (B_s) for each particle, and the number and size of all the individual broken pieces of particles. From this data, tables were created similar to those in Tables 6.6 and 6.7, which summarise the amount and severity of breakage for each nominal size of particle.

Using this data an approximate calculation was made of the volume change due to breakage. The assumptions used in the calculations are given below.

i) All pieces of ballast that break off from the mother particle, no matter what size, move into the surrounding void spaces. This is based on the argument presented by McDowell and Daniell (2001). They stated that where there were large particles with a low coordination number, there are large void spaces surrounding that

particle, and when there was a low coordination number the particle was more susceptible to breakage.

ii) The approximate volume of a ballast particle can be represented by a simple angular solid.

A summary of the calculations are given below:

- For each specimen the number of particles in the original specimen (n_i), the void ratio (e), the original volume of the specimen (V_i), and the total volumetric strain ($\Delta V_{\varepsilon,total}$) at the end of the test were recorded.
- The volume of the solids (V_s) was calculated ($V_s = V_i / (1+e)$) from which the average single particle volume was also calculated ($V_{sp} = V_s / n_i$).
- The solid used for the modelling was a right square pyramid (rsp). Where the height (h_o) of the pyramid is the same as the length of the sides of the square base then the volume of the pyramid, $V_{rsp} = 1/3\ (h_o)^3$.
- In test T40 the average height of a single particle calculated using the square based pyramid described above was 44.8mm. This may have been slightly high when considering the size of the particles in the specimen, possibly due to the very approximate choice of shape.
- From test T40 data was recorded as in Table 7.2. A Type II (T_{II}) breakage of the aforesaid right square pyramid was approximated to $1/10^{th}$ of the height of the pyramid, as shown in Figure 7.6. A Type III (T_{III}) breakage was approximated to $1/5^{th}$ the height. A Type IV (T_{IV}) breakage was approximated to $1/3^{rd}$ the height. A Type V (T_V) breakage was approximately equivalent to 1/2 of the height of the pyramid. The breakage height taken off the pyramid is given in Table 7.3.
- The total volume of breakage could then be calculated as the sum of the volumes of all of the breakages (the first three terms of which are given in Equation 7.2), where each breakage volume (ΔV_{bj}) is calculated as $1/3 n_{bi} \times h_{bi}^3$.

$$\Delta V_b = -\sum_{j=1}^{j=n_i}\left[\frac{n_{b28}T_{II}\times(h_{b28}T_{II})^3}{3}\times\frac{n_{b37}T_{II}\times(h_{b37}T_{II})^3}{3}\times\frac{n_{b50}T_{II}\times(h_{b50}T_{II})^3}{3}\times.....\right] \quad \text{Equ 7.2}$$

Where all the terms are as defined in Table 7.2 and 7.3.

- For test T40 the total volume of breakage was calculated as 23580mm^3, this is approximately 11% of the observed total volume change of 221200mm^3. Therefore the volumetric change due to shearing was 244780mm^3 according to Equation 7.1.
- In Equation 7.2 the calculation of the volume change due to breakage (ΔV_b) is dominated by the breakage of the larger (50mm) particles. One or two significant

breakages (Type IV or V) would have a large impact on the calculation of the volume change due to breakage (ΔV_b).

7.5.3 Volumetric strain model

The stress-strain and volumetric strain curves from test T40 are shown in Figure 7.7(a and b). The solid line in Figure 7.7(b) shows the total observed volumetric strain and the dashed line shows the proposed volumetric strain due to shearing alone where no breakage occurs ($\Delta V_{\varepsilon,s} = \Delta V_{\varepsilon,total} - \Delta V_{\varepsilon,b}$). The dotted lines show the expected total volumetric strain and the shearing volumetric strain behaviour past the end of the test. The volumetric strain due to breakage ($\Delta V_{\varepsilon,b}$) was calculated as 0.13% at the end of the test. The total observed volumetric strain ($\Delta V_{\varepsilon,total}$) recorded at the end of the tests was 1.21%. Using Equation 7.1 the volumetric strain due to shearing alone ($\Delta V_{\varepsilon,s}$) was calculated as 1.34%. From this proposed model there are four main points that emerged.

i) The breakage behaviour had little influence on the total volumetric strain behaviour at small strains (stage 1).
ii) The breakage of the particles caused the total volumetric strain curve to become flattened in the middle (stage 2), as postulated by Yamamuro and Lade (1993) (Figure 2.18).
iii) This flattening of the volumetric strain curve disguised the true volumetric strain behaviour due to shearing alone, and although from the total volumetric strain graphs it would appear that the specimen was far from approaching critical state it can be seen that it could in fact be very close to critical state (stage 3). It should be noted that on similar testing material Indraratna (1998) reported high rates of dilation were still occurring at 20% axial strain.
iv) The breakage behaviour was also considered to have flattened any possible peak in the stress-strain graph. The solid line in Figure 7.7(a) shows the stress-strain graph as observed from test T40. The dashed line shows a possible alternative should no breakage occur.

These calculations were carried out for all of the triaxial tests where the necessary data was available. The values for the observed total volumetric strain ($\Delta V_{\varepsilon,total}$), the calculated volumetric strain due to breakage ($\Delta V_{\varepsilon,b}$) and the calculated volumetric strain due to shearing at the end of the test ($\Delta V_{\varepsilon,s}$) are presented in Table 7.4, which for the monotonic load tests in Series 2 shows that the volumetric shear strain ($\Delta V_{\varepsilon,s}$) at 140kPa

was very close to that at 90kPa cell pressure. In Series 6 the volumetric shear strain ($\Delta V_{\varepsilon,s}$) at 140kPa cell pressure was greater than it was at 90kPa cell pressure. This would therefore suggest that the calculated volumetric strains due to breakage may have been slightly too high. This may have been partly due to the upper sieve size being used as the nominal particle size thus assuming bigger sized particles. Taking the average size between the sieve sizes may be more appropriate and give more realistic results.

As the stress-strain and volumetric strain behaviour of the wet and dry specimens in the monotonic load tests were similar (Figures 5.55 and 5.56), and the total breakage scores (B_{TBS}) were also similar one would also expect the volumetric strains due to breakage ($\Delta V_{\varepsilon,b}$) to be similar. From Table 7.4 it can be seen that the volumetric strain due to breakage ($\Delta V_{\varepsilon,b}$) for the wet and dry specimens are comparable, which shows the consistency of the model between specimens with like behaviour.

The model has been formulated based on some simple assumptions and a simple angular solid to represent the ballast particle. These may have caused an over-calculation of the volumetric strains due to breakage ($\Delta V_{\varepsilon,b}$). However it is proposed that the model itself is not at fault and could be developed further, possibly with the use of computer modelling and with more detailed information on the size and shape of the ballast particles before and after testing.

7.5.4 Relating the model to other tests

The model outlined above was based on the observations, trends and data recorded from the monotonic load tests on nominal 50mm ballast specimens. In the following sections the behaviour of the monotonic load tests on stone specimens, the behaviour of the cyclic load tests and the behaviour of the post cyclic monotonic load tests will be briefly discussed in the light of the proposed model.

7.5.4.1 Stone specimens

As described previously no breakage analysis was carried out on the 20mm stone, as there appeared to be minimal breakage. It can be seen in Figures 5.12 and 5.14 that similar stress-strain and volumetric strain behaviours were apparent in the stone specimens as with the ballast specimen (Figures 5.13 and 5.15). In light of the above proposed volumetric strain model this would suggest that breakage was occurring in the stone also, reducing the peak stress and flattening the volumetric strain curve. It is possible that minor breakage did occur in the stone and although the specimens could

not be analysed using the particle breakage scores as with the ballast particles some form of sieve analysis may have proved that a recordable amount of breakage was occurring. Unfortunately it was too late in the test programme to investigate this further.

Although Bishop (1966) agreed with the effect of particle breakage reducing the amount of dilation (at high cell pressures), he also found in tests using steel shot that there was still, to a lesser extent, a decrease in the amount of dilation even though there was no breakage or squashing of the particles. It is possible even at the low pressures used during this research that this was apparent in the 20mm stone specimen tests (Figures 5.12 and 5.14).

7.5.4.2 Post cyclic monotonic load tests

In the post cyclic monotonic load tests the stress-strain and volumetric strain behaviours were fairly similar to that in the monotonic load tests as described in Section 5.3.4. The main differences were that:

i) The initial stiffnesses in the post cyclic monotonic tests were significantly higher than in the initial monotonic load tests (Table 5.4). This caused a definitive peak to be formed in the lower cell pressure tests (40kPa and 90kPa – see Figure 5.24).

ii) There was virtually no initial compaction in the post cyclic monotonic load tests and the rate of dilation was significantly higher (Figure 5.26).

The curves from Figure 5.24 and 5.26 have been sketched in Figure 7.8(a) and 7.8(b). Figure 7.8(b) shows the observed total volumetric strain behaviour ($\Delta V_{\varepsilon,total}$) represented by the solid lines. The dashed lines show the proposed volumetric strain due to shearing alone ($\Delta V_{\varepsilon,s}$) for the 40kPa and 90kPa cell pressure tests as expressed by the model. From this two very clear trends were identified.

i) On the stress-strain curve Figure 7.8(a) the point at which the curve breaks away from the initial straight line (tangent at zero strain) in the post cyclic monotonic load tests was significantly higher than in the monotonic load tests. Some authors may refer to this point as the yield point. For the purposes of this work it was identified as the 'break point'. The higher 'break point' in the post cyclic monotonic load tests compared to the monotonic load tests suggests that many of the weaker particles/asperities had already fractured during the cyclic load tests. Hence there was only limited breakage occurring up to the break point and no associated reduction in the peak stress. The 'break point' stresses (approximately

between 480kPa and 600kPa) were much closer to the characteristic strengths (416kPa and greater) observed in the single particle crushing tests (Section 6.2).

ii) On the volumetric strain curve Figure 7.8(b) (also seen in Figure 5.26) it was noted that within the first 1% axial strain a peak rate of dilation occurred, after which there rate of dilation slightly dropped. As can be seen from the volumetric strain curve due to shearing alone ($\Delta V_{\varepsilon,s}$) it was proposed that this be attributed to the particle breakage behaviour. It is possible that the start of this behaviour was actually closely related to the 'break point' identified with the stress-strain behaviour in the previous paragraph.

7.5.4.3 Cyclic load tests

The model for the cyclic load tests needs to be slightly different, as the threshold stress value was never approached with the maximum deviator stress being some 50% less than the supposed 'threshold stress' defined in Figure 7.5(a) (250kPa compared to 500kPa respectively). As can be seen from Table 6.5 the amount of breakage recorded in each of the cyclic load tests was significantly lower than the breakage in the monotonic load tests with equivalent cell pressures. The proposed volumetric strain behaviour model described above would give a slightly different curve of volumetric strain due to shearing alone ($\Delta V_{\varepsilon,s}$) than that from the curve of the observed volumetric strain ($\Delta V_{\varepsilon,total}$) (see Figure 5.21), showing slightly less shearing. It was assumed that during the first few load cycles a significant proportion of the breakage occurred, which then continued slowly with the application of load cycles (see Series 3 results in Table 6.5). The breakage of particles was assumed to occur due to fatigue failure rather than a pure tensile fracture as was tested in the single particle crushing tests. The breakage behaviour (and also the strain behaviour) in Series 3 (Table 6.5) showed there to be a threshold in the number of load cycles after which an increase in particle breakage occurred due to the repetitive weakening of the particles.

In Table 7.5 the development of the volumetric strain behaviour due to breakage ($\Delta V_{\varepsilon,b}$) in the cyclic tests can be seen (as calculated according to the model). Also in Table 7.5 the observed total volumetric strains ($\Delta V_{\varepsilon,total}$) are reported and the volumetric strains due to shearing ($\Delta V_{\varepsilon,s}$) have been calculated using Equation 7.1. It can be seen that the volumetric shear strain ($\Delta V_{\varepsilon,s}$) continues to increase gradually with the application of load cycles.

7.5.5 The performance of layered and damped specimens in the model

There were no particular anomalies noticed in the monotonic load tests on layered specimens (Table 7.4). In the post cyclic monotonic load tests the amount of volumetric strain due to breakage ($\Delta V_{\varepsilon,b}$) was noted to drop with an increase in the amount of stone overlying the ballast. This was as expected as there would have been less ballast particles available to break. There was only one layered specimen cyclic load test (test T41) that did not have a post cyclic monotonic load test; there was nothing unusual about the results calculated.

Similarly no anomalies were noted with the damped specimens from Series 5. The two tests with ballast in Series 5 had relatively low levels of particle breakage, giving only slight differences between the total observed ($\Delta V_{\varepsilon,total}$) and shearing ($\Delta V_{\varepsilon,s}$) volumetric strains. The volumetric strain due to breakage ($\Delta V_{\varepsilon,b}$) was slightly higher for the damped ballast specimens in Series 5 than the ballast only specimens in Series 2. This was as would be expected, as the total breakage score (B_{TBS}) was higher in the damped ballast specimens than the ballast only specimens

7.5.6 Summary of volumetric strain model

In the light of what has been discussed above, this could explain the reasons for the original shakedown model (Figure 2.27) not being totally applicable to granular materials as discussed by Werkmeister et al. (2001) and seen in Figure 2.29. They showed that for an angular sand there was no elastic shakedown apparent in the initial stages of the test, i.e. cyclic loading with no permanent strain and that the zone of plastic shakedown was entered straight away. This was believed to be because during the first few load cycles there would have been a slight rounding/fracture of many of the asperities allowing plastic strains to occur. However the stresses induced in the cyclic load tests in the current work were a lot lower than the stresses needed to cause even initial fracture in the single-particle crushing tests. The reason for this may be quite simple. The breakage occurring at relatively low stresses is thought to be due to the arrangement of particles and the transfer of stress through the specimen as discussed by McDowell and Bolton (1998). The type of breakage most common in the triaxial tests (Type II asperity breakage) is unlikely to have been tested during the single-particle crushing tests. It is possible that the initial crushing values determined in the single-particle crushing tests were actually for larger breakages of Type III or higher.

The model has provided more insight into the behaviour of granular materials showing that the volumetric strain due to breakage ($\Delta V_{\varepsilon,b}$) can play a significant part in the total observed strain behaviour ($\Delta V_{\varepsilon,total}$). It also offers an explanation into why such materials may not conform to typical critical state soil mechanics predictions.

It is apparent from the above discussion that the model needs improving. However it has shown that the amount of volumetric shear strain may be approximately calculated. Further testing is required, especially in the monotonic load test with the tests being taken up to different amounts of strain and the breakage calculated. Greater detail about the size and shape of the individual particles in the tests may also be required to enhance the performance of the model.

7.6 Discussion of the current work in relation to shakedown theory

The shakedown model was described in detail in Section 2.7. Figure 5.5 shows possibly all three types of behaviour as described by Werkmeister et al. (2001) and discussed below. Range A, is that of plastic shakedown, where the rate of strain decreases to almost nothing (test T9, Bardon stone - 90kPa cell pressure). Range C, is that of incremental collapse or ratcheting (tests T11 and T13, Cloburn stone - 40kPa cell pressure). Werkmeister et al. observed that the closer the stress level was to the (assumed) monotonic load failure stress then the decrease in the strain rate was reduced. In Range C, they assumed particle abrasion and crushing occurred.

In the current work the average peak deviator stress of the Cloburn stone specimens at 40kPa cell pressure under monotonic loading (T1 and T6) was recorded as between 260kPa and 310kPa (Table 5.1), although the failure load could be as low as 125kPa – 175kPa (Figure 5.1). This average peak deviator stress was close to the controlled maximum cyclic load of 250kPa, although impact loads at the point of loading the specimen reached as high as 300kPa – 350kPa in some cases. Range B (after Werkmeister et al.), was termed intermediate response – plastic creep. The initially high strain rate rapidly reduced to a relatively low rate, which may have been approaching a constant strain rate. When plotted in terms of rate of strain versus accumulated strain the differences in behaviour were a lot more apparent as seen in Figure 7.9. From this it can be seen that all of the tests may actually only be in Ranges A and B.

The load regimes of the cyclic load tests have been plotted onto the model proposed by Werkmeister et al. (Figure 2.30), in Figure 7.10. The differences in the models are

verified in Figures 7.11 for the stone and ballast specimens. In the majority of cases the data fitted well within the model even though the model was designed for sandy gravel material with 4% moisture content. For the stone specimens it was seen that the cyclic load tests all head towards an asymptotic final axial strain value similar to that described by Range A. With the ballast specimens the tests at 90kPa, 140kPa and 240kPa cell pressure could also be described as Range A. The 40kPa cell pressure test however was more akin to Range B, where the specimen may have been heading for constant rate of axial strain.

With the wetted specimens in Series 6, as seen in Figure 7.12, the tests at 90kPa and 140kPa cell pressure could be described as Range A, however at 40kPa the specimen was definitely in Range B. A third axis could possibly be included onto the Werkmeister et al. (2001) model to include the effect of the moisture content. By carrying out a programme of cyclic load tests with a range of different deviator stresses and moisture contents this 3-D model could be developed.

7.7 Laboratory test conclusions

The results from triaxial tests on eighty three specimens and from one hundred and twenty single-particle crushing tests have been discussed. From the results and discussions on these laboratory tests the following conclusions have been made.

1) Although the observed patterns and trends in the triaxial test results were similar to those reported in other research the absolute values were not. It is possible that the differences were due to four main factors. i) The materials used were of differing strengths, shapes and sizes; ii) The grading of the specimens in the different test programmes varied; iii) The loading regimes were not comparable; iv) The majority of the specimens tested in other work were saturated or partially saturated; few authors reported tests on dry materials.

2) Assuming the specimens remained a right-angled cylinder when calculating the volume change with large sized granular material requiring higher axial strains was inappropriate due to significant barrelling of the specimen. In the monotonic load tests the new volume change unit proved that the measured volumetric strains were some three times lower (in dilation) than the calculated volumetric strains (Section 3.3.4).

3) Breakage of the ballast particles appeared to reduce the amount of dilation in the monotonic load tests even at a low cell pressure (40kPa). At higher cell pressures

(90kPa and 140kPa) increased breakage reduced the amount of dilatancy further. This reduction in dilation was thought to cause a flattening of the peak in the deviator stress-strain graphs (Section 7.5.3).

4) In the post cyclic monotonic load tests there were clear peaks in the stress-strain behaviour at 40kPa cell pressure. It was postulated that this was due to breakage having already occurred in the cyclic load tests and hence limited breakage occurring during the early stages of the post cyclic monotonic load tests (Section 7.5.4.2).

5) Particle breakage occurred at lower stress levels in the triaxial tests than in the single-particle crushing tests. This was due to the single-particle crushing test using two flat platens to crush the particles, which did not fully replicate the loading regime applied to the particles in a soil matrix (Section 7.3.3).

6) In the layered specimens at low cell pressures (40kPa) the amount of stone overlying the ballast did not affect the overall compressive strength in the monotonic load tests (Section 7.3.5). However the amount of dilation occurring did increase with the amount of stone overlying the ballast. These patterns were also observed in the cyclic load tests. Only a limited amount of migration of the overlying 20mm stone into the ballast layer was observed.

7) There was a clear relationship between the increase in the amount of stone overlying the ballast and the decrease in the amount of ballast breakage occurring in the specimens (Section 6.3.4).

8) The lower resilient modulus of the damped specimens using a rubber base mat and a wooden disc between the top cap and the material led to an increase in the amount of plastic strain under cyclic loading, which was associated with an increase in the amount of breakage. This behaviour was contrary to that proposed before the test series commenced (Section 7.3.6).

9) In the monotonic load tests with wetted specimens the compressive strengths and the amounts of particle breakage were similar to those observed with the dry specimens. However a significant increase in the amount of plastic strain and breakage was observed in the cyclic load test on the wetted specimens compared with the dry specimens (Section 7.3.7).

10) A model was developed to consider the mechanisms causing volumetric straining of the specimen (Section 7.5). An approximate volume change due to breakage

was calculated which gave insight into the reduction in the amount of dilation caused by the particle breakage. A similar pattern of total volumetric strain behaviour was also seen with the stone specimens, albeit to a lesser extent. Slight breakage was observed in the stone during the test programme and with an appropriate testing technique the amount of breakage occurring in the stone specimens may also be calculated.

11) The behaviour of the Bardon 20mm stone was significantly different to the Cloburn 20mm stone under cyclic loading (Section 7.3.2). There was no apparent difference in behaviour with monotonic loading.

Specimen	Key φ'	Current work φ'
Ballast 40kPa	49°	53°
Equal layers 40kPa	48°	53°-54°
Stone 40kPa	50°	52°

Table 7.1 - Comparing the value of angle of shearing resistance (φ') with Key's (1998)

Severity of breakage	for a 28mm particle (n_{b28})	for a 37mm particle (n_{b37})	for a 50mm particle (n_{b50})
Type II breakage (T_{II})	6	22	20
Type III breakage (T_{III})	2	20	18
Type IV breakage (T_{IV})	-	3	3
Type V breakage (T_V)	-	1	1

Table 7.2 - Summary table of the number of broken particles (n_b) in Test T40

Severity of breakage	for a 28mm particle (h_{b28}) (h_o = 28mm)	for a 37mm particle (h_{b37}) (h_o = 37mm)	for a 50mm particle (h_{b50}) (h_o = 50mm)
Type II breakage (T_{II})	(h_o * $^1/_{10}$ =) 3mm	(h_o * $^1/_{10}$ =) 4mm	(h_o * $^1/_{10}$ =) 5mm
Type III breakage (T_{III})	(h_o * $^1/_5$ =) 6mm	(h_o * $^1/_5$ =) 7mm	(h_0 * $^1/_5$ =) 10mm
Type IV breakage (T_{IV})	(h_o * $^1/_3$ =) 9mm	(h_o * $^1/_3$ =) 12mm	(h_o * $^1/_3$ =) 17mm
Type V breakage (T_V)	(h_o * $^1/_2$ =) 14mm	(h_o * $^1/_2$ =) 18mm	(h_o * $^1/_2$ =) 25mm

Table 7.3 - Approximated height of breakage (h_b) from the pyramid

		Test details and cell pressure (kPa)	Specimen no.	$(\Delta V_{\varepsilon,b})$ (%)	$(\Delta V_{\varepsilon,total})$ (%)	$(\Delta V_{\varepsilon,s})$ (%)
Series 2	mono tonic	90	T40	0.13	1.21	1.34
		140	T60	0.52	0.80	1.32
	cyclic	40	T38	0.02	-0.80	-0.78
		140	T64	0.01	-1.27	-1.26
	post cyclic mono.	40	T57	0.18	5.71	5.89
		140	T61 T62	0.54 0.78	4.75 2.15	5.29 2.93
Series 3	cyclic	90, 2Million cycles	T42	-	-	-
		90, 1Million cycles	T75	0.03	-1.44	-1.41
		140, 100 cycles	T65	0.00	-0.22	-0.22
		140, 1000 cycles	T66	0.01	-0.44	-0.43
		140, 10,000 cycles	T67	0.03	-0.72	-0.69
Series 4	monotonic	40, single layer 20mm	T50	0.10	2.64	2.74
		40, double layer 20mm	T52	0.08	2.52	2.60
		40, 1:2layered	T53	0.04	3.45	3.49
		40, 1:1layered	T44	0.02	4.92	4.94
		40, 2:1layered	T49	0.02	5.39	5.41
	cyclic	90, single layer 20mm	T41	0.02	-2.15	-2.13
	post cyclic monotonic	40, single layer 20mm	T48	0.32	4.12	4.44
		40, double layer 20mm	T51	0.19	6.90	7.09
		40, 1:2layered	T46	0.11	6.77	6.88
		40, 1:1layered	T45	0.06	7.70	7.76
		40, 2:1layered	T47	0.02	6.19	6.21
Series 5	cyclic	140, ballast with damping	T69	0.03	-1.67	-1.64
		140, double layer 20mm, with damping	T70	0.02	-1.52	-1.50
Series 6	monotonic	40, wet material	T81	0.14	2.46	2.60
		90, wet material	T82	0.24	0.92	1.16
		140, wet material	T79	0.47	0.80	1.27
	cyclic	40, wet material	T80	0.15	-0.68	-0.53
		90, wet material	T83	0.11	-1.84	-1.73
		140, wet material	T78	0.16	-2.64	-2.48

Table 7.4 – Summary of the volume change characteristics for the ballast specimens in Series 2, and Series 4-6

Test No.	No. of Cycles	$\Delta V_{\varepsilon,total}$	$\Delta V_{\varepsilon,b}$	$\Delta V_{\varepsilon,s}$
T65	100	-40,670	904	-39,766
T66	1000	-81,130	1387	-79,743
T67	10,000	-133,820	4782	-129,038
T64	100,000	-237,210	2485	-237,210

Table 7.5 - Summary of the volume change characteristics for the specimens in Series 3

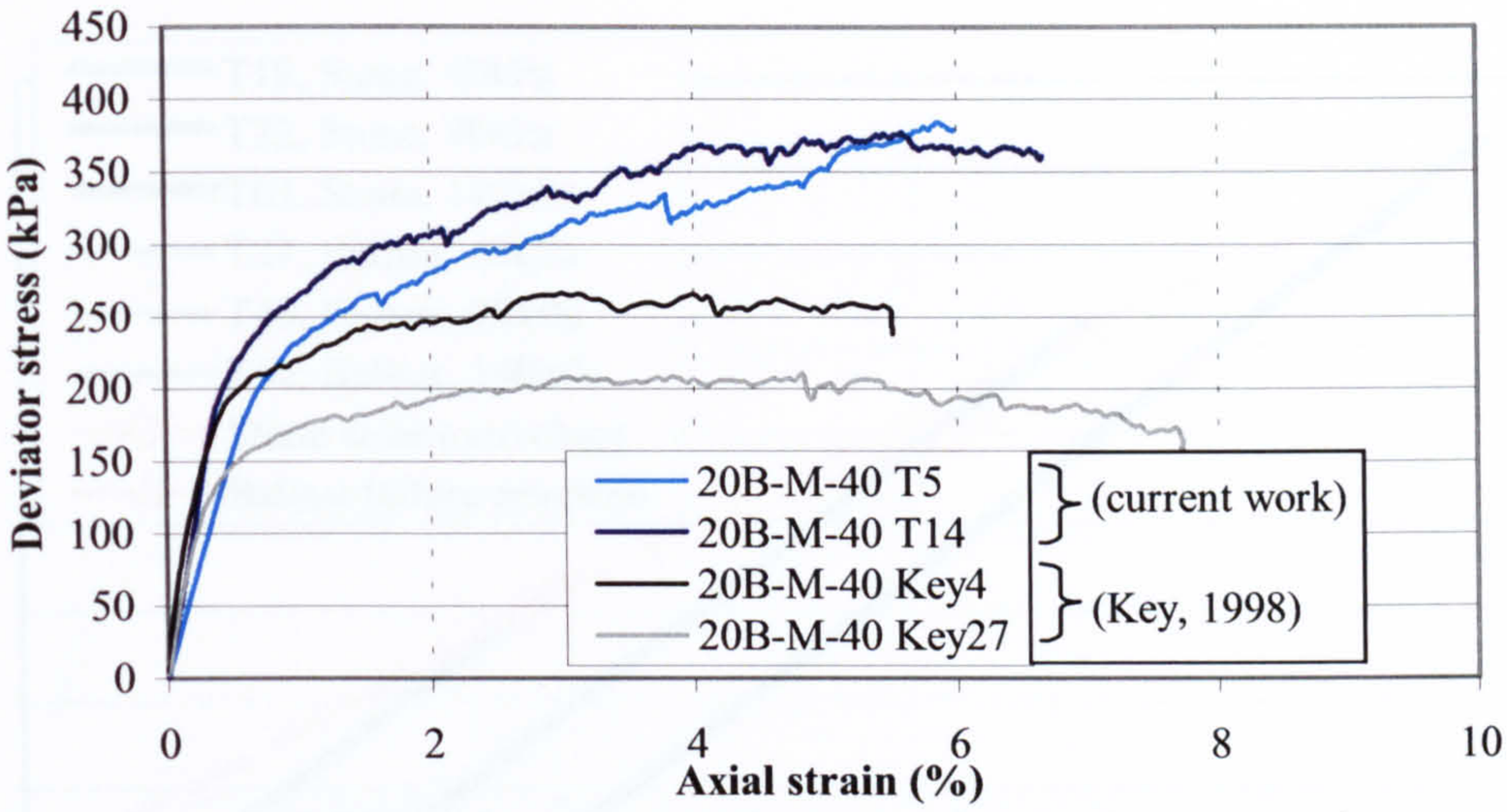

Figure 7.1 - Repeatability of stress-strain behaviour of monotonic tests in the current research and those of Key (1998)

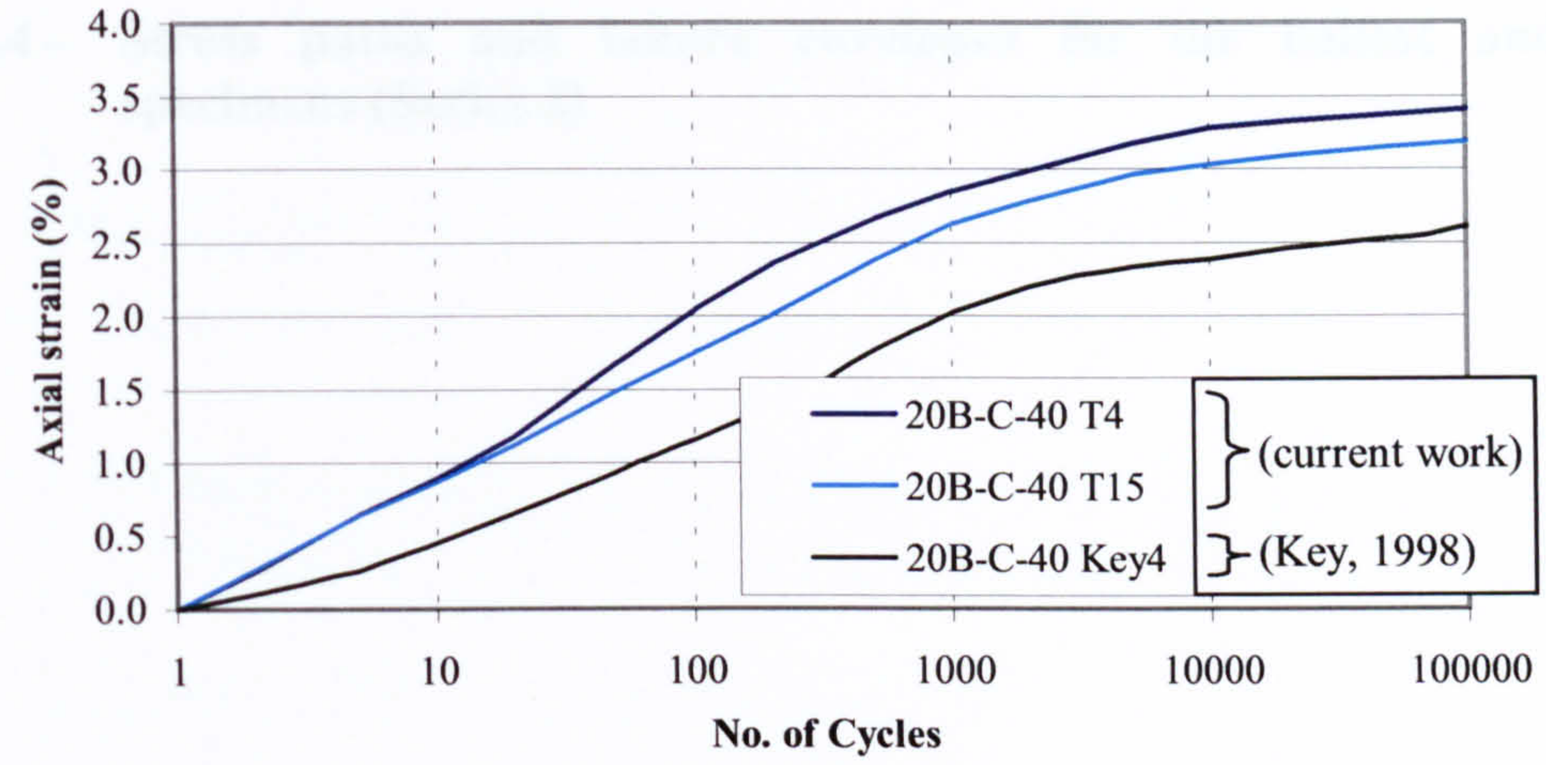

Figure 7.2 - Repeatability of axial strain behaviour of cyclic load tests in the current research and those of Key (1998)

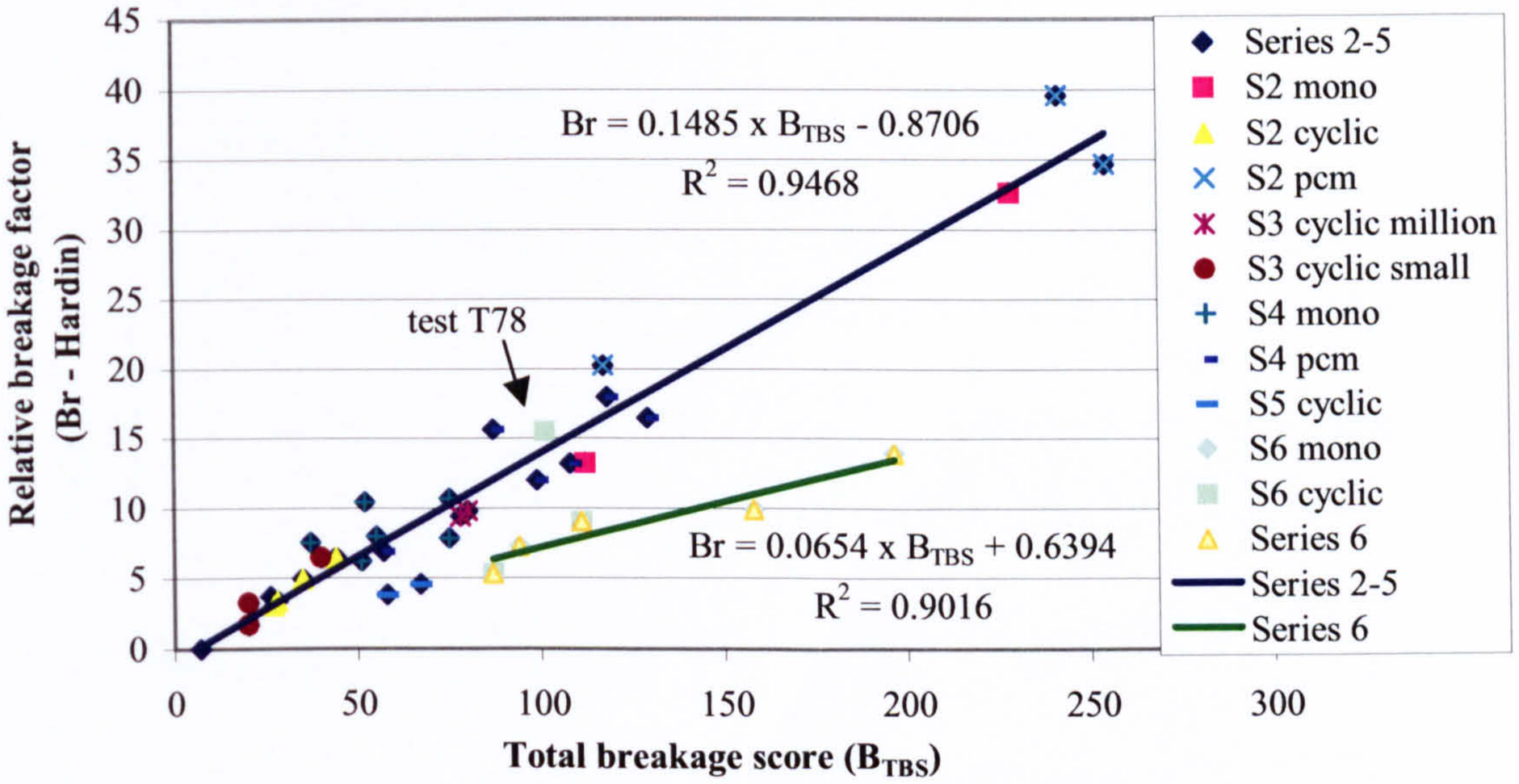

Figure 7.3 - Correlation between Hardin's (1985) relative breakage factor (B_r) and the total breakage score (B_{TBS})

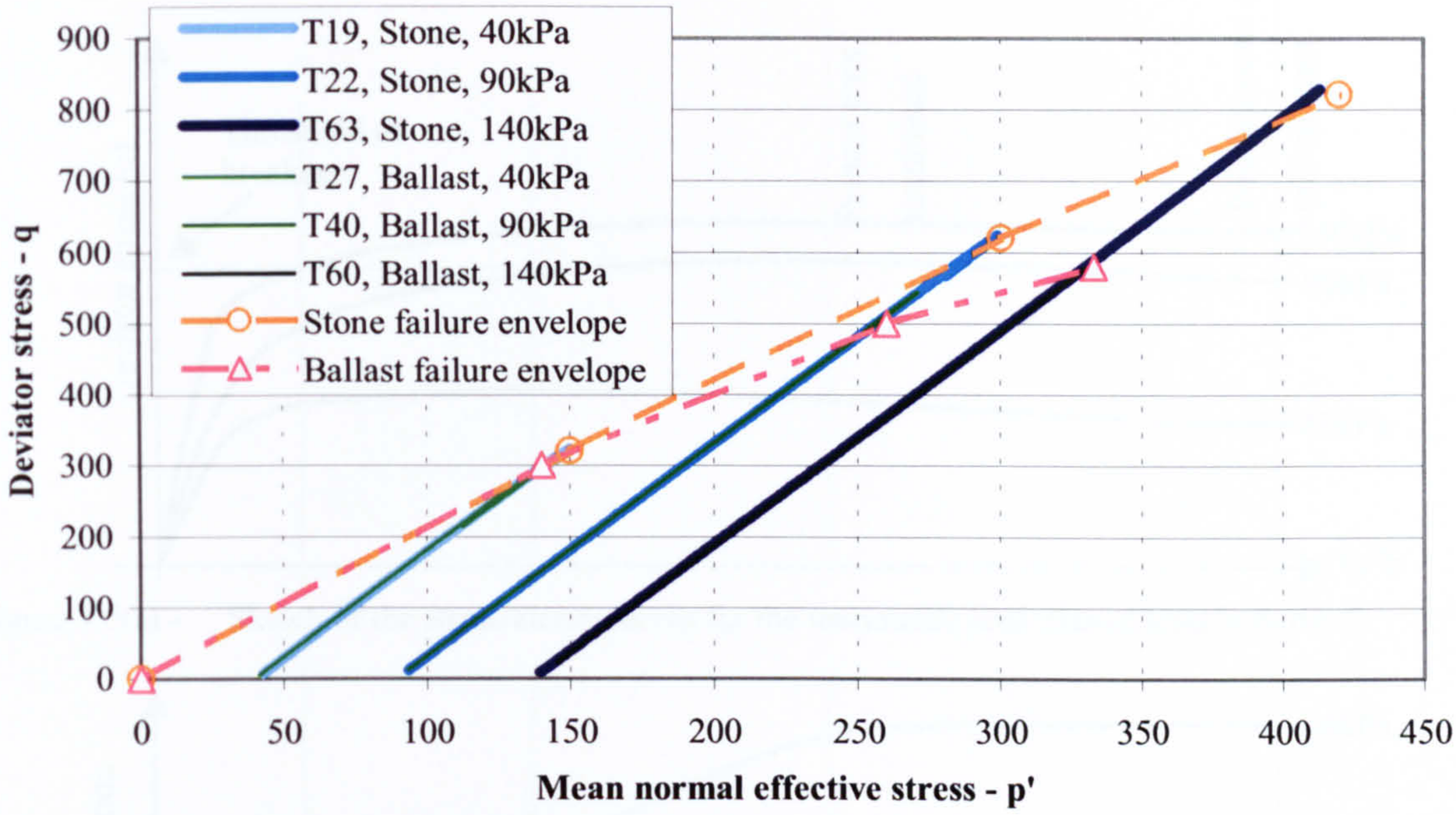

Figure 7.4 - Stress paths and failure envelopes for the ballast and stone specimens (Series 2)

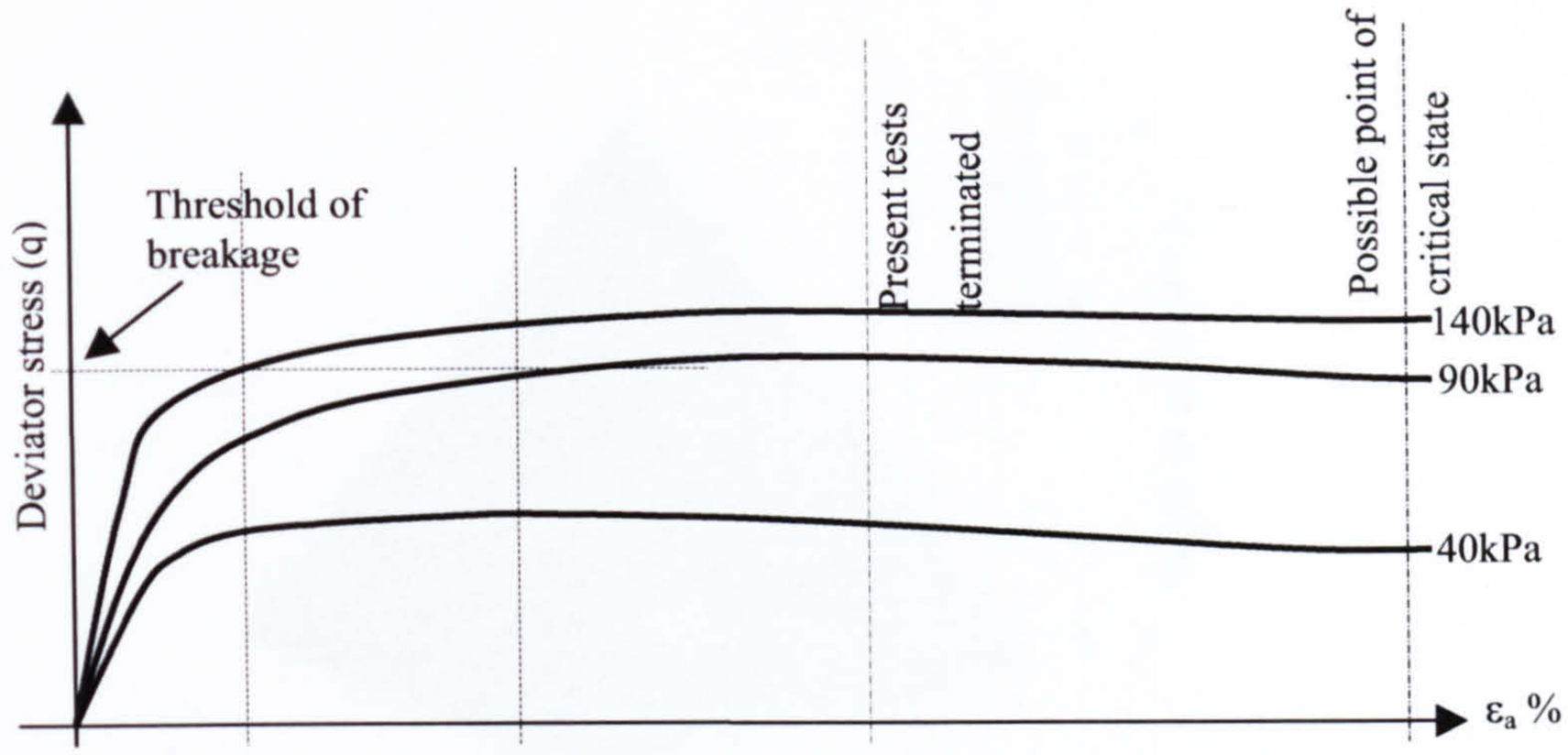

Figure 7.5(a) - Sketch of the stress-strain curves for the monotonic load triaxial tests in Series 2

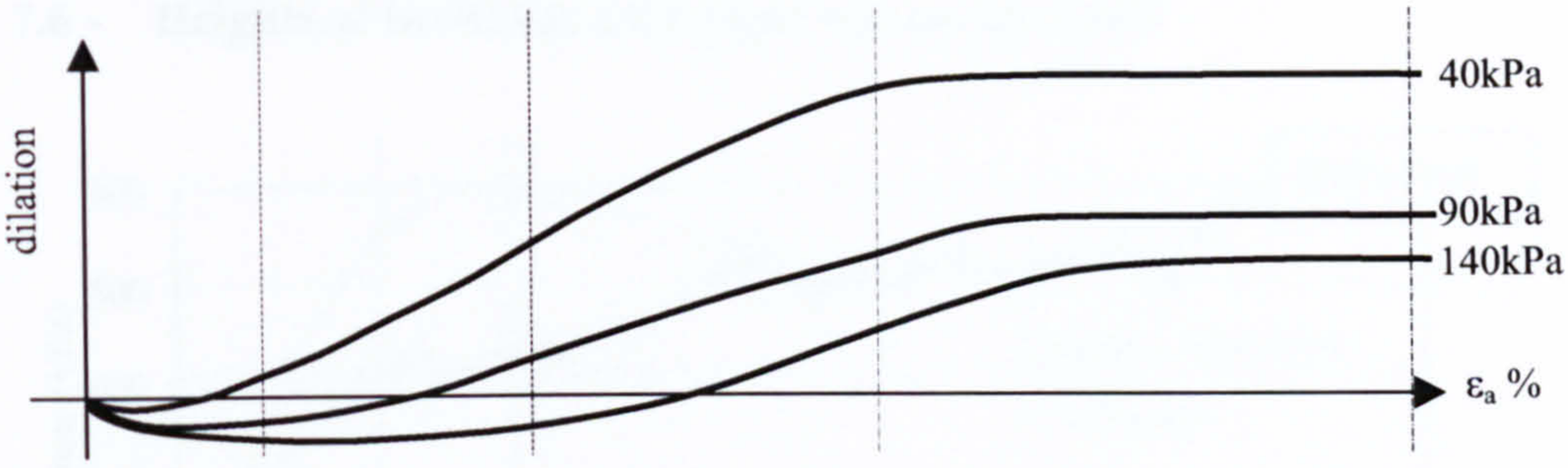

Figure 7.5(b) - Sketch of the observed volumetric strain curves ($\Delta V_{\varepsilon,total}$)

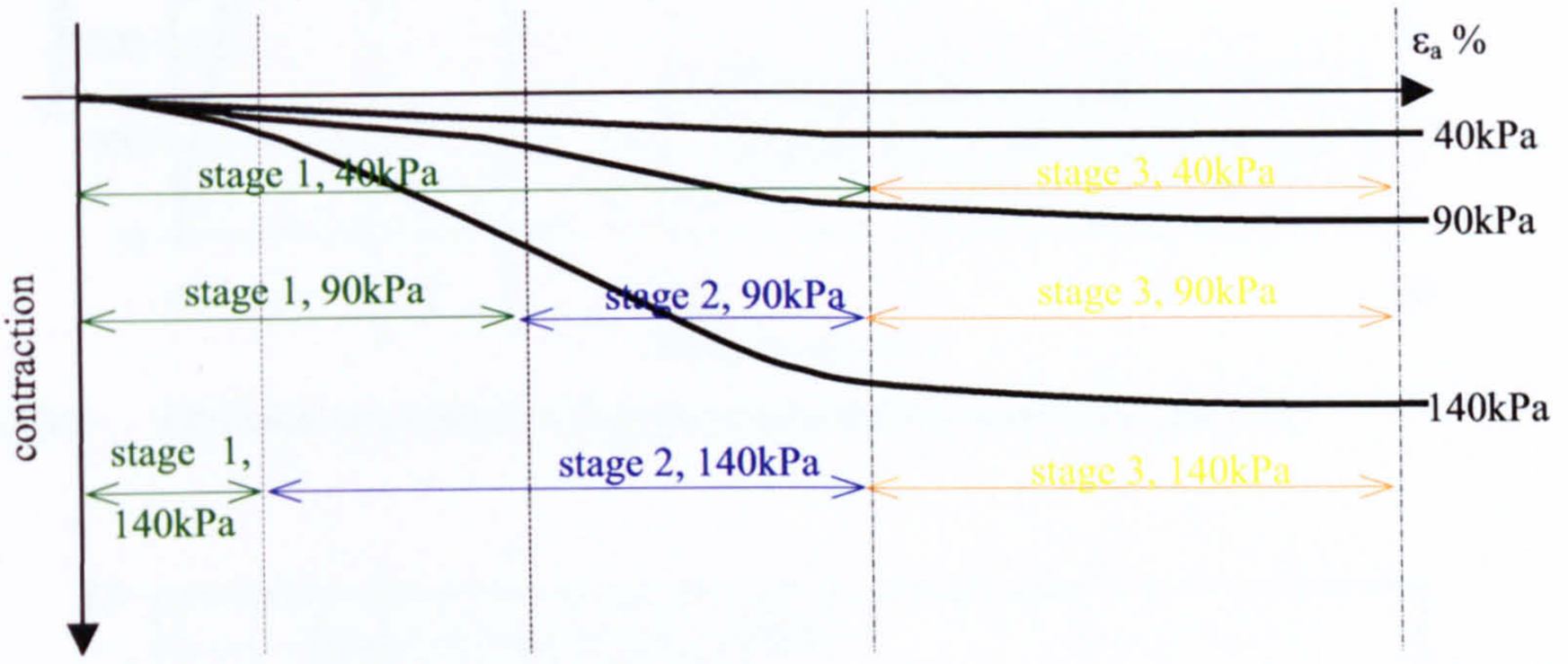

Figure 7.5(c) - Sketch of the proposed volumetric strain curves for breakage ($\Delta V_{\varepsilon,b}$)

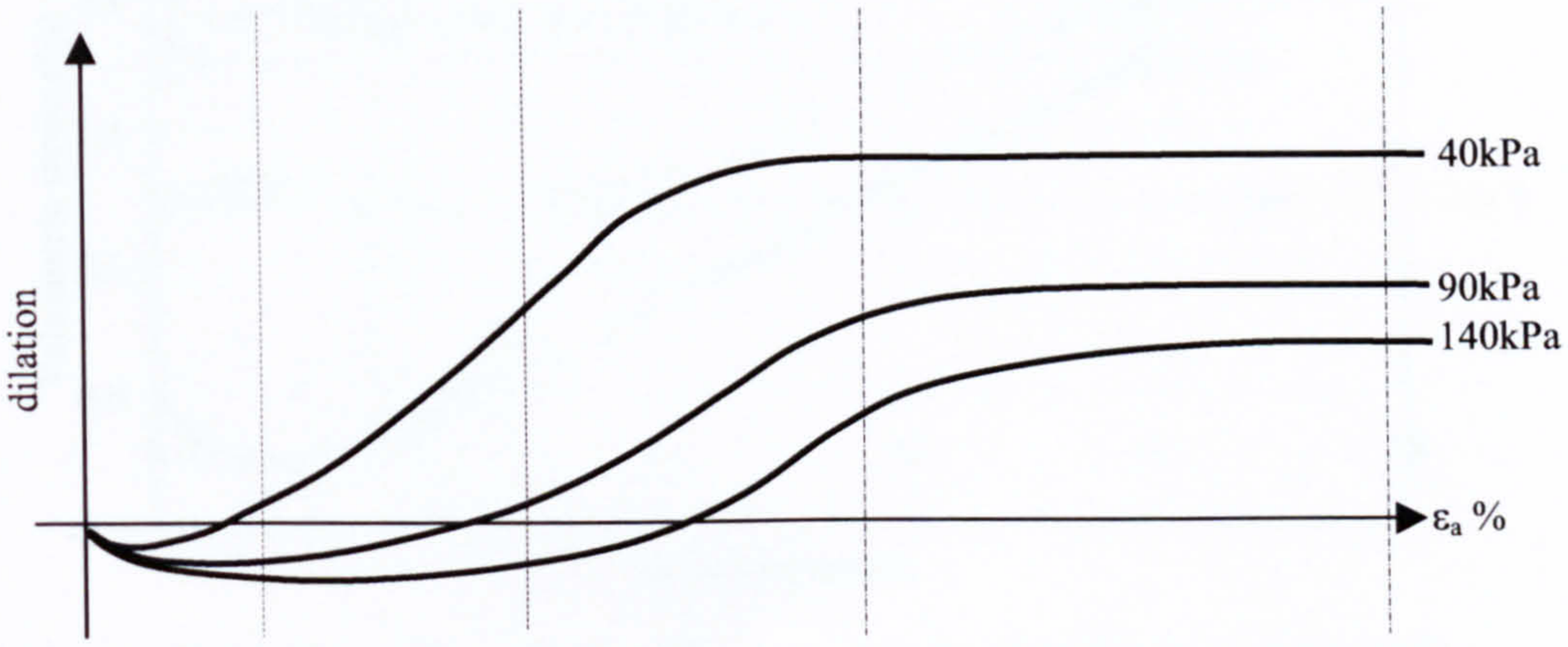

Figure 7.5(d) - Sketch of the proposed volumetric strain curves due to shearing ($\Delta V_{\varepsilon,s}$)

Figure 7.5 - Stress-strain and volumetric strain behaviour as proposed by the volumetric strain behaviour model

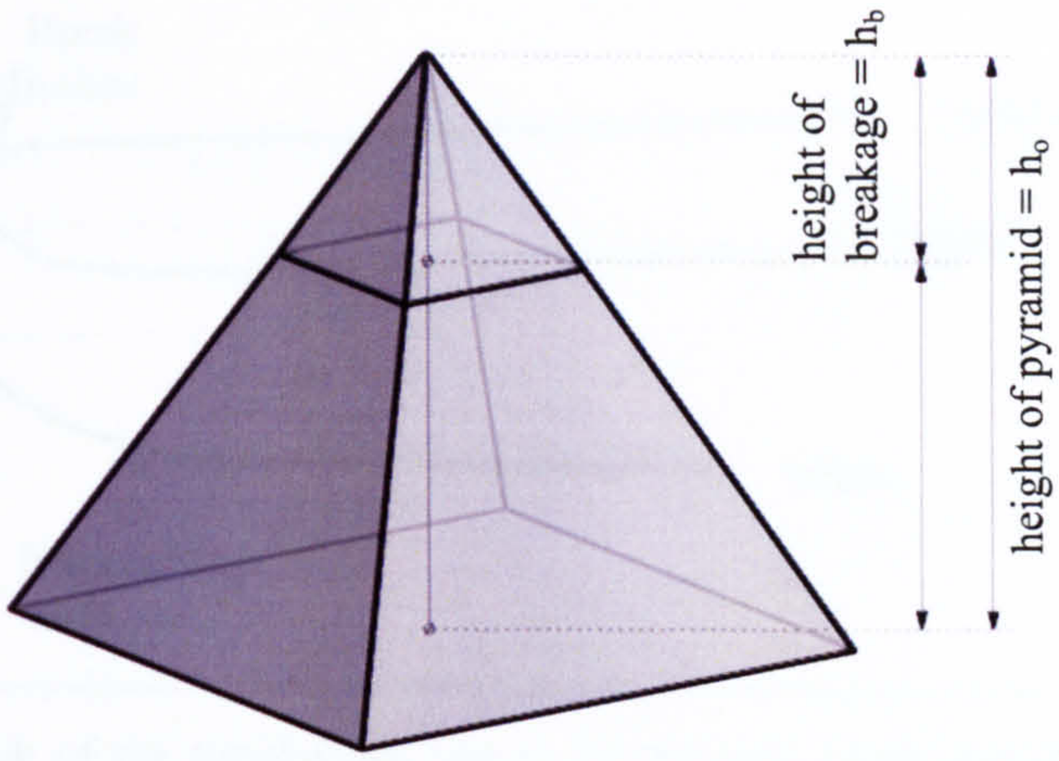

Figure 7.6 - Heights of breakage on a right square pyramid

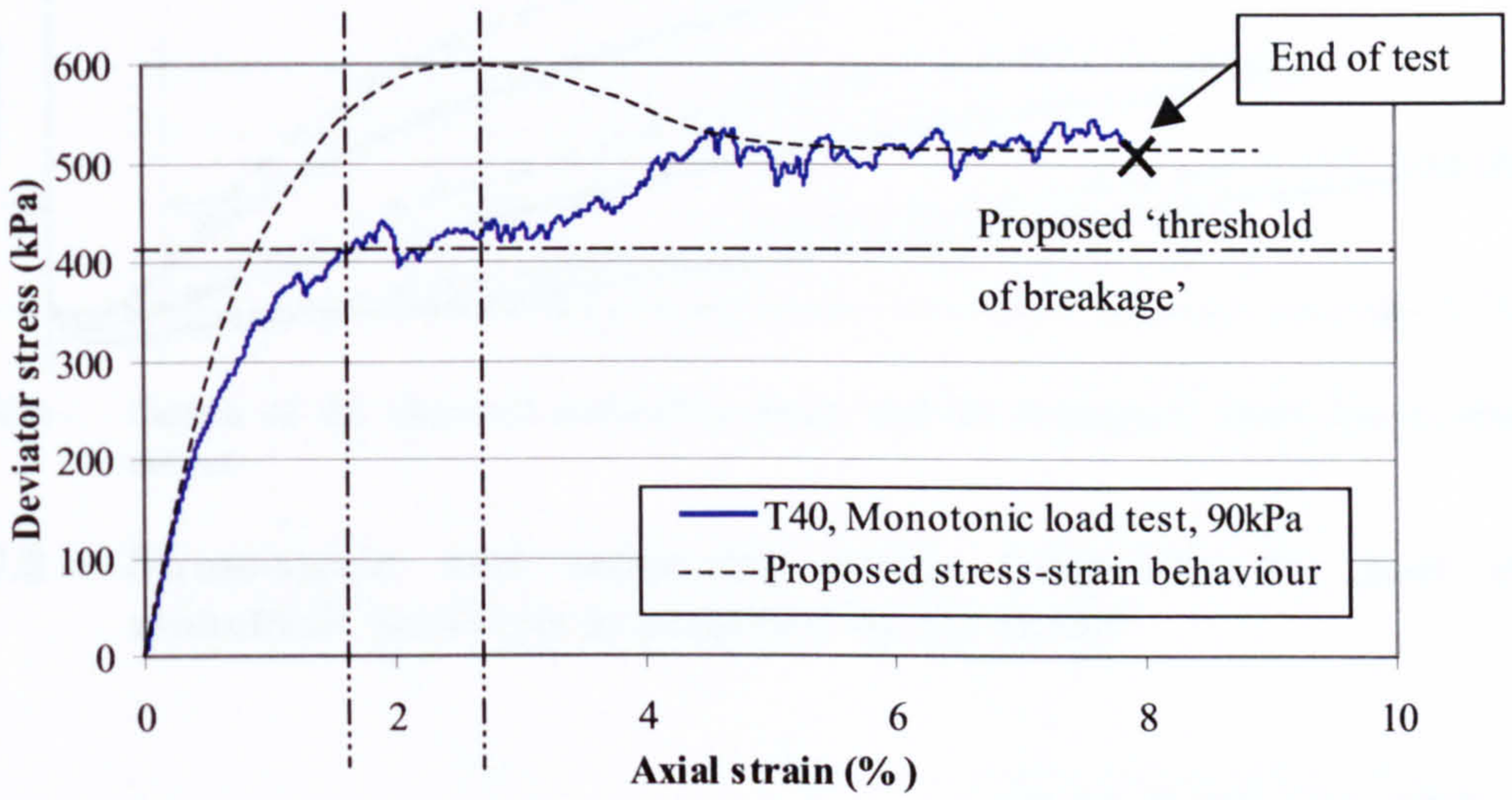

Figure 7.7(a) - Observed stress-strain and proposed stress-strain curves for test T40

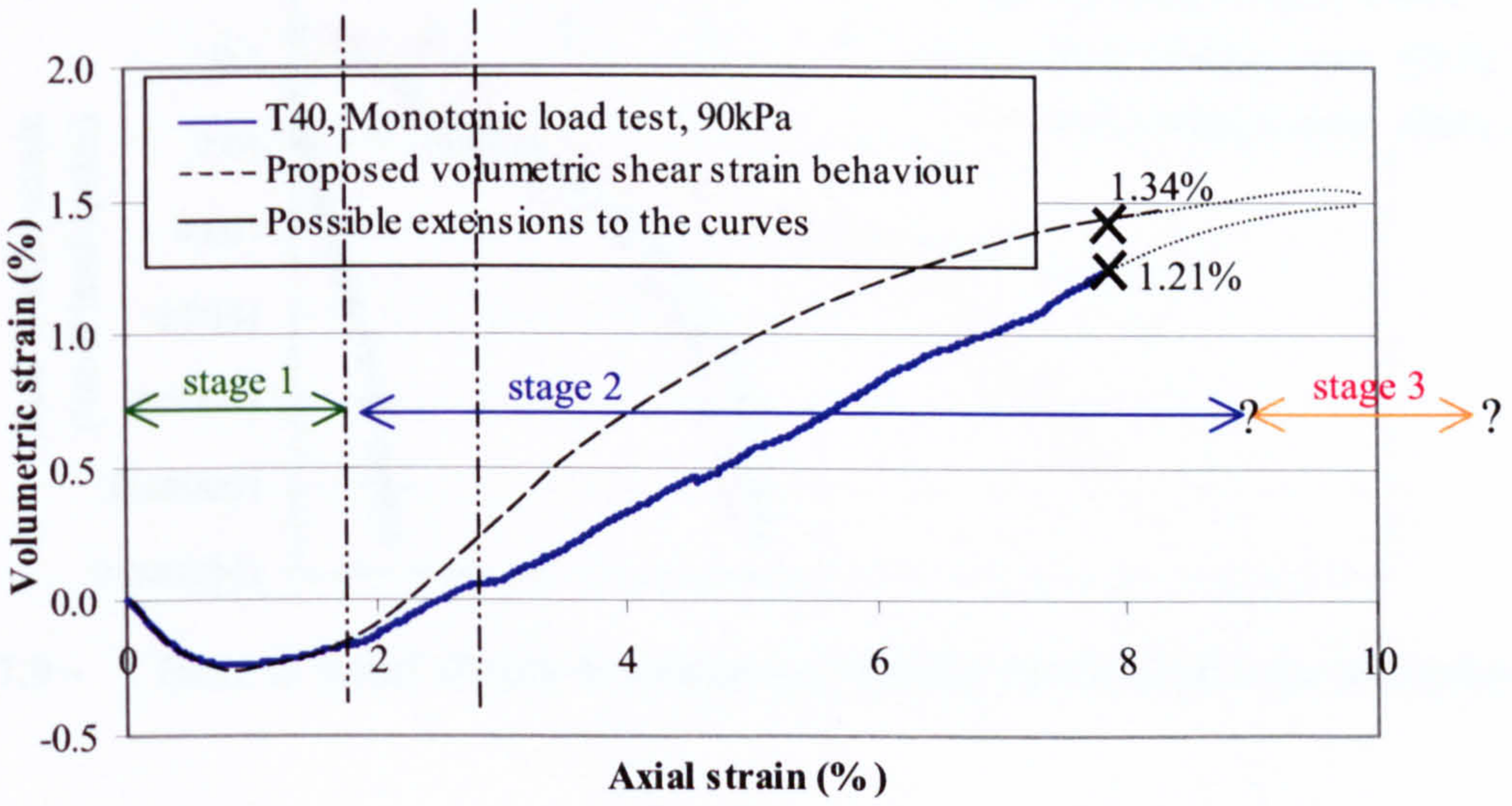

Figure 7.7(b) - Observed volumetric strain and proposed volumetric strain curves for test T40

Figure 7.7 - Observed and proposed specimen behaviour for a 90kPa cell pressure monotonic load test (T40)

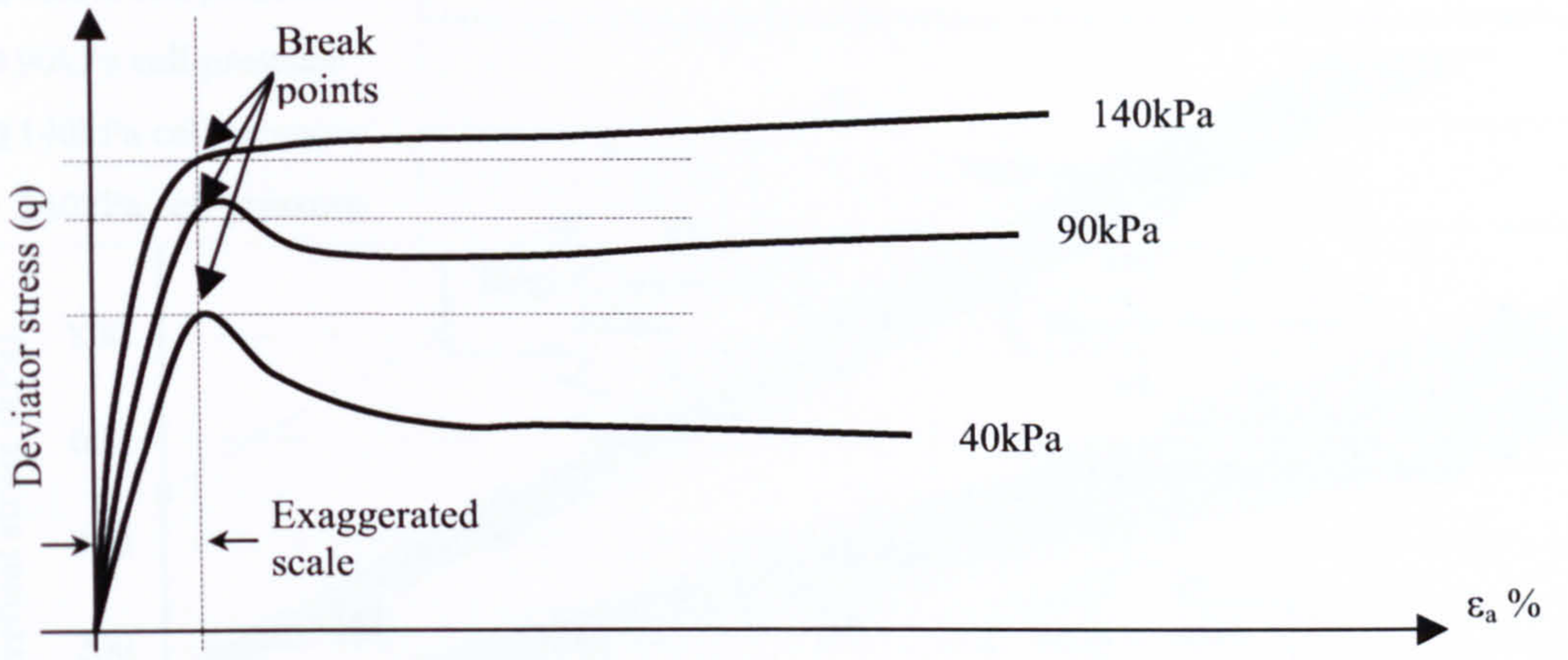

Figure 7.8(a) - Sketch of the stress-strain curves for the post cyclic monotonic load triaxial tests in Series 2

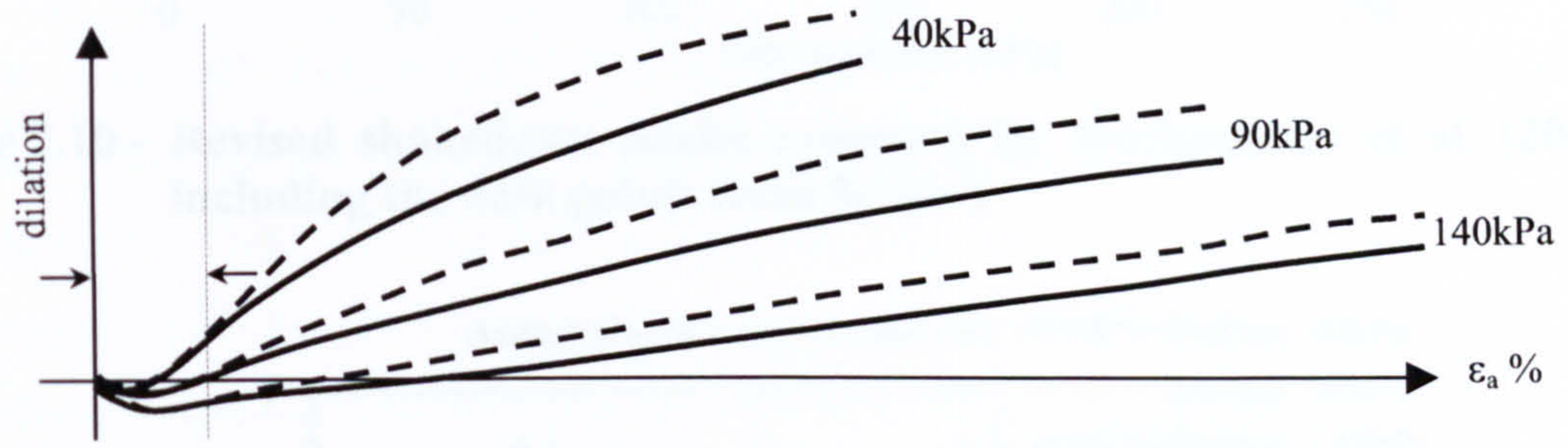

Figure 7.8(b) - Sketch of the observed volumetric strain and the volumetric strain due to shearing curves

Figure 7.8 - Stress-strain and volumetric strain behaviour for post cyclic monotonic load tests as proposed by the model

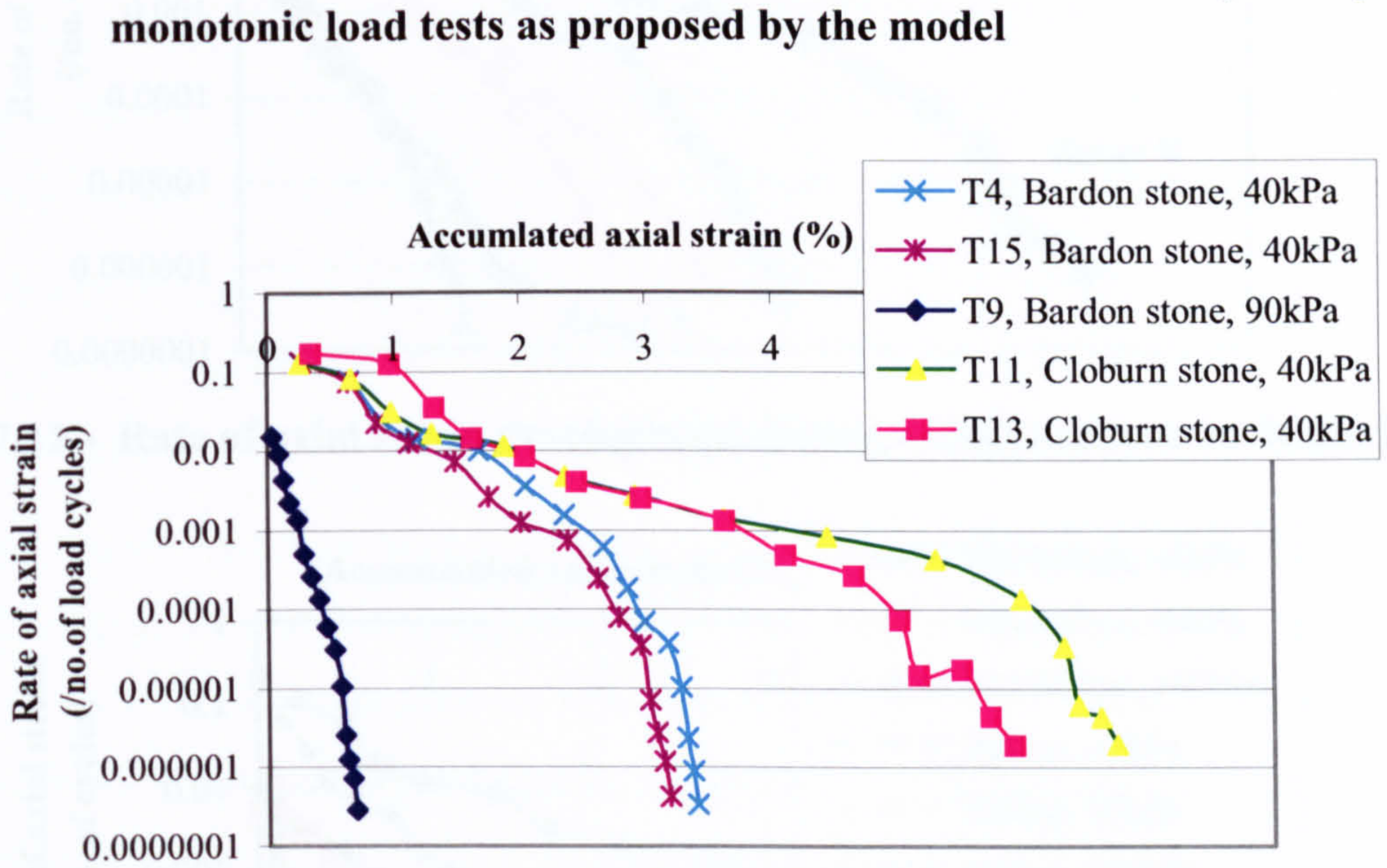

Figure 7.9 - Rate of axial strain development during cyclic load tests in Series 1

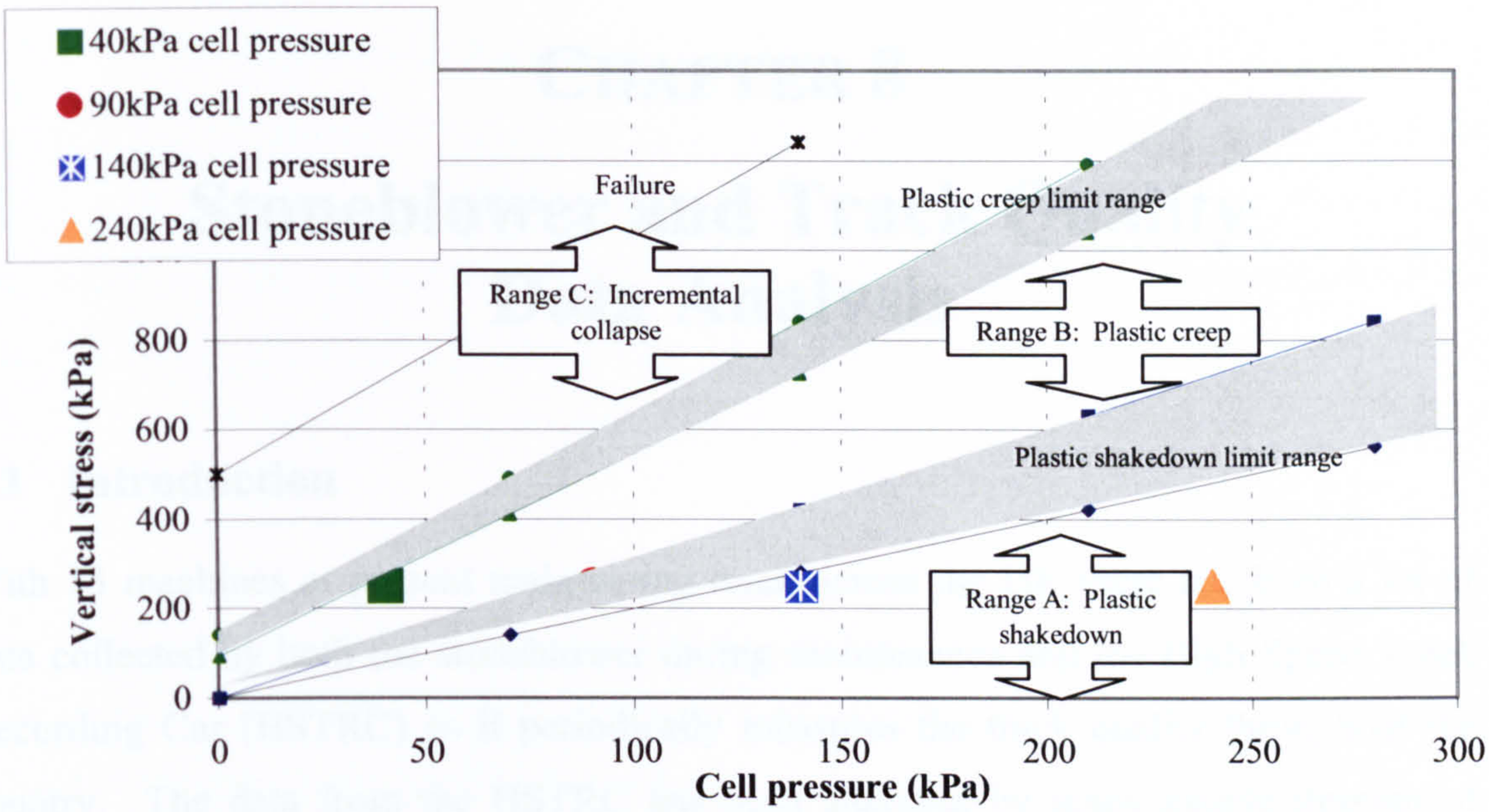

Figure 7.10 - Revised shakedown model proposed by Werkmeister et al. (2001) including the data points from Series 2

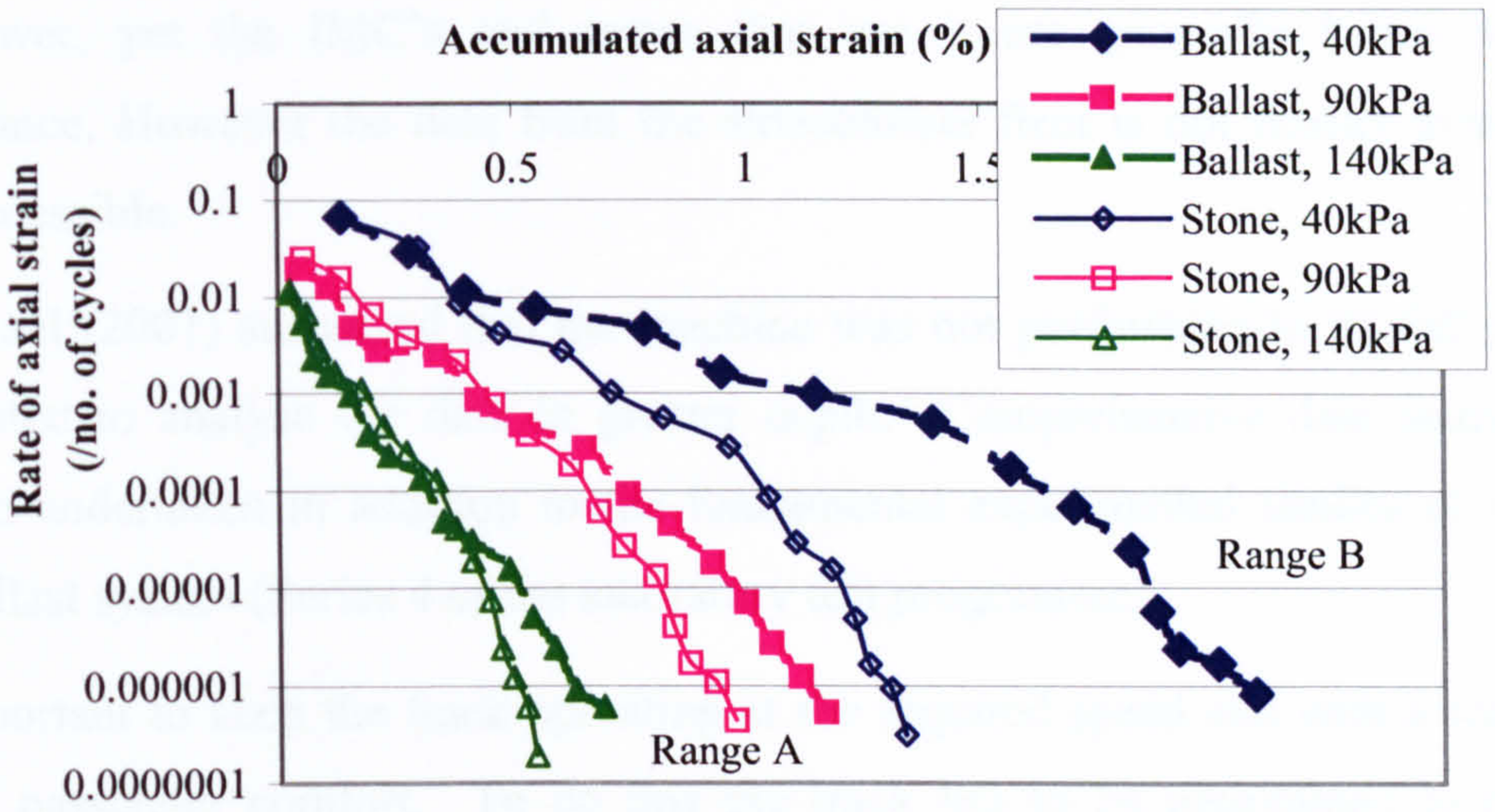

Figure 7.11 - Rate of axial strain development during cyclic load tests in Series 2

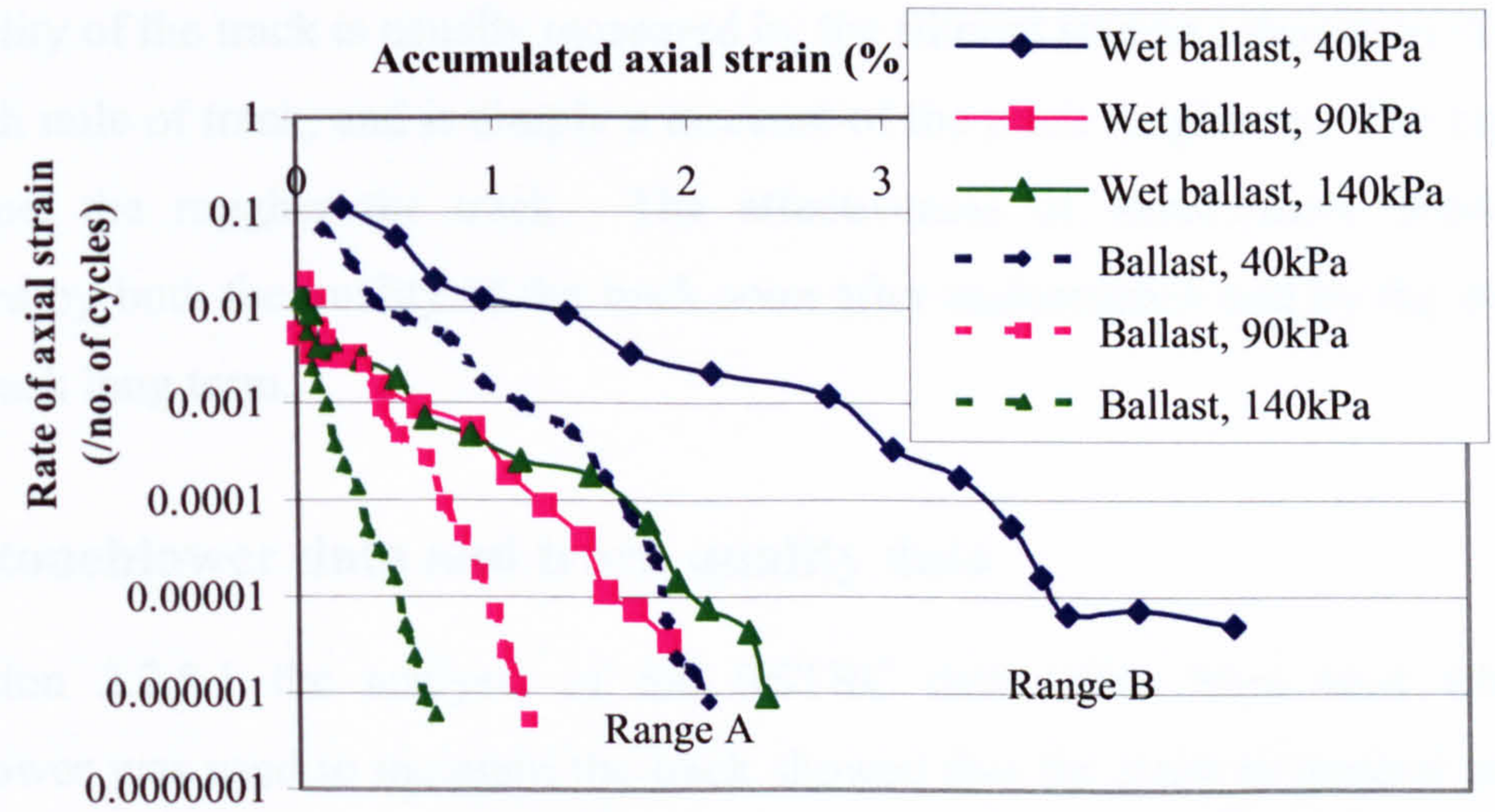

Figure 7.12 - Rate of axial strain development during cyclic load tests in Series 6

CHAPTER 8

Stoneblower and Track Quality Data Analysis

8.1 Introduction

With 13 machines at present maintaining track across the UK there has been a lot of data collected by both the stoneblower during maintenance and the High Speed Track Recording Car (HSTRC) as it periodically measures the track quality throughout the country. The data from the HSTRC has been analysed by many people throughout Railtrack and the Infrastructure Maintenance Companies (IMC's) who use the stoneblower. This has led to much speculation over the effectiveness of the stoneblower, yet the IMC's and crews that use it are generally happy with the performance. However the data from the stoneblower fleet is not readily available or easily accessible.

McMichael (2001) suspected that the machine was not performing to its full potential and wanted to analyse the data in greater depth. Comprehensive data analysis was therefore undertaken in addition to the fundamental experimental studies of the two-layer ballast system (Series 4 of the laboratory test programme).

It is important to keep the track operating at the required speed and with a reasonable level of passenger comfort. To do this the track has to be maintained to a certain standard of quality both in the vertical profile (top) and in the lateral profile (alignment).

The quality of the track is usually measured by the filtered standard deviation (SD) over an eighth mile of track, and is simply a measure of the track roughness. The higher the SD value, the rougher the track. The effectiveness of maintenance needs to be measured by both the quality of the track soon after maintenance and by the durability of the track long term.

8.2 Stoneblower data and track quality data

In Section 2.2.5.1 the analysis of the HSTRC data taken from sites where the stoneblower was used to maintain the track showed that the track in general improved (Baulk, 1999), although there was a large amount of scatter. The analysis also showed that there were many sites that did not appear to be responding to the maintenance. It is

for these two reasons that further analysis was required. To carry out this further analysis it was necessary to be aware of any parameters that might cause different sections of track to respond differently under this maintenance technique. Therefore a list of possible parameters that might affect the post-maintenance performance of the track has been included (Section 8.2.1). Secondly it was important to be certain that each piece of track that was included in the analysis had actually been maintained (Section 8.2.2).

8.2.1 Parameters of special stoneblowing interest

Below is a list of parameters that could potentially have an effect on the post maintenance performance of the stoneblower.

- Line speed, high / slow,
- Axle loads,
- Impact loading especially on jointed track,
- Sleeper / rail type,
- Traffic frequency / axle spacing, i.e. rate of loading,
- Height of lifts, i.e. the amount of stone being blown under individual sleeper ends,
- Mixed stoneblowing and tamping,
- The effect of ramping in and out during maintenance, e.g. end eighths,
- Climate conditions, i.e. temperature and moisture content,
- Subgrade type / modulus,
- Good / fouled ballast,
- Acceleration / braking, e.g. track on either side of a station or speed restriction,
- Transitions / curves / straight,
- Cant deficiency,
- Wavelengths of particular faults; there are discrete wavelengths that certain types of measurement systems do not pick up,
- Operating crews may have an affect on the machine's overall performance,
- Individual machine performance.

8.2.2 Sorting the track recording car data

Between January 1999 and December 2000 approximately 18,500 eighths were recorded as having been maintained using the stoneblowing technique. In total around 35,000 eighths had been maintained by stoneblowing by the end of 2001. Although the

overall results showed an improvement in track quality there were many eighths that did not appear to improve and some that appeared to have deteriorated.

From the original 18,500 eighths only 1441 eighths were actually analysed. Initially many eighths could not be used due to eighths with badly recorded mileage, i.e. where the mileage recorded during the measurement run by the machine was not within 80 metres of the distance between the start mileage and finish mileage recorded by the crew. Also where incorrect ELR's (Engineers Line Reference) and Track ID's had been recorded, i.e. when either the ELR was not recognised or something other than Fast or Slow and Up or Down was recorded in the appropriate box. Other sites were not used because only four ELR's selected from the main UK lines were analysed. Although 1441 eighths was only 8% of the original data it still represented a significant amount of track maintenance across a range of routes around the country.

8.3 Stoneblower data analysis

The analysis of the performance of the stoneblower as a track maintenance tool was not easy, as there were many difficulties in getting accurate, reliable data. Firstly, the stoneblower did not use the same techniques and calculations as the HSTRC for measuring the track quality. Secondly, the difficulty of knowing exactly where the machine was on the track within the UK made it difficult to compare data from the stoneblower with that of the HSTRC. When checks were carried out, the position of the stoneblower recorded by the crew in terms of ELR's and Track ID's often did not match up with the databank used in TrackMaster. Thirdly the stoneblower does not use the same techniques and calculations for maintaining the horizontal profile of the track as an Automated Lining System tamper (ALC) or an Automatic Track Top Alignment tamper (ATTA).

8.3.1 Primary Analysis - SUDA

The primary stoneblower data analysis was carried out by SUDA (Stoneblower User interface Data Analysis Macro), a piece of software programmed in Visual Basic for Applications - Excel (Fair, 2002, included in Appendix D on CD1)

In Fair (2002) the details of the SUDA macro were explained, including details of the files used and the calculations made.

Each file produced by SUDA contained, apart from the sheets containing the data;

- a maintenance summary sheet,

- two vertical profile charts,
- a vertical top 35m wavelength running standard deviation chart and a vertical top 70m wavelength running standard deviation chart,
- two versine charts,
- a lateral alignment 35m wavelength running standard deviation chart and a lateral alignment 70m wavelength running standard deviation chart,
- a twist check chart,
- a cant and curvature chart,
- a raw performance chart.

Further details from TrackMaster were then inserted manually into the file.

8.3.1.1 Maintenance summary

Table 8.1 shows a typical maintenance summary sheet. The title bar shows the ELR (SPC9 – one particular section on the Midland Main Line, St Pancras to Chesterfield), the track ID (Down Fast– also known as 2100), the mileage measured by the machine during the measurement run (145miles 5chains to 146miles 6chains). Due to the longstanding use of the nomenclature it would be inappropriate to convert mileage and chains into kilometres. The title then gives the date of the maintenance and finally the machine number (80206).

Under the title Design Information there were 12 categories set out.

1) The site file was a hexadecimal number, which with the date and the machine number gave a unique number to each separate site maintained.
2) The design category, which was input by the crew, was specified in terms of A*, A, B, C, or D. A* was recognised as the design for best quality of track and D for the worst quality. The design category determined the values for each parameter used in the design, including the following three categories.
3) The measured standard deviation (SD) cut off. If the value of the vertical top SD was worse than the measured standard deviation cut off then it would have been maintained.
4) The measured cord offset cut off. If the value of the lateral alignment SD was worse than the measured cord offset cut off then it would have been maintained.
5) The target SD was the SD that the machine was trying to achieve.
6) The sixth category gave details about the stoneblowing tubes; whether they were inserted on sections of track where no stone was blown – in the analysis no sites showed positive to this category.

7) The seventh category showed the sleeper type at the beginning of the maintenance.
8) The eighth category showed if there was a change in the sleeper type during the maintenance.
9) Likewise category nine showed the rail type at the start of the maintenance.
10) Category ten showed if there was a change in the rail type during the maintenance.
11) Category eleven showed the month in which the site was maintained. This was used in determining the weather (see Section 8.4.7).
12) Finally category twelve shows the operator. At present this information is not recorded.

The second part of the maintenance summary sheet (Table 8.2) gives the following details for each eighth.

1) The pre-maintenance SD, the design SD and the calculated post-maintenance SD, both vertical top and lateral alignment, for the 35m wavelength and the 70m wavelength parameters.
2) Details about any restrictions in an eighth were recorded. These details included maximum lifts (level) and slews (alignment) and also whether either system had been completely turned off during the maintenance (these are system overrides and are input by the crew during the measurement run).
3) The amount of stone blown in each eighth and whether the track was straight and flat, had a transition or cant. Where there was a cant on the track the amount of the cant was also recorded.

8.3.1.2 Vertical profile charts (x2)

There were two vertical profile charts produced by SUDA (Figure 8.1 and Figure 8.2). The charts show distance in miles along the x-axis, and profile in meters up the y-axis. This can cause the chart to look very busy and cramped – and therefore the track to look in poor condition especially when a significant length of track was maintained (i.e. over 1km). The vertical grid lines represent eighth miles of track. The first vertical profile chart (Figure 8.1) shows the level of both rails with the pre-maintenance measurement run, the design and the calculated post-maintenance profile. A section of track where the design profile was with the pre-maintenance profile indicates points where the machine was not trying to improve the track. With all the charts plotted by SUDA, start and finish markers were included for the range where the sleepers were lifted and for the range where stone was blown. Figure 8.2 shows the second of the two vertical profile charts. On this chart the data for one of the rails and the calculated post-

maintenance profile were removed so that it is clearer to see the details. Details about the rails and sleepers through the site were also plotted on this graph.

8.3.1.3 Vertical top 35m and 70m wavelength standard deviation charts

The vertical top 35m and 70m wavelength standard deviation charts (Figure 8.3 and Figure 8.4) show the distance in miles along the x-axis and the vertical top standard deviation in mm up the y-axis. Again the vertical grid lines represented one eighth of a mile. On these charts the track categories for 125mph track from the Group Standards were also displayed.

8.3.1.4 Versine (lateral alignment) charts (x2)

These charts were similar to the vertical profile charts with the distance in miles on the x-axis and the versines in mm up the y-axis and the vertical gridlines representing each eighth. The first versine chart (Figure 8.5) plotted the pre-maintenance versines, the design and the calculated post-maintenance versines, also the ranges of sleepers lifted and stone blown were shown, and the amount of stone blown. The second versine chart (Figure 8.6) had the post-maintenance plot deleted for clarity and also showed the quantity of stone blow throughout the site. The dashed line shows where the lining system had been active / turned off.

8.3.1.5 Lateral alignment 35m and 70m wavelength standard deviation charts

The lateral alignment 35m and 70m wavelength standard deviation charts (Figure 8.7 and Figure 8.8) were very similar to the vertical top standard deviation charts and showed up very clearly areas where the system as a whole was being ineffective. (i.e. where there was little difference between the pre-maintenance profile and the design profile.)

8.3.1.6 Cant and curvature chart

The cant and curvature chart (Figure 8.9) shows the distance in miles on the x-axis, with the cant in mm on the primary y-axis and the curvature represented as 1/radius (1/mm) on the secondary y-axis. Plotting these two graphs allowed a simple check to be made with the TrackMaster plots (see Section 8.3.1.7 below).

8.3.1.7 TrackMaster – cant, curvature and structures charts (x2)

After the SUDA macro had finished, two charts containing HSTRC information on the cant and curvature were then copied from TrackMaster into the file. The first chart

(Figure 8.10) allowed checks to be made with the cant and curvature information recorded by the stoneblower by assessing the accuracy of the longitudinal positioning between the two machines (the stoneblower and the HSTRC). The second of the two charts (Figure 8.11) allowed the user to see if there were any structures that may have had an effect on the performance of the stoneblower or the track in general.

8.3.1.8 Twist check chart

The twist check fault chart (Figure 8.12) shows the distance in miles along the x-axis and the twist check calculation on the primary y-axis. The secondary y-axis shows if there were any twist fault occurrences and the level of the fault during the maintenance. A fault was indicated by a marker over 250 on the secondary y-axis scale (seen here at about 180metres). Due to complications in the macro the twist check chart was not formatted in the same way as the other charts.

8.3.1.9 Raw performance chart

The raw performance chart (Figure 8.13) shows the distance along the x-axis and the elapsed time from the start of the measurement run to the finish of the maintenance run on the y-axis. It quickly highlights if there were any difficulties during the maintenance that might have had an affect on the performance of the machine (e.g. losing positioning or machine difficulties such as an auger jam etc).

8.4 Secondary analysis – patterns and trends

The HSTRC data was sorted to allow the option to compare the four track quality parameters (both vertical top and lateral alignment at 35m and 70m wavelengths) using the following data:

- The twelve month average HSTRC standard deviation (SD) pre-maintenance.
- The twelve month average HSTRC SD post-maintenance.
- The last recorded HSTRC SD pre-maintenance.
- The first recorded HSTRC SD post-maintenance.
- The best HSTRC record SD post-maintenance by three and six months.

All the stoneblower data from the maintenance summary sheets produced by SUDA were stored in a central file. Each stoneblown eighth was then matched with the corresponding HSTRC data and the secondary analysis was carried out.

Although all the data for the four track quality parameters mentioned above were available for analysis, only the vertical top 35m wavelength parameter was analysed in depth as this was considered as the most critical track quality parameter.

On all of the scatter graphs (Figure 8.14 – Figure 8.21), apart from where stated, the last HSTRC recorded SD pre-maintenance was on the x-axis and the best HSTRC recorded SD in the 6 month post-maintenance was on the y-axis for each eighth of track. On the scatter graphs a best fit regression line was drawn through the data. The shallower the gradient and the lower the intercept the better the maintenance. These graphs also showed the line of equality (line of no effect), therefore data points that appeared above this line either showed that the stoneblower had caused the track quality to deteriorate or that the track quality had continued to deteriorate as if it had not been maintained; the latter was the most probable. It was also important to note on the scatter graphs that one marker may represent many data points on the graph, especially those with reasonably low pre-maintenance SD's (1-2mm). The outliers, both good and poor, often only represented the performance of one eighth of track.

The cumulative frequency graphs (e.g. Figure 8.23) also used the last pre-maintenance and the best 6 month post-maintenance HSTRC SD's for each eighth of track. These graphs also show the track quality group standards for 125mph track (200km/h), where the markers (X) were used for further clarification. Note, not all sections of track analysed were required to be of this standard. These graphs show in a fairly unique way the performance of the maintenance, and with an increasing amount of data (and quality), they will be a very useful tool in future analysis. Further explanation of the cumulative frequency graphs will be covered in Section 8.4.3.

Initially the overall performance was considered (Section 8.4.1 – Section 8.4.4), then in Section 8.4.5 – Section 8.4.9 different parameters that may have had an influence on the post-maintenance performance have been addressed.

8.4.1 Scatter Plots – four parameters

Initially each route was analysed separately (ECML, WCML, BML, GWML and MML) and scatter graphs were drawn for the four parameters (vertical top and lateral alignment, for 35m and 70m wavelengths). With each parameter there was little difference between the routes as is shown by the 35m wavelength parameter in Figure 8.14, except that maintenance by the stoneblower on the ECML appears to have been

marginally better than average. From this a regression line was then drawn through all the data as seen in Figure 8.15.

With all the data together, i.e. 1441 eighth, the four parameters were plotted in Figure 8.16 to Figure 8.19. In Figure 8.16 the vertical top 35m wavelength showed significant track quality improvement, although the improvement was limited at lower pre-maintenance SD (less than 1.3mm, i.e. where the regression line crosses the line of equality). The gradient of the regression line was 0.396 and the intercept was 0.8 (where a lower intercept value and a lower gradient value represent better performance). The vertical top 70m wavelength (Figure 8.17) did not perform quite so well with a lower limit pre SD for improvement of around 1.9mm. The gradient of the regression line was 0.577 and the intercept was 0.8.

For the lateral alignment 35m and 70m wavelengths (Figures 8.18 and 8.19) the results were very encouraging with gradients of 0.443 and 0.453 and intercepts values of 0.40 and 0.54 respectively. The graphs show the 35m and 70m alignments with a lower limit pre-maintenance SD for improvement of around 0.7mm and about 1mm respectively.

To give a broader view of the data a vertical top 35m wavelength graph showing the 12 month average pre-maintenance standard deviation vs. the 12 month average post-maintenance standard deviation is shown in Figure 8.20. Once again this shows that the overall quality of the track improved over this two year period.

Figures 8.16 to Figures 8.19 show that the stoneblower was in general performing well in all four parameters, especially with the vertical top 35m wavelength; the lateral alignment 35m wavelength and the lateral alignment 70m wavelength all showing significant track quality improvements.

8.4.2 Scatter in the data

Figure 8.21 shows all of the data that AEA Technology (Rail) analysed (Baulk, 1999). When this data was compared with the data in the current work, Figure 8.15, it was clear that there was a reduction in the amount of scatter in this further analysis. The work by AEA Technology (Rail) recorded a correlation coefficient (R^2) value equal to 0.3306, which improved to 0.4444 in this work. This reduction in scatter has been explained in Section 8.2.2.

There were a larger number of data points in Baulk's previous analysis but not all of the points could be trusted as accurate records. With the reduced number of data points presented here one can be almost certain that each and every site has been maintained as

it was recorded. Although this reduction in the number of sites significantly reduced the number of poor performance eighths there were a few of the good performance eighths removed from the analysis also. In other words this reduction in the number of data points was systematic and logical, and did not just remove the poor sites.

There maybe several reasons for the scatter on the 'reduced' graphs (e.g. Figure 8.16). One fairly significant reason that became clear throughout the analysis was the accuracy of positioning of both machines (the stoneblower and the HSTRC). The significance of positioning errors can be seen in a typical vertical top 35m wavelength running standard deviation plot in Figure 8.22, which shows the running standard deviation throughout the site as measured by the stoneblower. However the HSTRC only gave a value for the centre of each eighth. When considering the eighth 145.125 – 145.25miles, if the HSTRC was only 50m out on consecutive runs it could, in this case, have read a value of 1.25mm at the centre of the eighth on the first run and up to 2.6mm at the centre of the eighth on the next. This was equivalent to two track quality bands on 125mph track, which in commercial terms was very significant. The jump in SD seen in this eighth was not unusual. Another possible reason for the scatter could still rest with the quality of the data and weaknesses in both measurement systems (McMichael, 2001).

8.4.3 Cumulative frequency graphs – 35m vertical wavelength

BR Research used cumulative frequency charts as a way to look at the distribution of track quality in the 1980's and 1990's. The method was then developed further for use in this analysis by the author. The standard deviation (SD) (mm) was plotted along the x-axis of the graph, with the percentage of the number of sites better than any particular SD value on the y-axis. Also included on these graphs were the track quality group standards for 125mph track. These were marked (X) for further clarification.

For example, in Figure 8.23 the SD for the last HSTRC recording pre-maintenance and the SD for the first HSTRC recording post-maintenance have been plotted. The percentage of pre-maintenance sites better than the 90% standard was only 70% (i.e. 20% below the standard). After maintenance this had increased to 93% (3% better than the standards).

Figure 8.24 shows additional plots for the best HSTRC recorded SD in the 3 months post-maintenance and 6 months post-maintenance. It could be seen that by 3 months up to 59% of the best post-maintenance SD recording was better than the 50% group standard and that one could still see improvements up to 6 months after stoneblower

maintenance. Caution needed to be exercised with the best 6 month post-maintenance HSTRC recording as it was unclear whether any further maintenance had been carried out within those 6 months. However, for the purposes of this report it was assumed that no further maintenance was carried out within the 6 months following the maintenance as it was considered that only a few sites maybe in this category.

8.4.4 Stoneblower vs. HSTRC track quality data

Figure 8.25 shows a scatter graph comparing the pre-maintenance standard deviations recorded by the HSTRC and the stoneblower for the vertical top 35m wavelength for each eighth analysed. The stoneblower pre-maintenance SD (mm) is on the x-axis and the HSTRC last recorded pre-maintenance SD (mm) is up the y-axis. The line of equality represents the line on which data points would lie should the stoneblower and the HSTRC have recorded the same track quality SD for a specific eighth of track. Therefore each point should ideally lie on the line of equality. However there was a lot of scatter, which was possibly due to slight differences in the positioning of the two machines (see Section 8.4.2) and the slight differences in the measurement systems and calculations used on the two machines. The best fit regression line is also shown on the graph. In Figure 8.26 the scatter has been removed and the vertical top 70m wavelength regression line has been included. It was clear from this graph that the overall comparison between the stoneblower measurement run and the HSTRC run for the 35m was fairly good (the regression line almost coinciding with the line of equality) but the 70m was not quite so good. It was interesting to note that for the ECML the vertical top 70m wavelength regression line lay parallel and slightly offset to the line of equality (Figure 8.27), suggesting that in general the stoneblower was recording a SD value of about 0.2mm below that of the HSTRC. With the lateral alignment for 35m and 70m wavelengths (Figure 8.28), there was a similar pattern, although the data was slightly less comparable than with the vertical wavelengths.

8.4.5 Effects of stone quantity on the post-maintenance performance

One of the main areas of interest that became apparent was the effect of the amount of stone blown under each sleeper end. Figure 8.29 shows the last HSTRC recording pre-maintenance on the x-axis and the best 6 month post-maintenance recording up the y-axis. The data was split down into 6 stone quantity categories by averaging the amount of stone blown in each eighth, from 0 up to 2 tonnes/km, 2 to 4, 4 to 6, 6 to 8, 8 to 10 and 10+ t/km. Apart from the 8-10 t/km category all the others showed a clear trend.

Through the different categories (0-2t/km up to 10+t/km) the gradient of the regression line became shallower indicating better post-maintenance performance. The intercept however, slightly increased, which suggested post-maintenance performance on sections of track with a low (good) pre-maintenance SD was not so good. This was especially clear on the 10+t/km category where the projected regression line crosses the line of equality at a pre-maintenance SD of about 1.4mm. However on reasonable quality of track such as one with an SD of 1.4mm then there would be no need to blow large quantities of stone.

Looking at the same data on a cumulative frequency graph, several extra insights were available. On each of the separate graphs (Figures 8.30 – 8.33) the 'CF 35v Pre' line shows the last HSTRC pre-maintenance recorded SD, the 'CF 35v 6 month Post' line shows the best 6 month HSTRC post-maintenance recorded SD (for the vertical top 35m wavelength) and the 'CF 35v Design' line shows the design SD of the stoneblower. Figure 8.30 (0 - 2t/km) shows that the majority (64%) of track that had only a little amount of stone blown was already in the good track quality band, which says that 50% should be better than 1.7mm SD. Therefore when the stoneblower measured these sections of track it would not be trying to improve the track very much as it was already better than the standards. This was clear when looking at the difference between the pre-maintenance and the post-maintenance SD values. Furthermore, up to 30% of the track experienced no improvement in standard. Therefore one could argue that with small amounts of stone there was a limited effect on the post-maintenance performance, especially at low (good) pre-maintenance SD values. In Figure 8.31 and Figure 8.32 the improvement seen between the pre and post-maintenance SD's (horizontal displacement on the graph between the pre and post-maintenance curves) was clearly better than that with lower stone usage. For example, in Figure 8.32 less than 20% of the track pre-maintenance was in the good track quality band for 125mph track (better than 1.7mm SD), yet the best HSTRC SD value up to 6 months after showed that up to 55% of track reached the good quality track band (<97% the satisfactory band and nearly 100% the poor). Furthermore, improvements were seen in pre-maintenance track quality with SD values as low as 1mm and even 0.8mm in Figure 8.31, which was a very encouraging result.

With 6 to 8t/km (Figure 8.33) the pre-maintenance track quality was very poor, where not even 50% of track was inside the poor track quality band (125mph track) and although significant improvements were made to the track quality, the group standards

were not quite meet. Similar patterns were seen with categories 8-10t/km and 10+t/km, although there was not really enough data to accurately draw a cumulative frequency graph. This track was most likely not 125mph quality track and therefore would not have been expected to meet such stringent standards.

It was worth noting that all of the graphs (Figures 8.30 – 8.33) show that the post-maintenance track quality curve fell short of the design curve (higher SD's). Part of the reason for this would be explained by considering the difference between the HSTRC pre-maintenance value and the stoneblower pre-maintenance value (Figure 8.34). This graph shows that the stoneblower read the vertical top 35m wavelength track quality at a slightly lower value than the HSTRC (about 0.2mm) and therefore the design was calculated on better track quality values. This difference was not picked up on the scatter graphs and the reason for this has not yet been established. Following the argument through, one could reduce the design SD value by 0.2mm so that the HSTRC pre and post-maintenance track quality values could be compared with the design values from the stoneblower. However this would still leave a shortfall between the design quality and the post-maintenance track quality. This was not perceived to have been due to the stoneblower but a natural drop off due to the complicated and unknown characteristics of the materials and stress regimes that were under consideration and could possibly be corrected within the algorithm.

8.4.6 Effects of design category on the post-maintenance performance

As the values of the design parameters were set by the design category selected on the night of maintenance, the performances of the different design categories was analysed (Note: the crew entered the design category into the machine) depending on the track being maintaining. Four different design categories were considered, A* being the highest category then A, B, and C. No data was analysed that used category D. Figure 8.35 shows the performance of each category on a scatter graph (vertical top 35m wavelength, with the last pre-maintenance SD (mm) on the x-axis and best 6 month post-maintenance SD (mm) on the y-axis.) The data points show the scatter from the A* category. Category C data was not included in Figure 8.35 as only a limited number of category C sites were analysed. From this graph it can be seen that as one moved through the design categories from B up to A* there was not much difference in the overall gradient of the graphs, but the intercept value had significantly decreased (better performance).

Using the cumulative frequency graph format the pattern became even more obvious (Figures 8.36 – 8.39). The differences were not so marked as with the different stone quantity categories (Figure 8.30 – 8.33), although the starting point for each graph was not the same (that is the CF 35v pre curve – pre-maintenance SD). There was also a significant improvement in SD with all of the different design categories.

When comparing Figure 8.36, category A* and Figure 8.30, stone quantity category 0-2t/km, the pre-maintenance data (CF 35v pre) were very similar, with the A* category showing slightly worse pre SD values. However the design curve (CF 35v design) for the A* category was much tighter (steeper gradient), with the horizontal distance between the pre-maintenance and the design being greater than with the 0-2t/km category; the A* category was therefore attempting to do a lot more to the track. One can see that this was achieved, with the post-maintenance curve (CF 35v 6 month post) for the A* category also being tighter. Therefore the A* category yielded better results.

Furthermore when comparing the A* and A design categories, Figure 8.39, showed that the improvement for both categories were similar (e.g. about 0.6mm improvement in SD on the 60% line). Where track had a low pre-maintenance SD (about 1.5mm or less i.e. better track) category A* showed a significantly greater improvement than that of A. A* gave improvements to the track up to a pre-maintenance SD of about 0.8mm, whereas with category A improvement was limited up to a pre-maintenance SD of about 1.2mm. This was similar to that of the 0-2t/km category in the stone quantity graphs (Figure 8.30).

With the A* category there was a range of different stone quantity categories used (Figure 8.40), suggesting that the design category may be a more appropriate way of assessing the performance of the machine than purely by stone quantity. This was because the machine was blowing the amount of stone most appropriate to each sleeper end.

8.4.7 Effects of weather on the post-maintenance performance

Laboratory research suggested that wet materials may perform worse than dry materials under loading. The weather conditions (wet ballast) may therefore have an adverse effect on the post-maintenance performance of stoneblown track (see Sections 2.5 and 5.7). As the weather was not recorded during the maintenance run or in the days thereafter a 'broad brush' approach was developed to allow an initial investigation. To do this the month of maintenance was recorded, the year was then split into quarters,

winter (December, January and February), spring (March, April and May), summer (June, July and August) and autumn (September, October and November). Using this method of weather analysis, Figure 8.41 shows that there was no noticeable difference in the post-maintenance performance of stoneblown track due to the seasons. However there were several important factors to consider in relation to this. Firstly, the weather in Britain is very unpredictable, where any one month could within reason receive a lot more rain than any other month of the year. There is also a variation throughout the country in weather conditions, generally the south is considered dryer than the north, and the west wetter than the east. Secondly, as yet it is not totally clear which are the important factors to consider, the weather before, during or after maintenance or possibly a combination of each. Further work on this data may allow examination of the weather conditions to be refined in such a way that the results can be better interpreted.

8.4.8 Effects of different machines on the post-maintenance performance

Within the railway maintenance industry there has been speculation that different machines perform better than others. Using a scatter plot, Figure 8.42 shows that there was very little difference between the different machines. However it was interesting to note that the best two performing machines, 80210 and 80206, mainly operated on the ECML where a significant amount of track was maintained using the A* design category (Section 8.4.6). Caution was necessary with machine 80205, as there was only a limited amount of data available.

8.4.9 Effects of restricted lifts and slews on the post-maintenance performance

It became apparent during the analysis that the performance of the machine was severely limited in eighths where restricted lifts and or slews had been imposed. Figure 8.43 shows two sets of data. The solid regression line shows the performance of all eighths using the vertical top 35m wavelength parameter and the dashed regression line shows the performance of just those eighths were the performance of the machine had been restricted. The difference between the two lines was clear as the gradient of the restricted lifts line was steeper i.e. worse than the general data. The same pattern would be seen, and was even more pronounced in Figure 8.44, which looked at the lateral alignment 35m wavelength parameter and the eighths with restricted slews.

This data set (Figures 8.43 and 8.44) clearly showed how important it was to carry out site inspections before the maintenance run to measure and check distances so that the

minimum amount of restriction was applied during the maintenance, or better still the restriction may be removed completely. There were 38 eighths that had restricted lifts and 54 eighths that had restricted slews, many of which had both.

8.5 Data analysis conclusions and best practice

8.5.1 Conclusions

From the data analysed the following conclusions have been drawn.

1) The chosen design category had a significant effect on the post-maintenance performance of the machine.
2) The post-maintenance performance was not solely related to the amount of stone being blown, although the stone quantity was closely linked with the design category.
3) The analysis suggested that the route had no effect on the post-maintenance performance of the track.
4) By splitting the months of the year up into seasons, and assuming that winter was wetter than summer, the results impled that the weather had no adverse effect on the post-maintenance performance of the track.
5) There was no significant effect on the post-maintenance performance of the track treated by different machines.

However it is important to remember there were limitations within the analysis, where some end eighths were excluded from the analysis others were not. Also the linear regression line was used as the best fit line in all the scatter graphs; this assumption was made in previous analysis and was again used here. The use of the best 6 month data recorded by the HSTRC after maintenance in the analysis may have allowed possible errors to creep in where further maintenance had been carried out within six months of the site being analysed.

8.5.2 Best Practice

From the analysis presented here it was possible to provide guidelines on best practice.

1. It is important that the machines can be fixed to a datum for accurate and repeatable positioning. This applies to the stoneblower, the HSTRC and any other track quality recording device.

2. It is extremely important that the ELR, the Track ID and the start and finish mileages are recorded accurately, so that proper planning and analysis can be carried out.
3. The number and amount of any fixed lifts or slews needs to be reduced to allow more eighths to be effectively targeted by the stoneblower.
4. At the end of the measurement run the crew need to check the proposed design. Where there is little or no stone blown then the design category should be revised and if appropriate the new design carried out.
5. Better planning is necessary. The data showed that some planning was particularly poor with certain sections of track being maintained within months if not days of previous maintenance.
6. An onboard shut down procedure needs to be implemented to make sure that files are not getting corrupted.
7. This work suggests that a practical way of recording the weather needs to be devised so that conclusions may be drawn on this question.
8. In the interest of best practice, the operator/crew needs to be recorded so that in the instance where one operator is doing better, then this knowledge may be disseminated to the rest of the fleet. Having said that the author is aware that there are commercial difficulties and possible implications of data being used to adverse effects.

It is important to conclude that the machine will only do as it is 'told' to do. Where the machine was trying to maintain good track using an inappropriate category (for instance A instead of A*) then the maintenance was ineffective. In other words if the machine is being asked to do nothing then it will do nothing.

SPC9 - DOWN FAST - 145m5ch to 146m6ch
Stoneblown on 17/01/00 by machine No: 80206

Design Information	Site File	165
Design Category		B
Measured SD Cut Off		1.8
Measured Cord Offset Cut Off		3
Target SD		1.3
Tubes Inserted where no stone blown		NO
Sleeper Type (start)		4
Sleeper Type changes		No
Rail Type (start)		2
Rail Type changes		No
Weather		January
Operator		

Table 8.1 - Maintenance summary sheet (part 1)

SPC9 - DOWN FAST - 145m5ch to 146m6ch
Stoneblown on 17/01/00 by machine No: 80206

Standard Deviations

Mileage		Vertical Alignment							Lateral Alignment							Quan. of stone (T/km)	Track type	
		Pre SD		Design SD		Post SD		restr	Pre SD		Design SD		Post SD		res		Straig ht (s)	
from	to	35m	70m	35m	70m	35m	70m	ic.	35m	70m	35m	70m	35m	70m	tric		Transi	Cant (r
145	145.125															1.986		, -25
145.125	145.25	2.17	2.01	0.92	1.13	2.63	2.94		0.64	1.13	0.05	0.14	0.45	0.62		2.478		
145.25	145.375	1.38	1.68	1.02	1.38	2.32	2.88		0.41	0.74	0.05	0.17	0.34	0.42		1.22		
145.375	145.5	2.98	3.97	1.28	2.85	2.98	3.23		0.68	1.19	0.05	0.17	0.53	0.67		5.392		
145.5	145.625	2.29	2.84	1.08	1.88	2.44	2.81		0.74	1.15	0.05	0.11	0.37	0.52		5.453		
145.625	145.75	2.18	3.05	1.16	2.24	2.47	2.91		1.18	2.21	0.87	1.52	1.07	1.86	LO,	3.049	TST, T	, -25, -45
145.75	145.875	1.19	1.59	0.99	1.46	2.18	2.65		0.58	0.89	0.06	0.25	0.35	0.48		0.68	TST,	, -45
145.875	146	2.12	2.44	1.05	1.47	2.17	2.60		0.73	1.15	0.05	0.24	0.54	0.76		2.761	TEND,	, 0
146	146.125														LO,	1.012		, 0

Table 8.2 - Maintenance summary sheet (part 2)

% better than	Last pre	First post	Group standards
50	2.1	1.7	1.6
90	3.2	2.4	2.2
100	6.0	3.0	3.7

Table 8.3 - Comparing pre and post-maintenance SD's with the group standards for 125mph track

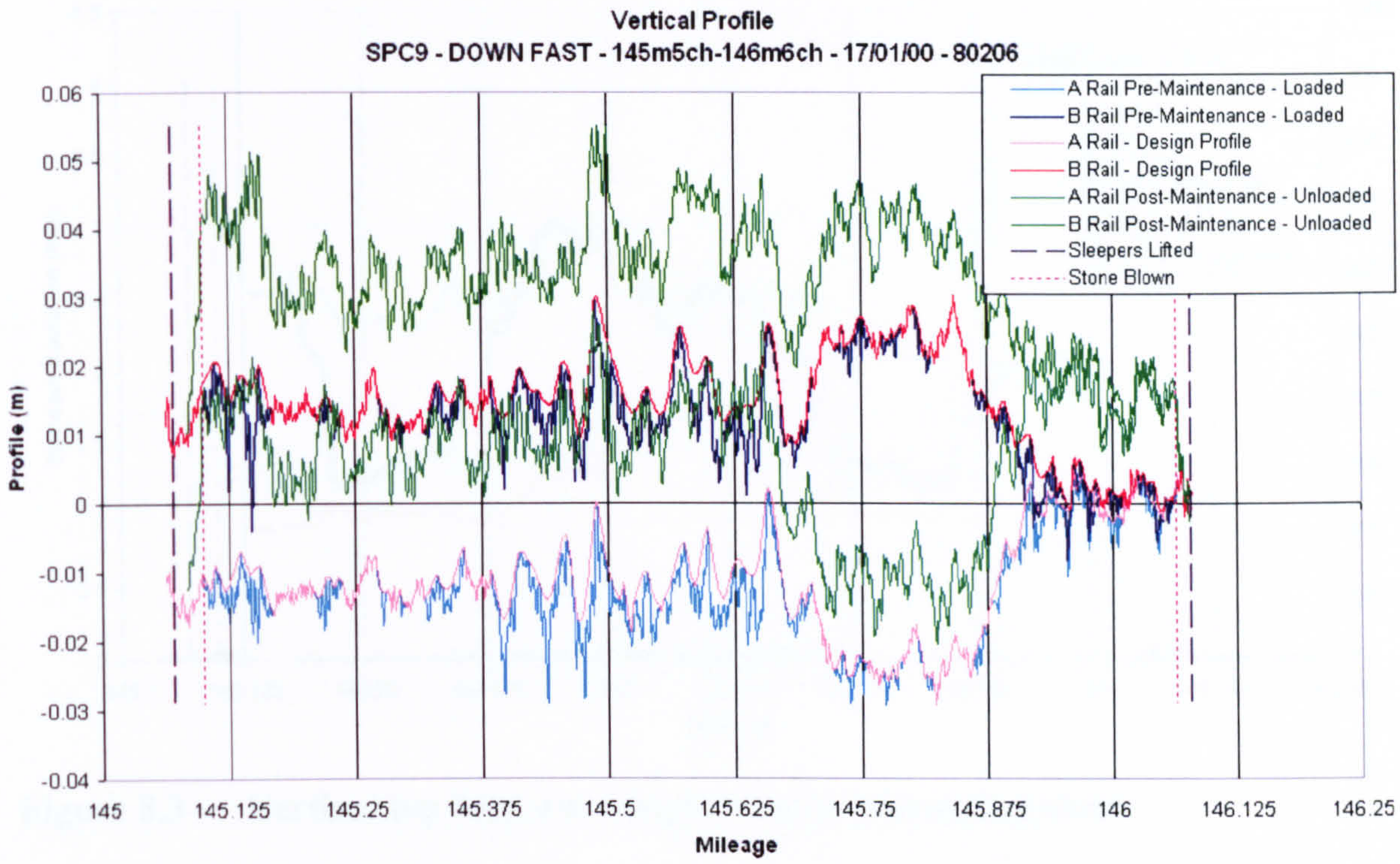

Figure 8.1 - Vertical profile as recorded by the stoneblower (Chart 1)

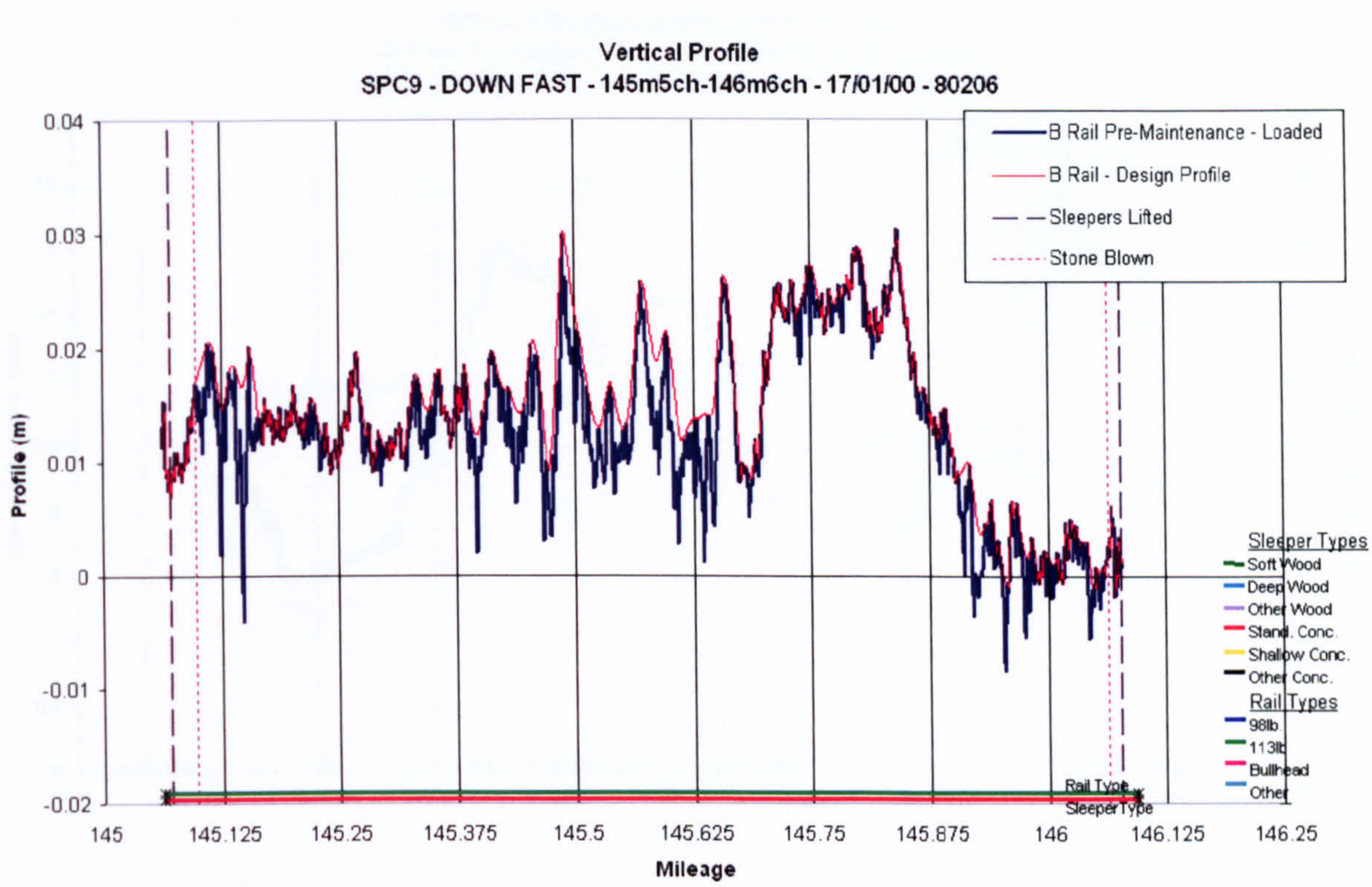

Figure 8.2 - Vertical profile as recorded by the stoneblower (Chart 2)

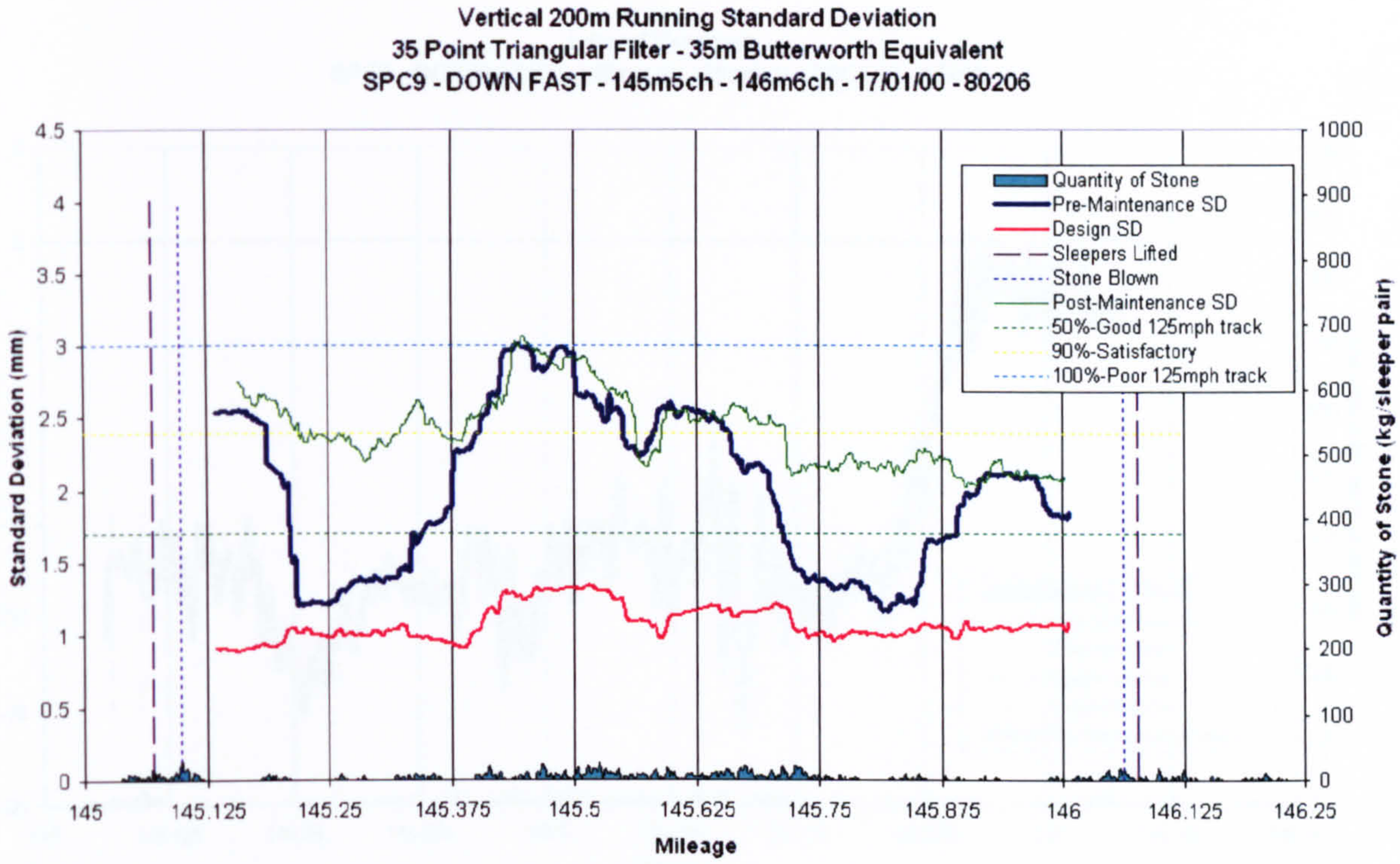

Figure 8.3 - Vertical top 35m wavelength standard deviation chart

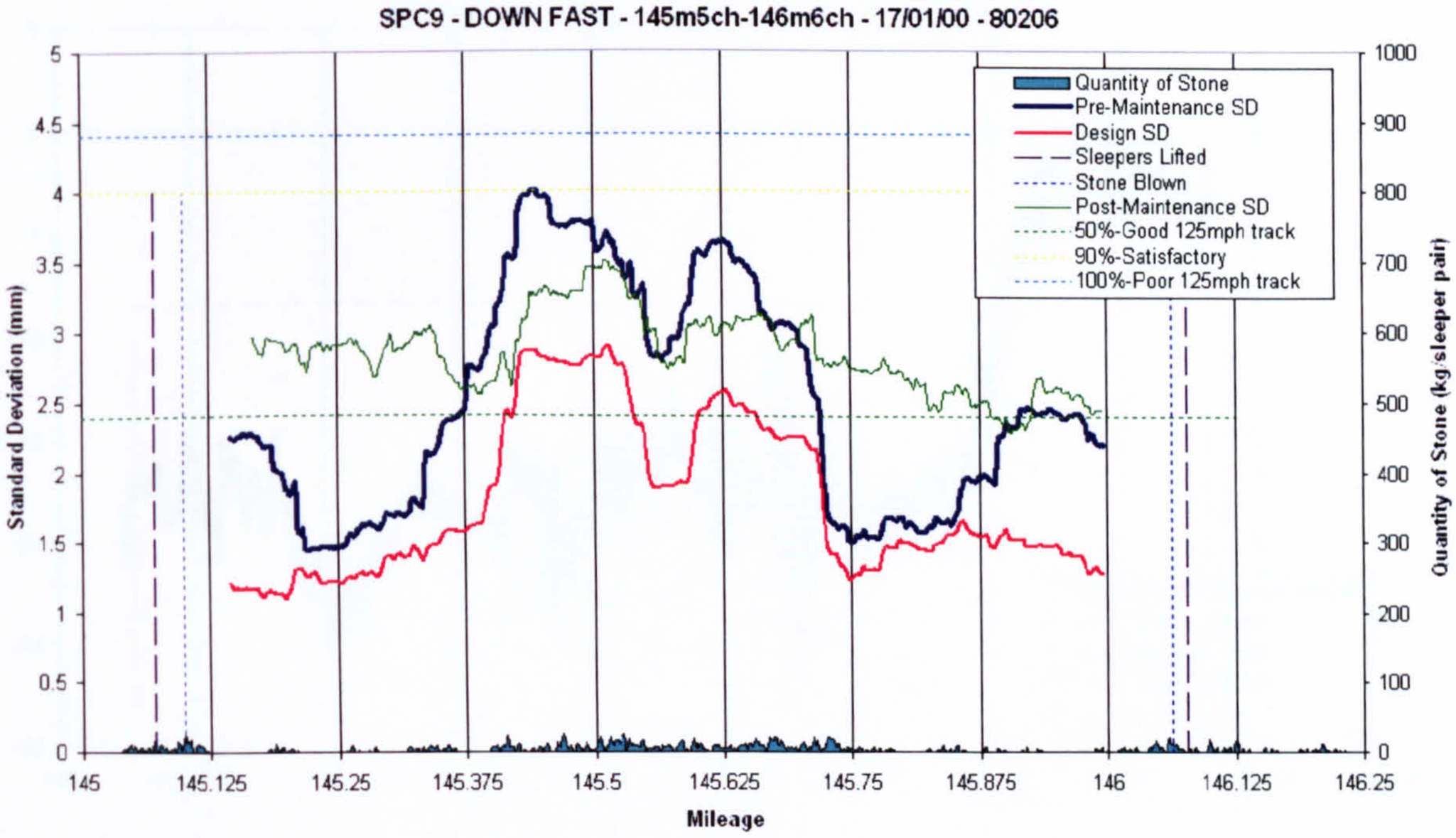

Figure 8.4 - Vertical top 70m wavelength standard deviation chart

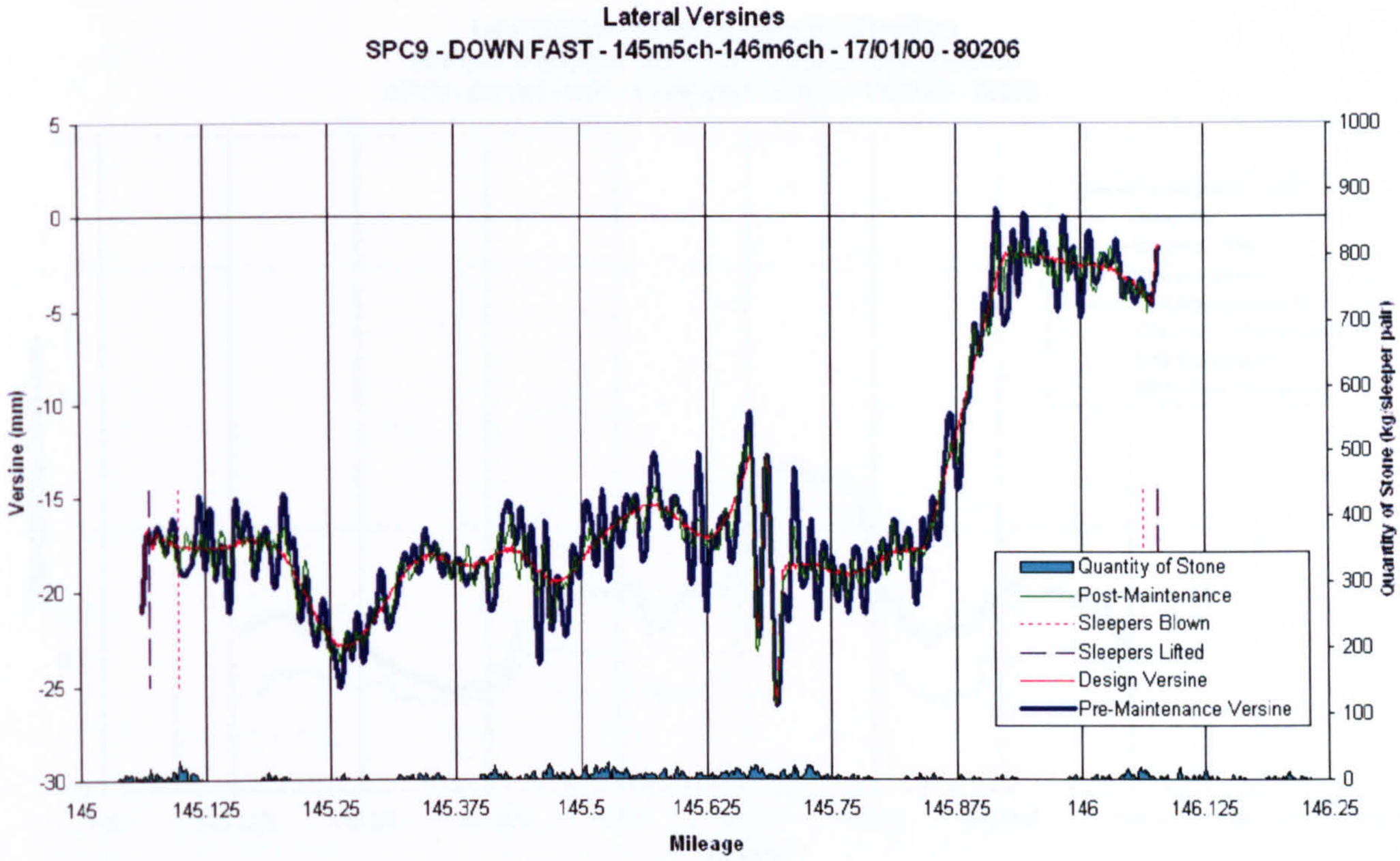

Figure 8.5 - Versine as recorded by the stoneblower (Chart 1)

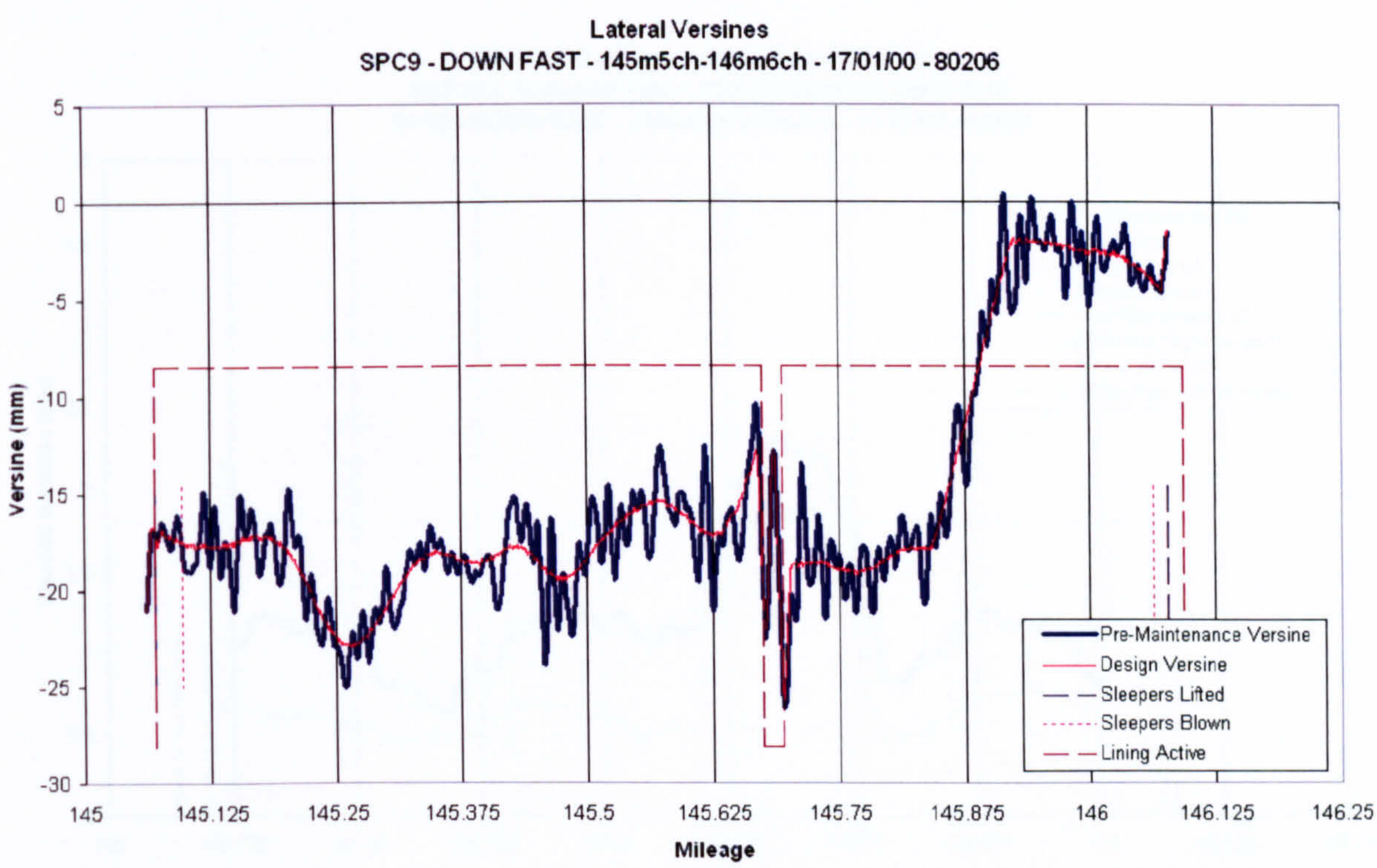

Figure 8.6 - Versine as recorded by the stoneblower (Chart 2)

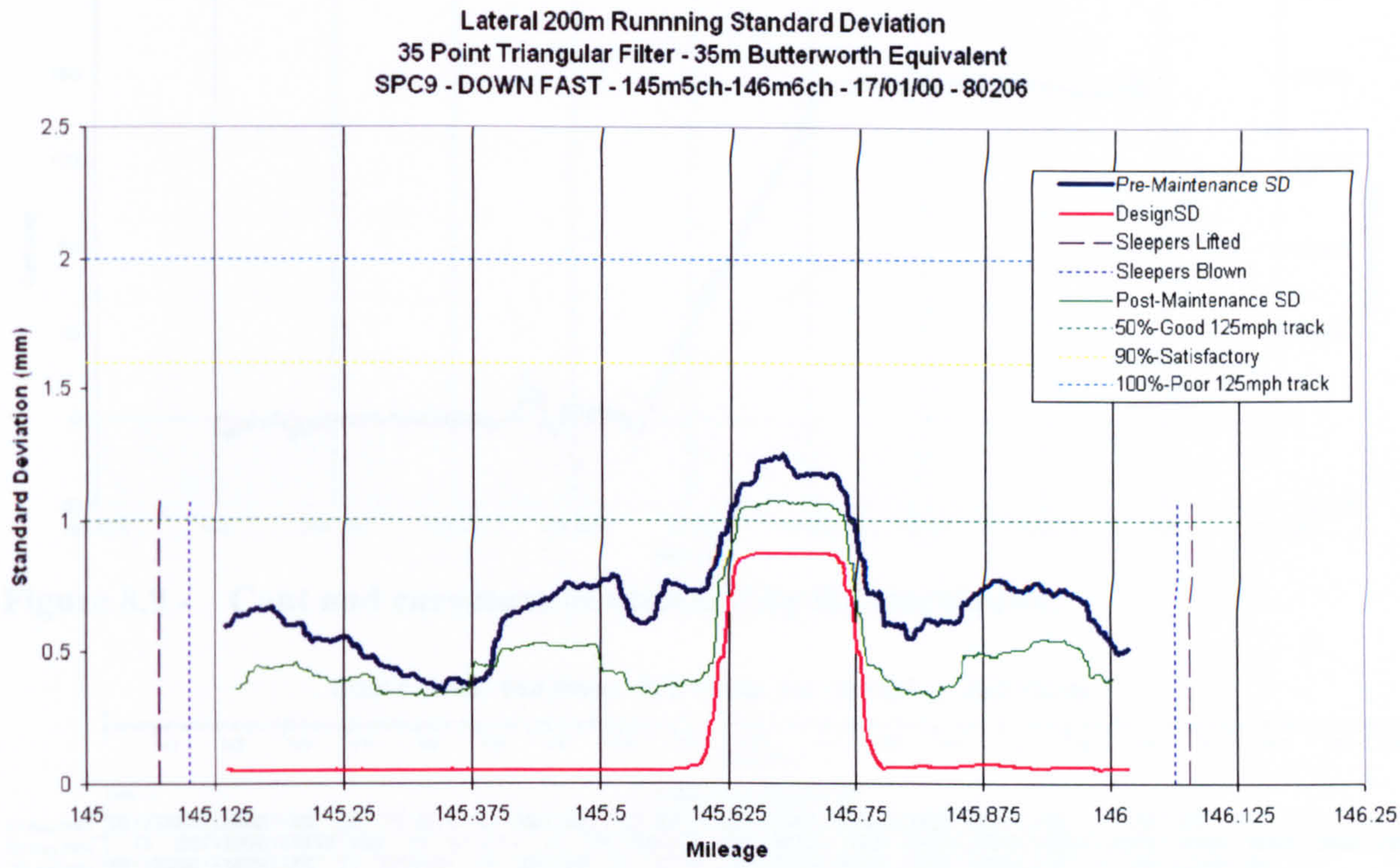

Figure 8.7 - Lateral alignment 35m wavelength standard deviation chart

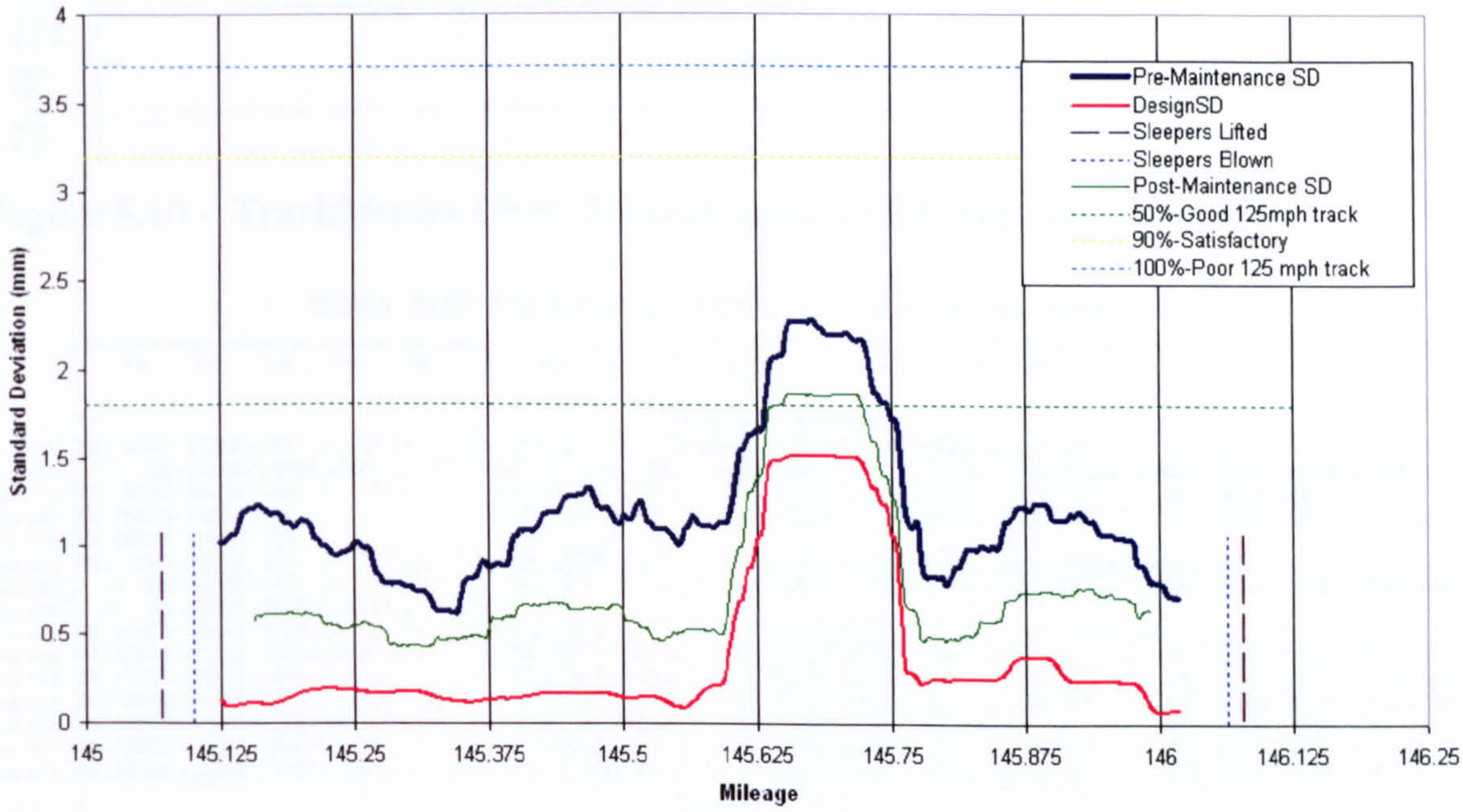

Figure 8.8 - Lateral alignment 70m wavelength standard deviation chart

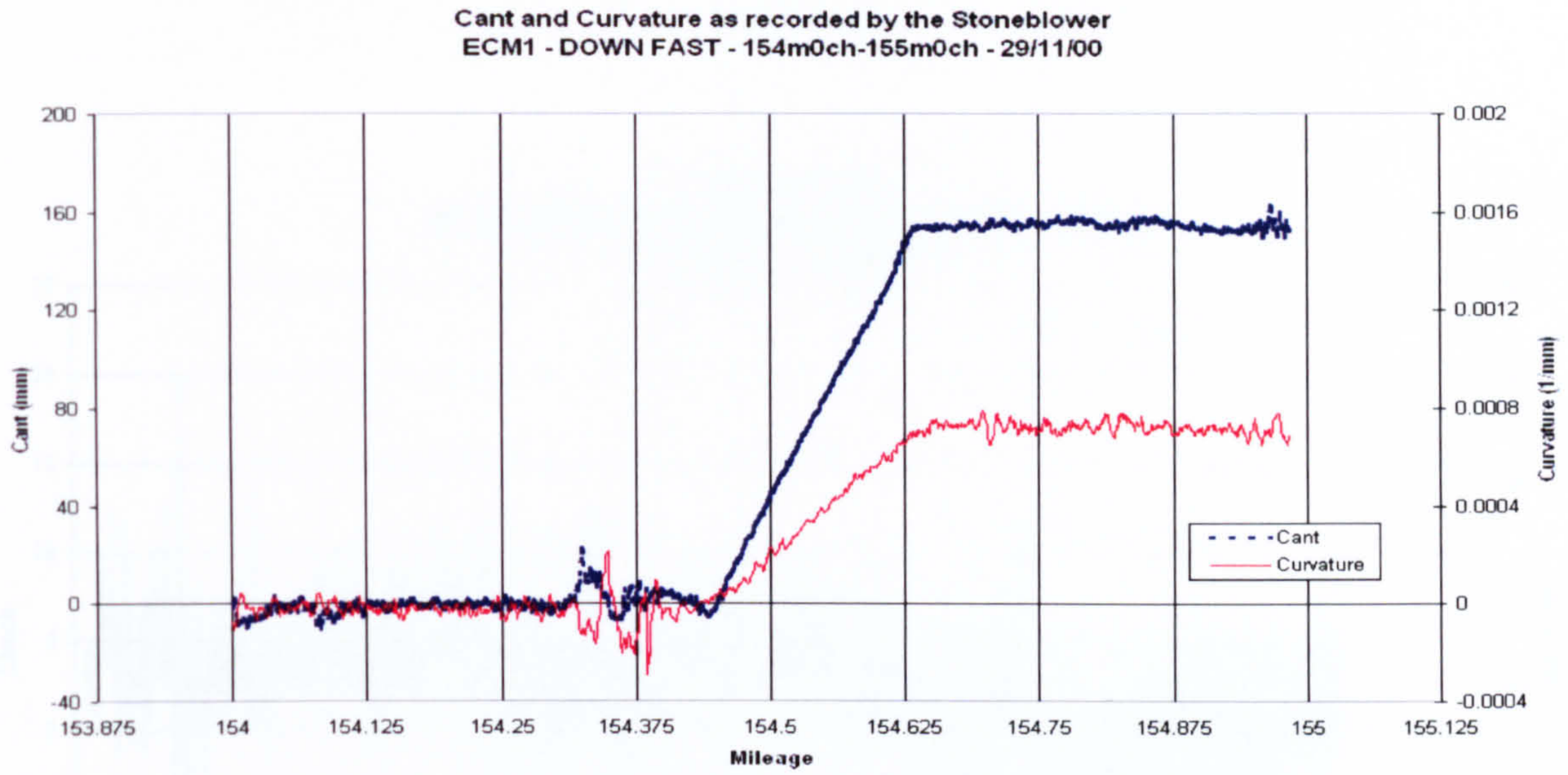

Figure 8.9 - Cant and curvature as recorded by the stoneblower

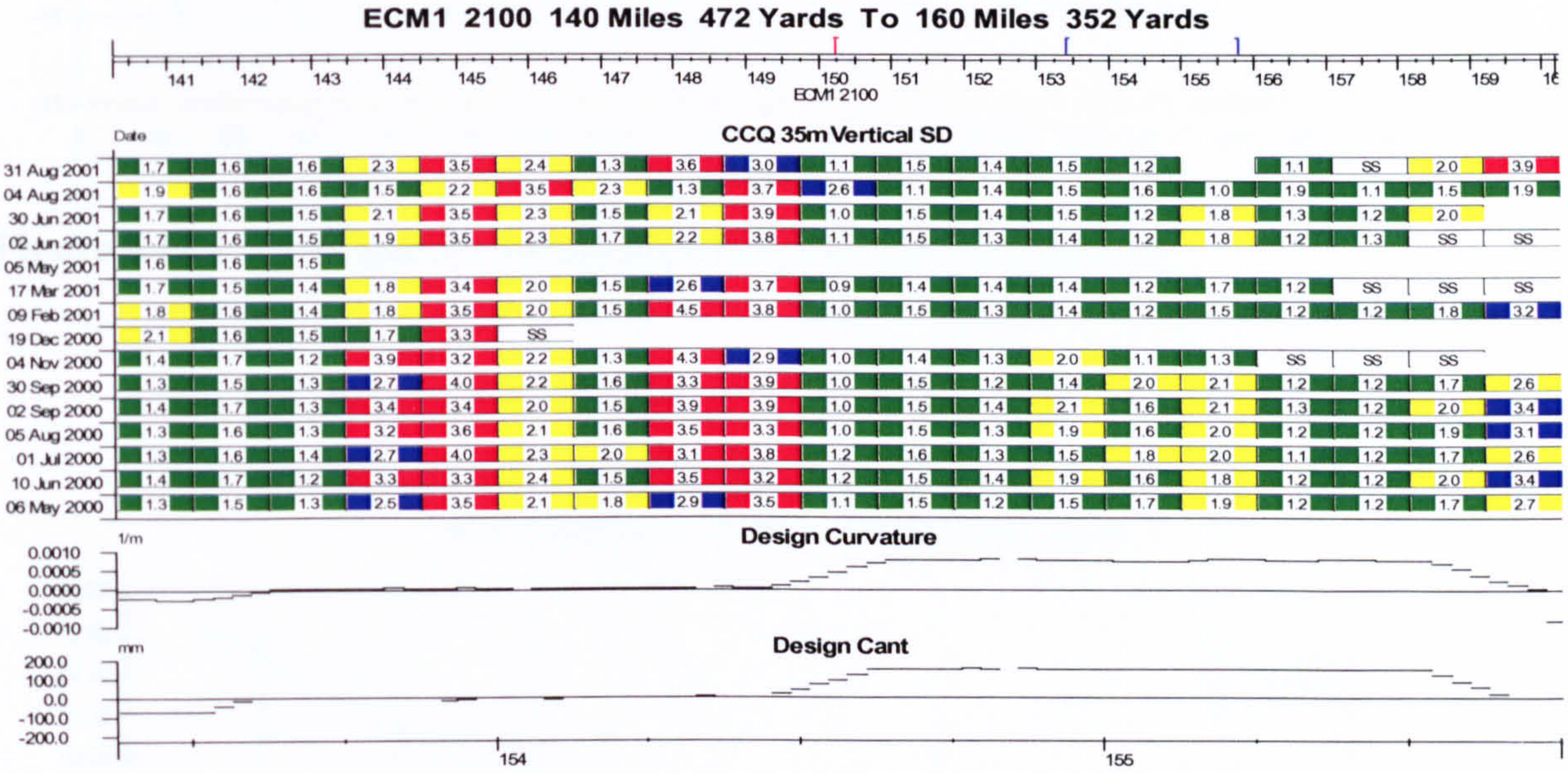

Figure 8.10 - TrackMaster Chart 1, track quality with cant and curvature

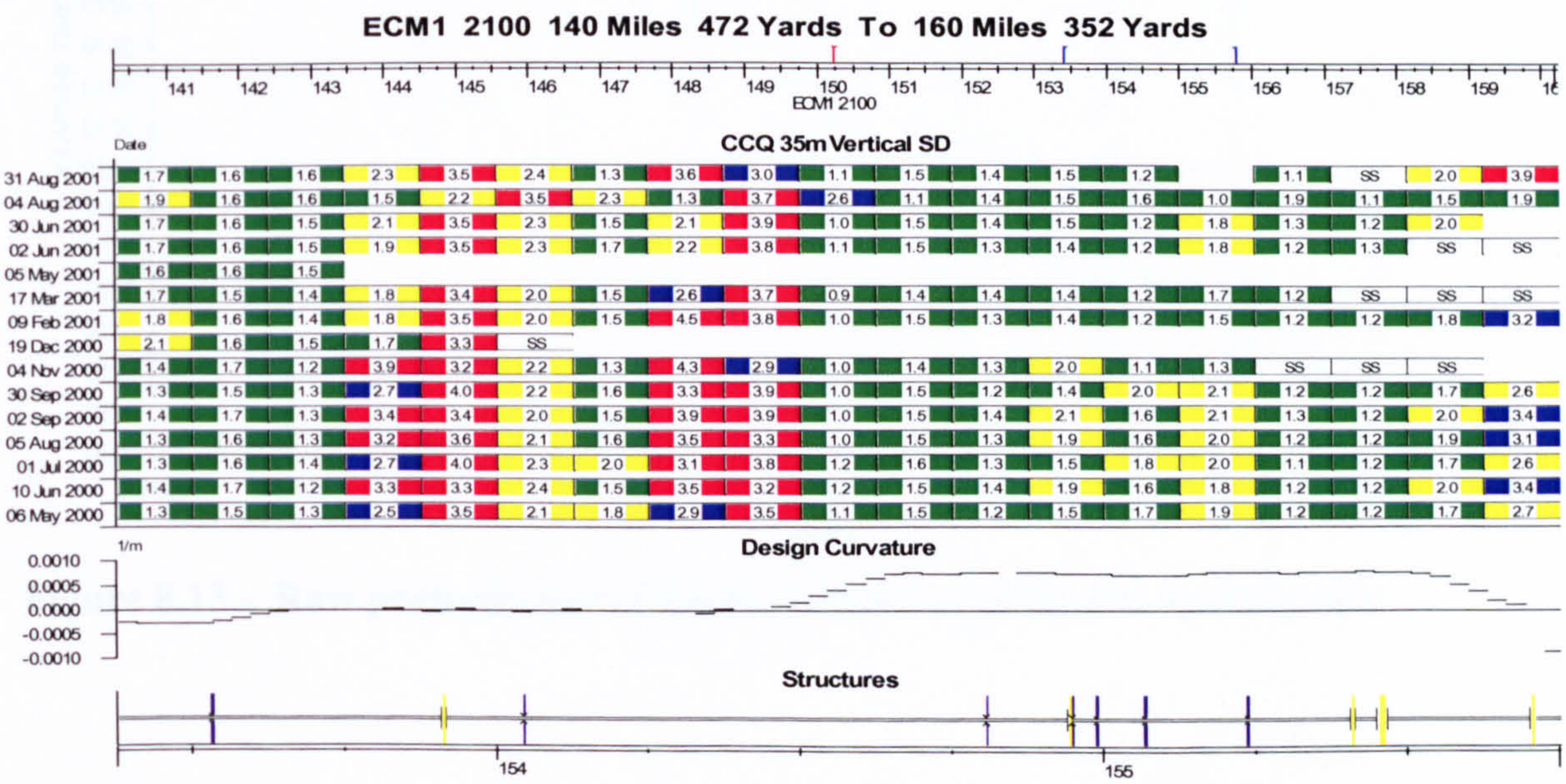

Figure 8.11 - TrackMaster Chart 2, track quality with curvature and structures

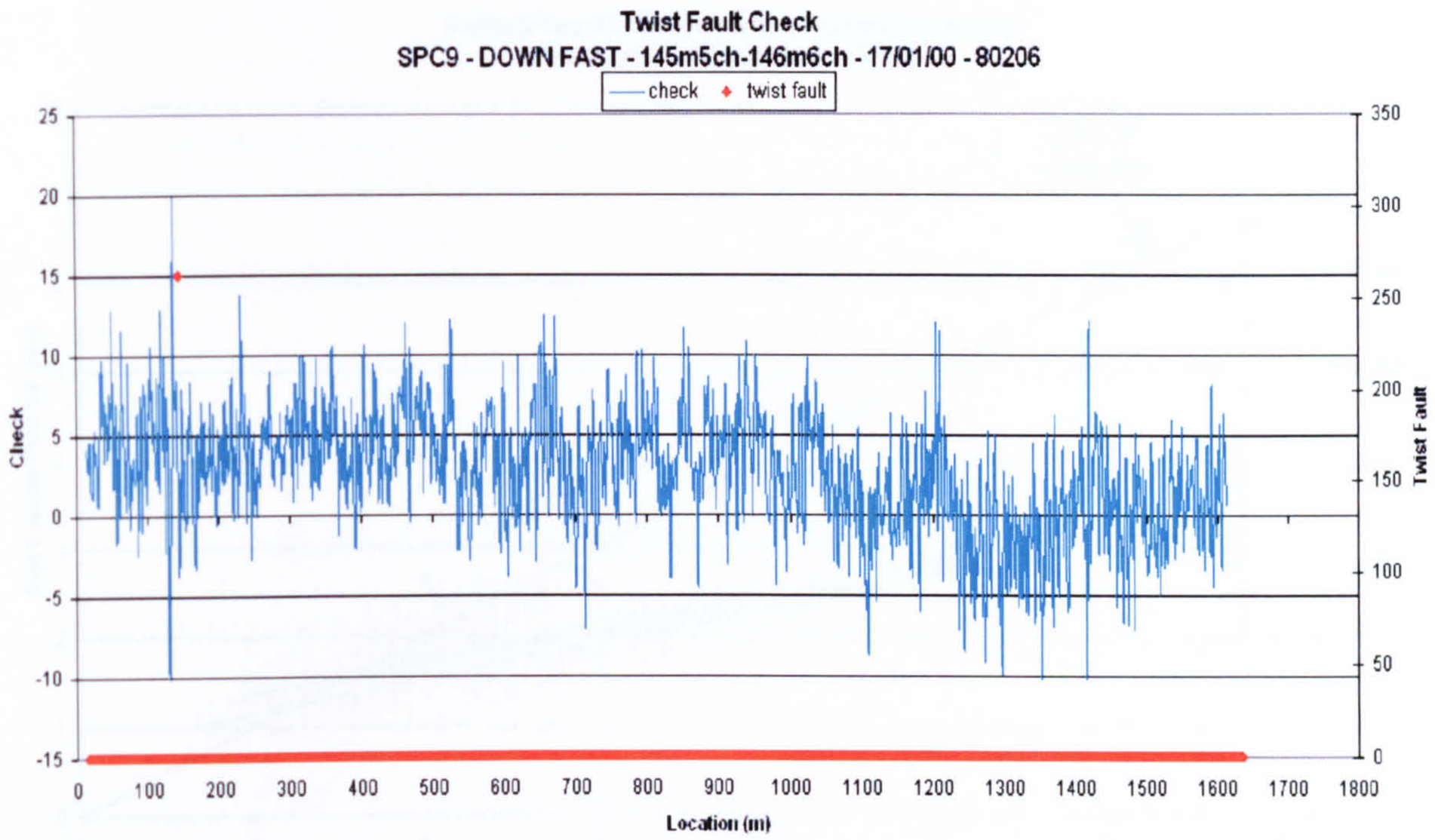

Figure 8.12 - Twist check chart as calculated by the stoneblower

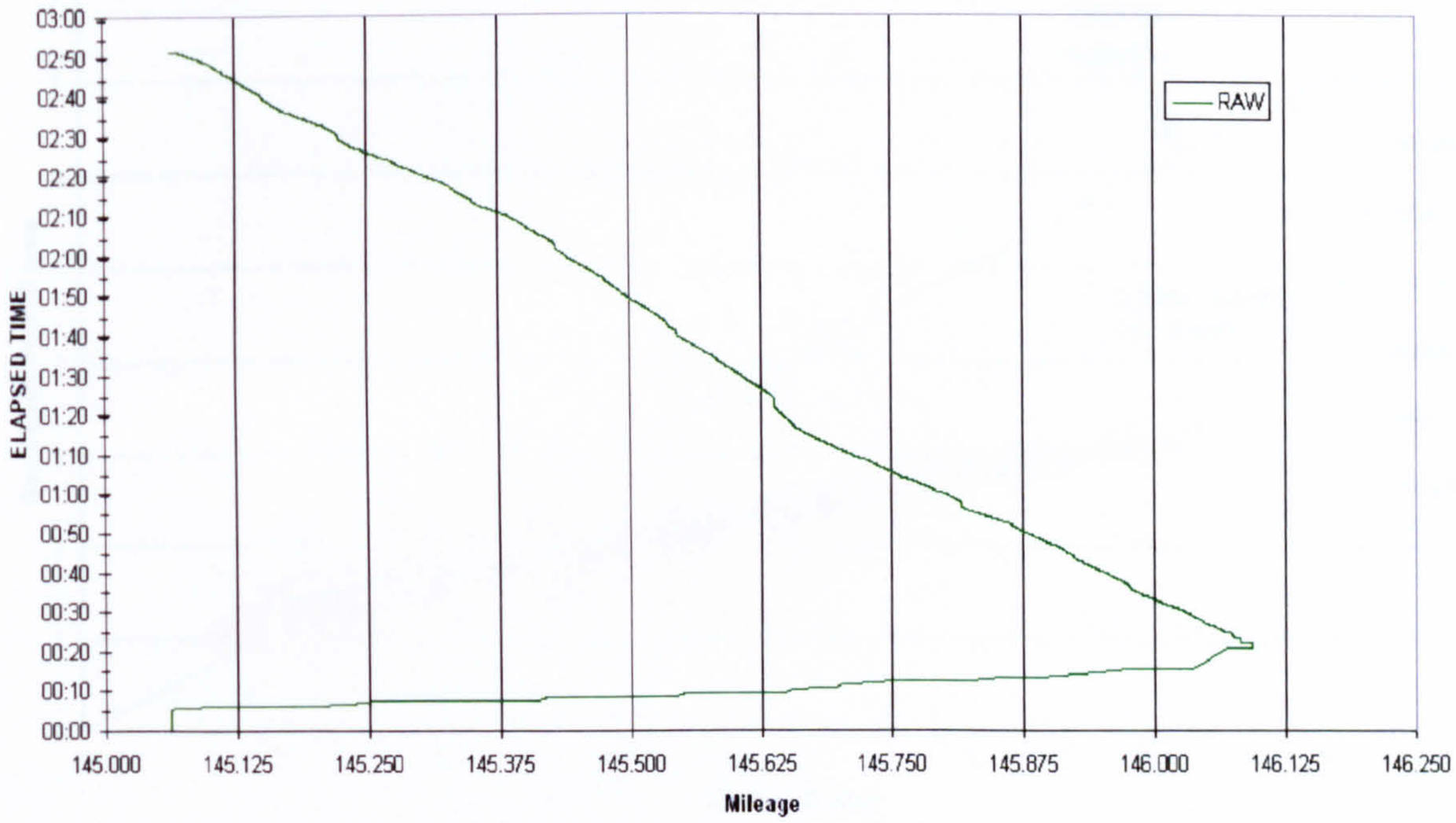

Figure 8.13 - Raw performance of the stoneblower during the maintenance

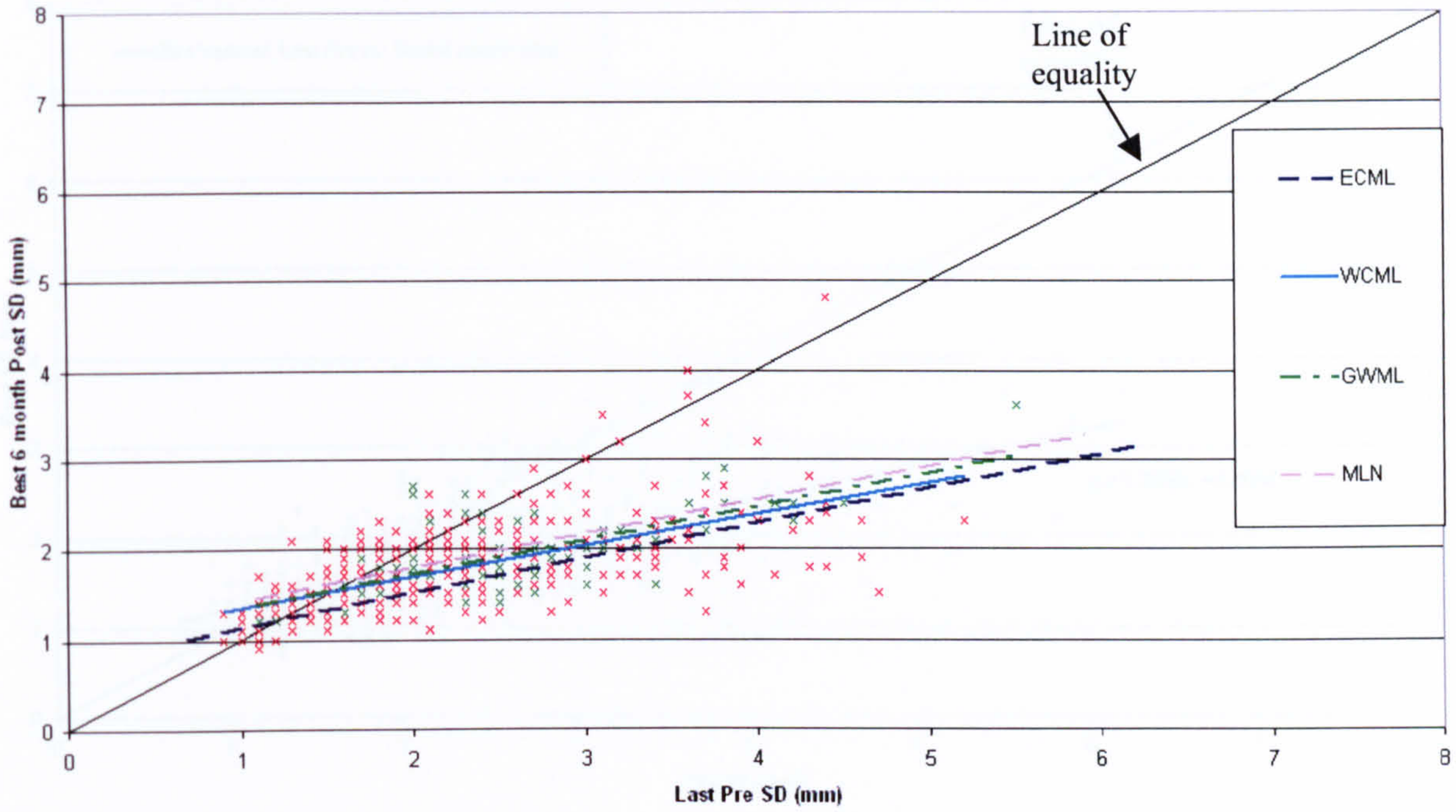

Figure 8.14 - Track quality improvement for each route analysed

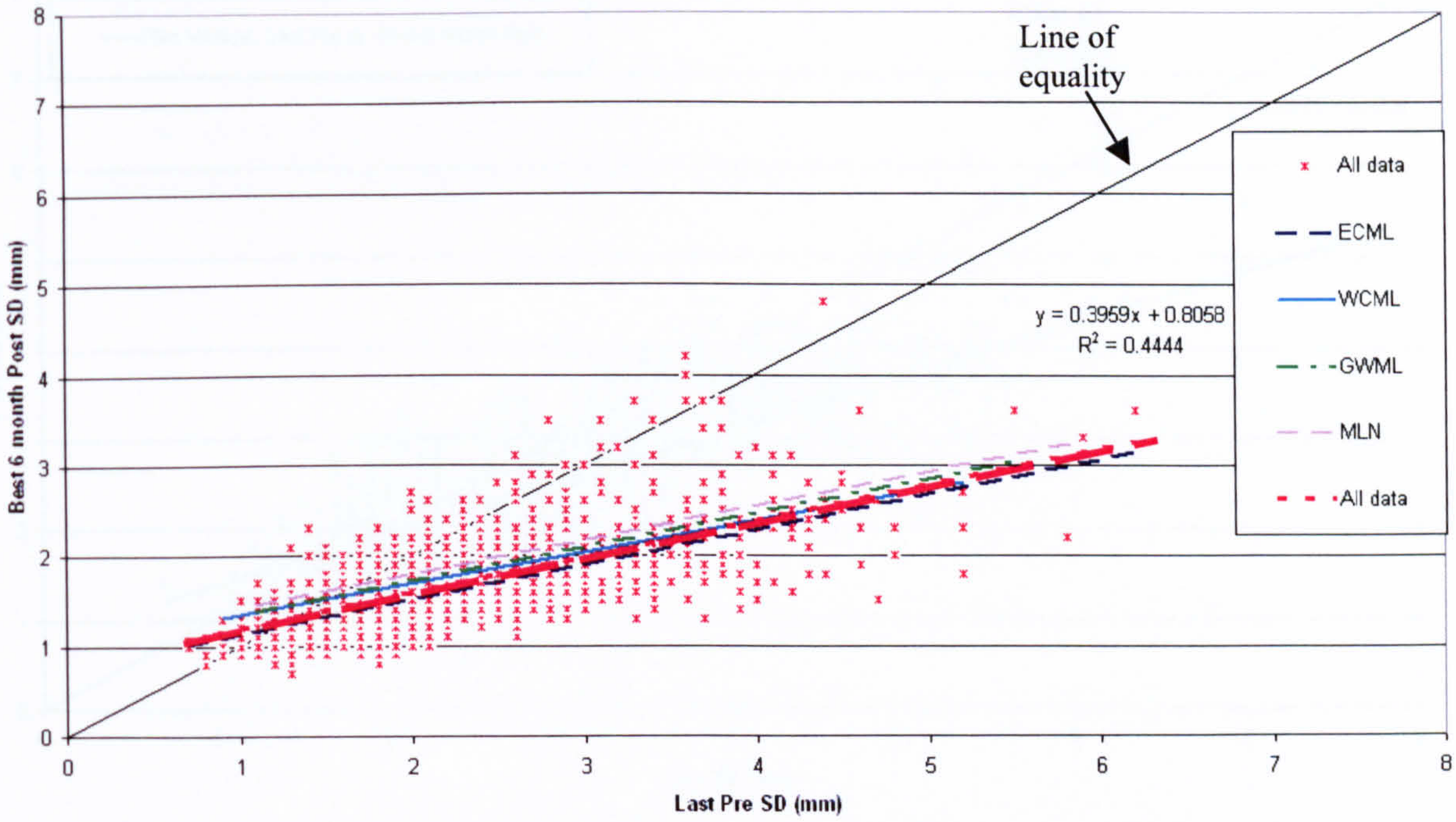

Figure 8.15 - Track quality improvement for all routes combined

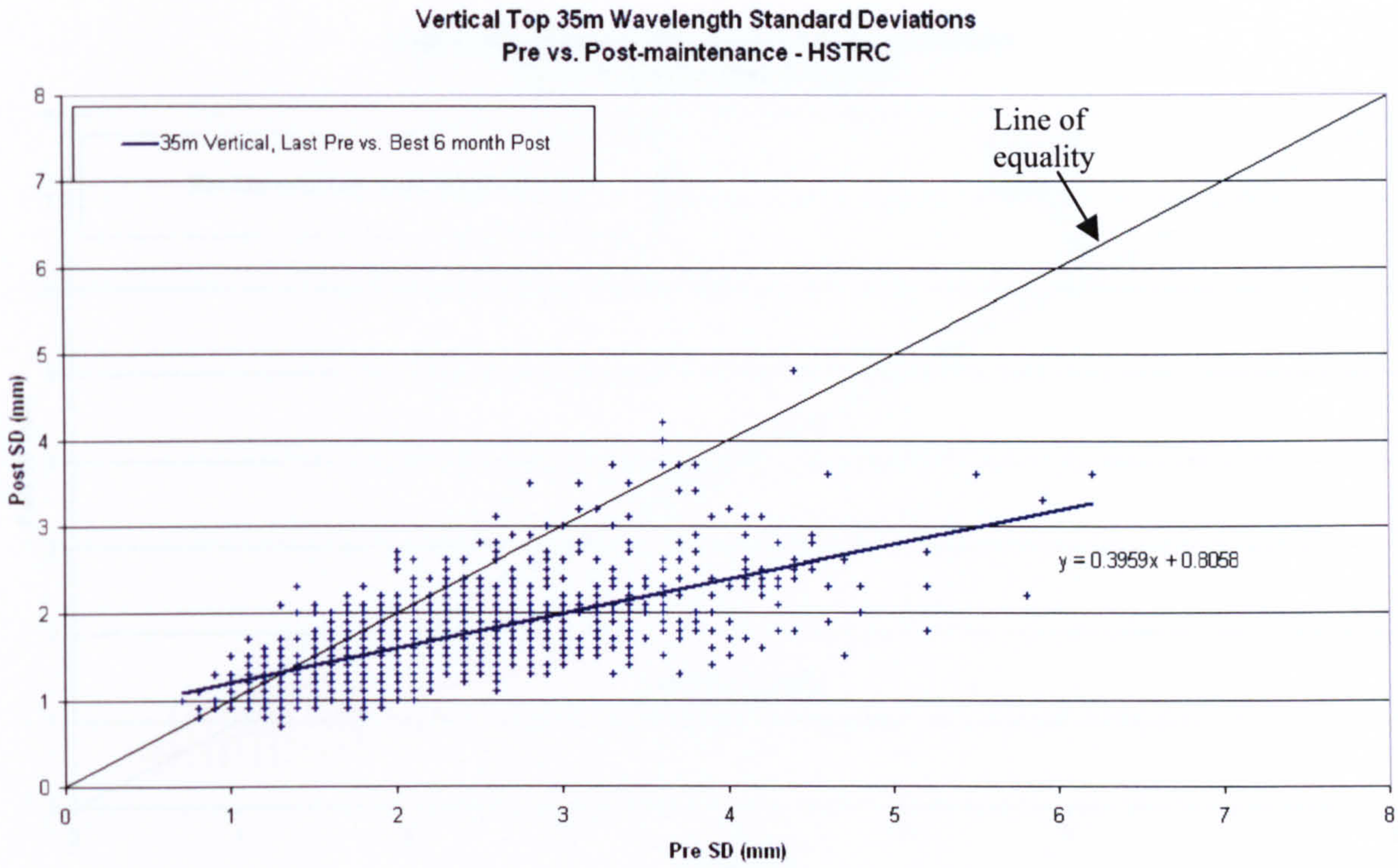

Figure 8.16 - Track quality improvement - vertical top 35m wavelength

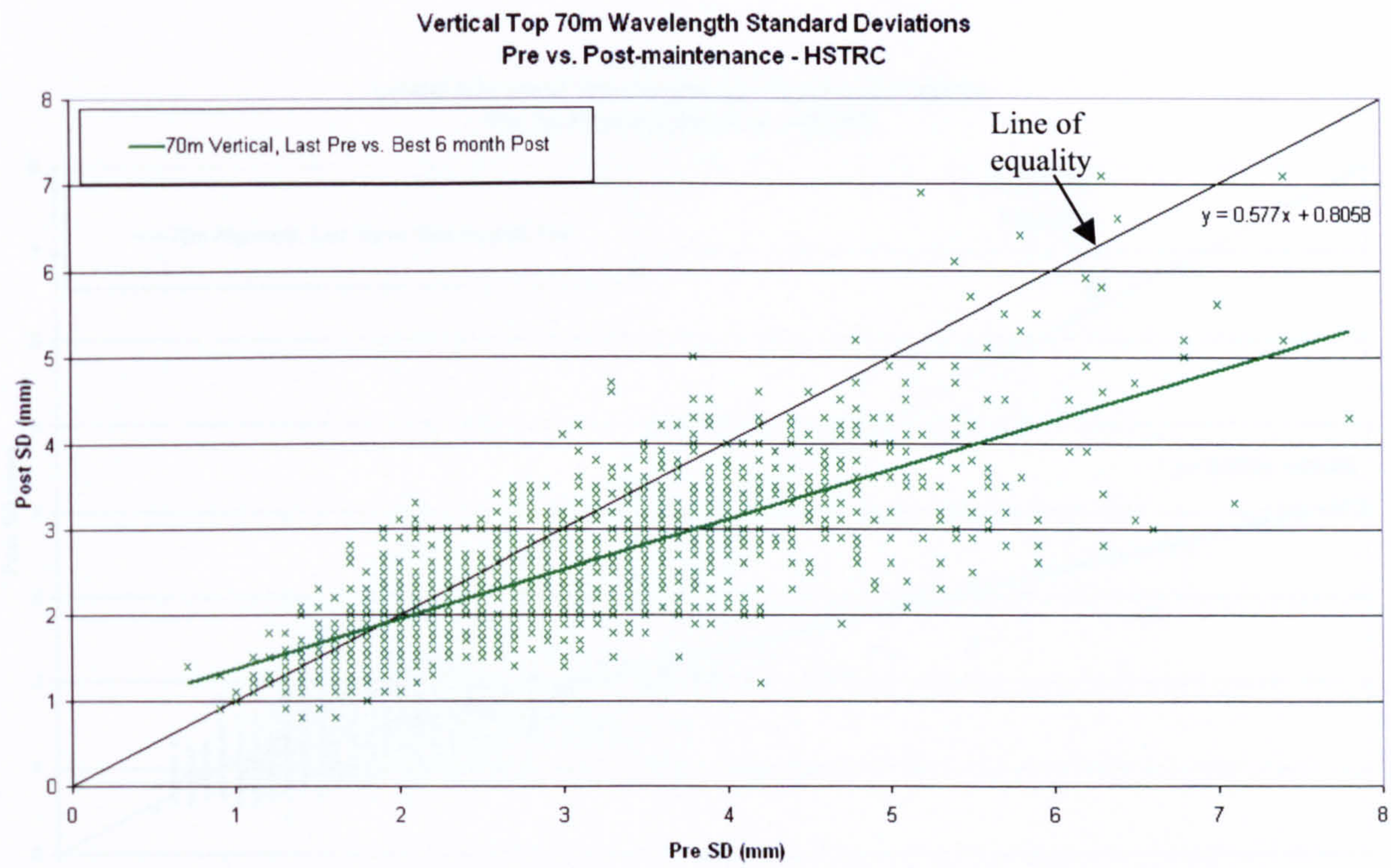

Figure 8.17 - Track quality improvement - vertical top 70m wavelength

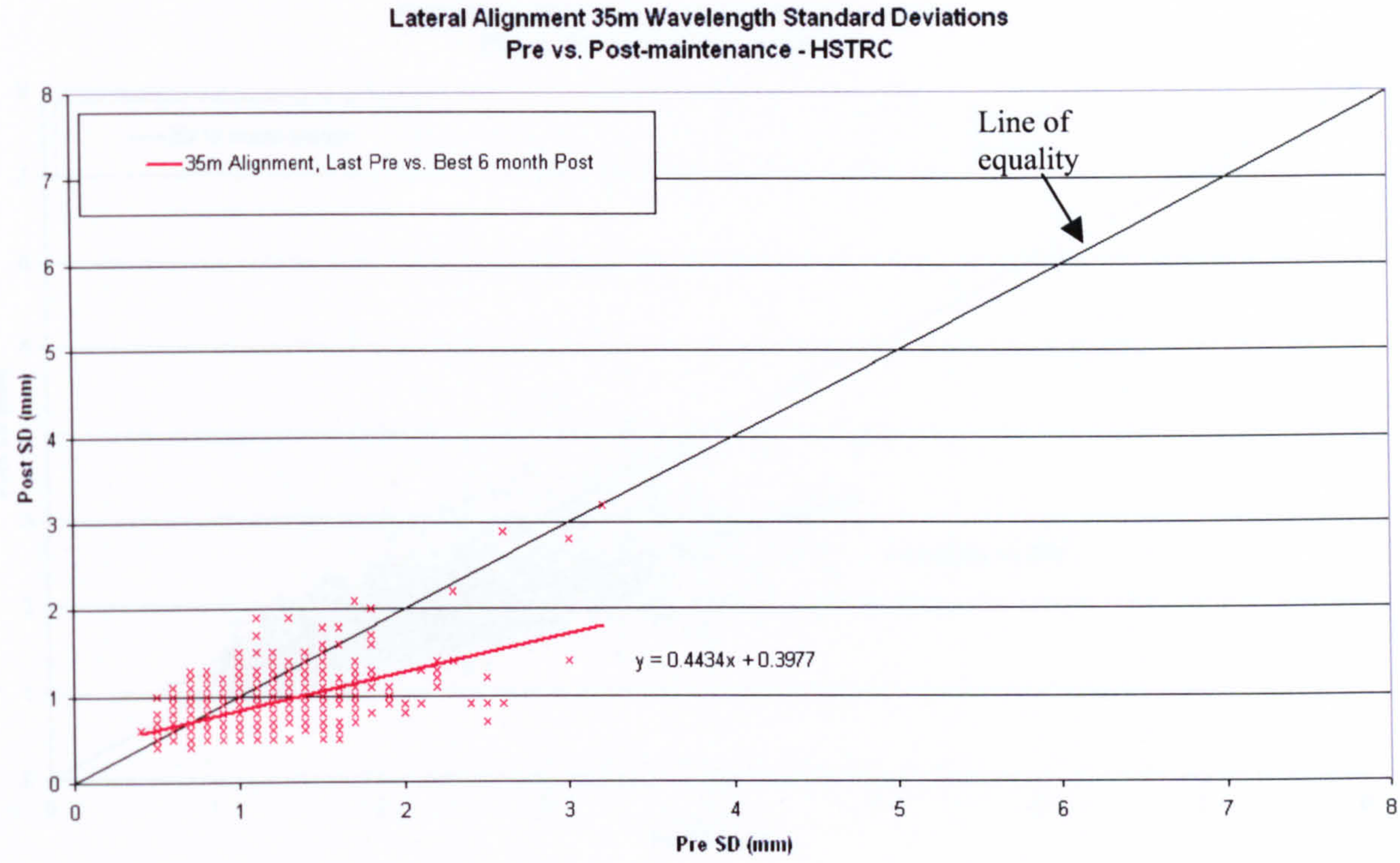

Figure 8.18 - Track quality improvement - lateral alignment 35m wavelength

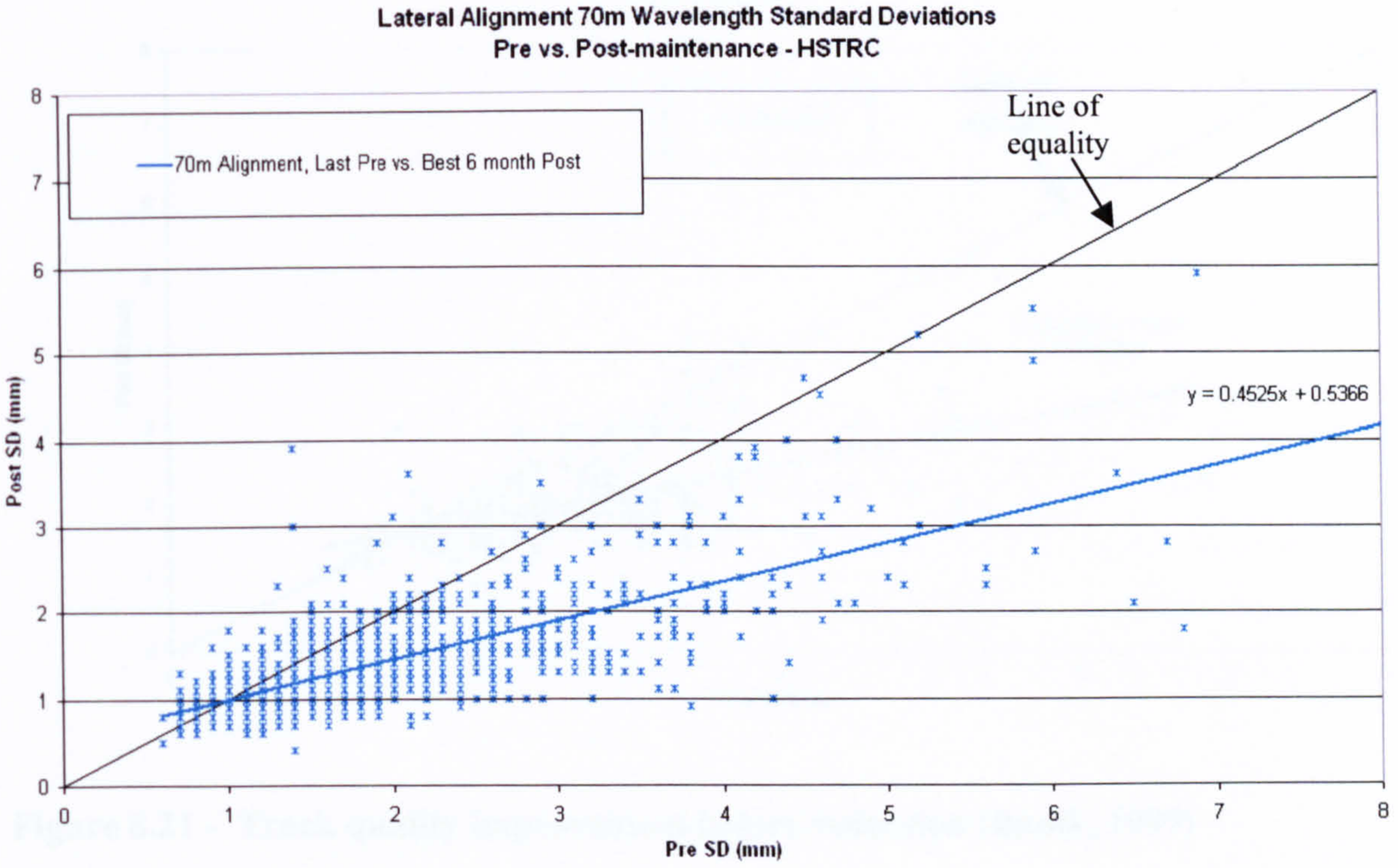

Figure 8.19 - Track quality improvement - lateral alignment 70m wavelength

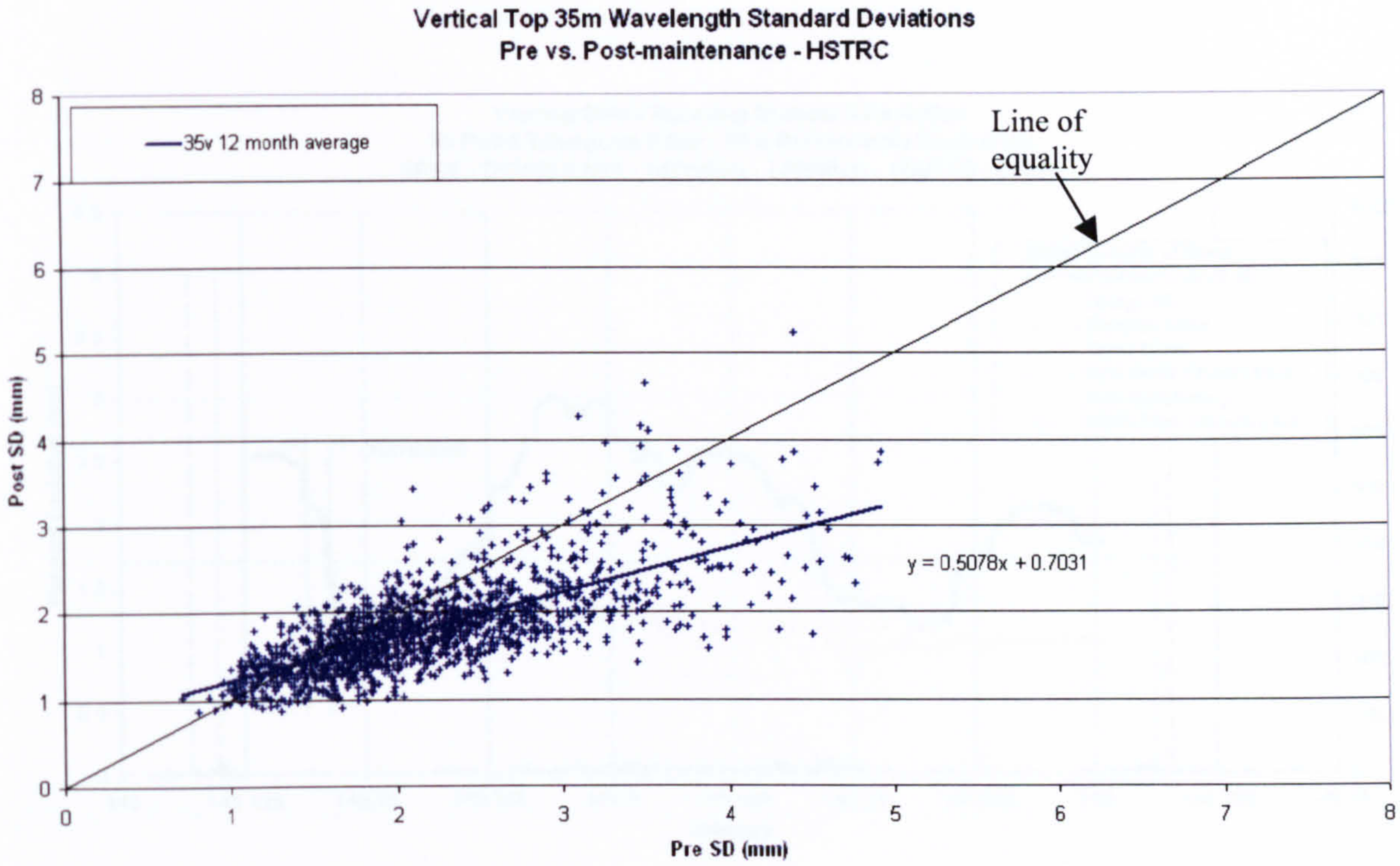

Figure 8.20 - Track quality improvement - 12 month average pre- and post-maintenance (vertical top 35m wavelength)

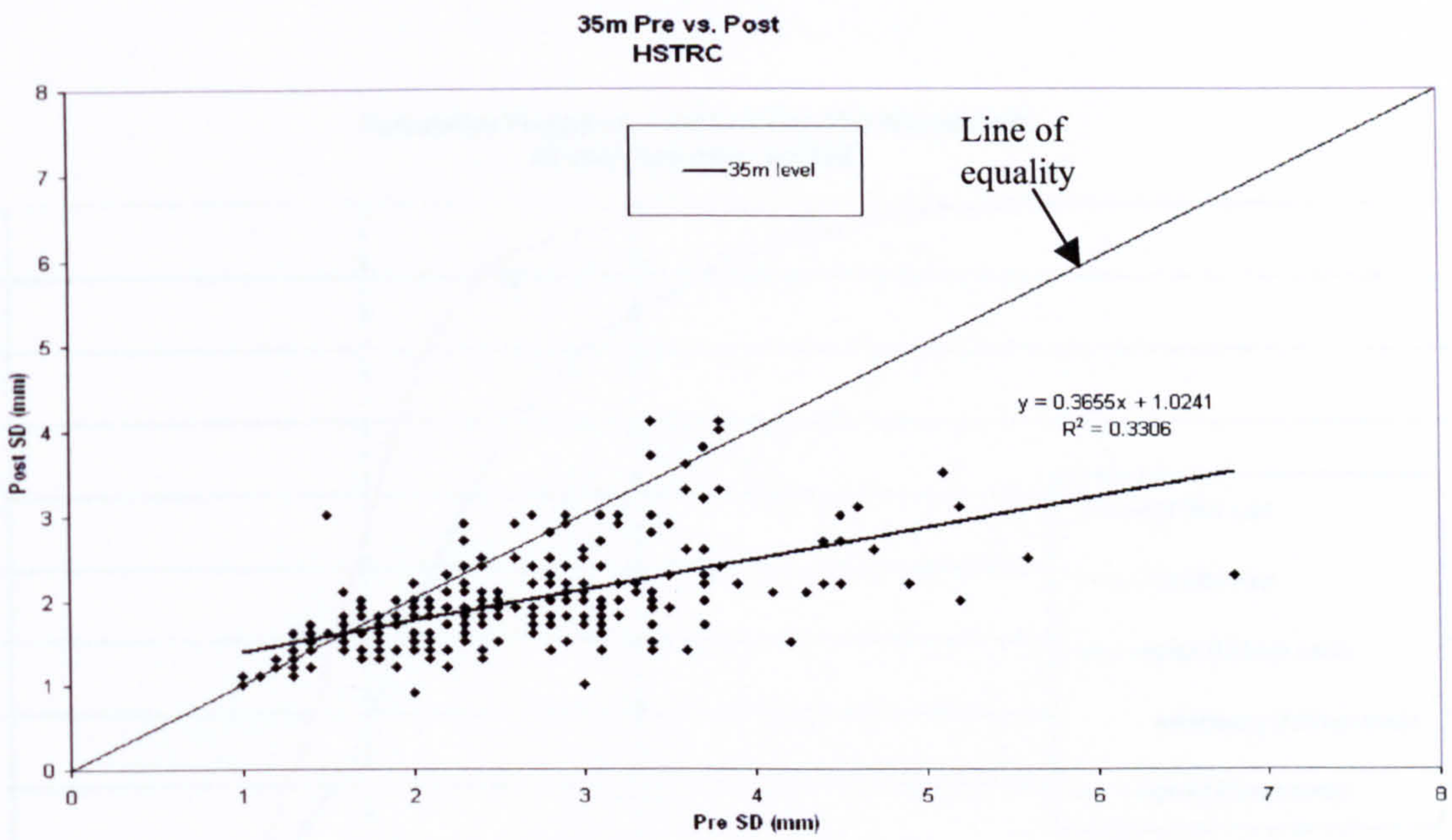

Figure 8.21 - Track quality improvement before reduction (Baulk, 1999)

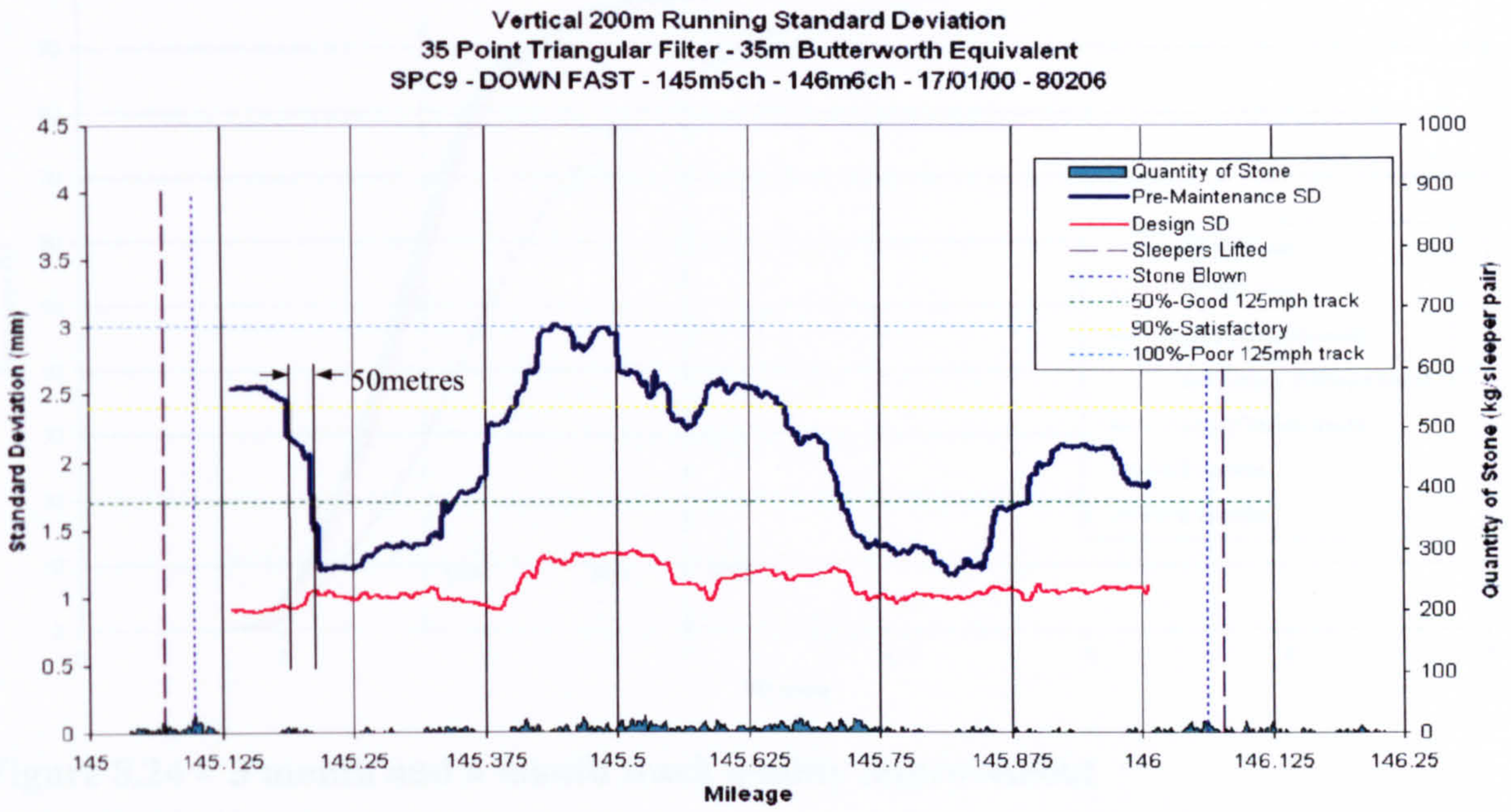

Figure 8.22 - Effect of positioning errors seen on a running standard deviation plot

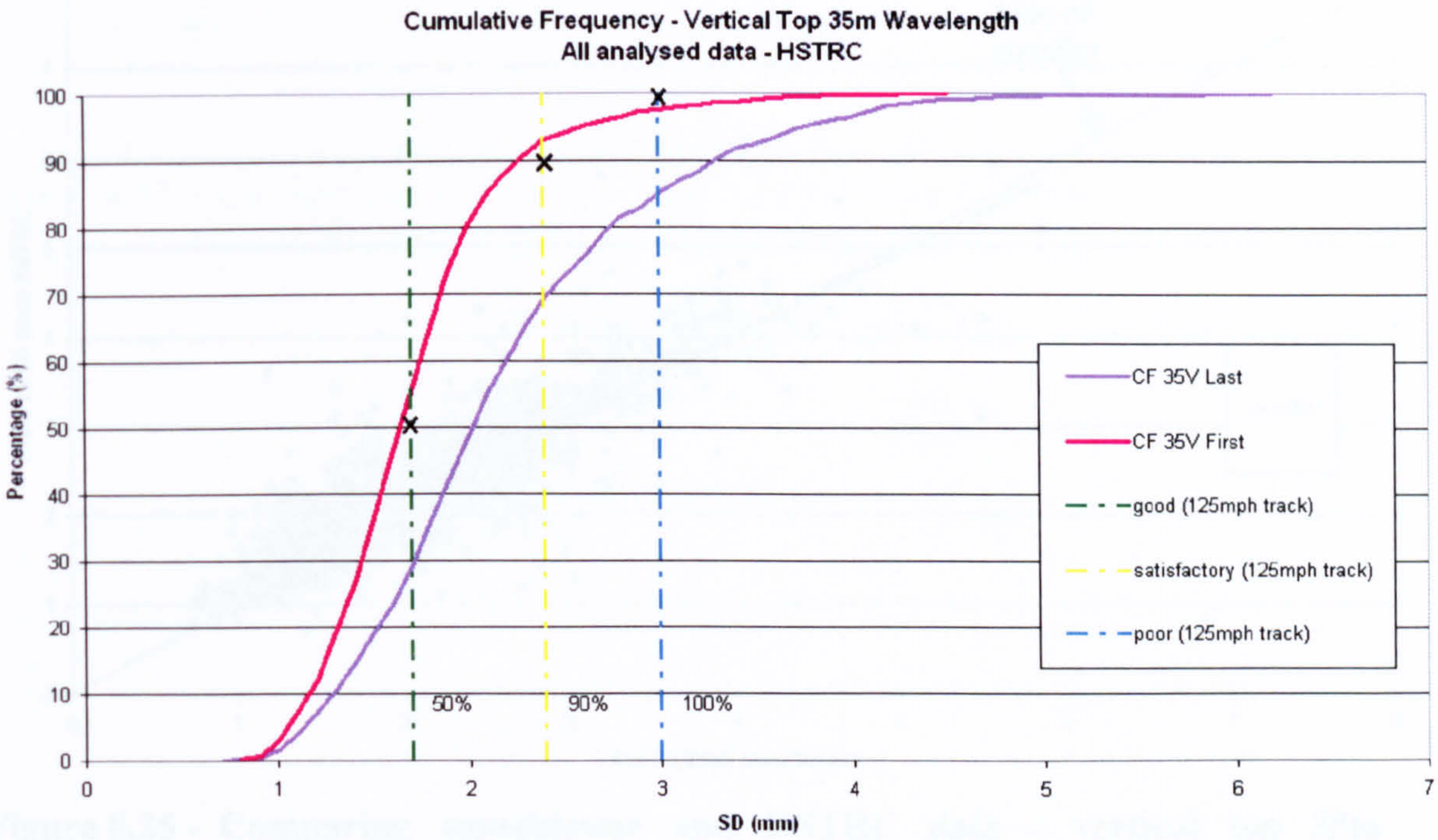

Figure 8.23 - Cumulative frequency plot showing track quality improvement - vertical top 35m wavelength

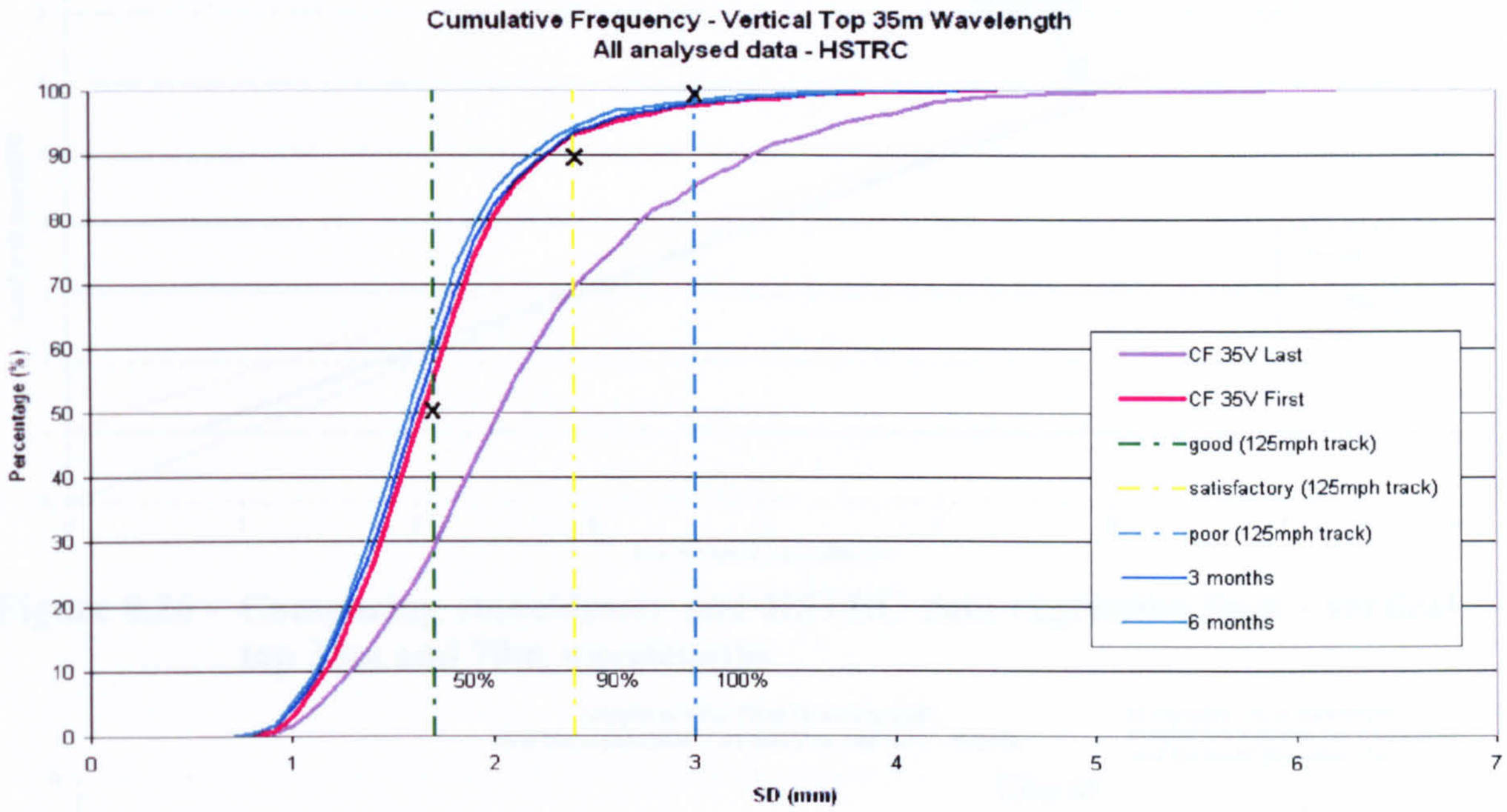

Figure 8.24 - 3 month and 6 month track quality improvement

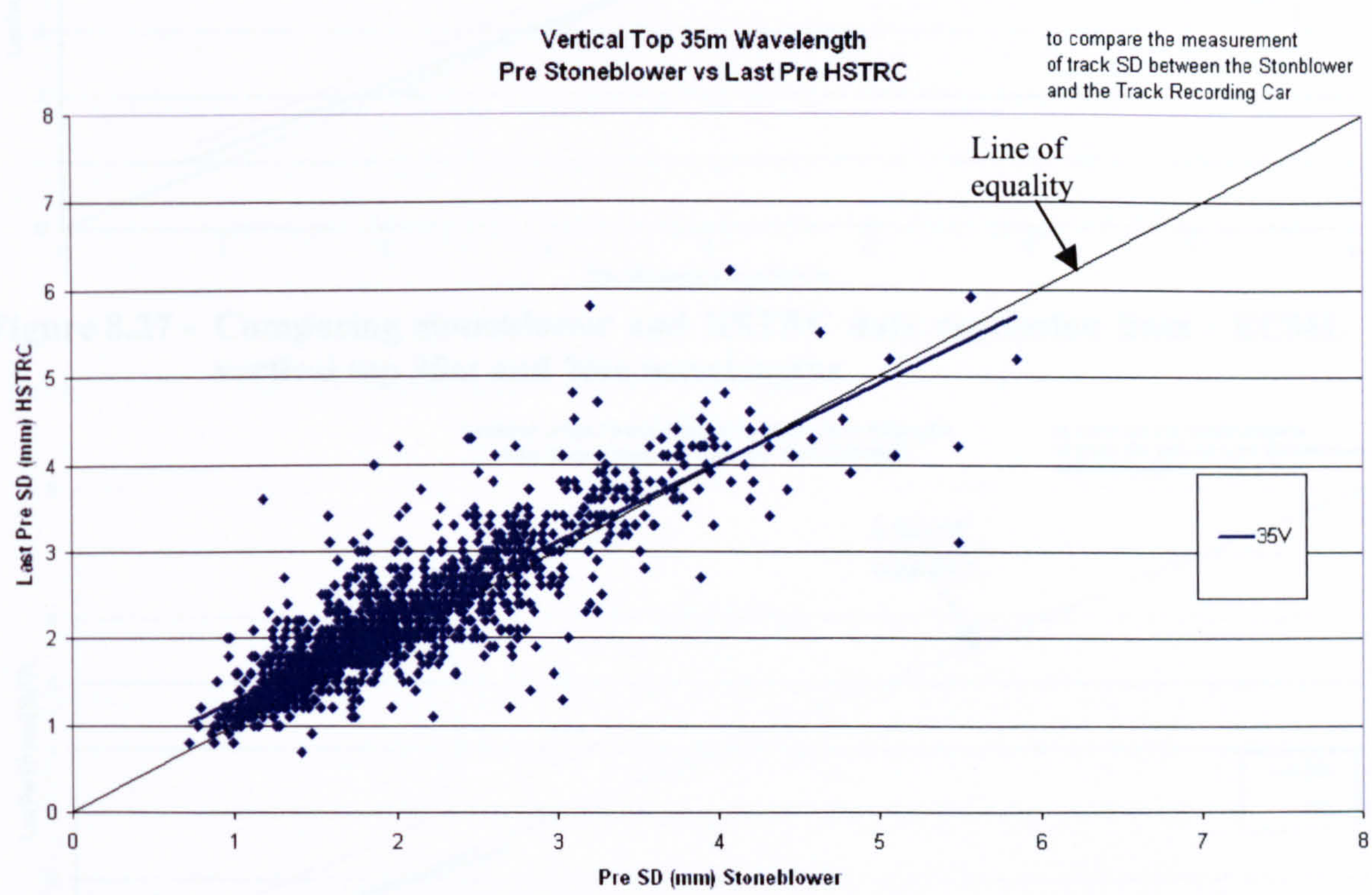

Figure 8.25 - Comparing stoneblower and HSTRC data - vertical top 35m wavelength

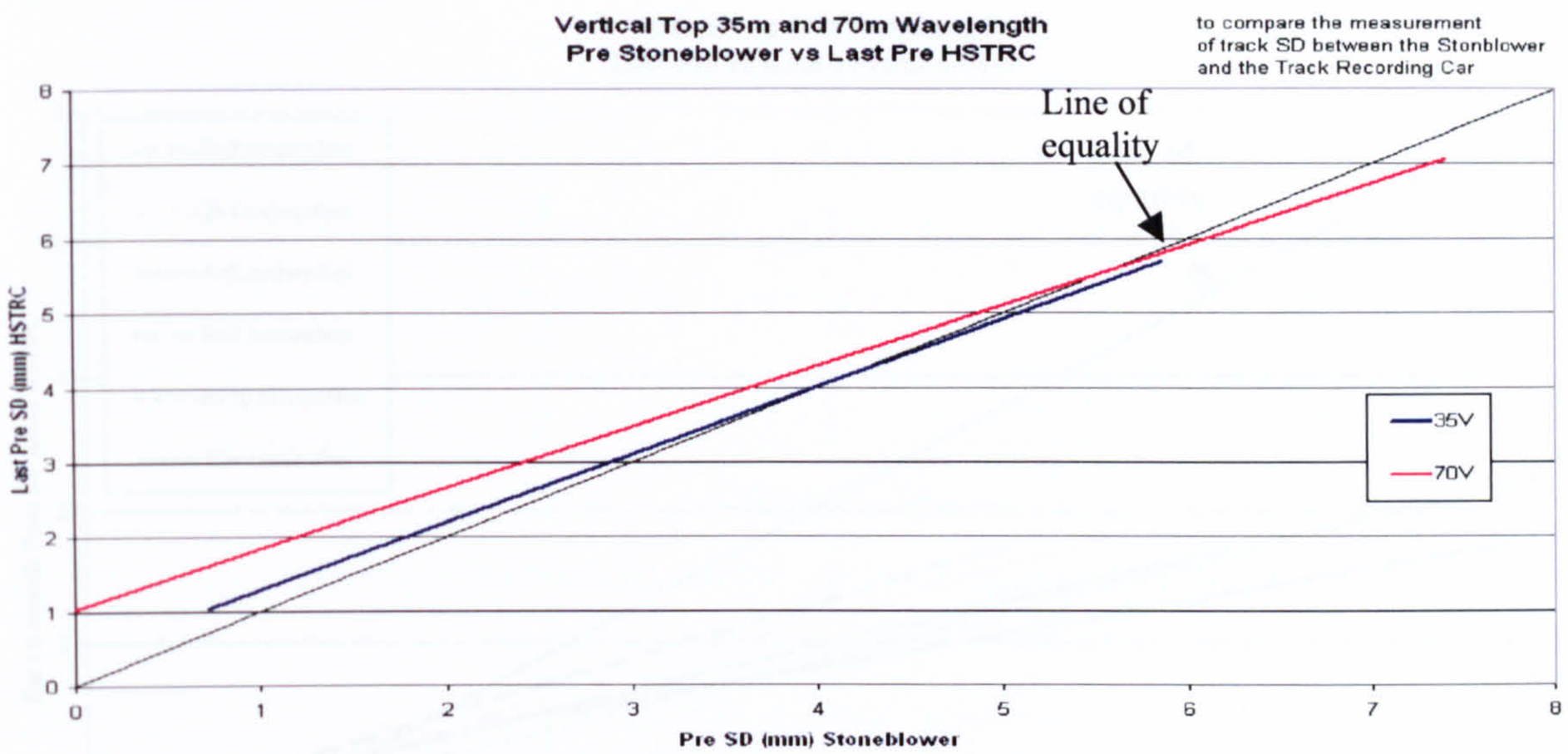

Figure 8.26 - Comparing stoneblower and HSTRC data regression lines - vertical top 35m and 70m wavelengths

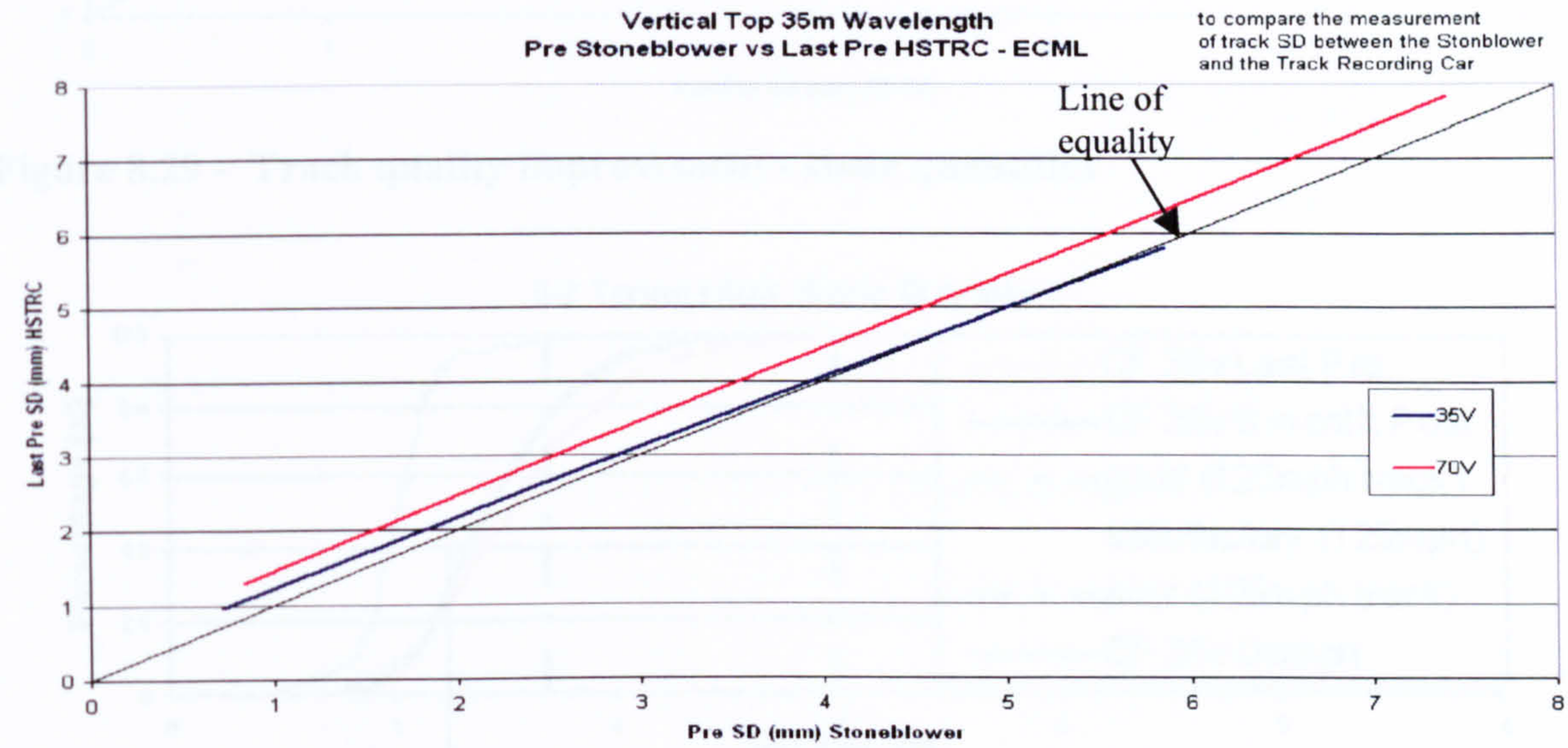

Figure 8.27 - Comparing stoneblower and HSTRC data regression lines - ECML vertical top 35m and 70m wavelengths

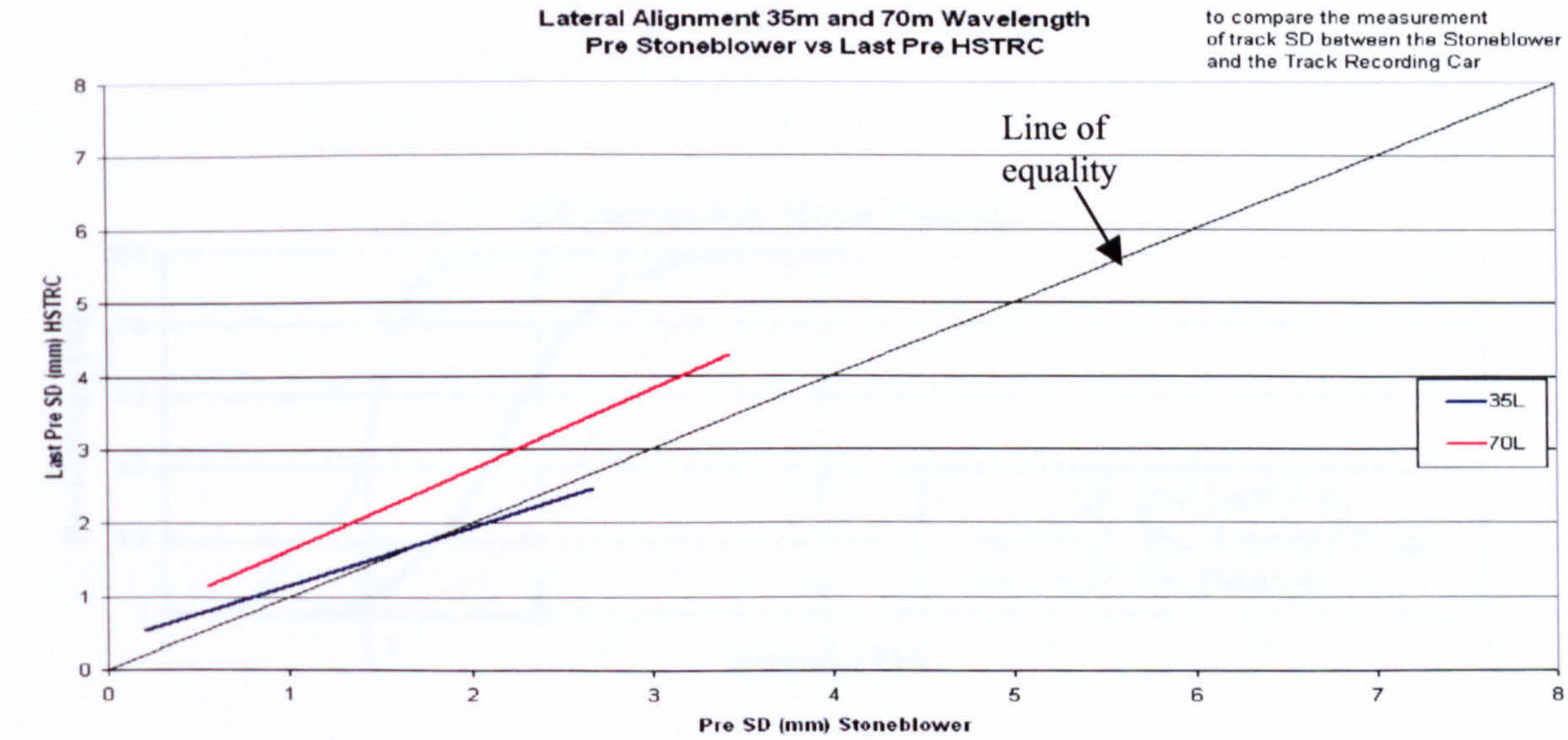

Figure 8.28 - Comparing stoneblower and HSTRC data regression lines - lateral alignment 35m and 70m wavelengths

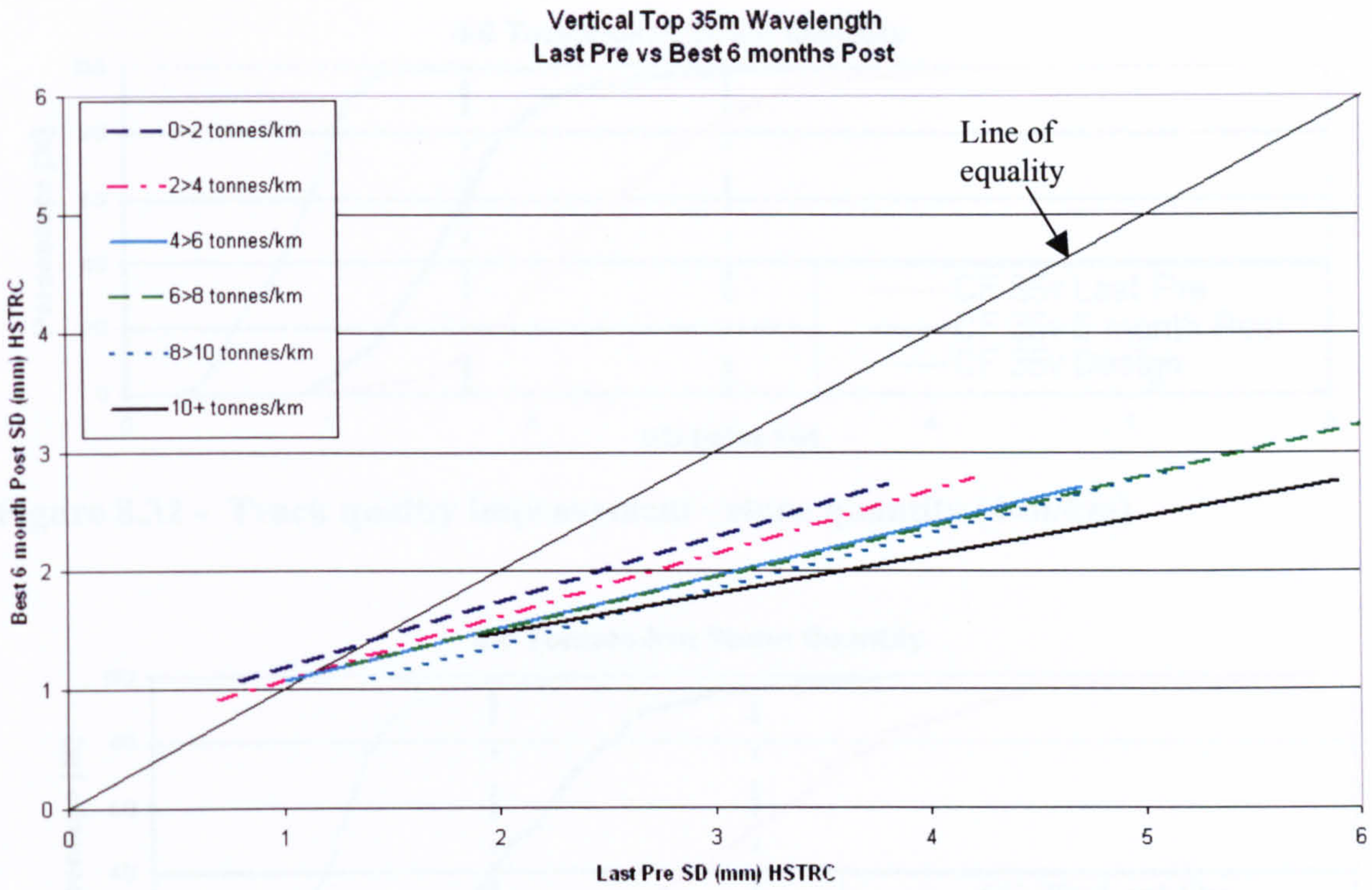

Figure 8.29 - Track quality improvement - stone quantities

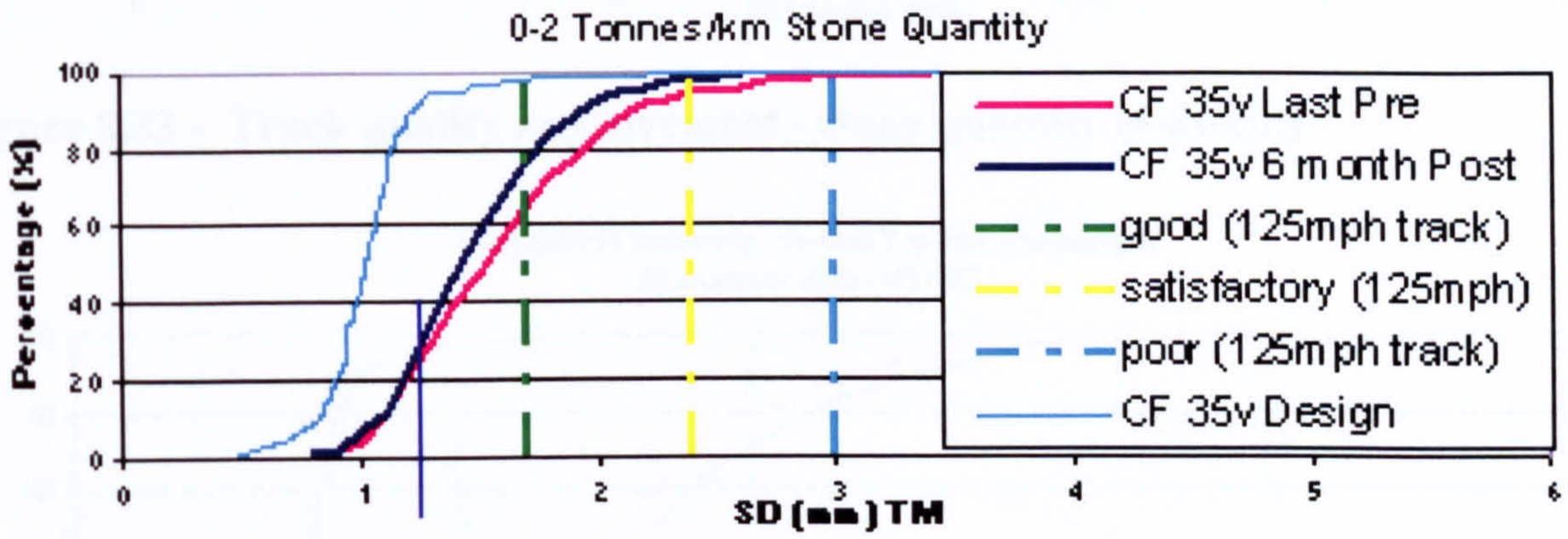

Figure 8.30 - Track quality improvement - stone quantity (0-2t/km)

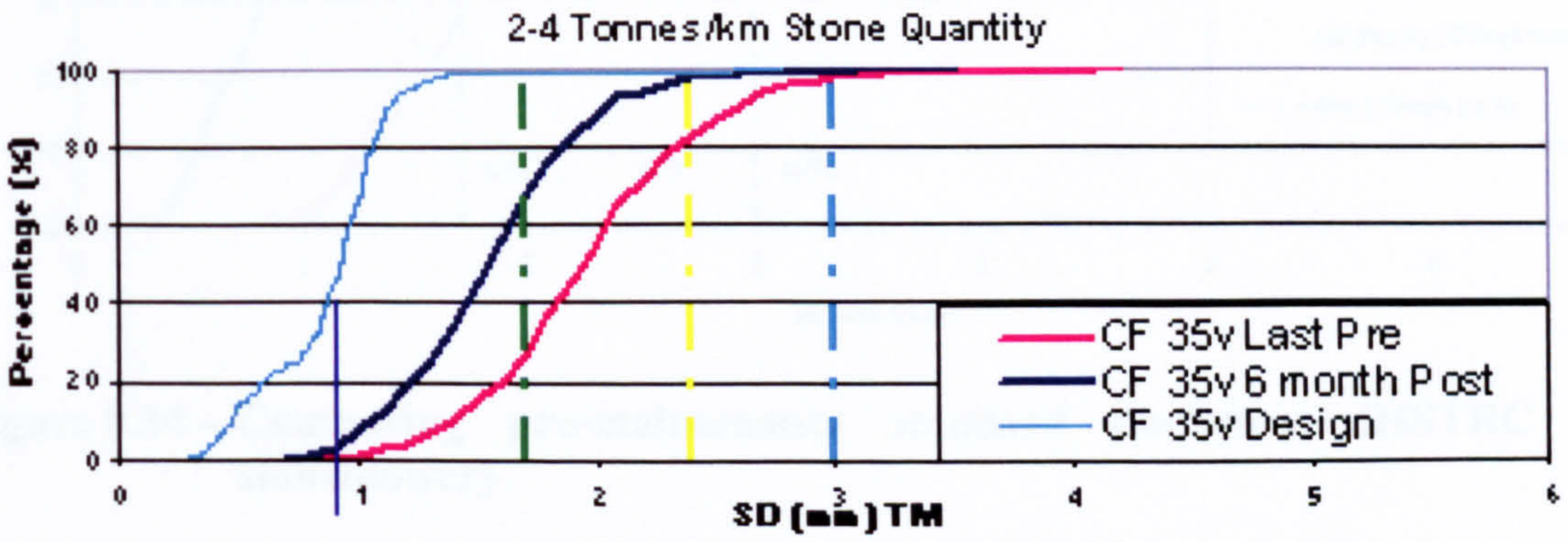

Figure 8.31 - Track quality improvement - stone quantity (2-4t/km)

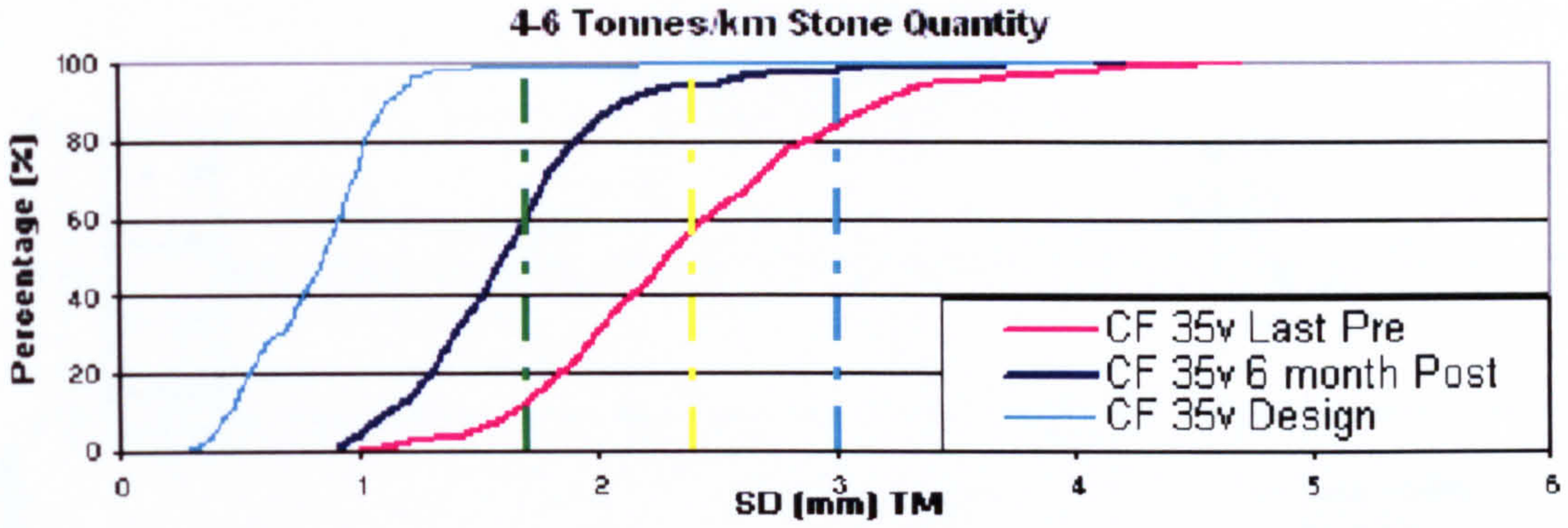

Figure 8.32 - Track quality improvement - stone quantity (4-6t/km)

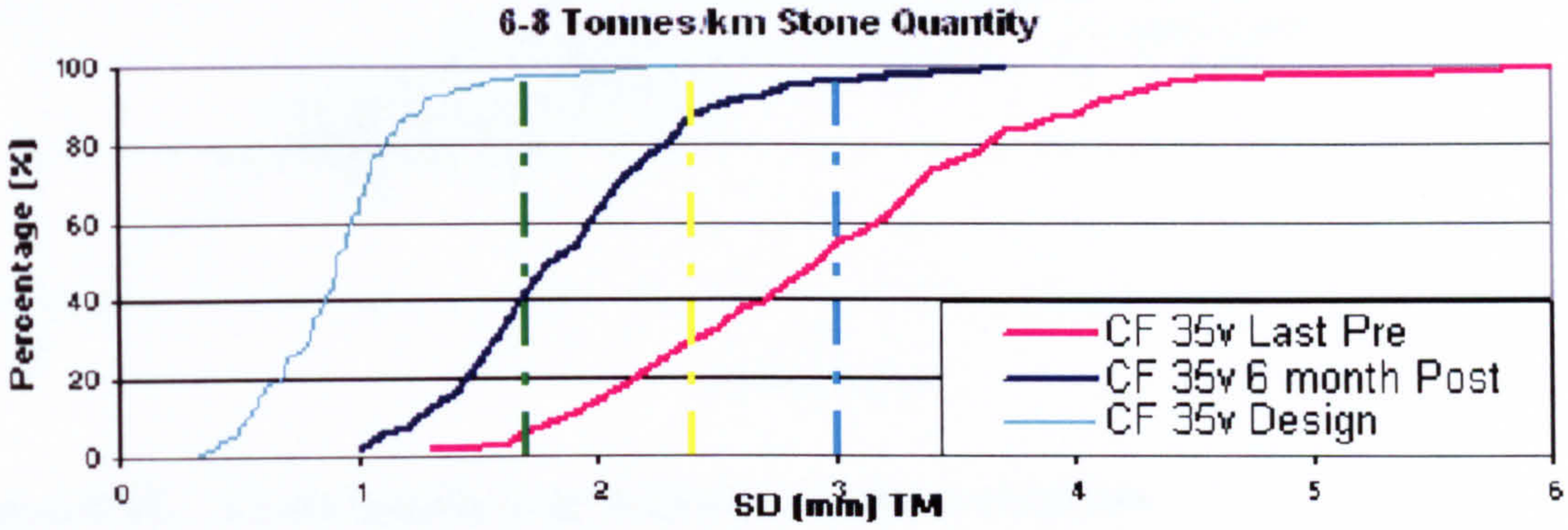

Figure 8.33 - Track quality improvement - stone quantity (6-8t/km)

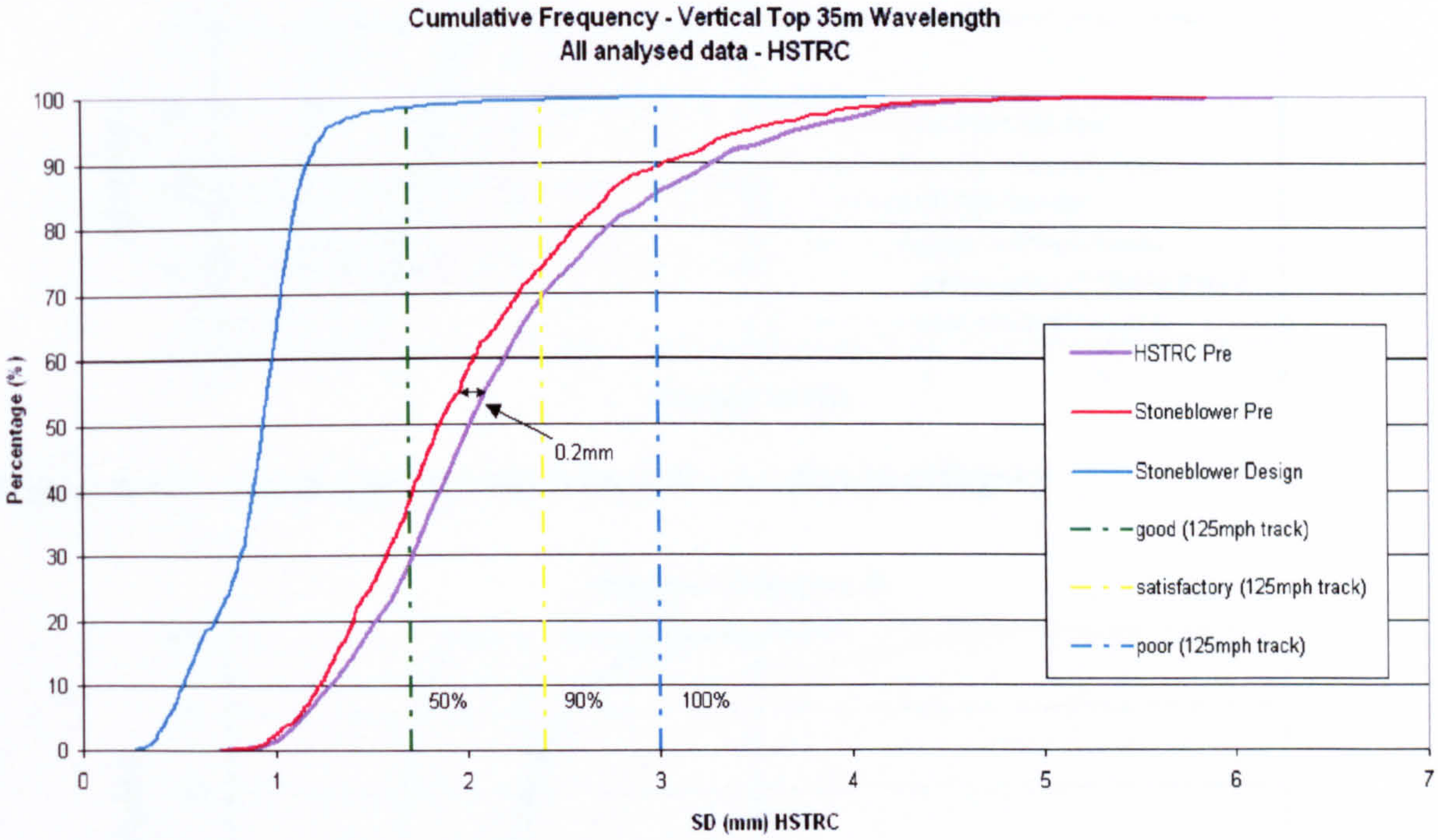

Figure 8.34 - Comparing pre-maintenance standard deviations (HSTRC & stoneblower)

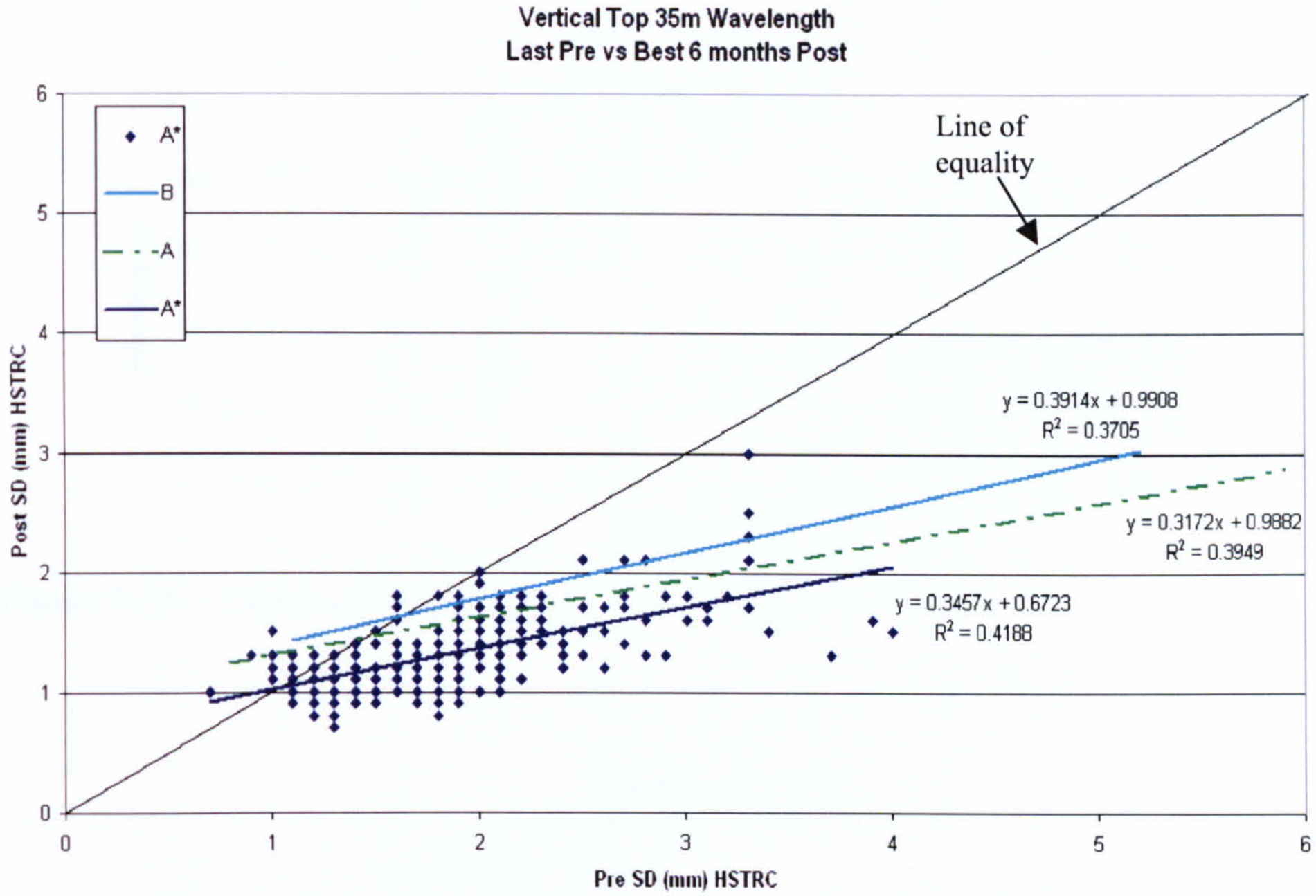

Figure 8.35 - Track quality improvement - design categories

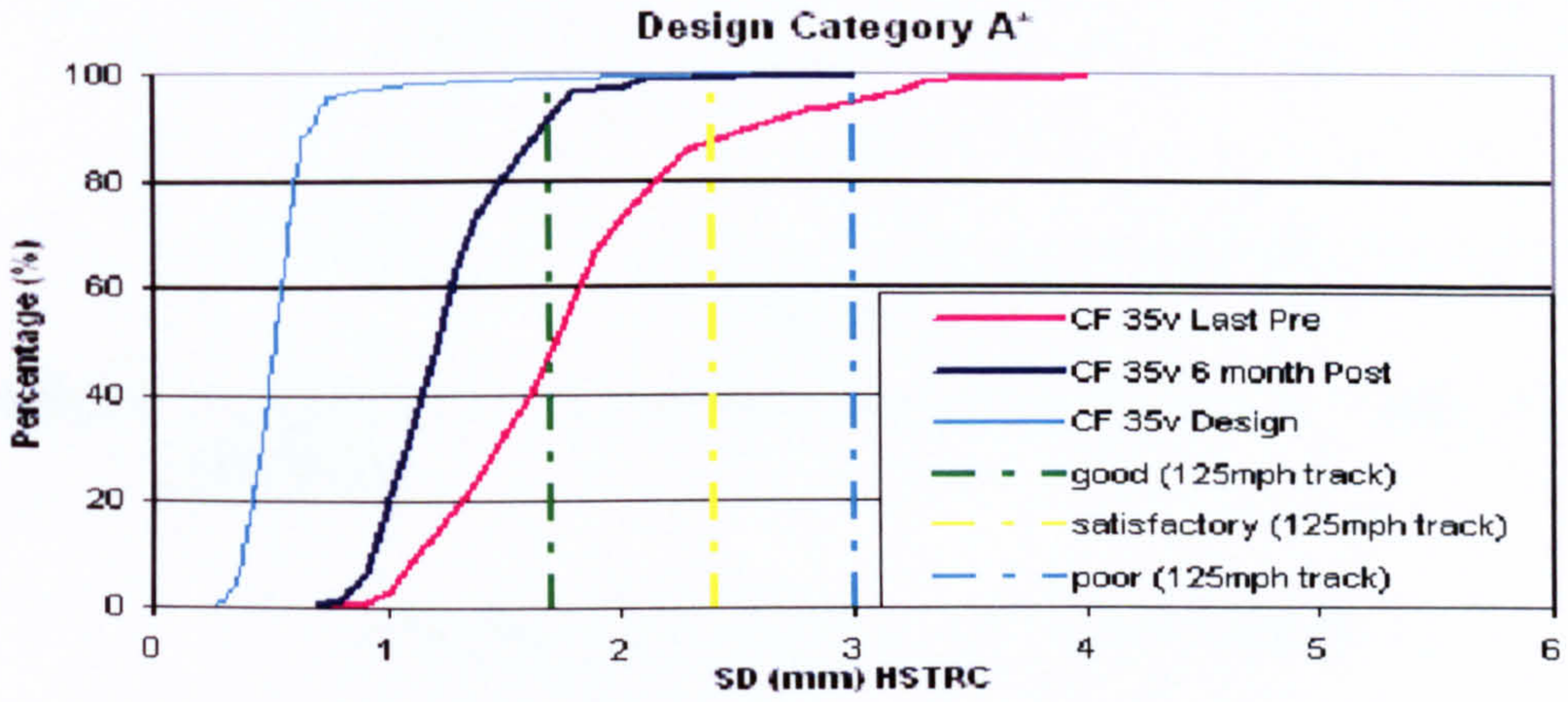

Figure 8.36 - Track quality improvement - A* design category

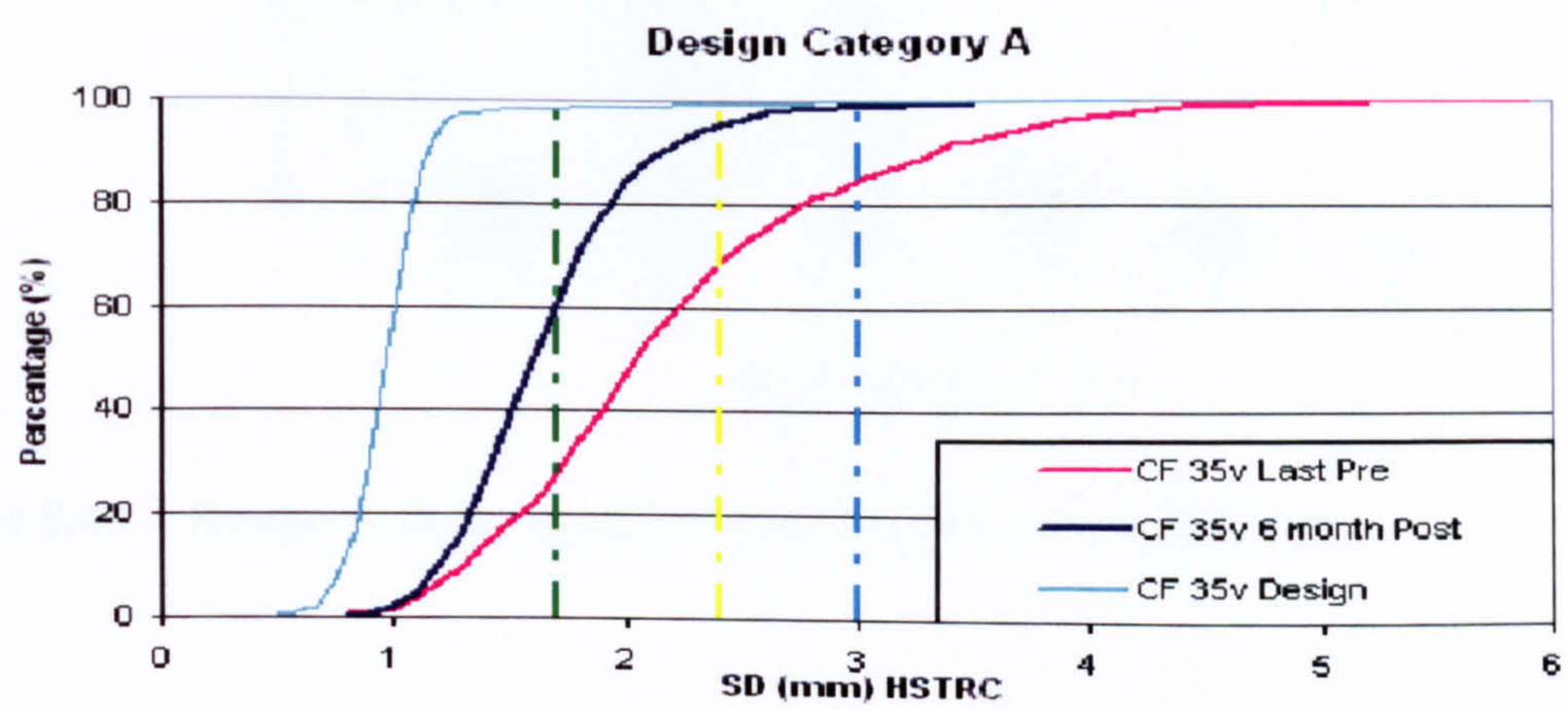

Figure 8.37 - Track quality improvement - A design category

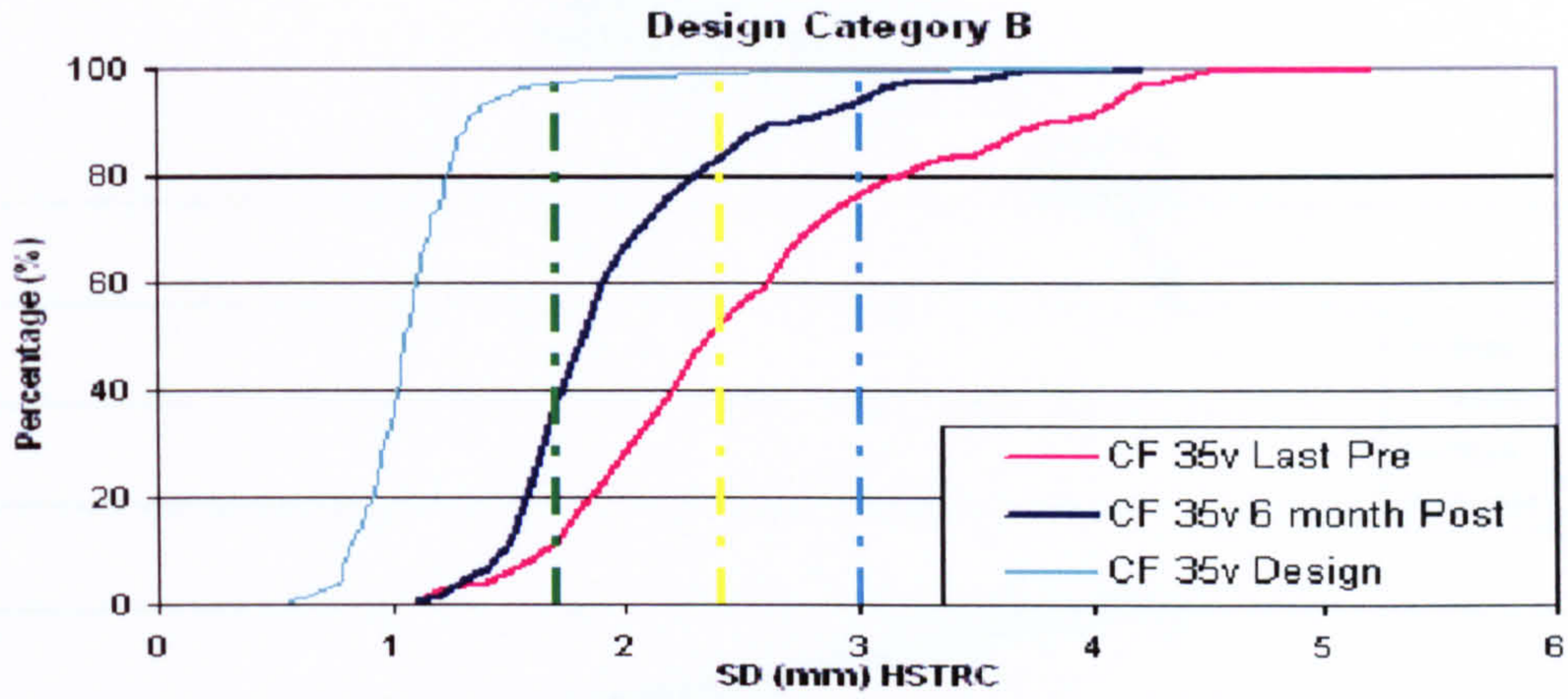

Figure 8.38 - Track quality improvement - B design category

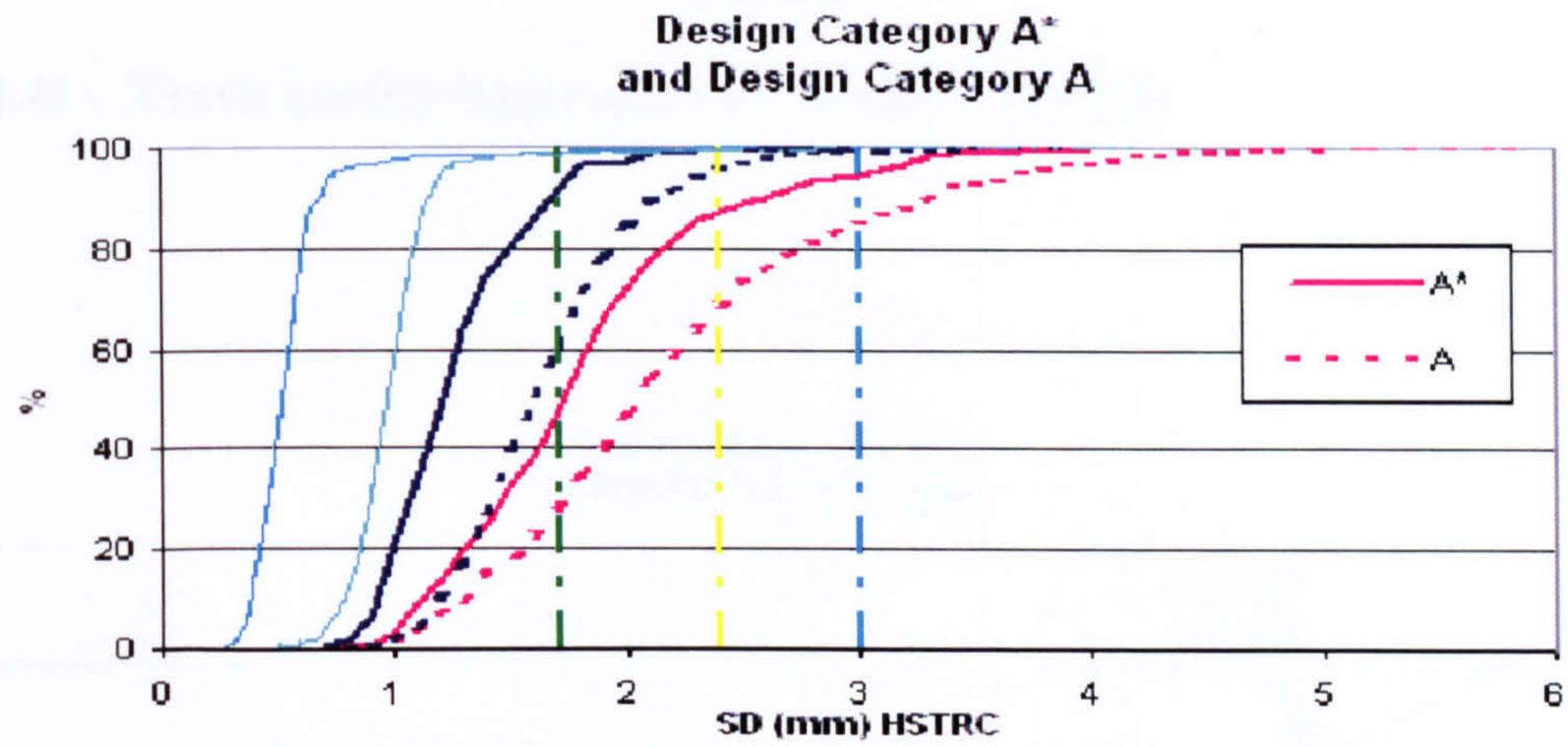

Figure 8.39 - Comparing track quality improvement for A* and A design categories

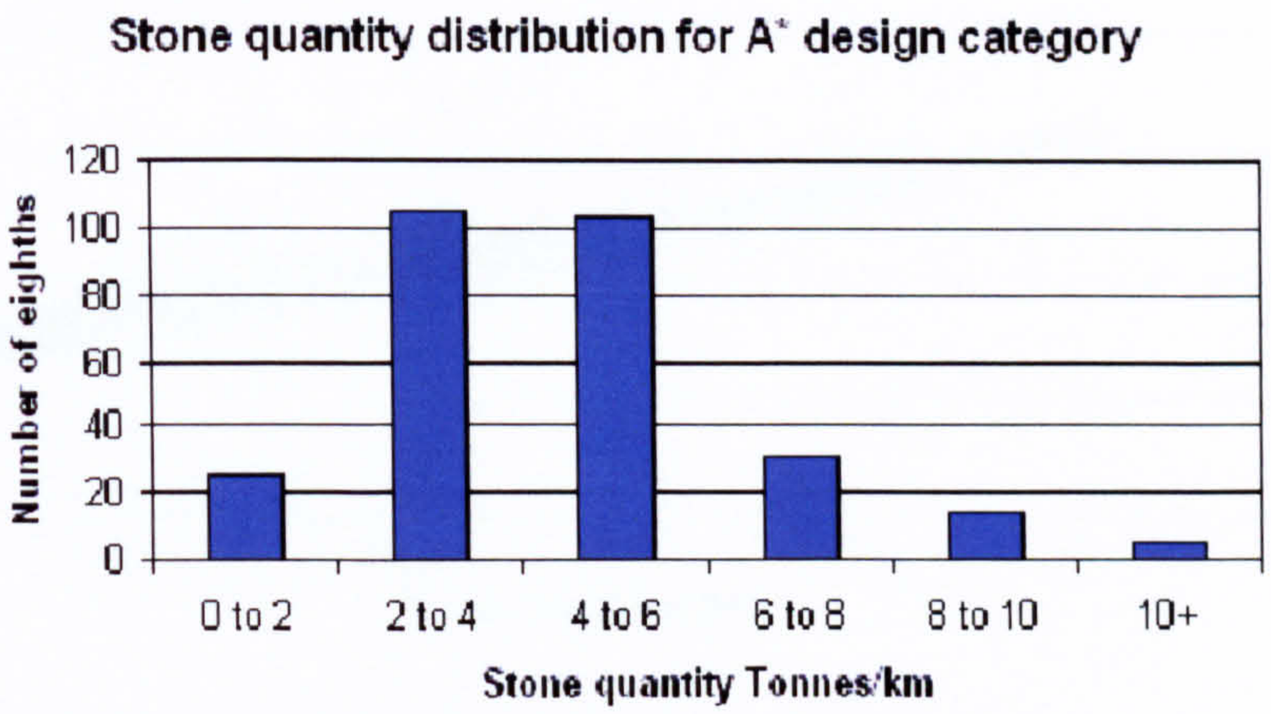

Figure 8.40 - Range of stone quantities used in the A* maintenance

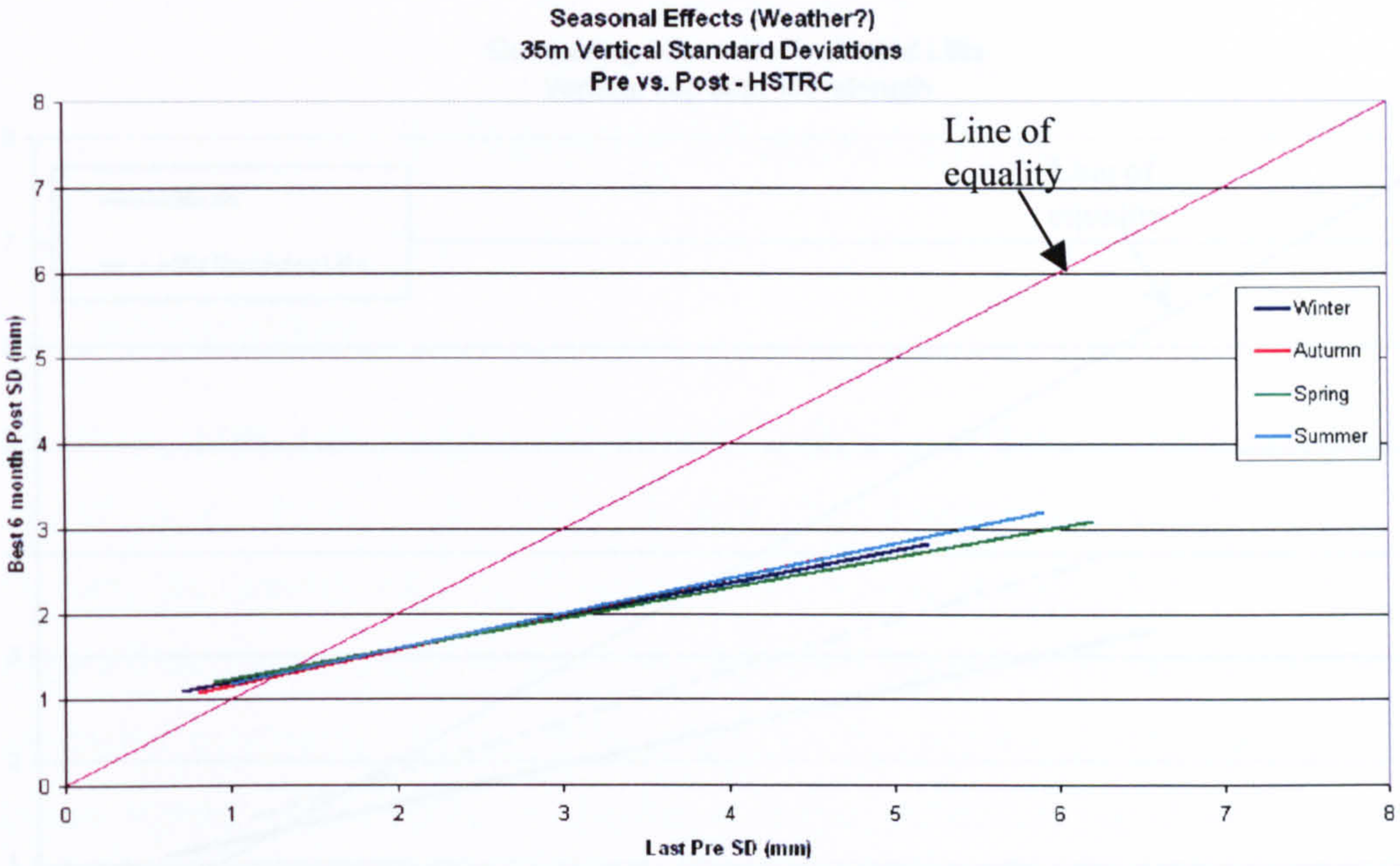

Figure 8.41 - Track quality improvement - weather analysis

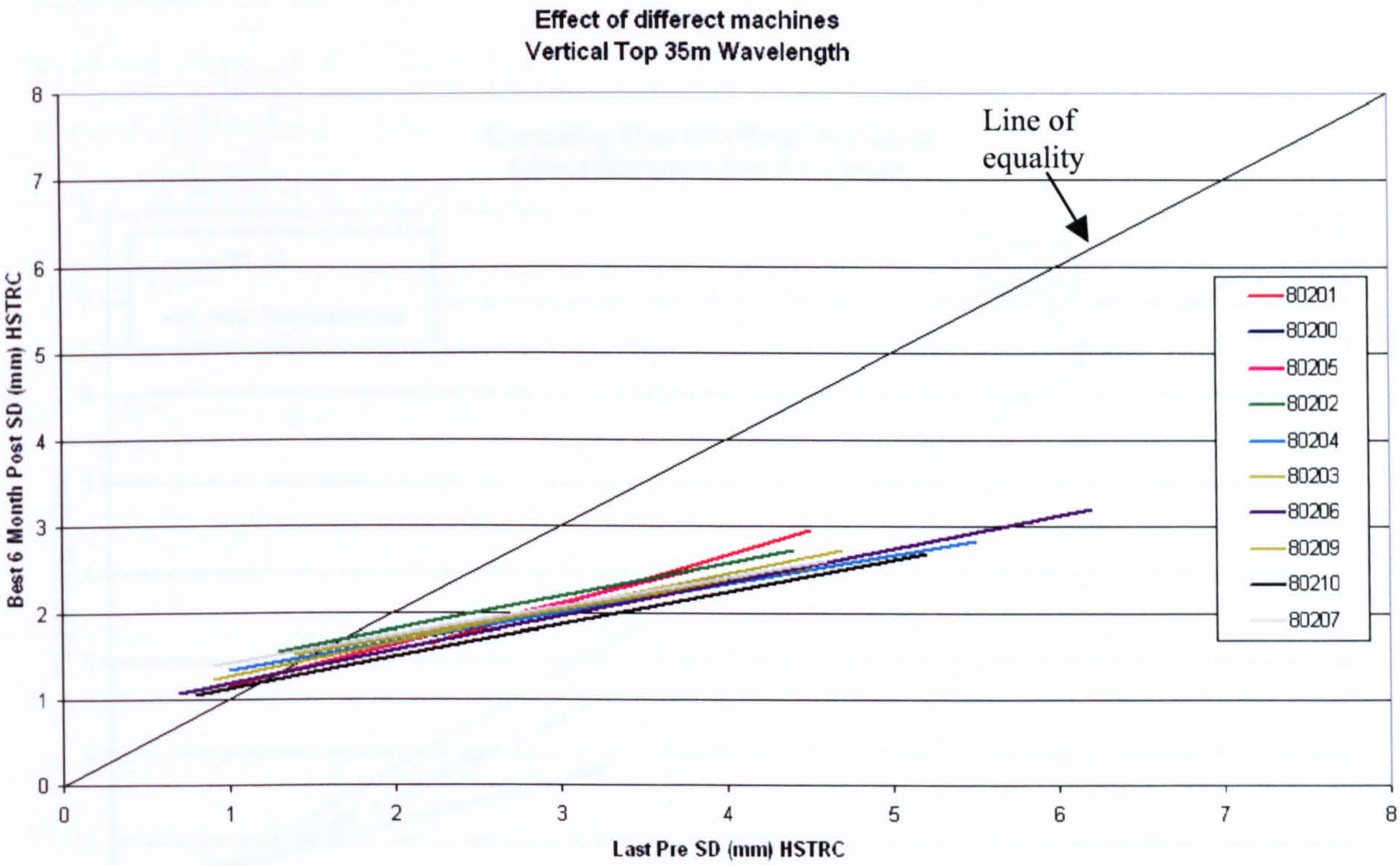

Figure 8.42 - Track quality improvement – performance of different stoneblowers

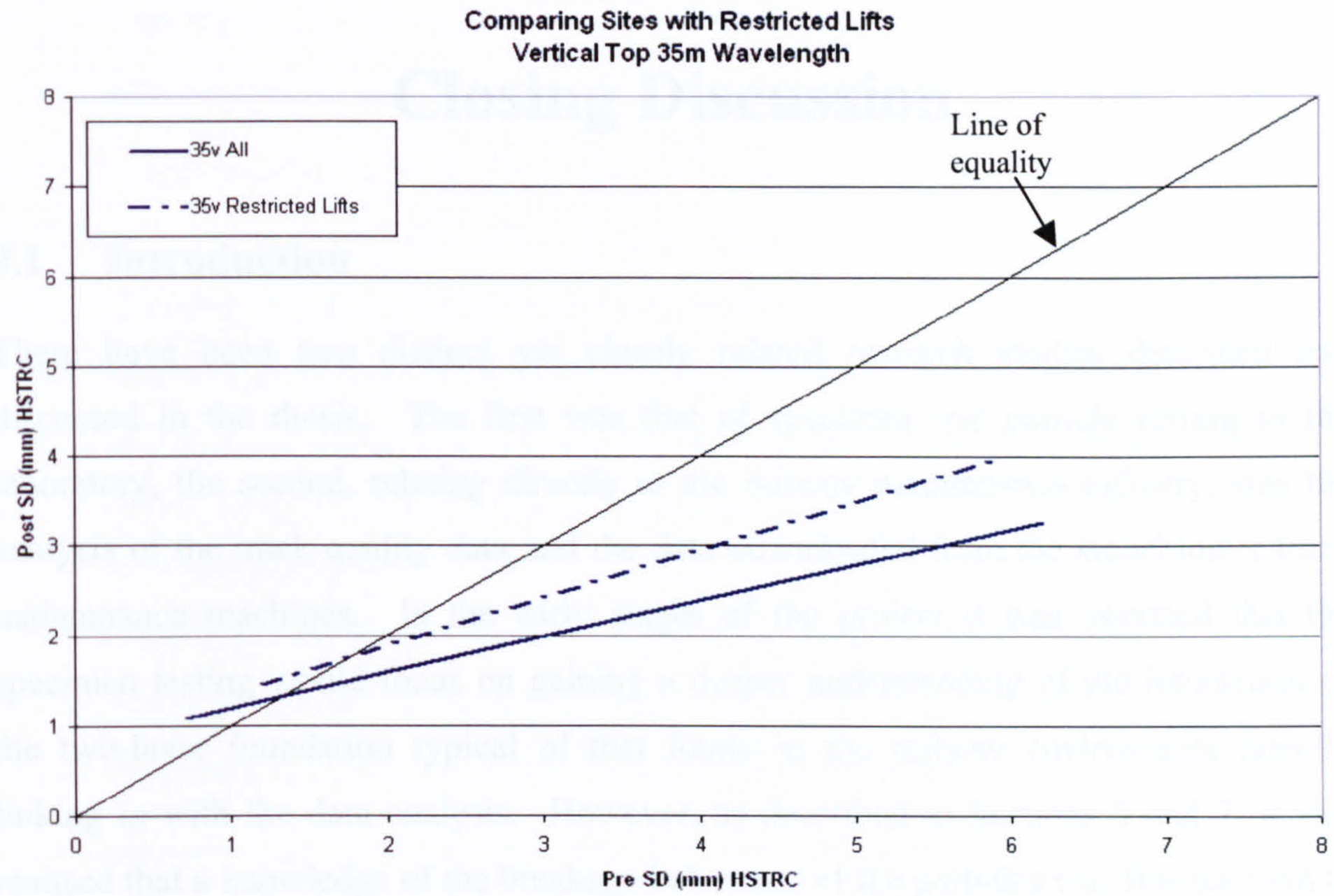

Figure 8.43 - Track quality improvement – effect of restricted lifts

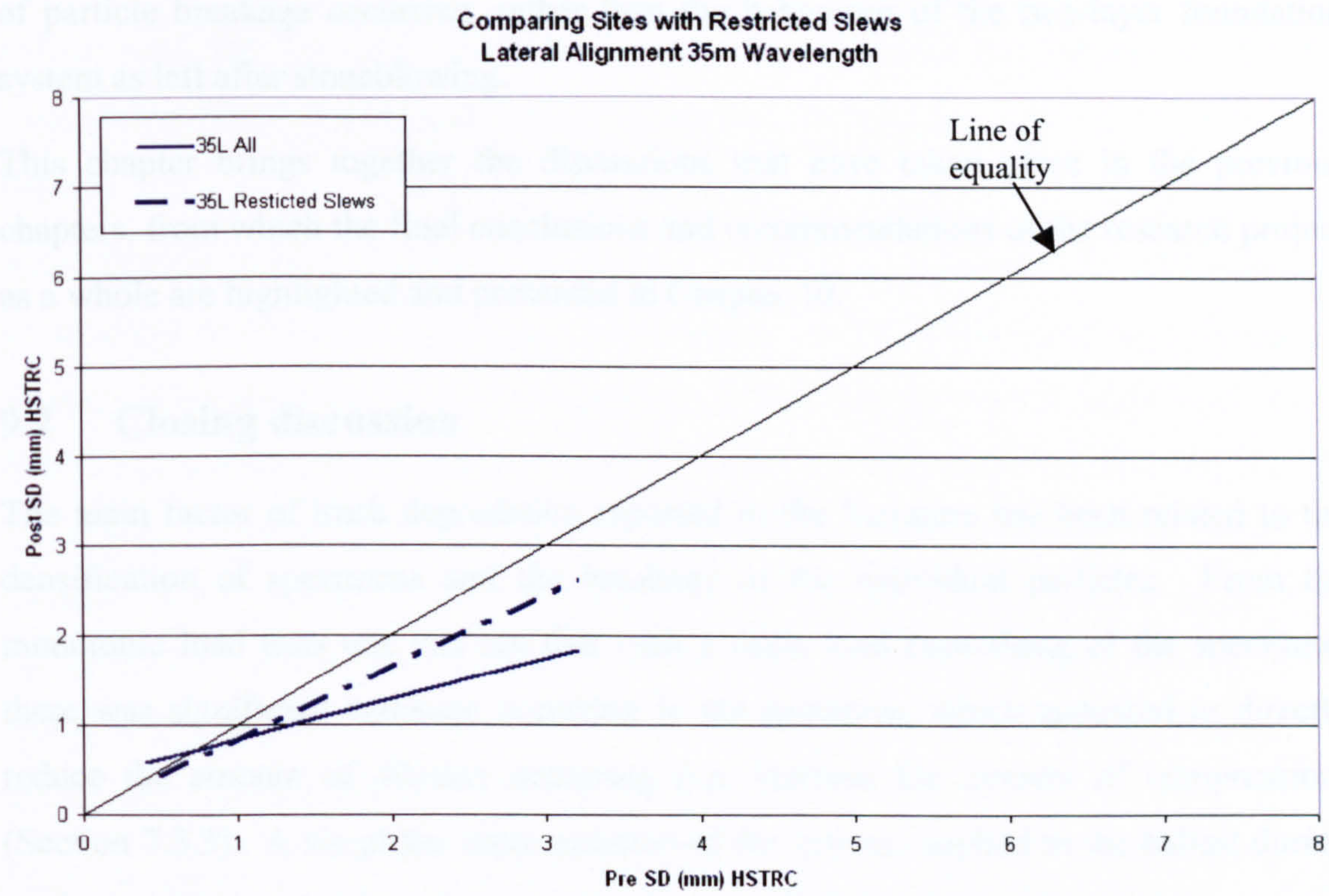

Figure 8.44 - Track quality improvement – effect of restricted slews

CHAPTER 9
Closing Discussion

9.1 Introduction

There have been two distinct yet closely related research studies described and discussed in the thesis. The first was that of specimen and particle testing in the laboratory, the second, relating directly to the railway maintenance industry, was the analysis of the track quality data and the data downloaded from the stoneblower track maintenance machines. In the early stages of the project it was assumed that the specimen testing would focus on gaining a deeper understanding of the interaction of the two-layer foundation typical of that found in the railway environment directly linking in with the data analysis. However, as described in Sections 5 and 7, it was realised that a knowledge of the breakage behaviour of the particles was fundamental to a deeper understanding of the overall behaviour and in particular the volume change and displacement of the material. A modification of the original programme of tests was therefore made, so as to concentrate on developing the understanding of the importance of particle breakage occurring, rather than the behaviour of the two-layer foundation system as left after stoneblowing.

This chapter brings together the discussions that have taken place in the previous chapters, from which the final conclusions and recommendations of the research project as a whole are highlighted and presented in Chapter 10.

9.2 Closing discussion

The main factor of track degradation reported in the literature has been related to the densification of specimens and the breakage of the individual particles. From the monotonic load tests one can see that with a static load (squashing of the specimen) there was significant breakage occurring in the specimen, which appeared to directly reduce the amount of dilation occurring (i.e. increase the amount of compression) (Section 7.3.3). A simplistic representation of the stresses applied to the ballast during track maintenance with a tamper may be modelled by a triaxial specimen rotated through 90° and loaded monotonically, as seen in Figure 9.1. The specimen would then be loaded in the horizontal plane rather than the vertical plane. Significant particle

breakage would occur, similar to that in the monotonic load tests in the current work. This would lead to a build up of fines and eventually to poor performance where the ballast bed would need renewing.

From the tests by Chrismer (1990) a Hardin breakage factor (B_r) (Hardin, 1985) for the amount of breakage occurring after 10 tamp cycles on granite ballast was calculated as $B_r = 12$. Using the correlation (Series 2-5) in Figure 7.3 the equivalent total breakage score (B_{TBS}) was determined as equal to approximately 87. Compared to the B_{TBS} values in Table 6.5 it can be seen that the breakage as measured in the above 10 tamp cycles ($B_{TBS} = 87$) was slightly lower than that seen in a single monotonic load test at 40kPa cell pressure ($B_{TBS} = 104$), and slightly more than the breakage seen in a 1 million load cycle test ($B_{TBS} = 80$). It can be assumed therefore from this that the actual strains and loads applied to the specimen in the monotonic load tests were significantly higher than those used by the tamper during track maintenance.

When comparing the amount of breakage occurring in the cyclic load tests to that of the monotonic load tests it was clear that the 100,000 load cycle tests at 40kPa cell pressure only induced a limited amount of breakage ($B_{TBS} = 35$), whereas in the monotonic load tests a significant amount of breakage occurred ($B_{TBS} = 104$) also under monotonic loading at 40kPa cell pressure. Furthermore, where stone was introduced between the ballast and the top cap, as with the two-layer foundations introduced by the stoneblower, there was a decrease in the amount of breakage seen in the underlying ballast.

Evans (1992) (Table 2.1) reports that passing traffic only produced $1/20^{th}$ of the amount of breakage of that of a single tamp maintenance. In the current work three times the amount of breakage occurred in the monotonic load test than in the cyclic load test at 40kPa cell pressure, where the maximum deviator stress was approximately 300kPa. At 140kPa cell pressure, where the maximum deviator stress reached approximately 580kPa, the amount of breakage in the monotonic load tests was 5.2 times higher than the amount of breakage occurring in similar cyclic load tests. From these results it would therefore appear that there was some disparity between the breakage behaviour occurring in the laboratory and that occurring in-situ.

From the limited number of damped specimens tested in Series 5 (Section 7.3.6), where a rubber mat was laid under the specimen to crudely simulate the subgrade and a wooden disc was inserted between the top cap and the material to represent the railway sleeper, it would appear that the action of reducing the resilient modulus caused an

increase in the amount of breakage and further plastic strains to occur. This would imply that a stiffer subgrade modulus would therefore decrease the amount of breakage and plastic strains occurring in the ballast bed. On the other hand a stiffer subgrade would cause increased wear to elements of the superstructure (Evans, 1992).

The breakage analysis in this current work has focused solely on the 50mm ballast particles and not on the 20mm stone particles. It remains to be seen whether the stone particles would also be more susceptible to breakage when wet than when dry. It is postulated that with the smaller particles there would be fewer cracks into which the pore fluid could enter, hence there would be little difference in the amount of breakage between the wet and dry 20mm stone with the pressure range considered here. However, at higher pressures the differences in behaviour may become more apparent.

In Chapter 8, describing the track quality and stoneblower maintenance data analysis, it was suggested that the weather had no obvious effect on the post-maintenance performance of the track (Section 8.4.7). However, it was clear from the laboratory work that under cyclic loading wet ballast particles appeared to be much weaker than dry particles and hence greater plastic strains and more breakage were observed (Section 7.3.7). The majority of the extra plastic straining above that of the dry specimens would appear to occur within the first 2,000 load cycles.

A possible explanation is that when new ballast is originally laid it requires maintenance one or two times in quick succession to re-level the track as the new material beds down. During this period any rain would increase the moisture content of the ballast bed. The ballast particles will be weakened due to the increase in moisture content and an increase in breakage will occur as the next train passes over the site. After this breakage has occurred then those ballast particles that have broken will not break further unless the stresses are significantly increased.

With tamping new ballast may be brought under the sleeper. These 'new particles' when wetted may also undergo degradation with loading. However with stoneblowing there is no new ballast in the load path and hence no further breakage will occur.

The necessity for completely reliable data to be recorded from the stoneblower, tamper and track recording car (HSTRC) in terms of the exact positioning of the machine and maintenance became apparent during the stoneblower data analysis (Chapter 8). Furthermore it is crucial that all details about all types of maintenance be recorded and passed on to the central database. From this good, reliable analysis of track

maintenance for both the stoneblower and the tamper can be made, from which good practice and long term management decisions may be made.

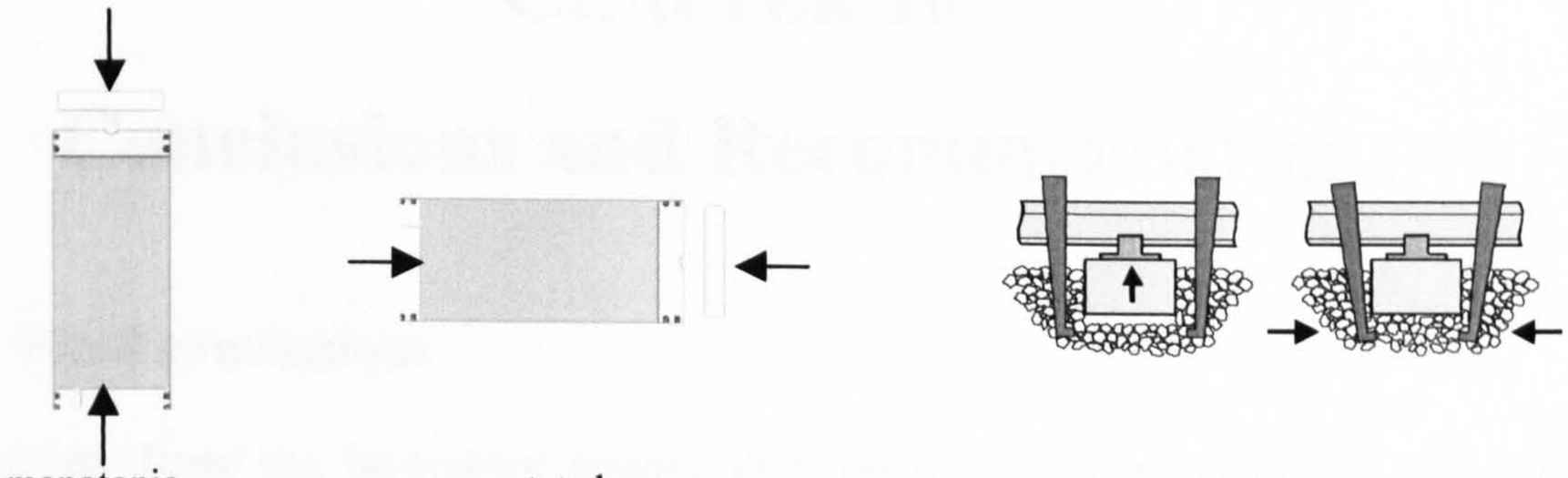

Figure 9.1 - Comparison between the loading applied in monotonic load triaxial tests and tamping maintenance

CHAPTER 10

Conclusions and Recommendations

10.1 Final conclusions

Conclusions from the laboratory studies and stoneblower data analysis have been presented in Sections 7.7 and 8.5 respectively. The following are the main conclusions drawn from the project as a whole:

1) Breakage behaviour has an important role to play in the performance of a granular material such as ballast, even at relatively low pressures.
2) Breakage led to a decrease in the rate of dilation (increased compression) under monotonic loading and increased permanent strain under cyclic loading.
3) A volumetric strain behaviour model has been proposed. This allowed the separation of the volumetric strain due to particle breakage and the volumetric strain due to shearing (particle rearrangement).
4) In the cyclic load tests a layer of smaller stone overlying the ballast decreased the amount of breakage occurring in the underlying ballast. The addition of a layer of stone also served to increase the resilient modulus, although any effect on the accumulation of plastic strain was not apparent.
5) In the monotonic load tests an increase in the thickness of stone gave a decrease in the amount of breakage occurring in the underlying ballast.
6) With a damped system (a rubber mat at the bottom of the specimen and a wooden disc at the top) there was an increase in the amount of breakage, an increase in the permanent strain and a decrease in the resilient modulus.
7) The addition of moisture to the material in the laboratory caused a significant increase in the permanent deformation under cyclic loading and an increase in the amount of breakage recorded, although in the monotonic tests there was little noted difference in stress-strain behaviour or in breakage behaviour. It is thought that under cyclic loading there may be a build up of internal pore water pressure, which is not quickly dissipated under rapid loading, causing a propagation in crack growth and weakening of the particles.
8) From the track quality data analysis it was clear that the design category was the single most important factor that controlled the quality and durability of the post

maintenance track. An enhanced A** algorithm should be installed on the stoneblower including lower measurement target values and tighter design target levels. Alongside this the lower design categories should also be upgraded in a similar manner to raise the performance of the machine.

9) Typically the post-maintenance performance was not influenced by either the route from which the data was analysed or the individual machine.
10) The appeared to be no effect due to the weather conditions, which was based on the month in the year.
11) Restricted pieces of track where maintenance could not be carried out had a significant effect reducing the post-maintenance performance.

10.2 Recommendations for future work

From the laboratory testing and the stoneblower and track quality data analysis carried out, several gaps have been identified in the understanding and knowledge regarding the geotechnical behaviour of ballast materials for railway track maintenance. The main areas that were considered to be most usefully investigated in the future are listed below.

1) Further specimen testing is required in the following four areas;

   i) To verify the volumetric strain model testing needs to be carried out over a greater range of cell pressures and by stopping the tests at different axial strains in the monotonic load tests. The amount of breakage may then be recorded and the volumetric strain due to breakage calculated.

   ii) To investigate the effects of moisture in the monotonic load tests, testing at higher cell pressures is required. Testing using different moisture contents is also necessary to gain a deeper understanding of the effect of moisture on the breakage and strains in the ballast. Furthermore, the behaviour of wetted 20mm stone needs to be investigated to see if it, like ballast, deforms more (and has greater breakage) than the dry specimens.

   iii) To clarify the effect of the rate of loading on the axial strains and breakage of the ballast further testing is needed with different load waveforms.

   iv) Further investigation is needed to establish the effect of 'damping' on the specimens.

2) The Werkmeister et al. (2001) revised shakedown model shows potential, but the model needs to be slightly adapted for ballast materials and to include the effects of moisture content before verification with a further testing programme.

3) Similar analysis needs to be carried out on data from track maintained with tamping.

REFERENCES

Adams, M. J., M. A. Mullier & J. P. K. Seville (1994). Agglomerate strength measurement using a uniaxial confined compression test. Powder Technology **78:** 5-13.

Al-Hussaini, M. (1983). Effects of particle size and conditions on the strength of crushed basalt. Canadian Geotechnical Journal **20**(4): 706-717.

Alva-Hurtado, J. E. D. & E. T. Selig (1981). Survey of laboratory devices for measuring soil volume change. Geotechnical Testing Journal, ASTM **4**(1): 11-18.

Anderson, W. F., P. I. Fair, A. J. Key & P. McMichael (2001). The deformation behaviour of two layer railway ballast beds. Proceedings of the XV International Conference on Soil Mechanics and Geotechnical Engineering, Istanbul.

Anderson, W. F. & A. J. Key (2000). Model testing of a two layer railway track ballast. Journal of Geotechnical and Geoenvironmental Engineering, ASCE **126**(4): 317-323.

Ansell, P. & S. F. Brown (1978). Cyclic simple shear apparatus for dry granular materials. Geotechnical Testing Journal, ASTM **1**(2): 82-92.

Araruna, J. T., Jr., A. H. Harwood & B. G. Clarke (1995). A practical, economical and precise volume change measurement device. Geotechnique **45**(3): 541-544.

Atkinson, J. H. (1993). An introduction to the mechanics of soils and foundations. London, McGraw-Hill.

Awoleye, E. O. A. (1998). A numerical model for the determination of track ballast life. Proceedings of the 1st International Conference Railway Engineering.

Barksdale, R. G. (1972). Laboratory evaluation of rutting in base-course materials. Proceedings of the 3rd International Conference on Structural Design of Asphalt Pavements, 161-174.

Barksdale, R. G. (1991). Compressive stress pulse times in flexible pavements for use in dynamic testing, Highway Research Record, Highway Research Board. **345:** 32-44.

Baulk, R. (1999). Stoneblower performance monitoring. Phase 1b., AEA Technology (Rail).

Billam, J. (1971). Some aspects of the behaviour of granular materials at high pressures. Stress strain behaviour of soils. Cambridge, Foulis**:** 69-80.

Billam, J. (1972). Some aspects of the behaviour of granular materials at high pressures. Stress-strain behaviour of soils. Proceedings of the Roscoe Memorial Symposium.

Bishop, A. W. (1950). Measurement of the shear strength of soils. Geotechnique **2**(1): 113-116.

Bishop, A. W. (1966). The strength of soils as engineering materials. Geotechnique **16**(2): 91-128.

Bishop, A. W. & A. K. G. Eldin (1953). The effect of stress history on the relation between ϕ and porosity in sand. Proceedings of 3rd International Conference in Soil Mechanics, 1: 126-130.

Bishop, A. W. & G. E. Green (1965). The influence of end restraints on the compression of cohesionless soils. Geotechnique **15**(3): 243-266.

Bolton, M. D. & G. R. McDowell (1996). Clastic mechanics. IUTAM Symposium on Mechanics of Granular and Porous Materials, Dordrecht, Kluwer.

Bowman, E. T., K. Soga & W. Drummond (2001). Particle shape characterisation using Fourier descriptor analysis. Geotechnique **51**(6): 545-554.

Boyce, J. R. (1976): The behaviour of granular material under repeated loading. PhD Thesis. Dept. Civil Engineering, University of Nottingham.

Boyce, J. R. & S. F. Brown (1976). Technical note: Measurement of elastic strain in granular materials. Geotechnique **26**(4): 637-640.

Boyce, J. R., S. F. Brown & P. S. Pell (1976). The resilient behaviour of a granular material under repeated loading. Proceedings of the Australian Road Research Board **28**: 8-19.

Braddick, H. J. J. (1963). The physics of experimental method. London, Chapman and Hall.

British Railways Board (1993): Track Maintenance Handbook GC/EH0005. British Railways Board, Group Standard: 207.

Brown, S. F. (1974). Repeated load testing of a granular material. Journal of Geotechnical Engineering Division, ASCE **100**(GT7): 825-841.

Brown, S. F. (1996). Soil mechanics in pavement engineering. Geotechnique **46**(3): 383-426.

Brown, S. F. & A. F. L. Hyde (1975). Significance of cyclic confining stress in repeated-load triaxial testing of granular material. Transportation Research Record **537**: 49-57.

Brown, S. F. & M. P. O'Reilly (1991). Cyclic loading of soils: from theory to design, Blackie.

Brown, S. F. & P. S. Pell (1967). An experimental investigation ot the stresses, strains and deflections in a layered pavement structure subjected to dynamic loads, Proceedings of the Second International Conference on Structural Design of Asphalt Pavements, University of Michigan, Ann Arbor, USA, 487-504.

Brown, S. F. & E. T. Selig (1991). The design of pavement and rail track foundations, Chapter 6. Cyclic loading of soils; from theory to design. M. P. O'Reilly & S. F. Brown. Glasgow and London, Blackie: 249-305.

Cedergren, H.R. (1989). Seepage, drainage and flow nets, Third Edition, John Wiley & Sons

Chan, F. W. K. & S. F. Brown (1994). Significance of principal stress rotation in pavements. Proceedings of the XIII International Conference of Soils Mechanics and Foundation Engineering, New Delhi, India.

Chandler, H. W. (1985). A plasticity theory without Druckers postulate, suitable for granular materials. Journal of Mech. Phys. of Solids **33**: 215-226.

Charles, J. A. & K. S. Watts (1980). The influence of confining pressure on the shear strength of compacted rockfill. Geotechnique **30**(4): 353-367.

Cheung, L. W. (1994). Laboratory assessment of pavement foundation materials. Civil Engineering, University of Nottingham.

Chrismer, S. M. (1990). Track surfacing with conventional tamping and stone injection. Chicago, Illinois, ARR Technical Center: 32.

Chrismer, S. M. (1991). Increased ballast maintenance life through stone injection. Railway Track and Structures: 32.

Chrismer, S. M., and E.T. Selig (1991). Computer model for ballast maintenance planning. Proceedings of the 5th International Heavy Haul Railway Conference, Beijing, China. 223-227.

Claisse, P. & C. Calla (2003). Tests on a two layered ballast system. Proceedings of the 6th International Conference Railway Engineering, Edinburgh.

Collins, I. F. & M. Boulbibane (2000). Geomechanical analysis of unbound pavements based on shakedown theory. Journal of Geotechnical and Geoenvironmental Engineering, ASCE **126**(1): 50-59.

Coop, M. R. & I. K. Lee (1993). The behaviour of granular soils at elevated stresses. Predictive soil mechanics, Wroth Memorial Symposium. London, Thomas Telford: 186-198.

Cope, D. L. (1992). Track: Its structural function in response to traffic forces. 4th RIA Track Sector Course. Nottingham. 1; Section 3: Design Paper 4.3.1.

Cundall, P. A. & O. D. L. Strack (1979). A discrete numerical model for granular assemblies. Geotechnique **29**(1): 47-65.

Datta, M., S. K. Gulhati & G. V. Rao (1979). Crushing of Calcareous sands during shear. Proceeding of the XI Annual Conference on Offshore Technology Conference, Houston, Texas.

Dawson, A. R. & S. D. Gillett (1998). Assessment of on sample instrumentation for repeated load triaxial tests. Transportation Research Record **1614**: 52-60.

Dawson, A. R. & A. Gomes Correia (1987). The effects of stress and pore water pressure states on the resilient properties of granular materials. Proceedings of 12th ICSMFE, Rio de Janeiro, Balkema, Rotterdam.

Dawson, A. R. & A. Gomes Correia (1996). The effects of subgrade clay condition on the stuctural behaviour of road pavements. Flexible Pavements. A. Gomes Correia, Balkema, Rotterdam: 113-119.

De Souza, J. M. (1958) Compressibility of sands at high pressures. Massachusetts Institute of Technology, Cambridge, Massachusetts: 63-64.

Eisenmann, J., G. Leykauf & L. Mattner (1993). Deflection and settlement behaviour of ballast. Proceedings of the fifth International Heavy Haul Railway Conference, Beijing.

Eisenmann, J. & L. Mattner (1989). Setzungsverhalten des schotters bei der simulation hoher fahrgeschwindigkeiten, Mitteilungen des Prüfamtes für Bau von Landverkehswegen der Technischen Universität München, Heft 55.

Esveld, C. (1989). Modern railway track, MRT productions, Germany.

Evans, E. (1992). The design of railway track foundations. 4th RIA Track Sector Course. Nottingham. 1; Section 3: Design; Paper 4.3.3.

Fair, P. I. & P. McMichael (2002). Understanding track quality in the light of stoneblower data files. Railtex 2002.

Fair, P. I. (2002). Comprehensive stoneblower data analysis (on track maintained in 1999 and 2000). Research report RF002490/1. Dept. of Civil and Structural Engineering. University of Sheffield, UK.

Festag, G. & R. Katzenbach (2001). Material behaviour of dry sand under cyclic loading. Proceedings of the XV International Conference on Soil Mechanics and Geotechnical Engineering, Istanbul, Balkema.

Field, W. G. (1963). Towards the statistics definition of a granular material. Proceedings of the 4th Australian and New Zealand Conference on Soil Mechanics, 143-148.

Ford, R. (1995). Differential ballast settlement, and consequent undulations in track caused by vehicle-track interaction. Vehicle System Dynamics Special Supplement 24: 222-233.

Freeme, C. R. & V. P. Servas (1985). Advances in pavement design and rehabilitation. Accelerated Testing of Pavements. Pretoria, CSIR.

Gaskin, P. N., G. P. Raymond & A. G. Powell (1978). Response of railroad ballast to vertical vibration. Transportation Engineering Journal, ASCE **104**(TE1): 75-87.

Gidel, G., D. Breysse, A. Denis & J.-J. Chauvin (2000). Material fabric and mechanical properties after compaction for unbound granular materials. International Workshop on Compaction of Soils, Granulates and Powders, Innsbruck, Balkema, Rotterdam, Brookfield.

Goto, S., F. Tatsuoka, S. Shibuya, Y. S. Kim & T. Sato (1991). A simple guage for local small strain measurements in the laboratory. Soils and Foundations, Japanese Society of Soil Mechanics and Foundation Engineering **31**(1): 169-180.

Griffith, A. A. (1920). The phenomena of rupture and flow in solids. Philos. Trans. R. Soc. London a(221): 163-198.

Hagerty, M. M., D. R. Hite, C. R. Ulrich & D. J. Hagerty (1993). One-dimensional high-pressure compression of granular media. Journal of Geotechnical Engineering, ASCE **119**(1): 1-18.

Hall, E. B. & B. B. Gordan (1963). Triaxial testing with large scale pressure equipment. Laboratory shear testing for soils. ASTM **STP 361**: 315-328.

Hardin, B. O. (1985). Crushing of soil particles. Journal of Geotechnical Engineering, ASCE **111**(10): 1177-1191.

Hafiz M. A. (1950). Strength characteristics of sands and gravels in direct shear. Ph.D. Thesis, London.

Head, K. H. (1992). Manual of soil laboratory testing. Portsmouth, Pentech Press Limited.

Hellawell, A. (1997). Stoneblower provides ballast maintenance solution. Railway Gazette International(September): 595-596.

Hendron, A. J. (1963). The behaviour of sand in one-dimensional compression. Urbana, Illinois, University of Illinois: 50-89.

Henkel, D. J. & G. D. Gilbert (1952). The effect of the Rubber membrane on the measured triaxial compression strength of clay samples. Geotechnique **3**: 20-29.

Hicks, R. G. & C. L. Monismith (1971). Factors influencing the resilient response of granular materials. Highways Research. Washington D.C., Highways Research Board. **345:** 15-31.

Hyde, A. F. L. & Y. Nakata (2001). Particle crushing and yielding of clastic materials. Proceedings of the XV International Conference on Soil Mechanics and Geotechnical Engineering, Istanbul, Balkema.

Indraratna, B., D. Ionescu & H. D. Christie (1998). Shear behaviour of railway ballast based on large scale triaxial tests. Journal of Geotechnical and Geoenvironmental Engineering, ASCE **124**(5): 439-449.

Indraratna, B., L. S. S. Wijewardena & A. S. Balasubramaniam (1993). Large scale triaxial testing of Greywacke rockfill. Geotechnique **43**(1): 37-51.

Insley, A.E. (1967). Discussion on compressibility and crushing of granular soils in anisotropic triaxial compression. Canadian Geotechnical Journal, Vol. 4 No. 1.

Jaeger, J. C. (1967). Failure of rocks under tensile conditions. International Journal of Rock and Mining Science **4**: 219-227.

Janardhanam, R. & C. S. Desai (1983). Three dimensional testing and modeling of ballast. Journal of Geotechnical Engineering, ASCE **109**(6): 783-796.

Johnson, D. M. (1983). The introduction of British Rail's stoneblowing technique as an alternative to tamping. 1983 AREA Conference, Chicago.

Kalcheff, I. V. & R. G. Hicks (1973). A test procedure for determining the resilient properties of granular materials. Journal of Testing and Evaluation **1**(6): 472-479.

Keubris, R. H. & Y. P. Vaid (1990). Corrections for membrane strength in the triaxial test, Geotechnical Testing Journal, Vol. 13, No. 4, December 1990, 361-369.

Key, A. J. (1998). Behaviour of two layer railway ballast under cyclic and monotonic loading. PhD Thesis. Dept. of Civil and Structural Engineering, University of Sheffield.

Khogali, W. E. I. & M. Zeghal (2000). On the resilient behaviour of unbound aggregates. Unbound aggregates in road construction. Dawson. Rotterdam, Balkema: 29-34.

Knutson, R. M. & M. R. Thompson (1978). Permanent deformation behaviour of railway ballast. Transportation Research Record **694**: 47-53.

Kohata, Y., G.-L. Jiang & E. Sekine (1999). Deformation properties of railroad ballasts subjected to monotonic and cyclic loadings. World Congress on Railway Research, Tokyo.

Kolisoja, P. (1997). Factors affecting the deformation properties of coarse grained granular materials. Proceedings of the XIV International Conference on Soil Mechanics and Foundation Engineering, Hamburg, Germany.

Lade, P. V. (1988). Automatic volume change and pressure measurement devices for triaxial testing of soils. Geotechnical Testing Journal, ASTM **11**(4): 263-268.

Lade, P. V., J. A. Yamamuro & P. A. Bopp (1996). Significance of particle crushing in granular materials. Journal of Geotechnical Engineering Division, ASCE **122**(4): 309-316.

La Rochelle, P., S. Leroueil, B. Trak, L. Blais-Leroux & F. Tavenas (1988), Area corrections in triaxial tests, Advanced |Triaxial Testing of Soil and Rock, ASTM, Philadelphia, STP 977, 715-731.

Lashine, A.K., S.F. Brown, P.S. Pell (1971). Dynamic properties of soils. Report No. 2 submitted to Koninklijke/Shell Laboratorium, Dept. Civil and Structural Engineering, University of Nottingham, UK.

Lau, C. Y. (2003): Behaviour of railway track foundation. Dept. of Civil and Structural Engineering, MEng dissertation. University of Sheffield.

Lee, D.M. (1992). The angles of friction of granular fills. PhD Thesis, Cambridge University, UK.

Lee, I. K. & M. R. Coop (1995). The intrinsic behaviour of decomposed granite soil. Geotechnique **45**(1): 117-130.

Lee, K. L. & I. Farhoomand (1967). Compressibility and crushing of granular soils in anisotropic compression tests. Canadian Geotechnical Journal **4**(1): 68-86.

Lee, K. L. & H. B. Seed (1967). Drained strength characteristics of sands. Journal of the Soil Mechanics and Foundations Division, ASCE **93**(SM6): 117-141.

Lee, K. L. & F. J. Vernese (1978). End restraint effects on cyclic triaxial strength of sand. Journal of Geotechnical Engineering Division, ASCE **104**(GT6): 705-719.

Lekarp, F., U. Isacsson & A. R. Dawson (2000a). State of the art. I: Resilient response of unbound aggregates. Journal of Transportation Engineering **126**(1): 66-75.

Lekarp, F., U. Isacsson & A. R. Dawson (2000b). State of the art. II: Permanent strain response of unbound aggregates. Journal of Transportation Engineering **126**(1): 76-83.

Leslie, D. D. (1963). Large scale triaxial tests on gravelly soils. Proceedings of the 2nd Pan-American Conference on SMFE, Brazil.

Leslie, D. D. (1975): Shear strength of rockfill

Physical Properties Engineering Study 526. Sausalito, US Army Corps of Engineers.

Leung, C. F., F. H. Lee & N. S. Yet (1996). The role of particle breakage in pile creep in sands. Canadian Geotechnical Journal **33**: 888-898.

Li, D. & E. T. Selig (1995). Wheel/Track dynamic interaction: Track substructure perspective. Vehicle System Dynamics Supplement 24: 183-196.

Lopez Pita, E. A. & P. Fonseca Teixeira (2002). Influence of ballast density on track deformation. 5th International Railway Engineering Conference, London, Railway Engineering.

Luzzani, L. & M. R. Coop (2001). On the relationship between particle breakage and the critical state of sands. Soils and Foundations, Japanese Society of Soil Mechanics and Foundation Engineering **42**(2): 71-78.

Marachi, N. D., C. K. Chan & H. B. Seed (1972). Evaluation of properties of rockfill materials. Journal of Soil Mechanics and Foundations Division, ASCE **98**(SM1): 95-114.

Marsal, R. J. (1966). Large scale testing of granular materials. ASCE Structural Engineering Conference, Miami.

Marsal, R. J. (1967). Large scale testing of rockfill materials. Journal of the Soil Mechanics and Foundations Division, ASCE **93**(SM2): 27-43.

McDowell, G. R. & M. D. Bolton (1998). On the micro mechanics of crushable aggregates. Geotechnique **48**(5): 667-679.

McDowell, G. R., M. D. Bolton & D. Robertson (1996). The fractal crushing of granular materials. Journal of Mechanics of Physical Solids **44**(12): 2079-2102.

McDowell, G. R. & C. M. Daniell (2001). Technical Note: Fractal compression of soils. Geotechnique **51**(2): 173-176.

McDowell, G. R. (2001). Statistics of soil particle strength. Geotechnique **51**(10): 897-900.

McMichael, P. L. (1998). The Stoneblower comes of age. Development, testing and operating of a new track maintenance system. Presented at the ICE.

McMichael, P. L. (1999a). Stoneblower Performance, Internal report Dv_aea2.doc, 11 June 1999, Railtrack.

McMichael, P. L. (1999b). Stoneblower Performance, Internal report SBREP.doc\pm6, Railtrack.

McMichael, P. L. (2001). Personal communication during the time spent working with the stoneblower project team, Railtrack, Derby UK.

Miura, N., H. Murata & N. Yasufuku (1984). Stress-strain characteristics of sand in a particle crushing region. Soils and Foundations, Japanese Society of Soil Mechanics and Foundation Engineering **24**(1): 77-89.

Miura, N. & S. O-Hara (1979). Particle crushing of decomposed granite soil under shear stresses. Soils and Foundations, Japanese Society of Soil Mechanics and Foundation Engineering **19**(3): 1-14.

Miura, N. & Y. Yamanouchi (1975). Effect of water on the behaviour of a quartz rich sand under high stresses. Soils and Foundations, Japanese Society of Soil Mechanics and Foundation Engineering **15**(4): 23-34.

Morris, B. H. (1992). Major track design factors. 4th RIA Track Sector Course, Nottingham, UK.

Nakata, Y., A. F. L. Hyde, M. Hyodo & H. Murata (1999). A probabilistic approach to sand particle crushing in the triaxial test. Geotechnique **49**(5): 567-583.

Nakata, Y., M. Hyodo, A. F. L. Hyde, Y. Kato & H. Murata (2001a). Microscopic particle crushing of sand subjected to high pressure one-dimensional compression. Soils and Foundations, Japanese Society of Soil Mechanics and Foundation Engineering **41**(1): 69-82.

Nakata, Y., Y. Kato, M. Hyodo, A. F. L. Hyde & H. Murata (2001b). One dimensional compression behaviour of uniform sand related to particle crushing strength. Soils and Foundations, Japanese Society of Soil Mechanics and Foundation Engineering **41**(2): 39-51.

Ng, C. W. W., L. T. Zhan & Y. J. Cui (2002). A simple system for measuring volume changes in unsaturated soils. Geotechnical Testing Journal **39**: 757-764.

Nobari, E. S. & J. M. Duncan (1972). Effects of reservoir filling on stresses and movements in earth and rockfill dams. Berkley, California, Ofc. of Res. Services. University of California.

Nutbrown, D. & R. Nicholas (1999). Stoneblower experiences. PWI Autumn Technical Seminar.

Oda, M. (1977). Co-ordination number and its relation to shear strength of granular materials. Soils and Foundations, Japanese Society of Soil Mechanics and Foundation Engineering **17**(2): 29-42.

Oldecop, L. A. & E. E. Alonso (2001). A model for rock compressibility. Geotechnique **51**(2): 127-139.

Pappin, J. W., S. F. Brown & M. P. O'Reilly (1992). Effective stress behaviour of saturated and partially saturated granular materials subject to repeated loading. Geotechnique **42**(3): 485-497.

Pestana, J. M. & A. J. Whittle (1995). Compression model of cohesionless soils. Geotechnique **45**(4): 611-631.

Ping, W. V. & Z. Yang (1998). Experimental verification of resilient deformation of granular subgrades. Transportation Research Record **1639.**

Raad, L., G.H. Minassian, and S. Gartin (1992). Characterisation of saturated granular bases under repeated loads. Transportation Research Record 1369, TRB, Washington, D.C. 73-82.

Ramamurthy, T., V. K. Kanitkar & K. Prakash (1974). Behaviour of coarse grained soils under high stresses. Indian Geotechnical Journal **4**(1): 39-63.

Raymond, G. P. (1985). Analysis of track support and determination of track modulus. Transportation Research Record **1022**: 80-90.

Raymond, G. P. & V.A. Diyaljee (1985). Railroad ballast load ranking classification. Journal of Geotechnical Engineering. ASCE. 105(10), 1133-1153.

Raymond, G. P. & R. J. Bathurst (1994). Repeated load response of aggregate in relation to track quality index. Canadian Geotechnical Journal **31**: 547-554.

Roberts, J. E. & J. M. De Souza (1958). The compressibility of sands. Proceedings of the ASTM **58**: 1269-1277.

Salman, T. H. (1994). Triaxial behaviour of partially saturated granular soils at low stress levels. PhD Thesis. Department of Civil and Structural Engineering, University of Sheffield, UK.

Sammis, C., G. King & R. Biegel (1987). The kinematics of guoge deformation. Pure Applied Geophysics **125**: 777-812.

Sato, Y. (1995). Japanese studies on deterioration of ballasted track. Vehicle System Dynamics Special Supplement 24: 197-208.

Scholey, G. K., J. D. Frost, D. C. F. Lo Presti & M. Jamiolkowski (1995). A review of instrumentation for measuring small strains during triaxial testing of soil specimens. Geotechnical Testing Journal, ASTM **18**(2): 137-156.

Seed, H. B., F. G. Mitry, C. L. Monismith & C. K. Chan (1967). Factors influencing the resilient deformations of untreated aggregate bases in two layered pavements subject to repeated loadings. Highways Research Record 140, Highways Research Board: 19-57.

Selig, E. T. & J. E. D. Alva-Hurtado (1982). Predicting effects of repeated wheel loading on track settlement. 2nd International Heavy Haul Railway Conference, Colorado Springs.

Selig, E. T. & J. M. Waters (1994). Track geotechnology and substructure management. London, Thomas Telford.

Selig, E. T., T. S. Yoo & C. M. Panuccio (1982). Mechanics of ballast compaction. Volume 3: Field test results for ballast physical state measurement. Washington D.C., Federal Railroad Administration, Office of Research and Development.

Shenton, M. J. (1975). Deformation of railway ballast under repeated load conditions. Railroad Track Mechanics & Technology. Oxford, UK, Pergamon Press.

Sowers, G. F., R. C. Williams & T. S. Wallace (1965). Compressibility of broken rock and settlement of rockfills. Proceedings of 6th Conference on Soil Mechanics and Foundation Engineering, Montreal.

Steacey, S.J. & C.G. Sammis (1991). An automaton for fractal patterns of fragmentation. Nature 353, No.6341, 250-252.

Stewart, H. E. (1986). Permanent strain for cyclic variable amplitude loadings. Journal of Geotechnical Engineering Division, ASCE **112**(6): 646-660.

Stewart, H. E. & E. T. Selig (1982). Predictions of track settlement under traffic loading. 2nd International Heavy Haul Railway Conference, Colorado Springs.

Sweere, G. T. H. (1990). Unbound granular bases for roads. PhD Thesis. Delft University of Technology.

Taylor, D. W. (1948). Fundamentals of soil mechanics. New York, John Wiley and Sons, Inc.

Thom, N. H. & S. F. Brown (1987). The effect of moisture on the structural performance of a crushed-limestone road base. Transportation Research Record 1121, Transportation Research Board, Washington, D.C., 50-56

Thom, N. H. & S. F. Brown (1988). The effect of grading and density on the mechanical properties of a crushed dolomitic limestone. Proceedings of the Australian Road Research Board **14**(Pt. 7): 94-100.

Thom, N. H. & S. F. Brown (1989). The mechanical properties of unbound aggregates from various sources. Unbound Aggregates in Roads, Jones and Dawson, Butterworths, London, 130-142.

Thompson, M. R. & K. L. Smith (1998). Repeated triaxial characterization of granular materials. Transportation Research Record **1278**: 61-69.

Tutumluer, E., N. Garg & M. R. Thompson (1998). Granular material radial deformation measurements with a circumferential extensometer in repeated load triaxial testing. Transportation Research Record **1614**: 61-69.

Ueng, T. S. & T.-J. Chen (2000). Energy aspects of particle breakage in drained shear of sands. Geotechnique **50**(1): 65-72.

Uzan, J. (1985). Characterisation of granular material. Transportation Research Record **1022**: 52-59.

Vesic, A. S. & R. D. Barksdale (1963). On shear strength of sand at very high pressures. Laboratory shear testing for soils. ASTM STP 361: 301-305.

Vesic, A. S. & G. W. Clough (1968). Behaviour of granular materials under high stresses. Journal of Soil Mechanics and Foundations Division, ASCE **94**(SM3): 661-688.

Weibull, W. (1951). A statistical distribution function of wide applicability. Journal of Applied Mechanics **18**: 293-297.

Werkmeister, S., A. R. Dawson & F. Wellner (2001). Permanent deformation behaviour of granular materials and the Shakedown concept. Transportation Research Record **1757**: 75-81.

Wright, S. E. (1983). Damage caused to ballast by mechanical maintenance techniques, British Railway Research.

Yamamuro, J. A. & P. V. Lade (1993). Effects of strain rate on instability of granular soils. Geotechnical Testing Journal **16**(3): 304-313.

Yamamuro, J. A. & P. V. Lade (1996). Drained sand behaviour in axisymmetric tests at high pressures. Journal of Geotechnical Engineering, ASCE **122**(2): 109-119.